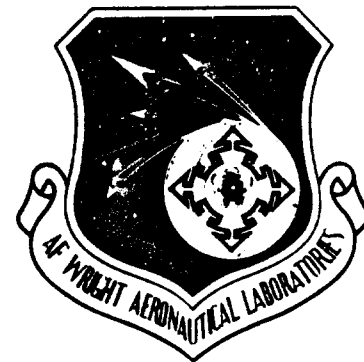


AFWAL-TR-84-2042
ESL-TR-84-29



ALTERNATE FUELS COMBUSTION RESEARCH

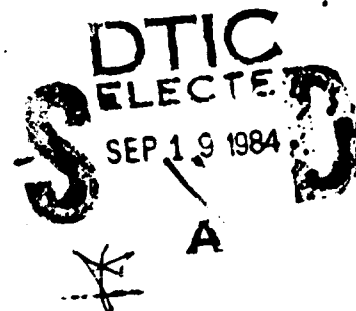
PRATT & WHITNEY CANADA
MISSISSAUGA, ONTARIO
CANADA

JULY 1984

Final Report for Period May 1980 - September 1983

Approved for public release; distribution unlimited.

AERO PROPULSION LABORATORY
AIR FORCE WRIGHT AERONAUTICAL LABORATORIES
AIR FORCE SYSTEMS COMMAND
WRIGHT-PATTERSON AIR FORCE BASE, OHIO 45433



REPRODUCED FROM
BEST AVAILABLE COPY

84 09 19 001

AD-A145 691

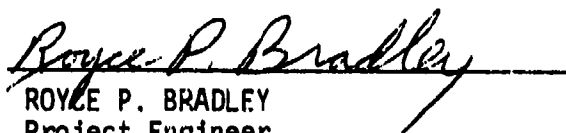
DTIC FILE COPY

NOTICE

When Government drawings, specifications, or other data are used for any purpose other than in connection with a definitely related Government procurement operation, the United States Government thereby incurs no responsibility nor any obligation whatsoever; and the fact that the government may have formulated, furnished, or in any way supplied the said drawings, specifications, or other data, is not to be regarded by implication or otherwise as in any manner licensing the holder or any other person or corporation, or conveying any rights or permission to manufacture use, or sell any patented invention that may in any way be related thereto.

This report has been reviewed by the Office of Public Affairs (ASD/PA) and is releasable to the National Technical Information Service (NTIS). At NTIS, it will be available to the general public, including foreign nations.

This technical report has been reviewed and is approved for publication.



ROYCE P. BRADLEY
Project Engineer
Fuels Branch
Fuels and Lubrication Division
Aero Propulsion Laboratory



ARTHUR V. CHURCHILL, Chief
Fuels Branch
Fuels and Lubrication Division
Aero Propulsion Laboratory

FOR THE COMMANDER



ROBERT D. SHERRILL, Chief
Fuels and Lubrication Division
Aero Propulsion Laboratory

"If your address has changed, if you wish to be removed from our mailing list, or if the addressee is no longer employed by your organization please notify AFWAL/POSF, W-PAFB, OH 45433 to help us maintain a current mailing list".

Copies of this report should not be returned unless return is required by security considerations, contractual obligations, or notice on a specific document.

Unclassified

SECURITY CLASSIFICATION OF THIS PAGE (When Data Entered)

REPORT DOCUMENTATION PAGE		READ INSTRUCTIONS BEFORE COMPLETING FORM									
1. REPORT NUMBER AFWAL-TR-84-2042 ESL-TR-84-29	2. GOVT ACCESSION NO. A145-691	3. RECIPIENT'S CATALOG NUMBER									
4. TITLE (and Subtitle) ALTERNATE FUELS COMBUSTION RESEARCH		5. TYPE OF REPORT & PERIOD COVERED Final Report for Period May 80 - Sep 83									
		6. PERFORMING ORG. REPORT NUMBER									
7. AUTHOR(s) M. Gratton, I. Critchley, P. Sampath		8. CONTRACT OR GRANT NUMBER(s) F33616-80-C-2002									
9. PERFORMING ORGANIZATION NAME AND ADDRESS Pratt & Whitney Canada, Mississauga, Ontario, Canada.		10. PROGRAM ELEMENT, PROJECT, TASK AREA & WORK UNIT NUMBERS PE62203F WU3048-05-06									
11. CONTROLLING OFFICE NAME AND ADDRESS Aero Propulsion Laboratory (AFWAL/POSF) Air Force Wright Aeronautical Laboratories (AFSC) Wright-Patterson AFB, Ohio 45433		12. REPORT DATE July 1984									
14. MONITORING AGENCY NAME & ADDRESS (if different from Controlling Office)		13. NUMBER OF PAGES 333									
		15. SECURITY CLASS. (of this report) Unclassified									
		15a. DECLASSIFICATION/DOWNGRADING SCHEDULE									
16. DISTRIBUTION STATEMENT (of this Report) Approved for Public Release: Distribution Unlimited											
17. DISTRIBUTION STATEMENT (of the abstract entered in Block 20, if different from Report)											
18. SUPPLEMENTARY NOTES											
19. KEY WORDS (Continue on reverse side if necessary and identify by block number)											
<table border="0"> <tr> <td>Fuels</td> <td>Combustion</td> </tr> <tr> <td>Alternate Fuels</td> <td>Emissions</td> </tr> <tr> <td>Gas Turbine Combustion</td> <td>PT6A-65</td> </tr> <tr> <td>Exhaust emissions</td> <td>JT15D-5</td> </tr> </table>				Fuels	Combustion	Alternate Fuels	Emissions	Gas Turbine Combustion	PT6A-65	Exhaust emissions	JT15D-5
Fuels	Combustion										
Alternate Fuels	Emissions										
Gas Turbine Combustion	PT6A-65										
Exhaust emissions	JT15D-5										
20. ABSTRACT (Continue on reverse side if necessary and identify by block number)											
<p>This report presents the results of the Alternate Fuels Combustion Research program. The effects of variations in fuel properties on the performance of a can, PT6A-65, and JT15D-5 combustion systems were determined. Sixteen different fuels were used, encompassing a wide range of chemical and physical properties. The tests covered current specification, broadened specification and alternate source (shale and tar sands derived) fuels. <</p>											

DD FORM 1 JAN 73 1473

EDITION OF 1 NOV 65 IS OBSOLETE

Unclassified

SECURITY CLASSIFICATION OF THIS PAGE (When Data Entered)

Combustor rig tests and gas generator tests were performed to determine the effects of fuel properties on stability, low temperature light-offs, gaseous emissions, smoke emissions, metal temperature and radiation heat loads. Attempts were also made to characterize fuel nozzle contamination and carbon formation, but these tests were somewhat inconclusive.

Lean blow-out stability limits were influenced by fuel hydrogen content and spray quality, and to a lesser extent by fuel volatility; cold start tests showed good correlation with properties affecting fuel atomization. Steady state tests indicated CO, HC and smoke emissions were strongly influenced by fuel hydrogen content; fuel effects on take-off NO_x emissions were small but were significant at idle due to changes in combustion efficiency. Radiation heat loads and liner temperatures were strongly influenced by hydrogen content and by properties affecting fuel atomization characteristics. Smoke emissions were sensitive to fuel hydrogen content, aromatic content, injector design, and also to the type of aromatics present within the fuel. Carbon check tests on the can combustor were inconclusive, possibly due to carbon shedding with several fuels. Combustor exit temperature distributions were found to be sensitive to changes in the composition as well as the physical properties of the fuels.

FOREWORD

This is the Final Report of the Alternate Fuels Combustion Research Program, conducted under contract No. F33615-80-C-2002. Program sponsorship was provided by the United States Air Force Wright Aeronautical Laboratories (AFWAL) and Engineering and Services Center (AFESC), and the Canadian Departments of National Defence (CDND) and Regional Industrial Expansion (DRIE). Mr. R. Bradley, AFWAL, and Dr. J. Coleman, CDND, were the project administrators.

Interim Report AFWAL-TR-83-2057 presented results of the Can Combustor Test Phase (Phase II) of the program. This report presents results of tests with turboprop and turboprop combustors (Phase III) and compares performance with that of the can combustion system.

Test fuel analysis was sponsored by CDND; results presented in Section II are based largely on inputs from Dr. J. Coleman and Mr. L.D. Gallop of CDND. Fuel nozzle hardware for the program was supplied by Delavan Manufacturing Co. (pressure) and Ex-Cell-O Corporation (airblast). The cooperation of these organizations is appreciated. Test fuels were supplied by AFWAL, CDND and PWC. Blending material for Jet A1 and JP4 were supplied by AFWAL.

Authors of this report wish to thank the following PWC personnel for their contributions to this program: Messrs. J.A. Saintsbury, J. Allan, F. Shum, J. Blondeau and M. Somji of Aerodynamics Engineering, Messrs. Y. Bergeron, R. Cyr, P. Sahu, A. Kong, R. Davis and R. Ouellette of Experimental Engineering, Mr. S. Monaghan, R&D Support, and Mr. W. Sidorenko of Contracts Administration. Test Support was provided by Messrs. A. Pascales, R. Pepin, J. Boyle, and D. Millard.

This report covers work conducted from 19 May 1980 through 9 September 1983.

Accession For	
NTIS GRA&I	<input checked="checked" type="checkbox"/>
DTIC TAB	<input type="checkbox"/>
Unannounced	<input type="checkbox"/>
Justification	
By _____	
Distribution/	
Availability Codes	
Dist	Avail and/or Special
A1	



TABLE OF CONTENTS

<u>SECTION</u>		<u>PAGE</u>
I	INTRODUCTION	1
II	TEST FUEL DESCRIPTION	3
	2.1 General Description	3
	2.2 Test Fuels	4
	2.3 Fuel Characterization	5
	2.4 Test Procedures	5
	2.5 Fuel Properties	6
III	RELATED STUDIES AND CAN COMBUSTOR TEST RESULTS	29
	3.1 Related Studies	29
	3.2 Small Engine Requirements	30
	3.3 Can Combustor Studies	32
	3.4 Impact of Fuel Property Changes on Can Combustion System	33
	3.5 Phase III Test Plan	37
IV	COMBUSTION SYSTEM HARDWARE	65
	4.1 JT15D-5 System	65
	4.2 PT6A-65 System	66
	4.3 Experimental Combustion Hardware	67
V	APPARATUS AND PROCEDURES	83
	5.1 JT15D-5 Atmospheric Rig Tests	83
	5.2 PT6A-65 Atmospheric Rig Tests	85
	5.3 PT6A-65 Cold Start Tests	86
	5.4 PT6A-65 Gas Generator Tests	88
	5.5 Fuel Handling Procedures	89
	5.6 Data Analysis Procedures	90
VI	RESULTS AND DISCUSSION	105
	6.1 JT15D-5 Atmospheric Rig Results	105
	6.2 PT6A-65 Atmospheric Rig Results	108
	6.3 PT6A-65 Cold Start Test Results	110
	6.4 PT6A-65 Gas Generator Test Results	111
	6.5 Comparison of Results	115

TABLE OF CONTENTS (Cont'd)

<u>SECTION</u>		<u>PAGE</u>
VII	CONCLUSIONS AND RECOMMENDATIONS	290
	7.1 Conclusions	290
	7.2 Recommendations	291
	REFERENCES	292
APPENDICES		
A	JT15D-5 Atmospheric Test Data	294
B	PT6A-65 Atmospheric Test Data	297
C	PT6A-65 Cold Start Test Data	302
D	PT6A-65 Gas Generator Test Data	304

LIST OF FIGURES

<u>FIGURE</u>		<u>PAGE</u>
2.1	Fuel Distillation Ranges (ASTM D2887)	21
2.2	Fuel Distillation Ranges (ASTM D2887)	22
2.3	Effect of Temperature on Fuel Density (ASTM D1298)	23
2.4	Effect of Temperature on Viscosity (ASTM D445)	24
2.5	Effect of Temperature on Surface Tension (Capillary Rise Technique)	25
2.6	Comparison of Fuel Freeze Points (ASTM D2386)	26
2.7	Comparison of Fuel Heating Values (ASTM D1405)	27
2.8	Comparison of Fuel Hydrogen Contents (ASTM D3710)	28
3. 1	Effect of Fuel Type on Smoke Levels	45
3. 2	Illustration of a Reverse-Flow Annular Combustor	46
3. 3	JT15D-5 Cross Section	47
3. 4	PT6A-65 Cross Section	48
3. 5	Projected Trends in Pressure Ratios	49
3. 6	Projected Trends in Turbine Inlet Temperatures	50
3. 7	Schematic of Can Combustion System	51
3. 8	Fuel Nozzles Used in Can Combustion Tests	52
3. 9	Can Combustor Rig Test Section Assembly	53
3.10	Impact of Fuel Properties on Lean Stability Limits (M simulation, Simplex 0.9 FN Nozzle)	54
3.11	Impact of Fuel Properties on Starting Characteristics (0.9 FN Nozzle)	55
3.12	Impact of Fuel Properties on Starting Characteristics (3.0 FN Nozzle)	56
3.13	Impact of Fuel Properties on Idle Combustion Efficiency (Power Level Simulation)	57
3.14	Impact of Fuel Hydrogen Content and Injector Types on HC and CO Emissions	58
3.15	Impact of Fuel Properties on NO _x Emissions at Simulated Take-Off Condition (Power Cycle)	59
3.16	Impact of Fuel Properties on NO _x Emissions at Simulated Idle Condition (Power Cycle)	60
3.17	Impact of Fuel Properties on Smoke Emissions at Simulated Take-Off Condition (Thrust Cycle)	61
3.18	Influences of Fuel Hydrogen Content and Injector Designs on Smoke Emissions	62

LIST OF FIGURES (Continued)

<u>FIGURE</u>		<u>PAGE</u>
3.19	Impact of Fuel Properties on Radiant Heat Loads (Parametric Tests)	63
3.20	Impact of Fuel Properties on Average Liner Temperatures (Thrust Level Tests)	64
4. 1	JT15D-5 Combustion System	73
4. 2	Cross Section of JT15D-5 Fuel Nozzle	74
4. 3	PT6A-65 Combustion System	75
4. 4	PT6A-65 Fuel Nozzle and Sheath Assembly	76
4. 5	PT6A-65 Fuel Manifold Arrangement	77
4. 6	JT15D-5 Air Flow Splits for Standard Combustor	78
4. 7	JT15D-5 Air Flow Splits for Rich Combustor	79
4. 8	Airblast Nozzle Cross Section	80
4. 9	PT6A-65 Standard Combustor Air Flow Splits	81
4.10	PT6A-65 Lean Primary Zone Combustor Air Flow Splits	82
5. 1	Layout of JT15D Atmospheric Rig	96
5. 2	General View of JT15D-5 Atmospheric Pressure Rig Test Section	97
5. 3	JT15D-5 Atmospheric Pressure Test Section	98
5. 4	Locations of JT15D-5 Liner Thermocouples	99
5. 5	PT6A-65 Atmospheric Pressure Rig Test Section	100
5. 6	Locations of Liner Thermocouples for PT6A-65 Atmospheric and Gas Generator Tests	101
5. 7	Layout of Cold Start Facility at NRC	102
5. 8	General View of PT6A-65 Gas Generator in Combustion Rig No. 2	103
5. 9	PT6A-65 Gas Generator Traversing Rig	104
6. 1	Effects of Fuel Properties on Idle CO Emissions (JT15D-5 Atmospheric, BOM, Simplex 2.25 FN)	124
6. 2	Effects of Fuel Properties on Idle HC Emissions (JT15D-5 Atmospheric, BOM, Simplex 2.25 FN)	125
6. 3	Effects of Fuel Properties on Idle CO Emissions (JT15D-5 Atmospheric, Rich P.Z. Simplex 2.25 FN)	126
6. 4	Effects of Fuel Properties on Idle HC Emissions (JT15D-5 Atmospheric, Rich P.Z. Simplex 2.25 FN)	127
6. 5	Effects of Fuel Properties on 30% Thrust CO Emissions (JT15D-5 Atmospheric, BOM, Airblast Nozzle)	128
6. 6	Effects of Fuel Properties on 30% Thrust HC Emissions (JT15D-5 Atmospheric, BOM, Airblast Nozzle)	129

LIST OF FIGURES (Continued)

<u>FIGURE</u>		<u>PAGE</u>
6. 7	Effects of Fuel Properties on 30% Thrust CO Emissions (JT15D-5 Atmospheric, Rich P.Z., Airblast Nozzle)	130
6. 8	Effects of Fuel Properties on 30% Thrust Emissions (JT15D-5 Atmospheric, Rich P.Z., Airblast Nozzle)	131
6. 9	Effects of Air Loading Parameter on Combustion Efficiency (JT15D-5 Atmospheric, BOM, Simplex 2.25 FN)	132
6.10	Effects of Air Loading Parameter on Combustion Efficiency (JT15D-5 Atmospheric, BOM, Airblast Nozzle)	133
6.11	Effects of Fuel Properties on Idle Combustion Efficiency (JT15D-5 Atmospheric, BOM, Simplex 2.25 FN)	134
6.12	Effects of Fuel Properties on Idle Combustion Efficiency (JT15D-5 Atmospheric, Rich P.Z., Simplex 2.25 FN)	135
6.13	Effects of Fuel Properties on 30% Thrust Combustion Efficiency (JT15D-5 Atmospheric, BOM, Airblast Nozzle)	136
6.14	Effects of Fuel Properties on 30% Thrust Combustion Efficiency (JT15D-5 Atmospheric, Rich P.Z., Airblast Nozzle)	137
6.15	Liner Temperature Variations Over Operating Range (JT15D-5 Atmospheric, BOM, Simplex 2.25 FN)	138
6.16	Effects of Fuel Properties on Average Liner Temperatures (JT15D-5 Atmospheric, BOM, Simplex 2.25 FN)	139
6.17	Effects of Fuel Properties on Average Liner Temperatures (JT15D-5 Atmospheric, BOM, Simplex 2.25 FN)	140
6.18	Effects of Fuel Properties on Peak Liner Temperatures (JT15D-5 Atmospheric, BOM, Simplex 2.25 FN)	141
6.19	Effects of Fuel Properties on Average Liner Temperatures (JT15D-5 Atmospheric, Rich P.Z., Simplex 2.25 FN)	142
6.20	Effects of Fuel Properties on Average Liner Temperatures (JT15D-5 Atmospheric, Rich P.Z., Simplex 2.25 FN)	143
6.21	Effects of Fuel Properties on Peak Liner Temperatures (JT15D-5 Atmospheric, Rich P.Z., Simplex 2.25 FN)	144
6.22	Effects of Fuel Properties on Average Liner Temperatures (JT15D-5 Atmospheric, BOM, Airblast Nozzle)	145
6.23	Effects of Fuel Properties on Average Liner Temperatures (JT15D-5 Atmospheric, BOM, Airblast Nozzle)	146

LIST OF FIGURES (Continued)

<u>FIGURE</u>		<u>PAGE</u>
6.24	Effects of Fuel Properties on Peak Liner Temperatures (JT15D-5 Atmospheric, BOM, Airblast Nozzle)	147
6.25	Effects of Fuel Properties on Average Liner Temperatures (JT15D-5 Atmospheric, Rich P.Z., Airblast Nozzle)	148
6.26	Effects of Fuel Properties on Average Liner Temperatures (JT15D-5 Atmospheric, Rich P.Z., Airblast Nozzle)	149
6.27	Effects of Fuel Properties on Peak Liner Temperatures (JT15D-5 Atmospheric, Rich P.Z., Airblast Nozzle)	150
6.28	Effects of Fuel Properties on Lean Limit Fuel-Air Ratio (JT15D-5 Atmospheric, BOM, Simplex 2.25 FN)	151
6.29	Effects of Fuel Properties on Lean Limit Fuel-Air Ratio (JT15D-5 Atmospheric, Rich P.Z., Simplex 2.25 FN)	152
6.30	Effects of Fuel Properties on Relative Profile Factor (JT15D-5 Atmospheric, BOM, Simplex 2.25 FN)	153
6.31	Effects of Fuel Properties on Relative Pattern Factor (JT15D-5 Atmospheric, BOM, Simplex 2.25 FN)	154
6.32	Effects of Fuel Properties on Relative Profile Factor (JT15D-5 Atmospheric, Rich P.Z., Simplex, 2.25 FN)	155
6.33	Effects of Fuel Properties on Relative Pattern Factor (JT15D-5 Atmospheric, Rich P.Z., Simplex 2.25 FN)	156
6.34	Effects of Fuel Properties on Relative Profile Factor (JT15D-5 Atmospheric, BOM, Airblast Nozzle)	157
6.35	Effects of Fuel Properties on Relative Pattern Factor (JT15D-5 Atmospheric, BOM, Airblast Nozzle)	158
6.36	Effects of Fuel Properties on Relative Profile Factor (JT15D-5 Atmospheric, Rich P.Z., Airblast Nozzle)	159
6.37	Effects of Fuel Properties on Relative Pattern Factor (JT15D-5 Atmospheric, Rich P.Z., Airblast Nozzle)	160
6.38	Liner Temperature Variations Over Combustor Operating Range (PT6A-65 Atmospheric, BOM, Simplex 0.65 FN)	161
6.39	Liner Temperature Variations Over Combustor Operating Range (PT6A-65 Atmospheric, BOM, Simplex 0.65 FN)	162
6.40	Effects of Fuel Properties on 70% Power Liner Temperatures (PT6A-65 Atmospheric, BOM, Simplex 0.65 FN)	163

LIST OF FIGURES (Continued)

<u>FIGURE</u>		<u>PAGE</u>
6.41	Effects of Fuel Properties on Liner Temperature Parameter (PT6A-65 Atmospheric, BOM, Simplex 0.65 FN)	164
6.42	Effects of Fuel Properties on 70% Power Liner Temperatures (PT5A-65 Atmospheric, BOM, Simplex 0.65 FN)	165
6.43	Effects of Fuel Properties on 70% Power Liner Temperature (PT6A-65 Atmospheric, Lean P.Z., Simplex 0.65 FN)	166
6.44	Effects of Fuel Properties on Liner Temperatures (PT6A-65 Atmospheric, Lean P.Z., Simplex 0.65 FN)	167
6.45	Effects of Fuel Properties on 70% Power Liner Temperatures (PT6A-65 Atmospheric, Lean P.Z., Simplex 0.65 FN)	168
6.46	Effects of Fuel Properties on 70% Power Liner Temperatures (PT6A-65 Atmospheric, BOM, Simplex 1.1 FN)	169
6.47	Effects of Fuel Properties on Liner Temperatures (PT6A-65 Atmospheric, BOM, Simplex 1.1 FN)	170
6.48	Effects of Fuel Properties on 70% Power Liner Temperatures (PT6A-65 Atmospheric, BOM, Simplex 1.1 FN)	171
6.49	Effects of Fuel Properties on 70% Power Liner Temperatures (PT6A-65 Atmospheric, Lean P.Z., Simplex 1.1 FN)	172
6.50	Effects of Fuel Properties on Liner Temperatures (PT6A-65 Atmospheric, Lean P.Z., Simplex 1.1 FN)	173
6.51	Effects of Fuel Properties on 70% Power Liner Temperatures (PT6A-65 Atmospheric, Lean P.Z., Simplex 1.1 FN)	174
6.52	Effects of Fuel Properties on Lean Limit Fuel-Air Ratio (PT6A-65 Atmospheric, BOM, Simplex 0.65 FN)	175
6.53	Lean Limit Fuel-Air Ratios vs Multiple Parameter Correlation (PT6A-65 Atmospheric, BOM, Simplex 0.65 FN)	176
6.54	Effects of Fuel Properties on Lean Limit Fuel-Air Ratio (PT6A-65 Atmospheric, Lean P.Z., Simplex 0.65 FN)	177
6.55	Lean Limit Fuel-Air Ratios vs Multiple Parameter Correlation (PT6A-65 Atmospheric, Lean P.Z., Simplex 0.65 FN)	178
6.56	Effects of Fuel Properties on Lean Limit Fuel-Air Ratio (PT6A-65 Atmospheric, BOM, Simplex 1.1 FN)	179
6.57	Effects of Fuel Properties on Lean Limit Fuel-Air Ratio (PT6A-65 Atmospheric, Lean P.Z., Simplex 1.1 FN)	180

LIST OF FIGURES (Continued)

<u>FIGURE</u>		<u>PAGE</u>
6.58	Lean Limit Fuel-Air Ratio vs Multiple Parameter Correlation (PT6A-65 Atmospheric, Lean P.Z., Simplex 1.1 FN)	181
6.59	Effects of Fuel Properties on Relative Profile Factors (PT6A-65 Atmospheric, BOM, Simplex 0.65 FN)	182
6.60	Effects of Fuel Properties on Relative Pattern Factors (PT6A-65 Atmospheric, BOM, Simplex 0.65 FN)	183
6.61	Effects of Fuel Properties on Relative Profile Factors (PT6A-65 Atmospheric, Lean P.Z., Simplex 0.65 FN)	184
6.62	Effects of Fuel Properties on Relative Pattern Factor (PT6A-65 Atmospheric, Lean P.Z., Simplex 0.65 FN)	185
6.63	Effects of Fuel Properties on Relative Profile Factors (PT6A-65 Atmospheric, BOM, Simplex 1.1 FN)	186
6.64	Effects of Fuel Properties on Relative Pattern Factor (PT6A-65 Atmospheric, BOM, Simplex 1.1 FN)	187
6.65	Effects of Fuel Properties on Relative Profile Factor (PT6A-65 Atmospheric, Lean P.Z., Simplex 1.1 FN)	188
6.66	Effects of Fuel Properties on Relative Pattern Factor (PT6A-65 Atmospheric, Lean P.Z., Simplex 1.1 FN)	189
6.67	Effects of Fuel and Air Inlet Temperatures on Times to Light (PT6A-65 Cold Start Tests)	190
6.68	Comparison of Time To Light at Fuel and Air Inlet Temperatures of 244K (PT6A-65 Cold Start Tests)	191
6.69	Effects of Fuel Properties on Time to Light (PT6A-65 Cold Start Tests)	192
6.70	Effects of Fuel and Air Inlet Temperatures on Time to Idle (PT6A-65 Cold Start Tests)	193
6.71	Comparison of Times to Idle at Fuel and Air Inlet Temperatures of 244K (PT6A-65 Cold Start Tests)	194
6.72	Effects of Fuel Properties on Time to Idle	195
6.73	Effects of Fuel Properties on Idle CO Emissions (PT6A-65 Gas Generator, BOM, Simplex 1.9 FN)	196
6.74	Idle CO Emission vs Multiple Parameter Correlation (PT6A-65 Gas Generator, BOM, Simplex 1.9 FN)	197
6.75	Effects of Fuel Properties on Idle HC Emissions (PT6A-65 Gas Generator, BOM, Simplex 1.9 FN)	198
6.76	Idle HC Emissions vs Multiple Parameter Correlation (PT6A-65 Gas Generator, BOM, Simplex 1.9 FN)	199

LIST OF FIGURES (Continued)

<u>FIGURE</u>		<u>PAGE</u>
6.77	Effects of Fuel Properties on Idle CO Emissions (PT6A-65 Gas Generator, 5% Bleed, Simplex 1.9 FN)	200
6.78	Idle CO Emissions vs Multiple Parameter Correlation (PT6A-65 Gas Generator, 5% Bleed, Simplex 1.9 FN)	201
6.79	Effects of Fuel Properties on Idle HC Emissions (PT6A-65 Gas Generator, 5% Bleed, Simplex 1.9 FN)	202
6.80	Effects of Fuel Properties on Idle CO Emissions (PT6A-65 Gas Generator, 5% Bleed, Simplex 2.2 FN)	203
6.81	Idle CO Emissions vs Multiple Parameter Correlation (PT6A-65 Gas Generator, BOM, Simplex 2.2 FN)	204
6.82	Effects of Fuel Properties on Idle HC Emissions (PT6A-65 Gas Generator, BOM, Simplex 2.2 FN)	205
6.83	Idle HC Emissions vs Multiple Parameter Correlation (PT6A-65 Gas Generator, BOM, Simplex 2.2 FN)	206
6.84	Effects of Fuel Properties on Idle CO Emissions (PT6A-65 Gas Generator, 5% Bleed, Simplex 2.2 FN)	207
6.85	Idle CO Emissions vs Multiple Parameter Correlation (PT6A-65 Gas Generator, 5% Bleed, Simplex 2.2 FN)	208
6.86	Effects of Fuel Properties on Idle HC Emissions (PT6A-65 Gas Generator, 5% Bleed, Simplex 2.2 FN)	209
6.87	Idle HC Emissions vs Multiple Parameter Correlation (PT6A-65 Gas Generator, 5% Bleed, Simplex 2.2 FN)	210
6.88	Combustion Efficiency Variations Over Operating Range (PT6A-65 Gas Generator, BOM, Simplex 1.9 FN)	211
6.89	Combustion Efficiency Variations Over Operating Range (PT6A-65 Gas Generator, BOM, Simplex 1.9 FN)	212
6.90	Combustion Efficiency Variations Over Operating Range (PT6A-65 Gas Generator, BOM, Simplex 1.9 FN)	213
6.91	Effects of Fuel Properties on Idle Combustion Efficiency (PT6A-65 Gas Generator, BOM, Simplex 1.9 FN)	214
6.92	Idle Combustion Efficiency vs Multiple Parameter Correlation (PT6A-65 Gas Generator, BOM, Simplex 1.9 FN)	215
6.93	Effects of Fuel Properties on 7% Power Combustion Efficiency (PT6A-65 Gas Generator, BOM, Simplex 1.9 FN)	216

LIST OF FIGURES (Continued)

<u>FIGURE</u>		<u>PAGE</u>
6.94	7% Power Combustion Efficiency vs Multiple Parameter Correlation (PT6A-65 Gas Generator, BOM, Simplex 1.9 FN)	217
6.95	Effects of Fuel Properties on Idle Combustion Efficiency (PT6A-65 Gas Generator, 5% Bleed, Simplex 1.9 FN)	218
6.96	Effects of Fuel Properties on Idle Combustion Efficiency (PT6A-65 Gas Generator, BOM, Simplex 2.2 FN)	219
6.97	Idle Combustion Efficiency vs Multiple Parameter Correlation (PT6A-65 Gas Generator, BOM, Simplex 2.2 FN)	220
6.98	Effects of Fuel Properties on Idle Combustion Efficiency (PT6A-65 Gas Generator, 5% Bleed, Simplex 2.2 FN)	221
6.99	Idle Combustion Efficiency vs Multiple Parameter Correlation (PT6A-65 Gas Generator, 5% Bleed, Simplex 2.2 FN)	222
6.100	Effects of Fuel Properties on Corrected NO _x Emissions (PT6A-65 Gas Generator, BOM, Simplex 1.9 FN)	223
6.101	Effects of Fuel Properties on Corrected NO _x Emissions (PT6A-65 Gas Generator, 5% Bleed, Simplex 1.9 FN)	224
6.102	Effects of Fuel Properties on Corrected NO _x Emissions (PT6A-65 Gas Generator, BOM, Simplex 2.2 FN)	225
6.103	Effects of Fuel Properties on Corrected NO _x Emissions (PT6A-65 Gas Generator, 5% Bleed, Simplex 2.2 FN)	226
6.104	Smoke Emission Variations Over Operating Range (PT6A-65 Gas Generator, BOM, Simplex 1.9 FN)	227
6.105	Smoke Emission Variations Over Operating Range (PT6A-65 Gas Generator, BOM, Simplex 1.9 FN)	228
6.106	Effects of Fuel Properties on Take-Off Smoke Number (PT6A-65 Gas Generator, BOM, Simplex 1.9 FN)	229
6.107	Take-Off Smoke Number vs Multiple Parameter Correlation (PT6A-65 Gas Generator, BOM, Simplex 1.9 FN)	230
6.108	Effects of Fuel Properties on Take-Off Smoke Number (PT6A-65 Gas Generator, 5% Bleed, Simplex 1.9 FN)	231
6.109	Take-Off Smoke Number vs Multiple Parameter Correlation (PT6A-65 Gas Generator, 5% Bleed, Simplex 1.9 FN)	232
6.110	Effects of Fuel Properties on Take-Off Smoke Number (PT6A-65 Gas Generator, BOM, Simplex 2.2 FN)	233

LIST OF FIGURES (Continued)

<u>FIGURE</u>		<u>PAGE</u>
6.111	Take-Off Smoke Number vs Multiple Parameter Correlation (PT6A-65 Gas Generator, BOM, Simplex 2.2 FN)	234
6.112	Effects of Fuel Properties on Take-Off Smoke Number (PT6A-65 Gas Generator, 5% Bleed, Simplex 2.2 FN)	235
6.113	Take-Off Smoke Number vs Multiple Parameter Correlation (PT6A-65 Gas Generator, 5% Bleed, Simplex 2.2 FN)	236
6.114	Liner Temperature Variations Over Operating Range (PT6A-65 Gas Generator, BOM, Simplex 1.9 FN)	237
6.115	Liner Temperature Variations Over Operating Range (PT6A-65 Gas Generator, BOM, Simplex 1.9 FN)	238
6.116	Effects of Fuel Properties on Average Liner Temperatures (PT6A-65 Gas Generator, BOM, Simplex 1.9 FN)	239
6.117	Average Liner Temperature vs Multiple Parameter Correlation (PT6A-65 Gas Generator, BOM, Simplex 1.9 FN)	240
6.118	Effects of Fuel Properties on Liner Temperature Parameter (PT6A-65 Gas Generator, BOM, Simplex 1.9 FN)	241
6.119	Effects of Fuel Properties on Peak Liner Temperatures (PT6A-65 Gas Generator, BOM, Simplex 1.9 FN)	242
6.120	Peak Liner Temperatures vs Multiple Parameter Correlation (PT6A-65 Gas Generator, BOM, Simplex 1.9 FN)	243
6.121	Effects of Fuel Properties on Average Liner Temperatures (PT6A-65 Gas Generator, 5% Bleed, Simplex 1.9 FN)	244
6.122	Average Liner Temperatures vs Multiple Parameter Correlation (PT6A-65 Gas Generator, 5% Bleed, Simplex 1.9 FN)	245
6.123	Effects of Fuel Properties on Liner Temperature Parameter (PT6A-65 Gas Generator, 5% Bleed, Simplex 1.9 FN)	246
6.124	Effects of Fuel Properties on Peak Liner Temperatures (PT6A-65 Gas Generator, 5% Bleed, Simplex 1.9 FN)	247
6.125	Peak Liner Temperatures vs Multiple Parameter Correlation (PT6A-65 Gas Generator, 5% Bleed, Simplex 1.9 FN)	248
6.126	Effects of Fuel Properties on Average Liner Temperatures (PT6A-65 Gas Generator, BOM, Simplex 2.2 FN)	249
6.127	Average Liner Temperature vs Multiple Parameter Correlation (PT6A-65 Gas Generator, BOM, Simplex 2.2 FN)	250

LIST OF FIGURES (Continued)

<u>FIGURE</u>		<u>PAGE</u>
6.128	Effects of Fuel Properties on Liner Temperature Parameter (PT6A-65 Gas Generator, BOM, Simplex 2.2 FN)	251
6.129	Effects of Fuel Properties on Peak Liner Temperatures (PT6A-65 Gas Generator, BOM, Simplex 2.2 FN)	252
6.130	Peak Liner Temperatures vs Multiple Parameter Correlation (PT6A-65 Gas Generator, BOM, Simplex 2.2 FN)	253
6.131	Effects of Fuel Properties on Average Liner Temperatures (PT6A-65 Gas Generator, 5% Bleed, Simplex 2.2 FN)	254
6.132	Average Liner Temperatures vs Multiple Parameter Correlation (PT6A-65 Gas Generator, 5% Bleed, Simplex 2.2 FN)	255
6.133	Effects of Fuel Properties on Liner Temperature Parameter (PT6A-65 Gas Generator, 5% Bleed, Simplex 2.2 FN)	256
6.134	Effects of Fuel Properties on Peak Liner Temperatures (PT6A-65 Gas Generator, 5% Bleed, Simplex 2.2 FN)	257
6.135	Peak Liner Temperatures vs Multiple Parameter Correlation (PT6A-65 Gas Generator, 5% Bleed, Simplex 2.2 FN)	258
6.136	Effects of Fuel Properties on Take-Off Relative Profile Factor (PT6A-65 Gas Generator, BOM, Simplex 1.9 FN)	259
6.137	Effects of Fuel Properties on Take-Off Relative Pattern Factor (PT6A-65 Gas Generator, BOM, Simplex 1.9 FN)	260
6.138	Effects of Fuel Properties on Take-Off Relative Profile Factor (PT6A-65 Gas Generator, 5% Bleed, Simplex 1.9 FN)	261
6.139	Effects of Fuel Properties on Take-Off Relative Pattern Factor (PT6A-65 Gas Generator, 5% Bleed, Simplex 1.9 FN)	262
6.140	Effects of Fuel Properties on Take-Off Relative Profile Factor (PT6A-65 Gas Generator, BOM, Simplex 2.2 FN)	262
6.141	Effects of Fuel Properties on Take-Off Relative Pattern Factor (PT6A-65 Gas Generator, BOM, Simplex 2.2 FN)	264
6.142	Effects of Fuel Properties on Take-Off Relative Profile Factor (PT6A-65 Gas Generator, 5% Bleed, Simplex 2.2 FN)	265
6.143	Effects of Fuel Properties on Take-Off Relative Pattern Factor (PT6A-65 Gas Generator, 5% Bleed, Simplex 2.2 FN)	266
6.144	Effects of Fuel Hydrogen Content on Relative Idle Combustion Efficiency	267
6.145	Effects of Fuel Volatility on Relative Idle Combustion Efficiency	268

LIST OF FIGURES (Continued)

<u>FIGURE</u>		<u>PAGE</u>
6.146	Effects of Fuel Volatility on Relative Combustion Inefficiency	269
6.147	Effects of Fuel Droplet Size on Relative Idle Combustion Efficiency	270
6.148	Effects of Relative Spray Droplet Size on Idle Emission	271
6.149	Effect of Fuel Hydrogen Content on Idle CO Emissions	272
6.150	Effect of Fuel Hydrogen Content on CO Emission Index (Can Combustor Tests, Nozzle Comparison)	273
6.151	Effect of Fuel Volatility on Idle CO Emissions	274
6.152	Effect of Fuel Properties on Relative HC Emissions	275
6.153	Effect of Fuel Hydrogen Content on Maximum Flame Temperature	276
6.154	Effect of Fuel Hydrogen Content on Take-Off NO _x Emissions	277
6.155	Effect of Fuel Hydrogen Content on Relative Smoke Number (PT6A-65 Nozzle/Stoichiometry Comparison)	278
6.156	Effect of Fuel Hydrogen Content on Take-Off Smoke Emissions	279
6.157	Effect of Fuel Hydrogen Content on Relative Smoke Number	280
6.158	Effect of Relative Spray Droplet Size on Starting Characteristics	281
6.159	Effect of Fuel Properties on Relative Lean Stability Limits	282
6.160	Effect of Fuel Hydrogen Content on Relative Lean Stability Limits	283
6.161	Effect of Fuel Hydrogen Content on Peak Liner Temperatures	284
6.162	Effect of Fuel Hydrogen Content on Average Liner Temperature	285
6.163	Effect of Fuel Hydrogen Content on Liner Temperature	286
6.164	Effect of Fuel Hydrogen Content on Liner Temperatures (JT15D-5 Nozzle/Stoichiometry Comparison)	287
6.165	Effect of Fuel Hydrogen Content on Liner Temperatures (PT6A-65 Nozzle/Stoichiometry Comparison)	288
6.166	Effect of Fuel Hydrogen Content on Liner Severity Parameter	289

LIST OF TABLES

<u>TABLE</u>		<u>PAGE</u>
2. 1	Test Fuels	11
2. 2	Test Fuels - Turboprop PT6A-65 Evaluation	12
2. 3	Test Fuels - Turbofan (JT15D-5) Evaluation	12
2. 4	Fuel Characterization Agencies	13
2. 5	Fuel Distillation Ranges (ASTM D86)	14
2. 6	Fuel Distillation Ranges (ASTM D2887)	15
2. 7	Fuel Properties I	15
2. 8	Fuel Properties II	15
2. 9	Fuel Properties III	18
2.10	Fuel Properties IV	19
2.11	Fuel Compositions	20
3. 1	Fuel Mainburner/Turbine Effects Test Scope (GE)	39
3. 2	Fuel Mainburner/Turbine Effects Test Scope (PWA)	40
3. 3	Comparison of Specifications for Jet-A and ERBS Fuels	41
3. 4	Performance Ratings of PT6A Turboprops	42
3. 5	Legend of Symbols Used in Section III Plots	42
3. 6	Influence Coefficients Corresponding to Observed Fuel Property Effects	43
3. 7	Minimum Light-off Temperatures	44
3. 8	Phase III Test Points	44
4. 1	JT15D-5 Combustor Operating Conditions in Engine at Thrust Levels Simulated in Test Program	69
4. 2	PT6A-65 Combustor Operating Conditions in Engine at Power Levels Simulated in Test Program	70

LIST OF TABLES (continued)

<u>TABLE</u>		<u>PAGE</u>
4. 3	Experimental Combustion Hardware Identification (JT15D-5)	71
4. 4	Experimental Combustion Hardware Identification (PT6A-65)	72
5. 1	JT15D-5 Atmospheric Rig Test Conditions	94
5. 2	PT6A-65 Atmospheric Rig Test Conditions	94
5. 3	PT6A-65 Gas Generator Test Setup Points	95
6. 1	Legend of Symbols Used in Section VI Plots	122
6. 2	Minimum Light-Up Temperatures	122
6. 3	Types of Combustion Tests (Alternate Fuels Research Program)	123

LIST OF SYMBOLS AND SUBSCRIPTS

<u>SYMBOL</u>	<u>DESCRIPTION</u>	<u>UNITS</u>
a	Constant	-
A	Area	cm ² , m ²
Aro	Aromatic Content	%
CO	Carbon Monoxide	-
CO ₂	Carbon Dioxide	-
EI	Pollutant Emission Index	g pollutant/kg fuel
far	Fuel-Air Ratio	g fuel/g air
FN	Flow Number	PPH/√PSI
h	Absolute Humidity	g H ₂ O/kg air
H	Fuel Hydrogen Content (mass fraction)	%
HC	Hydrocarbon (calculated as CH ₄)	-
JFTOT	Jet Fuel Thermal Oxidation Tester	-
K	Constant	-
LLFAR	Lean-Limit Fuel-Air-Ratio	g fuel/kg air
LSP	Liner Severity Parameter	-
LTP	Liner Temperature Parameter	-
M	Mach Number	-
M	Molecular Weight	-
\bar{M}	Air Velocity Parameter	lb.√ ^σ R/s/atm/ft ²
n	Number Of Points	-
Napht	Naphthalene Content	%
NO _x	Total Oxides of Nitrogen (-NO+NO ₂) Calculated as NO ₂	-
P	Pressure	Pa, atm
Q	Heat Flux	W/m ²
Q	Heat of Combustion (net)	MJ/kg
r	Correlation Coefficient	-
ASND	Relative Droplet Size	-
SHP	Shaft Horsepower	Hp
SMD	Sauter Mean Diameter	micron
SN	Smoke Number	-
t	Hypothetical Film Thickness	μm
T	Temperature	K

LIST OF SYMBOLS AND SUBSCRIPTS (CONT'D)

HC	Unburnt Hydrocarbon (expressed as CH ₄)	-
TIT	Turbine Inlet Temperature	K
T.P.	Temperature Parameter	-
TTI	Time-to-Idle	s
TTL	Time-to-Light	s
V	Volume	m ³
V	Velocity	m/s
W	Mass Flow Rate	kg/s
x	Independent Variable	-
y	Dependent Variable	-
α	Carbon-to-Hydrogen Atoms Ratio	-
ΔP	Pressure Drop	Pa
ΔT	Temperature Rise	K
η	Combustion Efficiency	%
ν	Kinematic Viscosity	centistokes
Ω	Air Loading Parameter	lb/ft ³ /atm ^{1.8}
ρ	Density	kg/m ³
σ	Surface Tension	dynes/cm
σ	Standard Error of Estimate	-
μ	Absolute Viscosity	centipoise

<u>SUBSCRIPT</u>	<u>DESCRIPTION</u>
1	Inlet
3	Compressor Exit Station
4	Combustor Exit Station
5	Turbine Inlet
10	10% Recovery
a	Air
AR	Relative to Standard Atmosphere

LIST OF SYMBOLS AND SUBSCRIPTS (CONT'D)

<u>SUBSCRIPT</u>	<u>DESCRIPTION</u>
ave	Average
c	Combustor
f	Fuel
FR	Relative to Standard Fuel Properties
g	Gas Generator
L	Liner (skin)
L	Liquid
LO	Liner with Baseline Fuel
max	Maximum
v	Vapor

SECTION I

INTRODUCTION

Almost all projections during the past decade forecasted reduced availability and increased cost of petroleum crudes. There have recently been some surplus in oil supply and reductions in oil prices, but the long term scenarios still appear valid. Only a limited amount of crude oil can be converted into aviation kerosene according to present specifications and there is also competition for middle distillate fuels from other product requirements. To ensure continued availability of jet fuels, there is a need to consider broadened specification fuels and fuels derived from new sources such as oil shales and tar sands. Several investigations have already been carried out, or are under way, to establish effects of fuel property changes on the performance of gas turbine systems. Many of the studies have involved commercial and military aviation power plants, which generally use straight-through highly-loaded annular combustion systems. However, most small aviation turbine engines used for helicopters, business jets, general aviation and auxiliary power units (APU) use reverse-flow annular combustion systems of moderate loadings and relatively high surface-to-volume ratios. The aim of this program was to evaluate and identify potential problems resulting from the use of relaxed specification fuels and fuels derived from unconventional sources in small engines with such combustion systems. Specifically, the objectives of the program were the following:

- Determine relationships between specific fuel properties and combustor performance, combustor durability, emissions, and fuel system performance and durability. The combustor and fuel systems shall correspond to requirements of small gas turbine engines of the type used in small utility and training aircraft, business jets, general aviation, and APU's.
- Determine the effects of fuel properties on the performance of single and dual-orifice pressure atomizing nozzles, airblast nozzles, and vaporizing nozzles. Examine the relationships among fuel properties, fuel nozzle types, engine combustor types and performance.
- Provide conclusions and recommendations concerning fuel specification limits for existing, conventional combustor and fuel nozzle designs, and for more advanced combustor and fuel nozzle designs which employ state-of-the-art concepts.

The program consisted of combustor rig and gas generator testing to evaluate effects of fuel property variations on performance of three small gas turbine combustion systems. These were:

- i) Can combustion system.
- ii) Turboprop reverse-flow annular combustion system.
- iii) Turbofan reverse-flow annular combustion system.

The results of investigations with the can combustion systems were described in the Interim Report, Reference 1. The experimental program was comprised of tests with 15 different fuels covering a range of fuel property variations, as well as shale and tar sand sources. Four different fuel preparation types were investigated with the can combustion system - single orifice pressure, dual orifice pressure, airblast and vaporizing nozzles. Over 1,000 tests were conducted during this phase of the program. Section III of this report summarizes results of the can combustor study. On the basis of these results, the program for Phase III work, involving two reverse flow annular combustors, was developed as described in Paragraph 3.5.

The remainder of this report, Sections IV to VI, describes in detail the results of investigations with turboprop and turbofan reverse-flow-annular combustor systems. The turboprop (PT6A) combustion system was evaluated with 12 different fuels, while the turbofan (JT15D) combustion system was tested with four different fuels. The fuel injectors considered were of the pressure atomizing and airblast types. Combustor performance, exhaust emissions, combustor wall temperatures, injection characteristics and similar data were obtained and analyzed. Detailed correlations were made relating selected fuel properties to the performance and durability parameters of the combustion systems. Observed effects with the reverse-flow annular combustion systems have been compared with those on the can combustor system (Phase II) and with published data concerning straight-through annular combustion systems.

SECTION II

TEST FUEL DESCRIPTION

2.1 General Description.

Sixteen test fuels were used for combustion system evaluation in this program, Table 2.1. The current specification fuels included JP4, Jet A1, Diesel 2 (provided commercially) and synthetic fuels RJ6 and JP10, supplied by AFWAL. Broadened specification fuels included ERBS-3, supplied by NASA, and low hydrogen blends produced by mixing JP4 and Jet A1 with AFWAL supplied 2040 Solvent.

To vary the viscosity and hydrogen content significantly, a blend of JP4 with Diesel 2 and 2040 solvent were supplied by AFWAL. Alternate source fuels included JP8 derived from oil shale, AFWAL supplied, and four blends of tar sand fuel, supplied by CDND, representing significant variations in aromatic content.

Can combustor tests were previously conducted on all the test fuels except RJ6 (1).

Turboprop combustor (PT6A) evaluation was undertaken on 13 test fuels, Table 2.2, while the turbofan combustor (JT15D) evaluation was conducted on four test fuels, Table 2.3.

The rationale for the selection of the test fuels matrix was to span systematically the feasible variations in key properties dictated by availability and cost, as well as use of non-petroleum sources for jet fuel production. The fuels selected for annular combustor (PT6A and JT15D) tests were based on observed combustion effects of all fuels (except RJ6) with the can combustion system, then eliminating fuels showing marginal, obvious or duplicating effects on liner performance¹.

Samples of fuels collected during the period of the test program were sent to CDND for further analysis. Additional samples are being retained at P&WC for purposes of future analysis if required.

2.2 Test Fuels

The specification fuels, a wide cut JP4 and a kerosene Jet A1, served as baseline or reference fuels. The properties of the other fuels were varied systematically beyond the specification limits imposed on the reference fuels, principally in the direction of higher final boiling point and higher aromatics content, which correspond to lower hydrogen content. In addition, there were fuels representing unconventional (non-petroleum) origin, and certain fuels not normally consumed in aircraft engines.

1. JP4 - a reference fuel, supplied by the contractor P&WC.
2. JP4/B1
3. JP4/B2

(2) and (3) were stocks of (1), JP4, to which two levels of an almost entirely aromatic solvent were added, with the object of reducing the hydrogen content to 13% and 12%, respectively. The 2040 solvent, supplied by AFWAL, had a boiling range approximately the same as that of typical kerosene gas turbine fuels.

4. Jet A1 - a reference fuel supplied by the contractor.
5. Jet A1/B1
6. Jet A1/B2

(5) and (6) were obtained by blending (4), Jet A1, with 2040 solvent, with targeted final hydrogen contents of 13% and 12%, respectively.

7. JP4/2040/Diesel - This fuel, provided by AFWAL, consisted of JP4 to which 2040 solvent and No. 2 Diesel fuel were added. This resulted in a fuel of 13% hydrogen by weight and an unusually wide boiling range.

8. Shale JP8 - A fuel prepared from oil shale and refined to meet Jet A1 specifications.

9. Tar Sands L-H
10. Tar Sands H-M
11. Tar Sands L-M
12. Tar Sands L-L

The four tar sands fuels were prepared by the research department of Imperial Oil at Sarnia, Ontario. The initial L or H signifies a low or high final boiling point; the final L, M or H signifies a (relatively) low, medium and high hydrogen content. As starting materials two products from Suncor's Athabaska operation

were employed: a kerocut, somewhat like JP5, with nominal boiling range of 473-573K, and an aromatic level of about 20%; and secondly a gas oil side stream of nominal boiling range 473-623K and considerably higher aromatic level, in excess of 40%.

(9), L-H, was the kerocut; (10), H-M, was a blend of kerocut and gas oil side stream. For the remaining two fuels the gas oil side stream was distilled, and a fraction taken off having the same boiling range as the kerocut. Two blends of the kerocut and this topping were made to make fuels (11), L-M, and (12), L-L, of the same boiling range as the kerocut but successively higher aromatic levels.

13. No. 2 Diesel was procured locally by the contractor.

14. ERBS-3 (Experimental Referee Broadened Specification) Fuel - provided by AFWAL, who obtained the fuel from NASA. The fuel in some ways resembled No. 2 Diesel, with final boiling and aromatic levels above specification limits for aviation fuels.

15. JP10 - hydrogenated dicyclopentadiene, a synthetic product supplied by AFWAL.

16. RJ6 - a blend of about 40% JP10 and 60% RJ5; RJ5 is a mixture of hydrogenated dimers of norbornadiene.

(15) and (16) were fuels of high volumetric energy density, employed in missiles and other applications in which space is at a premium; they were both supplied by AFWAL.

2.3 Fuel Characterization

Fuel characterization was organized by CDND. Agencies involved in the analysis are listed in Table 2.4. Complete specification testing was undertaken as well as non-specification property determinations, viz - simulated distillation by gas chromatography, thermal stability breakpoint, density, specific heat, viscosity, surface tension and true vapor pressure (all as functions of temperature), heats of combustion, hydrogen content and detailed hydrocarbon compositional analysis.

2.4 Test Procedures

Nearly all of the fuel test procedures were ASTM test methods or modifications of them. There was some redundancy or overlap, the source data being provided by two different methods. When partial data were furnished by one source and complete data for the same measurement by another, the complete data have been used for reasons of consistency. When data were obtained by variant or dissimilar methods, they have both been reported and commented on, particularly if there were disagreements to resolve.

2.5 Fuel Properties

2.5.1 D86 Distillation

Data are shown in Table 2.5. (RJ6 data not available).

2.5.2 D2887 Simulated Distillations by Gas Chromatography (G.C.)

The results of G.C. are listed in Table 2.6 and are graphically illustrated in Figures 2.1 and 2.2.

These distillations were carried out in two lots, fuels 1, 2, 5-8, 13-15 being examined some months before 3, 4 and 9-12. This accounts for the difference in presentation (in degrees and tenths of a degree), and may also be responsible for the discrepancy between JP4/B1 and JP4/B2; one would expect the boiling point at any level of recovery to be higher, not lower for JP4/B2 (as is observed in the Jet A1 blended fuels).

2.5.3 Thermal Stability

Fuels were examined in the Jet Fuel Thermal Oxidation Tester (JFTOT) in two ways (Table 2.7). First, a pass or fail test was conducted according to ASTM D3241 at the generally adopted temperature of 260°C (533K). Fuels were recorded (row 1) as pass (P) or fail (F), by one of two criteria, a pressure build-up (row 2) of greater than 25 mm during the 2.5 hour course of the test; or (row 3) a visual rating of 3 assuming the normal (N) sequence of color development is observed (row 4). It is generally accepted that certain abnormal (A) color developments or observation of a series of interference colors - peacock (P) are cause for failure regardless of the color rating. Several abnormal and peacock observations are listed in row 4. It is seen that all fuels that failed based on visual ratings, except for No. 2 Diesel, also failed by pressure build-up.

In addition, some tubes were examined in the Tube Deposit Rater (TDR), which gives an alternative, and more objective measurement of color density by reflectance. Averaged observations along the length of the tube while it was rotated (spun) and determination of the individual point of maximum light absorption (spot) were recorded.

A TDR spun reading of 15 has been proposed as a measure of failure. By this criterion, the JP4/B1 clearly failed while No. 2 Diesel, which failed on visual, passed by TDR.

The concept of breakpoint was introduced a few years ago in an attempt to quantify fuel thermal stability by defining a temperature at which some observation made with JFTOT exceeds a critical value. The fuel is run in the JFTOT at several temperatures, and by interpolation of results, the lowest temperature is found at which either pressure buildup exceeds 25 mm or the color rating (assuming the normal sequence of color development) reaches 3.

Breakpoints and failure modes are listed in the lower half of Table 2.7. The determination is not precise, and an uncertainty of at least $\pm 5^\circ\text{C}$ is to be expected. In principle a fuel with a breakpoint below 260°C should fail the specification test. As can be seen, JP4 which originally passed the specification test gave a breakpoint of 239°C based on visual ratings. In addition

JP4/B2, which failed the specification test on pressure was limited in breakpoint determination by color development. Several samplings of JP4 had been observed to contain sediments, and the testing agency reported extensive deposits of material on the prefiltering through Whatman filter paper that precedes JFTOT testing. The same agency reported a quite satisfactory breakpoint on the 2040 solvent (275-280°C, failure on color), so that blends of JP4 and 2040, even with the inherent uncertainty of the breakpoint method, are distinctly worse than either component alone. The most probable explanation of these irregular results is subsequent contamination of the stock of JP4, and variations in the method of sampling of JP4 and its blends.

Some thought has been given to the possible effects of this contamination on combustor test results. All fuels are filtered again before introduction to the combustor, therefore, blocked nozzles or distorted spray patterns due to gross contamination seems unlikely. As runs are at most several hours in duration, in power and thrust variation, with disassembly and examination of parts (e.g. for carbon buildup), the low thermal stability is not likely to have any effect, by deposition, during a run.

2.5.4 Density

Densities at 288K were determined at QETE using ASTM D1298, and at four other temperatures at Sherbrooke (Table 2.8, Figure 2.3). Sherbrooke tests used a Picker dynamic densimeter to determine density at the reference temperature of 298K. Thermal expansion coefficients were then measured for each fuel with high precision, and by an integration process densities at other temperatures could be calculated. QETE results fell quite satisfactorily on the curve obtained by plotting the Sherbrooke data.

2.5.5 Specific Heat

Specific heats as a function of temperature were determined at Sherbrooke, employing the Picker differential dynamic micro-calorimeter (Table 2.8).

2.5.6 Viscosity

Viscosities for fifteen fuels were determined at QETE, by ASTM D445. The viscosity of RJ6 at 219K (394°R) was 423.90 cSt, which is higher than the specification limit of 400 cSt at that temperature (Table 2.8, Figure 2.4).

2.5.7 Surface Tension

Surface tension was determined by Laval using a capillary rise technique, employing benzene as a reference fluid (Table 2.8, Figure 2.5).

2.5.8 Vapor Pressure

The method employed is a modification of the isoteniscopic procedure of ASTM D2879-75. For a mixture of many components such as a liquid fuel, the vapor pressure is not defined uniquely by temperature, but depends on the ratio of vapor to liquid volume. As this ratio approaches zero the contribution of the volatile components becomes increasingly important, and the vapor pressure approaches a limiting value. In the present work four isoteniscopes of V_v/V_l varying from 0.06 to 0.280 were used. These ratios are considerably smaller than those used in most previous work, and the results in consequence reflect more closely the limiting intrinsic value. Considerable manipulation of the experimental data is necessary in order to make correction for the air inevitably retained by the fuels. The original report² should be consulted for details of this data treatment. What is presented in Table 2.9 is a very small portion of the data generated, and is intended only to be representative of the information available in the report. Table 2.9 contains the experimental data at the two higher V_v/V_l ratios, 0.280 and 0.184, and the derived or corrected data at the highest V_v/V_l ratio (.280) and the limiting value $V_v/V_l = 0$. (The experimental data marked with an asterisk are derived by a short extrapolation from the experimental points in the original report).

The original report² comments on the extreme difficulty in getting error free results, and the fact that anomalies can occur even if meticulous care is exercised. An instance of this is found on comparing data for JP4/B1 and JP4/B2. The latter fuel contains more 2040 solvent, and in view of the boiling ranges of JP4 and 2040 solvent, it should have under the same conditions a lower vapor pressure than JP4/B1, not higher, as observed. This anomaly occurs both in the experimental and the derived data. Again, the experimental vapor pressure data for tar sands L-M appears abnormally high at $V_v/V_l = 0.280$, probably due to trapped air. The irregularity has disappeared in the corresponding derived data. JP10 is supposedly a pure compound, and one would expect to find its vapor pressure at any temperature independent of liquid-vapor ratio. Instead, some dependence similar to that of the other fuels is observed. This can be attributed either to residual air or to the presence of small amounts of light material not removed during production. The ASTM D2887 distillation of JP10 (Table 2.6) suggests that both light and heavy ends may be present.

2.5.9 Flash Point

Flash Point ASTM D56-11 (QETE), ASTM D3828 (Setaflash), (NRC)

There is significant disagreement between the two methods in the case of the less volatile fuels. (Table 2.10).

2.5.10 Freeze Point

ASTM D2386 (Table 2.10) records the disappearance of the last wax crystals on rewarming; it has been reported that the Setapoint reflects rather the wax appearance point, so that Setapoint measurements tend to be systematically lower than ASTM D2386. This observation is in general supported by examination of the data (omitting JP10 as anomalous). For fuels containing middle distillate fractions (JP4/2040/Diesel, tar sands fuels, No. 2 Diesel, and ERBS-3) Setapoint measurements are from 2 to 6°C lower than D2386. For the lighter JP4 and Jet A1 based fuels, the two measurements coincide within a degree, with the single exception of JP4/B1, in which the Setapoint reading is 2°C higher. A bar chart comparison of the ASTM D2386 data is shown in Figure 2.6.

2.5.11 Smoke Point

Smoke Point ASTM (D1322) data were provided by QETE and Gulf (Table 2.10). Gulf also provided luminometer data (ASTM D1740).

2.5.12 Heat of Combustion

Heats of Combustion by ASTM D2382 were provided by EMR and, for comparison, calculated heats of combustion by ASTM D1405 (Table 2.10 and Figure 2.7) from aniline-gravity product were provided by QETE. This latter determination is included as a matter of interest, as the aniline-gravity estimation applies only to petroleum-based fuels that meet a recognized specification (aviation gasoline, JP4, Jet A, etc.). Taking the ASTM D2382 heat of combustion figures as correct, and examining the ASTM D1405 figures, significant disagreement is seen with JP4 and its blends, and with Jet A1/B2. Calculated heating values for tar sands fuels are surprisingly good.

2.5.13 Fuel Composition

Hydrogen Content: The first two rows of Table 2.11 compare hydrogen content as determined by nuclear magnetic resonance (NMR) (ASTM D3701) at NRC, and by microcombustion at EMR. The latter figures are typical of the best that can be achieved by classical methods. Figure 2.8 is a bar chart comparison of NMR measured fuel hydrogen content values.

It is seen that attempts to reach 13 and 12% hydrogen by addition of 2040 solvent to the two base fuels were not completely successful. The location of the test laboratory (NRC in Ottawa), being remote from the blending site, made it difficult to adjust blend ratios to the required levels. The hydrogen content of JP10 was calculated from its formula and for RJ6 from its composition (39.9% RJ5) supplied by AFWAL.

Aromatics, Olefins and Paraffins: ASTM D1319 (Fluorescent indicator absorption) analysis provides a rough division into three fractions - aromatics, olefins and paraffins. Developed for gasoline and turbine fuel of petroleum origin, it provides an estimate of proportions. Results depend to some extent on

operator technique; only with considerable reservations can it be used with other fuels. The ASTM D1319 data provided by Imperial Oil for the four tar sands fuels are included with the QETE values (Table 2.11) and show the kind of variation that can be expected.

Naphthalenes: This estimation by ASTM D1840 (Table 2.11) is made by light absorption in the near ultraviolet. For the JP4 and Jet A1 blends with 2040 solvent, the naphthalene content can be calculated from the blend ratio, and the knowledge that 2040 solvent contains 57% naphthalenes. Results from ASTM D1840 come out in quite satisfactory agreement with these calculated values even though ASTM D1840 is a rather rough method of estimation.

Hydrocarbon Compositional Analysis: Detailed hydrocarbon compositional analysis was carried out by EMR, employing a modification of ASTM D2789. (ASTM D2789 is a gasoline analysis and this procedure was extended to include a mass spectrometric analysis of hydrocarbon composition). The original results were presented as paraffins, naphthenes in two categories, and aromatics broken into six categories. In this summary they have, for purposes of comparison, been reconsolidated into paraffins, naphthenes and aromatics (Table 2.11). The analytical program is so devised that olefins, low in any case, always appear as zero. Paraffins, naphthenes and aromatics add up to 100%, apart from rounding off errors. Again, naphthalenes are shown as a separate category.

Comparing data by the two methods, liquid chromatography (D1319) and gas chromatography-mass spectrometry (D2789 modified) it is seen that aromatic contents as determined by the latter are consistently lower, the more so the higher the aromatics level. This can be explained, in part as a difference in the treatment of molecules that have both an aromatic and an aliphatic component. D1319 assigns a side-chain aromatic, e.g. an alkylbenzene, entirely to the aromatic category, while mass spectrometry registers the presence of both aliphatic and aromatic moieties. The effect of this is apparent in examining the series of blends of 2040 solvent with Jet A1 and JP4. 2040 solvent contains about 35% alkylbenzenes, with the alkyl side chain on the average lying between butyl and amyl in length, and 39% of approximately monomethylnaphthalenes. In consequence, the range of aromatics levels determined by D2789 will be compressed compared to results by D1319.

Data from D1319 are in fact employed in deriving correlations with aromatics levels, but the same performance trends would be observed, using either method.

Sulfur and Nitrogen Content: The last three determinations; total sulfur (ASTM D1266), mercaptan sulfur (ASTM D1323) and nitrogen (ASTM D3228) were performed at QETE (Table 2.11). The sulfur determinations are all within specification for aviation turbine fuels. Nitrogen levels, for which no specifications exist, are in the range anticipated.

Table 2.1: Test Fuels

CURRENT SPEC.	BROADENED SPEC.	ALTERNATE FUELS
JP4/JET B	JP4/B1 JP4/B2 JP4/DF/2040	
JP8/JET A1	JET A1/B1 JET A1/B2	SHALE JP8
JP10 DIESEL 2 RJ6	ERBS-3	TAR SANDS L-H TAR SANDS L-M TAR SANDS L-L TAR SANDS H-M

Table 2.2: Test Fuels - Turboprop PT6A-65 Evaluation

Jet A1	JP4	ERBS-3
Jet A1/B1 *	JP4/B1 *	Tar Sands L-L
Jet A1/B2	JP4/B2	Tar Sands L-H
Shale JP8	JP4/2040/DF *	JP10
		RJ6 **
<p>* not used in gas-generator and cold-start tests</p> <p>** not used in atmospheric rig tests</p>		

Table 2.3: Test Fuels - Turbofan (JT15D-5) Evaluation

JP4

Shale JP8

ERBS-3

JP10

Table 2.4: Fuel Characterization Agencies

<u>PROPERTY</u>	<u>SOURCE</u>	<u>PROPERTY</u>	<u>SOURCE</u>
SPECIFIC GRAVITY	PWC CDND (QETE)	STOICHIOMETRY	PWC (CALCULATED)
DISTILLATION	CDND (QETE/EMR)		
FREEZING POINT	CDND (QETE)	TOTAL SULPHUR	CDND (QETE)
SPECIFIC HEAT VS TEMP	CDND (SHERBROOKE)	MERCAPTAN SULPHUR	CDND (QETE)
CHARACTERIZATION FACTOR	PWC (CALCULATED)		
THERMAL OXIDATIVE STABILITY	CDND (QETE)		
TOTAL AROMATICS	CDND (QETE)	WEIGHT % HYDROGEN	CDND (NRC/ERL-EMR)
VISCOSITY VS TEMPERATURE	CDND (QETE) (253 to 310K)	SURFACE TENSION	CDND (NRC/LAVAL)
HYDROCARBON COMPOSITION	CDND (ERL-EMR)	TRUE VAPOR PRESSURE	CDND (LAVAL)
SMOKE POINT	CDND (GULF)		
LUMINOMETER NUMBER	CDND (GULF)		
HEAT OF COMBUSTION	CDND (QETE)		
FLASH POINT	CDND (QETE/LAVAL)		

QETE = Quality Engineering Test Establishment (CDND)

LAVAL = Université Laval

SHERBROOKE = Université de Sherbrooke

CDND = Canadian Department of National Defence

NRC = National Research Council

PWC = Pratt & Whitney of Canada

ERL-EMR = Energy Research Laboratories,
Energy, Mines and Resources Canada

GULF = Gulf Oil Canada

Table 2.5: Fuel Distillation Ranges, ASTM D86

	1	2	3	4	5	6	7	8	9	10	11	12	13	14	15	16
	JP4	JP4 81	JP4 82	JP4 2040 DE2	JET A1	JET A1 81	JET A1 82	JP8 SMALL	KEROJET LN	KEROJET MN	KEROJET LN	KEROJET LN	DIESEL #2	EMULS-3	JP10	EMULS-3
D86																
1.B.P. °C	61	64	58	68.5	169	173	174	175	171	172	174	182	191	187	178	
5	88	92	91	99	177	189	183	184	197	192	194	197	223	197	181.5	
10	99	104	102	114	181	194	185.5	186	203	200	200	204	233	200	182	
20	117	126	131	141.5	186.5	191	192	189	211	214	210	213	246	208	182.5	
30	132.5	143	155	161	189.5	194	195	191	217	221	215	219	255	215	183	
40	147	160	173	194	193	197	209	195	223	227	223	225	263	220	183	
50	159	175	185	213	196	201	204	199	229	233	229	232	271	226.5	183	
60	169.5	186	197	230	200	206	210	204	234	240	236	238	280	235	183	
70	178	197	210	247	205	211	217	208	243	249	242	245	290	241	183	
80	187	209	223	265	210	218	224.5	217	249	259	249	254	302	260	183.5	
90	199.5	229	243	292	219	232	238	226	269	275	261	265	316	288	194	
95	210	248	258	319	229	245	253	235	278	296	271	278	334	309	184	
96	214	253	263	328	234	251	257	238	274	304	275	283	338	315	185	
E.P	218.5	263	268	328.5	244	265.5	272	248	283	311	288	285	346	329	195.5	
RECOVERY %	97.5	98	97.6	97.0	97.5	96	98.5	98.5	98.6	97.7	98.3	97.3	98.0	98.5	98.5	
RESIDUE	1.4	1.1	1.4	1.6	1.4	1.2	1.2	1.5	1.8	1.9	1.5	2.4	1.7	1.5	1.0	
LOSS	1.1	0.9	1.0	1.4	1.1	0.8	0.3	-	0.2	0.4	0.2	0.3	0.3	-	0.5	

Table 2.6: Fuel Distillation Ranges, ASTM D2867

°C	1	2	3	4	5	6	7	8	9	10	11	12	13	14	15	16
	JP4 B1	JP4 B1	JP4 B2	JP4 DF2	JET A1	JET A1 B1	JET A1 B2	JP8 SHARE	KEROJIT LH	KC+GSSS FM	KC+GSSS TOPPING LM	KC+GSSS TOPPING LL	DIESEL #2	ER35-3	JP10	RJ6
2287	30	44	29.9	33.9	131	133	135	146	131.5	178.8	123.7	132.9	148	145	169	188
0-52																
5	64	85	67.8	72.4	157	159	161	162	167.5	171.0	169.0	171.8	201	170	170	196
10	82	111	94.9	96.7	165	167	170	169	185.4	189.7	186.8	187.8	213	182	172	198
20	125	143	132.9	133.4	175	178	183	177	202.5	205.8	203.8	204.2	239	197	176	200
30	127	159	153.5	168.7	184	188	193	186	212.1	215.3	213.0	213.9	255	208	179	201
40	145	191	175.8	197.0	193	195	200	194	220.3	225.7	222.8	224.2	270	216	181	204
50	158	234	192.6	214.3	197	201	206	200	229.6	235.4	232.1	233.5	281	226	182	277
60	169	217	204.1	230.9	203	207	212	208	238.8	245.9	241.2	243.2	293	237	184	283
70	180	231	218.1	250.1	206	213	220	213	249.0	256.7	251.0	252.9	308	248	155	287
80	194	249	229.8	272.1	214	221	227	223	259.7	270.4	262.0	264.3	322	270	187	289
90	205	267	245.8	301.6	225	234	243	235	273.5	286.1	275.5	278.3	339	300	189	291
95	213	280	255.9	325.2	235	246	256	245	283.3	305.2	285.8	289.6	353	325	190	293
99.5	235	326	295.8	372.0	280	292	299	284	-	360.7	329.1	331.5	401	428	323	296

Note: Tests 3, 4, 9-12 were run at one time, the balance at another time, by the same agency.

Table 2.7: Fuel Properties I

	1	2	3	4	5	6	7	8	9	10	11	12	13	14	15	16
	JP4	JP4 B1	JP4 B2	JP4 2540 B2	JET A1	JET A1 B1	JET A1 B2	JP8 SHALE	KEROGUT UH	KC-80SS EX	KC-80SS TOPPING LN	KC-80SS TOPPING LL	DIESEL #2	EMSS-3	JP10	RJ5
FTET 02241 K: 260*	P	F	F	F	P	P	P	P	F	F	F	F	F	P	P	
P in H ₂	2.5	>254	>254	>254	3	7.5	1.0	0.5	36	>254	>254	>254	2.5	2	2	
VISUAL	1	3-4	4	3-4	<1	<1	<1	<1	1	1	1	4	1	1	<1	
A TIE	H	A	P	H	H	H	H	H	H	H	H	A	A	H	H	
(a) SPOT	3	43.5	-	-	<0	0	0	0	-	-	-	-	13.5	5	0	
(b) SPOT	4.5	45	-	-	2	0	1	1	-	-	-	-	17.5	7	0	
FREEPOINT °C	238	212	203	247	277	274	274	276	246	229	250	258	258	292	313	
P in H ₂	0	>25	1	>25	>25	6	5	>25	>25	>25	>25	>25	2	1	-	
VISUAL	3	1	3	2	1	3	3	1	1	1	1	1-2	3	3	-	

Table 2.8: Fuel Properties II

	1	2	3	4	5	6	7	8	9	10	11	12	13	14	15	16
	JP4	JP4 B1	JP4 B2	JP4 2040 DF2	JET A1	JET A1 B1	JET A1 B2	JP73 SWALE	KEROJUT LH	KC-6055 MH	KC-6055 TOPPING LM	KC-6055 TOPPING LL	DIESEL F2	ERBS-3	JP10	
DENSITY kg/L																
5°C	.77420	.81543	.84472	.82897	.81271	.83580	.85913	.81013	.84457	.85055	.84920	.85480	.85762	.84792	.84620	1.0245
15	.7558	.8078	.8359	.8215	.8048	.8289	.8518	.8033	.8380	.8436	.8434	.8481	.8509	.8417	.8377	1.0155
25	.75964	.80312	.82970	.81443	.79788	.82161	.84494	.79603	.83026	.83550	.83542	.84093	.8432	.83427	.83139	1.0100
45	.74447	.78520	.81362	.79267	.78372	.80740	.83053	.78192	.81714	.82244	.82153	.82074	.83100	.82061	.81657	.9955
65	.72935	.77002	.79767	.78532	.76957	.79318	.81623	.76781	.80342	.80638	.80764	.81315	.81769	.80696	.80175	.9815
SPECIFIC HEAT kJ/kg°K																
DIFFERENTIAL																
MICROCALORIMETRY																
5°C	1.9310	1.2498	-	1.8508	1.8913	1.8429	1.7983	1.9143	1.8246	1.8164	1.8168	1.8084	1.8468	1.8496	1.5185	1.34
25	2.3026	1.9185	-	1.9180	1.9580	1.9142	1.8625	1.9838	1.8992	1.8966	1.8906	1.8469	1.9193	1.9152	1.5999	1.43
45	2.0856	1.7563	1.9366	1.9701	2.0489	1.9873	1.9377	2.0650	1.9945	1.9744	1.9744	1.7630	1.5973	1.9922	1.6958	1.63
65	2.1216	2.0631	2.0212	2.0294	2.1455	2.0824	2.0208	2.1561	2.0985	2.0372	2.0332	2.0713	2.0833	2.0304	1.7955	1.62
VISCOSITY cSt																
D45 -20°C	1.85	2.15	2.52	3.05*	3.93	4.07	4.36	4.17	8.10	9.20	8.01	8.55	-	8.16	8.84	41.3
0°C (32°F)	1.29	1.45	1.66	2.35	2.39	2.46	2.56	2.52	4.15	4.55	4.06	4.31	8.63	4.19	5.03	15.9
21.1°C (70°F)	1.00	1.07	1.18	1.50	1.65	1.62	1.70	1.70	2.55	2.77	2.53	2.67	4.53	2.55	3.26	9.15
37.8°C (100°F)	0.730	.877	.955	1.26	1.28	1.27	1.30	1.35	1.85	1.96	1.82	1.83	3.03	1.85	2.37	7.05
SURFACE TENSION (dyne/cm)																
25	24.7	26.4*	26.0	24.4	27.95	22.2	29.2	26.95	23.5	29.1	28.8	28.5	25.5	30.2	32.1	35.8
50	22.5	24.1	23.9	23.4	25.35	26.2	26.55	25.1	23.4	26.3	26.6	26.2	26.3	27.2	29.8	33.8
75	20.35	21.4	21.4	21.4	22.9	24.3	24.8	23.1	24.3	24.7	24.6	24.2	25.3	24.4	27.4	30.8
	18.2	18.7	20.0	19.5	20.3	22.3	22.45	21.5	22.1	22.5	22.5	21.9	23.2	21.5	27.4	28.4

*interpolated

Table 2.9: Fuel Properties III

	1	2	3	4	5	6	7	8	9	10	11	12	13	14	15	16
	JP4	JP4 B1	JP4 B2	JP4 DF2	JET A1	JET A1 b1	JET A1 B2	JTP6 SHALE	KEROGUT LH	KC-GROSS HH	KC-GROSS TOPPING LR	KC-GROSS TOPPING LL	DIESEL #2	EBBS-3	JP10	RJ6
Vapour Pressure (mm Hg)																
322/9-75 Mc-Nified																
Experimental Data																
Vv/ML = 0.220	52*	39*	54*	30.5*	25.5*	33.5*	49*	20*	23*	17*	45.5*	22*	20.5*	35.5*	32*	
	112	87	111	80	42.5	53	63	56	46	28	67	40	35.5	57	43	
	220	17*	211	173	62	77	87	88	83	42.5	92	77	74	84	62	
	395	325	368	310	90	110	131	160	120	65	140	165	74	115	100	
Vv/ML = 0.184	73*	61*	77*	48*	31*	48*	67*	42.5*	78*	62*	51*	97*	37*	58*	42*	
	158	120	151	121	66	68	95	73	150	91	90	145	61	120	61	
	292	222	290	275	103	35	124	118	202	130	134	200	95	215	97	
	510	410	530	480	150	118	180	180	253	160	195	250	139	250	132	
Derived Data																
Vv/ML = 0.220	34	29	45	25.5	12	22	7	23.5	23	10	10	15	-	23	-	
	25	10	95	67.5	24	46	18	43.5	43	17.5	21	30.5	14	38.5	12	
	187	153	184	152	43	61	39	76	75	32.5	48	57.5	30	61	29	
	365	305	325	305	65	52	75	122	129	58	97	99	57	93	61	
Vv/ML = 0.0	74	94	152	70	73	164	60	78	217	44	87	198	93	207	25	
	173	150	360	183	157	290	137	149	400	92	305	355	208	380	66	
	200	370	770	465	310	478	290	263	675	175	435	610	425	650	155	
	740	650	-	930	545	725	540	440	-1050	395	825	910	750	1080	320	

* Derived by short extrapolation from experimental points.

Table 2.10: Fuel Properties IV

	1	2	3	4	5	6	7	8	9	10	11	12	13	14	15	16
	JM4	JM4 B1	JM4 B2	JM4 Z340 DF2	JET A1	JET A1 B1	JET A1 B2	JP8 SHALE	KEROBIT LN	KC-40SS NM	KC-40SS TOPPING LN	KC-40SS TOPPING LL	DIESEL #2	ERS-S-3	JP10	RJ5
FLASH POINT D 56-74G °C	-16	-14	-13.5	-7.5	53.5	55.0	57.0	54.5	63.0	63.5	62.0	64.0	68.0	66.0	50.5	65.5
FLASH POINT D 3820-SET/FLASH °C	-16	-14	-13.5	-7.5	55.5	56.0	59.0	55.5	66.0	67.0	64.5	67.5	73.0	69.0	52.5	
FREEZE POINT D 2386 °C	<73	-61	-47.5	-25	-60	-63	-53	-52	-48.5	-49	-48	-49	-13	-24	<73	-54
SET POINT D 2386 °C	<70	-59	-47.5	-31	-59.5	-62	-54	-51	-50.5	-52.5	-53.5	-53.5	-15.5	-26.5	<70	
SMOKE POINT D 1522 mm	28.5	14.9	10.0	14.5	22.8	15.9	11.5	24.2	16.0	17.0	16.0	15.0	15.7	15.5	16.6	
SMOKE POINT D 1322	27	14	12	14	22	17	12	22	17	16	16	14	15	14	17	
LUMINO-METER NO D 1740	63	34	19	31	46	29	21	51	35	31	32	28	29	28	30	
HEAT OF COMBUSTION D 2382 MJ/kg	43.82	43.16	41.90	42.80	43.04	42.99	41.79	43.30	42.87	42.66	42.80	42.80	43.21	43.07	42.81	41.93
ASHLINE POINT D 611 °C	52.5	35.8	22.4	46.1	56.1	44.4	31.8	56.9	55.4	52.2	50.0	45.9	62.5	53.3	(27)	
NET HEAT OF COMBUSTION (CALC) D 1405 MJ/kg	43.46	42.95	42.67	42.94	43.17	42.80	42.47	43.23	42.73	42.84	42.80	42.70	-	-	-	

* Re-measured due to previous sampling error

Table 2.11: Fuel Compositions

	1	2	3	4	5	6	7	8	9	10	11	12	13	14	15	16
	JP4	JP4 B1	JP4 B2	JP4 B2	JP4 B2	JP4 B1	JP4 B2	JP8 SHALE	KERO IN	KC-GROSS IN	KC-GROSS TOPPING LN	KC-GROSS TOPPING LL	DIESEL P2	EMBS-3	JP10	RJ6
HYDROGEN WT %	14.25	12.06	11.95	13.01	13.76	12.88	12.04	13.82	13.38	13.21	13.17	13.03	13.05	12.95	11.88 ¹	10.55 ¹
D3701 MICROCOMBUSTION	14.2	12.9	12.03	12.89	13.5	13.0	12.4	14.0	13.21	13.09	13.03	12.63	12.9	13.2	12.0	-
01319 COMPOSITION ²																
PARAFFINS % V	84.6	69.1	56.7	70.8	73.9	68.5	57.4	77.3	69.1 (78)	65.4 (70)	61.0 (66)	56.4 (63)	64.9	69.6	96.5	-
AROMATICS	14.5	30.2	42.5	28.3	19.7	30.2	41.7	21.1	29.1 (20)	33.4 (28)	37.2 (32)	41.8 (36)	31.2	29.1	0	-
OLEFINS	0.9	0.7	0.8	0.9	1.4	1.2	0.9	1.9	1.8 (2)	1.2 (2)	1.8 (2)	1.8 (1)	3.2	1.3	1.5	-
D1849 NAPHTHALENES 2V	0.3	11.0	17.6	10.7	8.7	9.2	17.3	0.6	1.0	1.7	1.3	1.6	7.8	12.5	0	-
D2763 MODIFIED PARAFFINS 2V	49.3	43.8	41.9	47.6	48.7	43.8	43.0	51.6	39.2	38.1	38.3	36.6	43.6	43.6	-	-
NAPHTHENES	35.9	27.0	25.1	29.0	35.1	30.7	28.4	30.8	41.3	40.7	40.0	38.7	28.4	27.2	-	-
AROMATICS	14.8	26.3	33.0	23.4	16.2	25.5	23.6	17.6	19.6	21.3	22.0	24.2	28.0	29.2	-	-
NAPHTHALENES (FROM AROMATIC FRACTION 1/2 P 2708)	1.1	10.1	16.2	8.9	1.3	9.0	11.7	1.2	1.0	1.3	1.4	1.5	4.9	7.5	-	-
D1266 TOTAL SULFUR % W/V	0.044	0.035	0.0034	0.085	0.004	0.005	0.003	0.003	0.003	0.024	0.019	0.024	0.241	0.050	0.002	-
9484 MERCAPTAN % W/V	0.0012	0.00029	0.00025	0.00058	0.00058	0.00038	0.00035	0.00042	0.0003	0.0003	0.0003	0.0003	0.00065	0.00052	0.00053	-
D3228 NITROGEN % W/V	0.0001	0.0001	0.0015	0.003	0.0020	0.0019	0.0019	0.0164	0.0013	0.007	0.019	0.021	0.0109	0.0009	0.0000	-

1. Calculated from the chemical formula.

2. Bracketed data for the four tar sands fuels were supplied by Imperial Oil, who prepared the fuels.

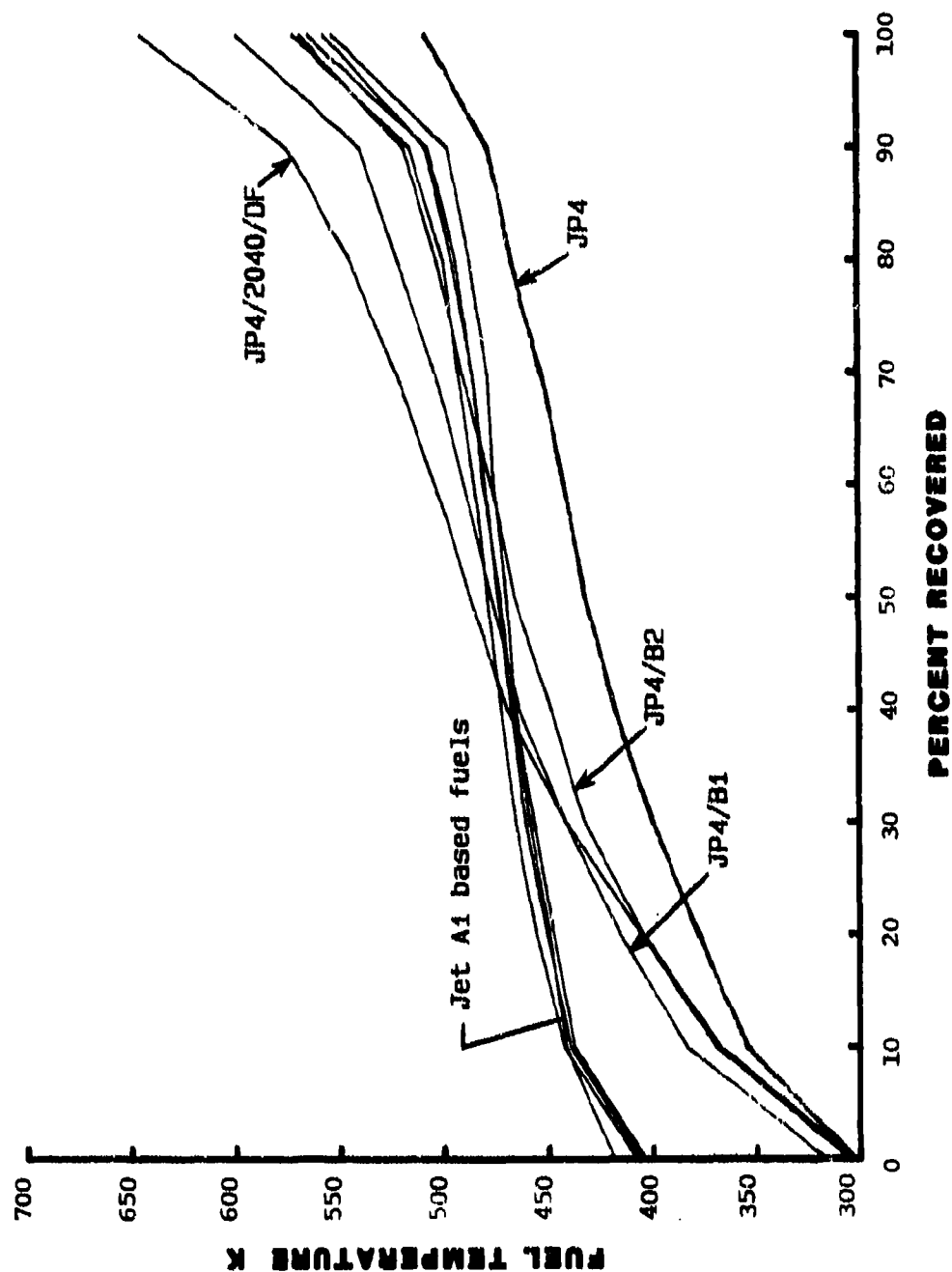


Figure 2.1: Fuel Distillation Ranges (ASTM D2887)

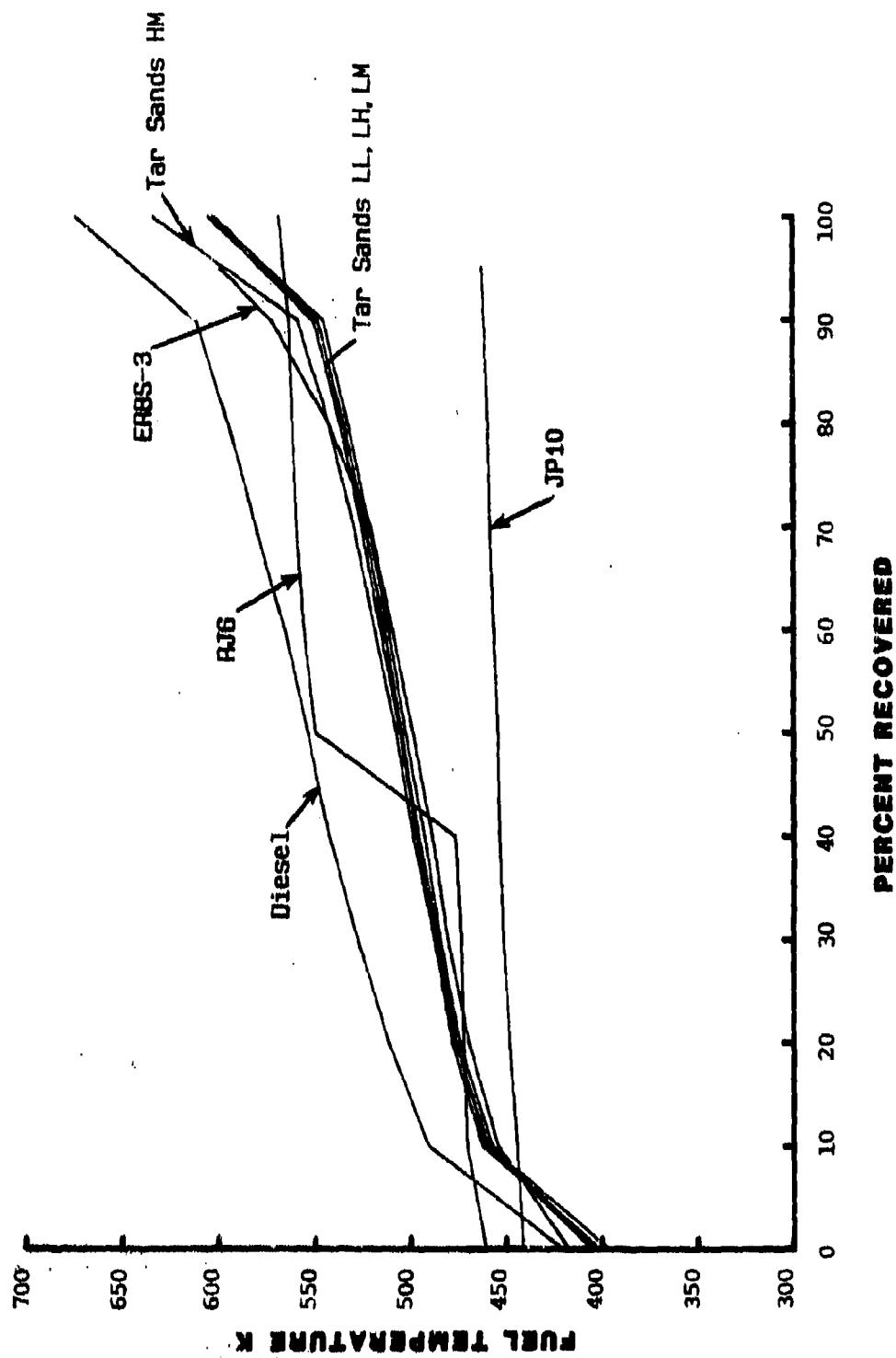


Figure 2.2: Fuel Distillation Ranges (ASTM D2887)

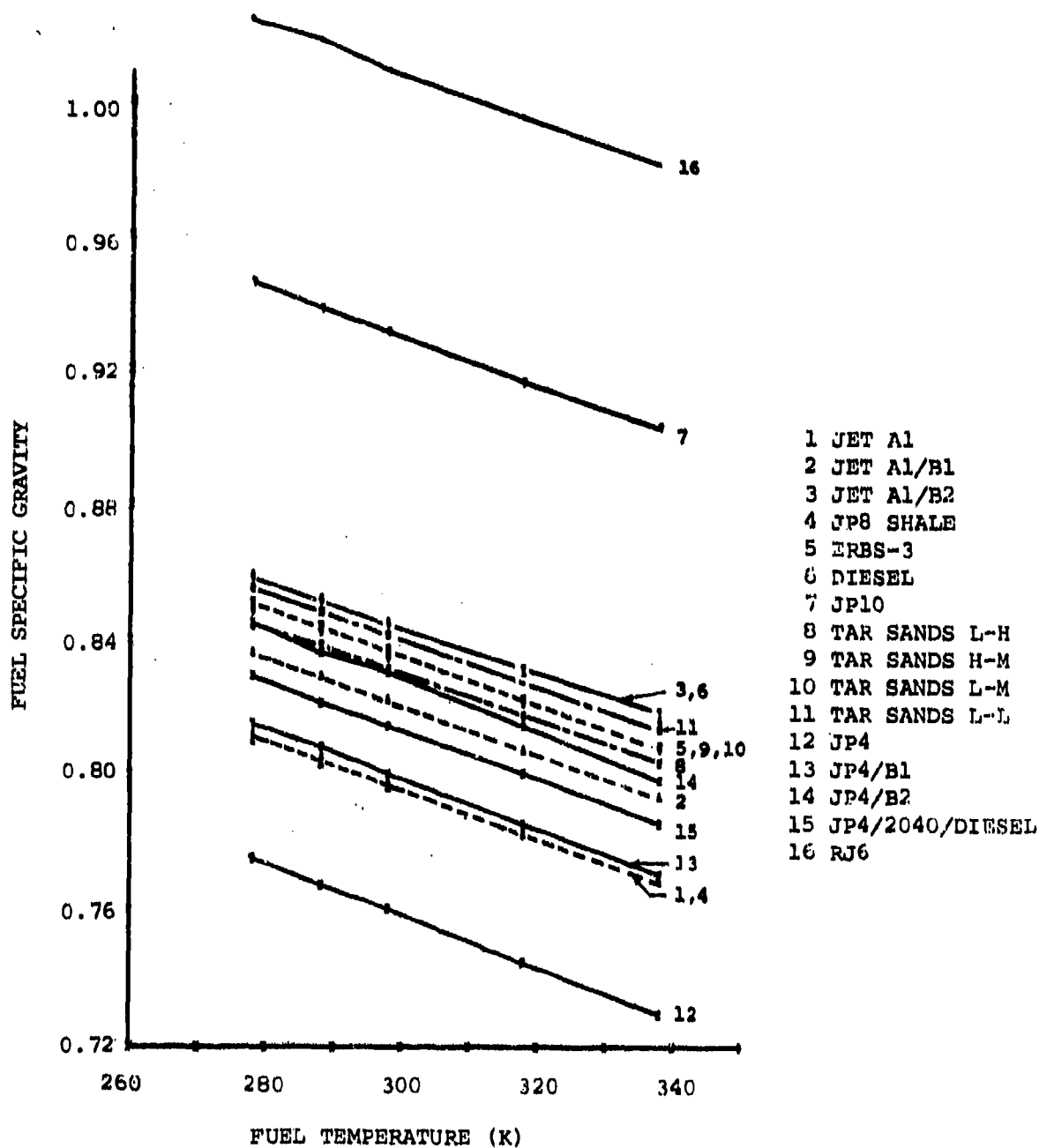


Figure 2.3: Effect of Temperature on Fuel Density (ASTM D1298)

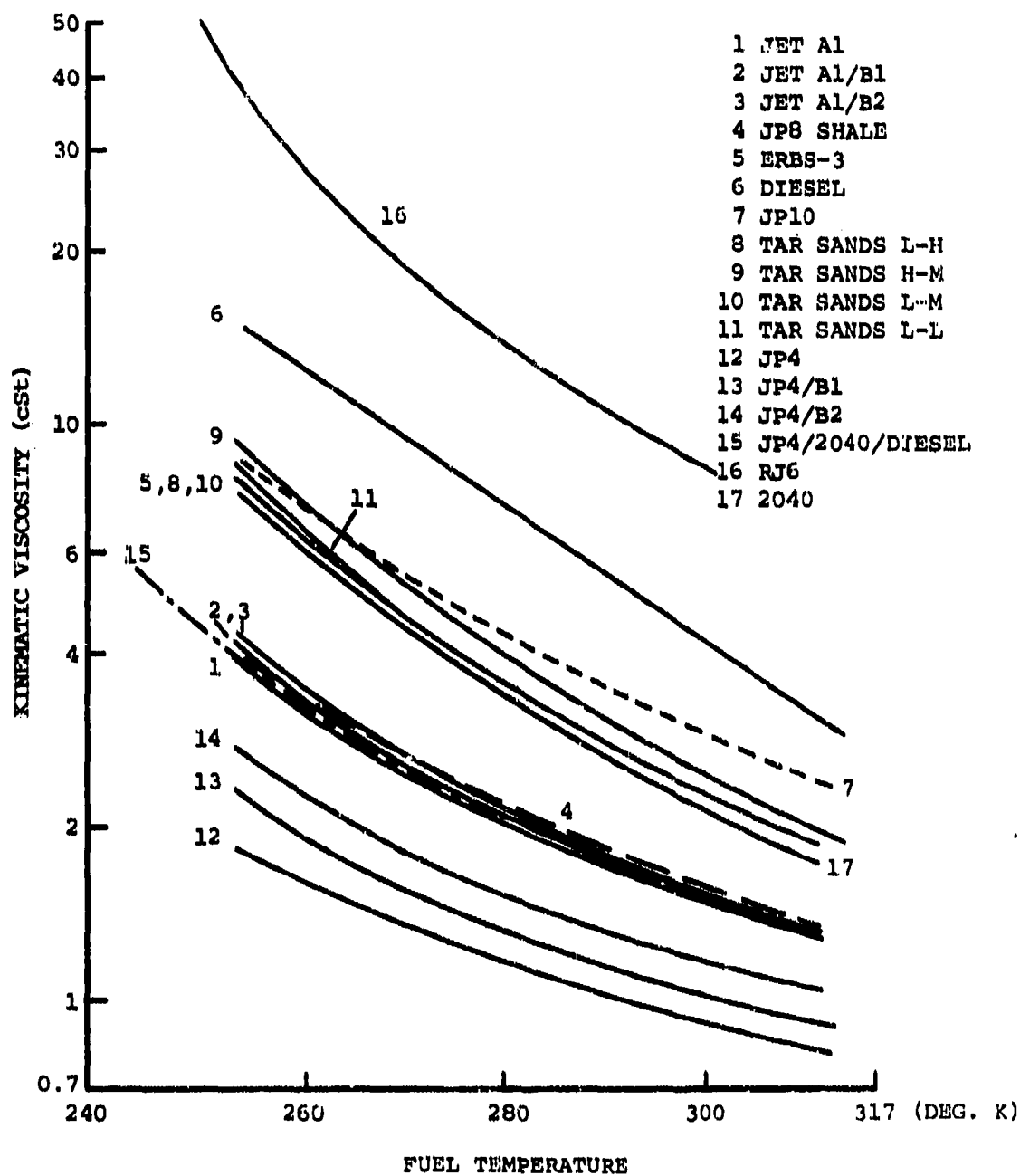


Figure 2.4: Effect of Temperature on Viscosity (ASTM D445)

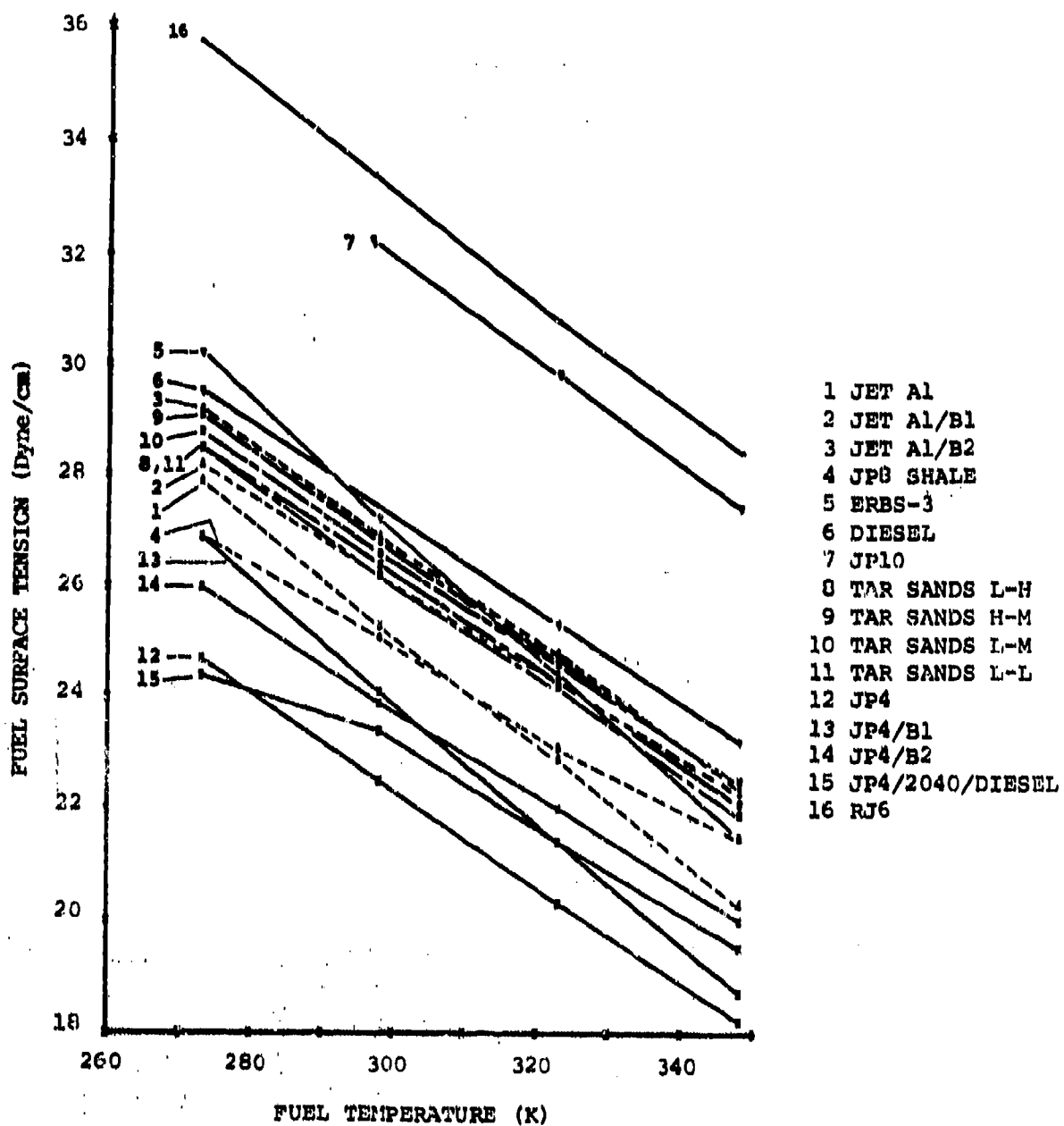


Figure 2.5: Effect of Temperature on Surface Tension
(Capillary Rise Technique)

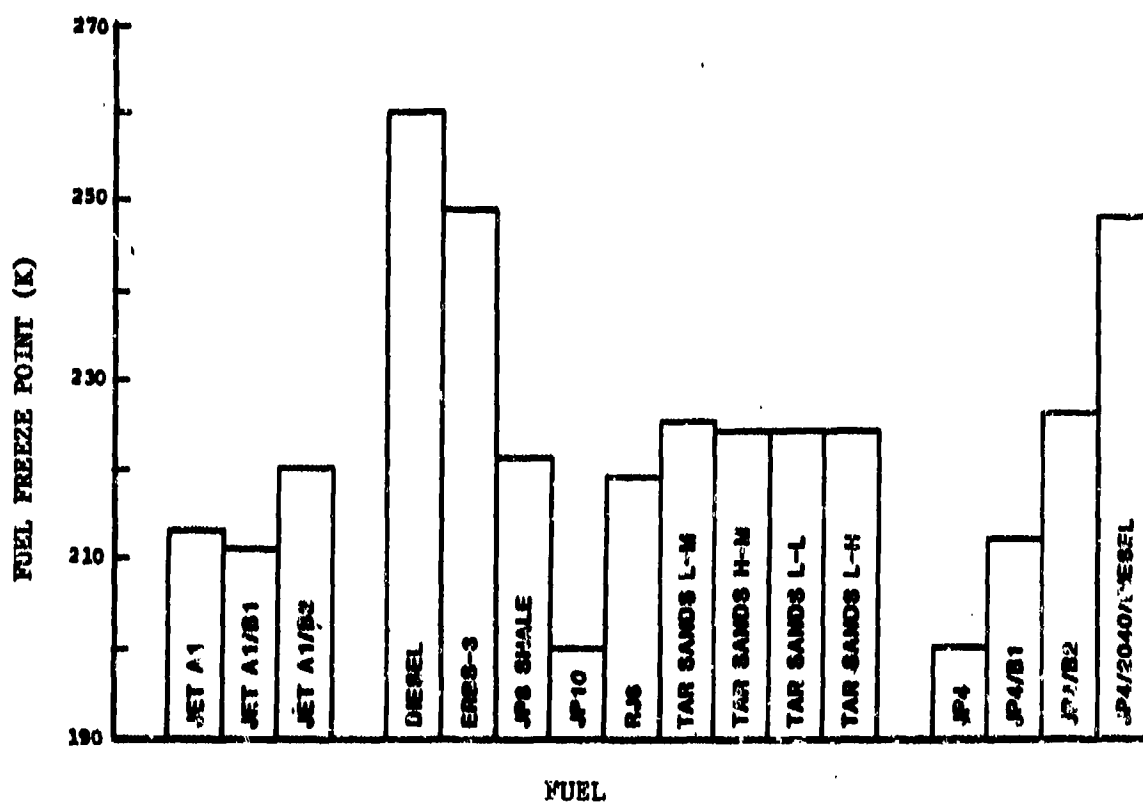


Figure 2.6: Comparison of Fuel Freeze Points (ASTM D2386)

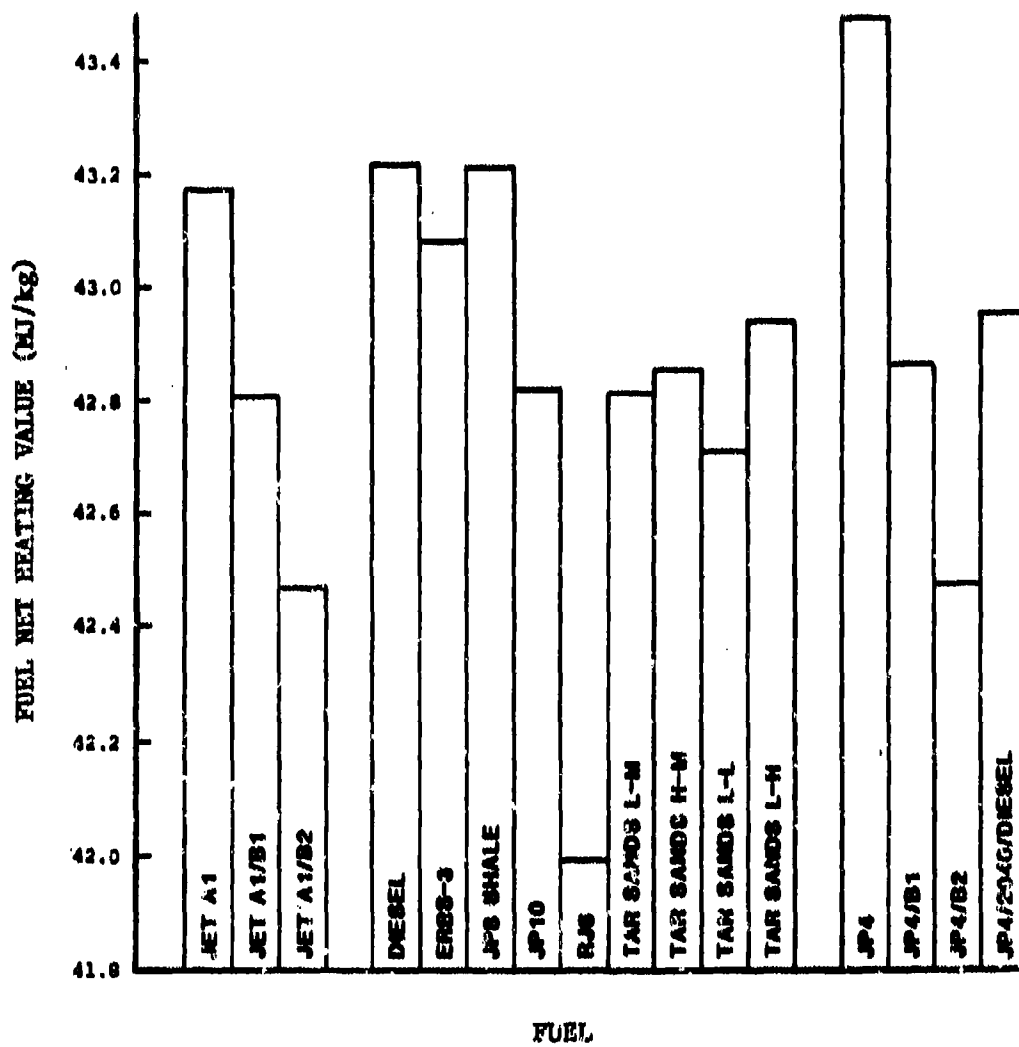


Figure 2.7: Comparison of Fuel Heating Values (ASTM D1405)

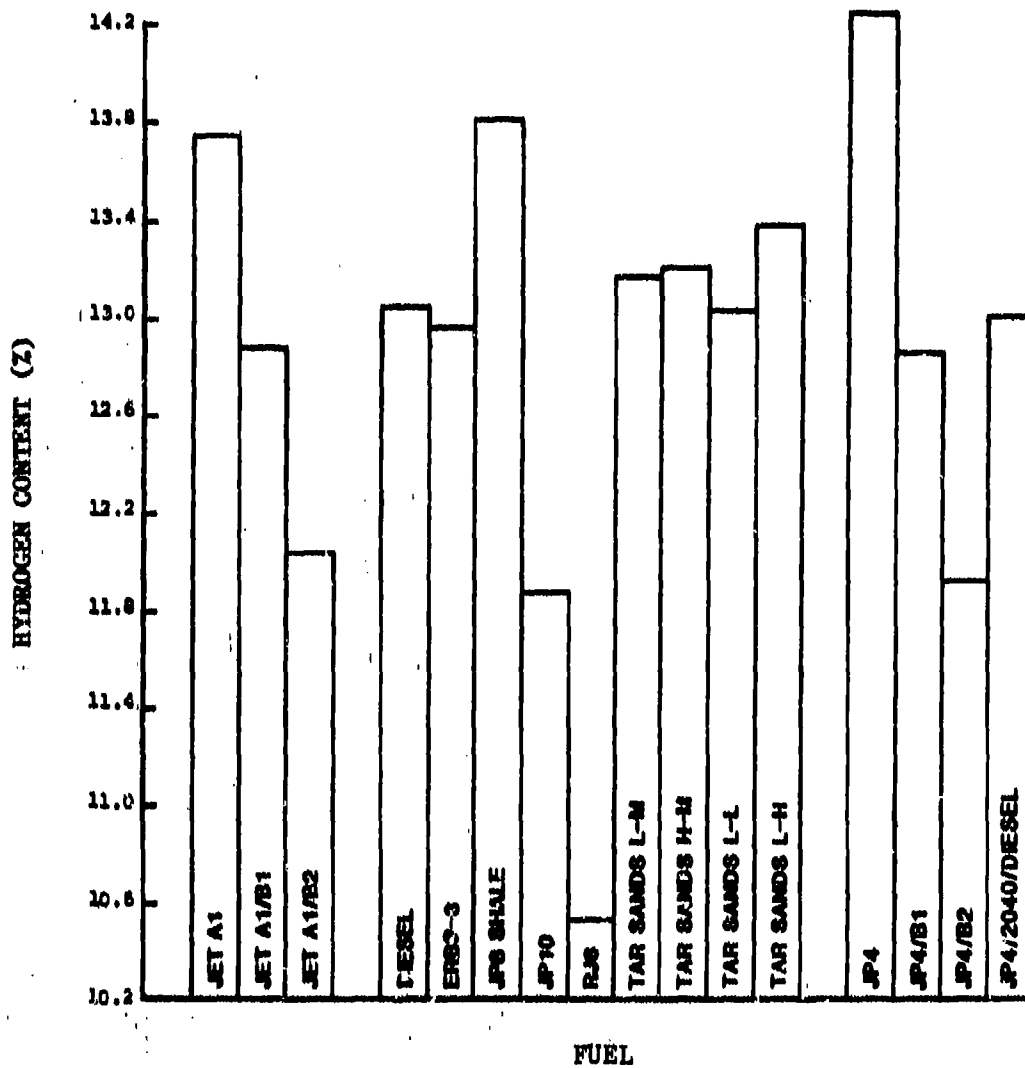


Figure 2.8: Comparison of Fuel Hydrogen Contents (ASTM D3710)

SECTION III

RELATED STUDIES AND CAN COMBUSTOR TEST RESULTS

3.1 Related Studies

This paragraph summarizes a number of investigations of fuel property effects on gas turbine engines, of which the present program is an extension. Jackson³ has summarized the investigations sponsored by AFWAL for the J-79, F-100, F-101, TF-41, J-57, J-85 and TF-39 combustion systems. In these programs the primary fuel properties varied were aromatics (single ring and multi-ring), hydrogen content (12% to 14.5% by weight), distillation range (JP4, JP8 and diesel fuel), and distillation end point (535-616K). Experimental shale oil derived fuels were also included in some of the more recent programs.

Tables 3.1 and 3.2 summarize the parameters studied in the different programs sponsored by AFWAL. The J79 program⁴ showed a strong effect of hydrogen content on smoke, carbon deposition, liner temperature, flame temperature and a moderate effect on NOx emissions; fuel volatility and viscosity effects were evident only in the low power operating range, while aromatic type and final boiling range produced no direct effect on emissions or combustor performance. The F-101 program⁵ found similar trends, although the effect of hydrogen content on smoke was somewhat less severe, see Figure 3.1, which is thought to be due to the more advanced form of fuel preparation (airblast) in the F-101 combustor.

An in-house program by AFWAL⁶ tested a T-56 single can combustor with a broad range of fuels, and these verified the strong effect of hydrogen content on combustor liner wall temperature. On the basis of extensive tests, a second order correlation was proposed between the fuel hydrogen content and combustor wall temperature:

$$T.P. = \frac{T_L - T_{L0}}{T_{L0} - T_3} = C_0 + C_1(H) + C_2(H)^2$$

Where T.P. = temperature parameter
T_L = liner temperature
T_{L0} = liner temperature with baseline fuel
T₃ = combustor inlet temperature
H = hydrogen content %

The equation derived for JP4 fuels, with 14.5% hydrogen as the baseline, was: T.P. = -.098 + .138H - .009H²

The tests also showed that irrespective of the hydrocarbon structure of the fuel blending component, combustor liner temperature varied primarily with fuel hydrogen content.

NASA Lewis Research center has sponsored a number of studies evaluating the impact of broadened specification fuels on commercial aircraft engine combustors. These have examined the Experimental Referee Broadened Specification (ERBS) fuel. Table 3.3 shows a comparison of specifications of Jet A and ERBS fuels. Significant property differences are the allowable aromatic/hydrogen content and the increase in allowable distillation temperatures. The increase in distillation temperature also necessitates a higher freeze point and increased viscosity, thus impacting atomization in the starting regime. The decrease in the minimum allowable breakpoint temperature implies that the thermal stability of ERBS fuel will be poorer than that of Jet A.

An analytical study of the impact of ERBS fuel on high bypass ratio commercial turbofan engines⁷ concluded that the use of ERBS fuel will have the following major consequences:

- Increased radiant heat load produced by ERBS will cause substantial deterioration in the life of the combustion liner and adverse effects on the durability of turbine aerofoils.
- Increased CO and THC emissions at low power, although use of improved fuel injector concepts may reduce the sensitivity of low power emissions to higher fuel viscosity.
- Increased smoke emissions. Since smoke formation is strongly dependent on detailed composition of fuel including cyclic and non-cyclic compounds, use of hydrogen content may not be an adequate parameter for characterizing fuel composition in this regard. This conclusion is at some variance with results of other studies⁶.
- Increased NO_x emissions due to higher adiabatic flame temperatures.
- No alteration will be required to the basic aerothermal definition of the combustors studied, although changes to better optimize the overall performance may be necessary.

3.2 Small Engine Requirements

This program was intended to extend the work described above into the small engine area, which has problems peculiar to itself. Small aviation turbine engines are largely used in small utility and training aircraft, auxiliary power units, cruise missiles and helicopters. Some of these typically have configurations as shown in Figure 3.2. The low pressure axial compressor stages and the high pressure centrifugal compressor stages are driven by an axial turbine. A separate power turbine provides output for turboprop or turboshaft applications. The combustor geometry most compatible with the geometric constraints of small engine

flow path is the reverse-flow annular configuration, although straight-flow annular and can combustors are found in some models. Advantages of the reverse-flow configuration are the ability to make use of the available volume, relatively low combustor loading and simpler maintenance due to accessibility of fuel injectors. The principal disadvantage, however, is the comparatively high surface-to-volume ratio inherent in the reverse-flow shape which makes liner cooling a difficult problem. Another difference on small engines is the relatively large pitching of fuel injectors which may affect exit temperature distribution. The low fuel flows result in small orifice sizes of pressure atomizers which may be prone to blockage and malfunction with usage of inferior fuels.

The overall aim of the test program is to examine effects of fuel properties on the performance of reverse-flow annular combustor type engines. Can combustor testing enabled quick and cost effective parametric investigations over a broad range of parameters from which a final test plan could be developed for investigation of reverse-flow annular combustion systems.

The JT15D family of turbofan engines has take-off ratings in the range of 2200-2900 lb thrust. The JT15D-1 engine with a take-off rating of 2200 lb thrust, has a bypass ratio of 3.3:1, pressure ratio of 9.7:1, and a total mass flow of 34 kg/sec (75 lb/sec). With the JT15D-5 engine, the thrust increase to 2900 lb has been achieved by the addition of an axial boost stage compressor. While the total airflow remains at 34 kg/sec (75 lb/sec), the overall pressure ratio is raised to 10.2:1, and the bypass ratio lowered to 2.68:1. A cross-section of the JT15D-5 is shown in Figure 3.3.

The PT6A family of gas turbine engines, with applications on both fixed wing aircraft and helicopters, has rated SHP in the range of 550 to 1375. Table 3.4 shows performance ratings of PT6A turboprop engines. While the basic engine envelope has remained largely the same, the increase in power has been achieved by successive increases in air mass flow, incorporation of cooled turbine vanes, and the addition of a second power turbine stage. Figure 3.4 shows a cross-section of the PT6A-65 engine, the operation of which was simulated during combustion testing, along with that of the JT15D-5 combustion system.

Figures 3.5 and 3.6 show the range of engine pressure ratio and turbine inlet temperature vs engine power level for small gas turbine engines currently in use. For small aircraft propulsion engines, pressure ratios range from 6:1 to 17:1 and turbine inlet temperatures range from 1200K to 1530K (2160°R to 2760°R). The engines chosen for the study are PT6A and JT15D with the following sea level take-off parameters:

PT6A-41 (250 SHP)	:	Pressure ratio 8.2:1,	TIT 1212K (2182°R)
PT6A-65 (1327 SHP)	:	Pressure ratio 10:1,	TIT 1333K (2400°R)
JT15D-4 (2500 lb)	:	Pressure ratio 10.2:1,	TIT 1280K (2304°R)
JT15D-5 (2900 lb)	:	Pressure ratio 12.1:1,	TIT 1355K (2440°R)

Thus the combustion system/engines chosen for the program are representative of small gas turbine power plants.

Both PT6A and JT15D engines use reverse-flow annular combustors. The JT15D series of engines have axial fuel injection - 12 dual orifice pressure jets with combined Flow Numbers (FN) ranging from 4.65 to 6.7 for the different models. The PT6A series of engines utilize 14 single orifice pressure jets spraying tangentially. The Flow Number of the PT6A-65 fuel nozzle is 1.9.

3.3 Can Combustor Studies

Evaluation of test fuels was initially undertaken on a can combustor system.

The can combustor was approximately 7 cm in diameter and 14 cm long with four cooling louvres located one each in the primary and intermediate zones, and two in the dilution zones, Figure 3.7. A single fuel nozzle was mounted axially at the combustor head where tangential entry holes provided swirling air to the primary zone. Four types of nozzles were tested with the can combustor to study the effects of fuel preparation, Figure 3.8; the simplex and duplex nozzles were pressure atomizers which use the fuel pressure drop to atomize the liquid into a fine spray. The airblast nozzle utilizes the energy of air flowing through the nozzle core to shear the relatively slow moving fuel into droplets. The vaporizing nozzle is a simple tube in the combustor, which allows transfer of thermal energy from the hot primary zone to the incoming fuel, thereby creating a rich vapor which enters the combustor through a small swirler and a mushroom shaped outlet.

Figure 3.9 shows a cross section of the can combustor rig. Combustion efficiency, gaseous emissions and smoke were monitored with a multi-point sampling probe in the exit plane of the combustor. The quartz windows at the back end of the rig allowed direct observation of flame behaviour both during steady state and transient performance tests. A transpiration radiometer probe was used to measure primary zone flame radiation⁹. Combustor metal temperatures were measured with twelve thermocouples, locations of which were determined using thermal paint at the beginning of the test program.

To accommodate the geometrical differences between the can combustor and the reverse-flow (PT6A and JT15D) combustors, two modelling parameters were used to define the can combustor rig air flows which simulated actual conditions on the full engine. The "air loading parameter" simulated emissions at low power and the "air velocity parameter" simulated general performance at high power. These parameters are defined as follows:

$$\begin{aligned} \text{"air loading parameter" } \Omega_c &= \frac{K_1 W_c}{P_3^{1.8} e^{T_3/K_2} V_c} \\ \text{"air velocity parameter" } \bar{M}_c &= \frac{K_3 W_c \sqrt{T_3}}{P_3 A_c} \end{aligned}$$

Thus the air mass flow for the can combustor rig test was determined from the modelling parameters, while inlet pressure, temperature, and overall fuel-air ratio were kept the same as in the engine. Fuel flows were adjusted according to the net heating value of the test fuel relative to that of Jet A1.

Steady-state performance tests were performed simulating five conditions on the turbofan (JT15D) cycle and three conditions on the turboprops (PT6A) cycle. At each condition gaseous emissions, smoke and liner skin temperatures were measured. Lean-limit tests were performed at four airflows bracketed around a (JT15D) ground idle condition, while ignition tests were performed at an airflow simulating engine cranking speed and temperature (air and fuel) between 289K (520°R) and 241K (435°R). Additional parametric tests were performed with four types of nozzles to evaluate the effects of inlet pressure and fuel-air ratio on gaseous emissions, smoke, liner skin temperatures, and flame radiation.

3.4 Impact of Fuel Property Changes on Can Combustion System

This section summarizes results from the can combustor phase¹ of the present research program. Table 3.5 is the legend which applies to all the plots in Section III. As well, regression coefficients were calculated for each plot, and are listed in Table 3.6. These describe the impacts of fuel properties on the following performance parameters.

3.4.1 Lean Stability

Fig 3.10 shows the impact of fuel properties on lean blow-off limits for simplex nozzle at air flows corresponding to idle condition. There is a fairly strong relationship between lean blow-off limits and volatility of the fuels, expressed as 10% recovery temperature (T10); this behaviour can be attributed to slower vaporization of higher boiling range fuels rendering combustion more unstable at equivalent fuel flows. However, between Jet A1/JP4 fuels and their blends, there are only small stability changes. The relationship of lean blow-off limit with hydrogen content shows a lot of scatter indicating other properties playing a role; by far the best correlation is with respect to relative droplet size of the pressure atomizer, defined as (SMD/SMD)_{JP4} where,

$$RSMD = \frac{SMD}{(SMD)_{JP4}} \cdot \left(\frac{\sigma_f}{\sigma_{JP4}} \right)^{.6} \left(\frac{v_f}{v_{JP4}} \right)^{.2} \left(\frac{\rho_f}{\rho_{JP4}} \right)^{.8}$$

The plot in Fig 3.10 shows a strong correlating effect of fuel properties through their influence on fuel droplet size. Thus fuel viscosity, density, and surface tension all affect lean blow-off limits. Tests with an airblast injector showed similar trends with fuel properties, although absolute lean blow-off limits were considerably higher, i.e. the combustor was less

stable. The lean blow-off limit is normally attained when there is insufficient excess heat from the combustion process to achieve adequate evaporation and initial pyrolysis of the incoming fuel, or when the residence time is not adequate for completion of the combustion process. Since both the fuel composition and fuel injector operation influence atomization and evaporation, variation in stability limits seen in these results is not surprising.

3.4.2 Ignition Performance

The ignition characteristics are critically influenced by evaporation of the fuel producing a local fuel-air mixture capable of immediate ignition and sustained combustion. The factors that can be expected to affect ignition include pressure and temperature of inlet air, fuel temperature which affects density and viscosity, and fuel properties influencing volatility, i.e. distillation temperature distribution. Ignition performance can be characterized by the minimum light-off temperature, minimum light-off fuel-air ratio and time-to-light.

Table 3.7 and Figures 3.11 and 3.12 describe light-off characteristics as a function of relative fuel properties, for two pressure atomizing nozzles. In the case of the fine (0.9FN) injector, satisfactory ignition was demonstrated down to a limited temperature of 242K (435°R) however both the minimum light-off fuel-air ratio and time to light were affected by fuel properties, Figure 3.11. Table 3.7 and Figures 3.12 show light-off performance with the coarse (3.0FN) fuel nozzle, strong dependence being apparent on volatility and relative droplet size and only poor correlation with hydrogen content. The data provides evidence of the significance of atomization characteristics and properties affecting vaporization of the fuel.

3.4.3 Combustion Efficiency and Gaseous Emissions

Steady state combustor performance was measured during operation simulating turboprop (PT6A) and turbofan (JT15D) cycles and typical test data are shown in Figures 3.13 - 3.16. Both CO and THC emissions were affected by fuel changes, the result apparently of differences in atomization and evaporation of the fuel. Figure 3.13 shows the influence of fuel properties on combustion efficiency while simulating idle condition on the turboprop cycle. In spite of considerable scatter, trends are toward lower combustion efficiency with reduced hydrogen content and volatility. However, there is a relatively strong correlation between combustion efficiency and relative droplet size of the pressure atomizer, indicating a strong effect of fuel viscosity and surface tension.

In general, the emission index of THC at idle revealed poorest correlation with hydrogen content¹; however better correlations were observed at higher power simulations, Figure 3.14. This indicates a major role of atomization and mixing on THC and CO emissions. At higher operating pressures, such mixing is more

easily achieved and changes in THC and CO emissions are then purely a function of fuel chemistry. Figure 3.14 shows the impact of injector geometry, the poorly optimized vaporizer showing relatively high THC and CO emissions.

Figures 3.15 and 3.16 show the impact of fuel properties on NO_x emissions at take-off and idle respectively. Published data¹² reveal a sensitivity of NO_x emissions to the fuel composition, the emissions generally increasing with reduction in the hydrogen content of the fuel. This trend suggests that the increased flame temperature with reduced hydrogen content is the governing mechanism. Test data from the present program however indicates that take-off NO_x emissions with a pressure atomizer are largely insensitive to fuel properties, Figure 3.15. Idle NO_x emissions, Figure 3.16, decrease with reduction in hydrogen content, which is probably the impact of lower reaction zone temperatures resulting from decreased combustion efficiencies at idle. Comparison of fuel nozzles showed no consistent NO_x trends with hydrogen content. Data from other engines however indicates that the trends are influenced by combustor design; for example, J85 combustion systems with pressure atomizers appear to show only a poor dependence of NO_x emissions with hydrogen content, whereas the F101 combustion system with airblast atomizers has a much stronger influence of hydrogen content⁵.

3.4.4 Smoke Emissions

Most published literature on broadened specification fuels reports an increase in the smoke levels when fuel hydrogen content is decreased. However there are differences of opinion as to whether hydrogen content is an adequate parameter for correlating smoke forming tendency of a fuel⁴.

Figure 3.17 shows variation of measured smoke number at take-off using the pressure atomizer. While the general trend indicates increased smoke as hydrogen content is decreased and aromatic content is increased, there is considerable scatter in the data. Further analysis indicates possible impact of naphthalene content; with Jet A1 and JP4 fuels, the addition of 2040 solvent raises both aromatic and naphthalene contents and results in a strong increase in smoke level. However, fuels such as L-H, H-M and L-M tar sands have a relatively low naphthalene content accompanying moderately high aromatic content, and these fuels seem to result in smoke level increases less severe than with Jet A1 and JP4 blends. Similarly ERBS-3 fuel with higher than average naphthalene content appears to result in higher smoke emissions. These results appear to indicate the types as well as overall levels of aromatics are significant, and that the presence of high concentrations of more complex multi-ring aromatic compounds may increase the propensity for smoke formation.

Figure 3.18 shows the effects of fuel injector type on smoke emissions. Airblast and vaporizer nozzles result not only in lower smoke emissions, but also appear to be less sensitive to hydrogen content. These trends are consistent with other published data comparing performance of airblast and pressure atomizing combustion systems¹².

3.4.5 Radiation and Liner Metal Temperatures

To evaluate the effect of fuel properties on radiation, measurements of radiation heat flux were made at two pressure levels using a transpiration radiometer. Figure 3.19 shows radiant heat flux as a function of fuel hydrogen contents and relative droplet size for a pressure atomizer. Good correlations are apparent with hydrogen content and droplet size at high pressure, whereas at lower pressures relative droplet size has little effect on radiation levels.

Liner temperature measurements were obtained with 12 thermocouples located on the cold side of the liner. The liner temperatures, in general showed wide variations from test to test, apparently in a random manner. For example, while some liner temperatures appeared to increase with decreasing hydrogen content at some power settings, the reverse occurred at other power levels. These effects are thought to be the result of local fuel-air ratios and flame front locations being influenced by fuel properties and operating conditions. Figure 3.20 shows the impact of fuel properties on average liner temperatures expressed as

$$\frac{T_L - T_{L_{JP4}}}{T_{L_{JP4}} - T_3}$$

Although the data show considerable scatter, the general trends indicate a substantial increase in metal temperature as the fuel hydrogen content is reduced, due mainly to increases in radiation levels. Also shown for comparative purposes are the engine correlations by Blazowski¹⁰, the dashed lines encompassing data from five combustors. It does appear from this comparison that there is good correlation between fuel hydrogen content and liner metal temperatures. There is also reasonable correlation with fuel aromatic content, although the purely synthetic JP10 fuel with no aromatics results in metal temperatures much higher than petroleum based fuels.

3.5 Phase III Test Plan

On the basis of the can combustor results, the following test plan was recommended for Phase III with PT6A and JT15D reverse-flow annular combustion systems, and agreed to by CDND and AFWAL Project managers.

3.5.1 Test Fuel

- a. PT6A Atmospheric Tests: Jet A1, Jet A1/B1, Jet A1/B2, JP4, JP4/B1, JP4/B2, JP4/DF/2040, ERBS-3, Shale JP8, L-L Tar Sands, L-H Tar Sands and JP10 (12 fuels).
- b. PT6A Full Pressure and Cold Start Tests: Jet A1, Jet A1/B2, JP4, JP4/B2, ERBS-3, Shale JP8, L-L, L-H Tar Sands, JP10 and RJ6(10 fuels).
- c. JT15D Atmospheric Tests: Shale JP8, JP4, ERBS-3 and JP10 (4 fuels).

3.5.2 PT6A Atmospheric Combustor Tests

- a. Combustor Configurations - 2 (Bill of Material and Lean Front End).
- b. Fuel Nozzle Types - 2 (Simplex with Different Flow Numbers).
- c. Operating Cycle - To simulate PT6A-65.
- d. Test Matrix simulating operation from idle to take-off to test the following performance parameters:
 - Two thermal paint tests to determine locations of thermocouples.
 - Temperature traversing and steady-state performance tests.
 - Transient tests to determine lean stability limits.

3.5.3 JT15D Atmospheric Combustor Tests

- a. Combustor Configurations - 2 (Bill of Material and Rich Front End).
- b. Fuel Nozzle Types - 2 (Simplex and Airblast).
- c. Operating Cycle - To simulate JT15D-5.
- d. Test matrix simulating operation from idle to take-off to test following performance parameters:

- Two thermal paint tests to determine locations for thermocouples.
- Temperature traversing and steady state performance tests.
- Transient tests to determine lean (stability) limits.

3.5.4 Cold Start Tests

- | | |
|----------------------------|--------------------------------------|
| a. Test Vehicle | - PT6A-65 Engine |
| b. Test Facility | - National Research Council, Ottawa. |
| c. Combustor Configuration | - PT6A-65 Bill of Material |
| d. Fuel Nozzles | - PT6A-65 Bill of Material |
| e. Minimum Temperatures | - -50°F or rig limit (228K) |

3.5.5 PT6A Full Pressure Tests

- | | |
|----------------------------|--|
| a. Test Vehicle | - PT6A-65 Gas Generator |
| b. Combustor Configuration | - 2 (Bill of material with and without cabin bleed) |
| c. Fuel Nozzle Types | - 2 (Simplex with different Flow Numbers). |
| d. Operating Cycle | - PT6A-65. |
| e. Test Parameters | - Metal Temperatures, Emissions, Smoke, Pattern Factors and Pressure Drop. |

A total of 536 data points were covered during Phase III tests as detailed in Table 3.8.

Table 3.1: Fuel Mainburner/Turbine Effects Test Scope (GE) (2)

TEST VEHICLE	Combustor Dome and Liner Temperature	Smoke and Gaseous Emissions	Combustor Exit Temp. Distribution	Combustor Stability at Idle	Cold Day Ground Start	Altitude Relight and Stability	Fuel Nozzle Plugging	Carbon Deposition	Transient Response	Turbine Material Erosion	Turbine Stator Heat Load	Fuels Tested
J79 Single Combustor High Pressure Rig	X	X						X				3
J85 Full Annular Combustor High/Low Pressure Rig	X	X	X	X	X	X		X				6
TF39 Full Annular Combustor Atmospheric-Pressure Rig		X	X									3
TF39 36° Sector Combustor High Pressure Rig	X	X						X				6
TF39 36° Sector Combustor Low Pressure Rig				X	X	X						6
J79/J85/TF39 Fuel Nozzle Fouling Rig							X					2
J79/J85/TF39 Turbine Material Erosion Rig									X			1
J79 Engine	X	X								X	X	2
J85 Engine	X	X						X		X	X	6
TF39 Engine	X	X								X	X	2

Table 3.2: Fuel Mainburner/Turbine Effects Test Scope (PWA) (2)

TEST VEHICLE	6*	Combusior Dome and Liner Temperatures	Smoke and Gaseous Emissions	Combusior Exit Temp. Distribution	Combusior Stability and Altitude Relight	Standard and Cold Day Ground Start	Carbon Deposition	Transient Response	Turbine Material Erosion
J57 (TF33) Single Can High Pressure Rig	6*	6	6	6			3	6	
J57 (TF33) Multiple Can Full Ann/Low Press Rig				6	6				
F100 90° Sector Rig	6	6	6	6	6	3	6	2	
Low Press Turbine Rig								2	

* Number of Test Fuels per Test

Table 3.3: Comparison of Specifications for Jet-A and ERBS Fuels⁽⁵⁾

	<u>Jet-A</u>	<u>ERBS</u>
Aromatic Content (% volume)	20 max.	-
Hydrogen Content (% weight)	*	12.8 \pm 0.2
Sulphur Mercaptan (% weight) max.	0.003 max.	0.003
Sulphur Total (% weight)	0.3 max.	0.3 max.
Naphthalene Content (% volume)	3.0 max.	-
Distillation Temperature (K)		
10 Percent	500 max.	477 max.
90 Percent	-	534 min.
Final Boiling Point	561 max.	-
Residue (% volume)	1.5 max.	-
Loss (% volume)	1.5 max.	-
Flashpoint (K)	311 min.	311/321
Freezing Point (K)	233 max.	244 max.
Maximum Viscosity (cs)	8 @ 253 K	12 @ 249 K
Heat of Combustion (J/kg)	42.8 x 10 ⁶ min.	-
Thermal Stability:		
JFTOT Breakpoint Temperature (K)	533 min.	511 min.
Method	Visual	TDR = 13

* For comparison to ERBS, the smoke point and luminometer limits result in a minimum hydrogen content of approximately 13.5%.

Table 3.4: Performance Ratings of PT6A Turboprops

Sea Level Static	Take-off/Max. Continuous			Max. Cruise			Weight lb.	Propeller
	Thermodynamic Performance		Max SHP Performance	Thermodynamic Performance		Max SHP Performance		
	ESHP	SFC(1)	SHP	ESHP	SFC(1)	SHP		
PT6A-20 PT6A-20A	610	0.640	550 TO 70°F	522	0.670	495 TO 59°F	289	2200
PT6A-27	751	0.595	680 TO 71°F	683	0.607	620 TO 69°F	300	2200
PT6A-28	751	0.595	680 TO 71°F	751	0.595	620 TO 91°F	300	2200
PT6A-34	886	0.562	750 TO 87°F	763	0.598	700 TO 67°F	311	2200
PT6A-41	1089	0.558	850 TO 106°F	1013	0.565	850 TO 84°F	370	2000
PT6A-45	1179	0.557	1120 TO 59°F	1004	0.570	956 TO 59°F	423	1620 TO 1700
PT6A-50	1174	0.560	1120 TO 59°F	1017	0.578	900 TO 74°F	546	1100 TO 1210
PT6A-65	1375	0.517	1294 TO 89°F	1022	0.522	956 TO 80°F	464	1700

(1) LB/ESHP/HR

Table 3.5: Legend of Symbols used in Section III Plots

○ Jet A1	▼ ERBS-3
● Jet A1/B1	▽ Diesel
① Jet A1/B2	▼ JP10
● Shale JP8	▲ Tar Sands L-H
□ JP4	▲ Tar Sands L-M
▣ JP4/B1	▲ Tar Sands H-M
▣ JP4/B2	△ Tar Sands I-L
■ JP4/2040/DF	

Table 3.6: Influence Coefficients Corresponding to Observed Fuel Property Effects.

Combustion parameter (Y)	Fuel property parameter (X)	Linear regression equation	Reference Figure No.
Lean limit far (LLFAR)	10% distillation temp. (K)	$Y = 2.24 \times 10^{-5}X - .0046$	3.10
Lean limit far (LLFAR)	Hydrogen content (%)	$Y = 0.0138 - .000669X$	3.10
Lean limit far (LLFAR)	Relative SMD	$Y = 0.00886X - .0055$	3.10
Minimum light-off far ($T_F=T_3=241K$)	10% distillation temp.(K)	$Y = 6.85 \times 10^{-5}X - .0073$	3.11
Minimum light-off far ($T_F=T_3=241K$)	Hydrogen content (%)	$Y = 0.0289 - .00055X$	3.11
Minimum light-off far ($T_F=T_3=241K$)	Relative SMD	$Y = 0.0135X - .0055$	3.11
Time-to-light (sec)	10% distillation temp.(K)	$Y = 0.0704X - 15.8$	3.11
Idle inefficiency (%)	10% distillation temp.(K)	$Y = 0.0235X - 6.4$	3.13
Idle inefficiency (%)	Hydrogen content (%)	$Y = 11.14 - 0.565X$	3.13
Idle inefficiency (%)	Relative SMD	$Y = 9.10X - 7.16$	3.13
EI-NO _x take-off (g/kg fuel)	10% distillation temp. (K)	$Y = 5.30 + 0.0060X$	3.15
EI-NO _x take-off (g/kg fuel)	Hydrogen content (%)	$Y = 5.98 + 0.154X$	3.15
EI-NO _x take-off (g/kg fuel)	Relative SMD	$Y = 5.55 + 1.96X$	3.15
Smoke (SN)	Hydrogen content (%)	$Y = 146 - 8.33X$	3.17
Average liner temperature	Hydrogen content (%)	$Y = 0.336 - 0.0189X$	3.20

Table 3.7: Minimum Light-Off Temperatures

FUEL	0.9 FN Simplex K (°R)	3.0 FN Simplex K (°R)
Jet A1	< 242 (435)	261 (470)
Jet A1/B2	< 242 (435)	269 (485)
JP4	< 242 (435)	< 242 (435)
JP4/R2	< 242 (435)	261 (470)
Tar Sands L-II	< 242 (435)	276 (497)
ERBS - 3	< 242 (435)	265 (477)
JP10	< 242 (435)	> 280 (520)

$$W_A = 0.023 \text{ kg/s}$$

$$W_{\text{max}} = 5.4 \text{ kg/hr}$$

Table 3.8: Phase III Test Points

PT6A-65	Atmospheric Rig (12 fuels):	194
PT6A-65	Gas Generator (10 fuels):	195
PT6A-65	Cold Start Tests (10 fuels):	81
JT15D-5	Atmospheric Rig (4 fuels):	66
TOTAL		536

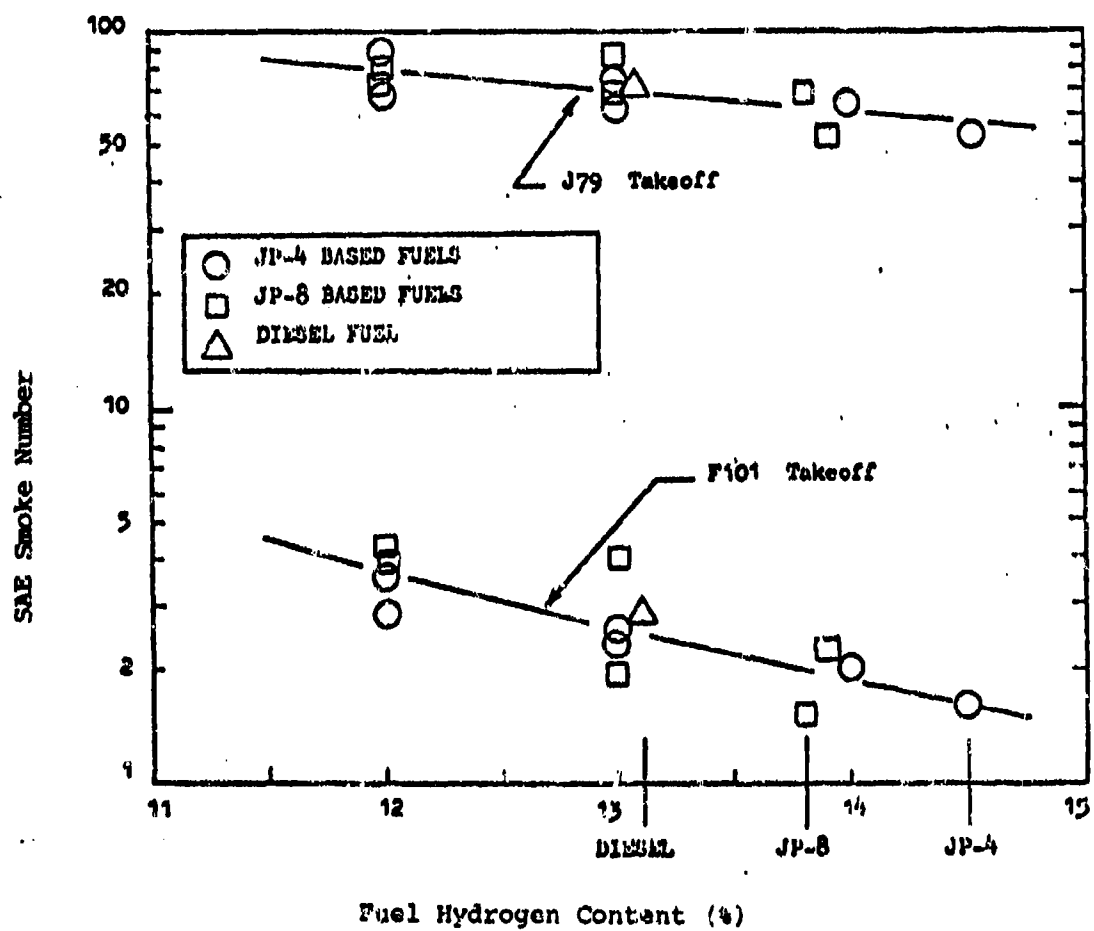


Figure 3.1: Effect of Fuel Type on Smoke Levels (2)

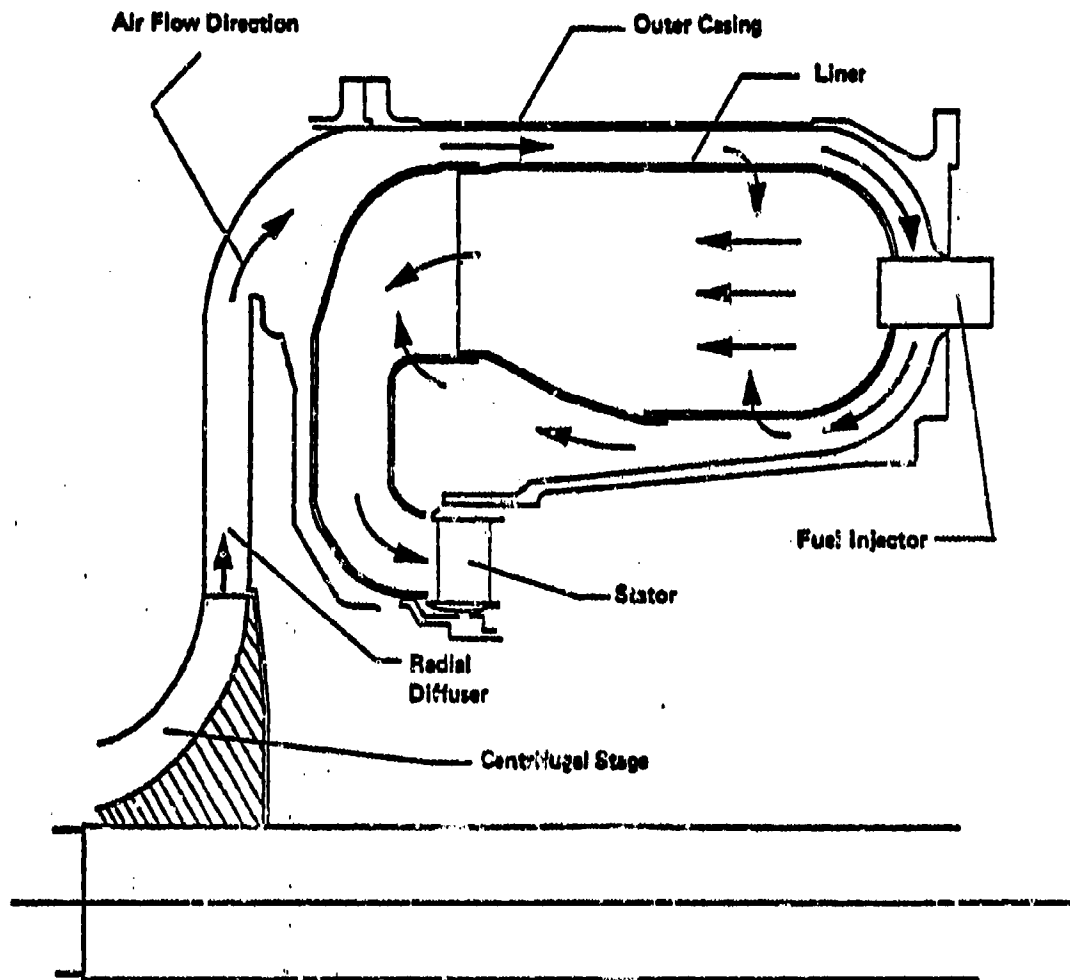


Figure 3.2: Illustration of a Reverse-Flow Annular Combustor

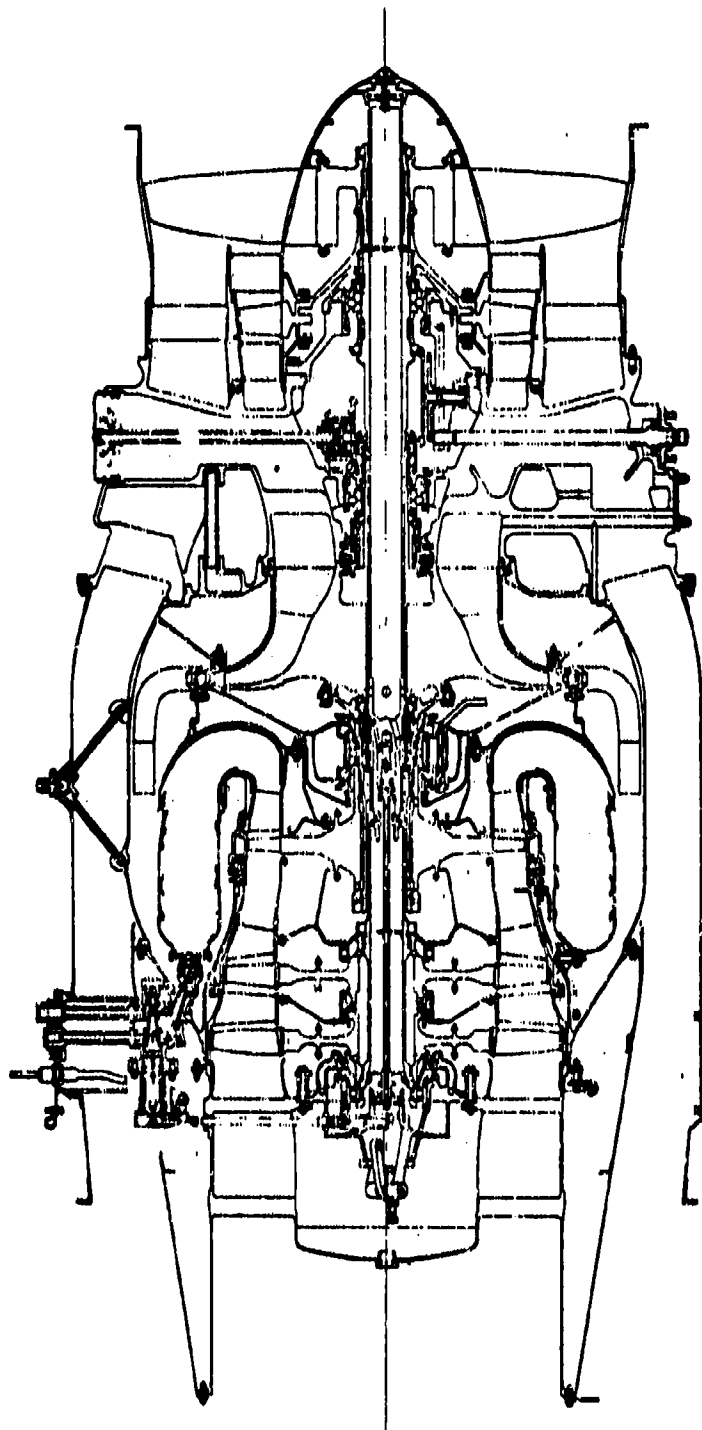


Figure 3.3: JT15D-5 Cross Section

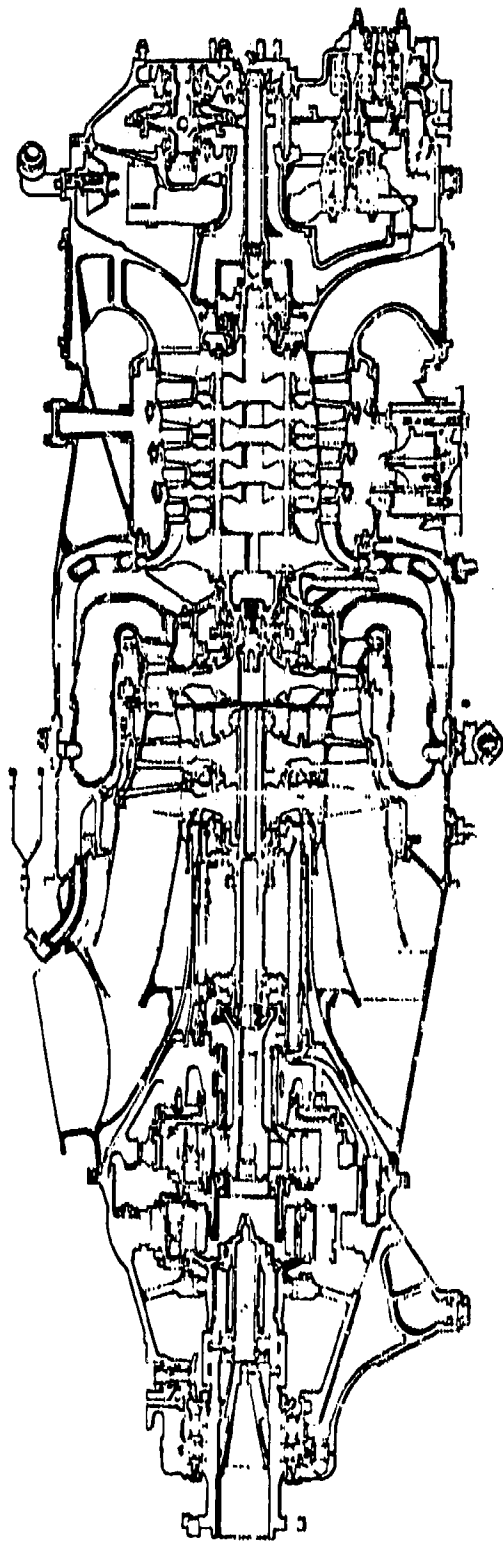


Figure 3.4: PT6A-65 Cross Section

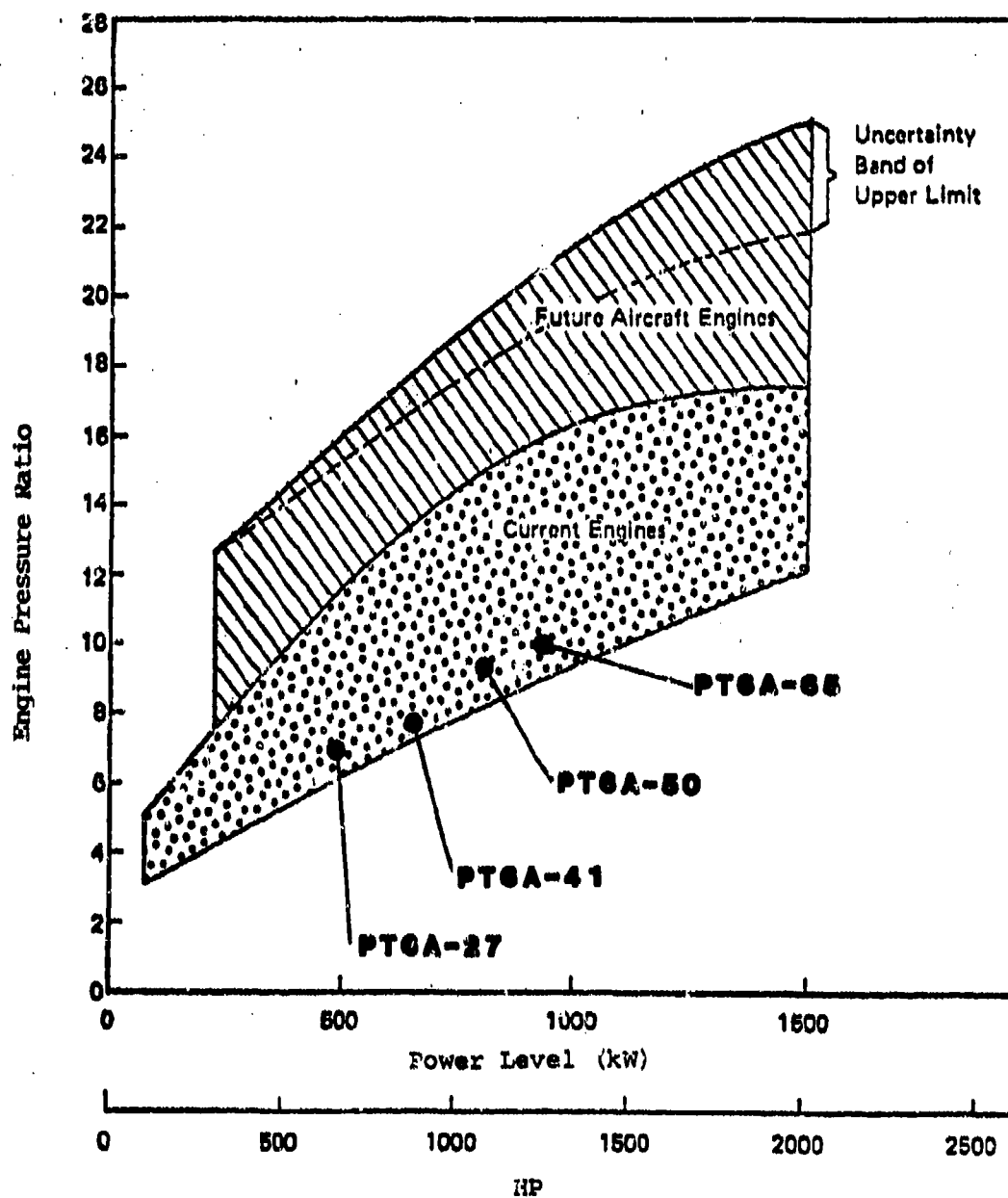


Figure 3.5: Projected Trends in Pressure Ratios

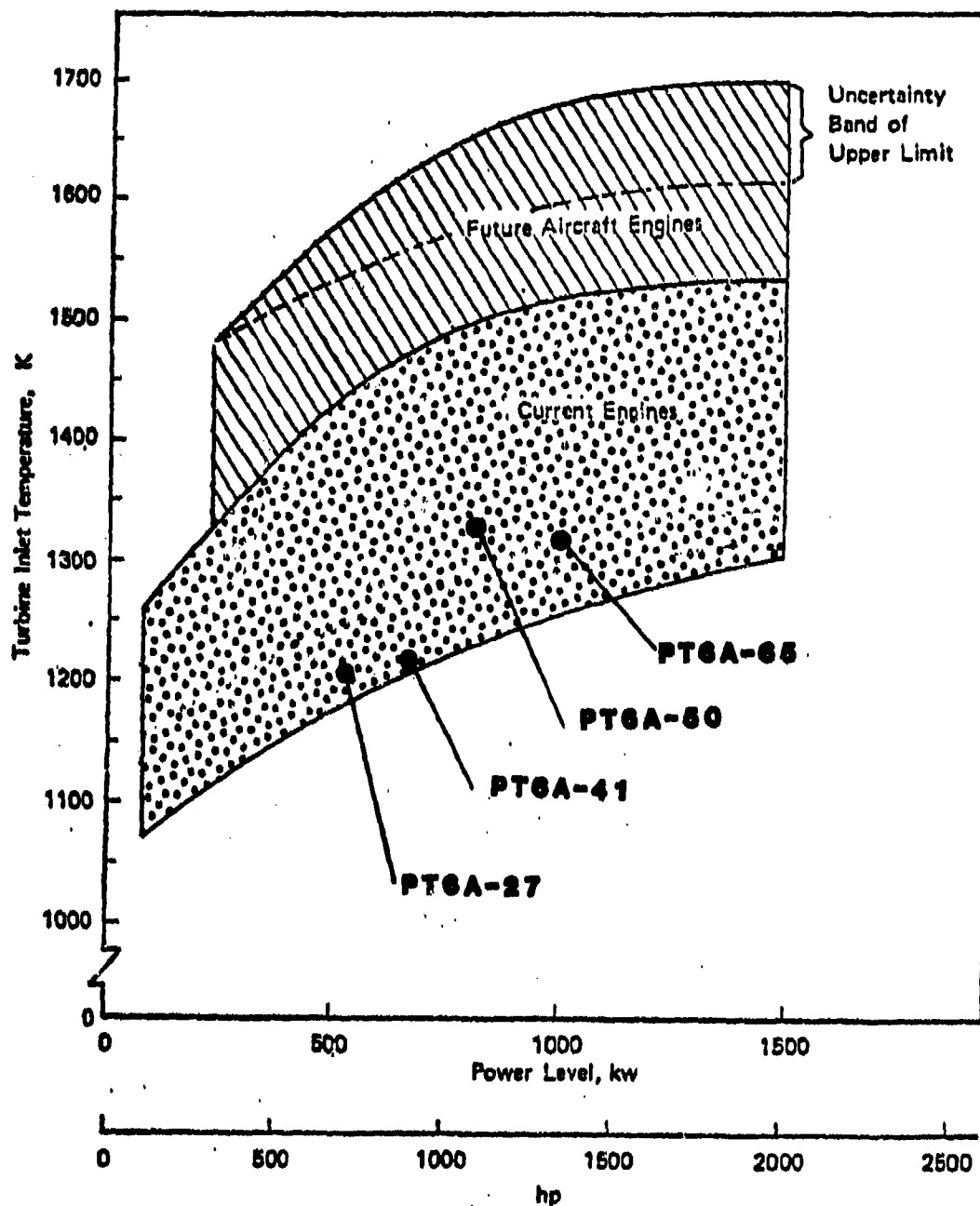


Figure 3.6: Projected Trends in Turbine Inlet Temperatures

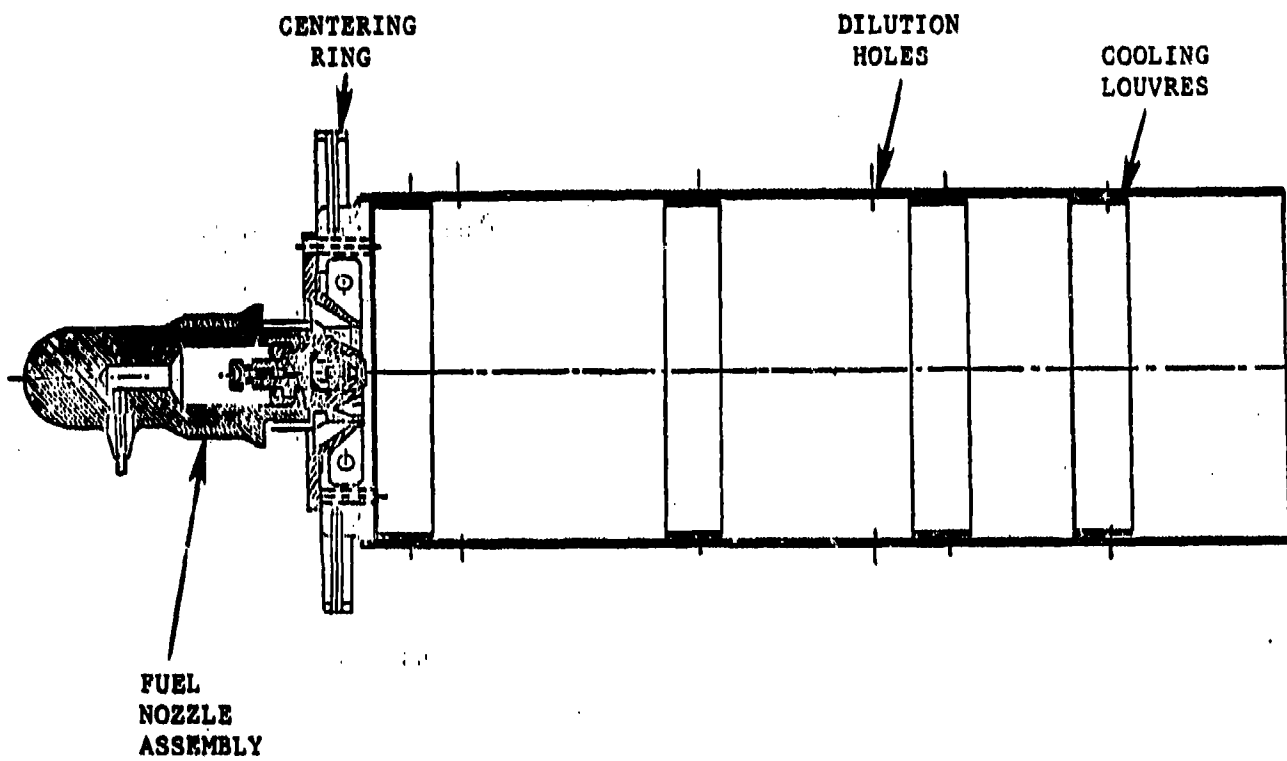


Figure 1.7: Schematic of Can Combustion System

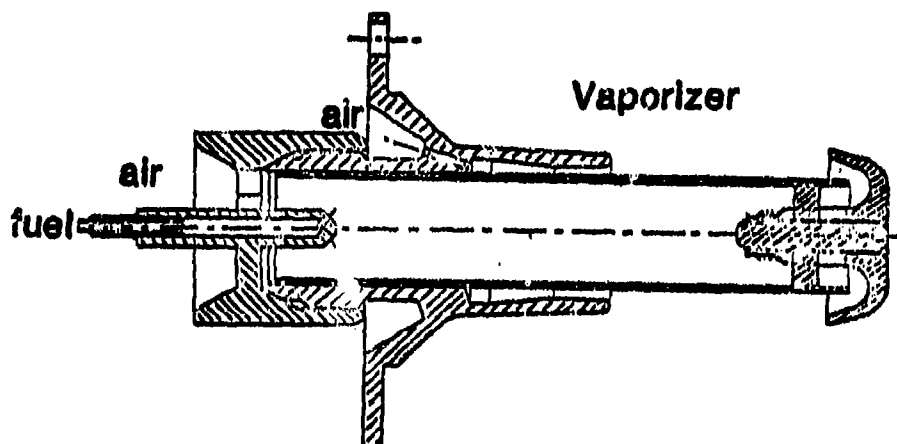
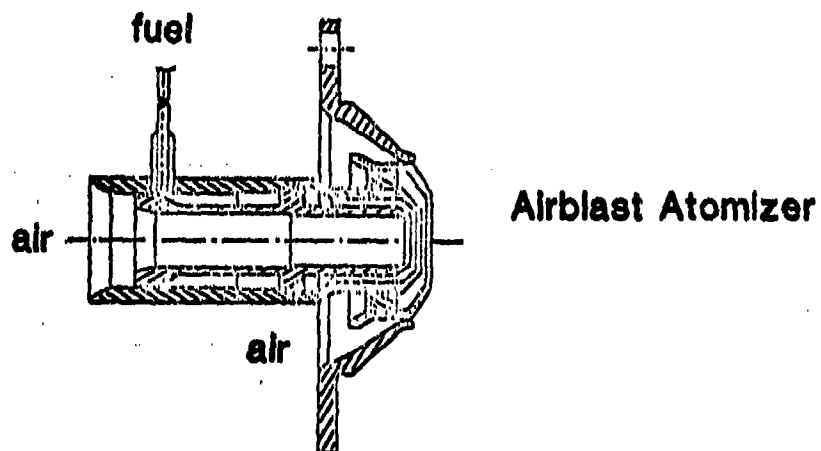
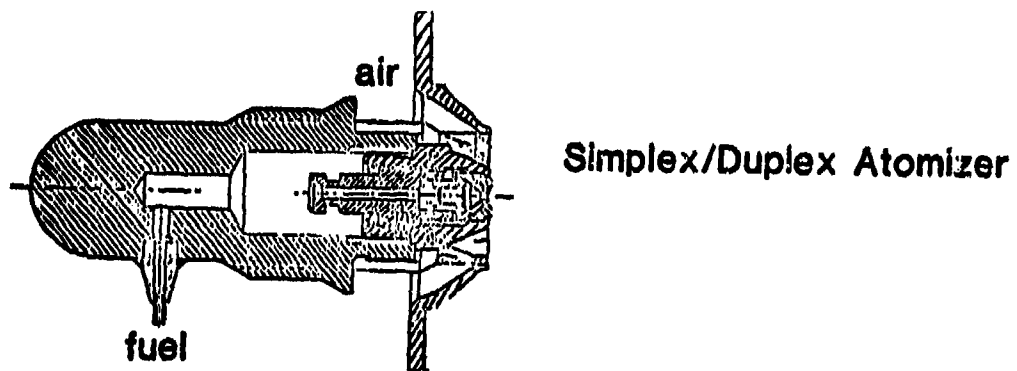


Figure 3.8: Fuel Nozzles Used in Can Combustor Tests

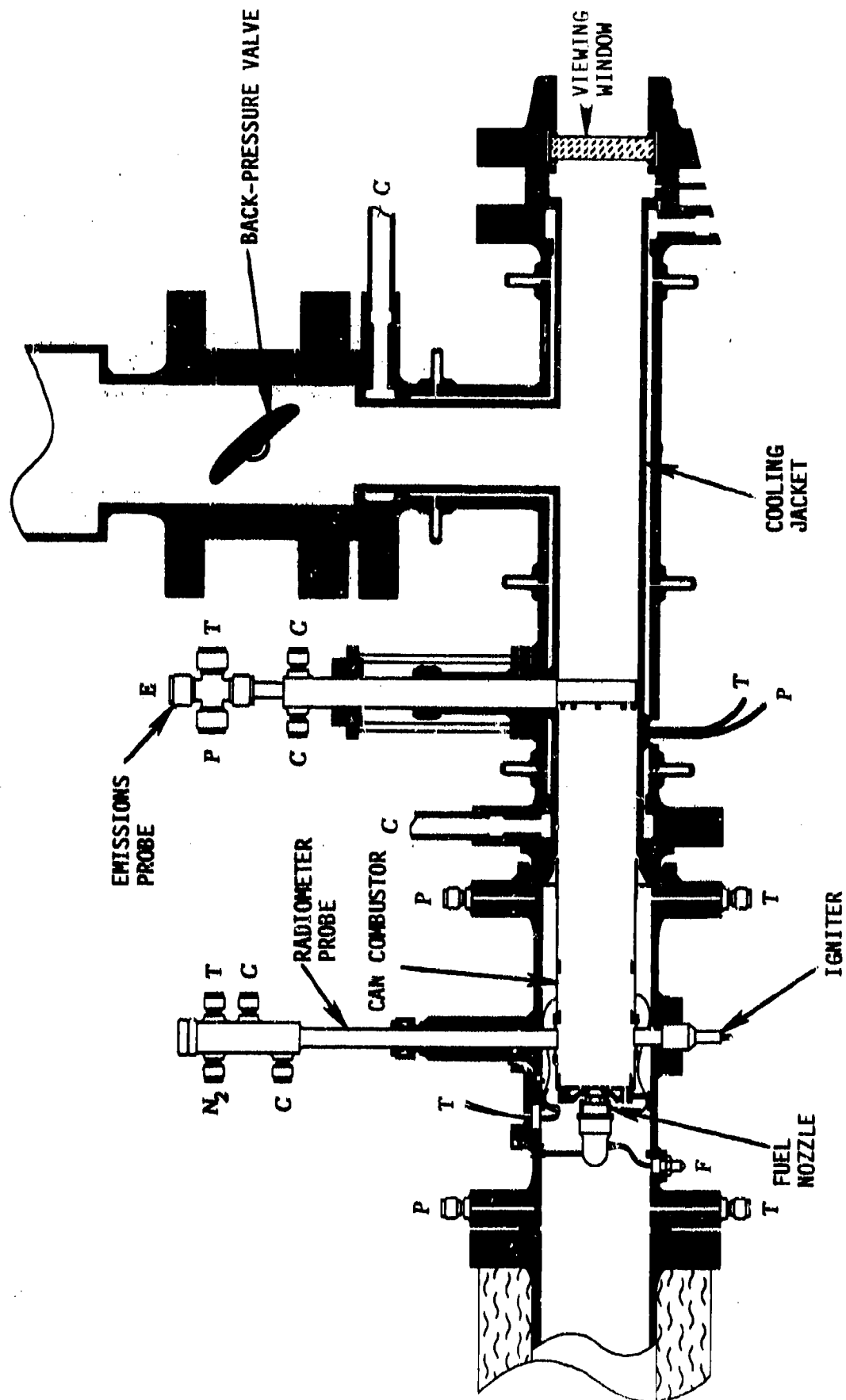


Figure 3.9: Can Combustor Rig Test Section Assembly

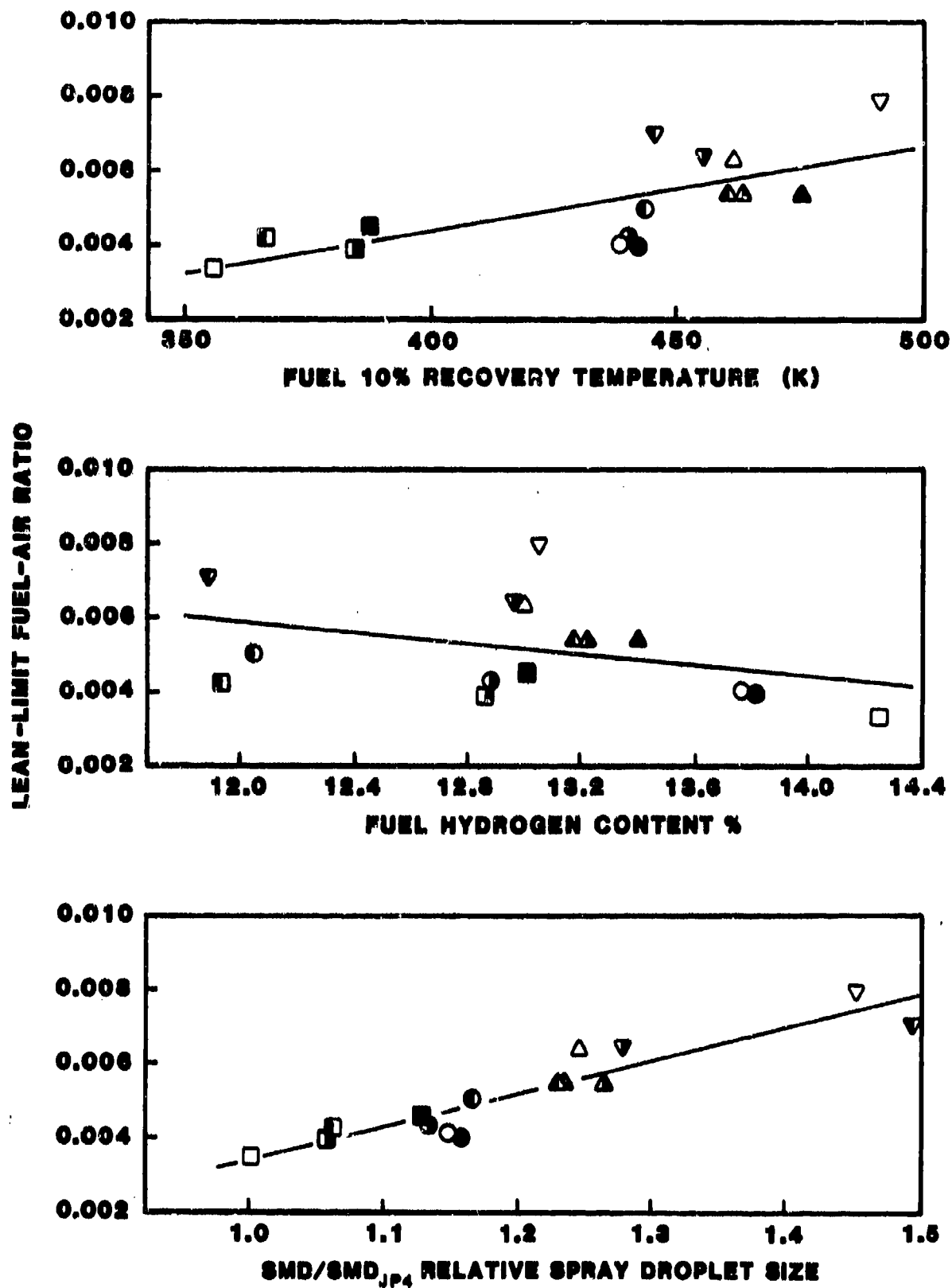


Figure 3.10 : Impact of Fuel Properties on Lean Stability Limits
(M Simulation, Simplex 0.9 FN Nozzle)

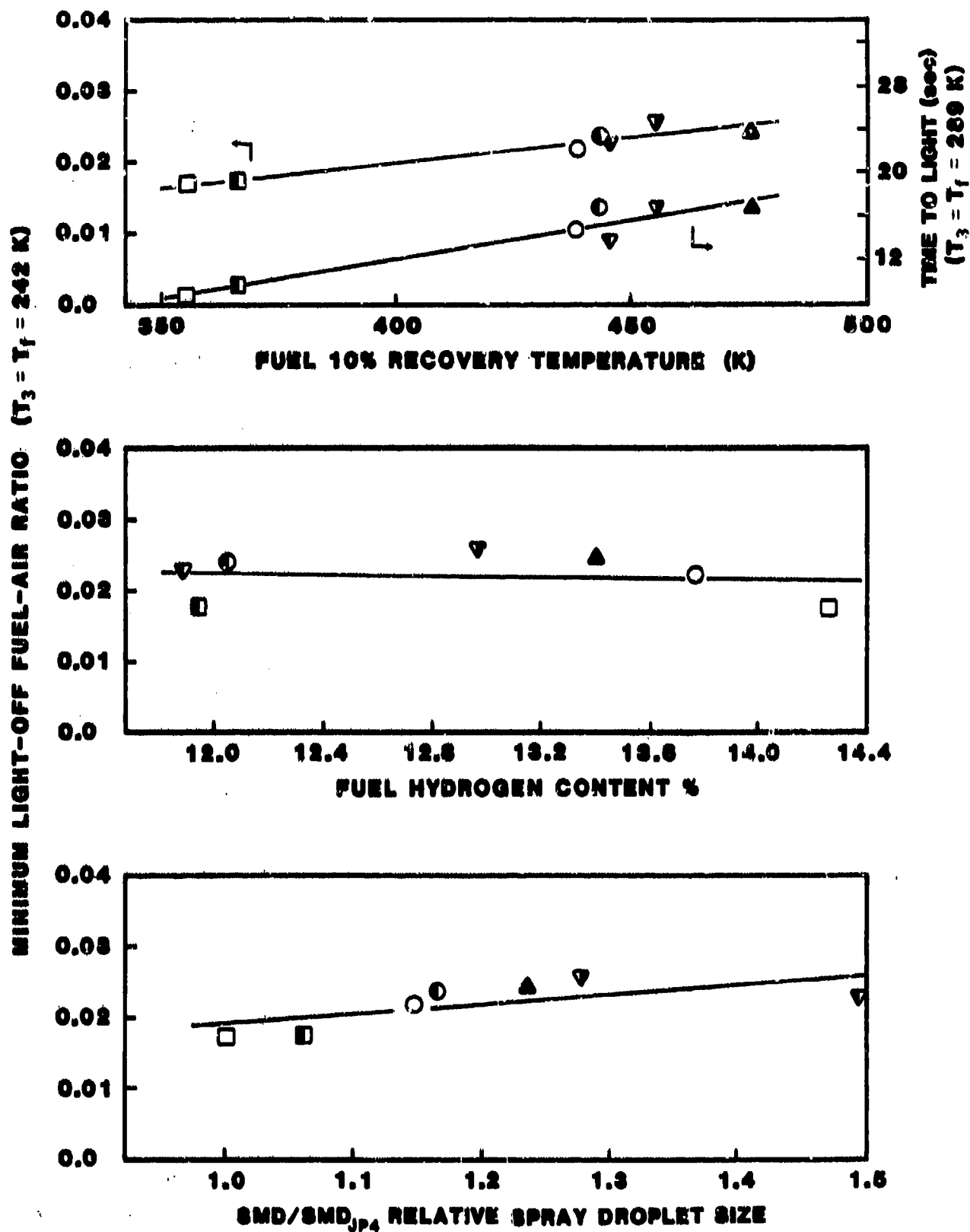


Figure 3.11: Impact of Fuel Properties on Starting Characteristics
(0.9 FN Nozzle)

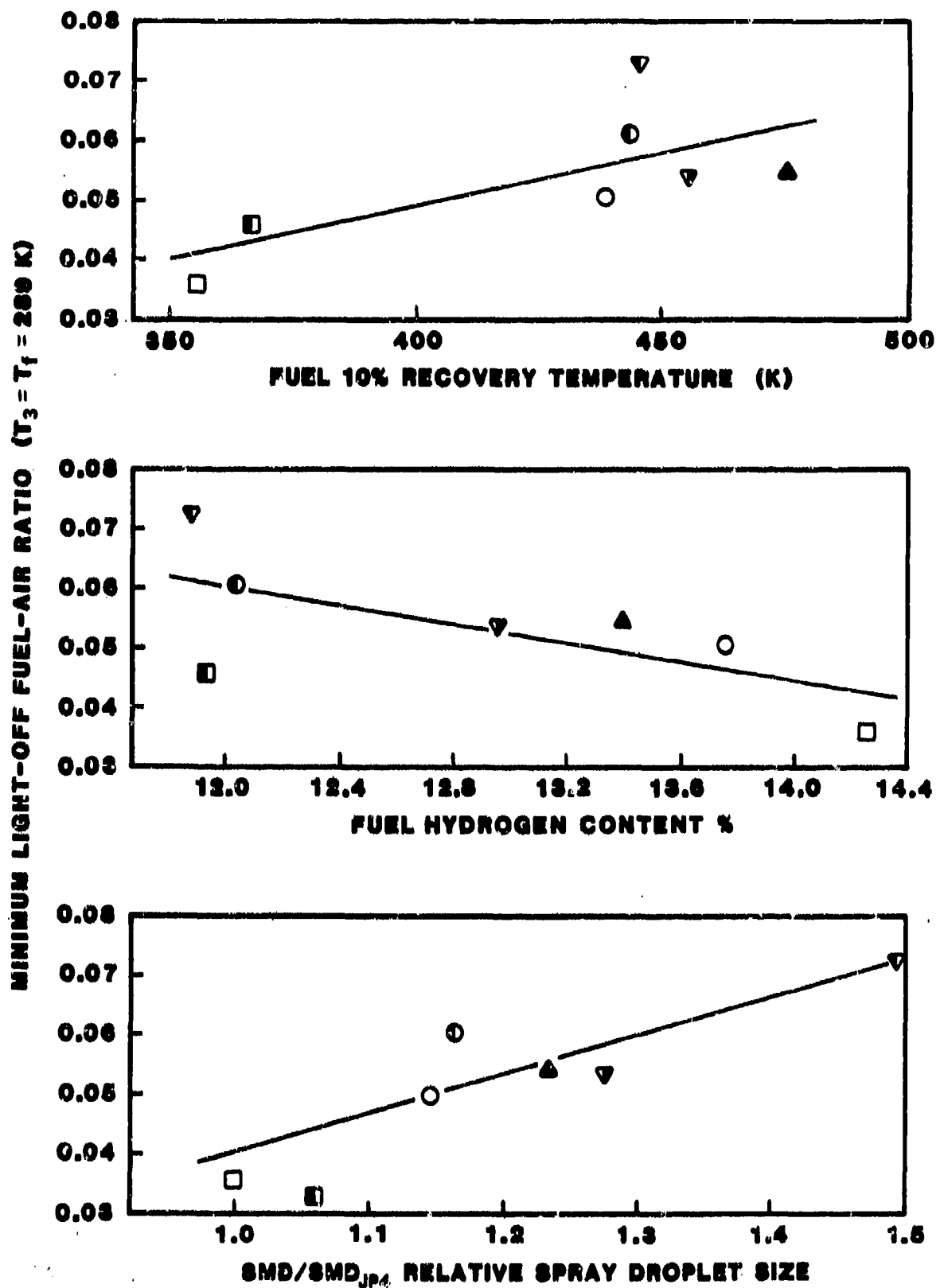


Figure 3.12: Impact of Fuel Properties on Starting Characteristics
(3.0 FN Nozzle)

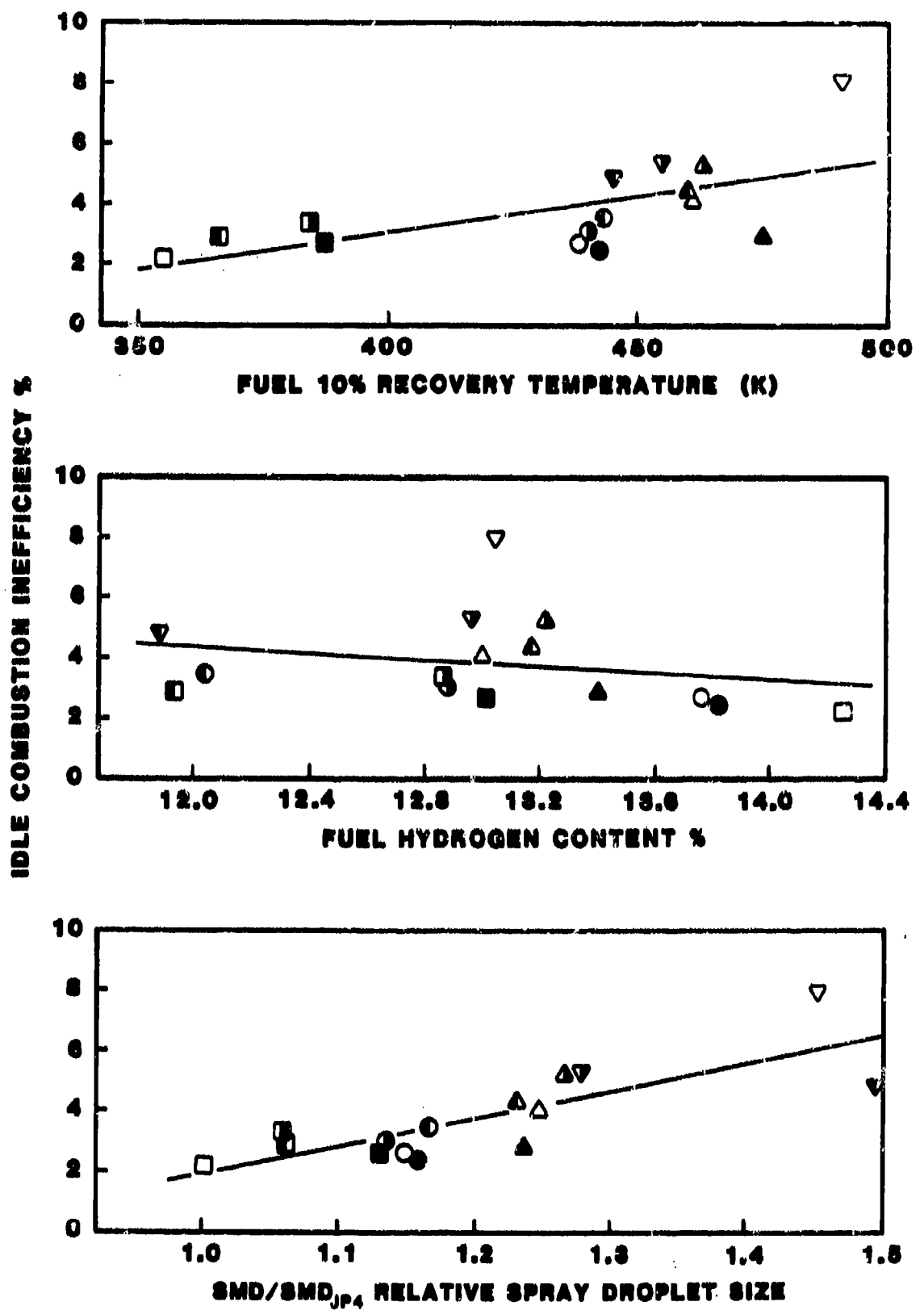


Figure 3.13: Impact of Fuel Properties on Idle Combustion Efficiency (Power Level Simulation, Simplex Nozzle)

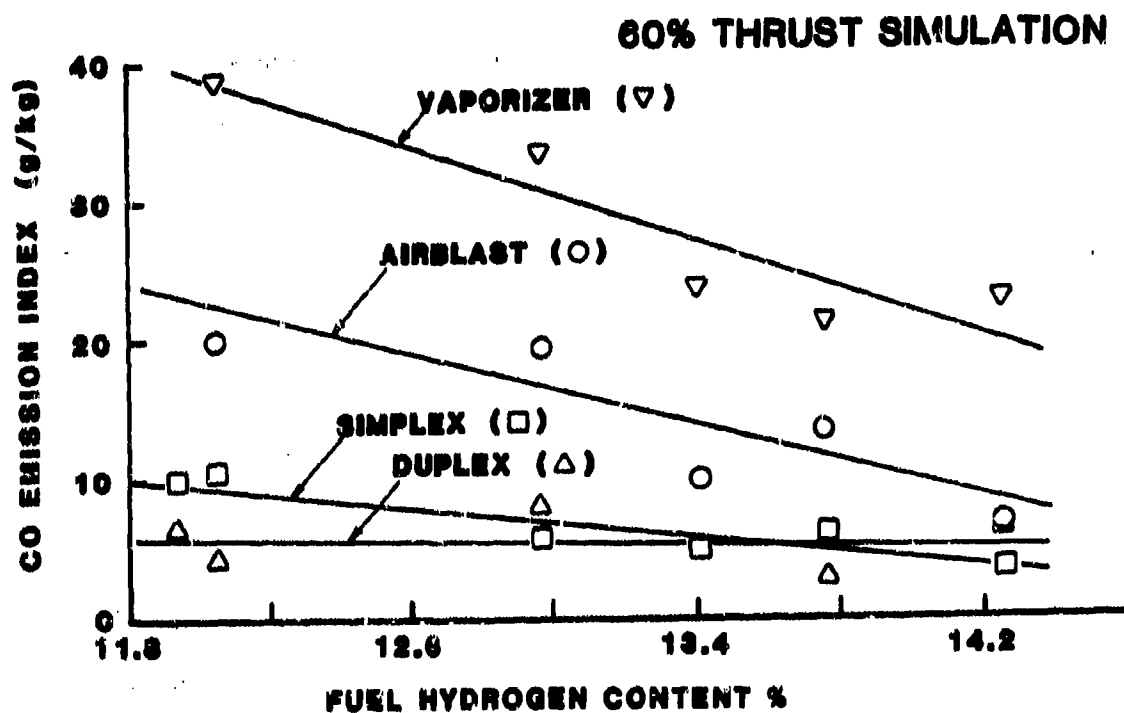
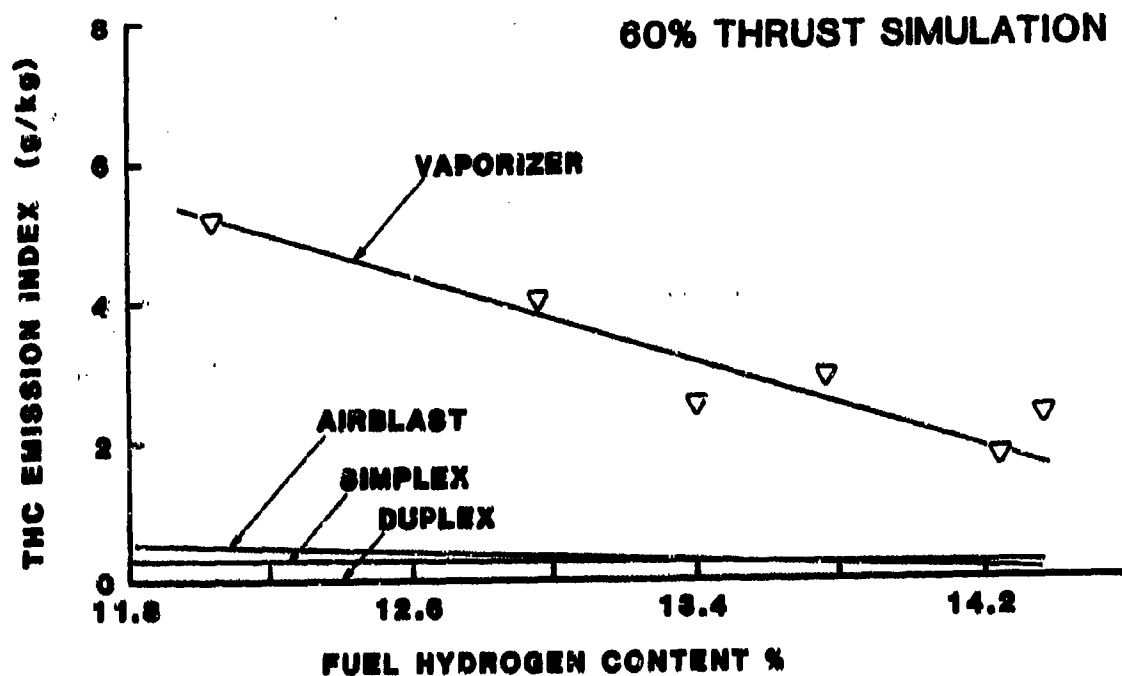


Figure 3.14: Impact of Fuel Hydrogen Content and Injector Types on HC and CO Emissions

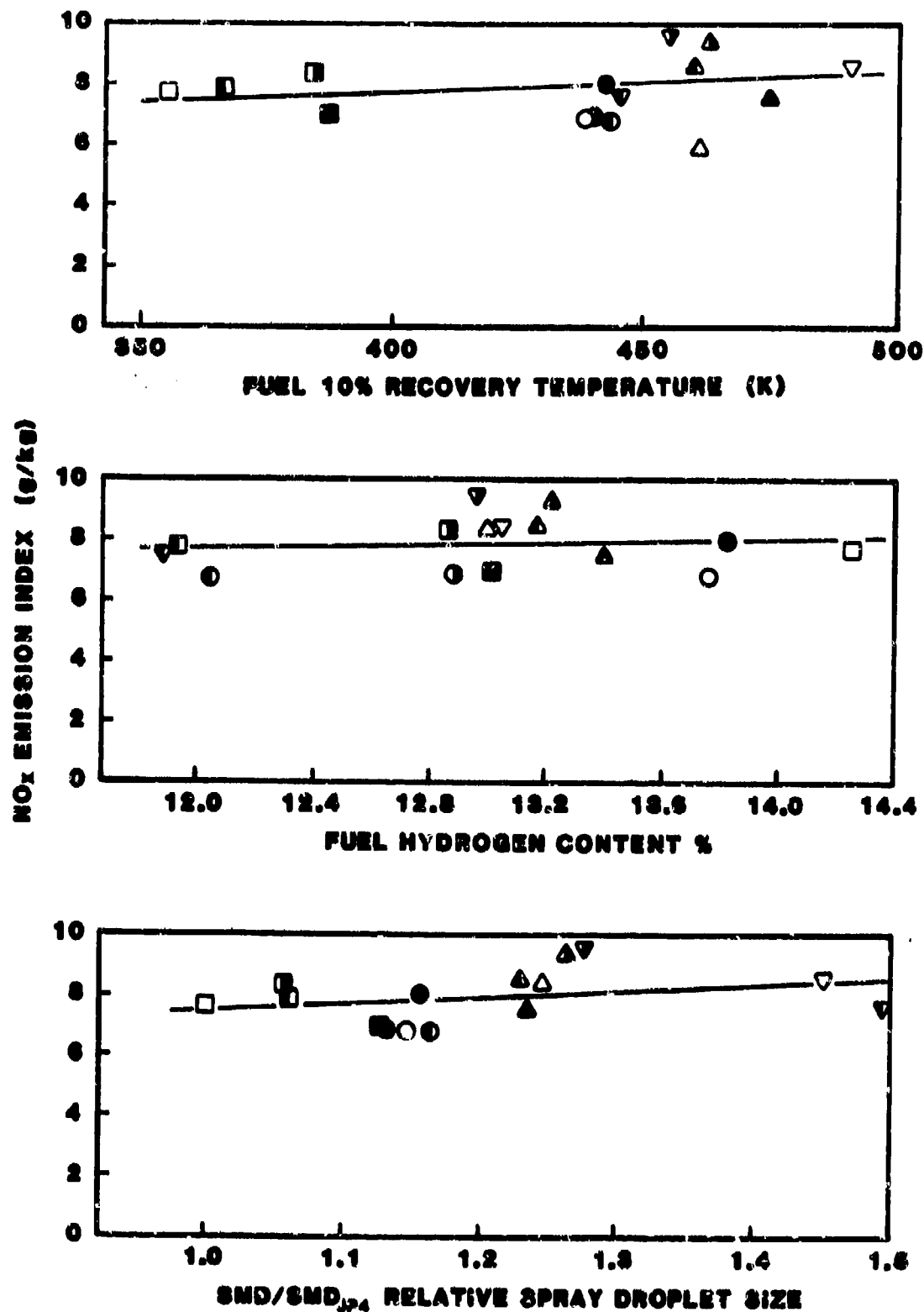


Figure 3.15 : Impact of Fuel Properties on NO_x Emissions at Simulated Take-Off Condition (Power Cycle, Simplex Nozzle)

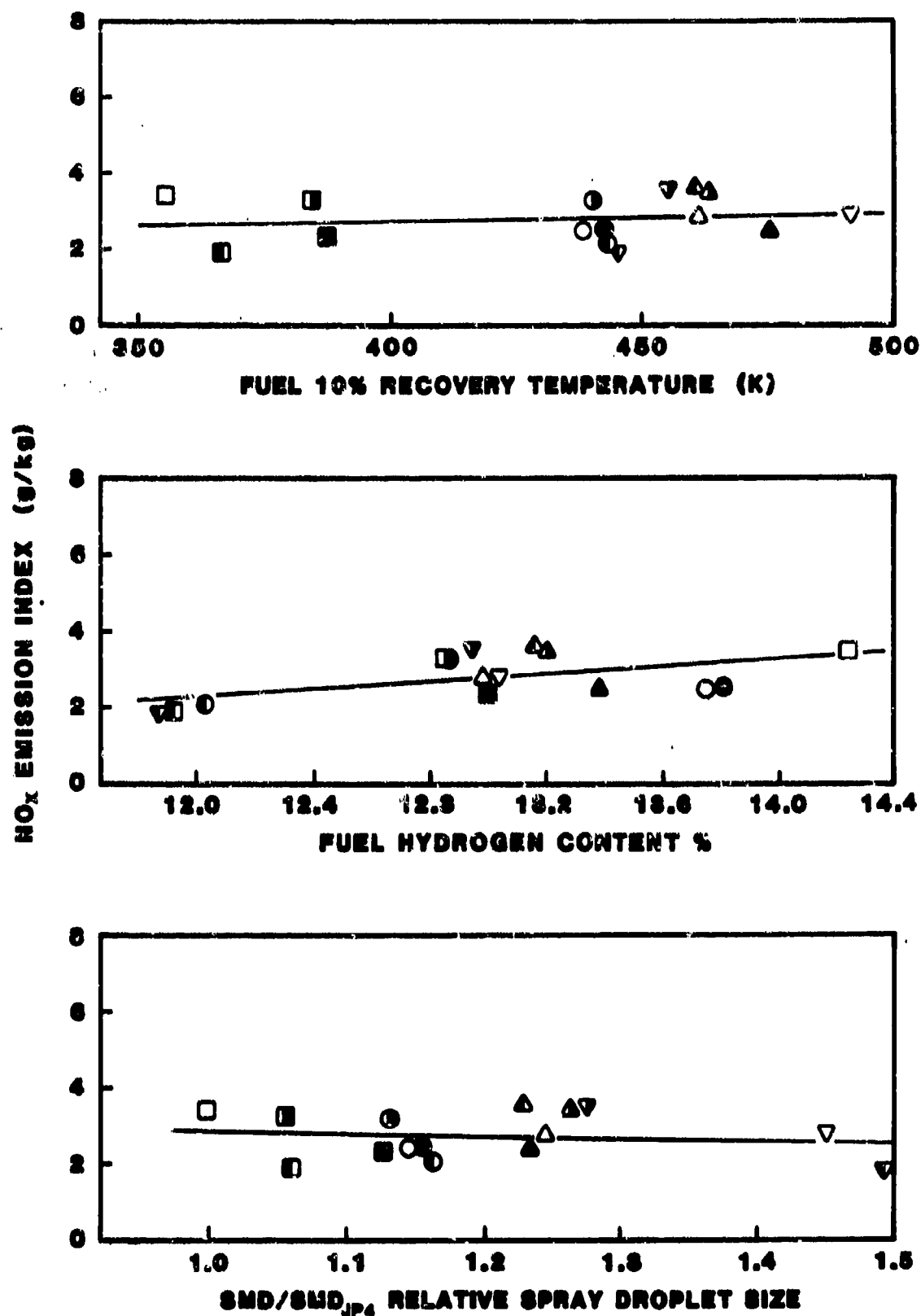


Figure 3.16: Impact of Fuel Properties on NO_x Emissions at Simulated Idle Condition (Power Cycle, Simplex Nozzle)

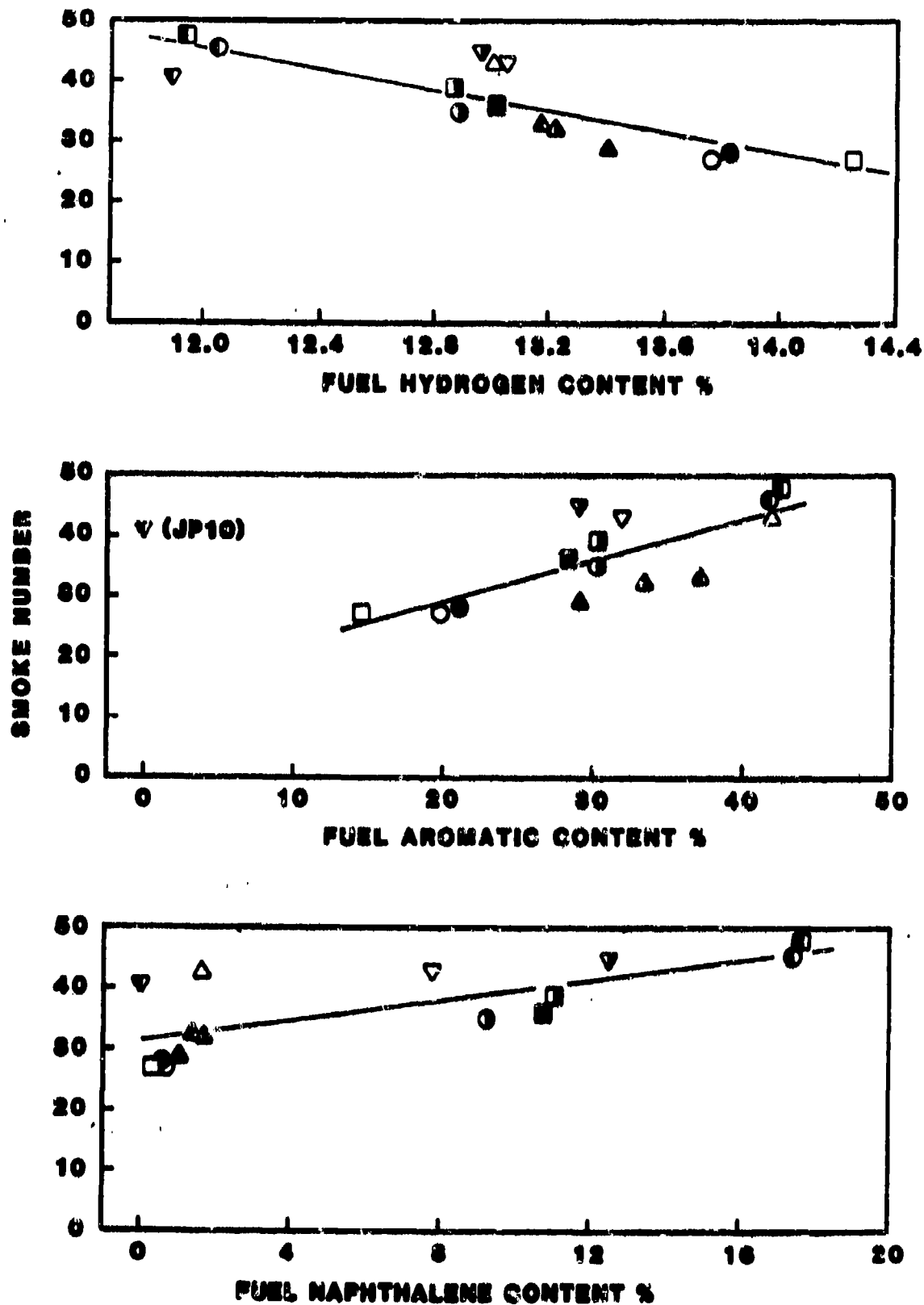


Figure 3.17: Impact of Fuel Properties on Smoke Emissions at Simulated Take-Off Condition (Thrust Cycle, Simplex Nozzle)

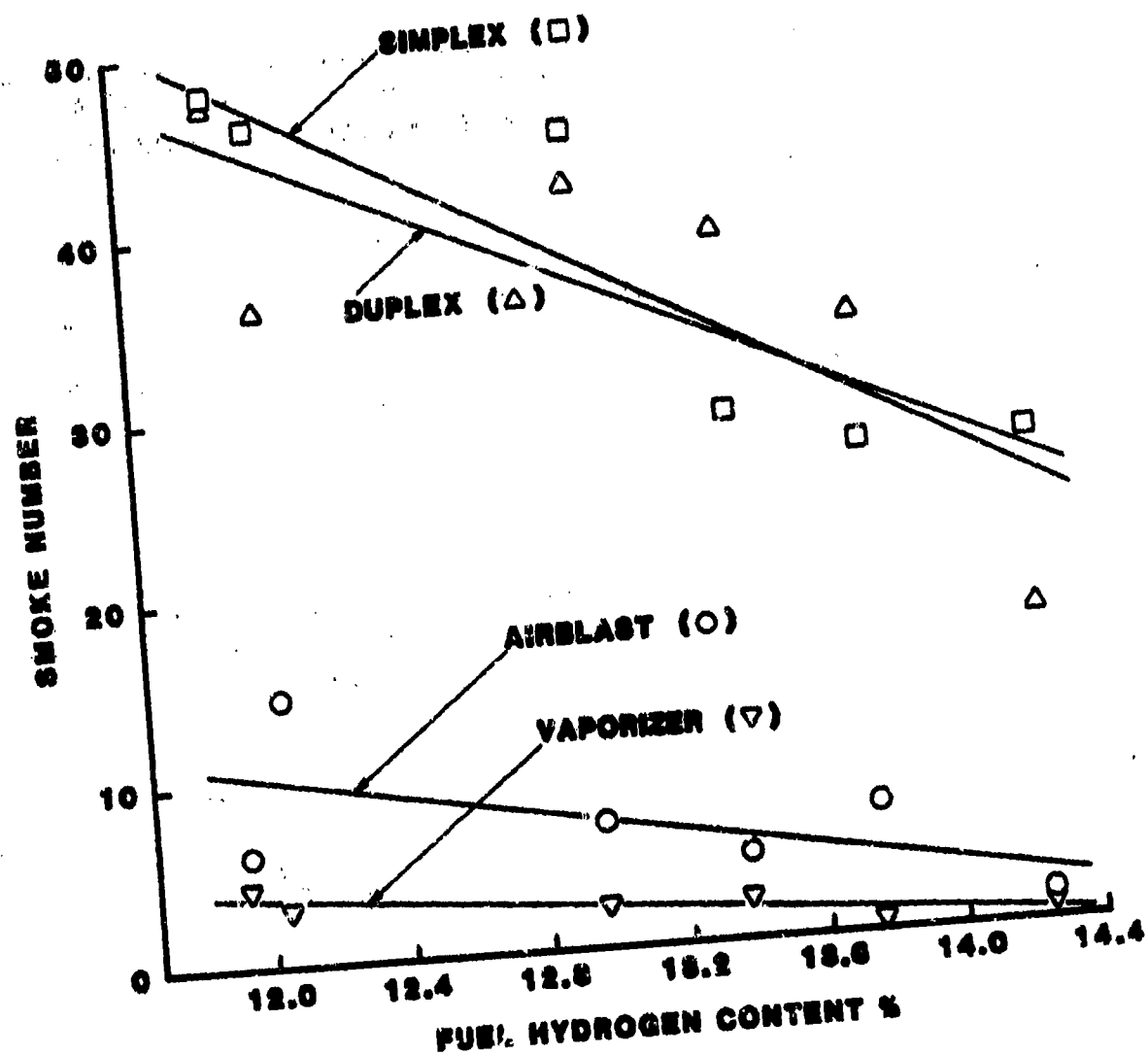


Figure 3.18: Influence of Fuel Hydrogen Content and Injector Designs on Smoke Emissions

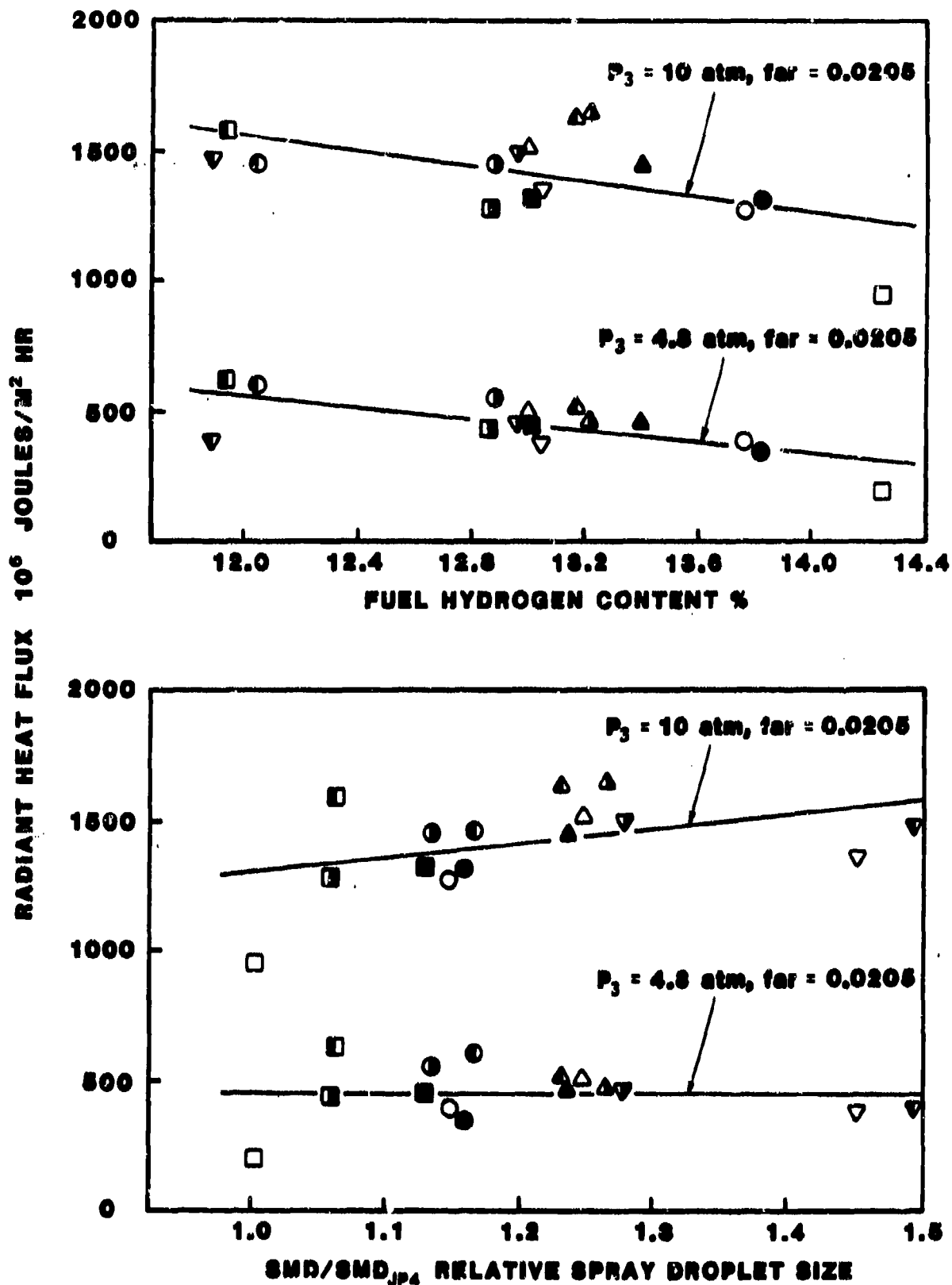


Figure 3.19: Impact of Fuel Properties on Radiant Heat Loads (Parametric Tests, Simplex Nozzle)

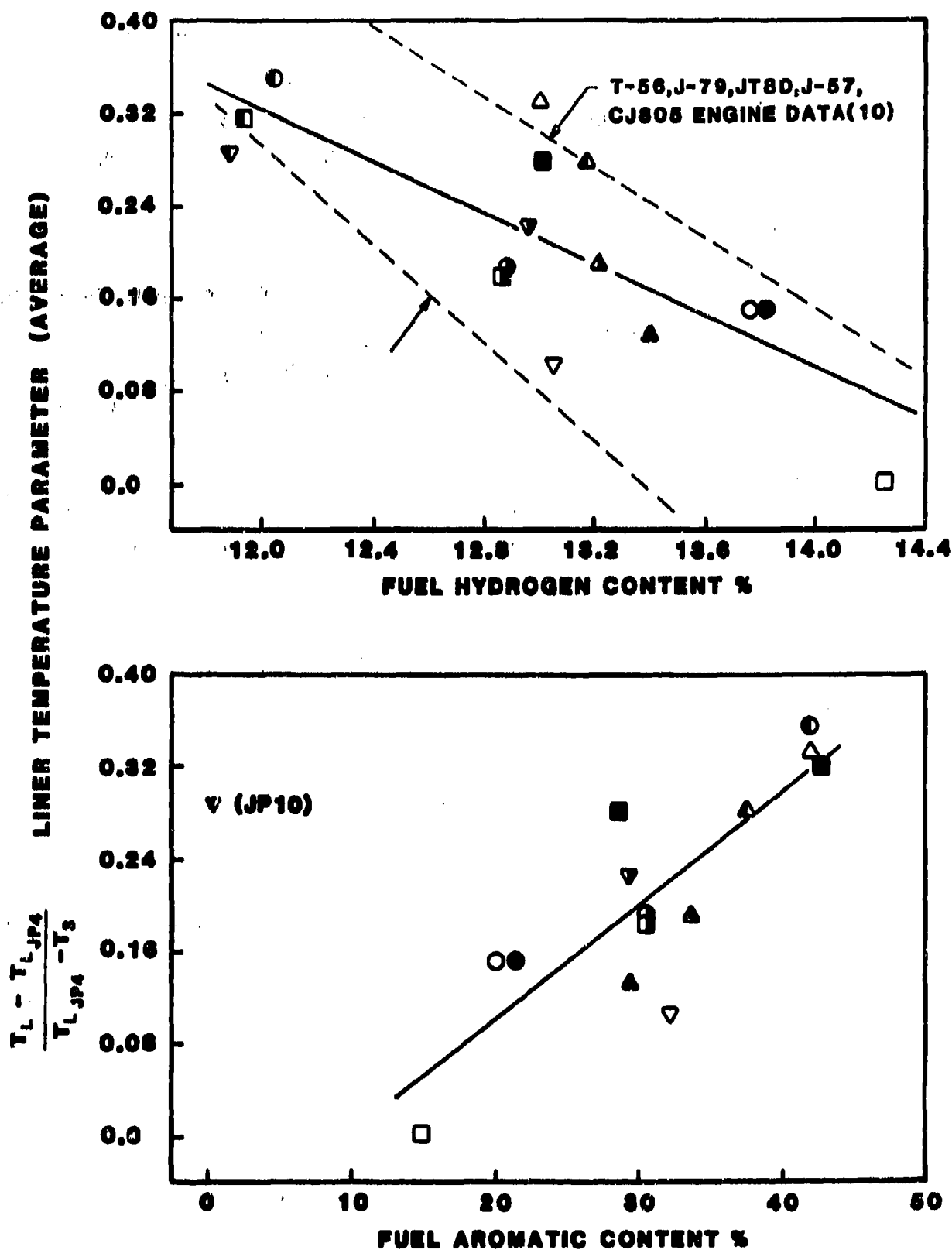


Figure 3.20: Impact of Fuel Properties on Average Liner Temperatures
(Thrust Level Tests, Simplex Nozzle)

SECTION IV

COMBUSTION SYSTEM HARDWARE

4.1 JT15D-5 System

4.1.1 The JT15D-5 engine was selected for turbofan combustion evaluation as described in Section III. This model has a take off thrust rating of 2,900 lbs. (12.9 kN) with a pressure ratio of 13.5:1. Fuel injection is with 12 duplex nozzles in the bill of materials configuration. Two spark igniters are used for lighting.

4.1.2 Standard Combustion System Description

The JT15D-5 combustor is of sheet metal construction using conventional splash louvres for film cooling. A sketch of the combustor is shown in Fig. 4.1. It features a machined joint between the outer liner and transition duct. This modification was incorporated to improve consistency of sealing and pattern factor.

Fuel is injected axially into a double vortex recirculation in the head of the combustor. This recirculation is driven by the cooling films and a swirler around the fuel nozzle. Reverse flowing louvres on the inner and outer wall act as trips to complete the recirculation. Combustion air in the primary zone is provided by cooling films, swirl air around the fuel nozzles and through jets which supplement the trip louvres. More air is added downstream for cooling and to complete combustion. Dilution jets mix the gases prior to entry into the curved transition ducts.

The transition duct turns the flow through 180° and accelerates the hot gases into the turbine inlet vane. The transition duct walls are also film cooled sheet metal. The larger duct incorporates a shield to reduce the radiative heat load on surrounding components.

Sliding seals are fitted around the fuel nozzles with the combustor being located by six pins on the head of the combustor. These allow radial growth whilst axial growth is accommodated by the sliding joints between the combustor liner and the transition ducts. Two igniters are provided, these are inserted through the outer casing to be flush-mounted in the dome of the liner.

Twelve axially spraying fuel nozzles are used. These are of the dual orifice, pressure atomizing type in order to provide good atomization over a wide range of fuel flows; details are shown in Fig. 4.2. Primary fuel for starting is injected through the central tip, the main secondary fuel is supplied through an annular passage around the primary nozzle. The flow number of the primary nozzles is 1.0. The secondary nozzles have a flow number of 5.7.

4.1.3 Combustor Operating Conditions

The combustor operating parameters at the simulated conditions are shown in Table 4.1.

4.2 PT6A-65 System

4.2.1 Engine Description

The turboprop combustor evaluations were based on the PT6A-65 engine, which has a power output of 1294 SHP. The engine is of the free turbine type incorporating a five stage compressor of approximately 10:1 pressure ratio, a single-stage compressor turbine and an independent two-stage power turbine driving the output shaft through an integral gearbox (Fig. 3.4). The combustion system consists of a single annular chamber in a reverse flow configuration. This is fitted with 14 simplex fuel nozzles and two spark igniters.

4.2.2 Standard Combustion System Description

A schematic of the PT6A-65 combustor is shown in Fig. 4.3. This combustor is also of splash louvre film cooled sheet metal construction, although some machined components are used in the head of the combustor. It differs from JT15D and earlier PT6 combustors in having an integral outer liner and outer transition duct. Outer and inner wrappers are joined by a machined, bolted flange in the head of the combustor, which eliminates the sealing problems of earlier designs. Machined sections are used around the fuel nozzle mountings, along with a machined seal between the inner liner and the smaller transition duct.

A single vortex recirculation is maintained in the combustor. The vortex is driven by the wall cooling flows and is tripped by jets and reverse flowing louvres on the inner wrapper. Combustion air in the primary zone is supplemented by cooling air from the fuel nozzle sheaths. Additional air is added downstream to complete combustion and for cooling purposes. Conventional dilution jets are used to set-up the exit temperature profile. The transition ducts are also of film cooled sheet metal construction. The combustor and transition duct used in the tests have hot side yttria-stabilized zirconia coating to maximize life.

The combustor is located by the fuel nozzle assemblies which are rigidly mounted off the casing. Bosses are provided on the combustor to spread axial loads on the sheaths. Holes in these bosses meter the cooling airflow over the nozzle sheaths. Two flush mounted igniters with sliding washers for sealing are located on the outer wrapper.

Fourteen single orifice pressure atomizers inject fuel tangentially into the combustor (Fig. 4.4). These protrude into the flame region, therefore a protective shroud is necessary. This is cooled by both internal and external airflows. The flow number of the nozzles is 1.9. A dual manifold system is used to

improve lighting performance (Fig. 4.5). The seven primary nozzles are grouped in two banks of four and three around each igniter, these are the first to receive fuel on starting. The seven secondary nozzles receive fuel once the primary system has been pressurized to approximately 20 psi. This pressure differential between the two manifolds is maintained throughout the operating range.

4.2.3 Combustor Operating Conditions

For the atmospheric pressure tests the conditions simulated were based on the PT6A-65R engine whilst the PT6A-65B version was simulated in the gas generator tests. These two engine types have identical combustion hardware and only differ in rated power outputs. The lower power version was simulated in the gas generator tests in order to maximize probe life at the high bleed condition. These conditions are listed in Table 4.2 for the engine conditions simulated.

4.3 Experimental Combustion Hardware

4.3.1 JT15D-5 Atmospheric Tests

In order to assess the effects of combustor stoichiometry, two combustors were used. The first was the standard JT15D-5 combustor as described above and shown in Fig. 4.1. This has a primary zone equivalence ratio of approximately 1.02, based on cold airflow analysis. The calculated airflow splits are given in Fig. 4.6.

The second combustor was a standard JT15D-5 modified to have a rich primary zone with a nominal equivalence ratio of 1.14. The airflow splits are shown in Fig. 4.7. It can be seen that the richening of the combustor was achieved by diverting air from the combustor into the large transition duct cooling films.

Fuel nozzle effects were investigated by using both airblast and pressure jet atomizers. The airblast nozzle was developed by Ex-Cell-O for PWC research purposes. A cross-section is shown in Fig. 4.8. Fuel enters a swirl chamber (through tangential holes) and is impacted by the swirling air flow at the exit of this chamber. The flow number of these nozzles is approximately 25. For the pressure jet nozzles it was necessary to test with lower flow number nozzles than standard. This was done in order to maintain reasonable atomization at the low fuel flows necessitated by the scaling procedure for atmospheric pressure testing. For this reason a single orifice nozzle with a flow number 1.2 was used. The spray cone angle of 90° was selected to be close to that of the standard nozzle. Part numbers of the hardware used are listed in Table 4.3.

4.3.2 PT6A-65 Atmospheric Tests

Here again two combustors were tested. The baseline was a standard engine combustor described in Section 4.2.2 and shown in Fig. 4.3. This has a primary zone equivalence ratio of approximately 1.0. Calculated airflow splits are given in Fig. 4.9. Contrary to the JT15D testing, the second combustor was designed to run leaner than the baseline. This combustor was modified by blanking cooling holes on the inner liner and opening extra holes in the primary zone. The resulting splits are shown in Fig. 4.10 and give a primary zone equivalence ratio of approximately 0.9.

Each combustor was tested with two sets of fuel nozzles. Both sets were pressure atomizing, one had a flow number of 0.6 per nozzle, the other had a flow number of 1.1 per nozzle. Like the JT15D tests, the flow numbers were lower than the standard engine hardware to compensate for the low fuel flow resulting from the scaling procedure. The use of two sizes of orifice allowed the effects of atomization quality to be observed.

Combustion hardware identification is given in Table 4.4.

4.3.3 PT6A-65 Cold Start Tests

A standard combustor and fuel nozzles were used for this testing; these have already been described in Section 4.2.2. The part identification is given in Table 4.4.

4.3.4 PT6A-65 Gas Generator Tests

Again the standard combustor as described in Section 4.2.2. was used, part identification is given in Table 4.4. Since gas generator testing is done at full engine pressures no scaling is necessary and therefore standard engine fuel nozzles (1.9 FN) were used. A second set of nozzles of 2.2 FN was also tested.

In order to minimize downtime the standard combustor was used throughout the gas generator tests. In this case the combustor stoichiometry was adjusted by running the engine both with and without cabin air bleed. The bleed case results in a richer overall fuel air ratio in the combustor. The fuel-air-ratios are also specified in Table 4.2.

Table 4.1: JT15D-5 Combustor Operating Conditions in Engine at Thrust Levels Simulated in Test Program

Standard Day Sea Level

Thrust Level (% max.)	W3 kg/s	P3/P1	T3 K	T4 K	Combustor far
Idle	3.12	2.59	409	758	.0090
30	5.92	5.33	508	900	.0105
70	9.40	9.52	606	1133	.0147
100	11.35	12.16	652	1263	.0174

Table 4.2: PT6A-65 Combustor Operating Conditions in Engine at Power Levels Simulated in Test Program

Atmospheric Pressure Tests: (PT6A-65R)

Power Level (% max. SHP)	W ₃ kg/s	P ₃ /P ₁	T ₃ K	T ₄ K	Combustor far
Ground Idle	1.40	2.59	417	812	.0104
40	3.12	6.83	557	1124	.0158
55	3.50	7.85	575	1182	.0172
70	3.77	8.63	588	1227	.0182

Gas Generator Tests: (PT6A-65B)

% Bleed	Power Level (% max. SHP)	W ₃ kg/s	P ₃ /P ₁	T ₃ K	T ₄ K	Combustor far
0	Ground Idle	1.23	2.34	407	853	.0118
0	5	1.59	3.24	451	912	.0127
0	45	3.05	6.76	560	1153	.0166
0	80	3.89	8.63	592	1242	.0186
0	100	4.05	9.50	605	1289	.0197
5	Ground Idle	1.17	2.30	405	903	.0132
5	5	1.54	3.13	450	972	.0140
5	45	2.90	6.60	558	1213	.0186
5	80	3.57	8.45	589	1305	.0207
5	100	3.86	9.31	603	1355	.0218

Table 4.3: Experimental Combustion Hardware Identification (JT15D-5)

JT15D-5 Atmospheric Tests

	<u>Part Number</u>
Standard Combustor	3021353
Rich Combustor	XSK 11901-1
Airblast Fuel Nozzles	Ex-Cello Research Nozzles 504P620 (Concept 2)
Pressure Jet Fuel Nozzles	3031278

Table 4.4: Experimental Combustion Hardware Identification (PT6A-65)

PT6A-65 Atmospheric Tests

Standard Combustor	Outer: 02X-3102528-01 Inner: 01X-3100686-01
--------------------	--

Lean Primary Zone Combustor	Outer: 02X-3102528-01 Inner: XSK 12228
-----------------------------	---

PT6A-65 Cold Start Tests

Standard Combustor	Outer: 23X-3102528-01 Inner: 3102514-01
--------------------	--

PT6A-65 Gas Generator Tests

Standard Combustor	Outer: 02X-3102528-01 Inner: 01X-3100686-01
--------------------	--

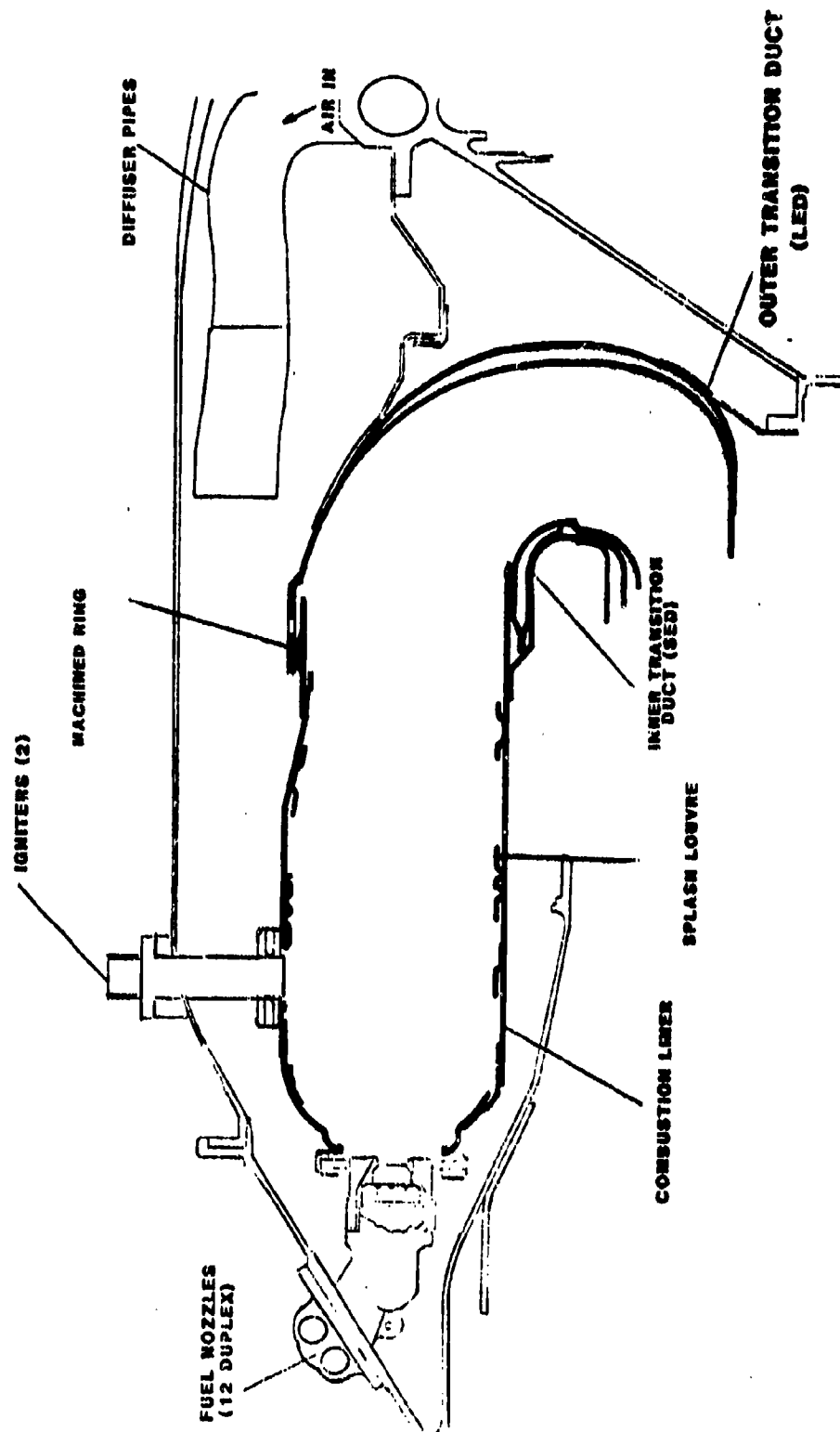


Fig. 4.1: JT15D-5 Combustion System

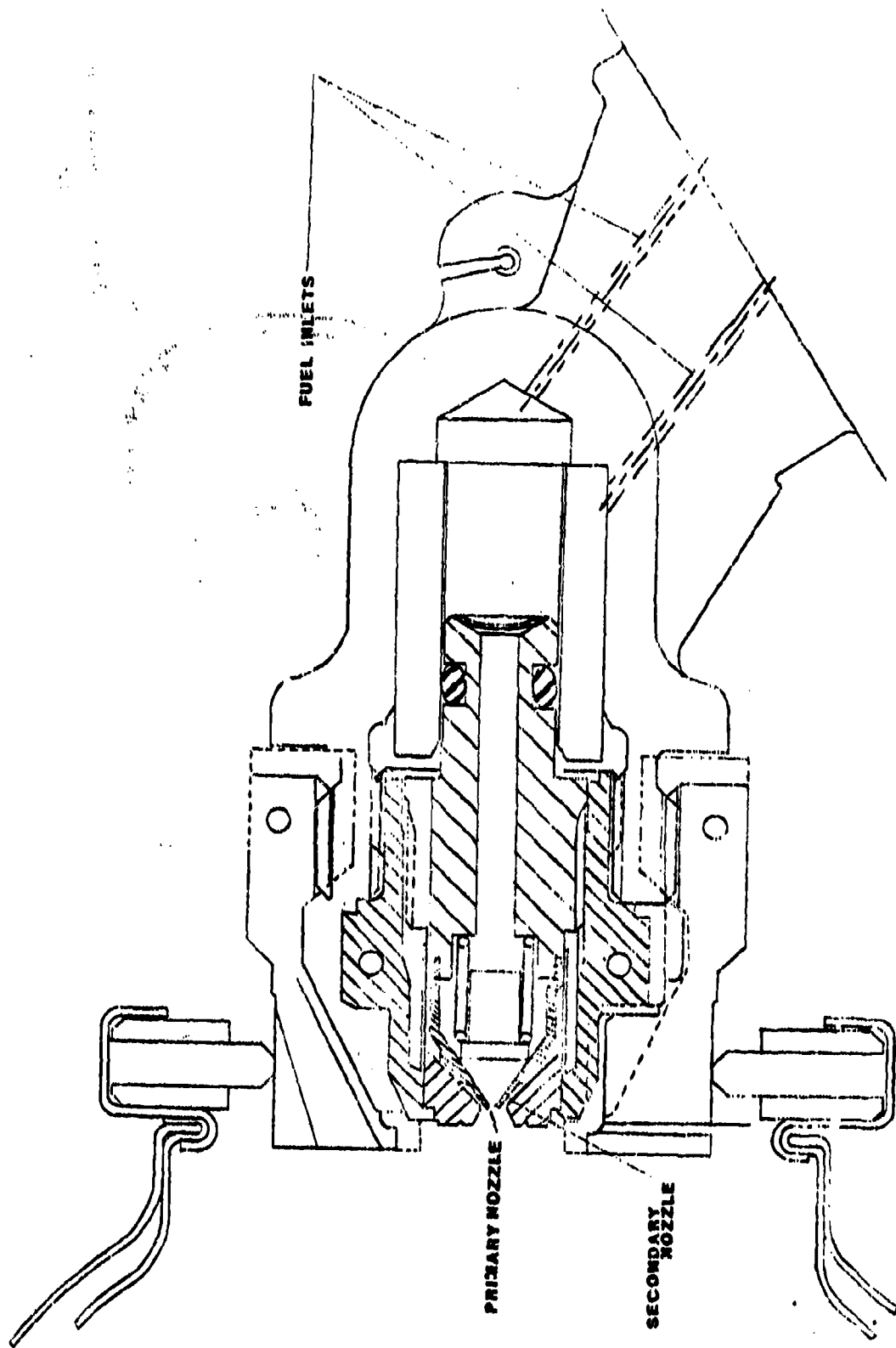


Fig. 4.2: Cross Section of JT15D-5 Fuel Nozzle

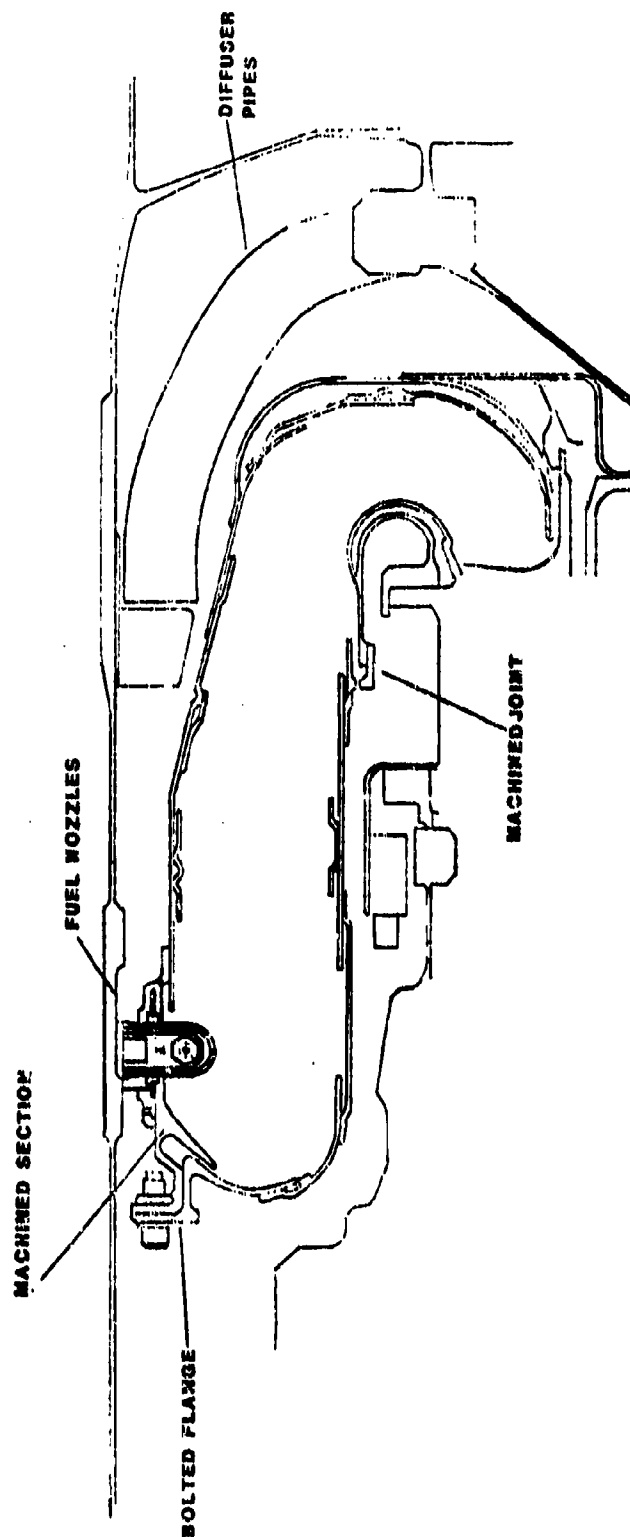


Fig. 4.3: PT6A-65 Combustion System

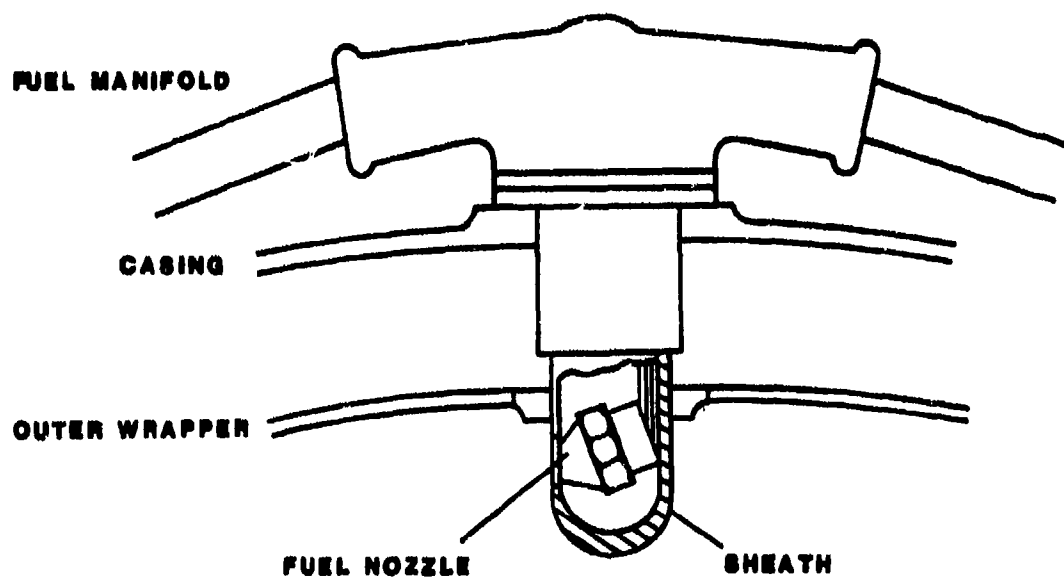


Fig. 4.4: PT6A-65 Fuel Nozzle and Sheath Assembly

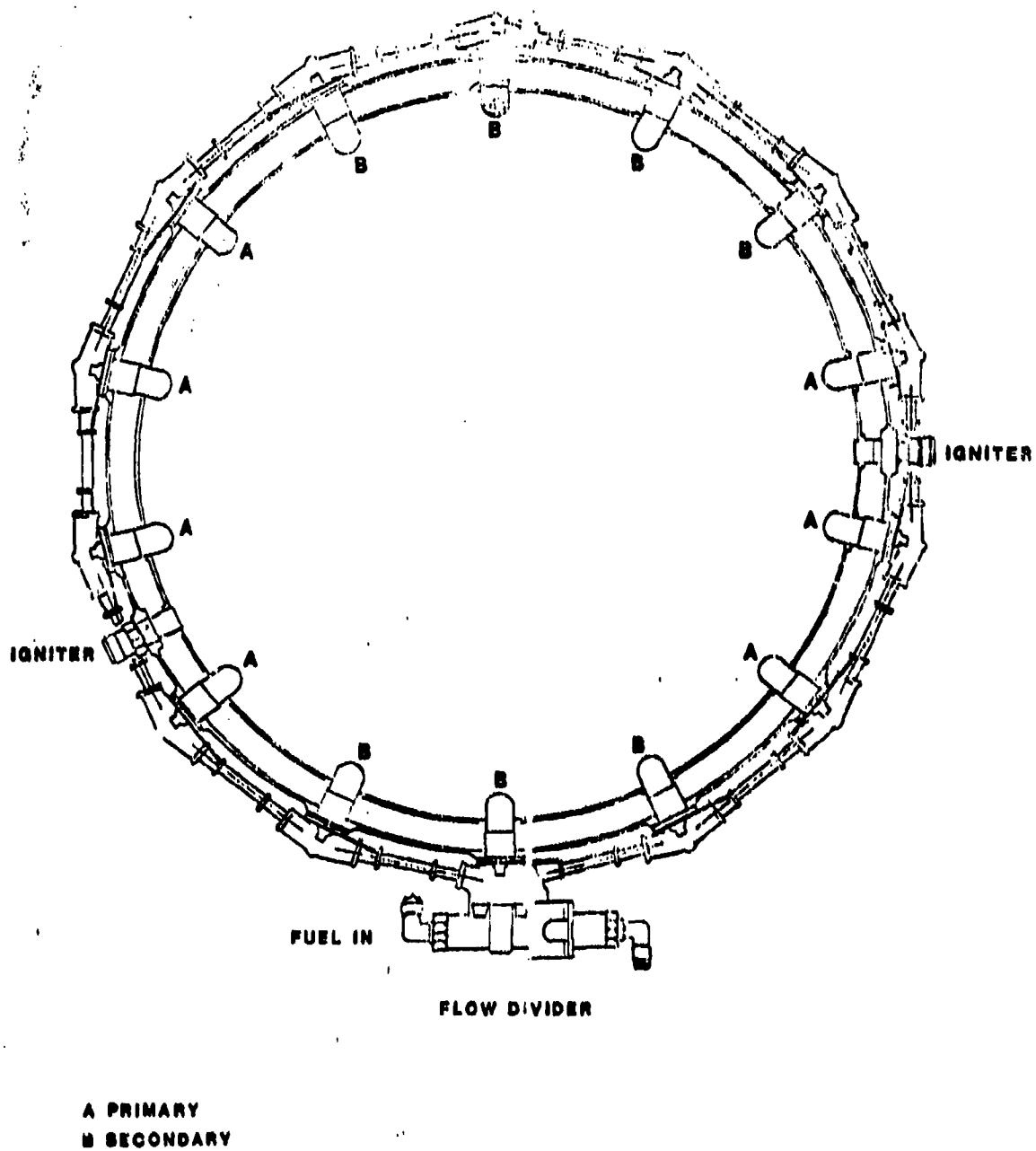


Fig. 4.5: PT6A-65 Fuel Manifold Arrangement

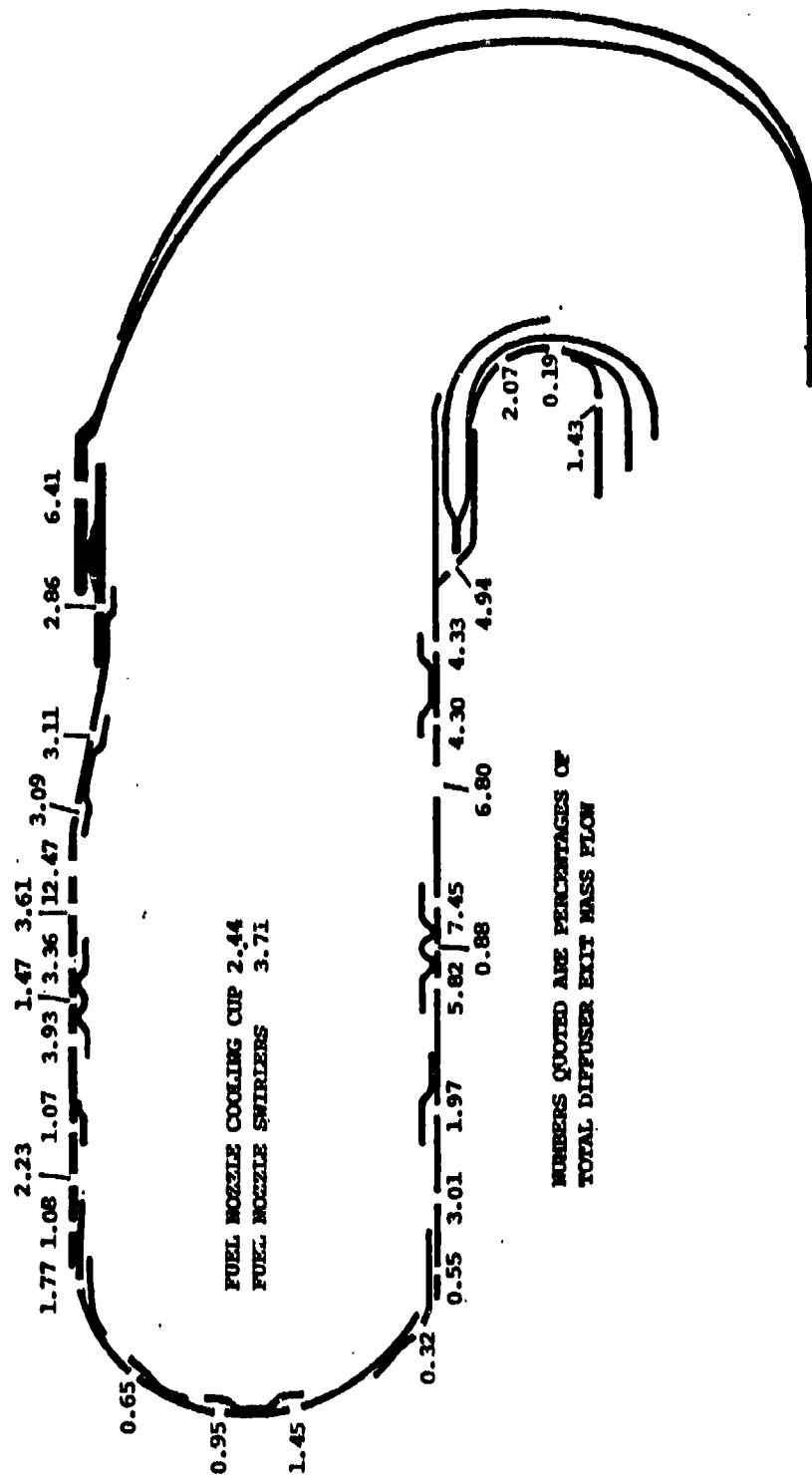


Fig. 4.6: JT15D-5 Air Flow Splits for Standard Combustor

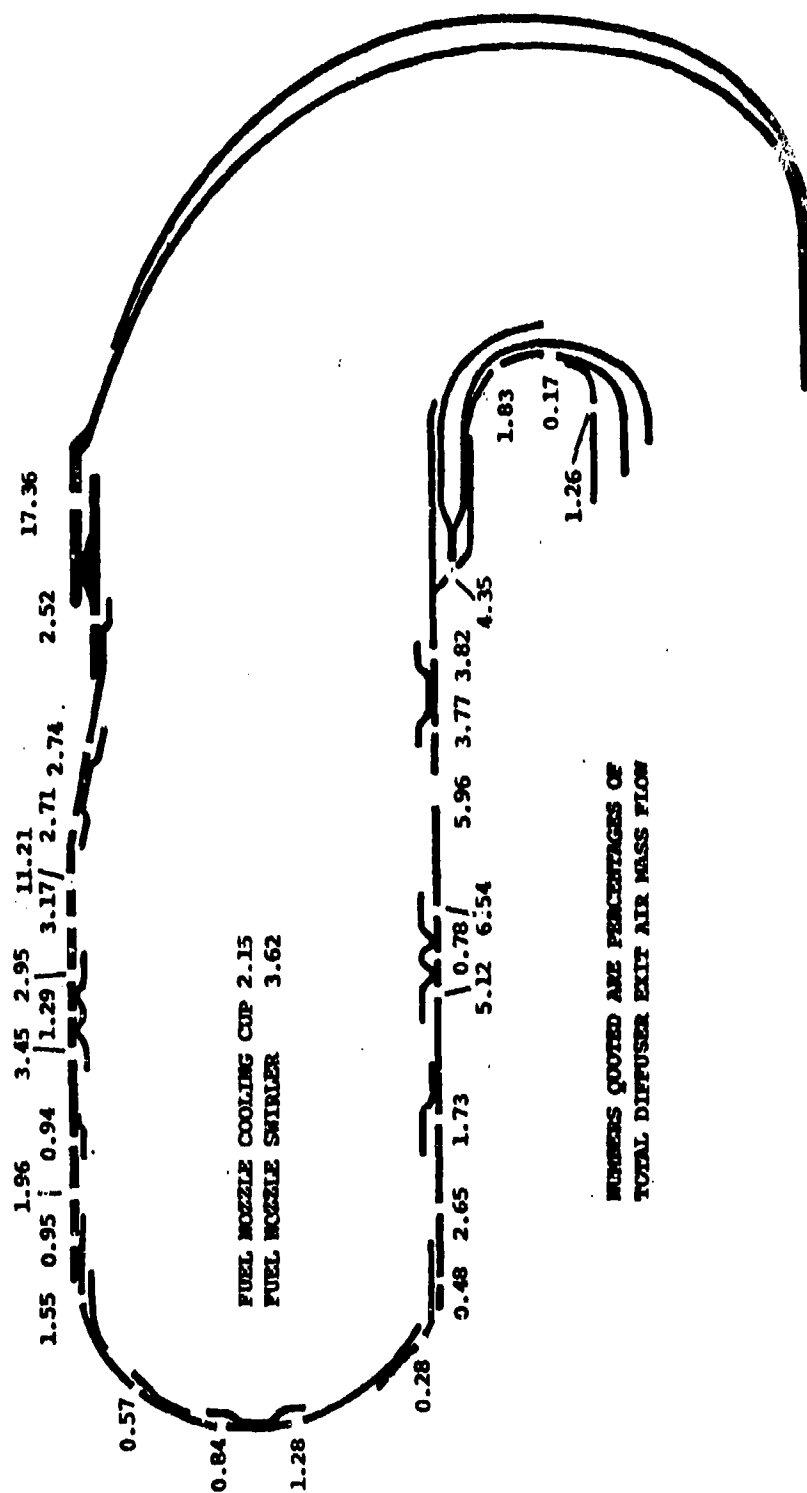


Fig. 4.7: JT15D-5 Air Flow Splits for Rich Combustor

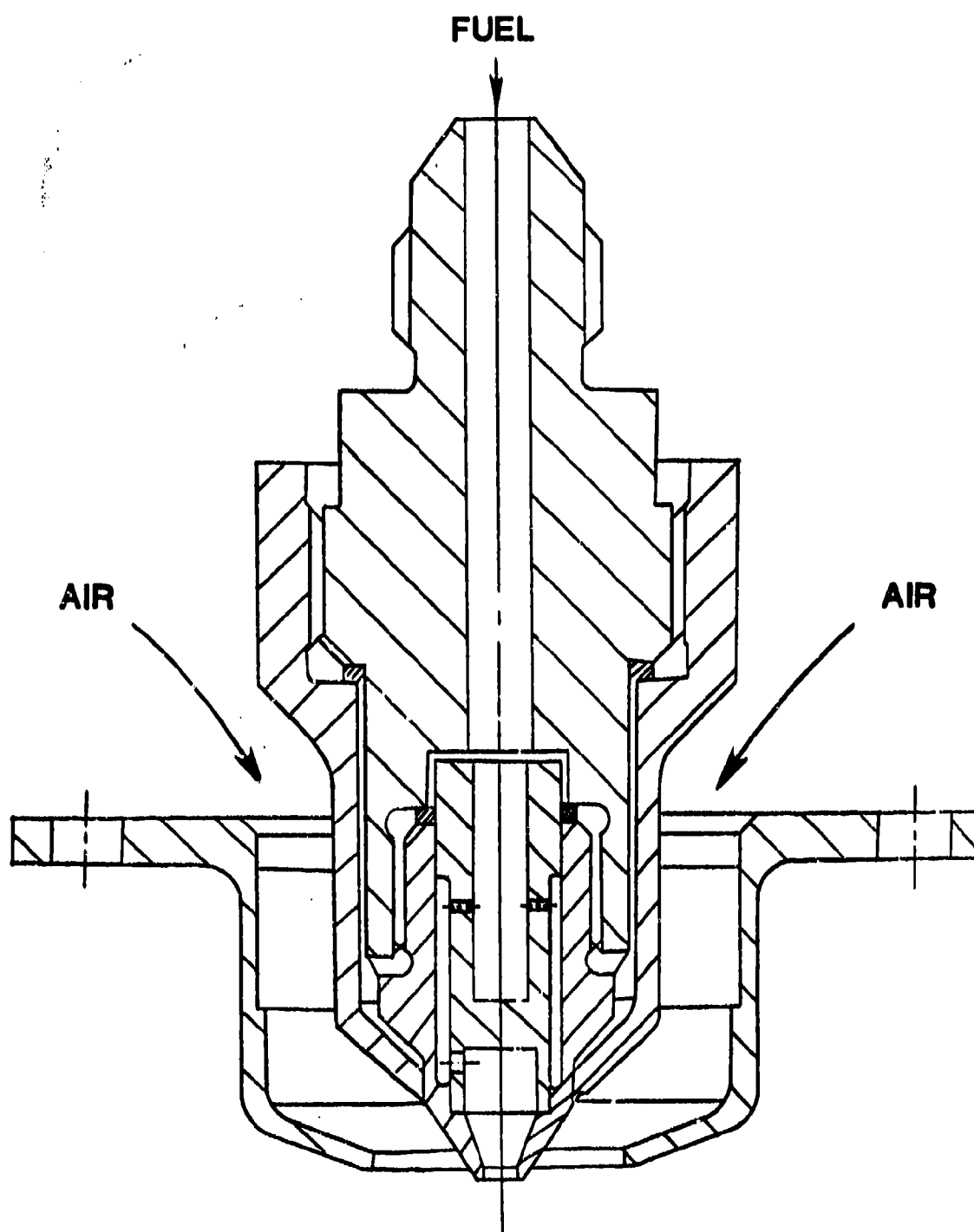


Fig. 4.8: Airblast Nozzle Cross Section

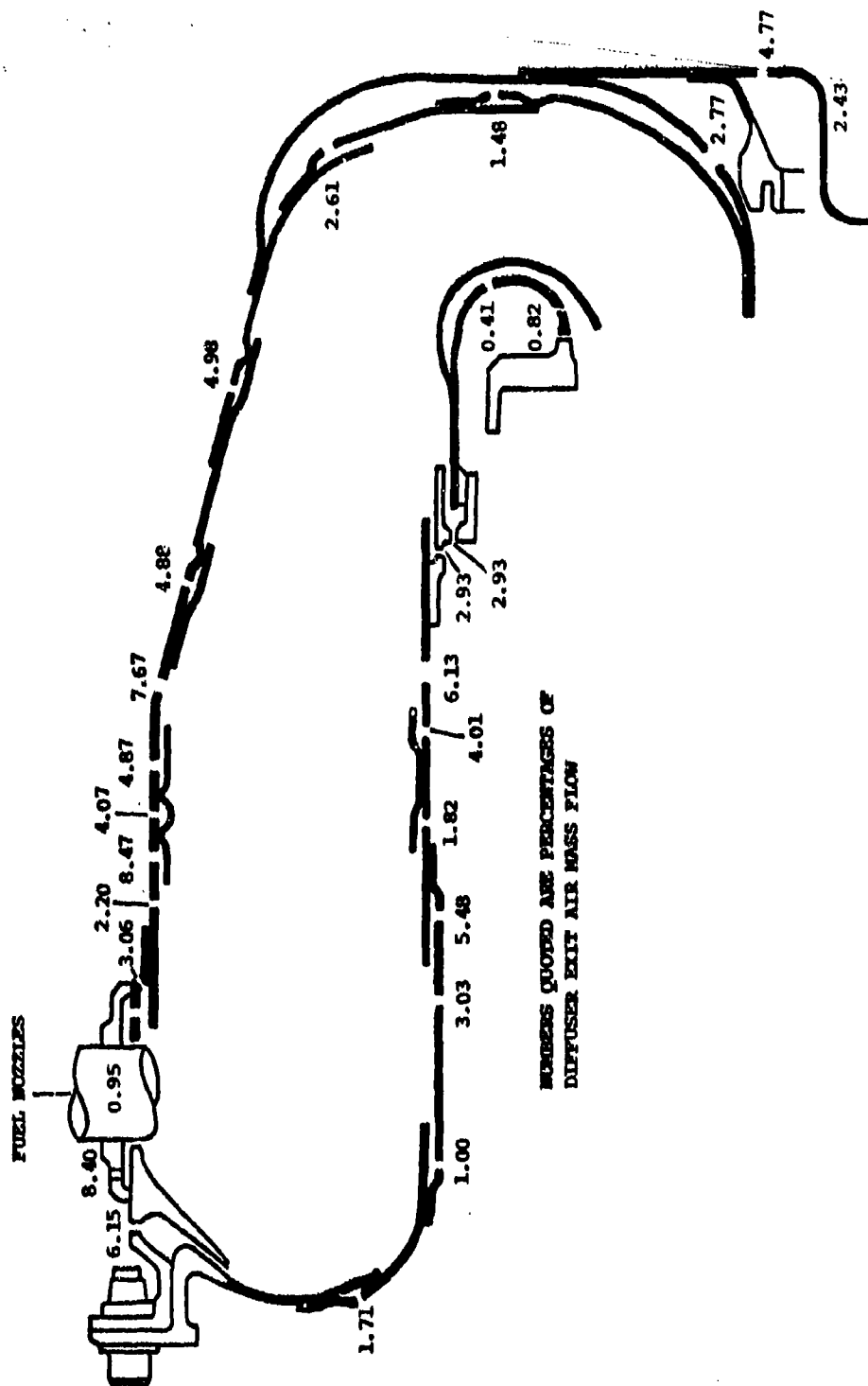


Fig. 4.9: PT6A-65 Standard Combustor Air Flow Splits

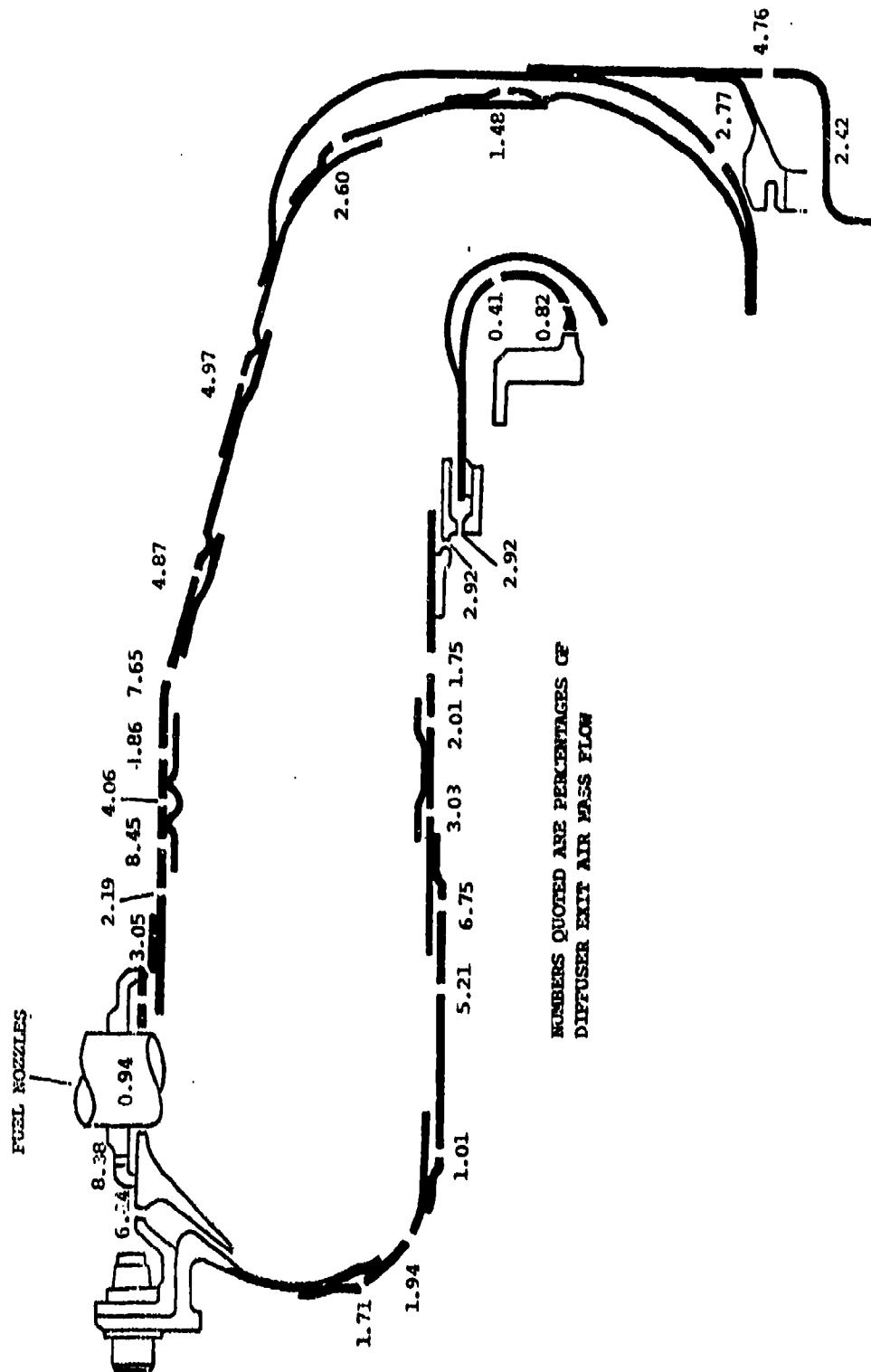


Fig. 4.10: PT6A-65 Lean Primary Zone Combustor Air Flow Splits

SECTION V

APPARATUS AND PROCEDURES

5.1 JT15D-5 Atmospheric Rig Tests

Atmospheric pressure tests were run on a full annular JT15D-5 combustor. The object of these tests was to observe the effect of four test fuels (Table 2.3) on the following parameters:

- Combustor metal temperatures
- Gaseous emissions
- Smoke emissions
- Lean flame stability limit (at idle)
- Exit temperature pattern factor

The tests were run over a range of conditions simulating engine running points from idle through to 100% power. These were carried out on two combustors and two types of fuel nozzles as specified in Section 4.3.1.

5.1.1 JT15D-5 Atmospheric Rig Description

The testing was carried out in Combustion Rig No. 3, located in the Experimental Test facility at Plant 7 in Mississauga. This test cell is equipped with fuel and air supplies, exhausts, controls and instruments for a variety of test configurations. For atmospheric pressure testing, air is supplied by a blower through an electric heater and a metering section to the test section. The layout of the rig is shown in Fig. 5.1. The air and fuel supplies are able to match combustor fuel-air ratio, inlet Mach numbers (M) and temperatures from idle up to the maximum power condition of the JT15D-5 engine.

The test section, Fig. 5.2, duplicates the engine geometry around the combustor from air inlet to the transition duct exit. A schematic is shown in Fig. 5.3. Inlet vanes are used to simulate the residual swirl from the diffuser pipes used on the engine. On leaving the transition duct, the hot combustion gases pass into an annular duct housing the traversing thermocouple array and thence into the cylindrical exhaust ducting. There are no significant flow restrictions downstream of the combustor so the test section remains only slightly above atmospheric pressure.

5.1.2 JT15D-5 Atmospheric Rig Instrumentation

Air mass flow was measured by an ASME standard orifice upstream of the test section, with standard upstream and downstream pressure tapings.

Fuel flow rates were measured using calibrated turbine flowmeters; readings were corrected for density at the measured fuel temperature.

Static pressure taps were used to measure air inlet pressure and combustor exit pressure in the transition duct. Inlet temperatures were measured using Type K thermocouples. Pattern factors were determined from a rotatable array of eight shielded Type K thermocouples positioned in the annular duct immediately downstream of the transition duct. These were located on radial centres of equal area.

Liner metal temperatures were initially determined using Thermin-dex OG6 thermal paint on the combustor exterior surfaces. The thermal paint tests were carried out on both combustors running at the 100% thrust simulation with the pressure jet fuel nozzles using Jet A1 fuel. The results of these tests allowed positioning of an array of 20 Type K thermocouples which were used for subsequent liner metal measurements. The locations of these thermocouples on the liner are shown in Fig. 5.4.

Combustor emissions were measured with a fixed array of probes giving 13 sampling points positioned at radial centres of area. These probes were positioned 2.6 cm. downstream of the transition duct exit plane. The probe sample lines were manifolded to a heated line leading to the emissions analyzer. The analyzer used was a Beckman Emissions Analyzer incorporating the following instruments:

- NO, NO_x - Chemiluminescent analyzer.
- THC - Flame ionization detector.
- CO, CO₂ - Infrared analyzer.

The instruments were checked with calibration gases before and after each test. The readings were verified by comparison of the measured fuel-air ratios with those calculated from the emissions analysis.

The same probes were used to sample the exhaust smoke. These samples were collected using a filter type smoke meter conforming to EPA specifications.

The reflectivities of the stained filter papers were measured using a Photovolt meter and converted to smoke numbers.

5.1.3 Experimental Procedure for JT15D-5 Atmospheric Tests

The baseline and rich primary zone combustors were each tested with both airblast and pressure jet nozzles. Four fuels were tested with each configuration, giving a total of 16 tests. Initial calibration runs were carried out using Jet A1.

A four-point test procedure was followed for each test. The set-up conditions for these points are given in Table 5.1. These conditions were used in order to simulate engine combustor inlet temperatures, Mach number and fuel-air ratios over a range of engine thrusts from idle to 100%. Fuel-air ratios were adjusted to allow for the variation in Lower Heating Value (LHV) of the different fuels.

A full set of readings, including smoke and emissions, was taken at each of the test points. Full temperature traverses were only taken at points 3 and 4. Lean flame stability limits were determined at idle inlet conditions by setting up to point 1 and reducing the fuel flow until flameout occurred at which point the fuel flow rate was noted. A repeat of each blowout test was carried out.

5.2 PT6A-65 Atmospheric Rig Tests

Atmospheric pressure tests were also carried out on a PT6A-65 combustor. The objectives were to study the effects of various test fuels (see Table 2.2) on the following parameters:

- combustor metal temperatures
- gaseous emissions
- smoke emissions
- lean flame stability limit (at idle)
- combustor exit temperature pattern factor

Engine conditions ranging from idle to 70% power were simulated. The combustors and fuel nozzles were as specified in Section 4.3.2. Twelve different fuels were used.

5.2.1 PT6A-65 Atmospheric Rig Description

The tests were run in Combustion Rig No. 2, located in Plant 1 at Longueuil. The test cell has similar facilities and capabilities to that used for the JT15D atmospheric tests. The layout of the atmospheric rig is essentially the same as shown in Fig. 5.1.

The test section is similar in concept to the JT15D atmospheric rig except that PT6A-65 engine geometry is simulated. The schematic is shown in Fig. 5.5. Note that the traversing thermocouple array is now mounted in a bifurcated exhaust.

5.2.2 PT6A-65 Atmospheric Rig Instrumentation

Instrumentation was similar to that described in Section 5.1.2 for the JT15D atmospheric tests. One exception was that the rotatable thermocouple array for pattern factor determination contained ten Type K thermocouples.

Thermal paint runs were carried out using the plant supply Jet A1 fuel with the smaller 0.6 FN nozzles on both baseline and lean primary zone combustors. Therminex OG6 paint was used for this purpose. An array of 20 Type K thermocouples was placed on the outer liner on the basis of these results. The locations of these probes are shown in Fig. 5.6. Liner thermocouples were confined to the outer liner since this part was common to both

combustion configurations. Thus, the build and strip times were greatly reduced.

Emissions and smoke sampling equipment and procedures were as for the JT15D atmospheric tests except that the probes were mounted downstream of the bifurcated exhaust duct.

5.2.3 Experimental Procedures for PT6A-65 Atmospheric Tests

Both the baseline and lean primary zone combustors were tested with the two sizes of pressure jet fuel nozzles. The twelve fuels were tested with each configuration giving a 48 point matrix.

Again four conditions were run on each test, as shown in Table 5.2. These simulated engine combustor inlet temperatures, Mach numbers and fuel-air ratios over a range of engine power levels from ground idle to 70% power. Fuel-air ratios were adjusted to allow for the LHV variations in the fuels. Initial runs were done at the 100% power simulation, however, problems were experienced with burning of the traversing thermocouples. Therefore further tests were limited to the 70% power simulation. Pattern factor determinations were made at this condition. Full sets of readings including smoke and emissions were taken at all test points. The lean flame stability limiting fuel air ratios were measured at the idle condition by reduction of the fuel flow until flameout occurred. Repeat blowout checks were performed.

5.3 PT6A-65 Cold Start Tests

A series of low temperature starting tests were conducted using a PT6A-65 engine to determine the cold day starting characteristics of the test fuels. The fuels used are listed in Table 2.2. The range of test conditions covered inlet temperatures ranging from warm ambients to -50°F (228K).

5.3.1 Cold Start Rig Description

The test program was carried out in the Pratt and Whitney altitude test cell annexed to the M10 building at the National Research Council of Canada plant in Ottawa.

This facility consists of an enclosed chamber, see Fig. 5.7, in which the engine is positioned. A three stage refrigerator and drier cools the air taken in from ambient. Air from a high pressure shop air supply is throttled down to approximately 1 psi above atmospheric and blown over the refrigeration coils into the test chamber. The cold air then passes through and around the engine into the exhaust system allowing the engine to soak down to the desired temperature. The refrigeration system has sufficient capacity to satisfy the idle air consumption rates of a PT6A-65 down to -50°F (228K).

For this program a PT6A-65 engine was installed with its gearbox connected to a dynamometer fixed in the chamber. The engine was built to PT6A-65 standard specification, including the fuel nozzles, combustion and ignition systems. The only variations were that heat exchangers were incorporated in the fuel and lubricating oil systems to shorten the soak down times.

For the purposes of this program a special fuel supply system was rigged up. This consisted of a portable pump which drew fuel direct from the supply drums. A return line and a feed line to the engine were provided.

Starter voltages were controlled by using a variable dropping resistor across a ground start motor-generator unit.

5.3.2 PT6A-65 Cold Start Test Instrumentation

The facility has the equipment to monitor and control the test chamber temperature and humidity levels.

The following engine parameters were measured and recorded during the starting transients using strip chart recorders:

- Engine speed (N_g) of the shaft.
- Combustor inlet pressure (P_3) from static tapings in the combustor casing.
- Fuel flow (W_f) measured by turbine flowmeter in the engine feed line.
- Fuel pressure in primary (P_{f1}) and secondary (P_{f2}) manifolds.
- Engine inlet temperatures (T_1) from Type K probe in inlet duct.
- Compressor turbine outlet temperatures (T_5) using an eight probe array between compressor turbine and second stage vane ring. These were harnessed together and the average temperature recorded.
- Fuel temperature measured between engine fuel pump and fuel control unit.

5.3.3 PT6A-65 Cold Start Test Procedures

Tests were conducted using ten fuels as detailed in Table 2.2. The tests were all performed at an approximate cranking speed of 16% NG(6000 rpm).

For each cold start, the engine was cold soaked until the fuel, lubricating oil and internal air (T_5) temperatures were within 5°F of the desired start temperature. Dry motoring cycles were performed to speed this process by circulating the engine oil and increasing the proportion of the system air flow passing through

the engine. Once the required temperature was reached, the recorders were started and the engine cranked to the desired speed. The ignition system was switched on, followed by the fuel. In the case of a successful start, the time-to-light and idle speed were noted. Once a no-light or hang was confirmed by repeat tests, no further attempts were made with that fuel. For each fuel, initial check starts were carried out at ambient temperature and then at temperatures corresponding to 10°F (5.5K) decrements starting at 30°F (272K).

5.4 PT6A-65 Gas Generator Tests

Tests were conducted on ten fuels (see Table 2.2) operating a PT6A-65 gas generator using a back pressuring device to attain engine full power conditions in the combustion section. Tests were performed to establish the effects of the test fuels on the following parameters:

- combustor metal temperatures
- gaseous emissions
- smoke emissions
- combustor exit temperature pattern factor

The engine was run between idle and 100% power levels with and without cabin air bleed. Two fuel nozzle sizes were tested.

5.4.1 PT6A-65 Gas Generator Arrangement

This program was run in Combustion Rig No. 2 in Plant 1 at Longueuil. For gas generator running, the cell has a suitably sized air intake, the engine then draws its own air from the cell (see Fig. 5.8). The engine gas path is complete up to the high pressure turbine outlet. The hot gases then pass through an annular duct containing a rotatable array of ten Type K thermocouples for pattern factor measurements. A schematic of the gas generator and traversing arrangement is shown in Fig. 5.9. Downstream of these thermocouples the flow is split into a bifurcated duct. This arrangement allows rapid access to the entire combustion system and traversing probes when necessary. Further downstream a remotely controlled, cooled butterfly valve was fitted. This valve simulates the restriction of the power turbine section and can be adjusted to set the gas generator on the full engine running line at any desired power level.

5.4.2 PT6A-65 Gas Generator Instrumentation

Engine air mass flow was measured by monitoring the pressure drop across the previously calibrated engine intake duct. Intake static pressure and temperature were also measured. The fuel flow rate was obtained from a turbine flowmeter after correction for density. Fuel manifold pressures were monitored to maintain a check on the condition of the fuel nozzles.

As for the atmospheric pressure tests, static pressure taps were used to measure combustor inlet and exit pressures. Type K thermocouples were used to measure combustor inlet temperatures and also in the rotatable array of ten probes for pattern factor determination. These ten probes were located at radial centres of area immediately downstream of the compressor turbine blades.

The outer combustion liner was taken from the PT6A-65 atmospheric rig test program (Paragraph 5.2) so that the liner thermocouple positions were as shown in Fig. 5.6.

Gaseous and smoke emissions from the engine were measured by probes mounted in the exhaust duct. The probes, analysis equipment and procedures were as described for the atmospheric tests in Section 5.2.2.

5.4.3 PT6A-65 Gas Generator Test Procedure

In order to minimize downtime the combustor liners were not changed in this program. Changes in the overall combustion fuel-air ratio at a given power level simulation were achieved by running with and without cabin air bleed. When flowing, the cabin bleed flow was set to a nominal value of 5% of engine intake air mass flow. Two sizes of fuel nozzles were used. This gave a 40 point test matrix for the ten fuels used.

In each test a five point schedule was followed. The conditions are given in Table 5.3. These reproduce engine conditions for power levels from ground idle (GI) to 100%. The gas generator was set on the engine running line by setting up the required fuel-air ratio (adjusted for fuel LHV) and overall engine pressure ratio. The normal procedure is to set up on engine speed and overall pressure ratio. However, in this case, it was deemed more important to maintain correct fuel-air ratios.

A full set of measurements was taken at each condition and the pattern factor determined for the 100% condition.

5.5 Fuel Handling Procedures

In order to prevent contamination of test fuels, certain procedures had to be adopted for handling and transport. The following fuels were stored in drums: Jet A1, ERBS-3, JP8 Shale, Diesel, Tar Sands, JP10, JP4/2040/DF, and RJ6. The remaining fuels, viz., Jet A1/B1, Jet A1/B2, JP4, JP4/B1, and JP4/B2 were stored in underground tanks. The samples used for analysis were collected at the onset of the can combustor tests. More samples were drawn during gas generator testing, however, contamination occurred since the samples were collected downstream of the fuel control unit filter which could not be changed between fuels. Investigations have shown that contamination was quickly cleaned out, therefore, test results were not affected. Fuel samples should have been collected at the end of each test rather than at the start.

All the rig tests covered by this report were fed by fuel from drums. For those fuels stored in drums this presented no

problem, however, the fuels stored in tanks had to be transferred to drums. In these cases the drums used had only been used for storage of clean distillate fuels. These were carefully drained and rinsed with new fuel several times before filling. For each fuel tested, a standard flushing procedure was adopted. First, all fuel lines were drained using compressed air. Then all fuel filters were replaced by "flushing filters" (these filters were only used for flushing). The lines were then flushed using the new fuel, then drained once again. The appropriate filters were then installed (each fuel was assigned a specific set of filters). Finally, the entire system was flushed using the new fuel.

5.6 Data Analysis Procedures

5.6.1 Combustion Efficiency Calculations

The measured emissions (ppm) were converted to emission indices using an in-house data reduction computer program. Wet concentrations of CO, HC, and CO₂ were used to compute sample fuel-air ratios based on the following relationships:

$$far = \left[\frac{M_C + \alpha M_H}{M_{AIR}} \right] \left[\frac{(1+h) [10^{-4}(CO) + (CO_2) + 10^{-4}(HC)]}{100 - 0.25\alpha [10^{-4}(CO) + (CO_2) + 10^{-4}(HC)]} \right]$$

where: h = Humidity of air, moles of water per mole of dry inlet air

α = Carbon/hydrogen ratio

M_C = Carbon molecular weight

M_{AIR} = Air molecular weight

M_H = Hydrogen molecular weight

Combustion efficiency and emission indices were computed using the following relationships:

$$\eta = 100 - [0.0232 EI_{CO} + 0.0908 EI_{HC}]$$

$$EI_{CO} = \left[\frac{(CO)}{10^{-4}(CO) + (CO_2) + 10^{-4}(HC)} \right] \left[\frac{M_{CO}}{10(M_C + \alpha M_H)} \right]$$

$$EI_{HC} = \left[\frac{(HC)}{10^{-4}(CO) + (CO_2) + 10^{-4}(HC)} \right] \left[\frac{M_{HC}}{10(M_C + \alpha M_H)} \right]$$

$$EI_{NOX} = \left[\frac{(NO_x)}{10^{-4}(CO) + (CO_2) + 10^{-4}(HC)} \right] \left[\frac{M_{NO_2}}{10(M_C + \alpha M_H)} \right]$$

The program was modified to calculate a net temperature rise for each set condition. The temperature rise is from a kinetics

routine which uses all relevant fuel properties. (C-H ratio, heat of combustion, specific gravity, sulphur content, enthalpy of evaporation, etc) and calculates an ideal temperature rise. The previously calculated combustion efficiency is then applied to the ideal temperature rise to arrive at an actual gas exit temperature. This information was used in NO_x vs T_4 correlations which will be discussed in Section VI dealing with test results. NO_x emissions indices which have been corrected to standard humidity of 0.0063 lb H_2O /lb air were calculated as follows:

$$\text{EI}_{\text{NO}_x(c)} = \text{EI}_{\text{NO}_x} * e^{19(h-0.0063)}$$

5.6.2 Fuel Property Correlations

The main thrust in the data analysis was to try to correlate such performance parameters as emissions, liner temperatures, flame radiation, and combustion efficiency to such fuel properties as hydrogen content, droplet size, volatility, etc. A central data base was therefore established which would permit comparisons between any two parametric sets of data (smoke emissions and fuel hydrogen content, for example). A computer program was then set up to plot any combinations of these data sets on an X-Y plotter. This greatly accelerated the task of trying to draw correlations from the data. In most cases, a straight line was drawn through data points using a linear regression technique. These lines were meant only as trend indicators and were not meant to dictate the type of correlation (linear, second order, etc.) present. The plotting capability proved to be a valuable tool in the data analysis.

5.6.3 Profile and Pattern Factor Determinations

Throughout this report the pattern factor is defined as the ratio of the average elevation of the peak temperatures above the mean, to the temperature rise from the combustor inlet, i.e.,

$$\text{Pattern Factor} = \frac{\hat{T} - \bar{T}}{\bar{T} - \bar{T}_{in}}$$

where \hat{T} = average of the twelve (PT6A) or fourteen (JT15D) peak temperatures

\bar{T} = thermodynamic combustor exit temperature (calculated)

\bar{T}_{in} = average of all combustor inlet temperatures.

The relative pattern factor was calculated by dividing the specific pattern factor by the JP4 pattern factor. In the case of defective probes the affected readings were not included in the calculations. No attempt was made to extrapolate from the remaining data to cover the missing points.

Radial profile factors are defined as the ratio of the highest probe average reading to the overall average temperature, i.e.;

Profile Factor = T_n/\bar{T}

where T_n is the highest of the circumferentially averaged temperatures. Once again, the relative profile factors were calculated relative to the JP4 profile factor.

5.6.4 Combustor Liner Temperature Parameters

Peak liner skin temperatures are expressed as the difference between the highest reading thermocouple in the array and the combustor inlet temperature, i.e. ($\bar{T}_L - T_3$).

Average liner skin temperatures are expressed as the difference between the average temperature reading of all the functioning thermocouples in the array and the combustor inlet temperature, i.e. ($\bar{T}_L - T_3$).

An average liner temperature parameter has also been used to express liner temperatures relative to those measured with the reference fuel JP4. This is defined as

$$\frac{\bar{T}_L - \bar{T}_{LJP4}}{\bar{T}_{LJP4} - T_3}$$

Similarly, the peak liner temperature parameter expresses peak temperatures relative to the reference fuel JP4 as follows:

$$\frac{\hat{T}_L - \hat{T}_{LTP4}}{\hat{T}_{LTP4} - T_3}$$

5.6.5 Droplet Size Correlations

In order to study the effects of atomization on combustor performance, Relative Sauter Mean Diameter (RSMD) is defined as the ratio of SMD of the fuel in question and SMD of JP4 at the same fuel mass flow and temperature. The SMD of the spray produced by a pressure atomizer has been correlated using the following in-house relationship:

$$SMD = \frac{K\sigma_f^{0.8} \nu_f^{0.2} W_f^{0.25}}{\Delta P_f^{0.4}}$$

$$\text{and, } \Delta P_f = \left(\frac{W_f}{FN} \right)^2$$

Thus, the relative droplet size is given by:

$$RSMD = \frac{SMD_f}{SMD_{JP4}} = \left(\frac{\sigma_f}{\sigma_{JP4}} \right)^{.6} \left(\frac{\nu_f}{\nu_{JP4}} \right)^{.2} \left(\frac{\rho_f}{\rho_{JP4}} \right)^{.8}$$

For the airblast injector, SMD was computed using the following relationship¹⁰:

$$SMD = K t^{0.375} \sigma_{AR}^{-.325} \left[\frac{W_f}{W_f V_f + C W_a V_a} \right]^{0.55} \rho_{FR}^{.25} \mu_{FR}^{.06} \sigma_{FR}^{.375}$$

For relative droplet sizes of airblast nozzles, all terms cancel except for the fuel properties such that:

$$RSMD = \frac{SMD_f}{SMD_{JP4}} = \left(\frac{\rho_f}{\rho_{JP4}} \right)^{.25} \left(\frac{\mu_f}{\mu_{JP4}} \right)^{.06} \left(\frac{\sigma_f}{\sigma_{JP4}} \right)^{.375}$$

5.6.6 Linear Regression Techniques

In comparing fuel property effects and trying to correlate them to performance parameters, linear regressions were performed which determined least square coefficients for the linear model:

$$y = a x + b$$

In order to evaluate the magnitude of data scatter about this line, a sample standard error of estimate (σ) was calculated:

$$\sigma = \left[\frac{\sum (y_i - y_{ic})^2}{n - 2} \right]^{1/2}$$

where y_i = actual values of y
 y_{ic} = values of y computed from the line equation
 n = number of points

Also, multiple line regressions were calculated to correlate three fuel properties to a performance parameter. Once again, least square coefficients were calculated to fit the following model:

$$y = a_0 x_1^{a1} x_2^{a2} x_3^{a3}$$

The associated correlation coefficient (r) is simply the ratio of the sample standard deviation and the standard error of estimate.

It should be noted that regressions are only valid within the parametric ranges of the samples and should never be extrapolated.

Table 5.1: JT15D-5 Atmospheric Rig Test Conditions

Simulated Power Setting (% Max. Thrust)	\bar{M}_c	T_3 K	far*
Idle	.0373	154	.009
30	.0384	252	.0105
70	.0373	350	.0147
100	.0365	396	.0174

Table 5.2: PT6A-65 Atmospheric Rig Test Conditions

Simulated Power Setting (% Max. SHP)	\bar{M}_c	T_3 (K)	far*
GI	.0302	417	0.0104
40	.0295	557	0.0158
55	.0293	575	0.0172
70	.0290	588	0.0180

* Fuel-air ratios quoted are for Jet A1. For other fuels these values were adjusted to allow for LHV variations using:

$$far_{\text{Fuel N}} = far_{\text{Jet A1}} \left[\frac{LHV_{\text{Jet A1}}}{LHV_{\text{Fuel N}}} \right]$$

Table 5.3: PT6A-65 Gas Generator Test Setup Points

Simulated Power Setting (% Max.SHP)		$N_g/\sqrt{\theta}$ * (rpm)	P_3/P_1	W_f Normalized (kg/hr)
No Bleed	GI	21750	2.34	52.3
	5	25500	3.24	72.5
	45	33049	6.76	182.8
	80	34960	8.63	250.3
	100	36121	9.50	286.3
5% Cabin Bleed	GI	21653	2.30	60.1
	5	25460	3.13	77.9
	45	33024	6.60	195.4
	80	34954	8.45	267.0
	100	36151	9.31	306.0

* Fuel flows quoted are for Jet A1. For other fuels these values were adjusted to allow for LHV variations using:

$$W_{fFuel\ N} = W_{fJet\ A1} \left[\frac{LHV_{Jet\ A1}}{LHV_{Fuel\ N}} \right]$$

$$* \theta = T_1/288.15$$

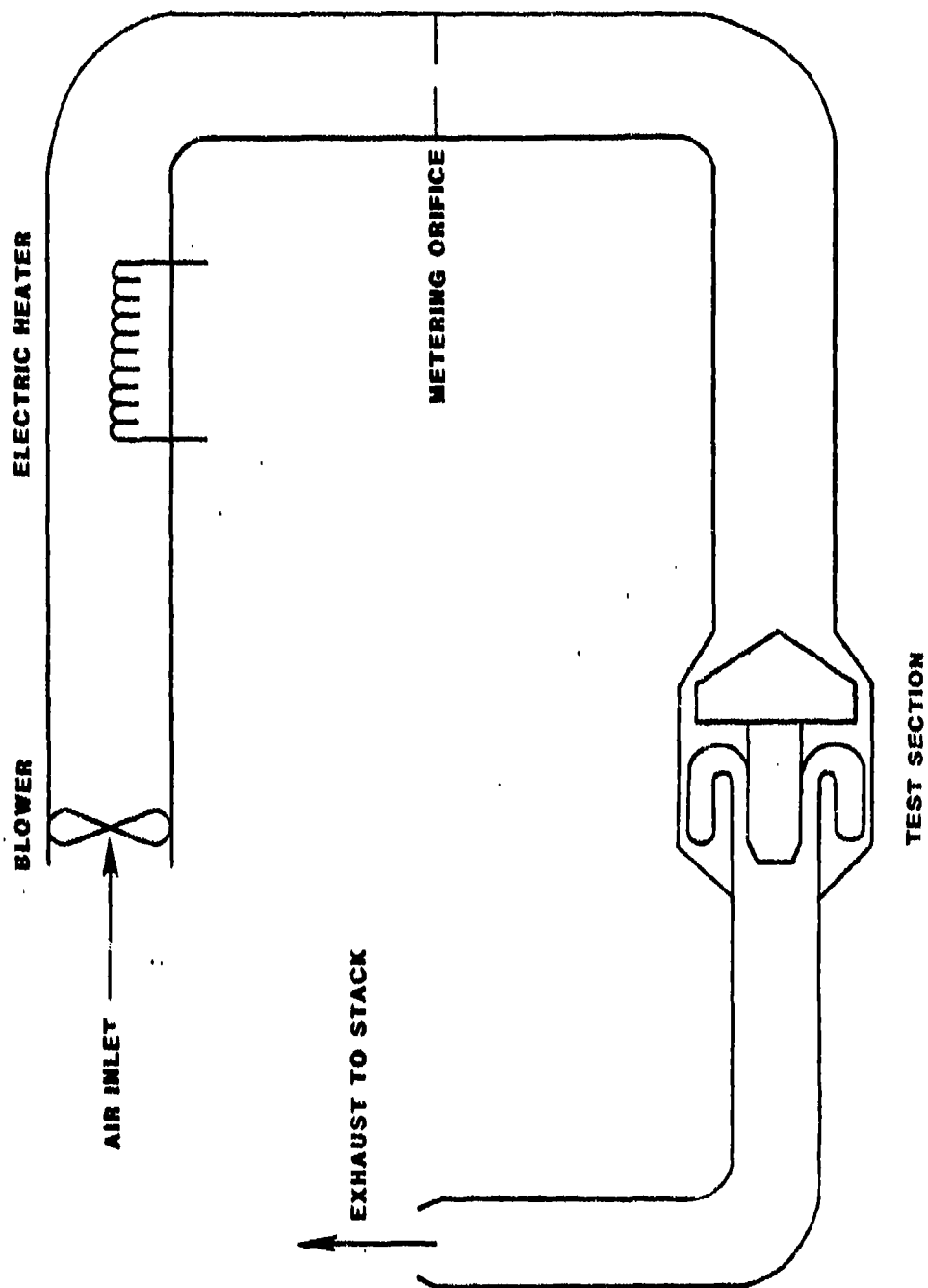


Figure 5.1: Layout of JT15D Atmospheric Rig

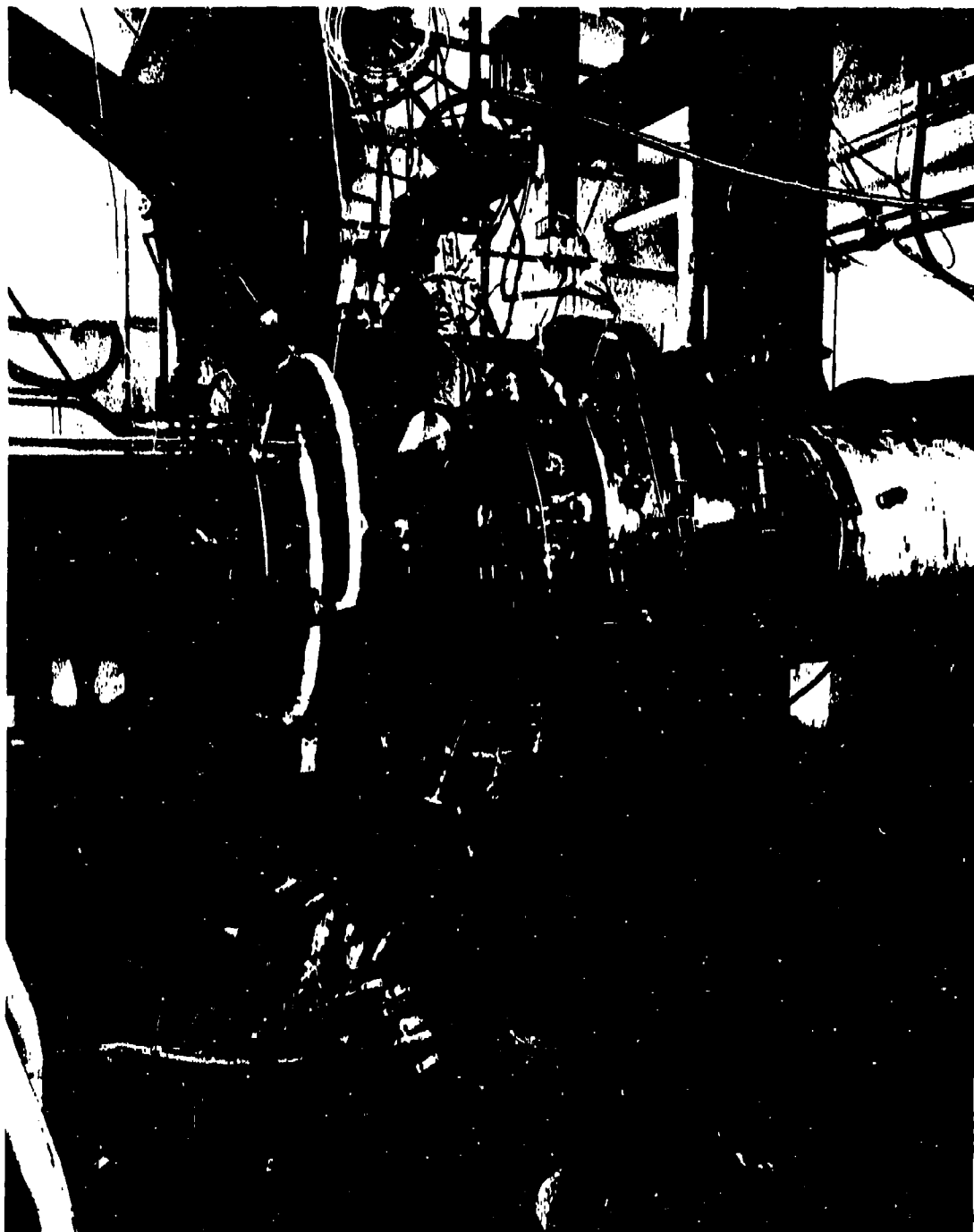


Figure 5.2: General View of JT15D-5 Atmospheric Pressure Rig Test Section

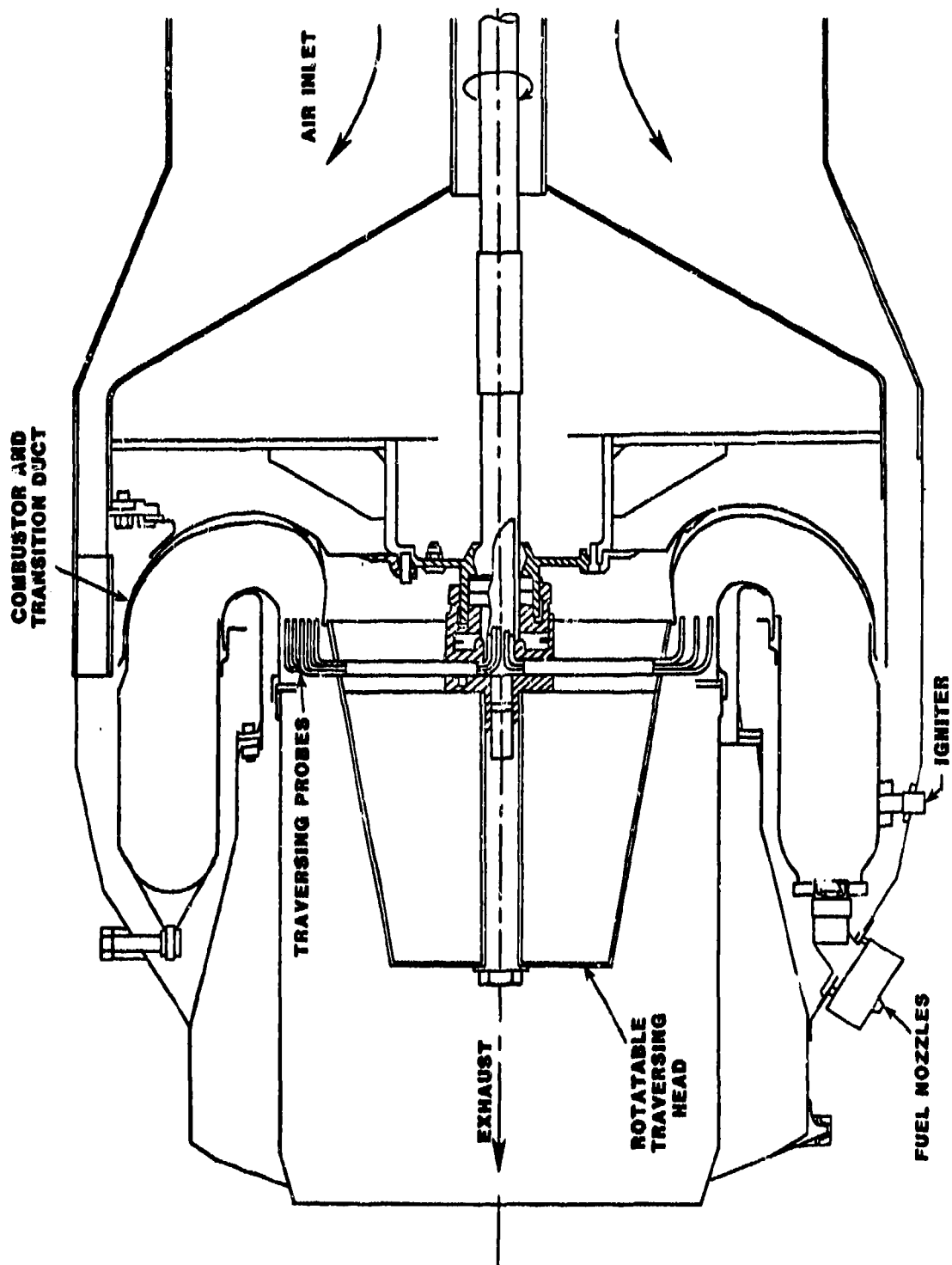
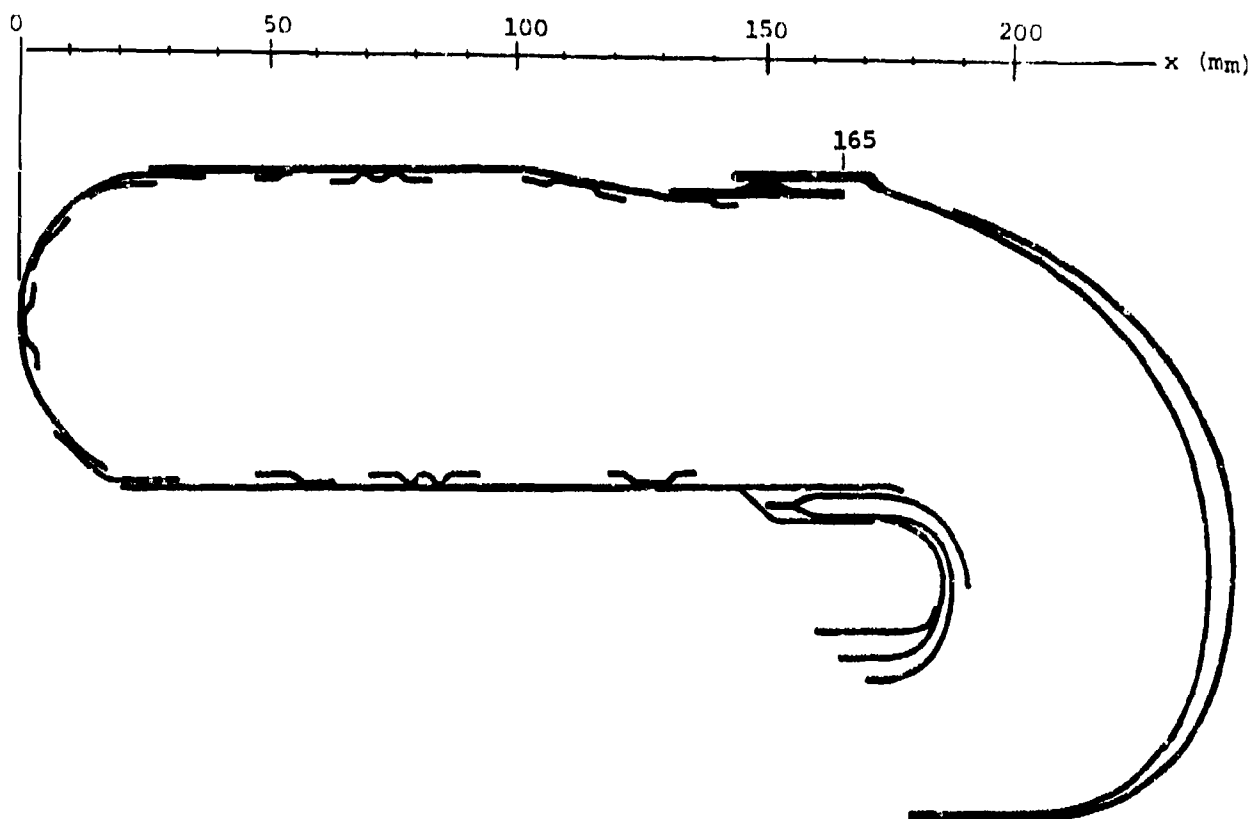


Figure 5.3: JT15D-5 Atmospheric Pressure Test Section



<u>Probe Number</u>	<u>Axial Position (mm)</u>	<u>Inner (I) or Outer (O) Wrapper</u>	<u>Circumferential Location (θ°) *</u>
1	0	-	13.000
2	0	-	105.000
3	0	-	133.000
4	0	-	193.000
5	0	-	343.000
6	33	I	0.000
7	33	I	120.000
8	33	I	330.000
9	1	O	75.000
10	1	O	345.000
11	12	O	75.000
12	12	O	345.000
13	32	O	75.000
14	32	O	345.000
15	49	O	75.000
16	49	O	345.000
17	100	O	75.000
18	100	O	345.000
19	137	O	75.000
20	137	O	345.000

* θ values measured clockwise from TDC;
Looking in direction of increasing x

Figure 5.4: Locations of JT15D-5 Liner Thermocouples

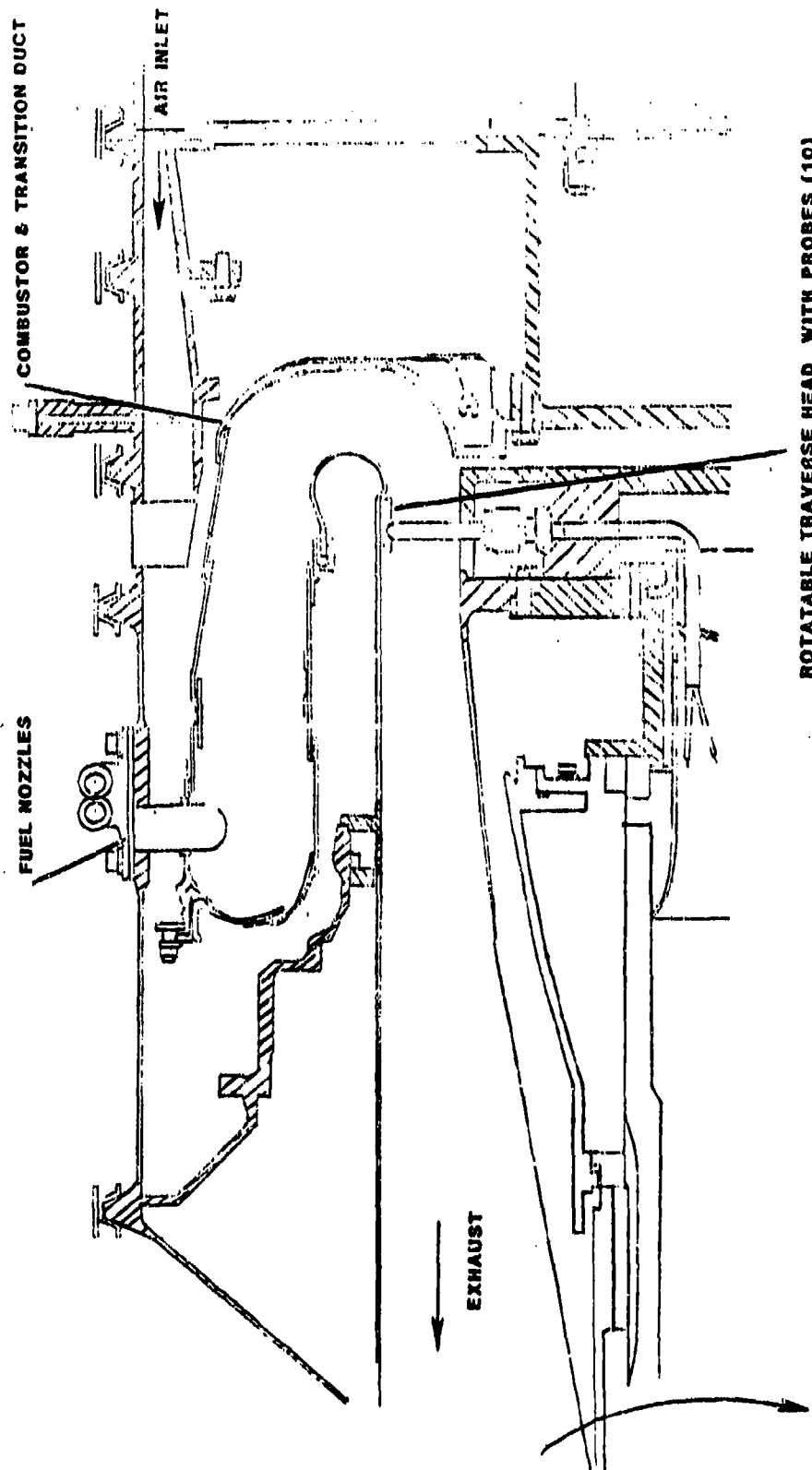
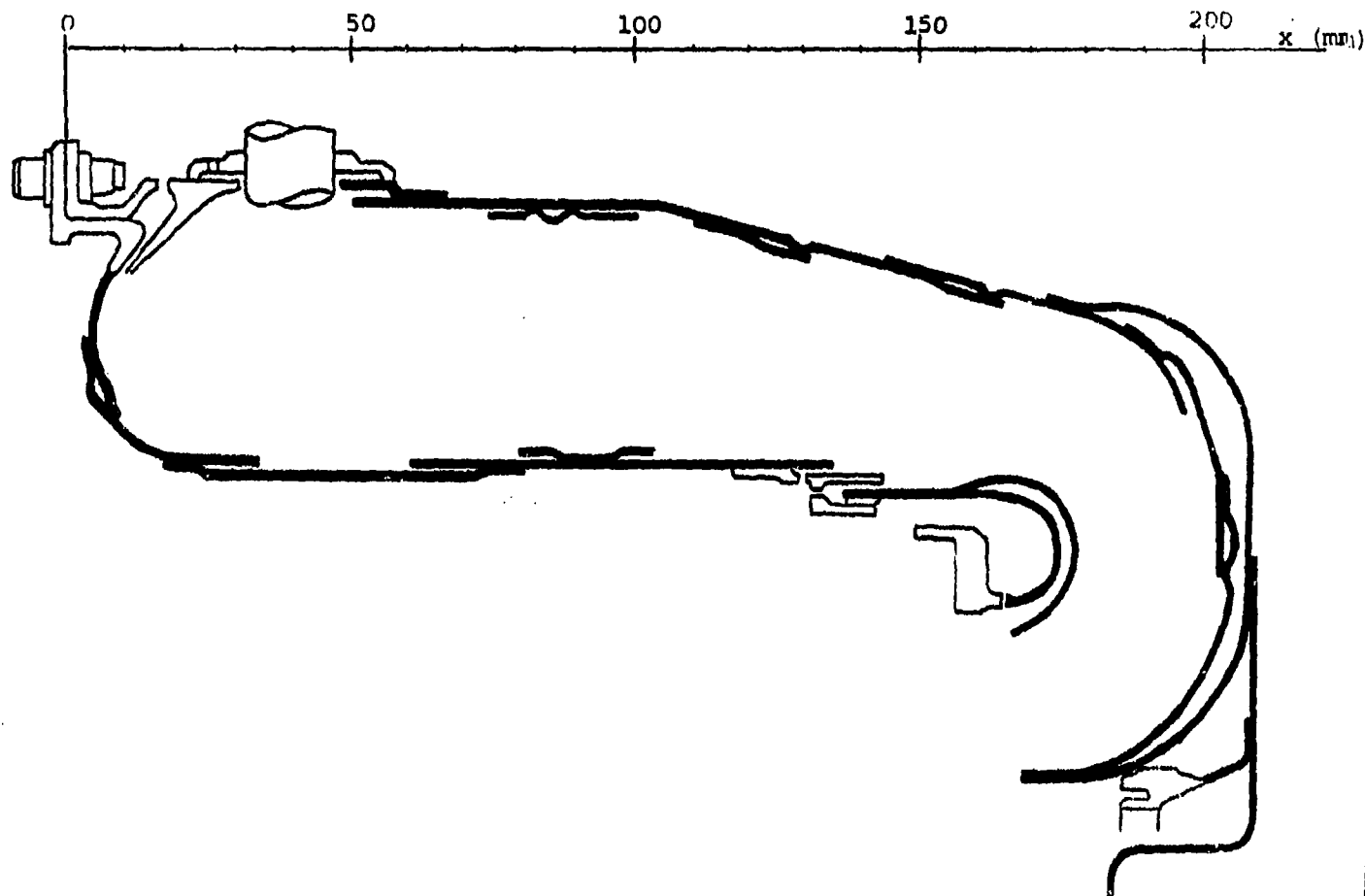


Figure 5.5: PT6A-65 Atmospheric Pressure Rig Test Section



Probe Number	Axial Position (x mm)	Circumferential Position (θ°)
1	27	347
2	31	167
3	29	218
4	42	116
5	31	90
6	64	347
7	64	218
8	64	90
9	118	0
10	120	193
11	121	128
12	143	347
13	144	193
14	141	128
15	186	347
16	186	218
17	186	116
18	208	0
19	208	257
20	208	154

Note: All thermocouples were positioned on the outer wrapper

Figure 5.6 Locations of Liner Thermocouples for PT6A-65 Atmospheric and Gas Generator Tests.

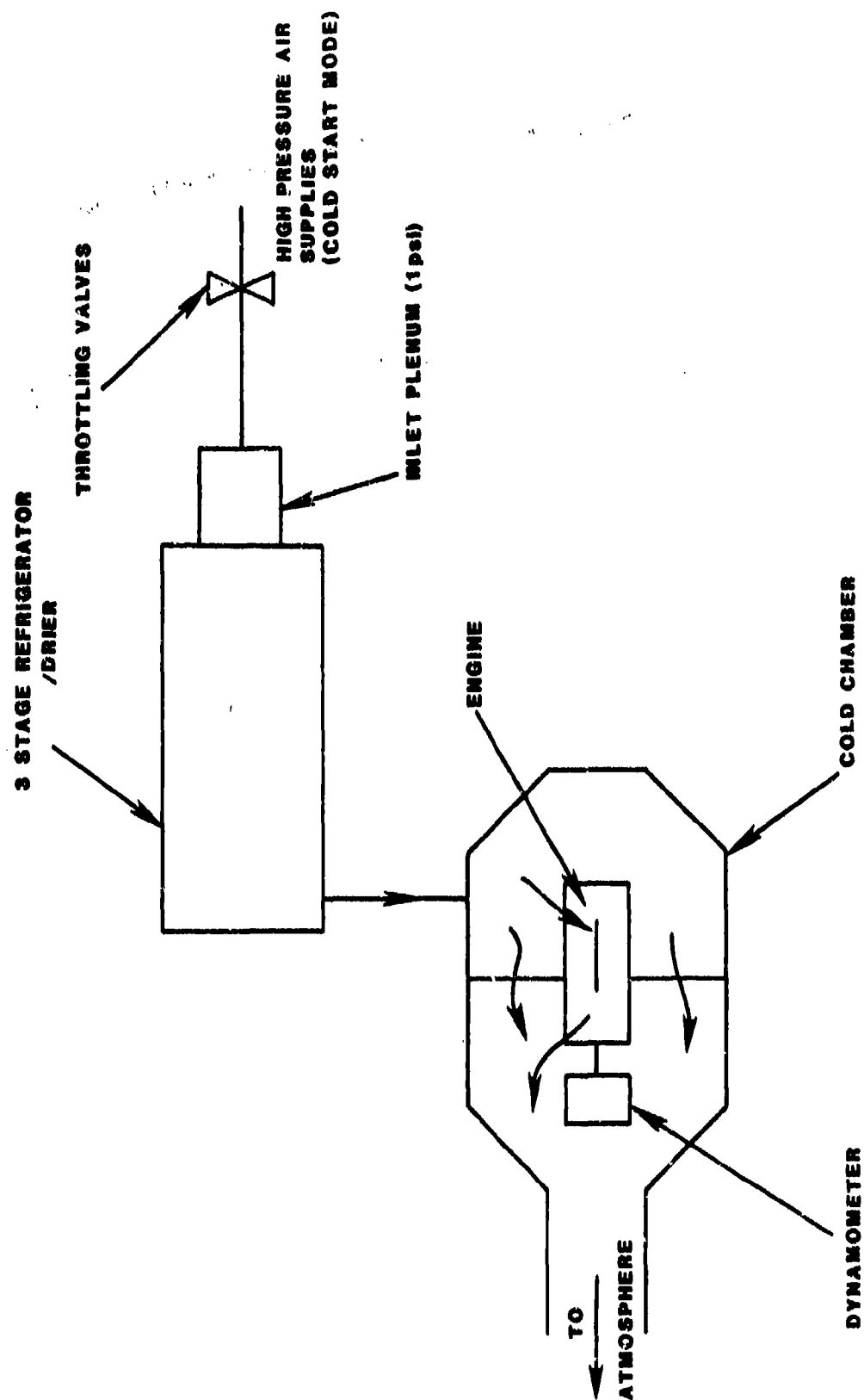


Figure 5.7; Layout of Cold Start Facility at NRC



Figure 5.8: General View of PT6A-65 Gas Generator in Combustion. Rig No. 2

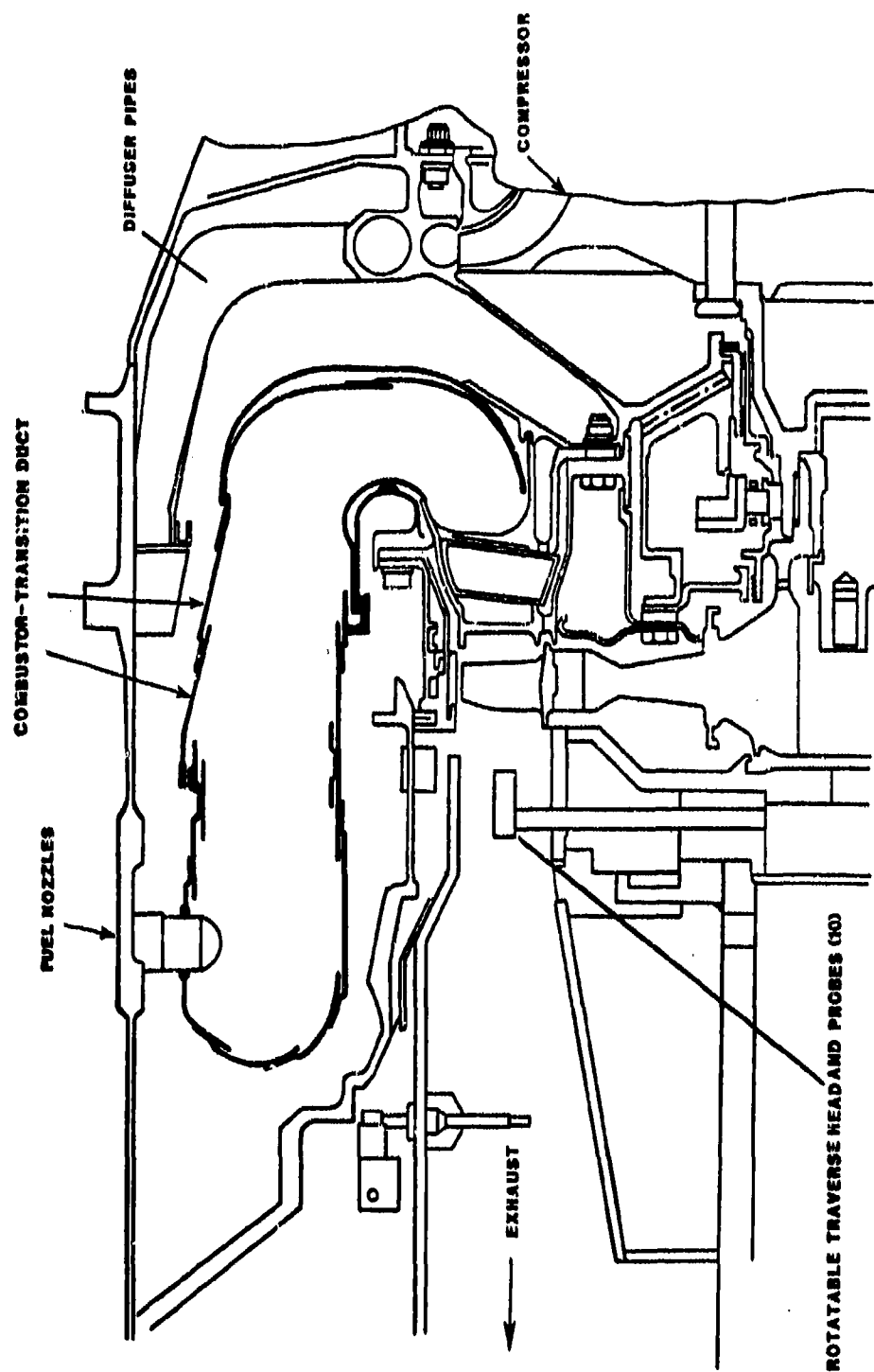


Figure 5.9: PT6A-65 Gas Generator Traversing Rig

SECTION VI

RESULTS AND DISCUSSION

Sections 6.1 through 6.4 describe results obtained during the various test activities with the PT6A and JT15D combustion systems. Section 6.5 presents comparisons and discussions of these test results with reference to the 'can' combustor data obtained during Phase II of the program and other published data on straight-through annular combustion systems. Detailed test data are presented in Appendices A through D. Table 6.1 is the legend of symbols used in Section VI plots.

6.1 JT15D-5 Atmospheric Rig Results

Atmospheric rig tests were conducted with JP4, Shale JP8, ERBS-3 and JP10, simulating operating conditions on the JT15D-5 engine running line. Simulation at atmospheric pressure was obtained in the manner described in Section V, maintaining values of rig Mach number, combustor inlet temperature and exit temperature to engine levels. Tests were conducted with pressure and airblast atomizing nozzles, and with two sets of combustor hardware conforming to bill of materials (BOM) and rich primary zone (rich P.Z.) configurations (Section IV). Test data are detailed in Appendix A and key variations of performance with fuel properties are described below.

6.1.1 CO and HC Emissions

Carbon monoxide (CO) and unburned hydrocarbons (HC) are both products of incomplete combustion and are generally highest at low power operating conditions (e.g. idle). Figure 6.1 shows variation of CO emissions at idle with hydrogen content, volatility and relative droplet size for the bill of material combustor with pressure atomizing fuel system. The trends indicate increasing CO emissions with reduced hydrogen content, reduced volatility and increased fuel droplet size relative to baseline (JP4) fuel. Correlations describing these effects were:

$$\text{Idle EI(CO) vs H (\%)} \quad Y = 324 - 12.2 x, \quad \sigma = 24.20$$

$$\text{Idle EI(CO) vs } T_{10}(\text{K}) \quad Y = .390 x - 3.66, \quad \sigma = 18.35$$

$$\text{Idle EI(CO) vs RSMD} \quad Y = 85.5 + 62.1 x, \quad \sigma = 24.11$$

Figure 6.2 shows variations of hydrocarbon emissions at idle with fuel properties for bill of material configurations using pressure atomizing nozzles, with trends similar to those for CO emissions:

$$\text{Idle EI(HC) vs H (\%)} \quad Y = 591 - 29.7 x; \quad \sigma = 45.05$$

$$\text{Idle EI(HC) vs } T_{10}(\text{K}) \quad Y = 1.03 x - 238; \quad \sigma = 8.02$$

$$\text{Idle EI(HC) vs RSMD} \quad Y = 166 x - 6.98; \quad \sigma = 41.18$$

Figures 6.3 - 6.8 show CO and HC emission variations with fuel properties for bill of material with airblast nozzle, and rich primary zone configuration with pressure atomizing and airblast nozzles. Trends in most cases are similar to bill of material configuration trends except in the rich configuration the emission levels are lower because of the richer front end conditions. The 30% comparison was used in the case of airblast nozzles because of their poor stability at conditions simulating ground idle operation. The fuel property effects in Figure 6.6 appear to influence HC emissions abnormally in that, trendwise, there is a reduction of HC emissions with reduced H content, reduced volatility and increased relative droplet size. Closer observations, however, reveal that this abnormal behaviour is due to the recorded level of HC emissions with JP4 fuel and that the other three fuels display the normally expected behaviour with change in fuel properties. As well, comparison of Figures 6.5 and 6.6 indicates that the trends of CO and HC emissions with fuel properties are different, whereas they should have been similar. It is therefore believed that the measured HC emission for JP4 fuel and the correlations shown in Figure 6.6 are erroneous.

6.1.2 Combustion Efficiency

Figures 6.9 and 6.10 show a reduction of combustion efficiency with increasing air loading parameter (Paragraph 3.3) for the four test fuels using pressure atomizing and airblast atomizing nozzles. Figure 6.11 shows variation of combustion efficiency at idle with fuel properties for bill of materials configuration using pressure atomizing nozzles. As expected, efficiencies decrease with reduced hydrogen content, reduced volatility, and increased relative droplet size:

Comb. Eff. vs H (%)	$Y = 38.8 + 2.98x;$	$\sigma = 4.54$
Comb. Eff. vs T_{10} (K)	$Y = 122 - 0.102x;$	$\sigma = 1.15$
Comb. Eff. vs RSMD	$Y = 98.6 - 16.5x;$	$\sigma = 4.19$

Figures 6.12-6.14 show combustion efficiency variations with fuel properties for rich primary zone combustor and bill of material combustor with airblast nozzles. Trends are very similar to those of the bill of material combustor except for Figure 6.13 which shows a reversal of trends as discussed in Paragraph 6.1.1.

6.1.3 Smoke Emissions

The smoke measurements indicated smoke levels below measurable levels, in all cases. This is quite a normal result from atmospheric rig tests, wherein the droplet distribution, and residence times are significantly different to operation under full pressure conditions, when simulation is based on constant approach Mach number.

6.1.4 Liner Metal Temperatures

Figure 6.15 shows variation of differential average liner temperature ($T_L - T_3$) with the metered fuel-air ratio for the four test fuels. Figure 6.16 shows ($T_L - T_3$) variation with fuel

volatility, aromatic and hydrogen contents for take-off simulation. JP10, a synthetic fuel, is anomalous in having both a low hydrogen content and zero aromatics. Correlation of $(T_L - T_3)$ at 'take-off' with fuel hydrogen content (Figure 6.16) results in,

$$(T_L - T_3) \text{ vs. } H (\%): \quad Y = 190 - 4.93 x; \quad \sigma = 2.39$$

Figure 6.17 shows correlation of average liner temperature parameter (see Para. 3.4.5) at take-off with fuel volatility, hydrogen and aromatic contents. Peak temperatures, Figure 6.18, do not correlate in the same fashion as average temperatures, presumably because of varying locations of flame fronts with different fuels. Figures 6.19 to 6.27 show variations of average and peak differential liner temperatures with fuel properties for rich front end pressure atomizer, bill of material airblast and rich front end airblast configurations respectively.

6.1.5 Lean Stability Limits

Figure 6.28 shows variation of lean limit fuel-air ratios with hydrogen content, volatility and relative droplet size, for bill of materials combustor with pressure atomizing fuel system. Trends indicate poorer lean limit stability with reduced hydrogen content, reduced volatility and increased relative droplet size. Correlations describing these effects are:

$$\text{LLFAR vs } H (\%) : \quad Y = 14.5 - .626 x; \quad \sigma = 0.47$$

$$\text{LLFAR vs } T_{10} (K): \quad Y = .941 + .124 x; \quad \sigma = 0.60$$

$$\text{LLFAR vs RSMD} : \quad Y = 2.07 + 3.37 x; \quad \sigma = 0.36$$

Figure 6.29 shows lean limit variations for rich primary zone configuration with pressure atomizing nozzles.

Poor stability performance of airblast injectors at idle prevented lean limit measurement for this fuel system.

6.1.6. Pattern Factors and Radial Profiles.

Exit temperature distributions were measured by traversing in the exit plane of the combustor at conditions simulating 70% and 100% thrust levels. Figures 6.30 and 6.31 show variations in radial profile factors and pattern factors with fuel properties and relative droplet size for bill of materials combustor with pressure atomizing fuel systems. Measured combustor exit temperatures were often in excess of 2200°F (1480K) for the 100% thrust condition, thereby causing probe failure in several cases. While data for this condition has been listed in Appendix A, data from the 70% thrust condition has been used in the analysis. The trends indicate significant influence by properties which affect atomization of the fuel. Even at this relatively high thrust simulation where the combustion efficiency is high, the droplet distribution and combustor characteristics appear to influence exit temperature quality significantly.

Similar trends were observed for the other combustor/nozzle combinations (Figures 6.32 to 6.37).

6.2 PT6A-65 Atmospheric Rig Results

As described in Section II, atmospheric rig tests were conducted with 12 fuels, Table 2.2, simulating operating conditions on the PT6A-65 engine running line. Simulation at atmospheric pressure was obtained in the manner described in Section V maintaining values of rig Mach number, combustor inlet temperature and exit temperature to engine levels. Tests were conducted with two sets (0.65 FN and 1.1 FN) of pressure atomizing nozzles, and with two sets of combustor hardware conforming to bill of material and lean primary zone configurations (Section IV). Test data are detailed in Appendix B and variations of performance parameters with fuel properties are described below.

6.2.1 CO, HC Emissions and Combustion Efficiency

Tests were undertaken measuring CO and HC emissions and calculating combustion efficiencies at simulated conditions along the PT6A-65 operating line. Test results are detailed in Appendix B, which shows the emissions expressed as Emission Indices. Results of atmospheric tests showed considerable scatter therefore correlations and plots have been confined to gas generator tests where measurements were undertaken under full pressure operating conditions and these are presented in detail in Paragraphs 6.4.1 and 6.4.2.

6.2.2 Smoke Emissions

As with JT15D-5 tests, smoke levels were below discernable levels at all conditions. This is consistent with normal results from atmospheric rig tests, where the droplet distribution and residence times are different to operation under full pressure conditions.

6.2.3 Liner Metal Temperatures

Figures 6.38 and 6.39 show variations of differential average liner temperature ($T_L - T_3$) with inlet temperature T_3 for the 12 test fuels, using 0.65 FN fuel nozzles and bill of materials combustion system.

Figure 6.40 shows the effects of fuel hydrogen content, volatility and aromatic content on average differential liner temperatures. Strong effects of hydrogen content and aromatic content corresponded to:

$$\begin{aligned} (T_L - T_3)_{\text{Ave. vs H Content (\%)}} & Y = 434 - 21.4x; \sigma = 15.53 \\ (T_L - T_3)_{\text{Ave. vs Aromatic Content (\%)}} & Y = 111.5 + 1.40x; \sigma = 16.57 \end{aligned}$$

Figure 6.41 shows the same data expressed in terms of liner temperature parameter defined as $(T_L - T_{LJP4}) / (T_{LJP4} - T_3)$, trends once again showing influence of fuel hydrogen and aromatic contents. Figure 6.42 shows variation of peak differential liner temperatures expressed as $(T_L - T_3)$ with fuel properties.

As with average temperatures, the peak liner temperatures increase with reduced fuel hydrogen content and increased fuel aromatics, corresponding correlations being,

$$(T_L - T_3) \text{ Peak vs H Content (\%)} \quad Y = 597 - 23.9 x; \sigma = 31.8$$

$$(T_L - T_3) \text{ Peak vs Aromatic Content (\%)} \quad Y = 250 + 1.08 x; \sigma = 33.7$$

Figures 6.43 to 6.51 show variations of average and peak differential liner temperatures with fuel properties for lean primary zone combustor (Lean P.Z.) with 0.65 FN pressure atomizers, bill of materials combustor with 1.1 FN pressure atomizers and lean primary zone with 1.1 FN pressure atomizers.

6.2.4 Lean Stability Limits

Figures 6.52 - 6.53 show the effects of fuel properties on lean stability performance of PT6A-65 bill of materials combustion system. Figure 6.52 shows the influence of fuel hydrogen content, volatility and relative droplet size on lean limit fuel-air ratios using a 0.65 FN pressure atomizing fuel system. The data indicate poorer stability with reduced hydrogen content, increased volatility and increased relative droplet size. However, the correlating factors show relatively small influence, the trends being well within experimental scatter in test data. Figures 6.54 and 6.55 show lean limit performance using 0.65 FN pressure atomizing fuel system with lean primary zone combustor, trends once again indicating relatively small influence of fuel properties on combustor stability. Figures 6.56 to 6.58 show lean limit performance of bill of material and lean primary zone configurations with 1.1 FN pressure atomizing nozzle, trends being similar to .65 FN nozzles.

6.2.5 Pattern Factors and Radial Profiles

Exit temperature distributions were measured by traversing in the exit plane of the combustor simulating 70% power level. Figure 6.59 shows the variation in combustor exit radial profile factor (RPF) with fuel hydrogen content, volatility and relative droplet size for bill of materials configuration with 0.65 flow number fuel injectors. The trends indicate significant influence of hydrogen content and relative droplet size as follows:

$$\text{RPF vs H\%} \quad Y = 6.85 - 0.382 x ; \sigma = 0.35$$

$$\text{RPF vs RSMD} \quad Y = 2.50 X - 1.04 ; \sigma = 0.31$$

Figure 6.60 shows effects of fuel properties and relative droplet size on combustor exit pattern factor for bill of materials combustor with 0.65 FN pressure atomizing nozzles. Like the radial profiles, the pattern factors appear strongly influenced by fuel hydrogen content and relative droplet size as follows:

$$\text{RPF vs H\%} \quad Y = 3.55 - 0.171 x ; \sigma = 0.12$$

$$\text{RPF vs RSMD} \quad Y = 0.254 + 0.91 x ; \sigma = 0.13$$

Figures 6.61 - 6.66 show effects of fuel properties on radial profile and pattern factors for lean primary zone configuration with .65 FN fuel nozzles, bill of materials with 1.1 FN fuel nozzles, and lean primary zone with 1.1 FN fuel nozzles. With some of the configurations the effects of fuel properties appear insignificant or display large amounts of scatter. It is suspected that in some cases rig asymmetries may have affected the quality of exit profile measurements.

6.3 PT6A-65 Cold Start Test Results

Start-up tests were conducted for ten fuels using PT6A-65 bill of material combustion and engine hardware, as described in Section V. Nozzles used were standard 1.9 FN pressure atomizers. Tests were done for a constant starting fuel flow to establish starting parameters such as minimum light up temperatures, time to light and time to idle.

Table 6.2 shows minimum light-up temperatures for the various test fuels. JP4, JP4/B2, Jet A1, Jet A1/B2 and Shale JP8 had successful ignitions at temperatures to below 231K (-44°F) and since this represented the lowest temperature achieved in the test facility, minimum light-up temperatures could not be established. ERBS-3 and Tar Sand fuels had minimum ignition temperatures in the 238 to 243K (-31 to -22°F) range. JP10 had successful lights down to 241K (-26°F) and RJ6 showed consistent light-offs only down to 271K (27°F). It appears from these results that minimum ignition temperatures are strongly influenced by fuel properties, the higher viscosity fuels resulting in poorer ignition performance.

Figure 6.67 shows time to light as a function of average fuel-air temperature. The effect of 2040 solvent blend with JP4 and Jet A1 appears minimal. ERBS-3 and Tar Sands fuels showed longer time to light even at higher light-up temperatures. Performance of JP10 was somewhat worse than ERBS-3 while RJ6 performed very poorly with 16 seconds time to light even at 269K (+25°F) air and fuel temperatures.

Figure 6.68 shows comparisons of time-to-light at a constant air-fuel average temperature of 244K (-20°F), some of the data being interpolated from tests at other temperatures. The relatively poor performance of ERBS-3, L-L Tar Sand and JP10 is evident from this comparison. Figure 6.69 shows variation of time-to-light at 244K as a function of fuel hydrogen content, volatility and relative droplet size. The times-to-light quoted include a fuel system filling time of approximately two seconds. Thus JP4 and Jet A1 fuels are lighting almost instantaneously at 244 K. Figure 6.69 therefore does not distinguish between these fuels hence they should not be considered in the correlation. For the other fuels, in spite of considerable scatter, longer times-to-light can be observed with reduced hydrogen content, larger droplet size, and reduced volatility.

Figure 6.70 shows time-to-idle as a function of average fuel-air temperature. Here the effect of 2040 solvent appears more

significant, the blended JP4/B2 and Jet A1/B2 fuels showing significantly poorer performance than baseline JP4 and Jet A1 fuels. Surprisingly, Shale JP8 performed worse than Jet A1/B2. The performance of ERBS-3 and Tar Sand fuels was considerably worse. Although JP10 showed poor ignition characteristics, the propagation (light-around) performance was extremely good, resulting in time-to-idle similar to Jet A1. Figure 6.71 shows comparison of time-to-idle at a constant average air-fuel temperature of 244K (-20°F), once again some of the data being interpolated from tests at other temperatures. The relatively good performance of JP10 and poor performance of ERBS-3 is evident from this comparison. Correlations of time-to-idle with fuel properties, Figure 6.72, show strong influence of volatility and droplet size. Again, the JP4 and Jet A1 fuels are not well differentiated and should not be considered in the correlation.

6.4 PT6A-65 Gas Generator Tests

Full pressure evaluation of PT6A-65 combustors was undertaken with a gas generator and the same ten fuels used for cold start tests were evaluated for steady state performance. The tests covered the operating range from ground idle to sea level take-off with the bill of material combustor and two sets (1.9 FN and 2.2 FN) of pressure atomizing nozzles. Tests were also run with 5% cabin bleed to simulate the case of richer overall fuel-air ratio. Due to a shortage of RJ6 fuel, only the bill of material configuration was tested. Only the first three conditions were completed on the 5% bleed 2.2 FN configuration, while no data is available for the 5% bleed 1.9 FN configuration. Plots which have no data for RJ6 have been marked "RJ6 data not available". Test data are detailed in Appendix D and observed fuel property effects are described below.

6.4.1 CO and HC Emissions

Figures 6.73 and 6.74 show the effects of fuel hydrogen content, volatility and relative droplet size on CO emissions at idle for bill of material configurations with 1.9 FN nozzles. The data show strong correlation with fuel hydrogen content and droplet size, and modest influence of volatility.

$$\text{EI-CO (idle) vs H Content (\%)} \quad Y = 189 - 9.94 x; \quad \sigma = 6.24$$

$$\text{EI-CO (idle) vs } T_{10} \text{ (K)} \quad Y = 3.83 + .134 x; \quad \sigma = 12.41$$

$$\text{EI-CO (idle) vs RSMD} \quad Y = 21.2 + 31.2 x; \quad \sigma = 6.14$$

$$\text{EI-CO (idle) vs (H, } T_{10}, \text{RSMD)} \quad Y = 45.7 \left(\frac{H}{14.25} \right)^{-1.41} \left(\frac{T_{10}}{355} \right)^{.389} (\text{RSMD})^{.211}$$

Figures 6.75 and 6.76 show effects of fuel properties on HC emissions at idle. Data from Jet A1/B2 and L-H Tar Sand were deleted due to suspected errors in measurement. Trends once again demonstrate the strong influence of fuel hydrogen content and droplet size on hydrocarbon emissions.

EI-HC (idle) vs H Content (%): $Y = 78.2 - 5.28 x$; $\sigma = 4.31$

EI-HC (idle) vs T_{10} (K): $Y = .0797 x - 23.3$; $\sigma = 7.49$

EI-HC (idle) vs RSMD: $Y = 18.2 x - 13.6$; $\sigma = 1.98$

EI-HC (idle) vs (H, T_{10} , RSMD):

$$Y = 2.13 \left(\frac{H}{14.25} \right)^{-1.98} \left(\frac{T_{10}}{355} \right)^{0.526} (RSMD)^{1.38}$$

Figures 6.77 to 6.87 show effects of fuel properties on CO and HC emissions for 5% bleed with 1.9 FN fuel nozzles, bill of materials with 2.2 FN injectors and 5% bleed with 2.2 FN injectors. Trends similar to bill of materials with 1.9 FN injectors were observed in all cases.

6.4.2 Combustion Efficiency

Figures 6.88 through 6.90 show combustion efficiency variation with air loading parameters. Figures 6.91 and 6.92 show effects of fuel properties on idle combustion efficiency for bill of material configuration with 1.9 FN nozzles after deleting the Jet A1/B2 and L-H Tar Sands data. Trends indicate strong correlation with both hydrogen content and relative droplet size.

Idle η (%) vs H Cont (%): $Y = 88.4 + .719 x$; $\sigma = 0.50$

Idle η (%) vs T_{10} (K): $Y = 102.4 - .0112 x$; $\sigma = 0.96$

Idle η (%) vs RSMD: $Y = 100.7 - 2.38 x$; $\sigma = 0.28$

Idle η (%) vs (H, T_{10} , RSMD):

$$Y = 97.6 \left(\frac{H}{14.25} \right)^{0.0268} \left(\frac{T_{10}}{355} \right)^{0.00635} (RSMD)^{-0.0316}$$

Figures 6.93 and 6.94 show correlations relating combustion efficiency at 7% power with fuel hydrogen content, volatility and fuel spray quality, the test corresponding to constant 7% (EPA recommended) idle condition. Combustion efficiency for bill of materials combustor with 1.9 FN fuel nozzles correlates with fuel properties as follows:

Idle η (%) vs H Cont (%): $Y = 93.7 + 0.386 x$; $\sigma = 0.44$

Idle η (%) vs T_{10} (K) : $Y = 101.2 - 0.00607 x$; $\sigma = 0.62$

Idle η (%) vs RSMD: $Y = 100.6 - 1.53 x$; $\sigma = 0.21$

Figures 6.95 to 6.99 show effects of fuel properties on idle combustion efficiency for 5% bleed with 1.9 FN nozzles, bill of materials with 2.2 FN nozzles and 5% bleed with 2.2 FN nozzles.

Trends in each case were similar to bill of materials configuration with 1.9 FN fuel nozzles.

6.4.3 NO_x Emissions

Figure 6.100 shows attempted correlations of take-off NO_x emissions corrected to 0.0063 lb H₂O/lb air standard humidity, for the bill of material combustor with 1.9 FN fuel system. Reduced hydrogen content of fuel results in marginal increases in NO_x emissions which also appear to be slightly influenced by spray quality, fuel properties producing a poorer spray resulting in higher NO_x emissions; NO_x emissions appear to be relatively insensitive to volatility expressed as 10% distillation temperatures.

$$EI (NO_x) \text{ vs H Content (\%)} \quad Y = 12.6 - .343 x; \quad \sigma = 1.44$$

$$EI (NO_x) \text{ vs RSMD} \quad Y = 6.56 + 1.30 x; \quad \sigma = 1.41$$

$$EI (NO_x) \text{ vs } T_{10} (K) \quad Y = 10.6 - .00540 x; \quad \sigma = 1.48$$

Similar trends were observed with other combinations of combustors and fuel systems, Figures 6.101 to 6.103.

6.4.4 Smoke Emissions

Figures 6.104 and 6.105 show variation of smoke emissions across the engine operating range for the ten fuels investigated, with bill of material configuration and 1.9 FN fuel nozzles. Figures 6.106 and 6.107 show correlations of Smoke Numbers at take-off condition with fuel hydrogen content, fuel aromatic content and fuel naphthalene content. Trends indicate strong sensitivity not only to aromatic and hydrogen levels, but also to the nature and type of aromatics.

$$SN \text{ vs H Content (\%)} \quad Y = 110.4 - 6.52 x; \quad \sigma = 4.62$$

$$SN \text{ vs Aro. Content (\%)} \quad Y = 11.2 + .455 x; \quad \sigma = 6.49$$

$$SN \text{ vs Napht. Content (\%)} \quad Y = 19.2 + .88 x; \quad \sigma = 3.92$$

$$SN \text{ vs (H, Aro, Napht)}$$

$$Y = 16.8 \left(\frac{H}{14.25} \right)^{1.48} \left(\frac{ARO}{14.5} \right)^{.045} \left(\frac{NAPHT}{0.3} \right)^{.215}$$

Figures 6.108 to 6.113 indicate similar trends of smoke emissions against fuel properties for 5% bleed with 1.9 FN fuel nozzles, bill of materials with 2.2 FN nozzles and 5% bleed with 2.2 FN nozzles.

6.4.5 Liner Metal Temperatures

Liner temperature measurements were obtained with 20 thermocouples located on the cold side of the outer wrapper and transition duct of the liner. As described in Section V, the

thermocouples were located in the primary, intermediate and dilution zones of the combustor and were based on thermal paint tests with the liner at (simulated) PT6A-65 take-off conditions. The liner temperatures, in general, showed wide variations from test to test, at times in an apparently random manner. For example, while some liner temperatures appeared to increase with decreasing hydrogen content at some power settings, at other settings the reverse occurred. These effects are thought to be the result of local fuel-air ratios and flame fronts being influenced by fuel properties. While all the 20 thermocouples were operative in all fuel cases during the atmospheric rig conditions, six of the thermocouples (No's 1, 5, 6, 10, 11 and 14) were erratic and at times inoperative during the gas generator tests. For purposes of analysis, data from all 20 liner thermocouples were considered from atmospheric rig measurements, while data from 14 thermocouples were considered from gas generator tests.

Figures 6.114 and 6.115 show variations of average differential liner temperatures ($T_L - T_3$) with calculated combustor exit temperatures for the ten test fuels, using 1.9 FN nozzles and bill of materials combustion system. From these plots average differential liner temperatures corresponding to the take-off combustor exit temperature of 1326K were interpolated. Figures 6.116 and 6.117 show the effects of fuel hydrogen content, volatility and aromatic content on average differential liner temperatures at take-off. A strong influence of hydrogen and aromatic contents was observed, similar to atmospheric pressure tests.

$$(T_L - T_3)_{\text{Ave}} \text{ vs H Content (\%)} \quad Y = 410 - 15.1 x; \quad \sigma = 8.33$$

$$(T_L - T_3)_{\text{Ave}} \text{ vs Aromatic Content (\%)} \quad Y = 179.5 + 1.12 x; \sigma = 7.50$$

Figure 6.118 expresses the same data in terms of liner temperature parameter $(T_L - T_{LJP4}) / (T_{LJP4} - T_3)$, trends once again showing strong influence of fuel hydrogen and aromatic contents.

$$\text{LTP vs H Content (\%)}: \quad Y = 1.14 - .0789x; \quad \sigma = .044$$

$$\text{LTP vs Aromatic Content (\%)}: \quad Y = .00583x - .0634 \quad \sigma = 0.039$$

Figures 6.119 and 6.120 show effects of fuel properties on peak differential liner temperatures expressed as $(T_L - T_3)$ peak, trends once again showing strong influences of fuel hydrogen content and aromatic content.

Figures 6.121 to 6.135 are plots of average and peak differential liner temperatures as functions of fuel properties sequentially for 5% bleed with 1.9 FN nozzles, bill of materials with 2.2 FN nozzles and 5% bleed with 2.2 FN nozzles. In each case both average and peak differential liner temperatures appear strongly influenced by fuel hydrogen and aromatic contents.

6.4.6 Pattern Factors and Radial Profiles

Exit temperature distributions with the gas generator were measured by traversing downstream of the compressor turbine, at conditions corresponding to 100% power condition. Figure 6.136 shows variations in relative turbine exit radial profile factor with fuel hydrogen content, fuel volatility and relative droplet size for bill of material configurations with 1.9 FN fuel injectors. The trends once again indicate significant influence of hydrogen content and relative droplet size as follows:

$$\text{RPF vs H Content (\%)} \quad Y = 1.87 - .0570x; \quad \sigma = 0.150$$

$$\text{RPF vs RSMD} \quad Y = 0.756 + 0.294x; \quad \sigma = 0.119$$

Thus, reduced hydrogen content and fuel properties increasing droplet size both result in larger radial profile factors. Figure 6.137 indicates relative insensitivity of relative turbine exit pattern factor to fuel properties. Figures 6.138 to 6.143 show variations of radial profile and pattern factors for other combinations of combustor and fuel injector system. In all cases radial profile factors appear significantly influenced by fuel hydrogen content and fuel relative droplet size. As with atmospheric data, pattern factor results are inconclusive, in some cases showing influence of fuel properties and in other cases small influence accompanying a lot of data scatter.

6.5 Comparison of Results

Three significantly different combustion systems have been investigated for the effects of fuel composition on combustor performance. Table 6.3 summarizes the tests conducted on the three combustion systems. Significant effects of fuel properties have been identified in the following areas:

- Emission increases (CO, HC, NO_x and smoke)
- Combustion efficiency (at idle) decreases
- Liner temperatures increase, which can result in reduced liner life
- Reduced starting capability
- Reduced flame stability, i.e. poorer lean limit performance

Other parameters have also been investigated for fuel effects, with mixed results. These include carbon deposition, nozzle coking and combustor exit temperature distribution. Flame radiation measurements were confined to the can combustion system and showed significant increases with poorer quality fuels. Alternate fuels (Shale, Tar Sands, etc) generally exhibited effects corresponding to changes in individual fuel properties relative to current specification fuels. In the following sections, an attempt has been made to compare the performances of the three combustion systems, together with observed effects on

straight-through annular combustion systems, mainly from the General Electric investigations described in References 4, 5, and 12.

6.5.1 Idle Combustion Efficiency

Combustion efficiency is a measure of the effectiveness in which chemical reactions between the fuel and air are completed within a given volume. The effectiveness is strongly influenced by fuel preparation, evaporation and reaction rates. At high power conditions, operation of most fuel injectors is optimum and vaporization of the fuel is enhanced by high combustor inlet temperatures, thus resulting in high combustion efficiency. At low power conditions, such as idle, the same factors result in reduced combustion efficiencies.

The present investigations have demonstrated hydrogen content of the fuel significantly influencing combustion efficiency at idle. Figure 6.144 shows combustion efficiency variations with respect to hydrogen content for turboprop PT6A, turbofan JT15D and corresponding can combustor simulations. The similarity of trends between the three combustion systems indicate that in all cases reduced hydrogen content of the fuel results in lower combustion efficiency at idle.

Figure 6.145 shows the influence of fuel volatility on combustion efficiency at idle. It appears from these comparisons that the magnitude of the volatility effect varies with the type of combustor and the fuel injector operation. Generally, however, poorer volatility (i.e. higher distillation temperature) results in reduced combustion efficiency. The large scatter in data is also evident in Figure 6.146 which shows a plot of $(1-\eta)/(1-\eta)_{JP4}$ against T_{10} temperatures¹². One reason for the scatter may be the varying contributions of hydrocarbon and carbon monoxide fractions to the combustion inefficiency, these two being influenced to varying degrees by the different boiling fractions.

Figure 6.147 shows the effect of droplet size on combustion efficiency at idle. The comparisons generally indicate a strong influence as well as the effect of combustor characteristics. It is interesting in the PT6A comparison that the bill of material and 5% bleed configurations show trends with significantly different slopes, whereas changing the fuel injector does not appear to change the slope of the trend lines. The trends of the can combustor variations appear similar to those of the JT15D-5 turbofan combustion systems, whereas they are significantly different to those of the PT6A-65 turboprop combustion systems. The differences in surface to volume ratios between the combustion systems do not appear to explain this performance variation. It is most likely that the differences in fuel injection methods are a contributory factor: the can combustor and JT15D having axial fuel injection, whereas PT6A has tangential fuel injection.

6.5.2 CO and HC Emissions

Carbon monoxide may be found in the exhaust either as a product of incomplete combustion or as a product resulting from frozen equilibrium. Thus it may be a function of residence time and reaction rates, or may result from quenching mechanisms at cool surfaces and dilution planes. As with combustion efficiency, CO emissions correlate well with SMD and volatility. Figure 6.148 presents comparisons of nondimensional SMD effects for various combustors¹². Annular combustors with airblast injectors (F101 and J79-17C) show stronger effects than annular combustors with pressure atomizing injectors (J79-17A and TF39). Both the reverse flow annular combustors with pressure atomizers (PT6A and JT15D) show stronger effects than straight-thru annular combustors with pressure atomizing systems.

Figure 6.149 shows comparison of fuel hydrogen effects for various combustors, once again, reverse-flow annular combustors show stronger effects than annular combustors^{4,5,12}. Figure 6.150 shows comparison of hydrogen effect on CO emissions for various atomizers using the PWC can combustor. The stronger effects of hydrogen content for airblast and vaporizing systems are evident from this comparison. This agrees with the generally observed behaviour with large engine combustors wherein emissions of carbon monoxide were more sensitive to fuel composition in experimental low emission combustors with advanced fuel injection systems than they were in more conventional combustors.

Figure 6.151 shows a comparison of fuel volatility effects for various combustors. In all cases, reduced volatility increases CO emission levels. The PT6A combustion system showed less sensitivity to volatility than the JT15D system.

Unburnt hydrocarbons in the exhaust may be due to poor atomization, poor mixing, insufficient evaporation and quenching of reactions in cool zones. Results from present programs generally indicate poor trends with fuel properties. Similar trends have been observed on other combustion systems as well, Figure 6.152. An exception appears to be the F101 combustor which shows good HC trends with SMD as well as volatility. The poor trends in many combustors would suggest that the presence of hydrocarbons in these combustors is much more a function of mixing/quenching than fuel properties.

6.5.3 NO_x Emissions

Oxides of nitrogen resulting from the combustion of hydrocarbon fuels may be formed by any of the following mechanisms. Prompt NO is usually a very small part of total NO_x production and is a result of reactions between hydrocarbon fragments and molecular nitrogen under rich mixture conditions. Thermal NO_x is formed by the reaction of O₂ and N₂ in air, whereas organic NO_x is the result of oxidation of fuel bound nitrogen. Since the fuels investigated did not contain significant bound-nitrogens, thermal NO_x may be considered to be main mechanism of NO_x formation. Temperature is by far the major factor contributing to the

formation of thermal NO_x . From a kinetic viewpoint, the formation is generally expressed in terms of the Zeldovich mechanism



Both the above reactions are strong functions of temperature, so much so, nearly all the thermal NO_x is produced at the highest temperature within the combustor. Figure 6.153 shows variations of maximum temperature during reaction as a function of hydrogen content, corresponding to PT6A-65 take-off condition. Since maximum reaction temperature increases as the fuel hydrogen content is reduced, the general trends are for NO_x to increase as hydrogen content is reduced. Figure 6.154 shows comparison of fuel effects on NO_x emissions for various combustion systems¹². In most cases NO_x decreases with increasing hydrogen content. The can combustor data, however, show NO_x emissions to be largely insensitive to fuel hydrogen content. The PT6A-65 trends show NO_x sensitivity to hydrogen content despite a lot of data scatter. Idle NO_x emissions with all three combustion systems show increases with hydrogen content, which is probably the impact of reaction zone temperatures being affected by combustor efficiencies at idle. The differences in sensitivity between the can and the PT6A-65 reverse flow annular combustor may be related to combustor design. The J-85 combustion system showed weak influence of hydrogen content, whereas the F101 systems had much stronger dependence of NO_x emissions on hydrogen content.

6.5.4 Smoke Emissions

Measurements of smoke emissions with both the can and reverse-flow-annular combustion systems indicate a strong influence of both fuel aromatic and hydrogen contents (Sections III and 6.3).

The data with the can combustor also shows that fuels with low naphthalene contents (L-H, H-M, L-M Tar Sands) resulted in correspondingly lower smoke emissions in spite of their high aromatic contents. The results appear to indicate that the types as well as overall levels of aromatics are important, and that the presence of high concentrations of complex multi-ring aromatic compounds may increase the propensity for smoke formation.

Figure 6.155 shows the similarity of smoke trends with hydrogen content for the four configurations of PT6A-65 combustion systems. Figures 6.156 and 6.157 compare PT6A-65 engine and can combustor smoke emissions with data from several other combustion systems^{12, 14}. As shown in Figure 6.157 the rate of increase of smoke number with decreasing hydrogen content is essentially the

same for TF41, F100, F101 and TF33. However, the ratio for TF30, J79, PT6A-65 and PWC can combustors are about twice as great. The trends are believed to be geometry related.

The influence of fuel injector design on smoke emissions was investigated with the can combustor. The data presented in Section III (Figure 3.18), show that airblast and vaporizing fuel nozzles resulted in lower smoke emissions and were less sensitive to hydrogen content than pressure atomizing systems. These trends are consistent with other data comparing performance of airblast and pressure atomizing combustion systems¹².

6.5.5 Ignition Characteristics

The ignition of liquid fuel in a gas turbine combustor is a complicated process depending on atomization, pyrolysis, and evaporation. Since the ignition of a combustible mixture takes place in the gas phase, the liquid fuel will have to be evaporated prior to ignition. For a constant energy supply from an ignition source, the gas phase fuel-air ratio in the ignition region will be the primary rate-controlling parameter and this is the result of the evaporation process which depends on volatility of the fuel and the spray characteristics of the injector. Thus the influence of fuel properties on ignition can be discussed in terms of volatility and spray characteristics.

The ignition process in a practical combustor cannot be investigated easily because of the difficulties in making measurements in the immediate ignition region. Ignition characteristics are therefore expressed in more general parameters such as time-to-light, ignition fuel-air ratio, flow velocity, minimum fuel-air temperatures and ignition energy.

Starting characteristics with multi-nozzle combustion systems are dependent not only on initial ignition characteristics but also on the efficiency of flame propagation, or light-around. This once again is a difficult process to characterize; in global terms, one can compare performance with parameters such as time-to-idle and maximum flame/exit temperature.

The can combustor investigations showed strong influences of fuel volatility and relative spray droplet size on minimum ignition fuel-air ratio. The correlation with hydrogen content was generally poor. Since the reverse-flow-annular combustor investigations were undertaken with a full engine having a fixed starting flow, minimum fuel flows for ignition could not be established. Instead, time-to-light, time-to-idle and minimum fuel-air ignition temperatures were compared. Figure 6.158 shows comparison of minimum light-off temperatures of various engines¹². The trends generally indicate poorer performance with increased spray droplet size. Differences in performance of the combustion systems have been attributed to variations of atomization quality at the light off conditions (Ref. 11).

6.5.6 Lean Blow-out Limits

There is comparatively little data available on the influence of fuel properties on the stability limits of combustion. However, ignition and blow-out processes are mechanistically similar. In both cases the gaseous fuel-air ratio is the important parameter. With ignition it is normally the fuel-air ratio near the igniter sparks that is critical, whereas the fuel-air ratio in the stabilizing recirculation zone exerts influence on blow-out characteristics. Present investigations have shown an influence of volatility and relative droplet size on lean limit fuel-air ratios. (Figure 6.158). The effect of hydrogen content seems more pronounced on lean limits than on ignition characteristics (Figure 6.160), possibly because of strong influence of hydrogen content on combustion efficiency of near limit flames. Trends also indicate less sensitivity with multi-fuel-nozzle annular combustion systems than with the single fuel nozzle can combustor; the latter may be due to stronger wall quenching effects and absence of thermal interaction between adjacent injector flows.

6.5.7 Combustor Liner Temperatures

Fuel property effects on average and maximum liner temperatures were investigated. Maximum liner temperature is the proper way of assessing the overall level of fuel effect, in that it can be a measure of liner durability. Figure 6.161 shows a comparison of hydrogen effects on maximum liner temperatures for various combustors¹² and indicates a drawback in this method of comparison. Since the location of flame front varies with the fuel, the instrumentation on the combustor will need to be quite extensive to pick up the location and magnitude of the peak temperature. It appears that the reversal of slope in the JT15D data is a result of insufficient thermocouple instrumentation in determining maximum liner temperatures.

Figure 6.162 shows a comparison of average liner temperatures for various combustors¹². While the trends in Figures 6.161 and 6.162 are similar (except for JT15D), the average liner temperature rise indicates somewhat lower standard errors of estimate. The data on the can combustor (Section III), also showed a good correlation of average liner temperature with fuel hydrogen content.

Figure 6.163 is a comparison of average liner temperature parameter

$$\frac{(T_L - T_{LJP4})}{(T_{LJP4} - T_3)}$$

for a number of aircraft combustors¹³ and clearly establishes the strong effect of hydrogen content on the liner temperature. Plots against aromatic content (Sections III, VI), show good

correlations as well; since aromatic content is generally related to hydrogen content, this agreement is not surprising.

Figure 6.164 is a comparison of fuel hydrogen effects on liner differential temperatures and liner temperature parameters for the various JT15D configurations. While the trends are similar, liner differential temperatures are considerably lower for airblast injectors. Figure 6.165 shows similar comparisons for PT6A-65 configurations, all with pressure atomizing injectors.

A parameter which can be used in durability analysis has been defined as liner severity parameter¹⁴ (LSP):

$$LSP = \frac{T_{metal, Max} - T_3}{T_4 - T_3}$$

When plotted against the hydrogen content of the fuel, the liner severity parameter indicates the sensitivity of liner durability and hot spot temperatures. The comparison in Figure 6.166 shows that for a variety of combustors, the liner severity parameter increases as the fuel hydrogen content is decreased. Although the rate of change of this parameter with respect to hydrogen content is generally small, the magnitude of the parameter differs significantly for each combustor.

Table 6.1: Legend of Symbols used in Section VI Plots

- JP4, JP4/B1, JP4/B2, JP4/2040/DF
- Jet A1, Jet A1/B1, Jet A1/B2, Shale JP8
- △ Tar Sands LL, LH
- ▽ JP10, RJ6, ERBS-3

Table 6.2: Minimum Light-Up Temperatures

Fuel	Temperature K (°F)	
Jet A1	< 231	(-44)
Jet A1/B2	< 228	(-50)
Shale JP8	< 229	(-47)
ERBS-3	239	(-30)
JP4	< 227	(-51)
JP4/B2	< 229	(-48)
Tar Sands L-H	238	(-31)
Tar Sands L-L	243	(-22)
JP10	241	(-26)
RJ6	271	(+27)

Idle CO Emission Index (g/kg)

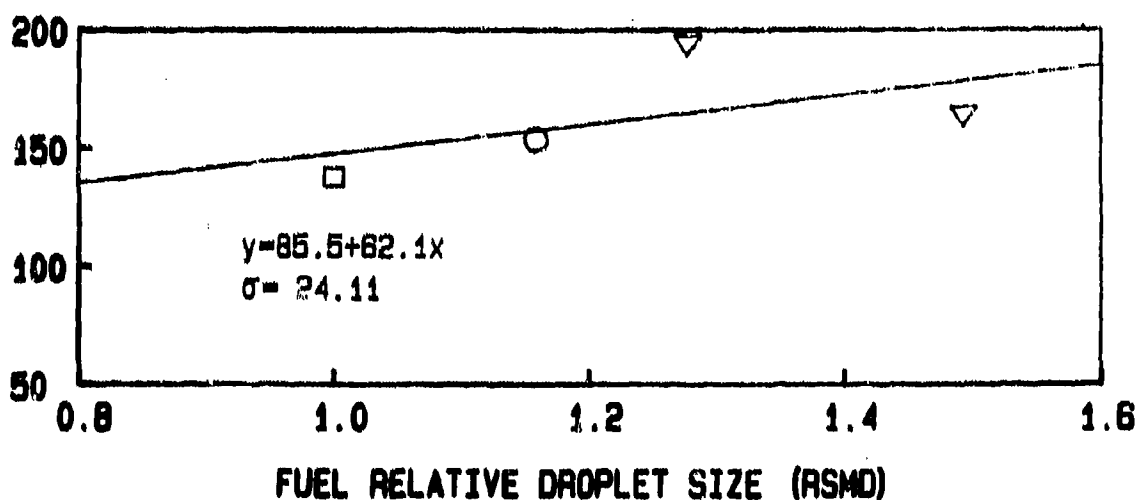
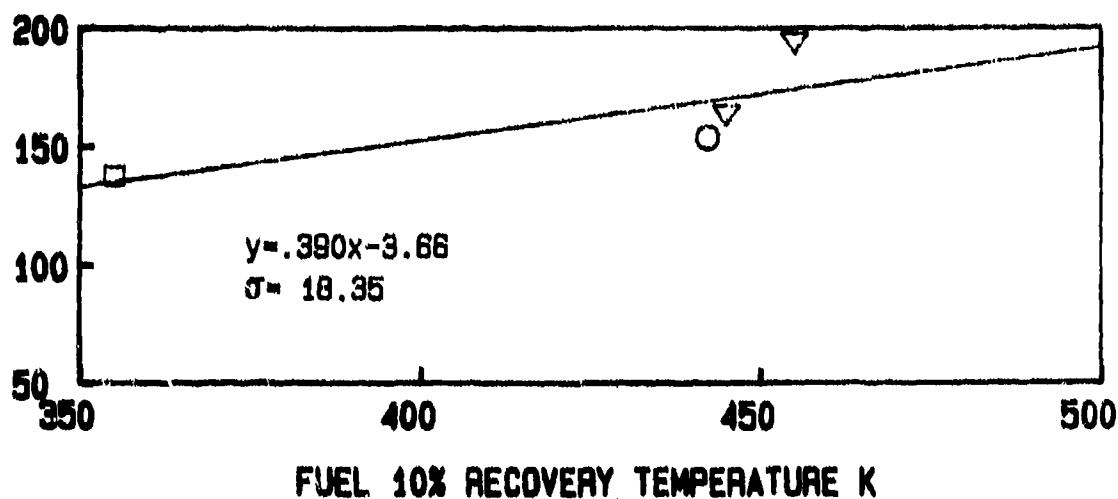
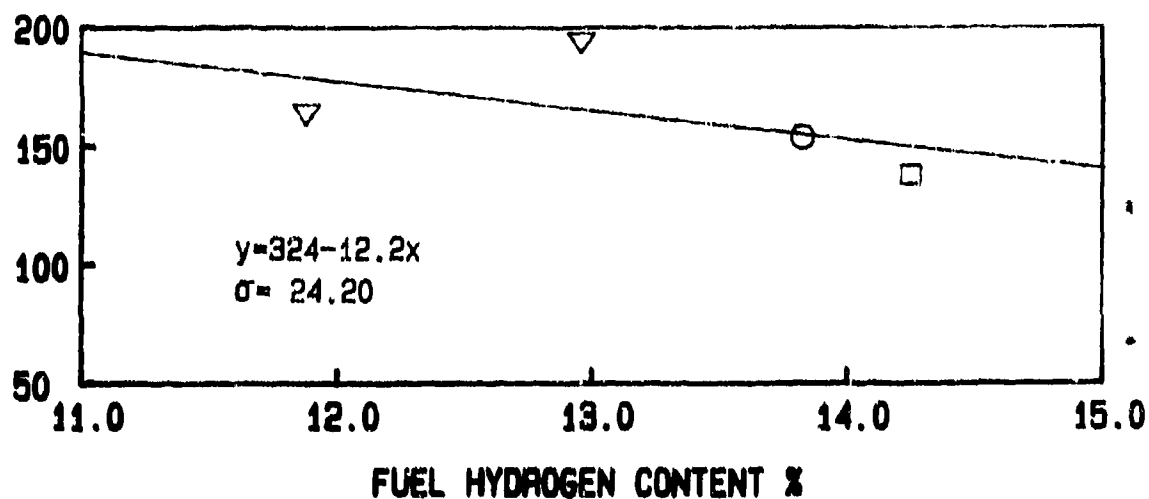


Figure 6.1: Effects of Fuel Properties on Idle CO Emissions
(JT15D-5 Atmospheric, BOM, Simplex 2.25 FN)

Idle HC Emission Index (g/kg)

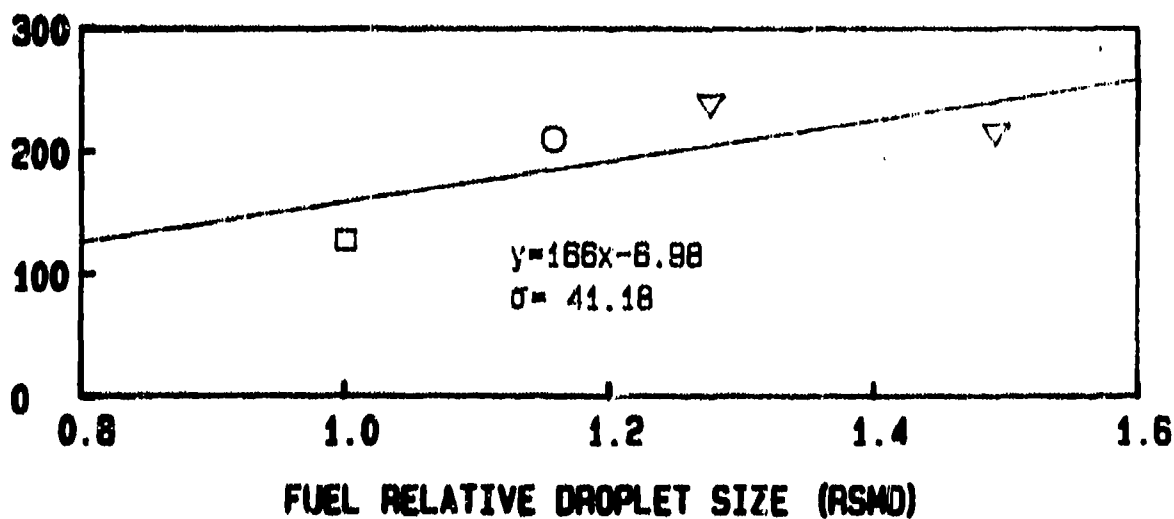
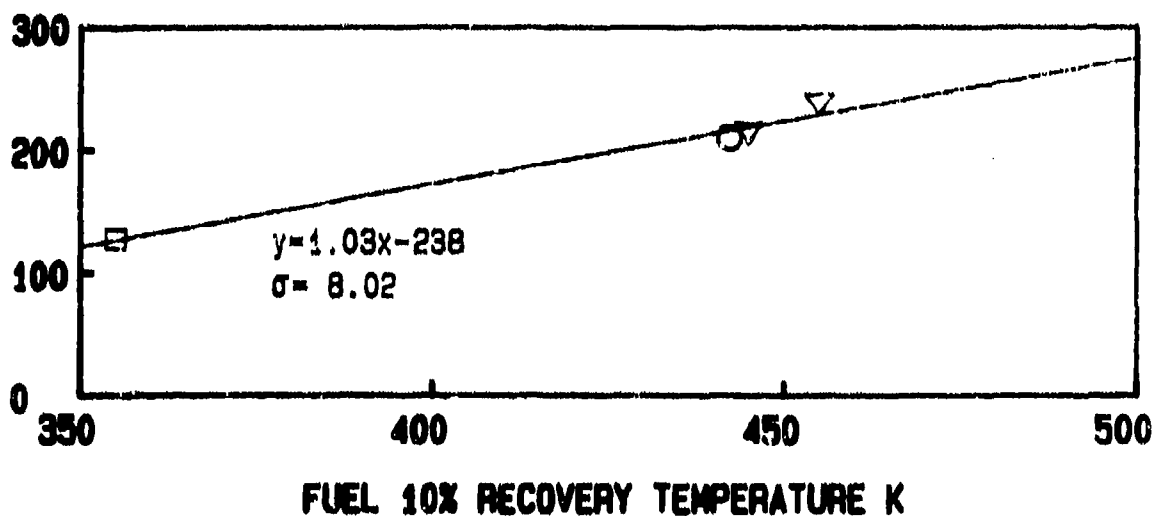
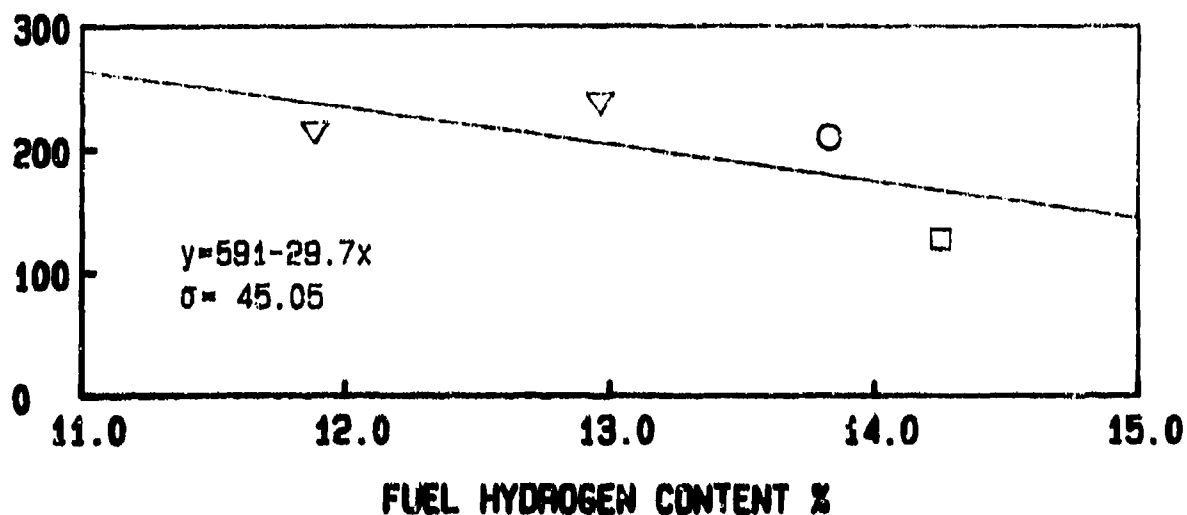


Figure 6.2: Effects of Fuel Properties on Idle HC Emissions
(JT15D-5 Atmospheric, BOM, Simplex 2.25 FN)

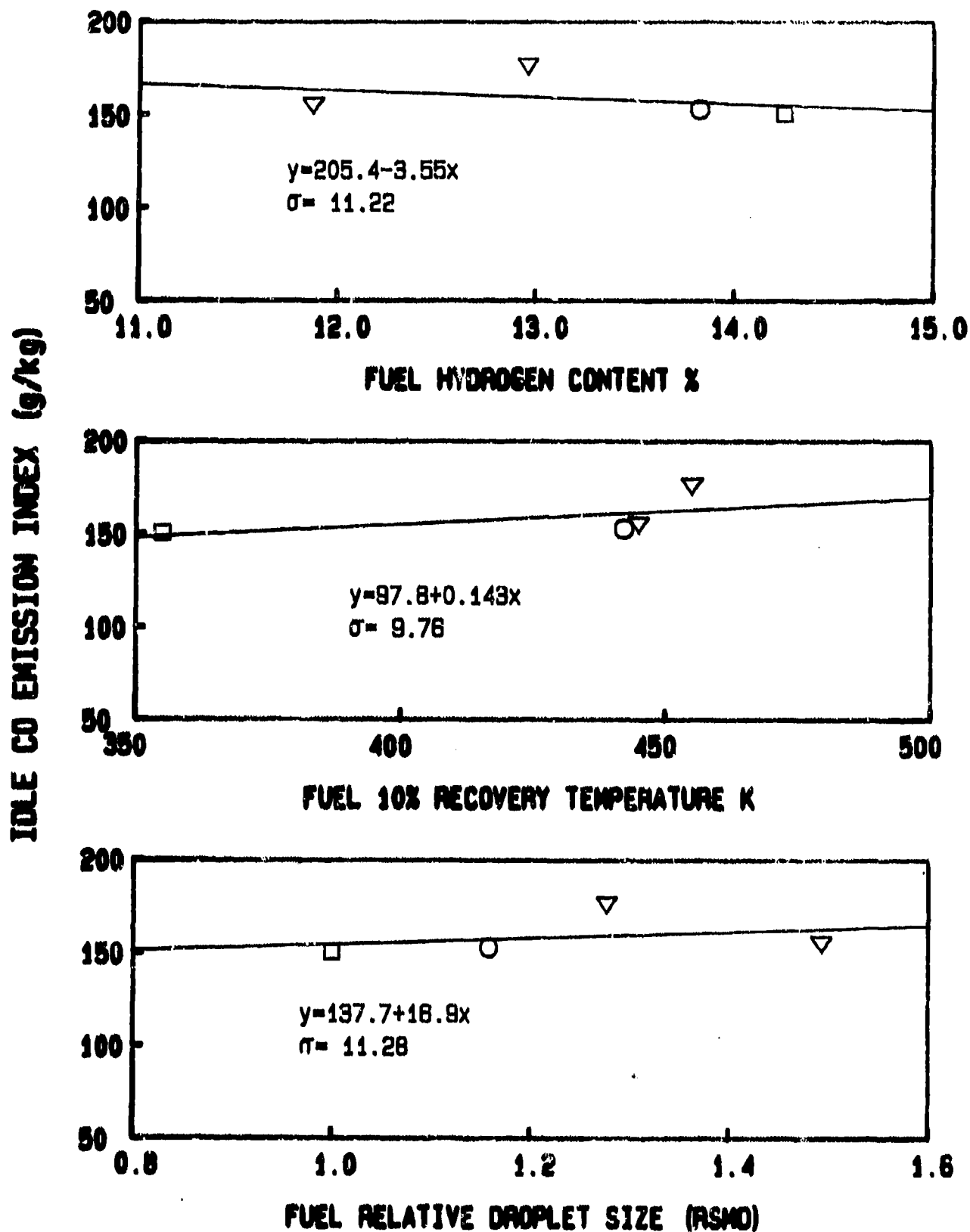


Figure 6.3: Effects of Fuel Properties on Idle CO Emissions
(JT15D-5 Atmospheric, Rich P.Z., Simplex 2.25 FN)

Idle HC Emission Index (g/kg)

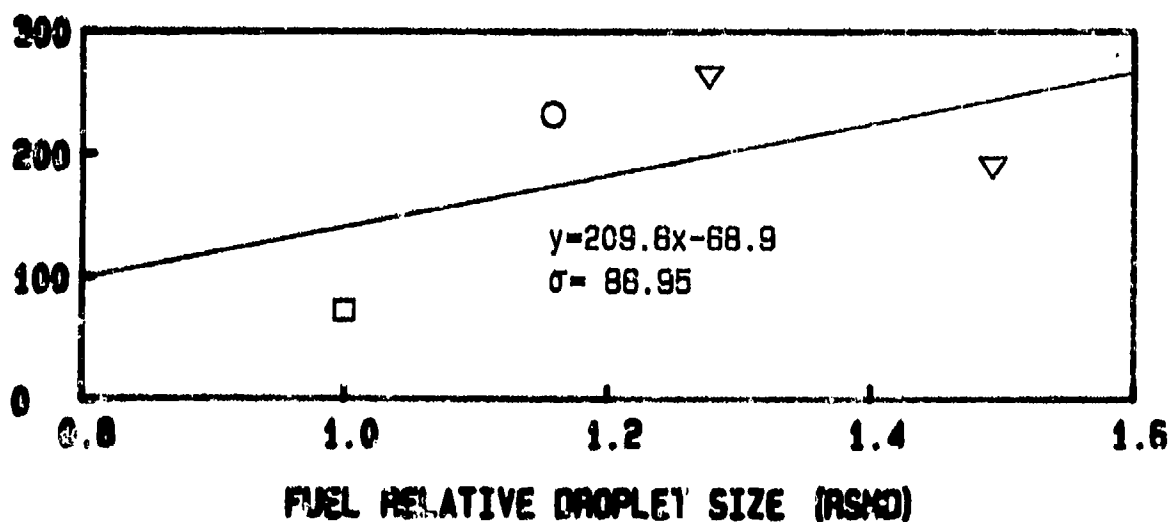
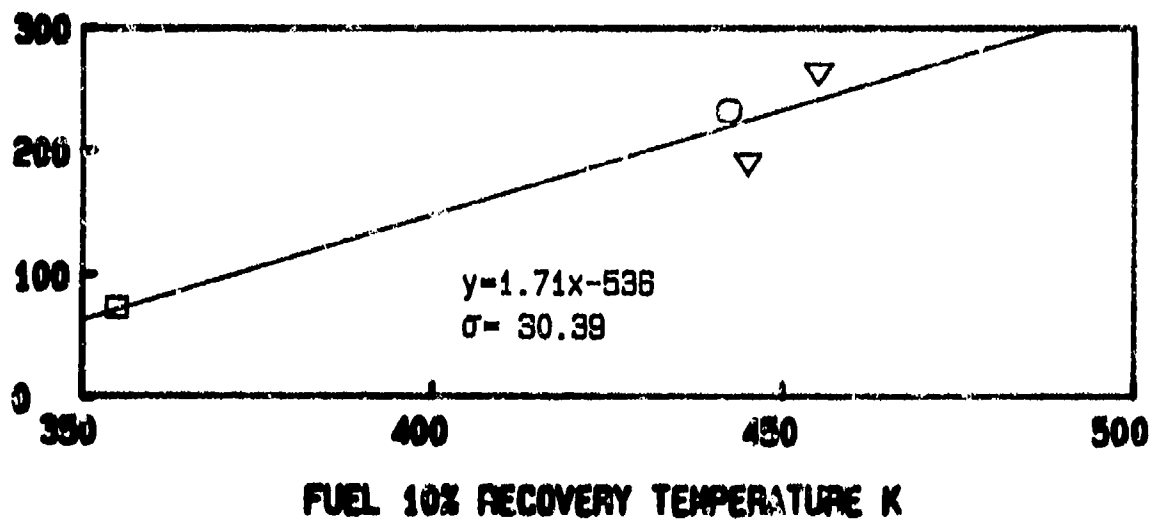
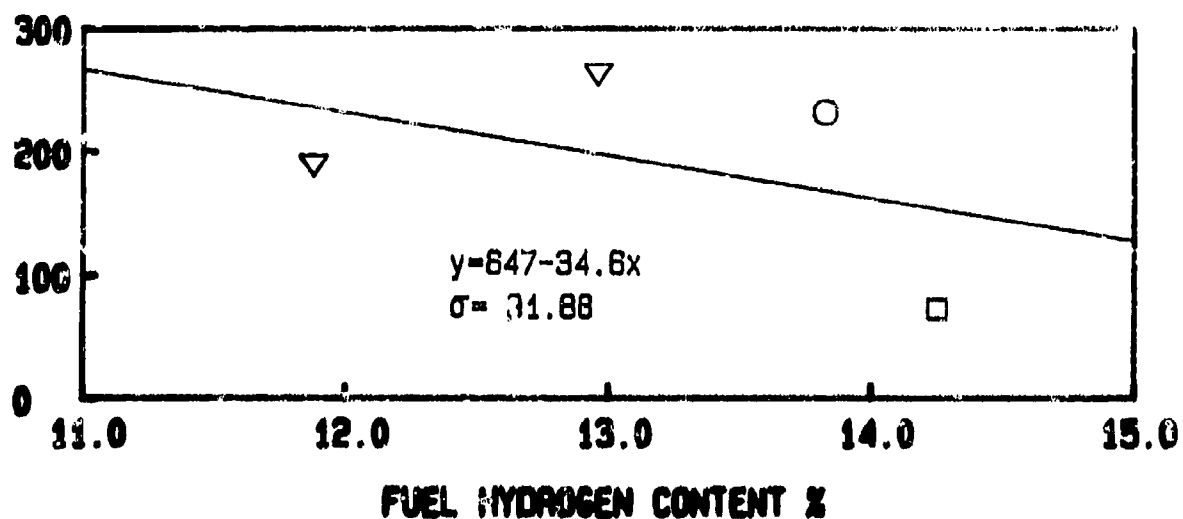


Figure 6.4: Effects of Fuel Properties on Idle HC Emissions (JT15D-5 Atmospheric, Rich P.Z., Simplex 2.00 FN)

30% THRUST CO EMISSION INDEX (g/kg)

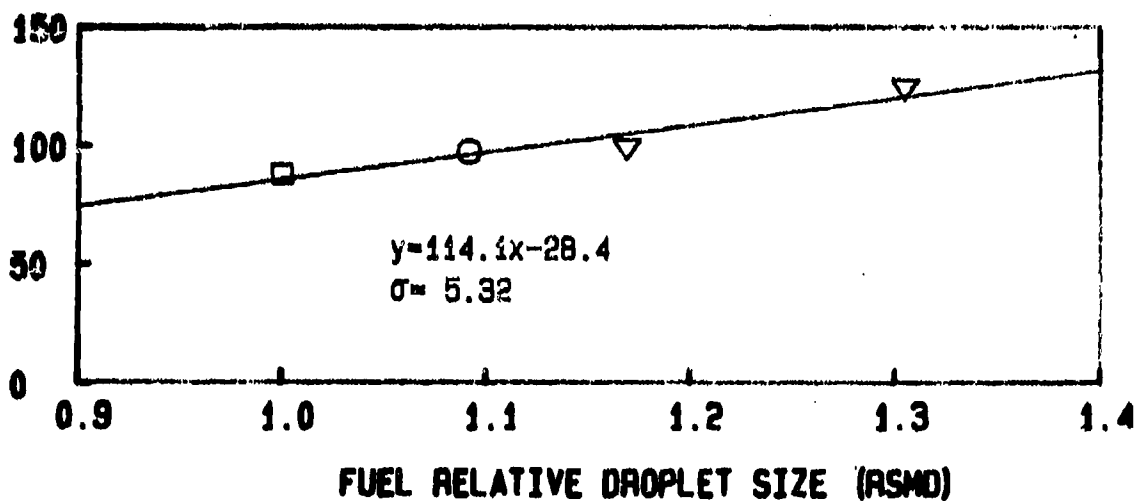
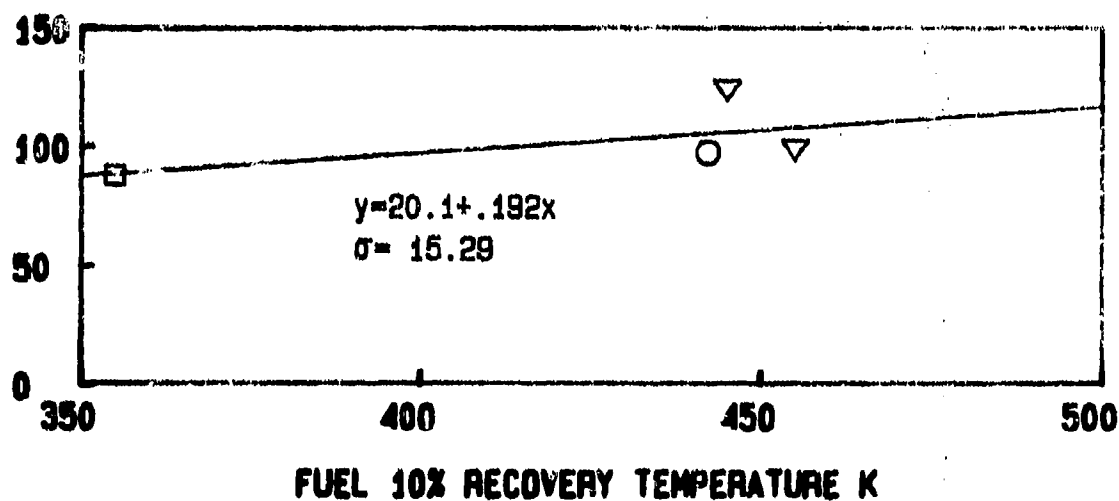
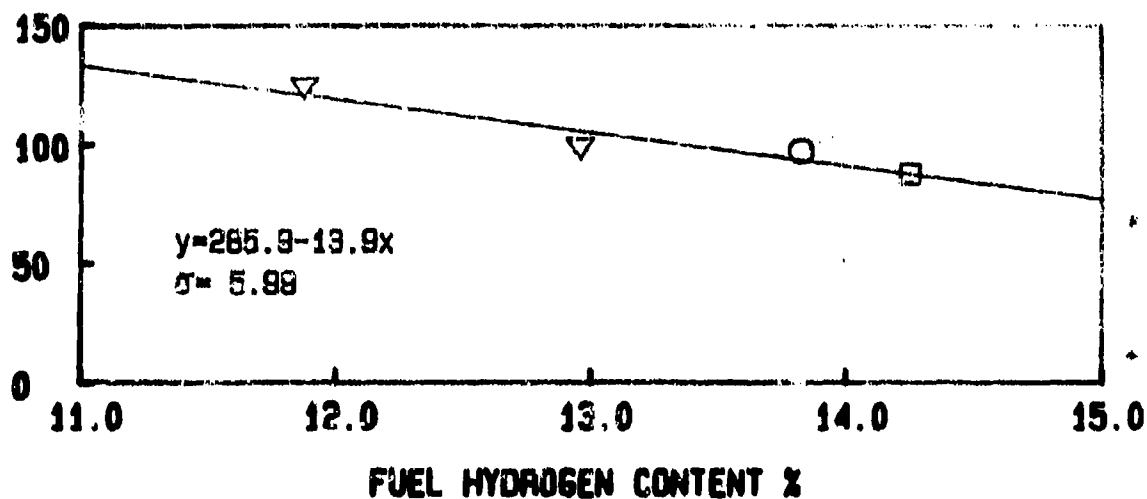


Figure 6.5: Effects of Fuel Properties on 30% Thrust CO Emissions (JT15D-5 Atmospheric, BOM, Airblast Nozzle)

30% THRUST HC EMISSION INDEX (g/kg)

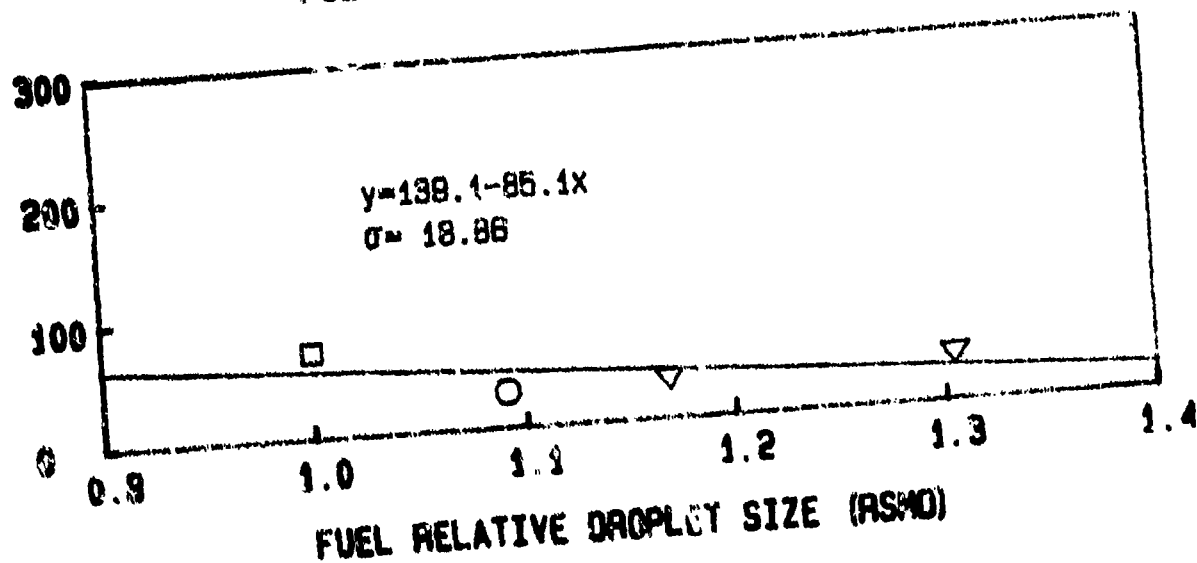
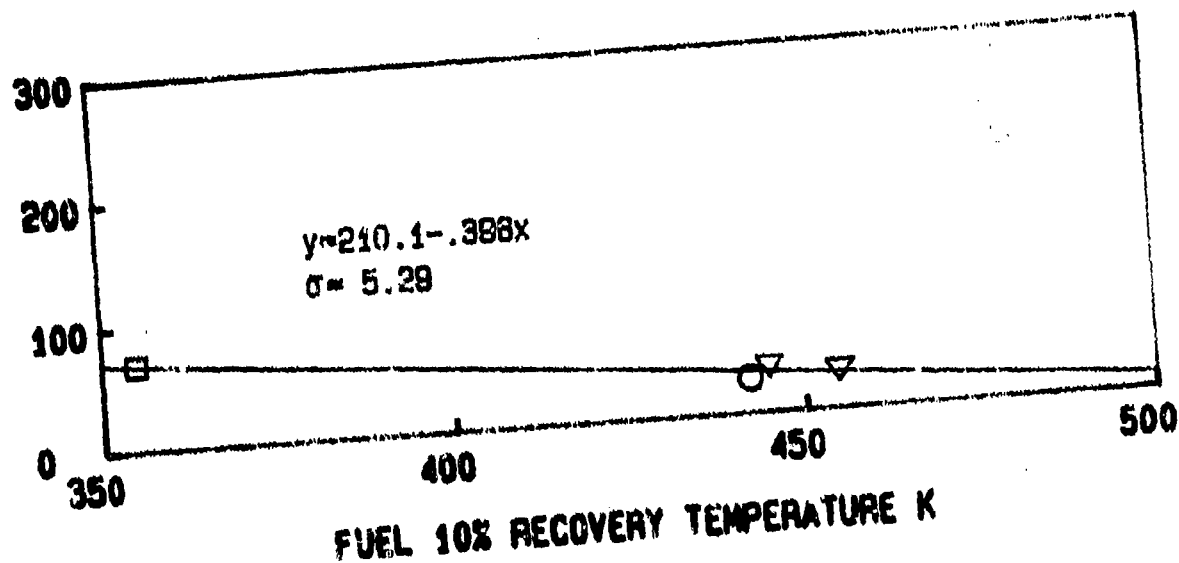
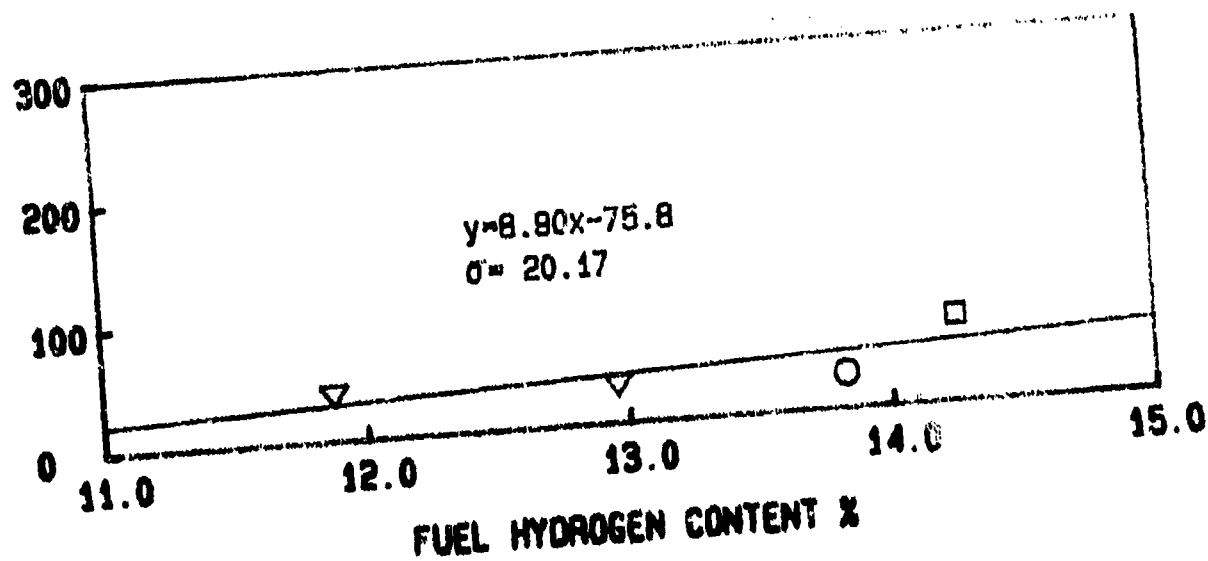


Figure 6.6: Effects of Fuel Properties on 30% Thrust HC Emissions (JTL15D-5 Atmospheric, BOM, Airblast Nozzle)

30% THRUST CO EMISSION INDEX (g/kg)

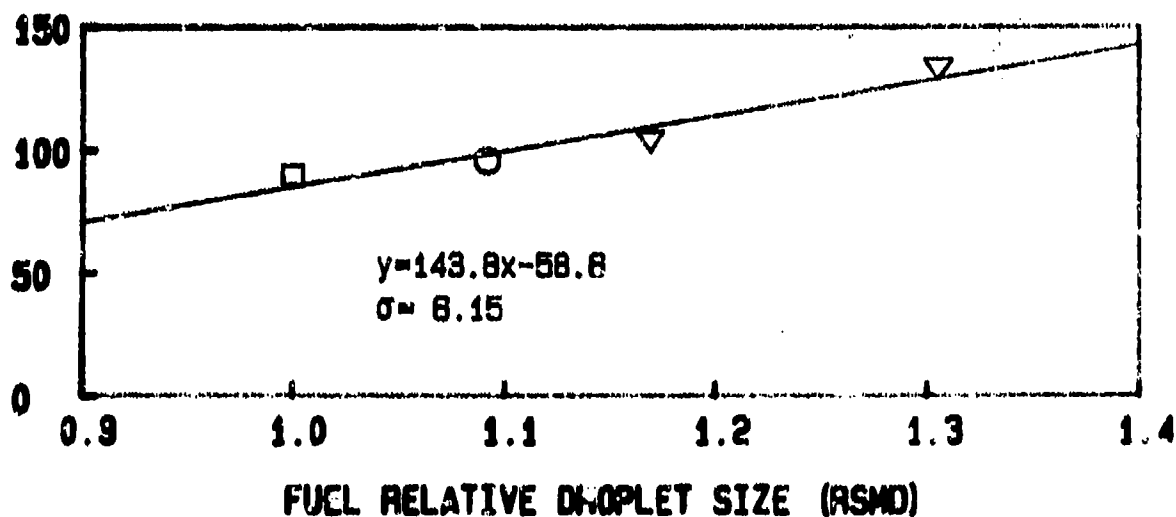
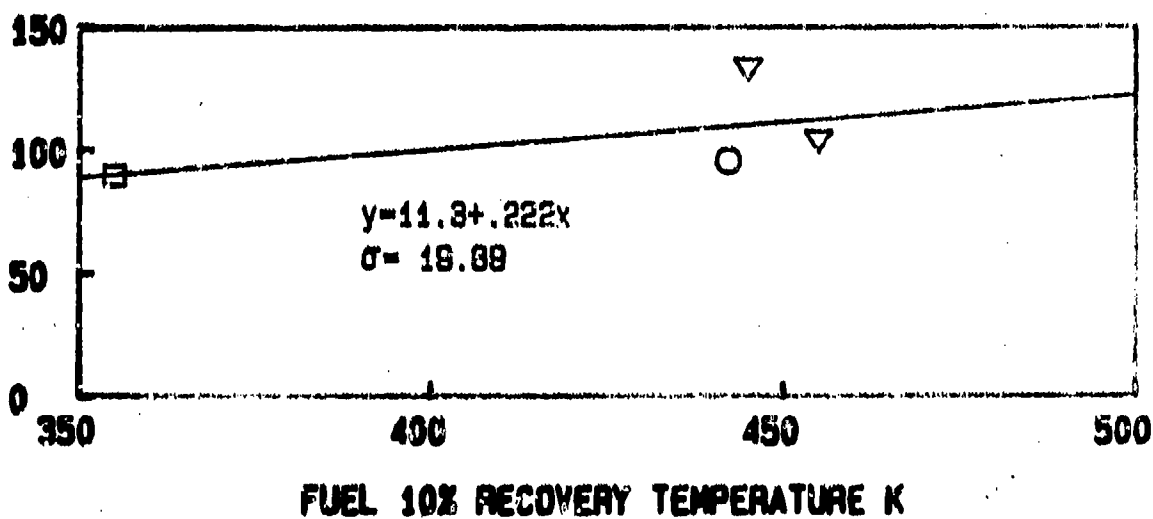
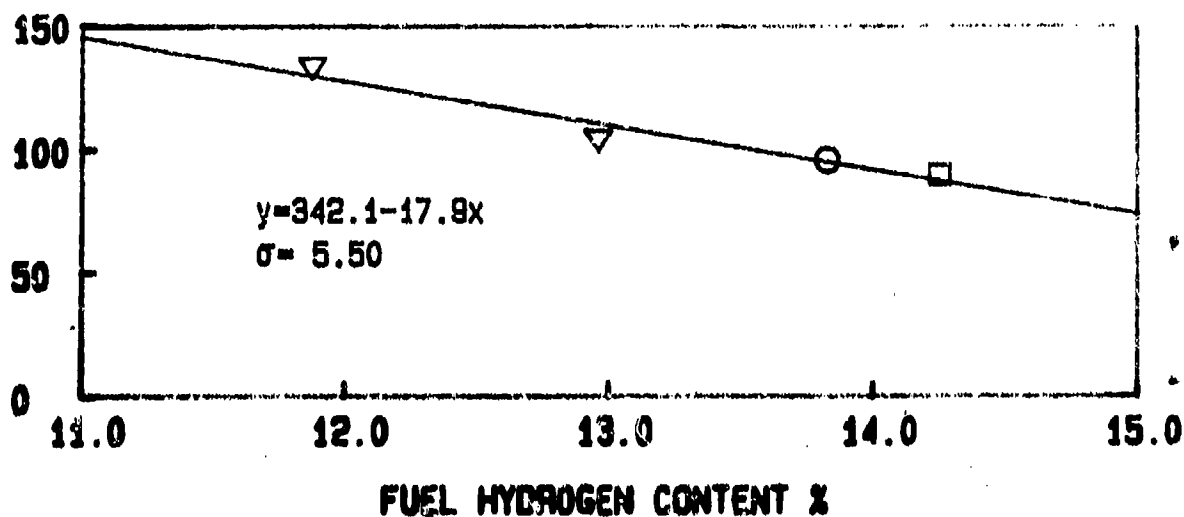


Figure 6.7: Effects of Fuel Properties on 30% Thrust CO Emissions (JT15D-5 Atmospheric, Rich P.Z., Airblast Nozzle)

30% THRUST HC EMISSION INDEX (g/kg)

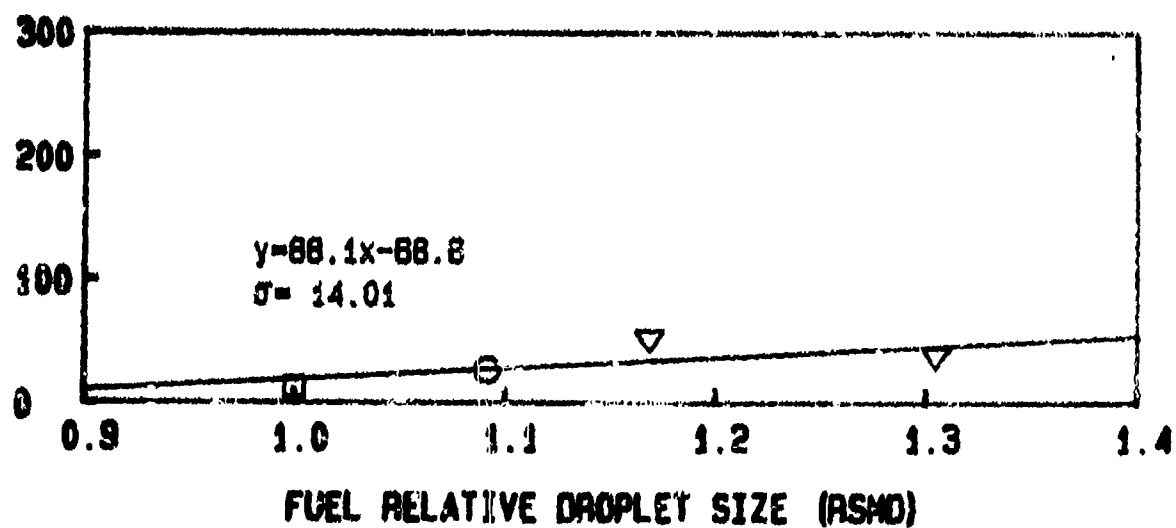
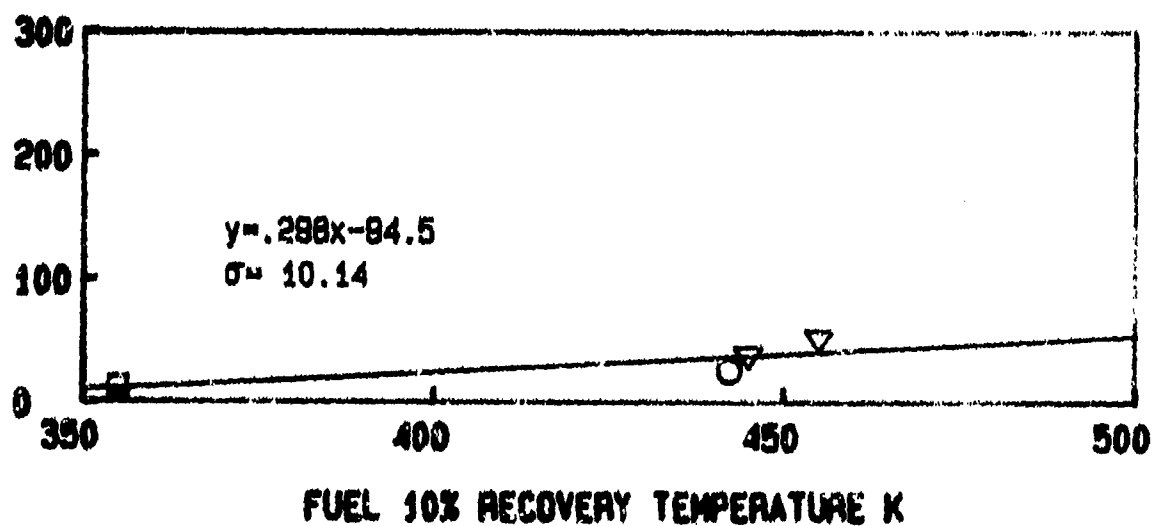
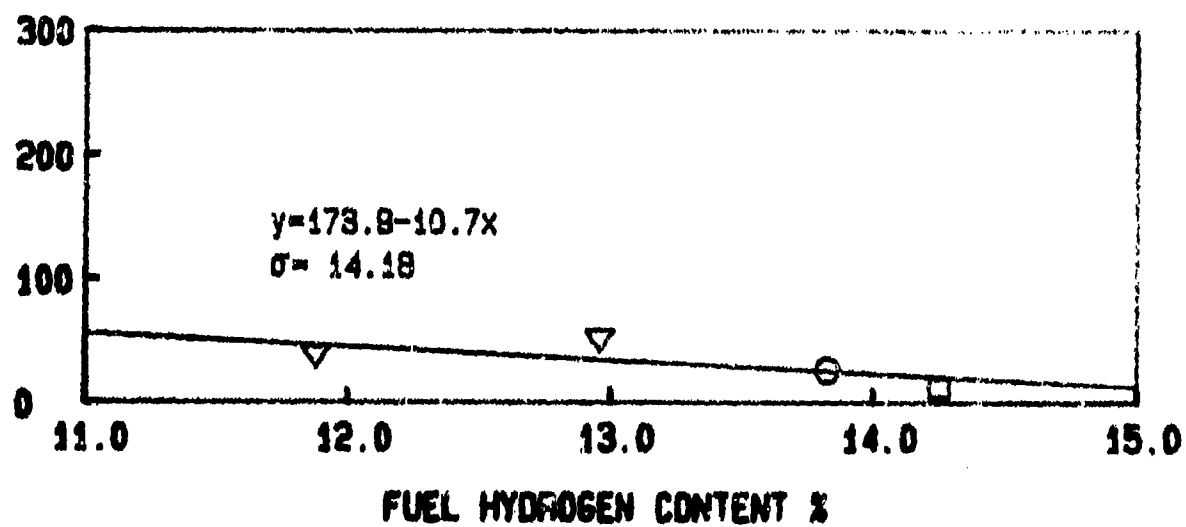


Fig. 3: Effects of Fuel Properties on 30% Thrust HC Emissions (JT15D-5 Atmospheric, Rich P.Z., Airblast Nozzle)

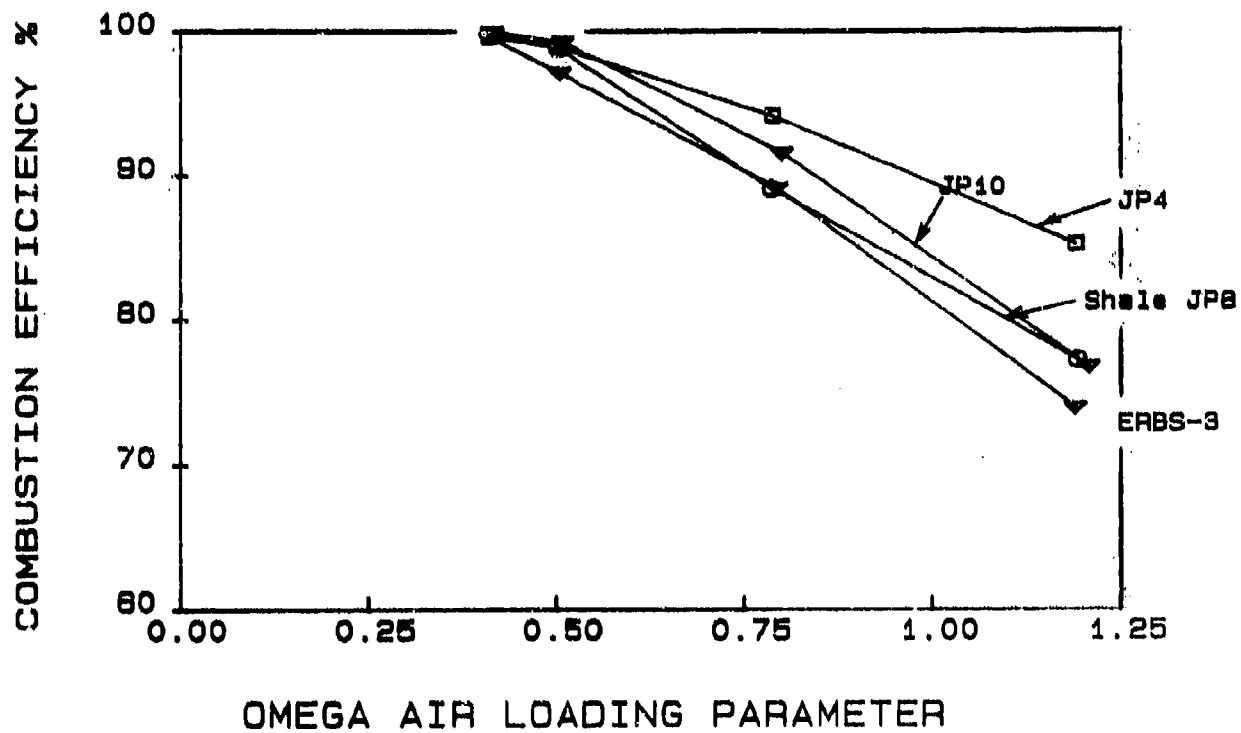


Figure 6.9: Effects of Air Loading Parameter On Combustion Efficiency
(JT15D-5 Atmospheric, BOM, Simplex 2.25 FN)

COMBUSTION EFFICIENCY %, AIRBLAST

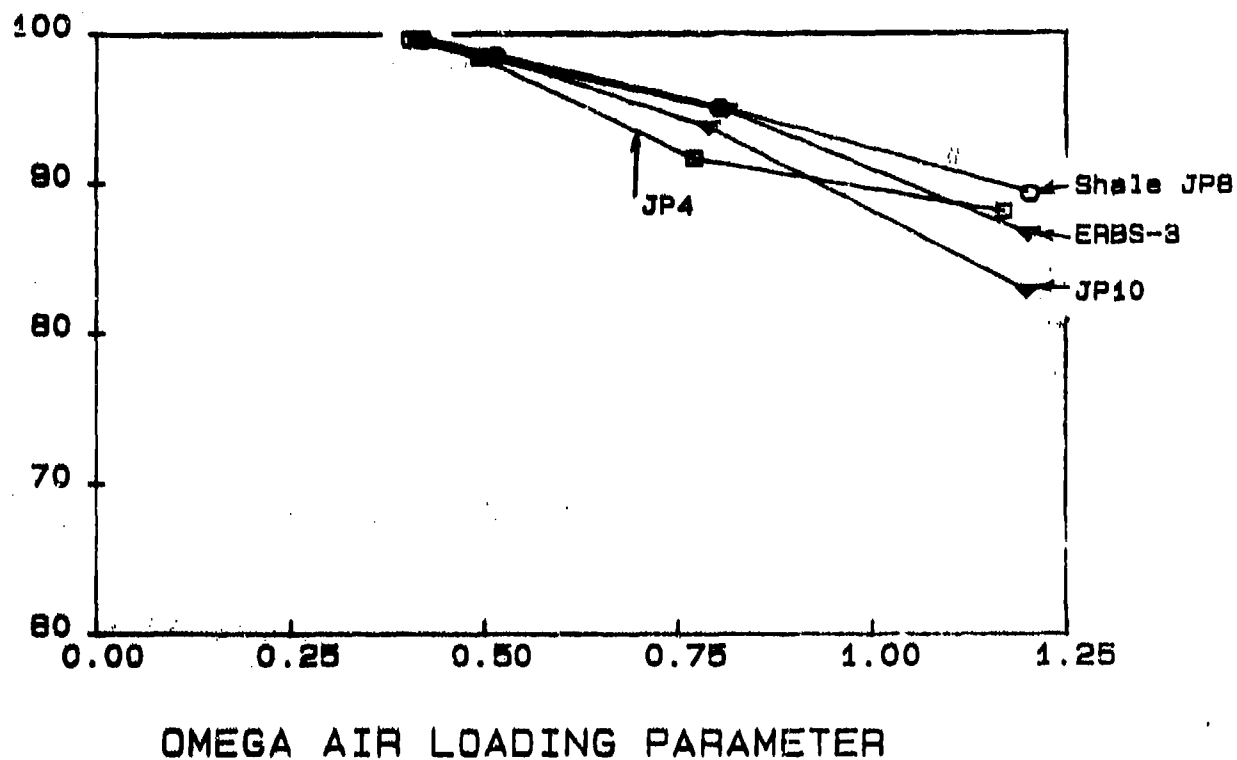


Figure 6.10: Effects of Air Loading Parameter on Combustion Efficiency (JT15D-5 Atmospheric, BOM, Airblast Nozzle)

IDLE COMBUSTION EFFICIENCY %

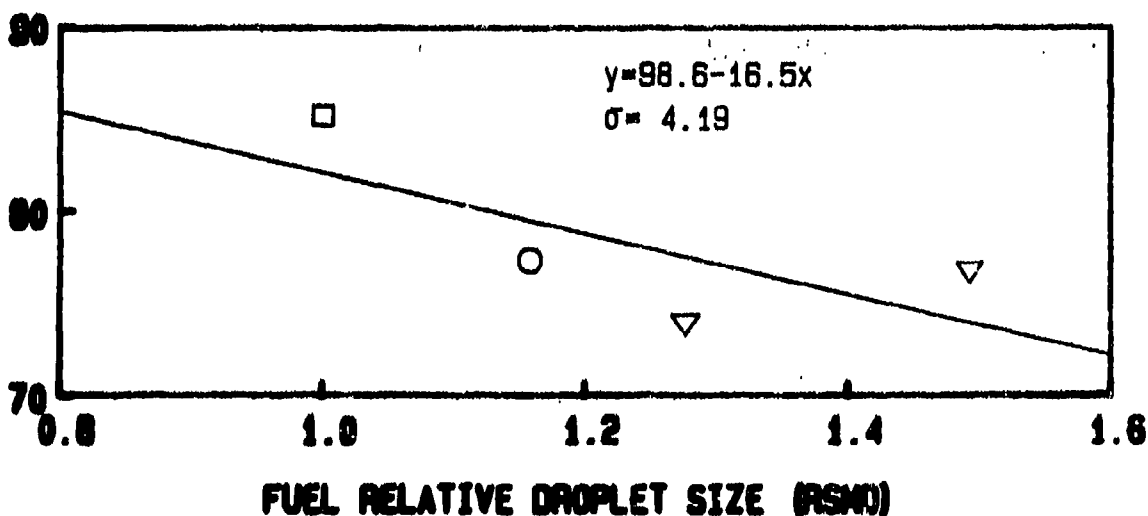
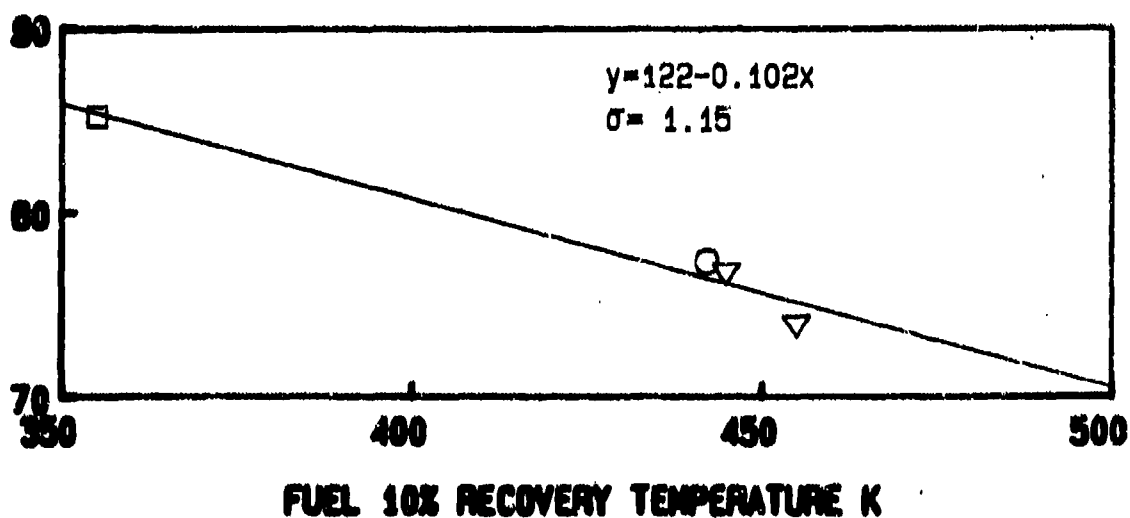
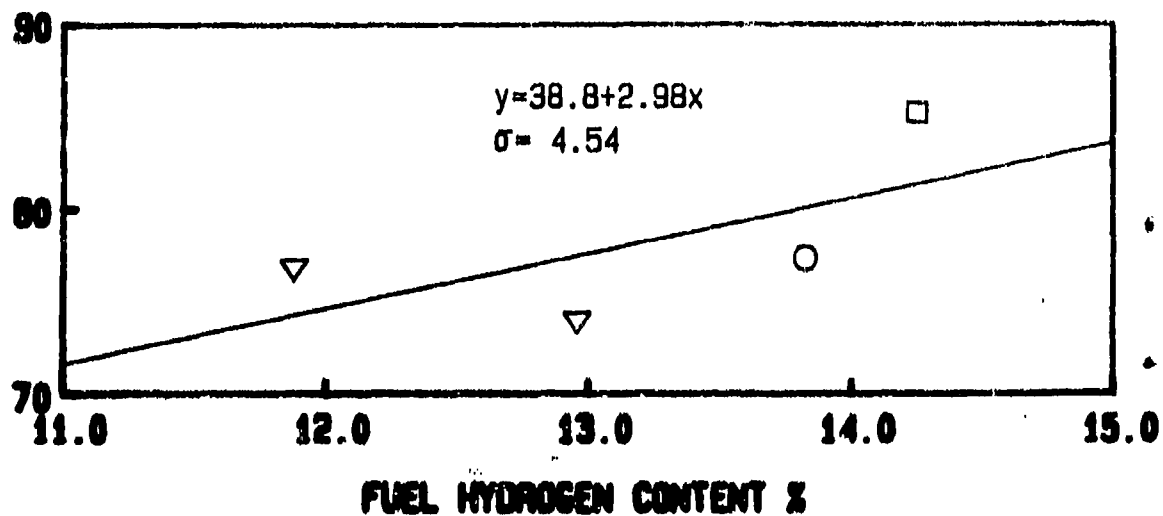


Figure 6.11: Effects of Fuel Properties on Idle Combustion Efficiency (JT15D-5 Atmospheric, BOM, Simplex 2.25 FN)

IDLE COMBUSTION EFFICIENCY %

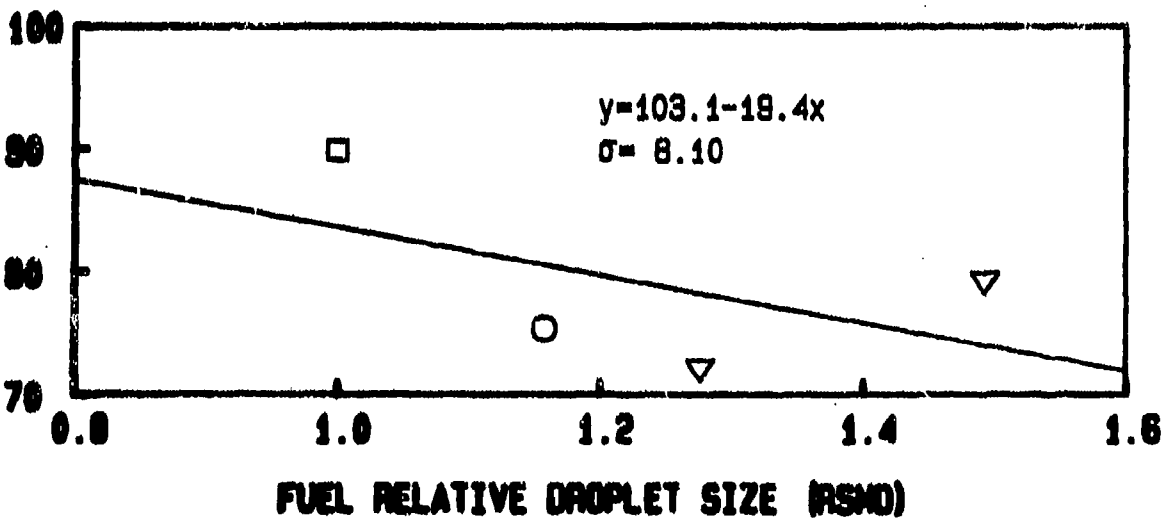
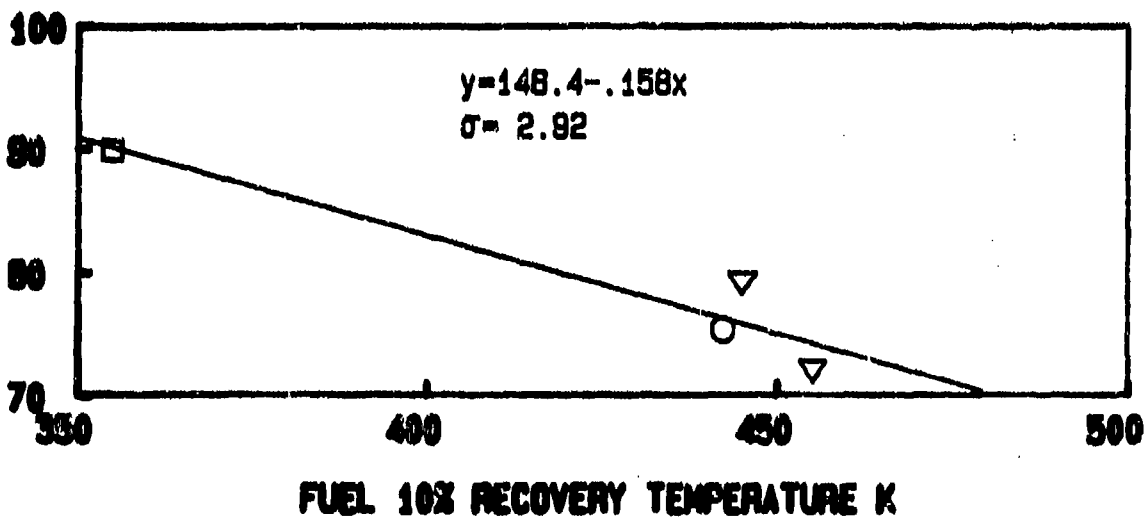
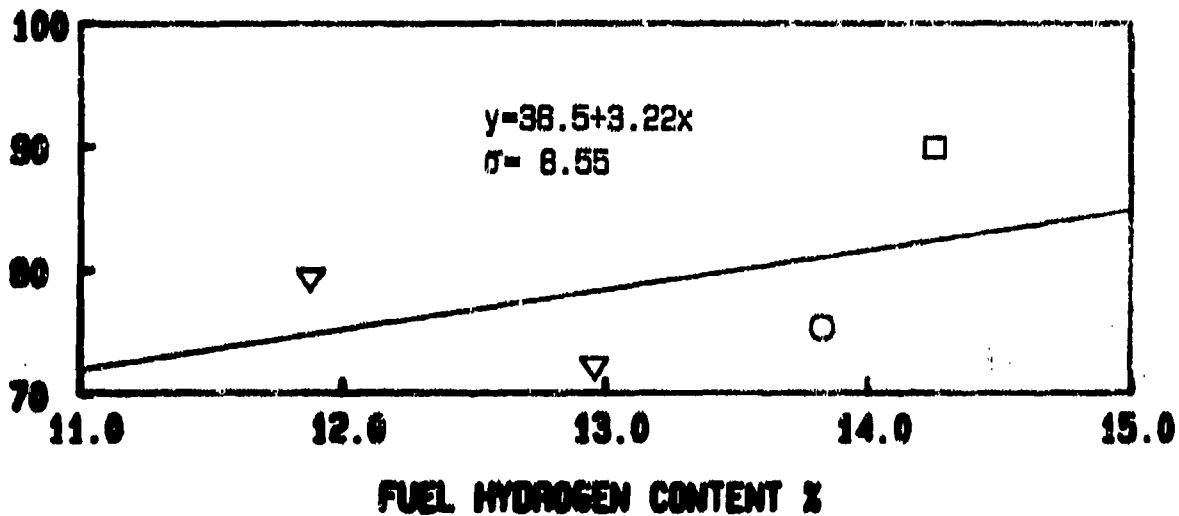


Figure 6.12: Effects of Fuel Properties on Idle Combustion Efficiency (JT15D-5 Atmospheric, Rich P.Z., Simplex 2.25 FN)

30% THRUST COMBUSTION EFFICIENCY %

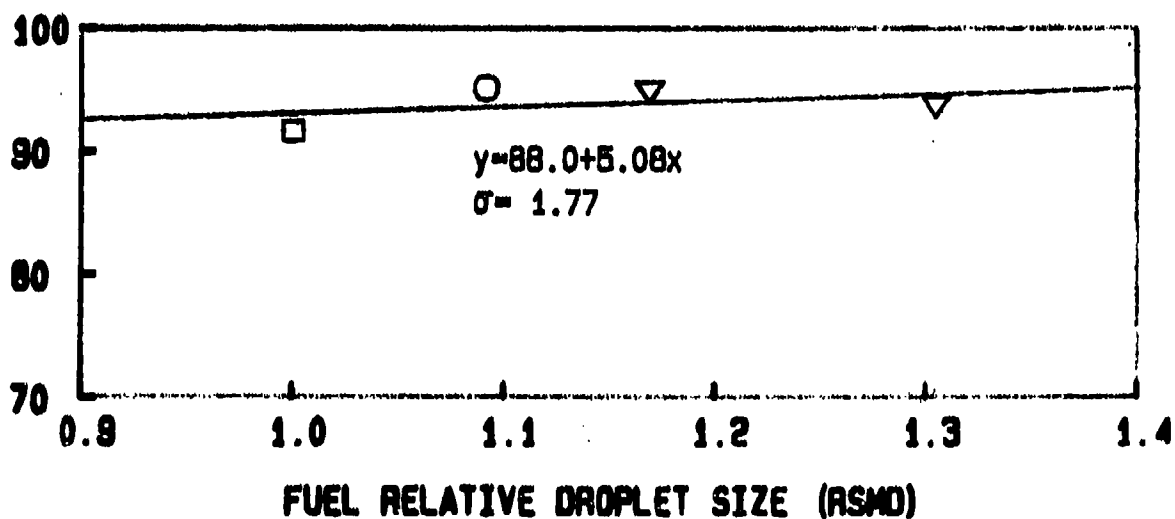
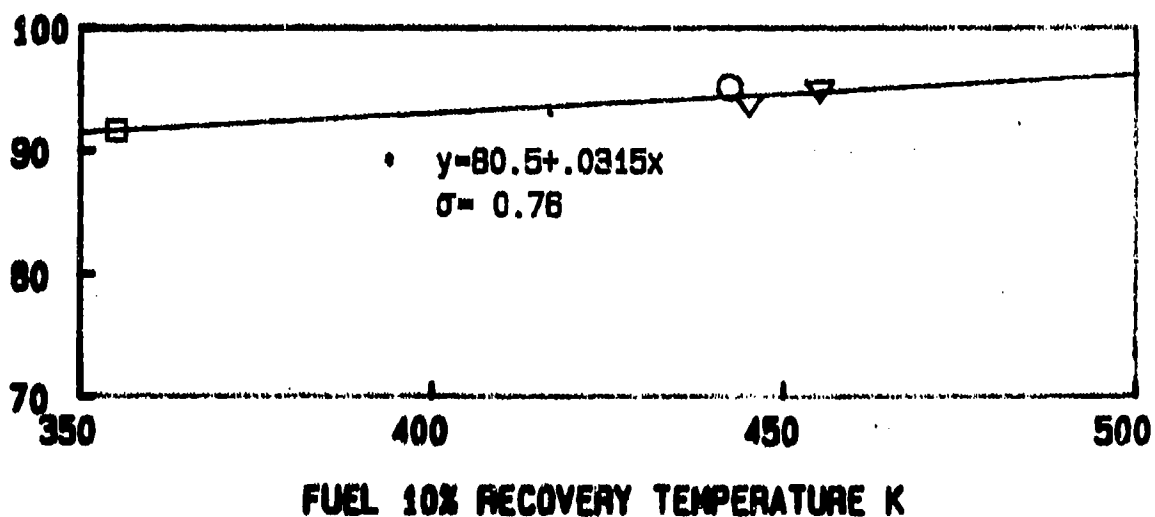
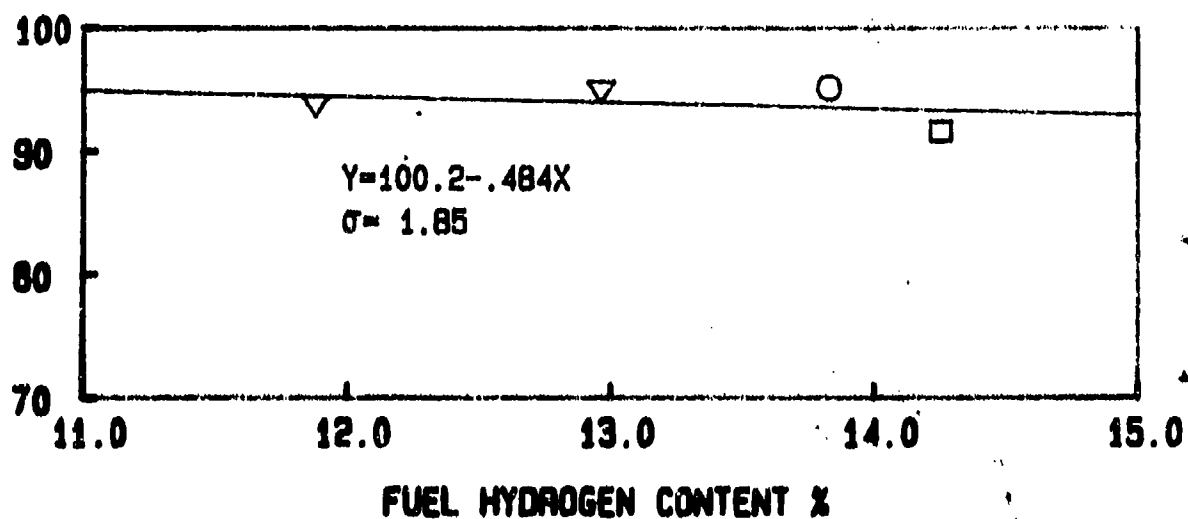


Figure 6.13: Effects of Fuel Properties on 30% Thrust Combustion Efficiency (JT15D-5 Atmospheric, BOM, Airblast Nozzle)

30% THRUST COMBUSTION EFFICIENCY %

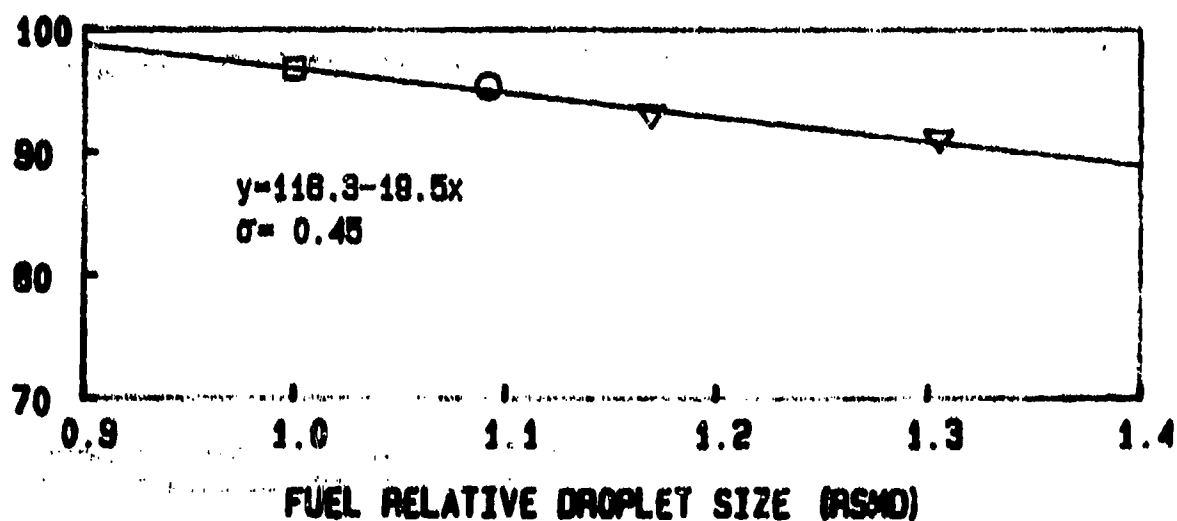
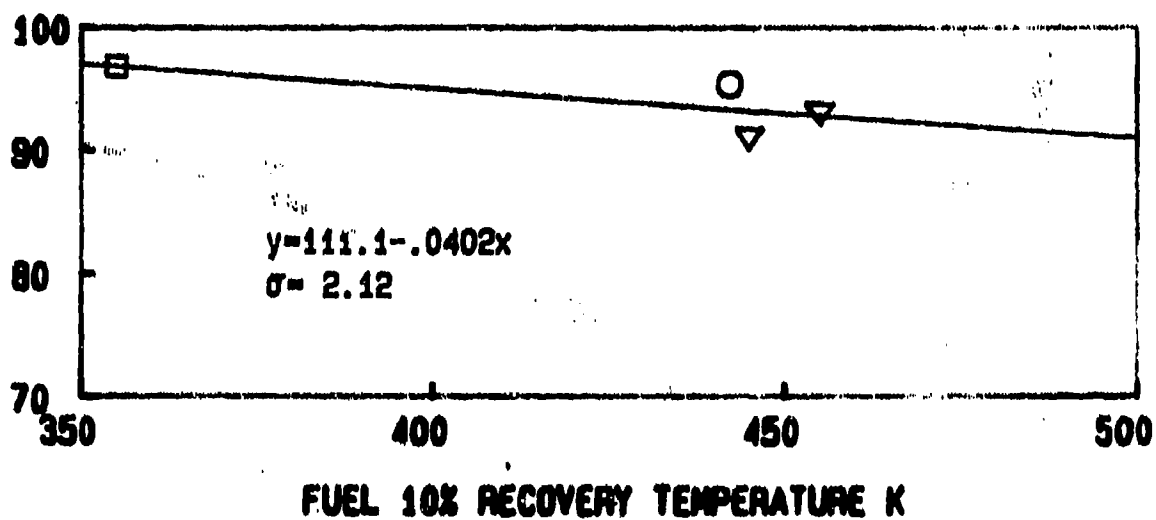
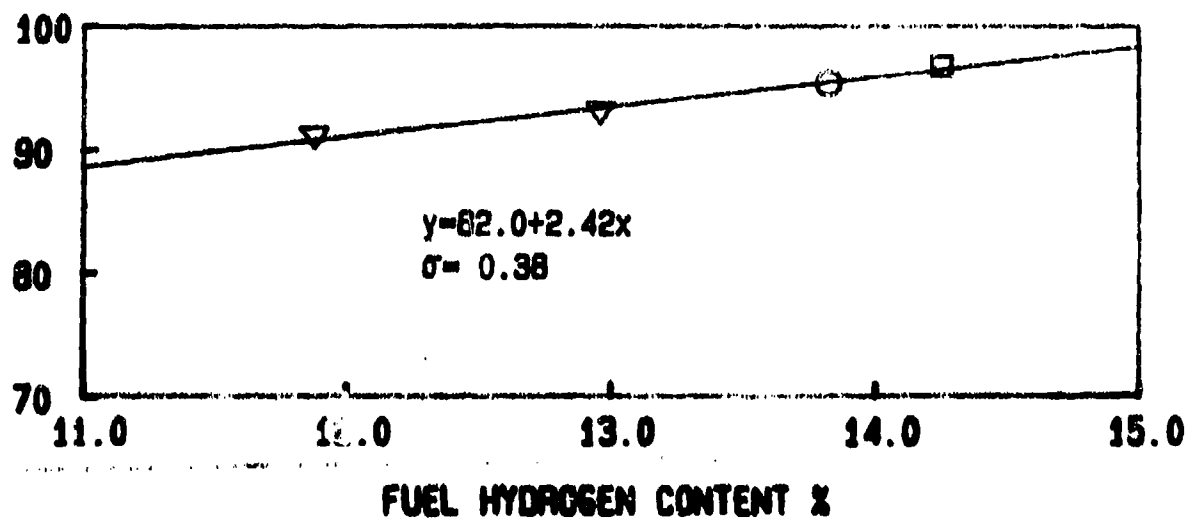


Figure 6.14: Effects of Fuel Properties on 30% Thrust Combustion Efficiency (JT15D-5 Atmospheric, Rich P.Z., Airblast Nozzle)

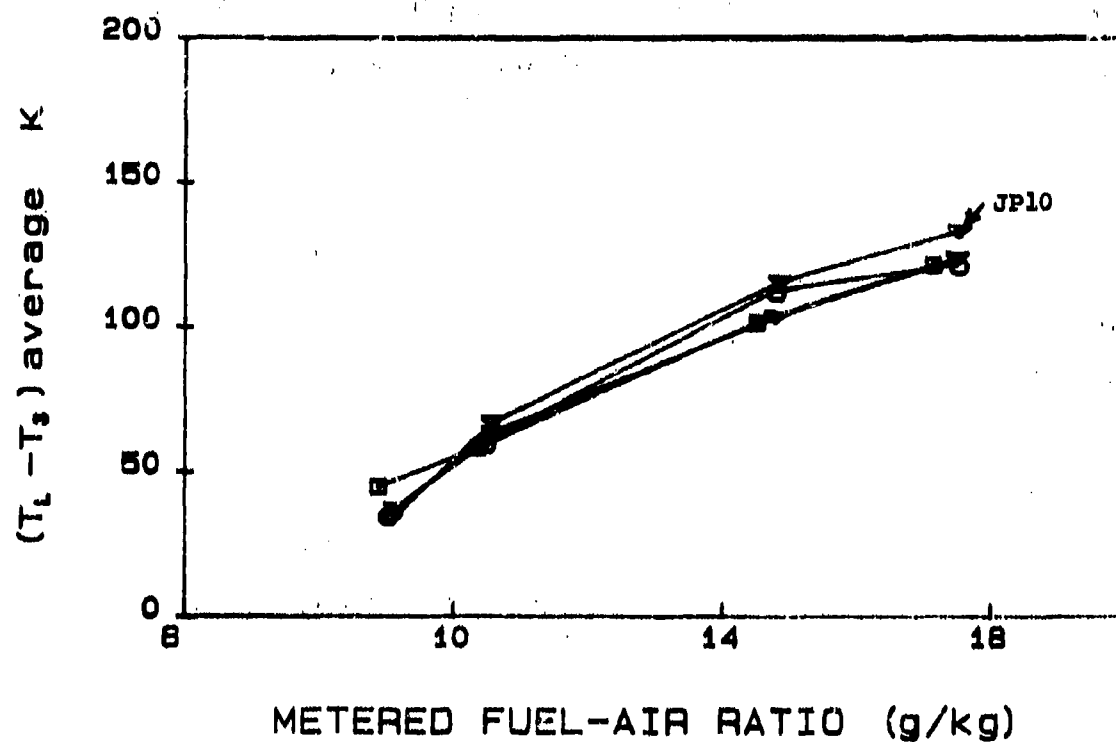


Figure 6.15: Liner Temperature Variations Over Operating Range
(JT15D-5 Atmospheric, BOM, Simplex 2.25 FN)

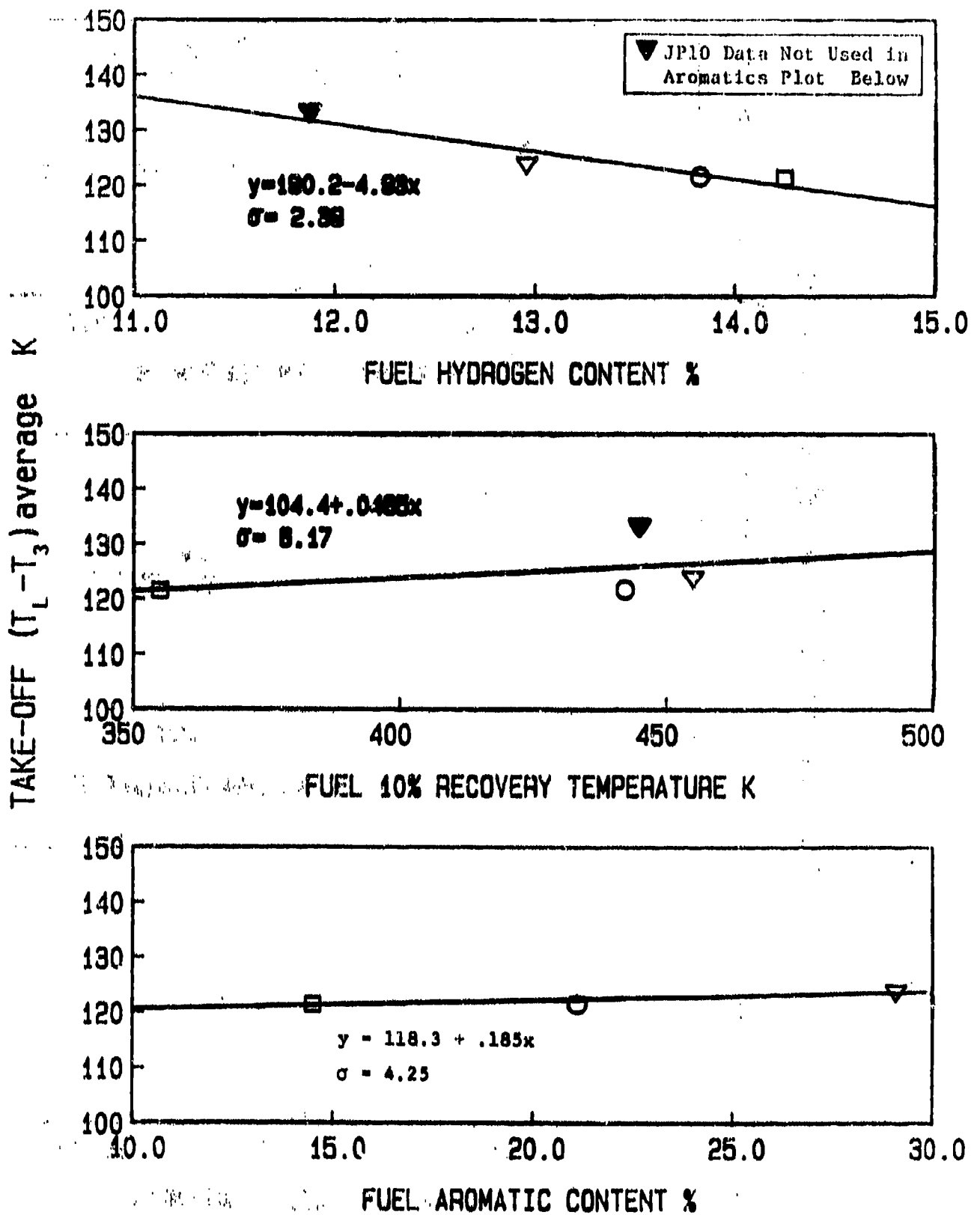


Figure 6.16: Effects of Fuel Properties on Average Liner Temperatures (JT15D-5 Atmospheric, BOM, Simplex 2.25 FN)

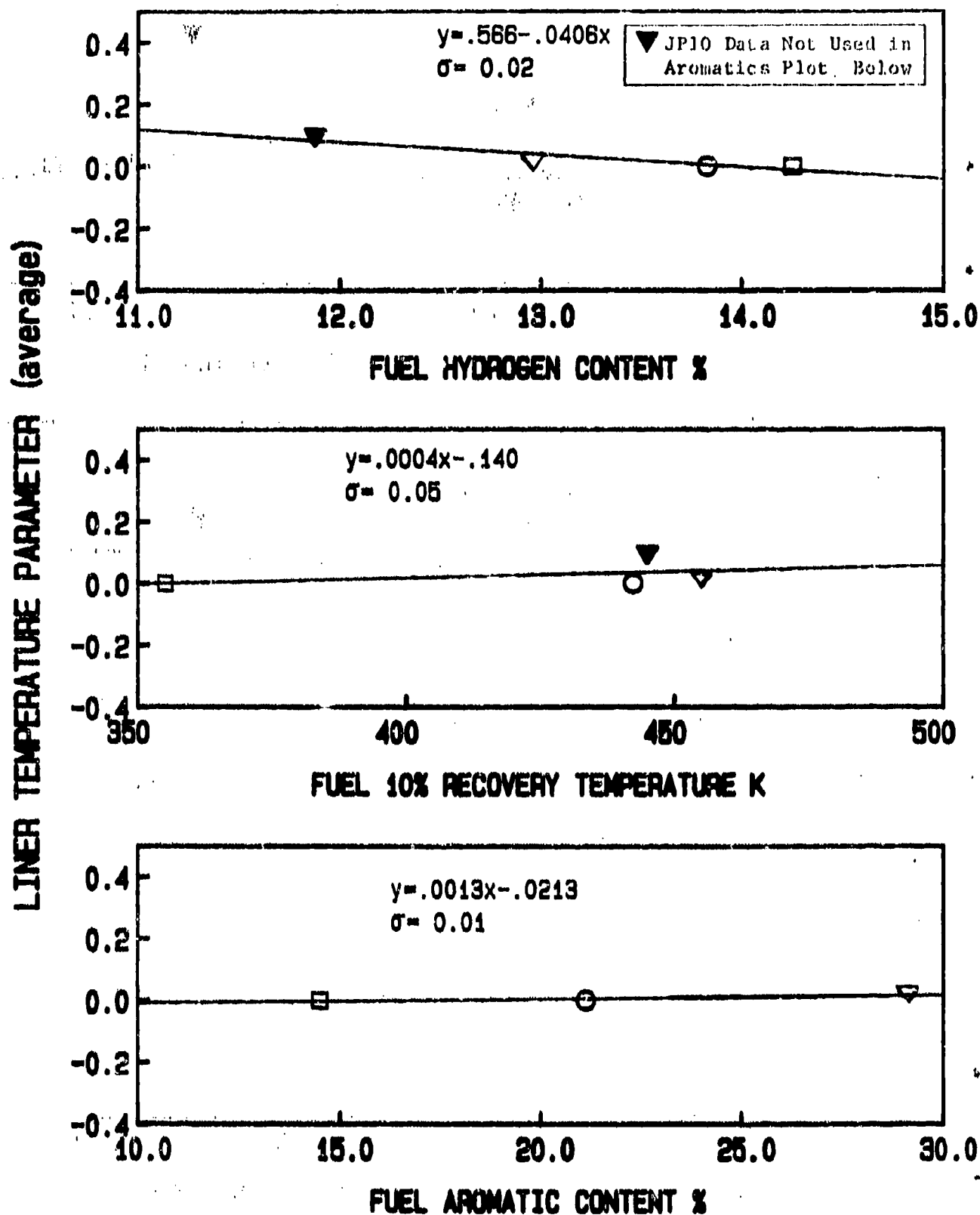


Figure 6.17: Effects of Fuel Properties on Average Liner Temperatures (JT15D-5 Atmospheric, BOM, Simplex 2.25 FN)

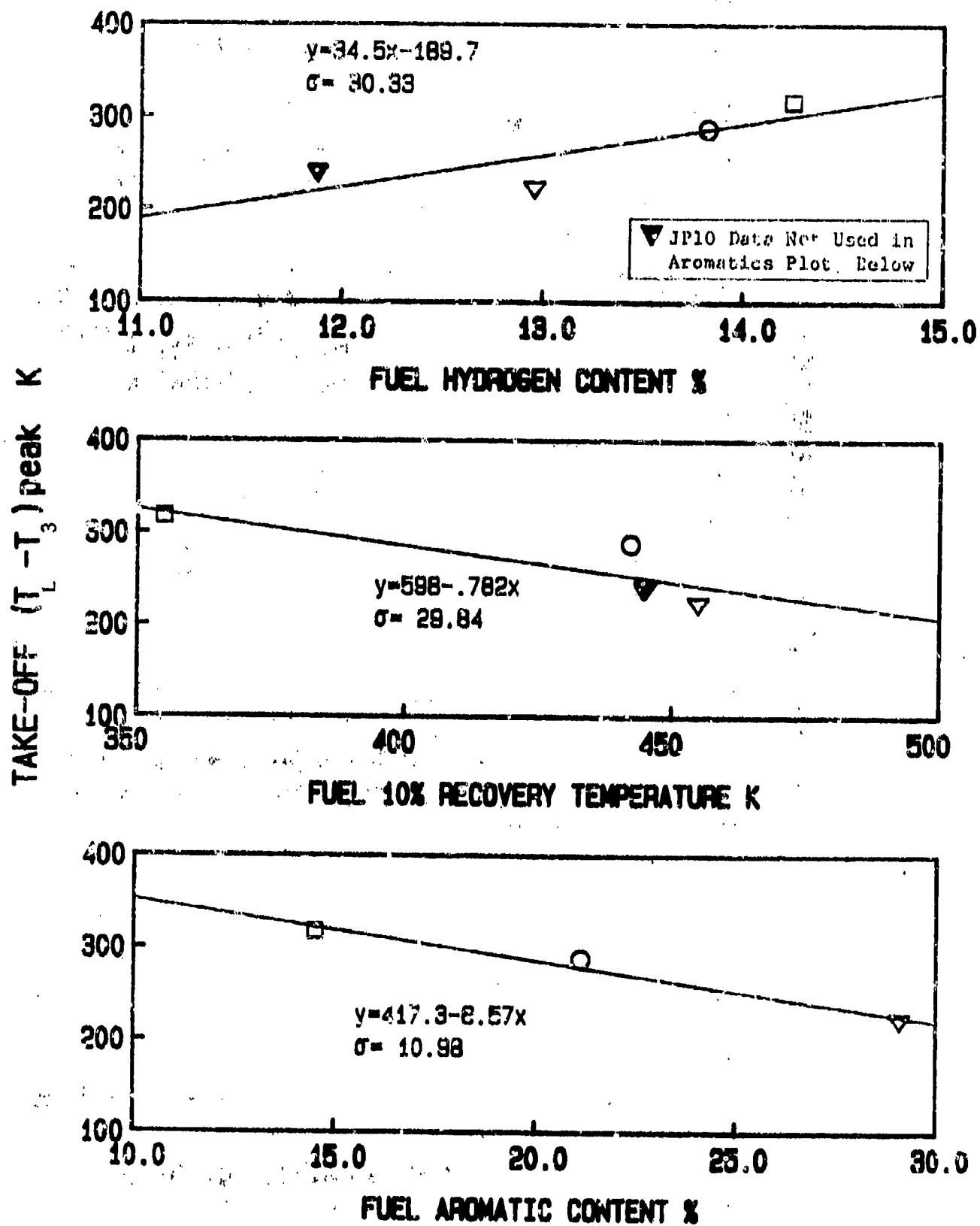


Figure 6.18: Effects of Fuel Properties on Peak Liner Temperatures (JT15D-5 Atmospheric, BOM, Simplex 2.25 FN)

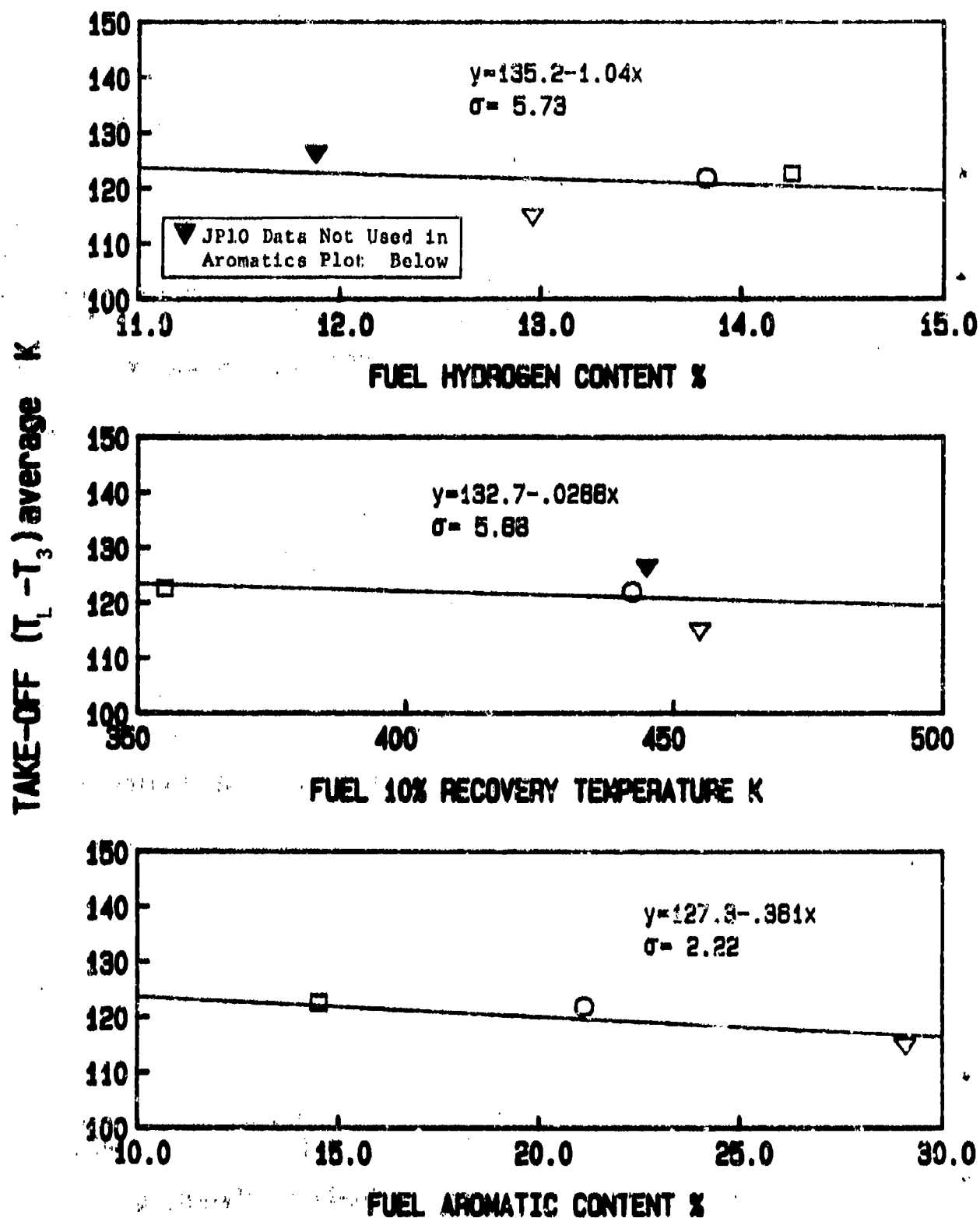


Figure 6.19: Effects of Fuel Properties on Average Liner Temperatures (JT15D-5 Atmospheric, Rich P.7., Simplex 2.25 FN)

LINER TEMPERATURE PARAMETER (average)

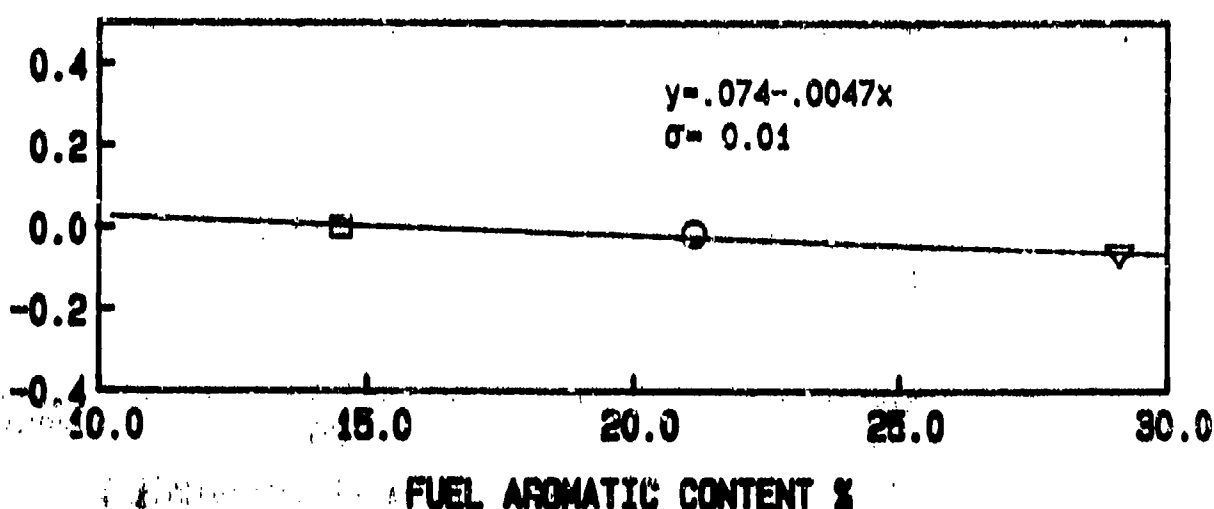
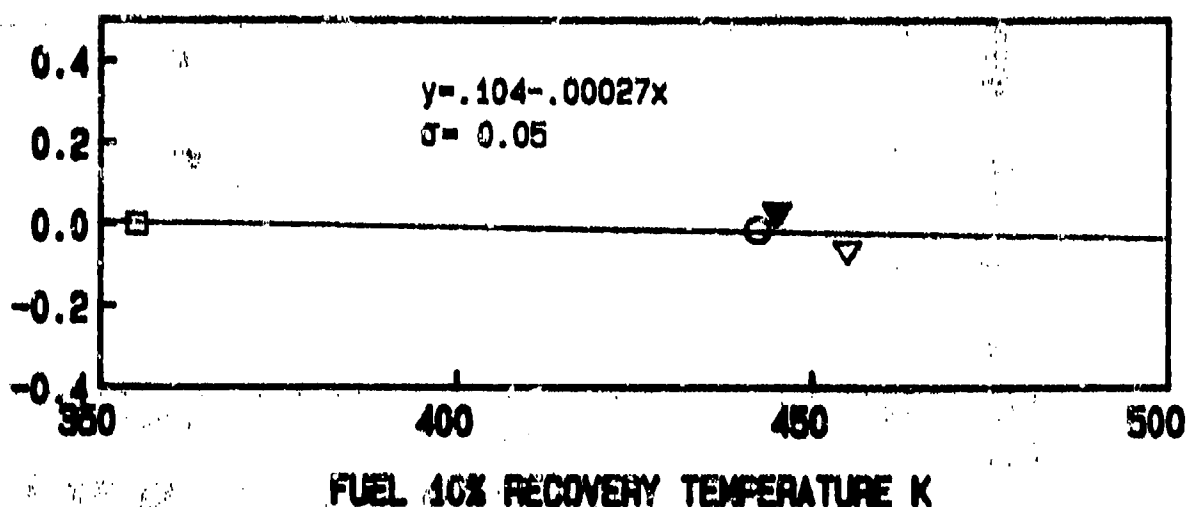
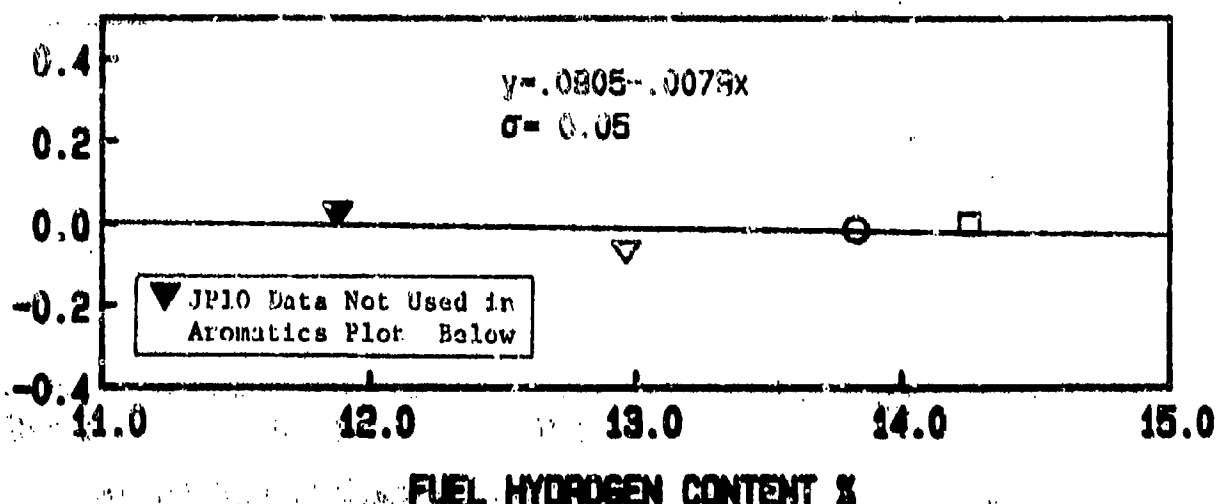


Figure 6.20: Effects of Fuel Properties on Average Liner Temperatures (JT15D-5 Atmospheric, Rich P.Z., Simplex 2.25 FN)

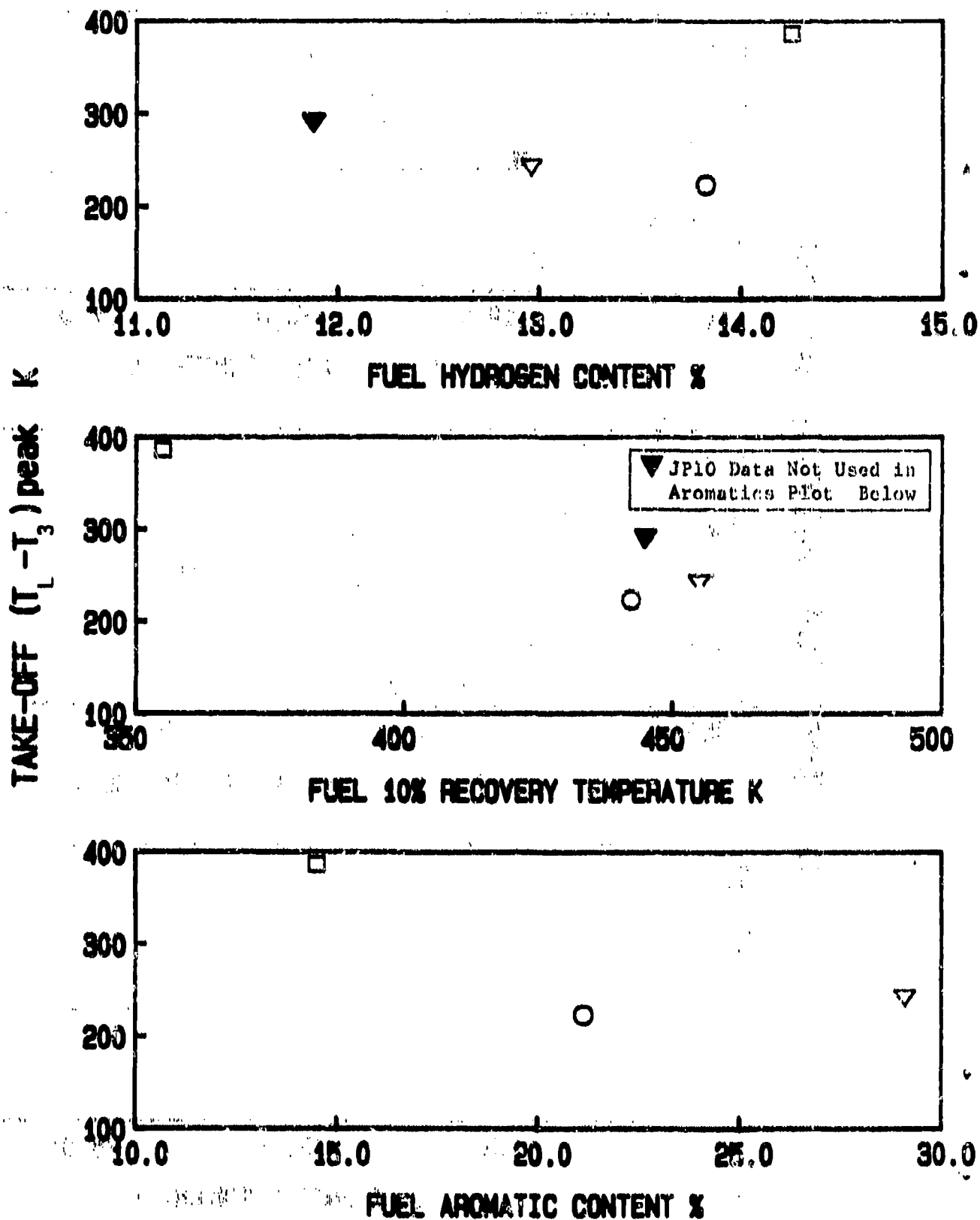


Figure 6.21: Effects of Fuel Properties on Peak Liner Temperatures (JT15D-5 Atmospheric, Rich P.Z., Simplex 2.25 FN)

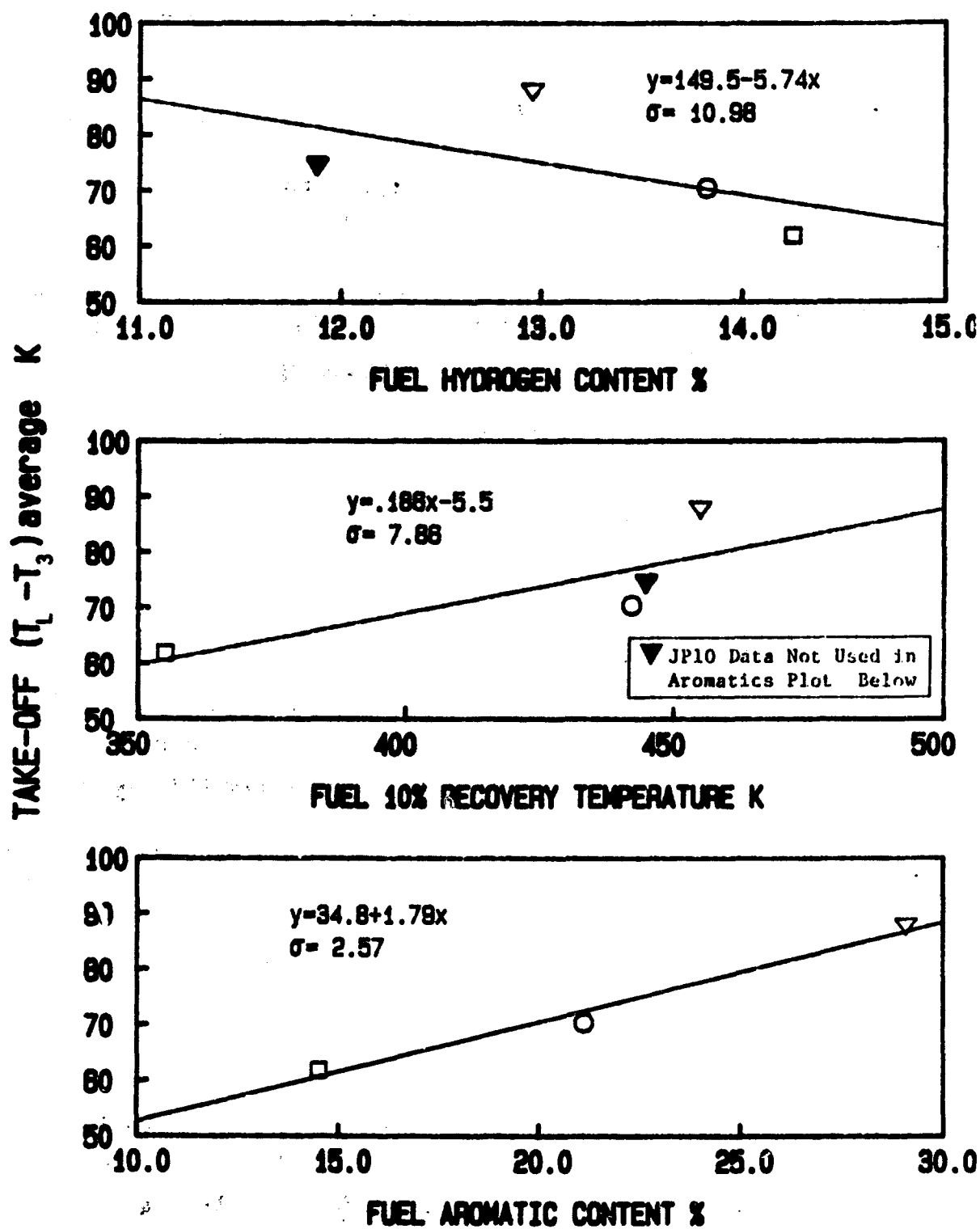


Figure 6.22: Effects of Fuel Properties on Average Liner Temperatures (JT15D-5 Atmospheric, BOM, Airblast Nozzle)

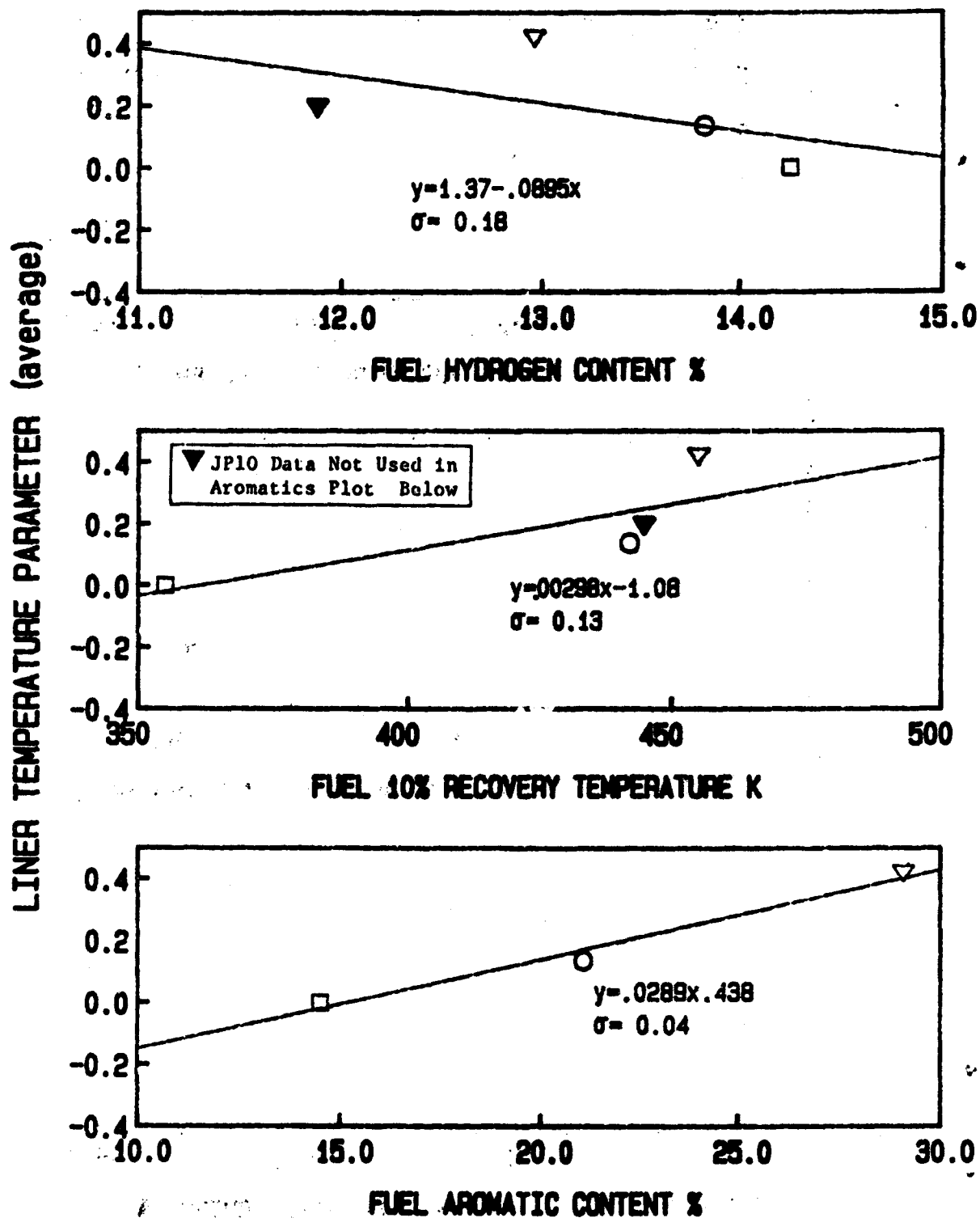


Figure 6.23: Effects of Fuel Properties on Average Liner Temperatures (JT15D-5 Atmospheric, BOM, Airblast Nozzle)

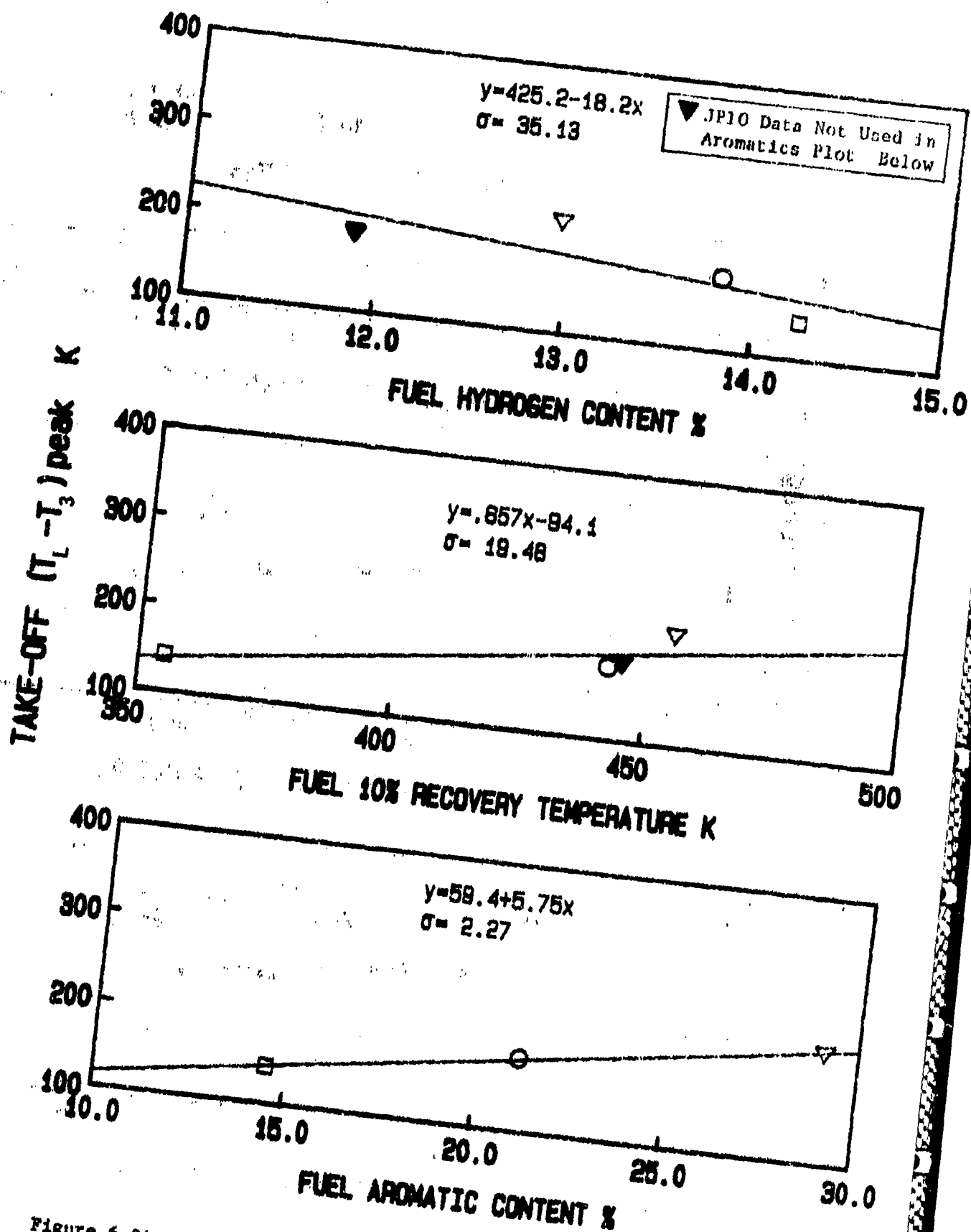


Figure 6.24: Effects of Fuel Properties on Peak Liner Temperatures (JT15D-5 Atmospheric, BOM, Airblast Nozzle)

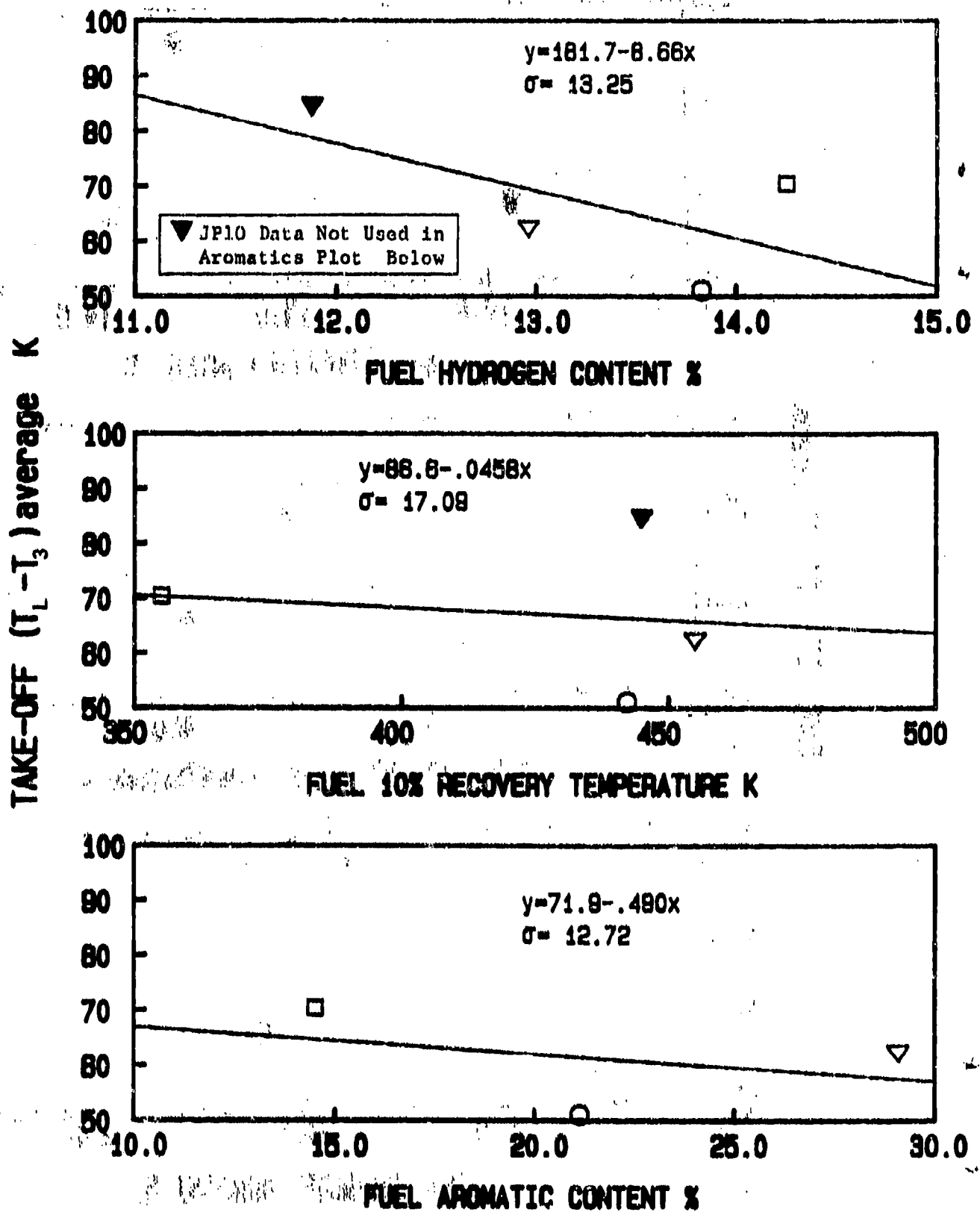


Figure 6.25: Effects of Fuel Properties on Average Liner Temperatures (JT15D-5 Atmospheric, Rich P.Z., Airblast Nozzle)

LINER TEMPERATURE PARAMETER (average)

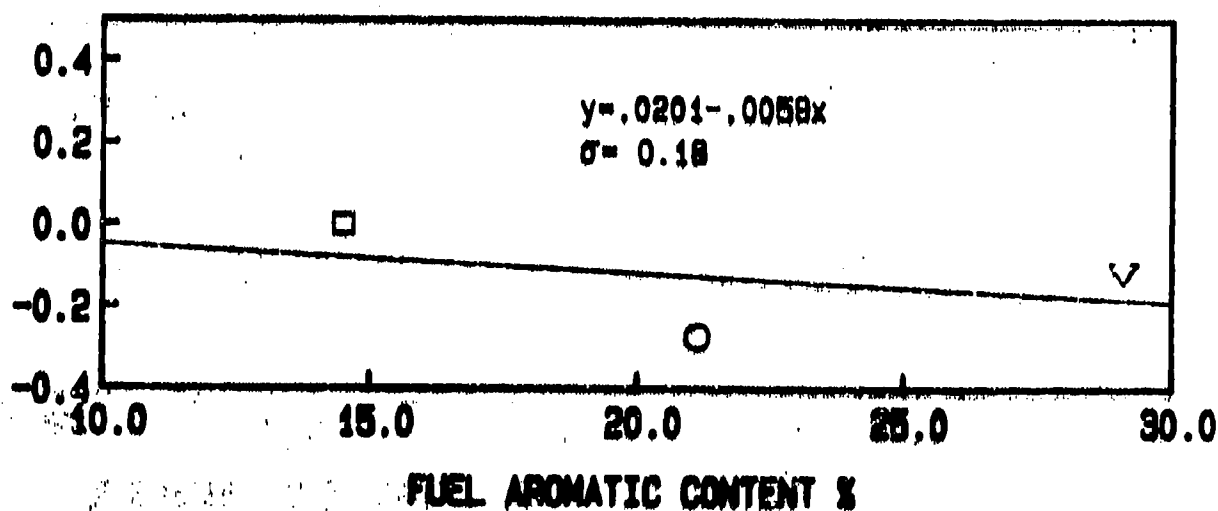
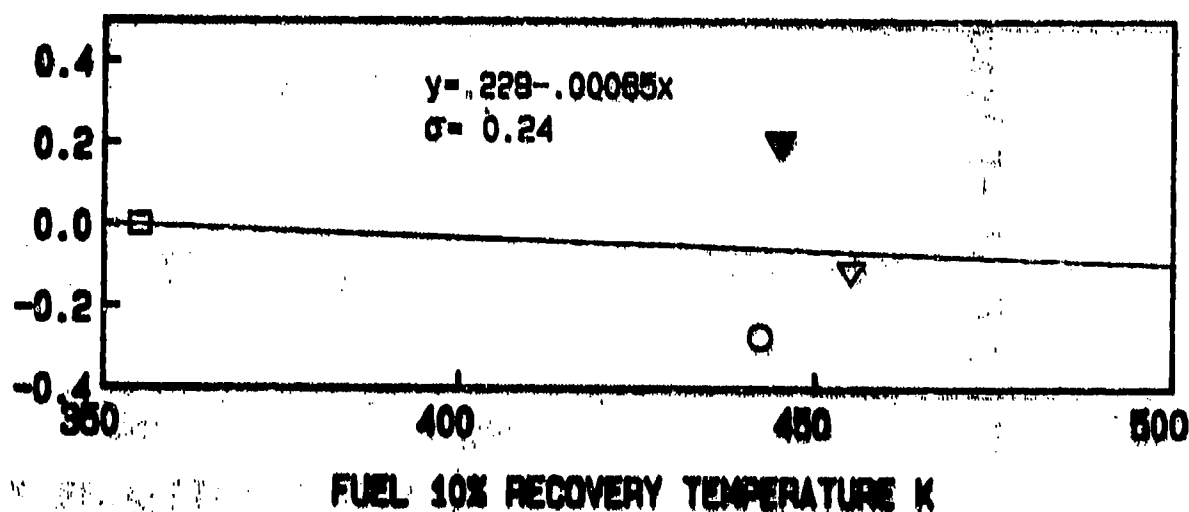
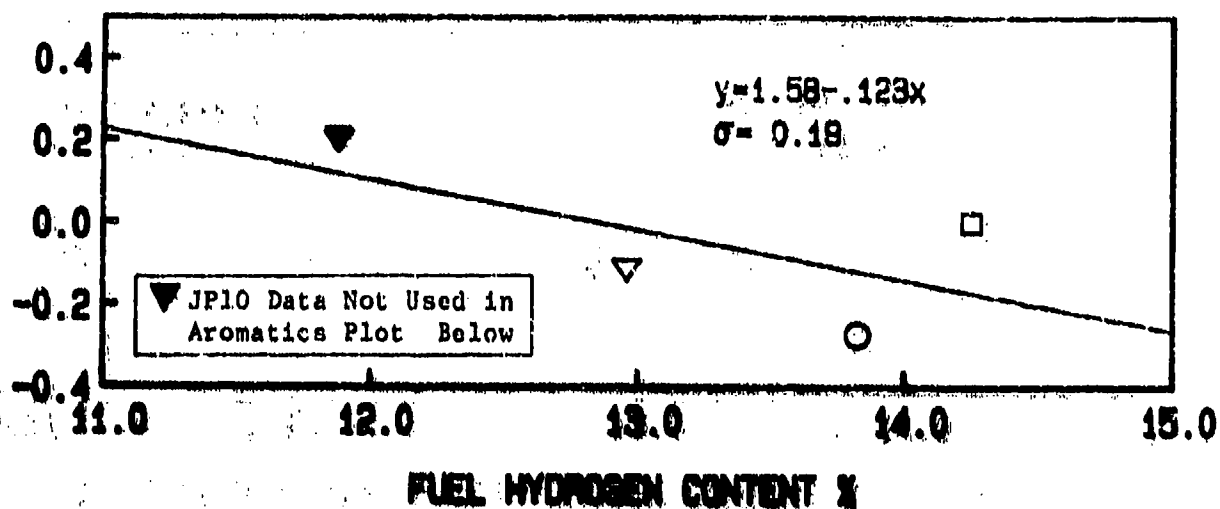


Figure 6.26: Effects of Fuel Properties on Average Liner Temperatures (JT15D-5 Atmospheric, Rich P.Z., Airblast Nozzle)

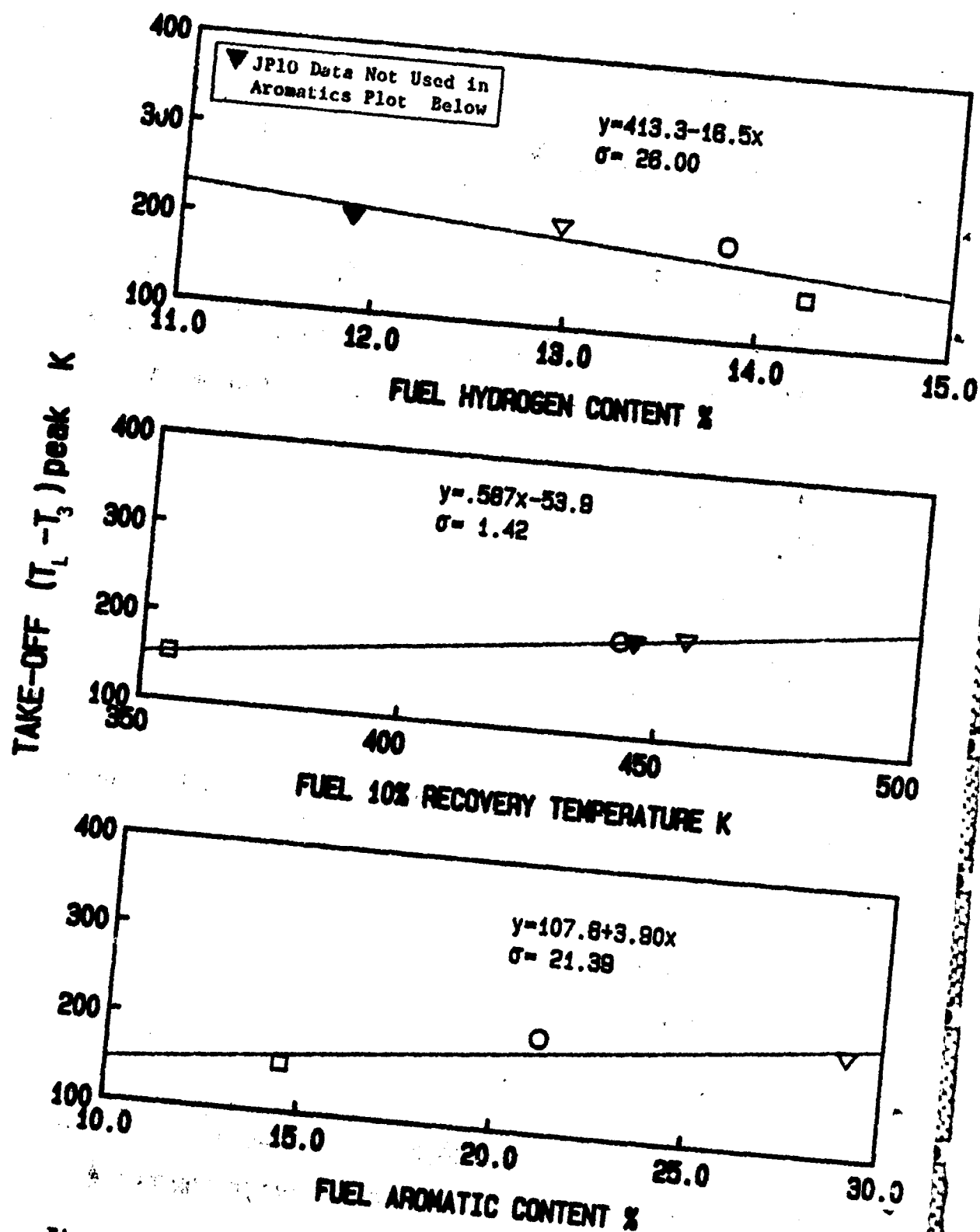


Figure 6.27: Effects of Fuel Properties on Peak Liner Temperatures (JT15D-5 Atmospheric, Rich P.Z., Airblast Nozzle)

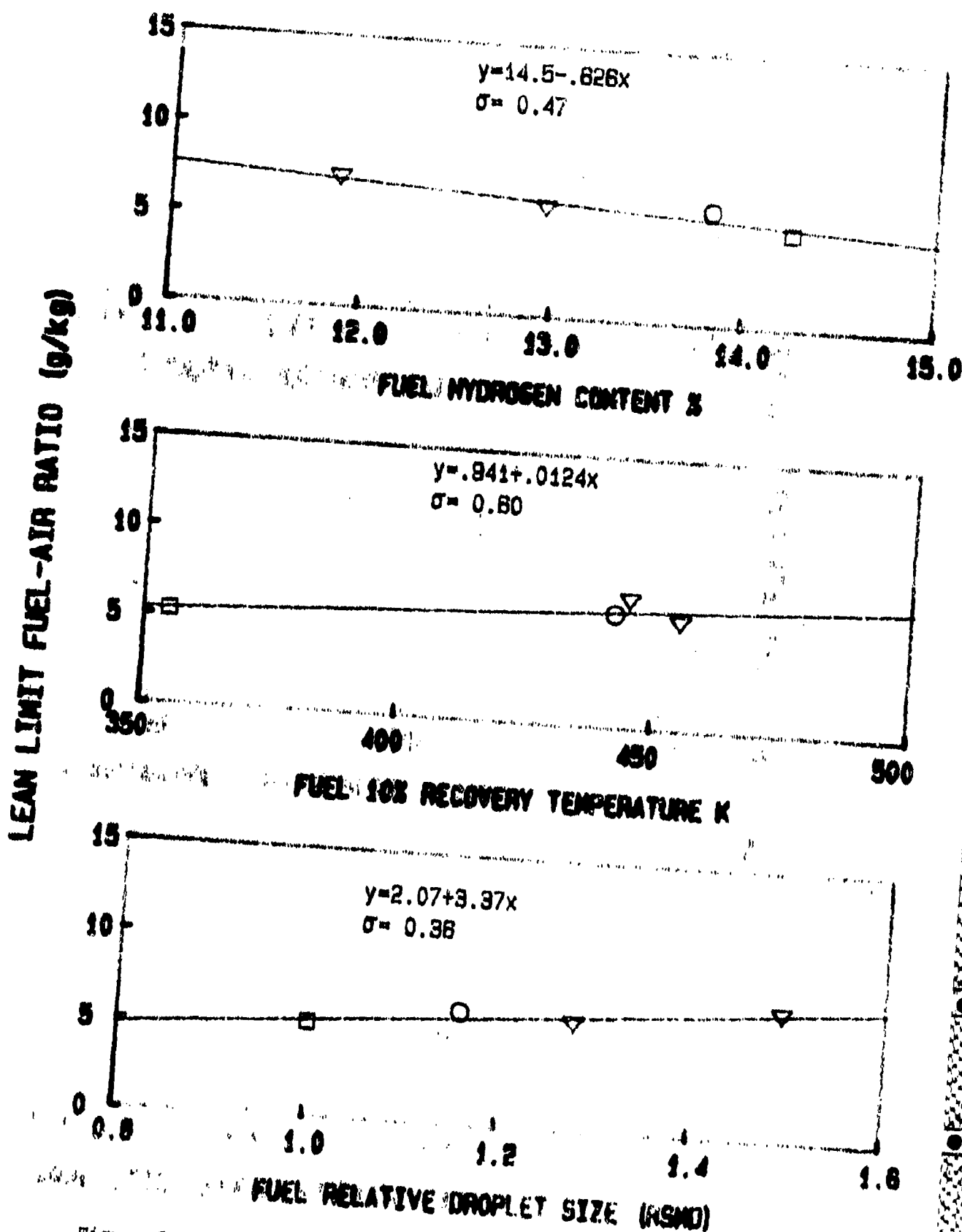


Figure 6.28: Effects of Fuel Properties on Lean Limit Fuel-Air Ratio
(JT15D-5 Atmospheric, BOM, Simplex 2.25 FN)

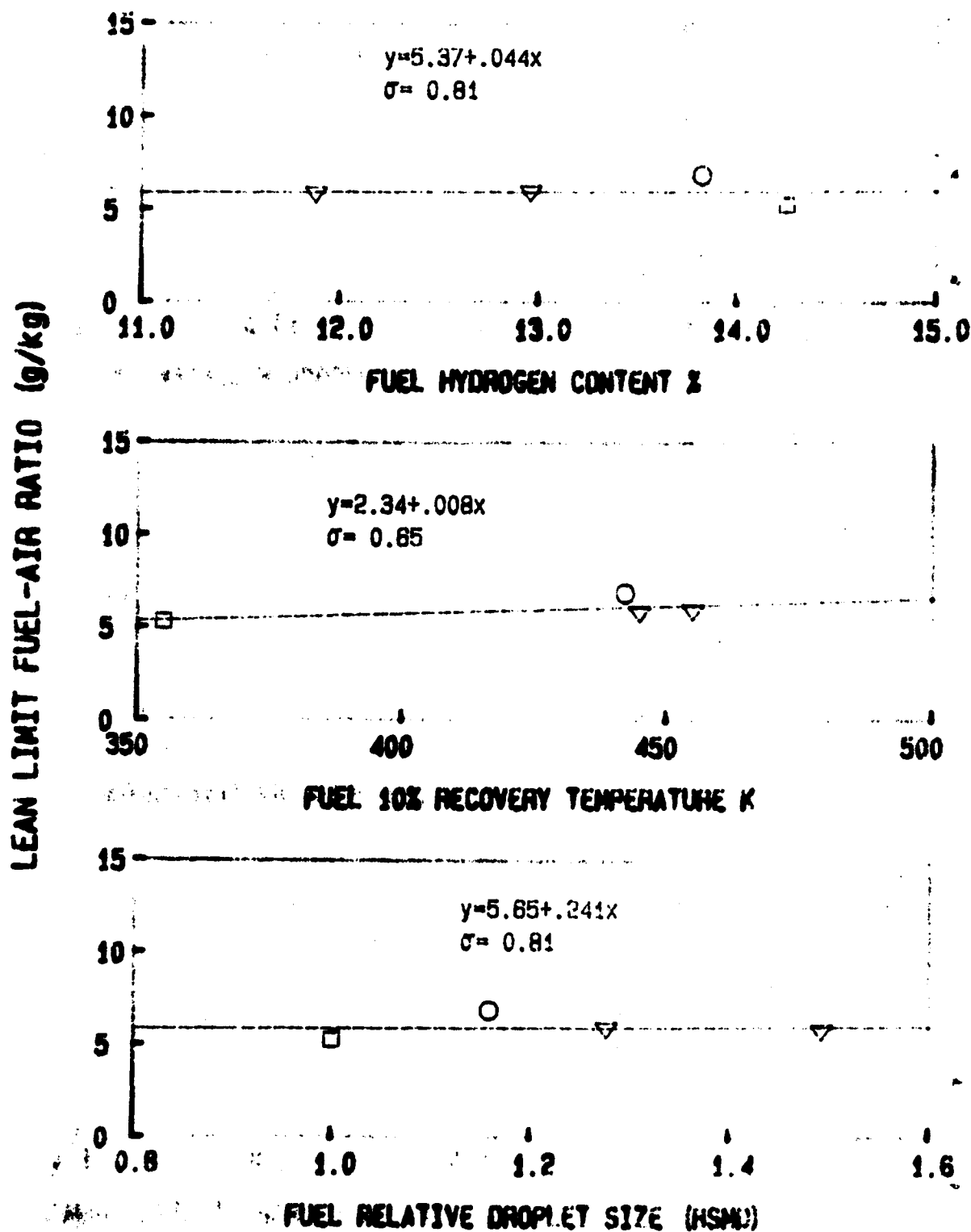


Figure 6.29: Effects of Fuel Properties on Lean Limit Fuel-Air Ratio
 (JT15D-5 Atmospheric, Rich P.Z., Simplex 2.25 FN)

70% RELATIVE PROFILE FACTOR

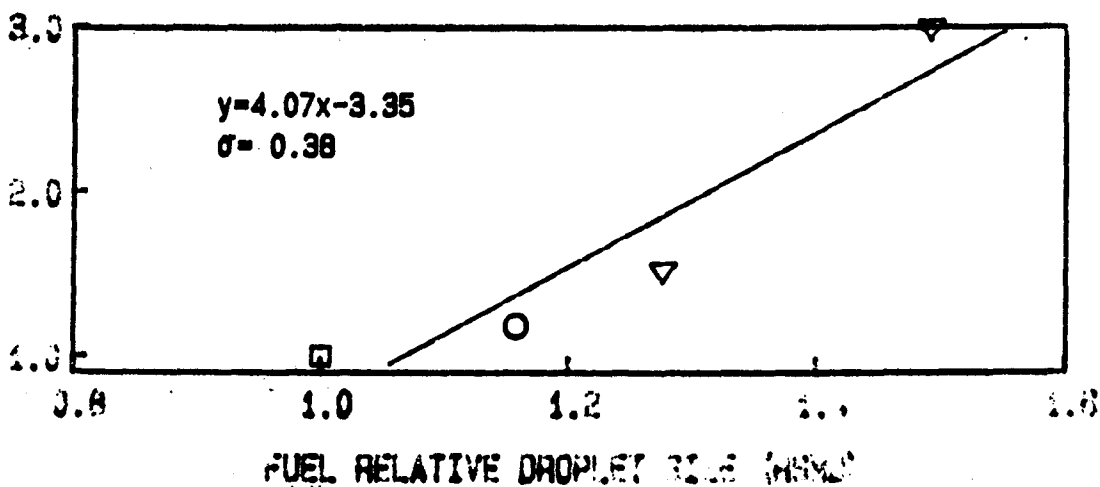
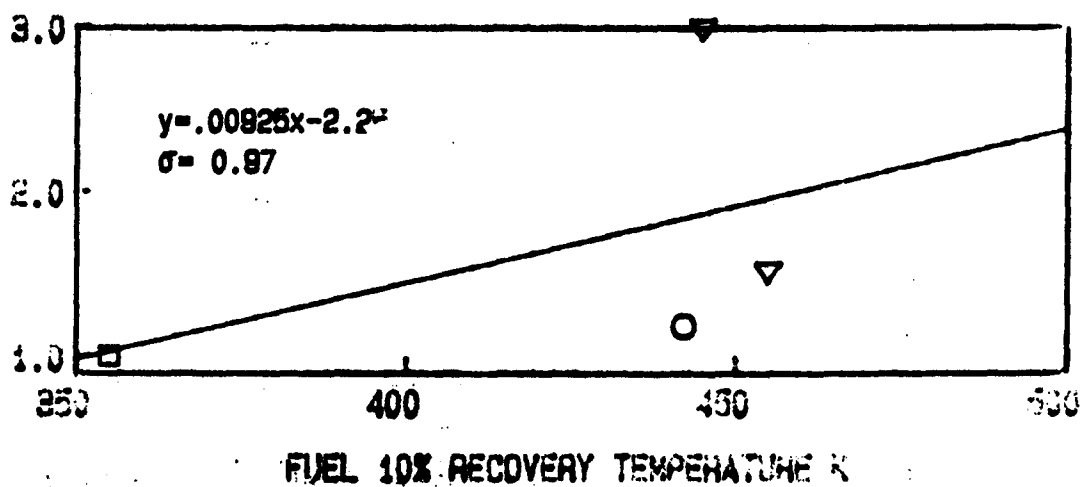
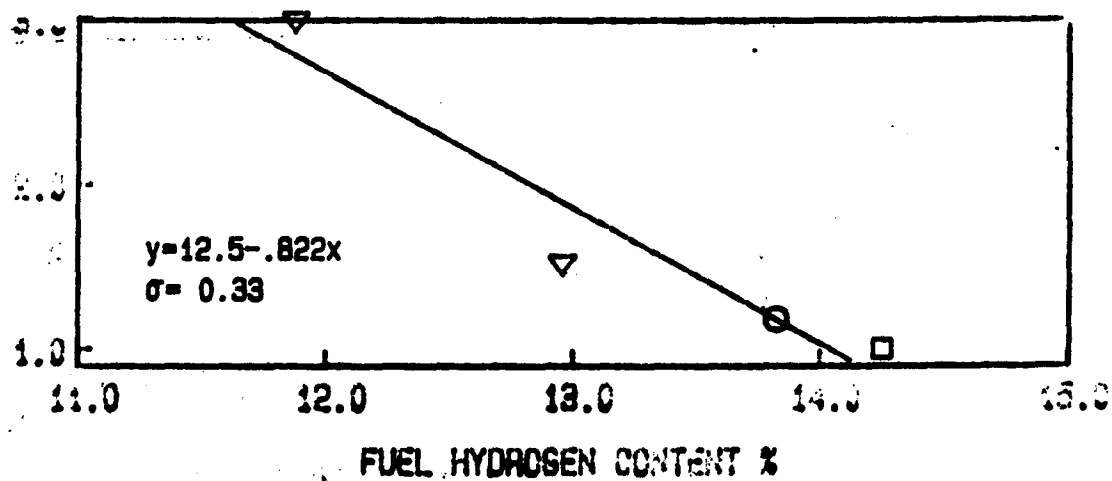


Figure 6.30: Effects of Fuel Properties on Relative Profile Factor (JT15D Atmospheric, BOM, Simplex 2.25 FN)

70% RELATIVE PATTERN FACTOR

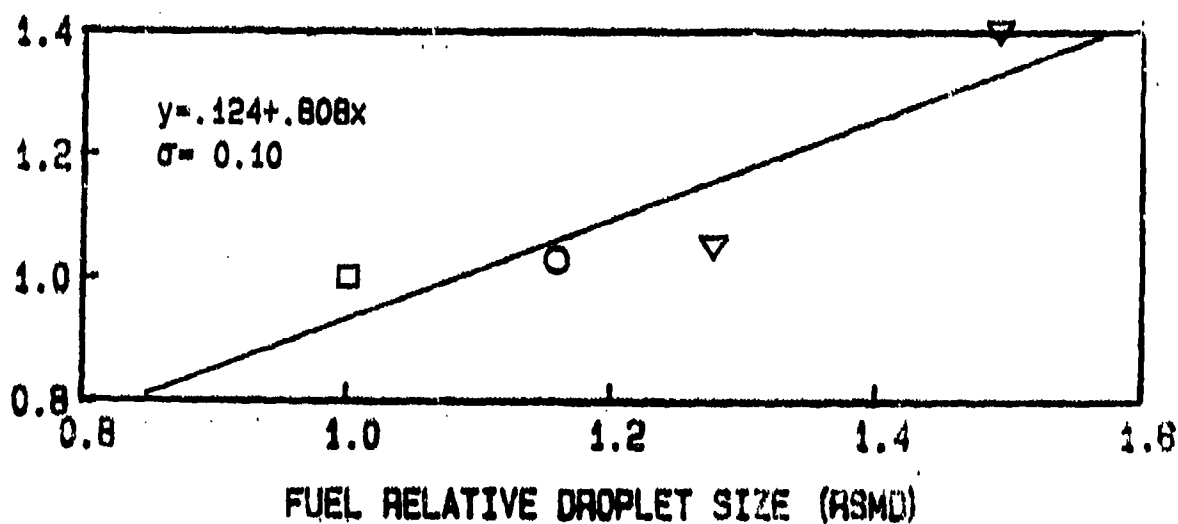
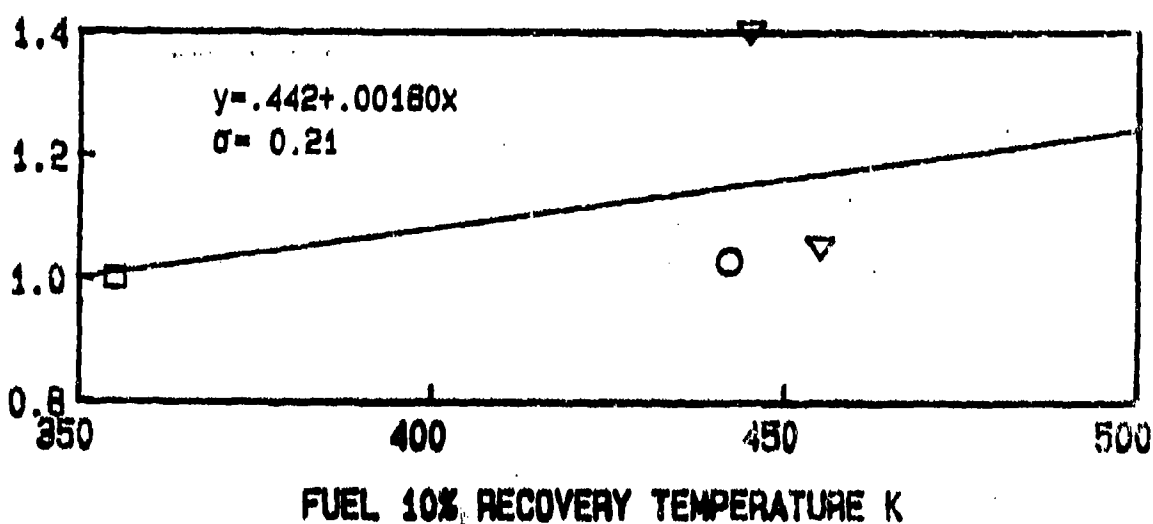
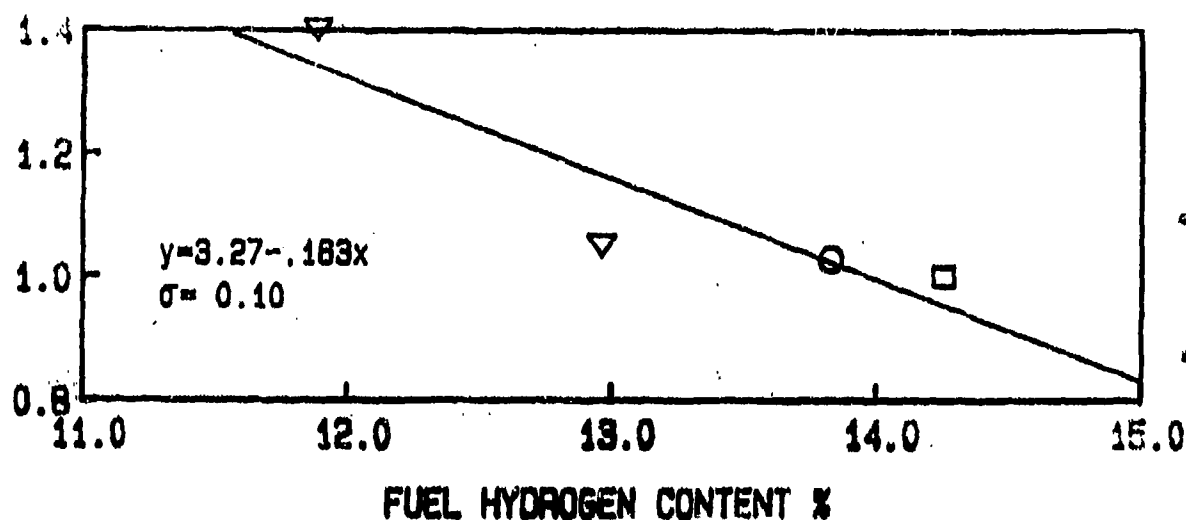


Figure 6.31: Effects of Fuel Properties on Relative Pattern Factor (JT15D-5 Atmospheric, BOM, Simplex 2.25 FN)

70% RELATIVE PROFILE FACTOR

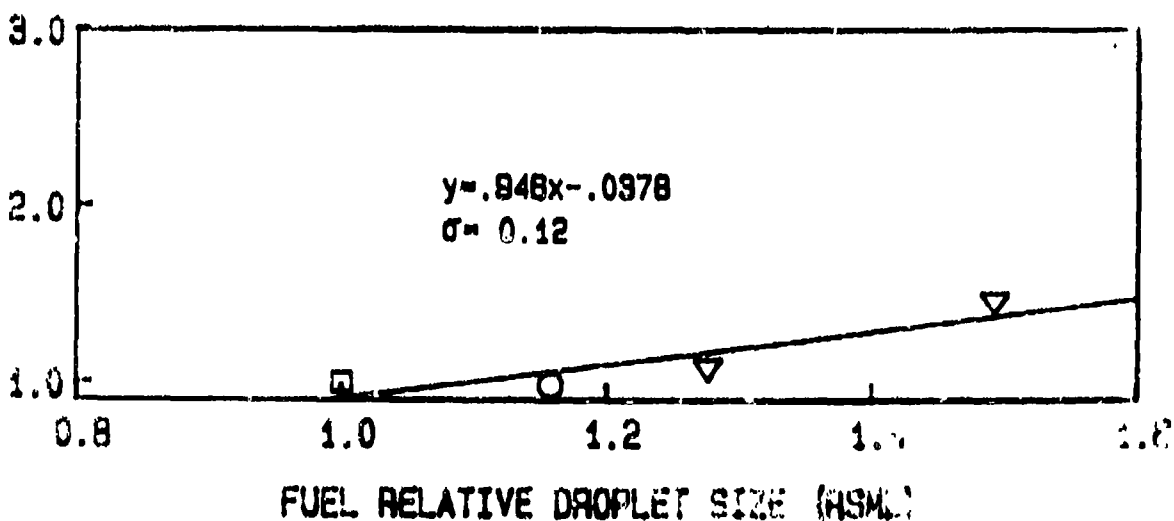
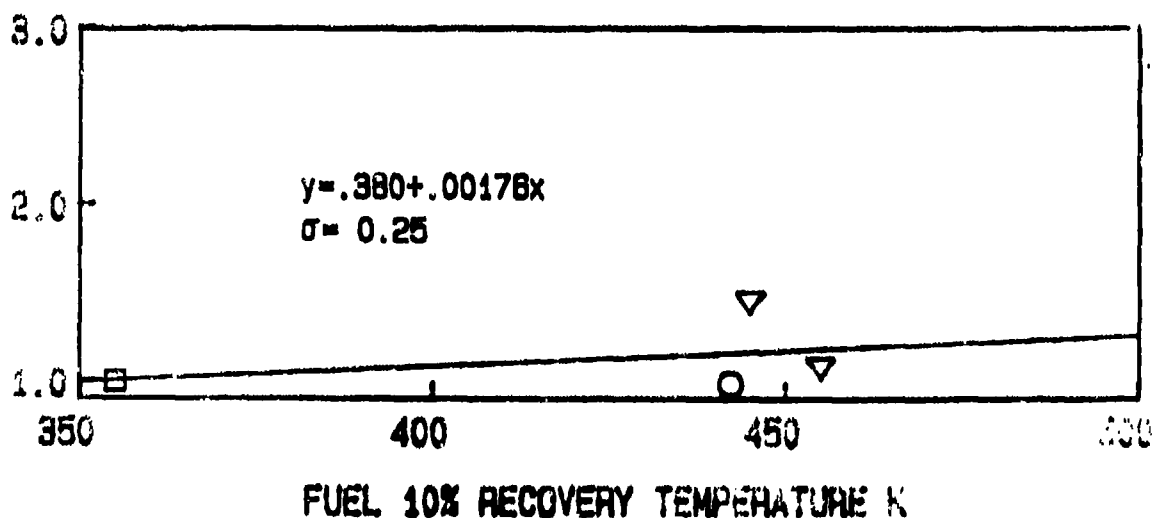
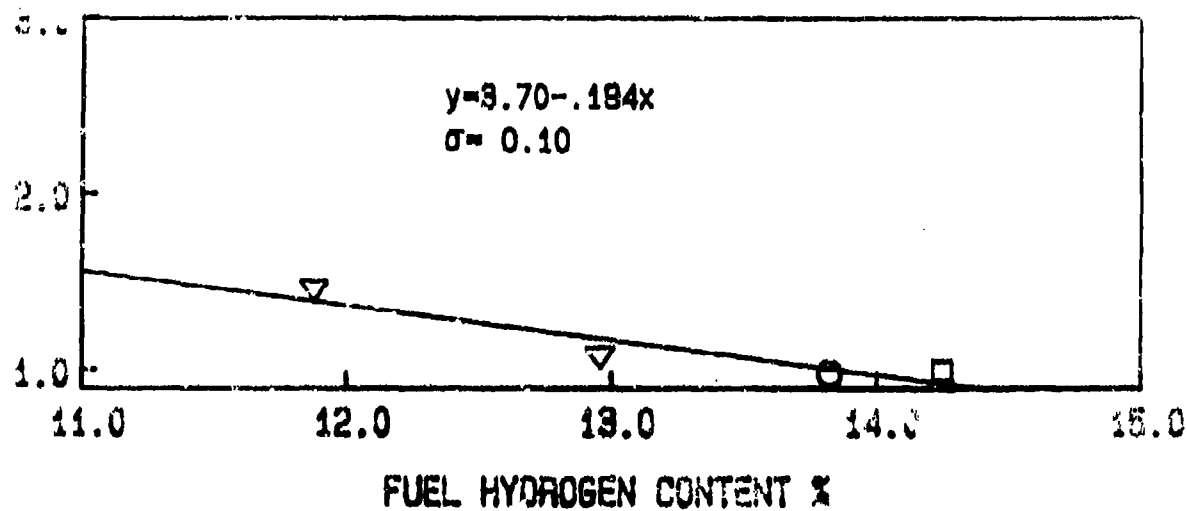


Figure 6.32: Effects of Fuel Properties on Relative Profile Factor (JT15D-5 Atmospheric, Rich P.Z., Simplex 2.25 FN)

10% RELATIVE PATTERN FACTOR

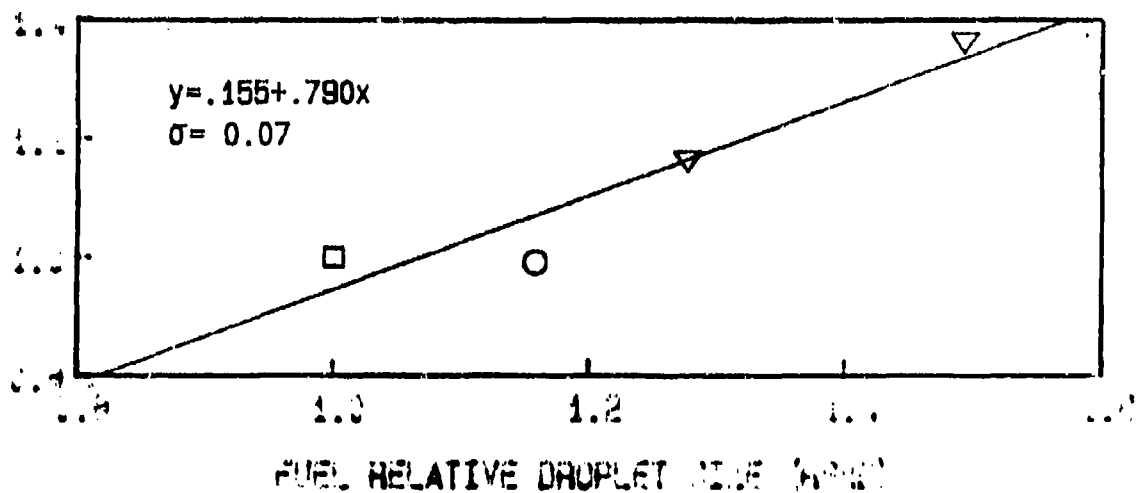
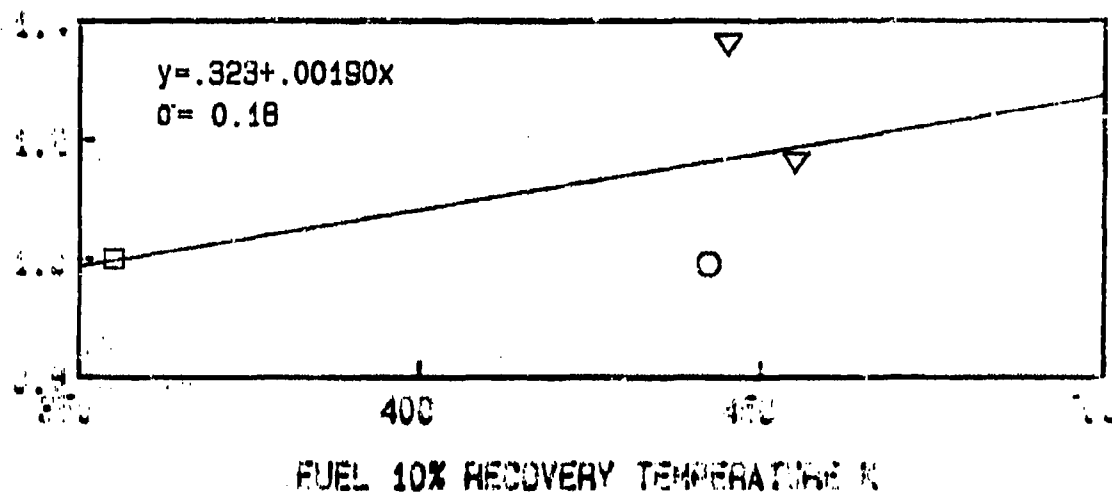
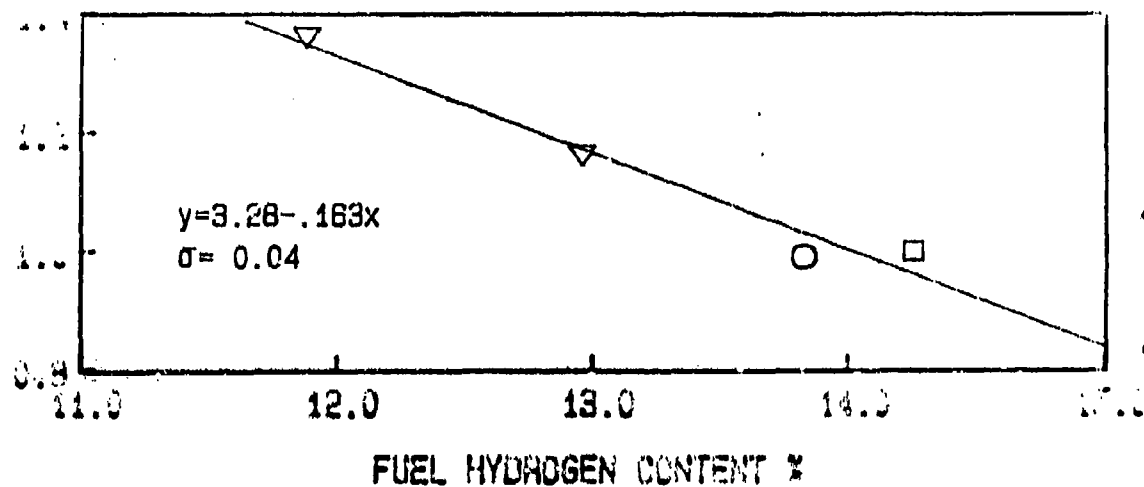


Figure 6.33: Effects of Fuel Properties on Relative Pattern Factor (JT15D-5 Atmospheric, Rich P.Z., Simplex 2.25 FN)

70% RELATIVE PROFILE FACTOR

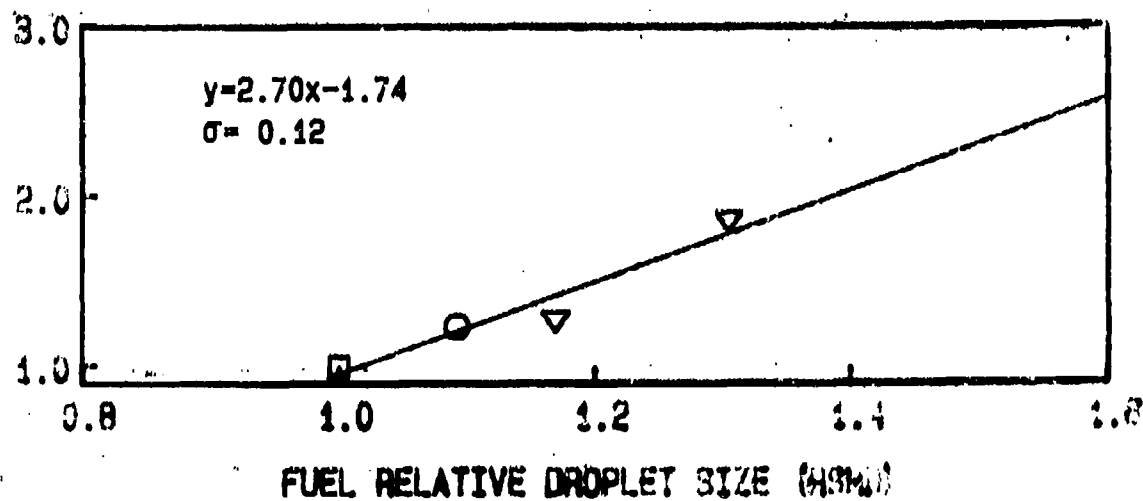
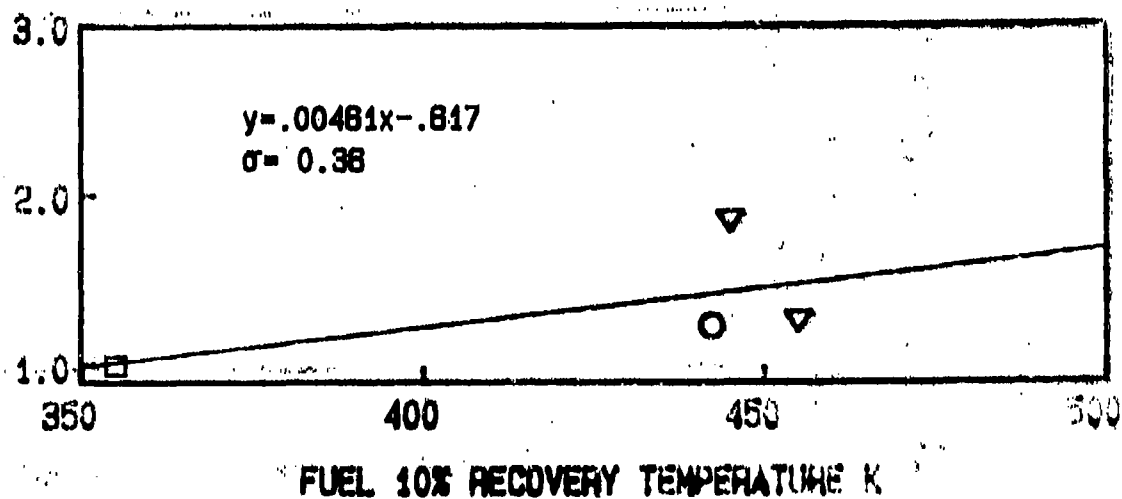
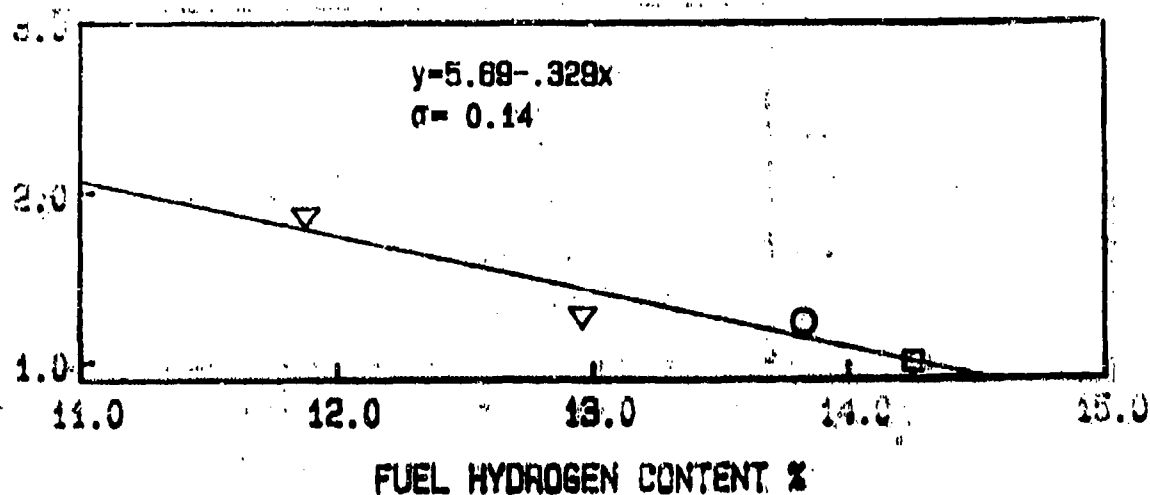


Figure 6.34: Effects of Fuel Properties on Relative Profile Factor (JT15D Atmospheric, BOM, Airblast Nozzle)

70% RELATIVE PATTERN FACTOR

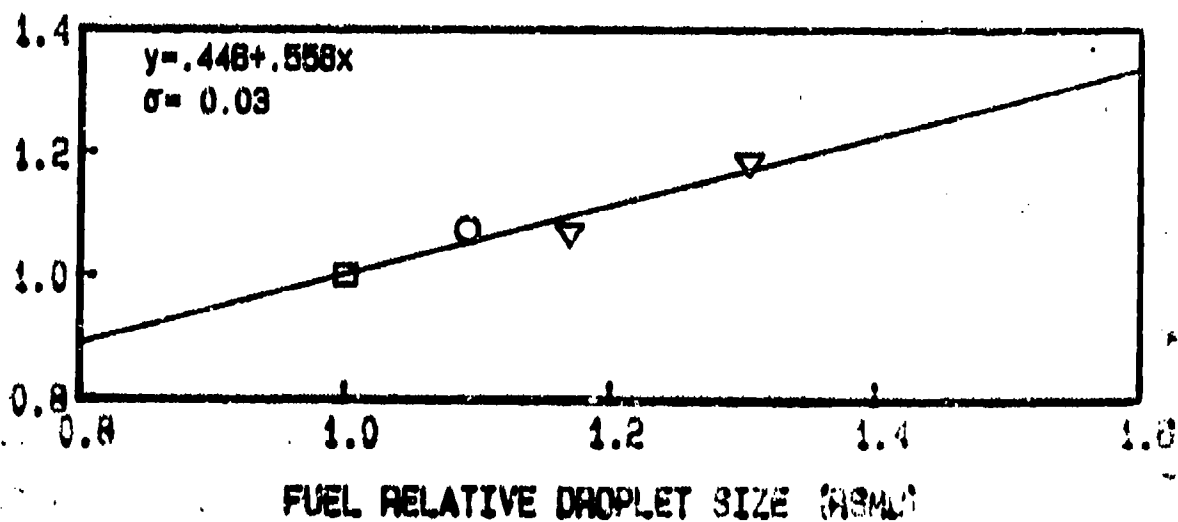
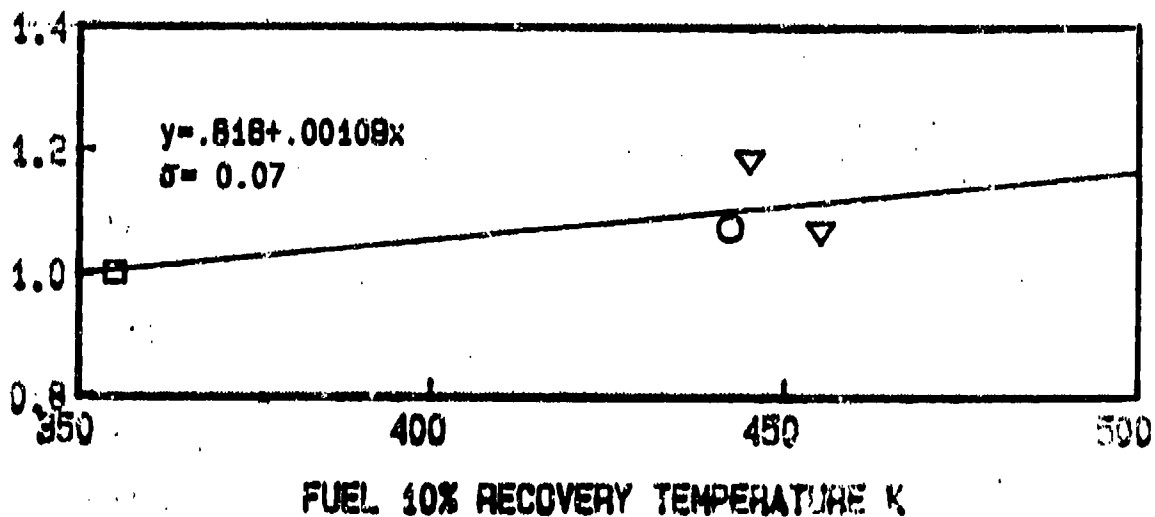
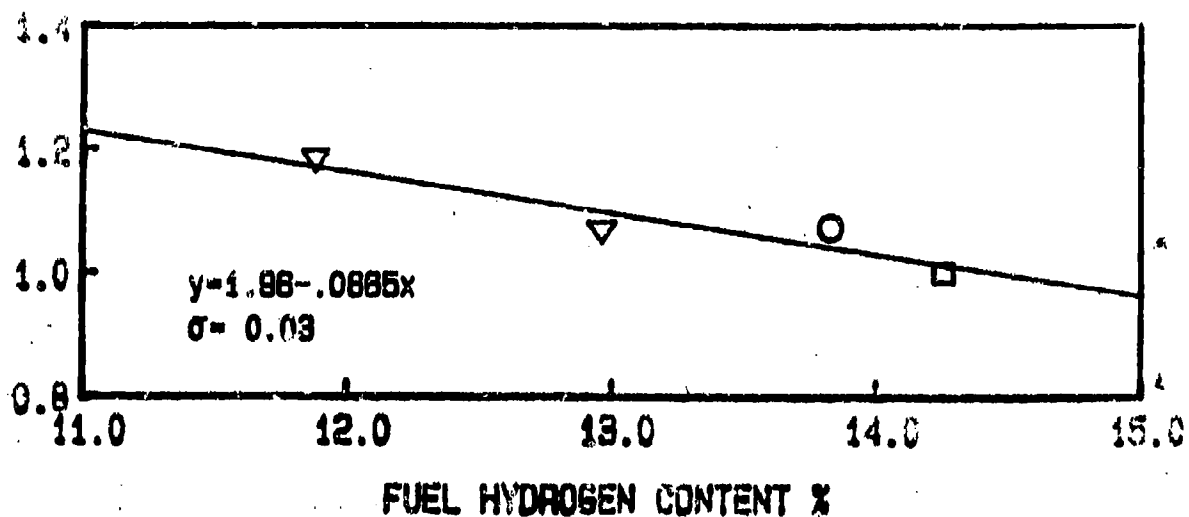


Figure 6.35: Effects of Fuel Properties on Relative Pattern Factor (JT15D-5 Atmospheric, BOM, Airblast Nozzle)

70% RELATIVE PROFILE FACTOR

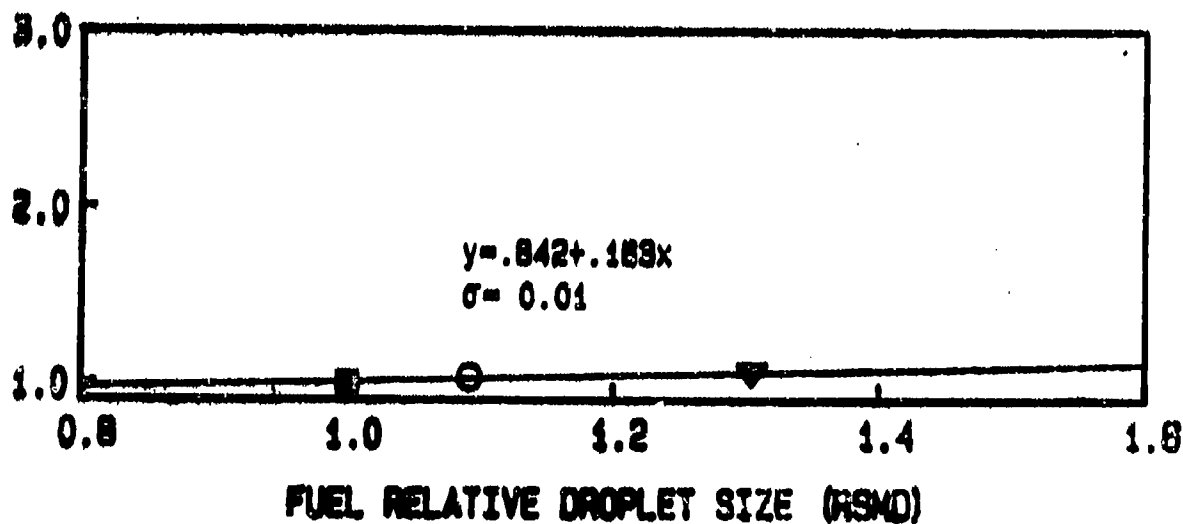
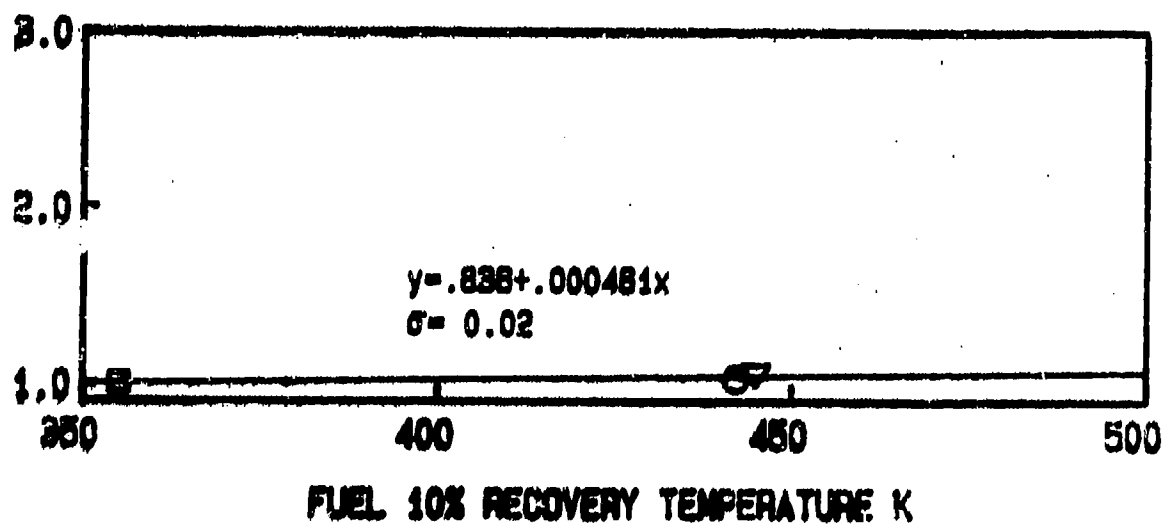
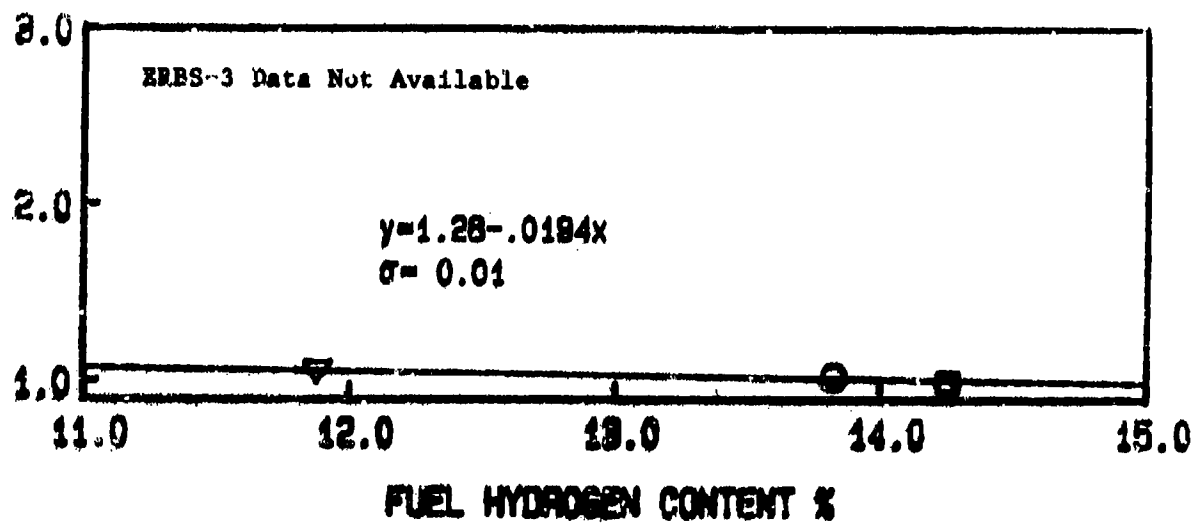


Figure 6.36: Effects of Fuel Properties on Relative Profile Factor (JT15D-5 Atmospheric, Rich P.E., Airblast Nozzle)

70% RELATIVE PATTERN FACTOR

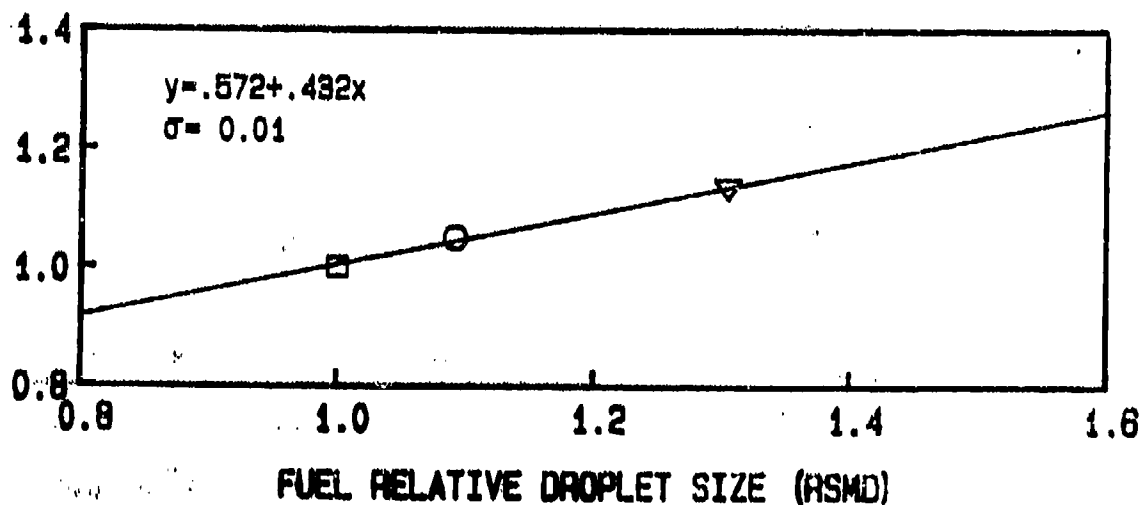
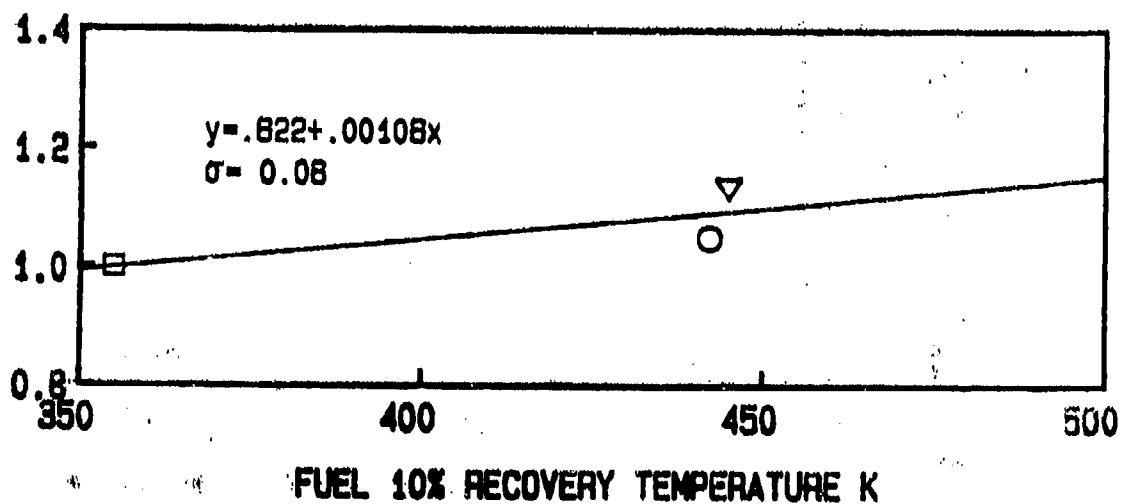
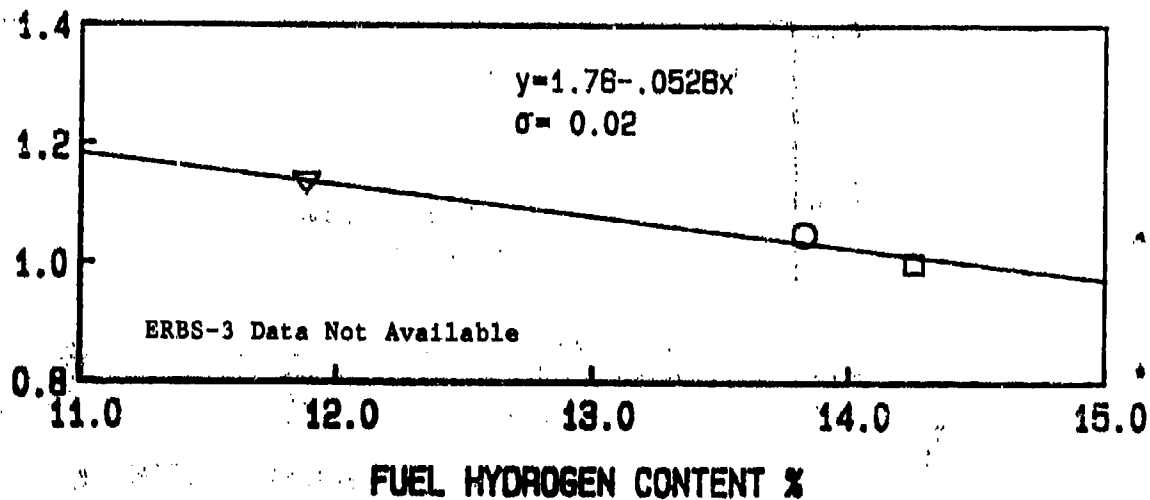
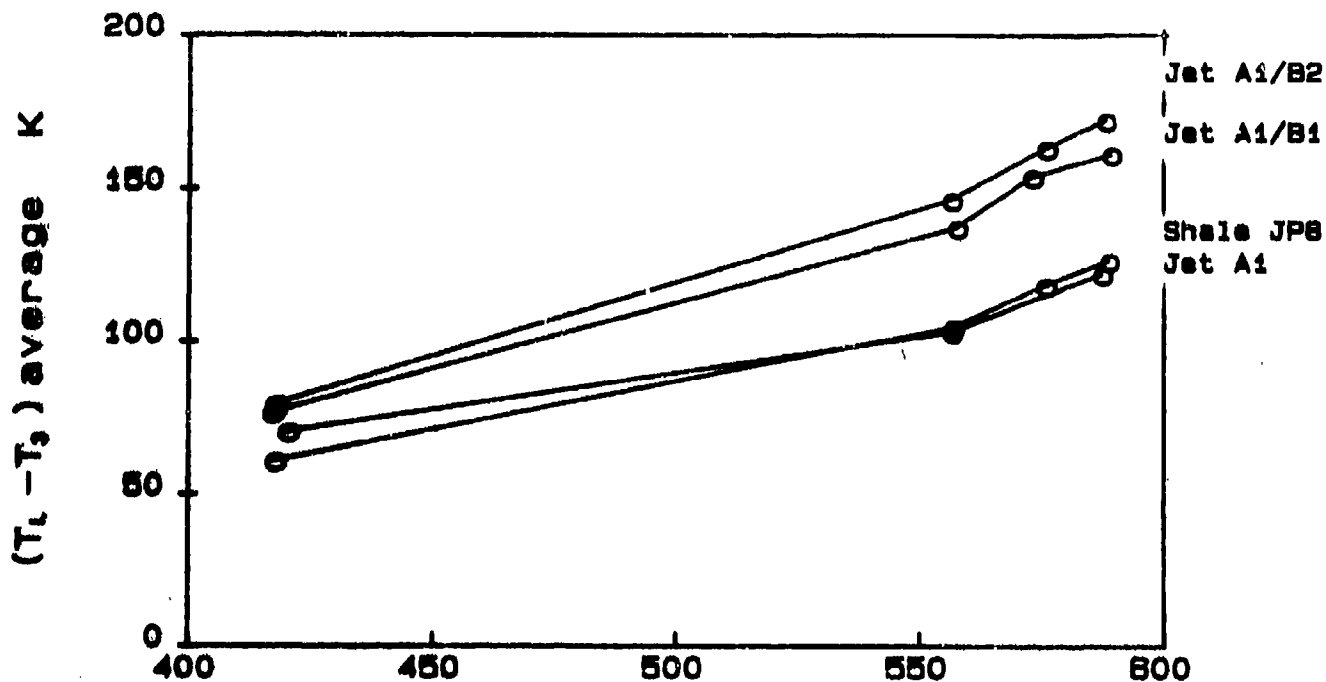
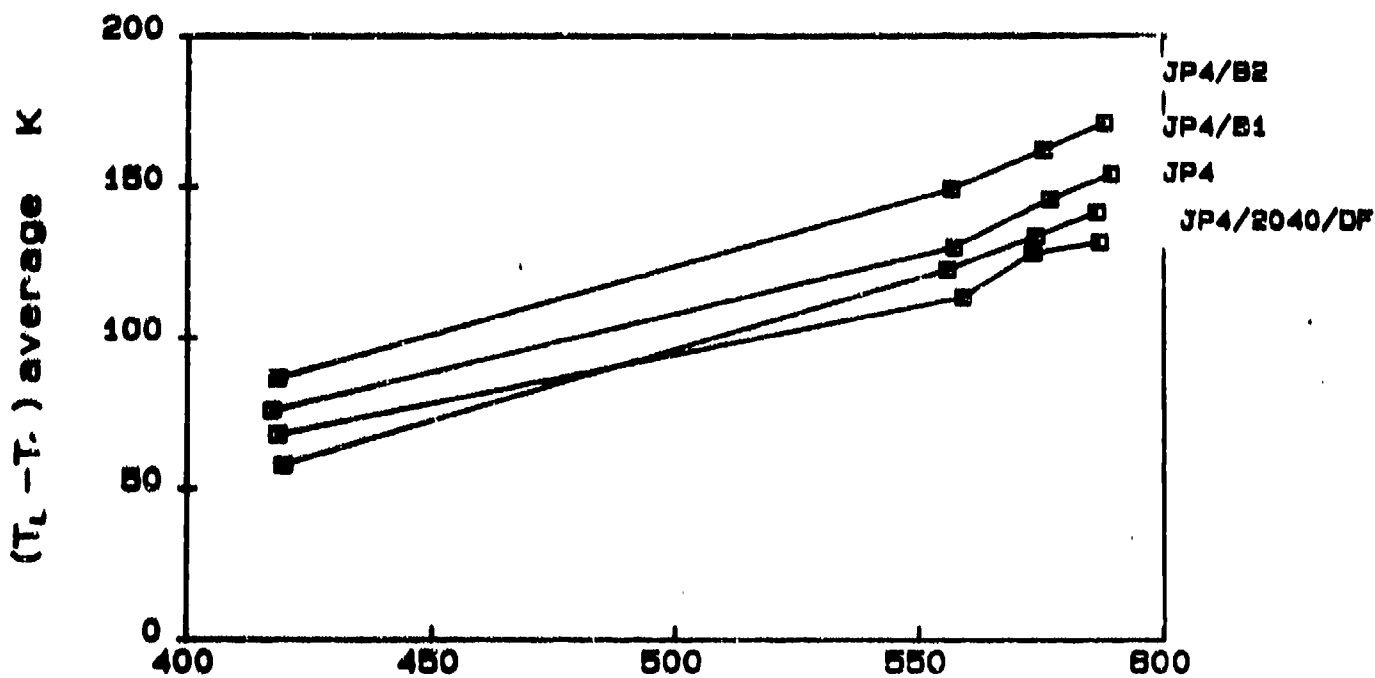


Figure 6.37: Effects of Fuel Properties on Relative Pattern Factor (JT15D-5 Atmospheric, Rich P.Z., Airblast Nozzle)

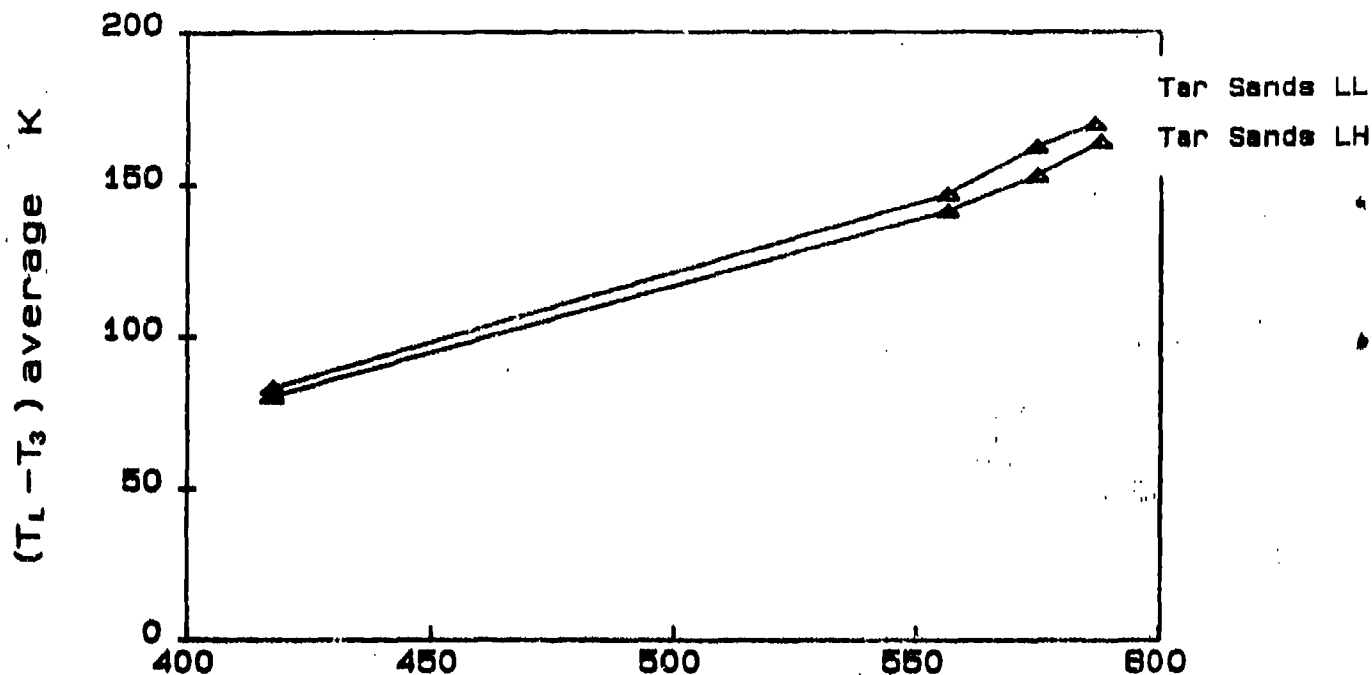


T_3 COMBUSTOR INLET TEMPERATURE K

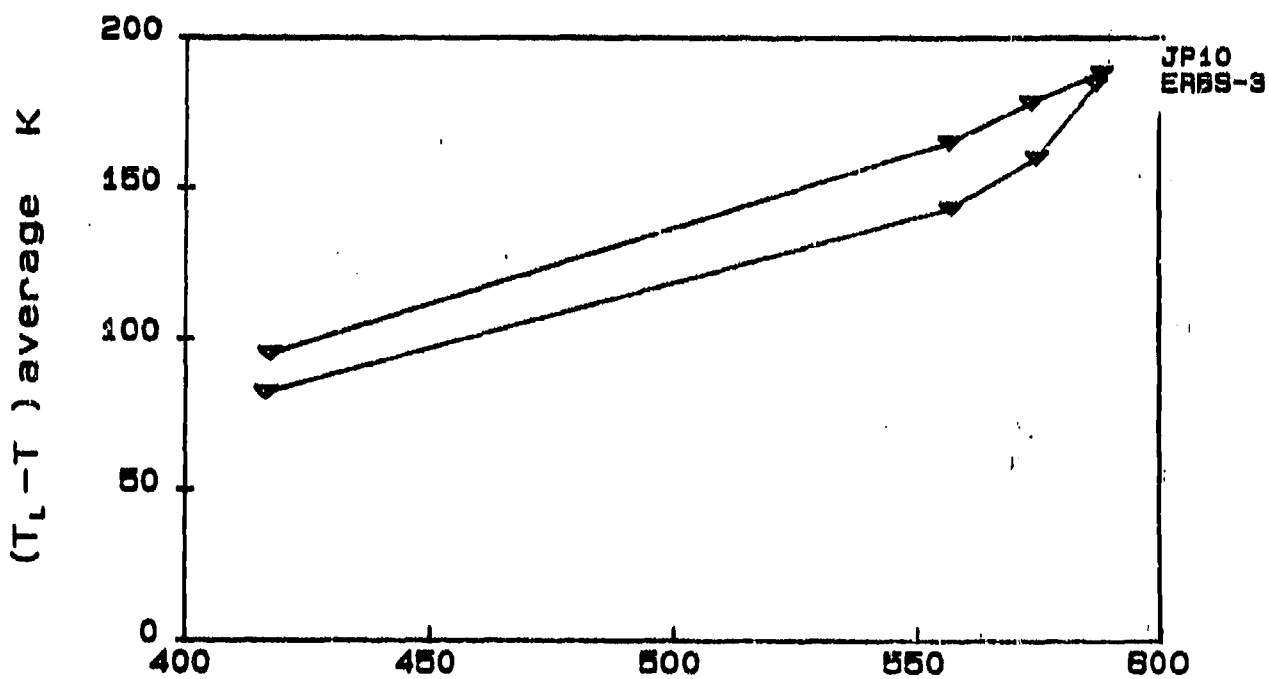


T_3 COMBUSTOR INLET TEMPERATURE K

Figure 6.38: Liner Temperature Variations Over Combustor Operating Range (PT6A-65 Atmospheric, BOM, Simplex 0.65 FN)



T3 COMBUSTOR INLET TEMPERATURE K



T3 COMBUSTOR INLET TEMPERATURE K

Figure 6.39: Liner Temperature Variations Over Combustor Operating Range
(PT6A-65 Atmospheric, BOM, Simplex 0.65 FN)

70% POWER, $(T_1 - T_2)$ average K

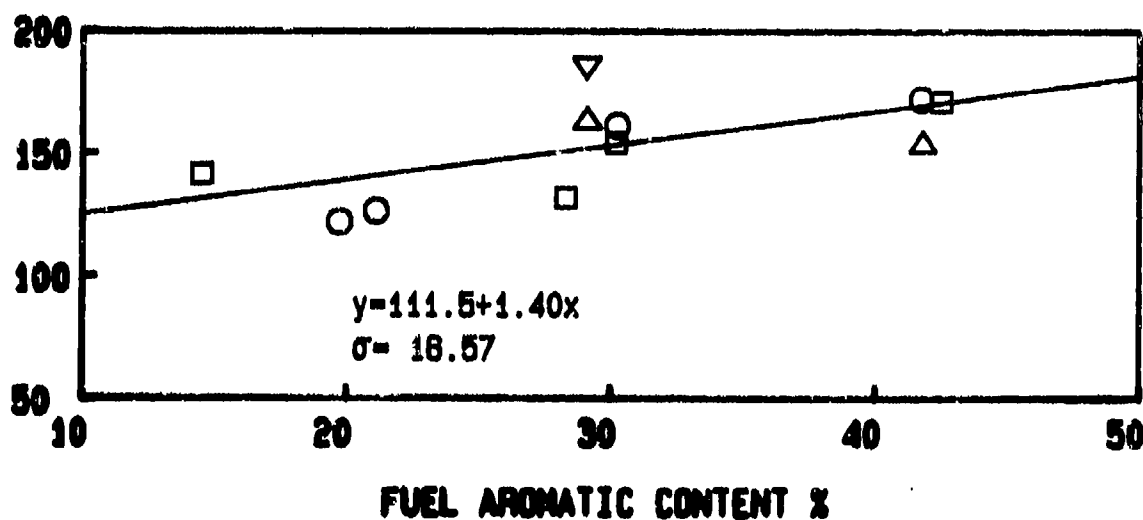
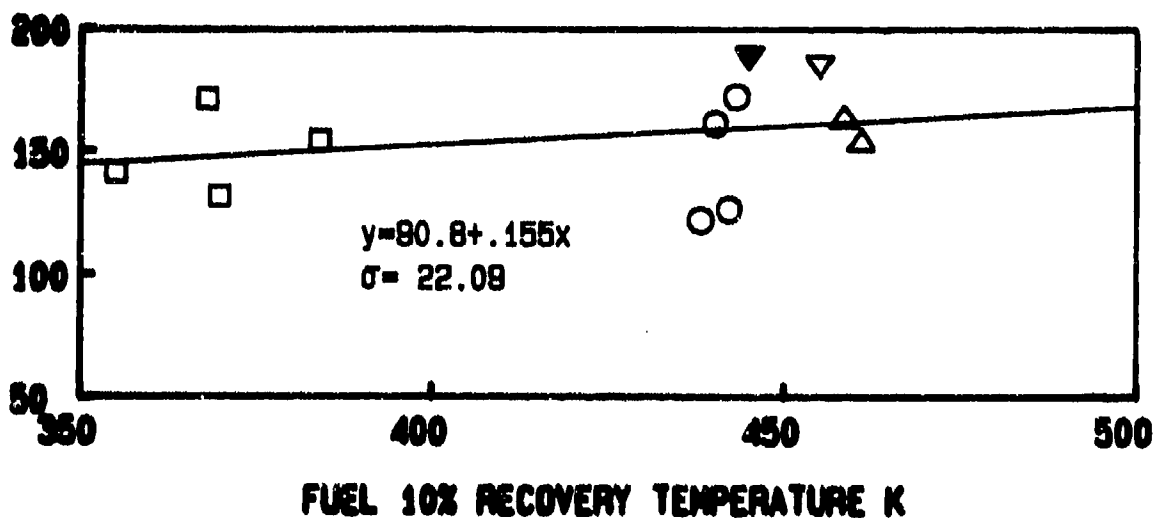
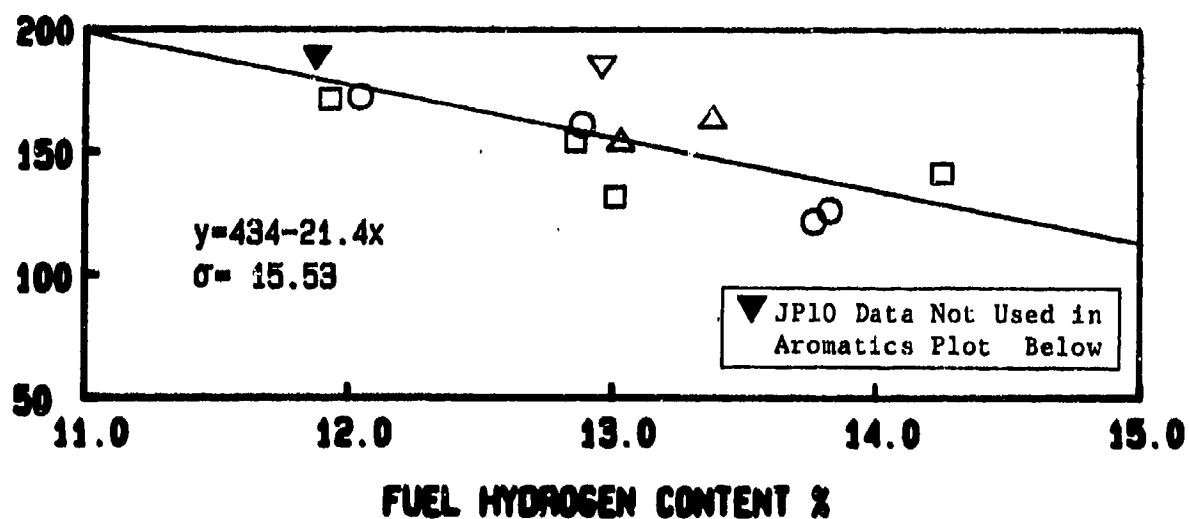


Figure 6.40: Effects of Fuel Properties on 70% Power Liner Temperatures (PT6A-65 Atmospheric, BOM, Simplex 0.65 FN)

LINER TEMPERATURE PARAMETER (average)

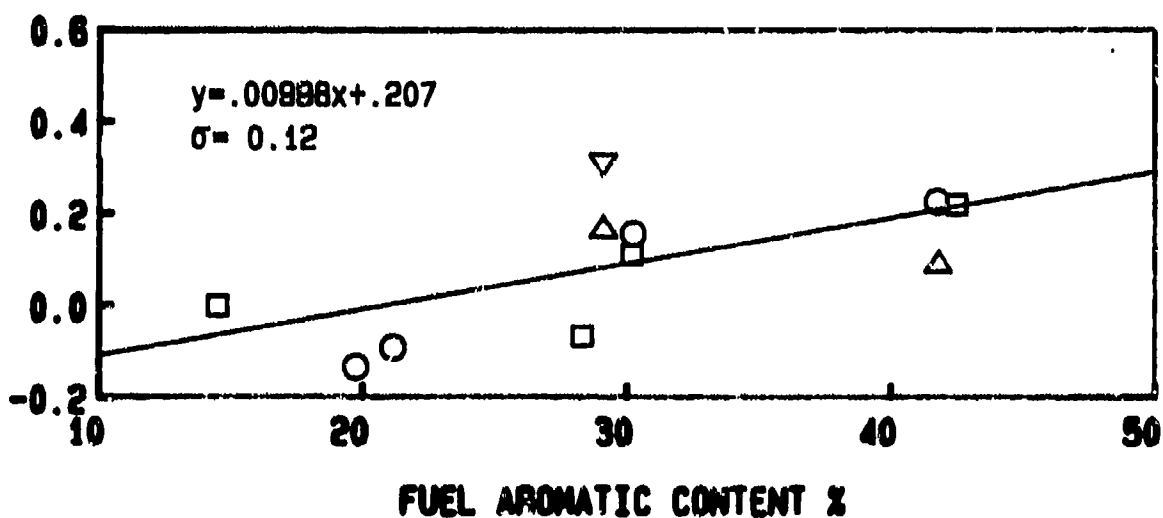
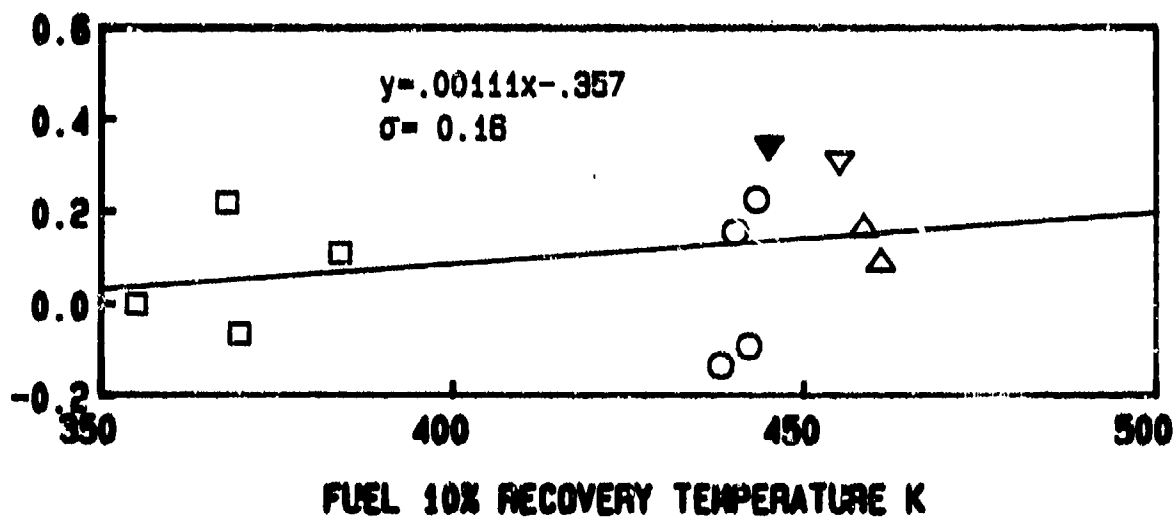
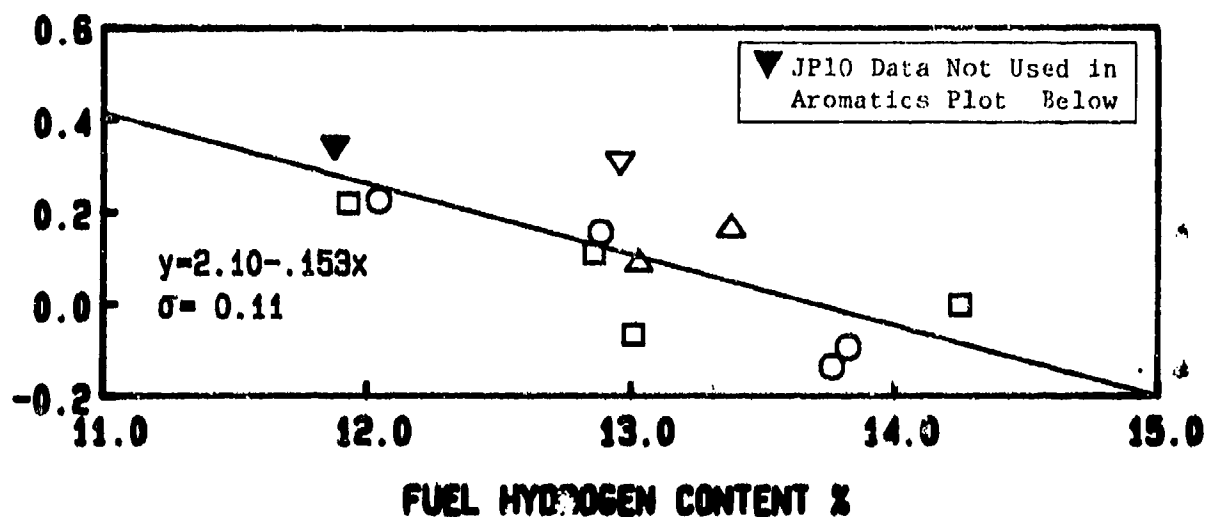


Figure 6.41: Effects of Fuel Properties on Liner Temperature Parameter (PT6A-65 Atmospheric, BOM, Simplex 0.65 FN)

70% POWER, $(T_L - T_3)$ peak K

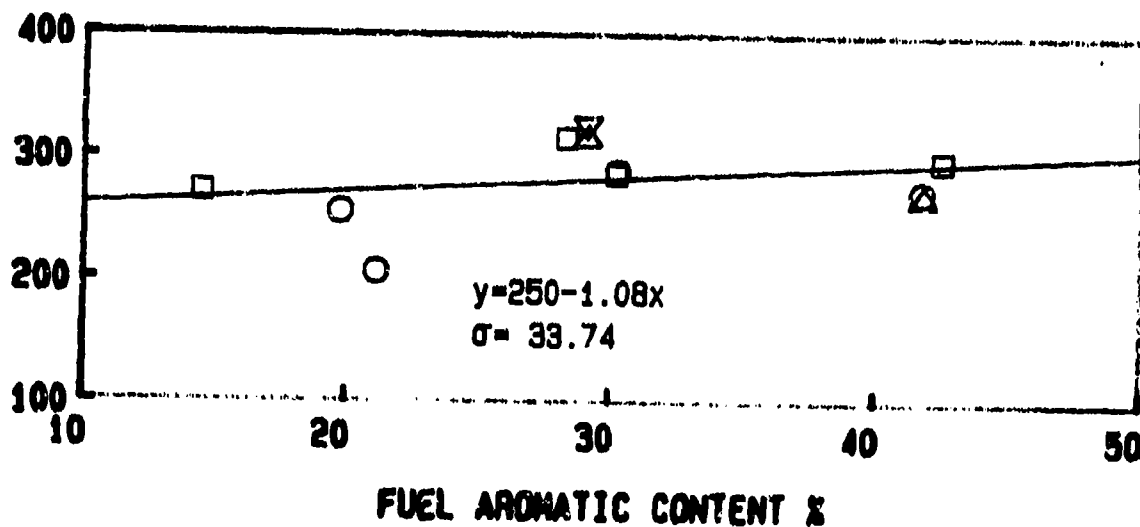
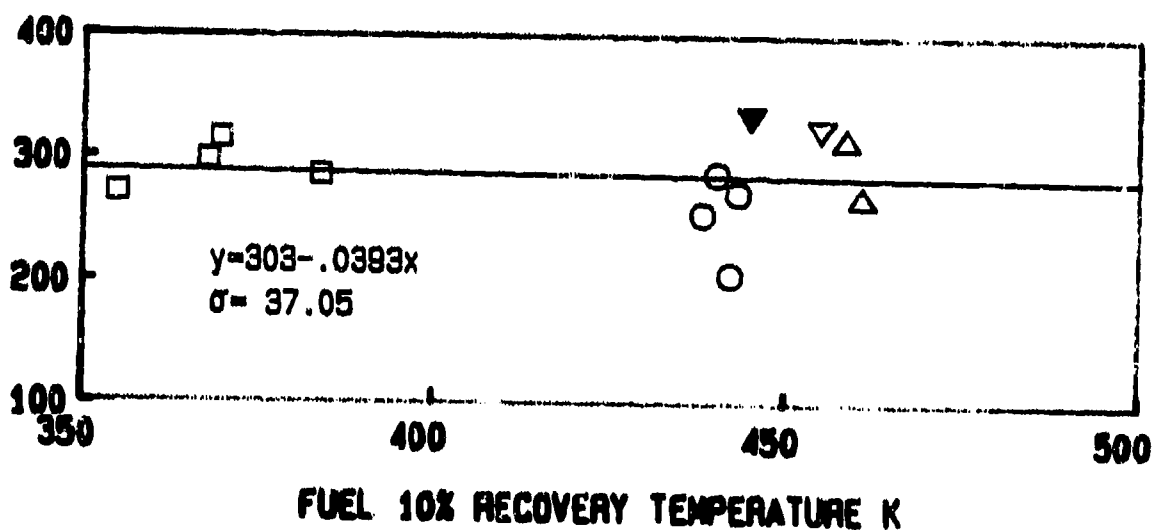
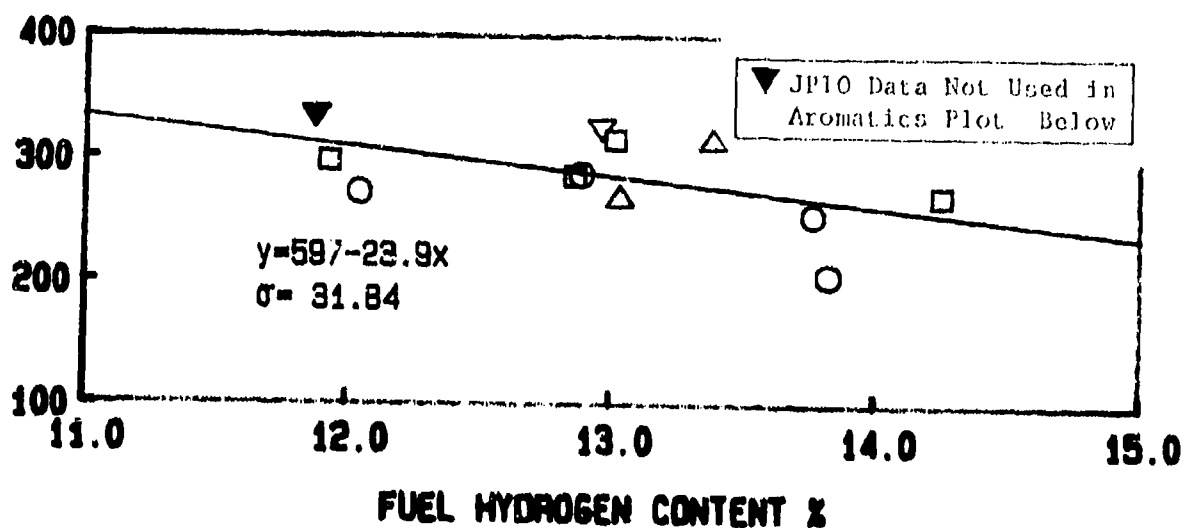


Figure 6.42: Effects of Fuel Properties on 70% Power Liner Temperatures (PT6A-65 Atmospheric, BOM, Simplex 0.65 FN)

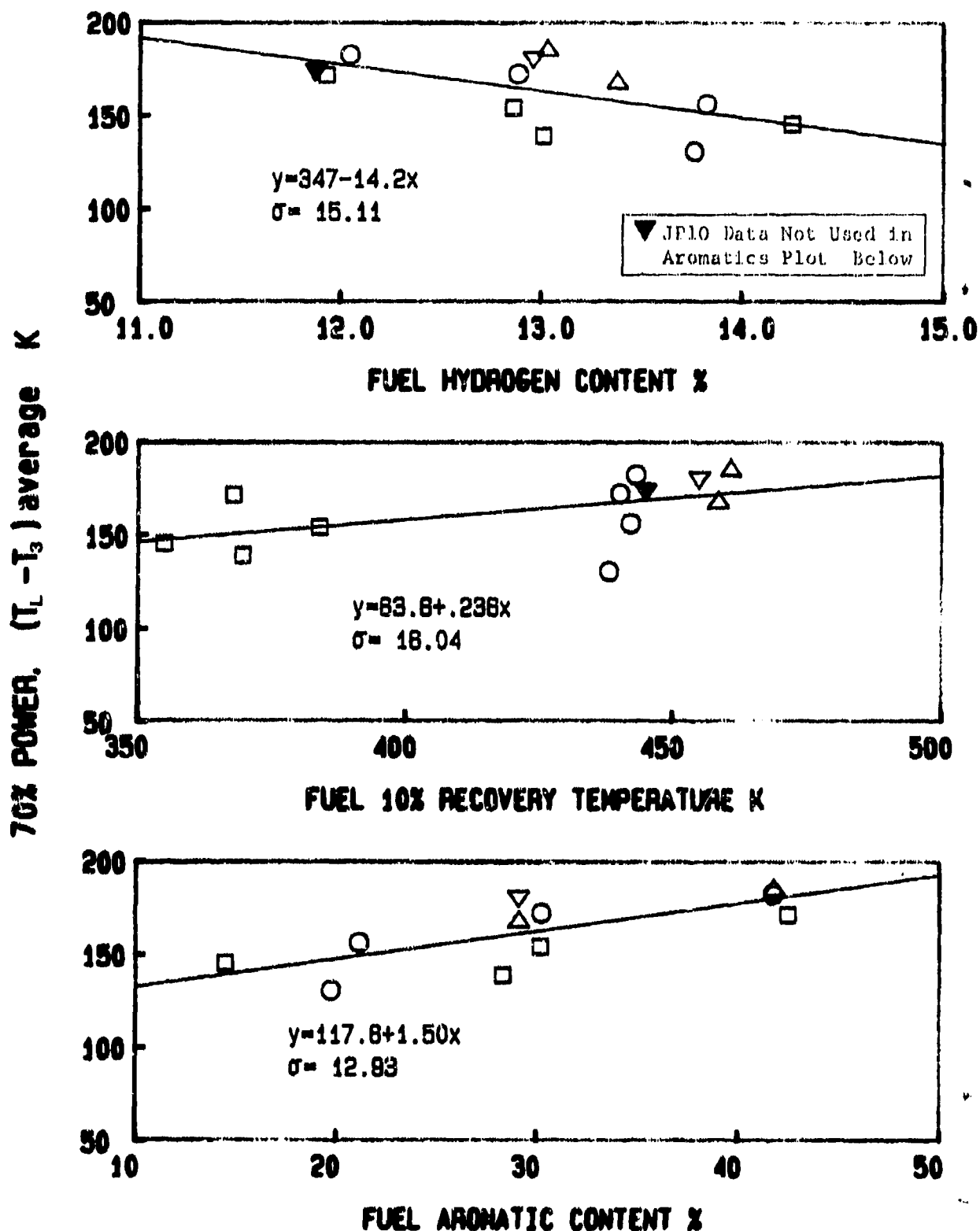


Figure 6.43: Effects of Fuel Properties on 70% Power Liner Temperature (PT6A-65 Atmospheric, Lean P.Z., Simplex 0.65 FN)

LINER TEMPERATURE PARAMETER (average)

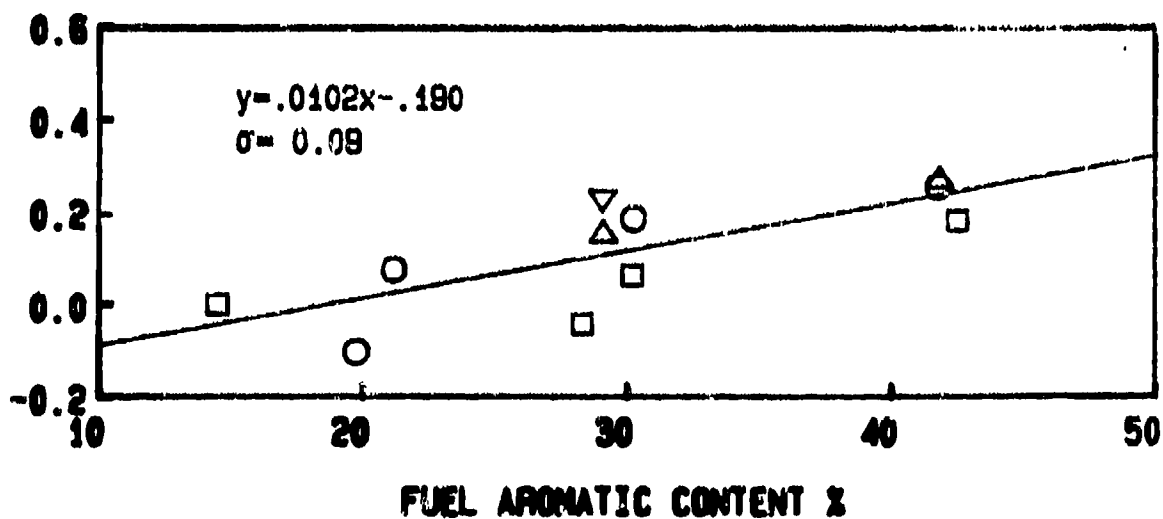
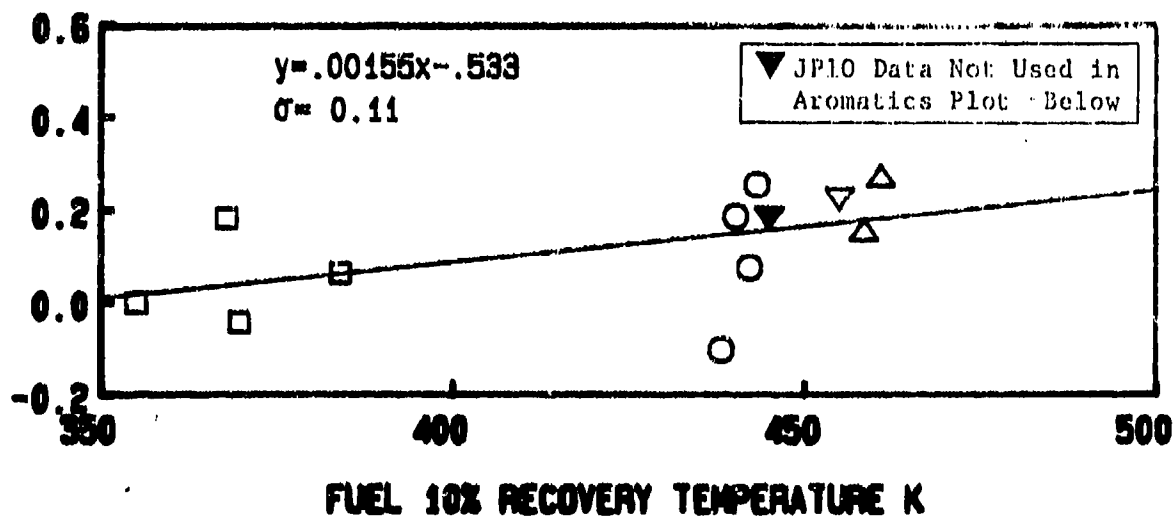
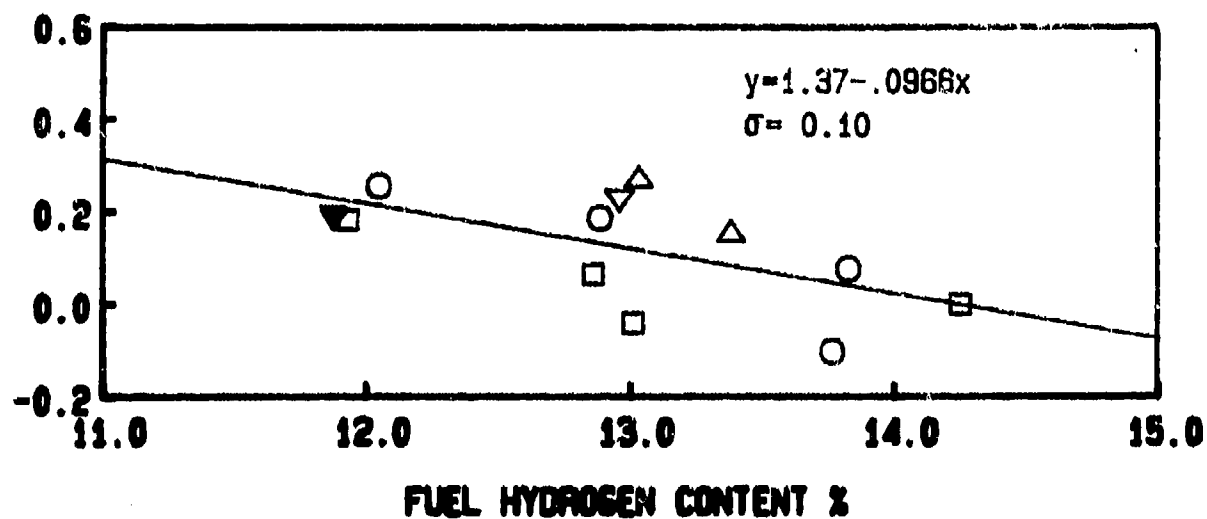


Figure G.44: Effects of Fuel Properties on Liner Temperatures (PT6A-65 Atmospheric, Lean P.Z, Simplex .65 FN)

70% POWER, $(T_L - T_3)$ peak K

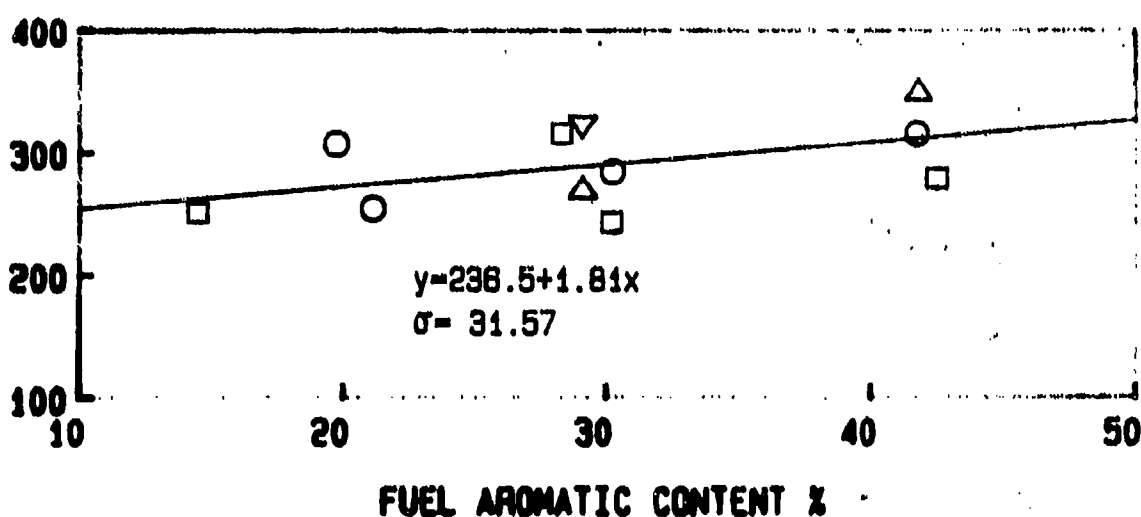
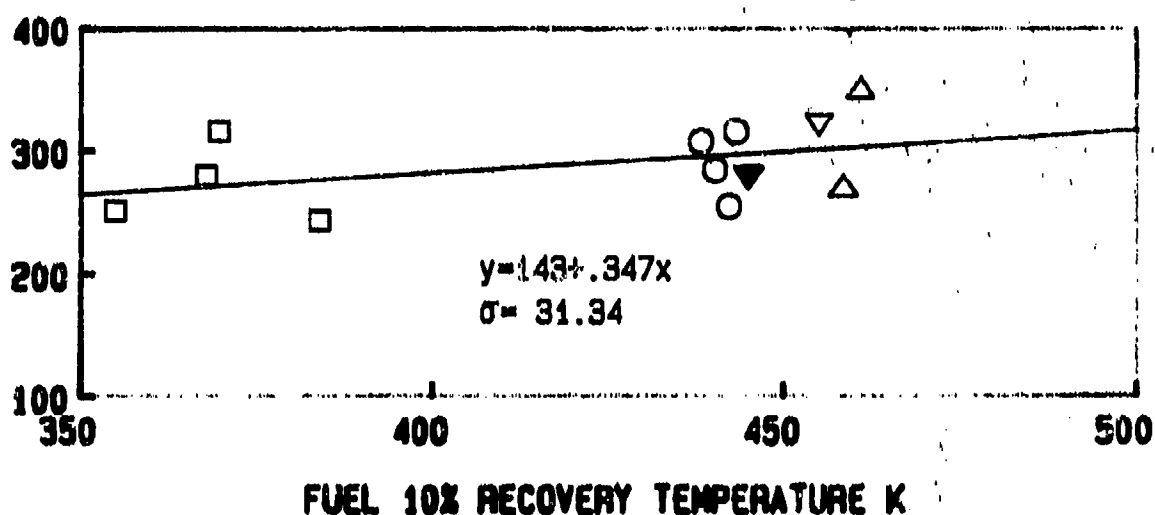
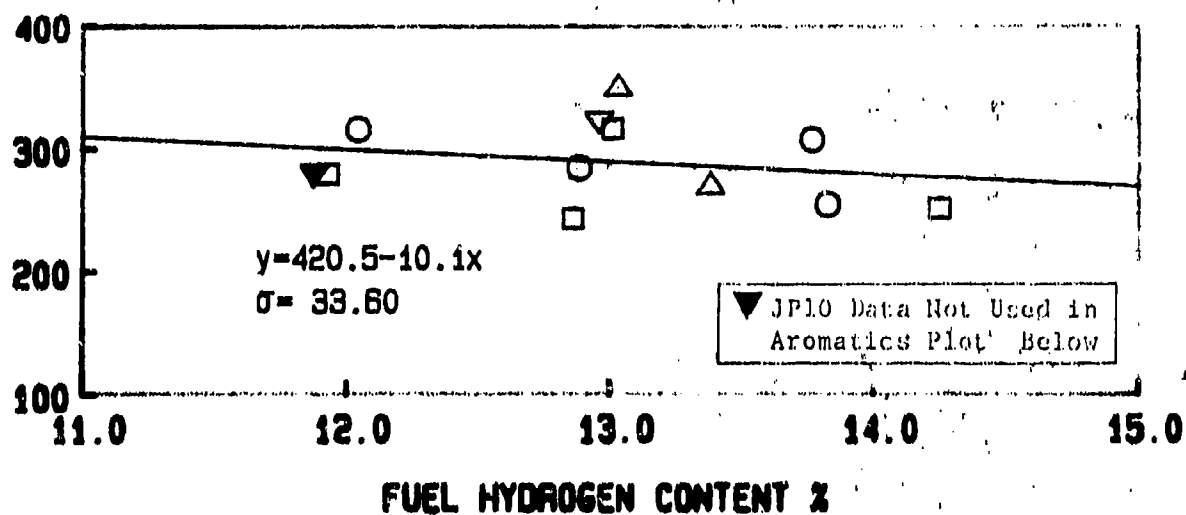


Figure 6.45: Effects of Fuel Properties on 70% Power Liner Temperatures (PT6A-65 Atmospheric, Lean P.Z., Simplex 0.65 FN)

70% POWER, $(T_L - T_3)$ average K

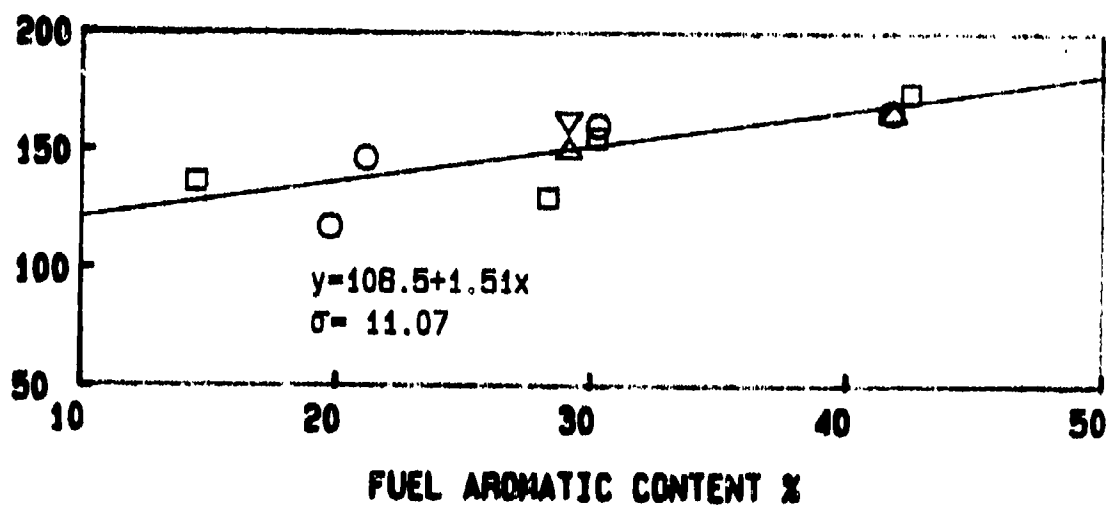
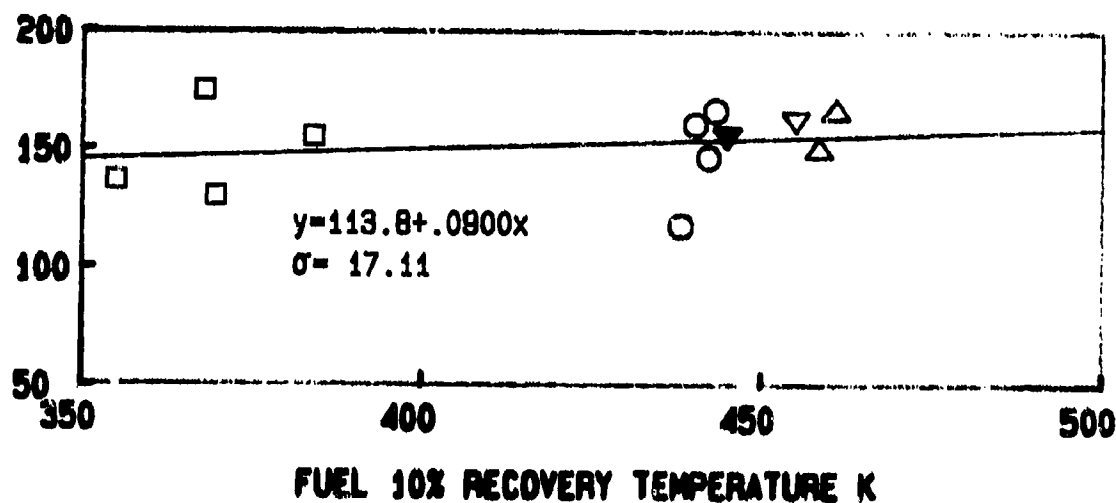
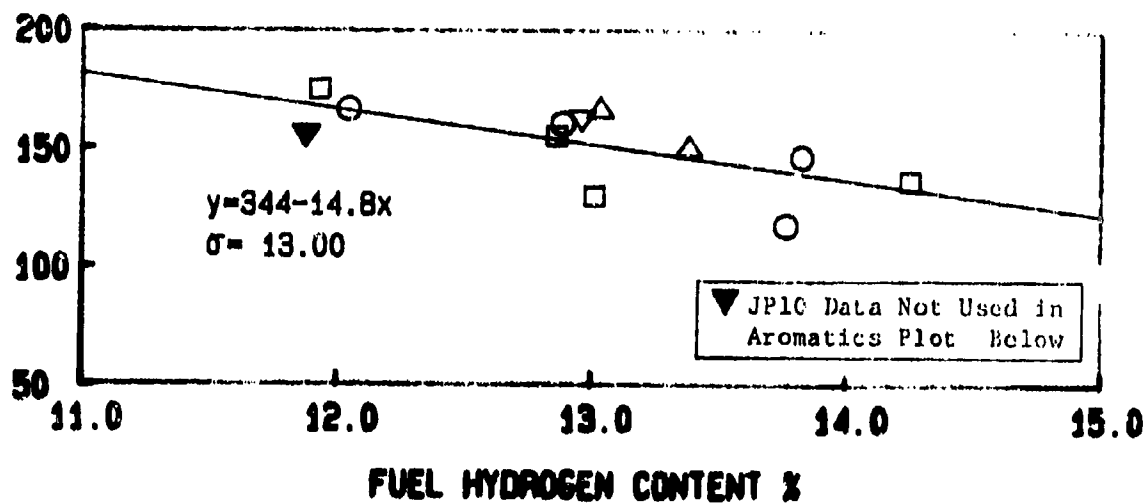


Figure 6. 46: Effects of Fuel Properties on 70% Power Liner Temperatures (PT6 5 Atmospheric, BOM, Nozzle, Simplex 1.1 FN)

LINEAR TEMPERATURE PARAMETER (average)

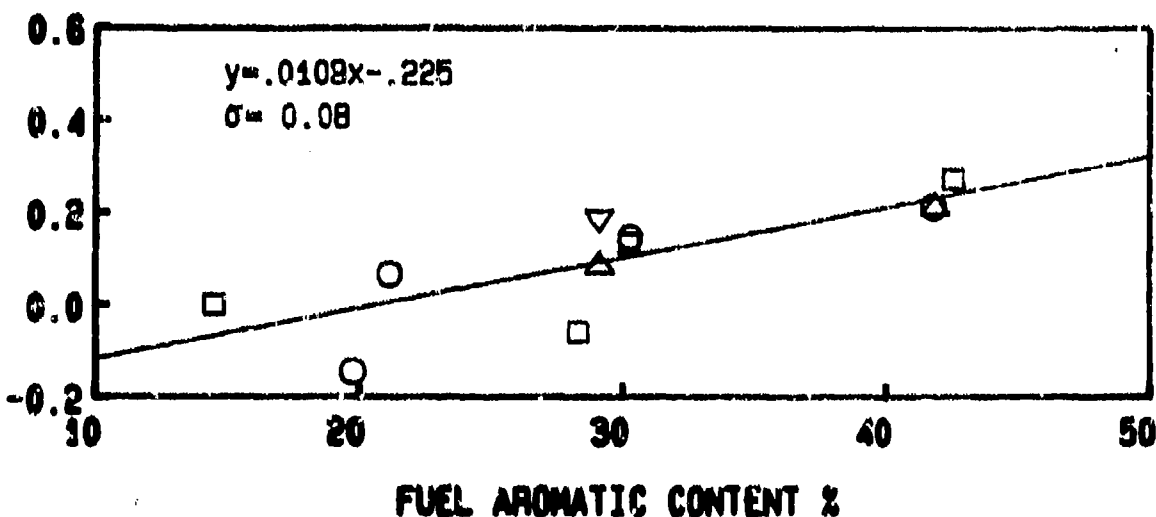
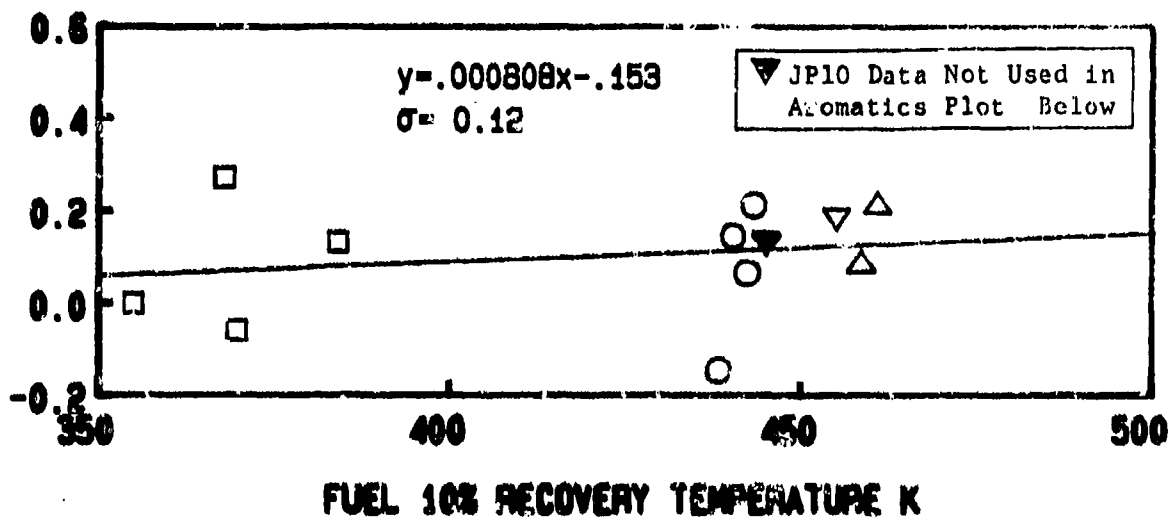
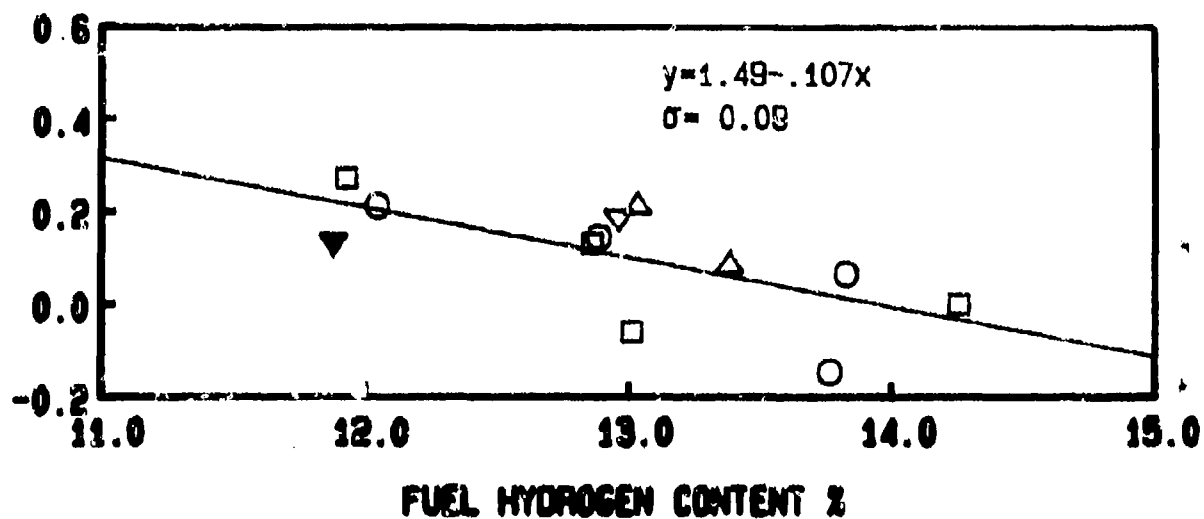


Figure 6.47: Effects of Fuel Properties on Liner Temperatures (PT6A-65 Atmospheric, BOM, Simplex 1.1 FN)

70% POWER, $(T_L - T_3)$ peak K

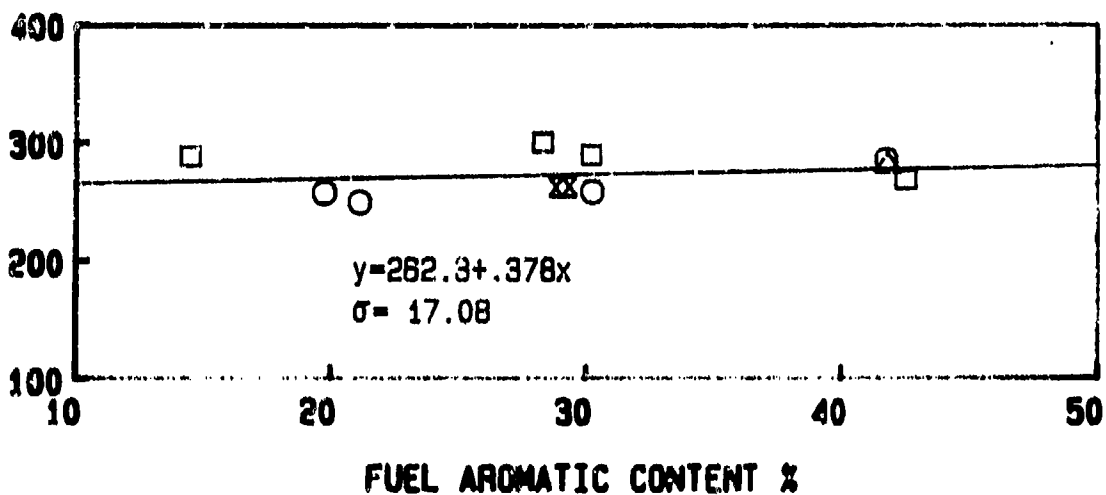
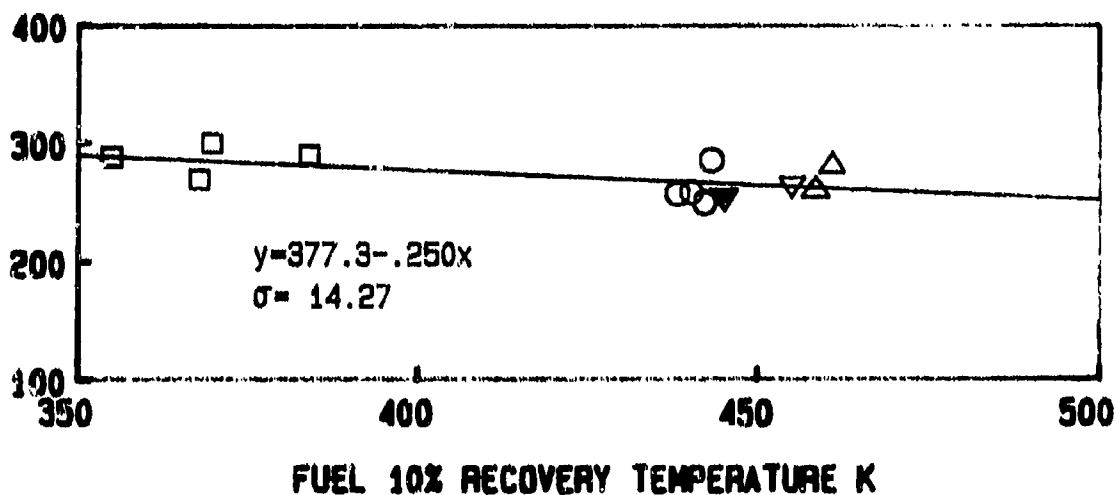
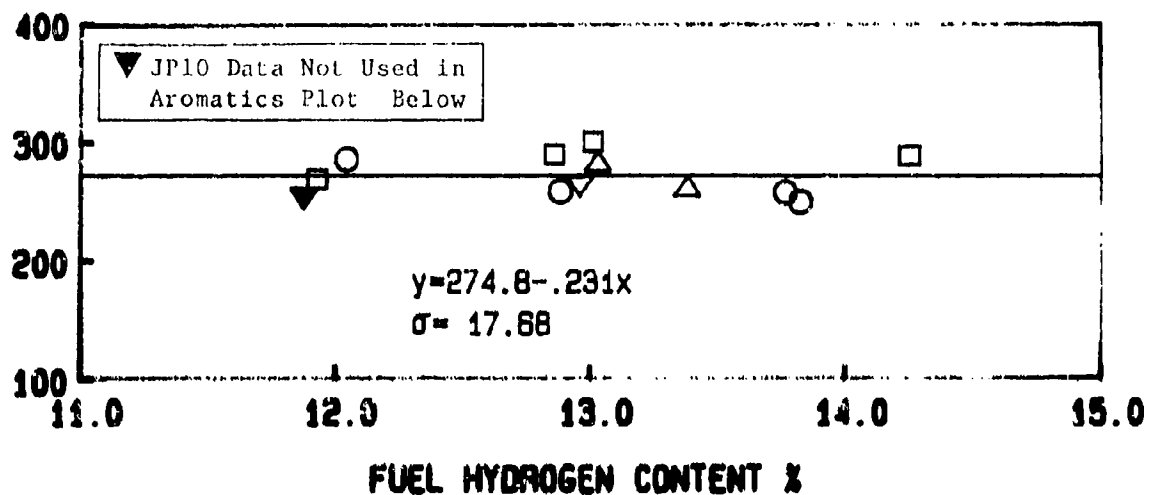


Figure 6.48: Effects of Fuel Properties on 70% Power Liner Temperatures (PT6A-65 Atmospheric, BOM, Simplex 1.1 FN)

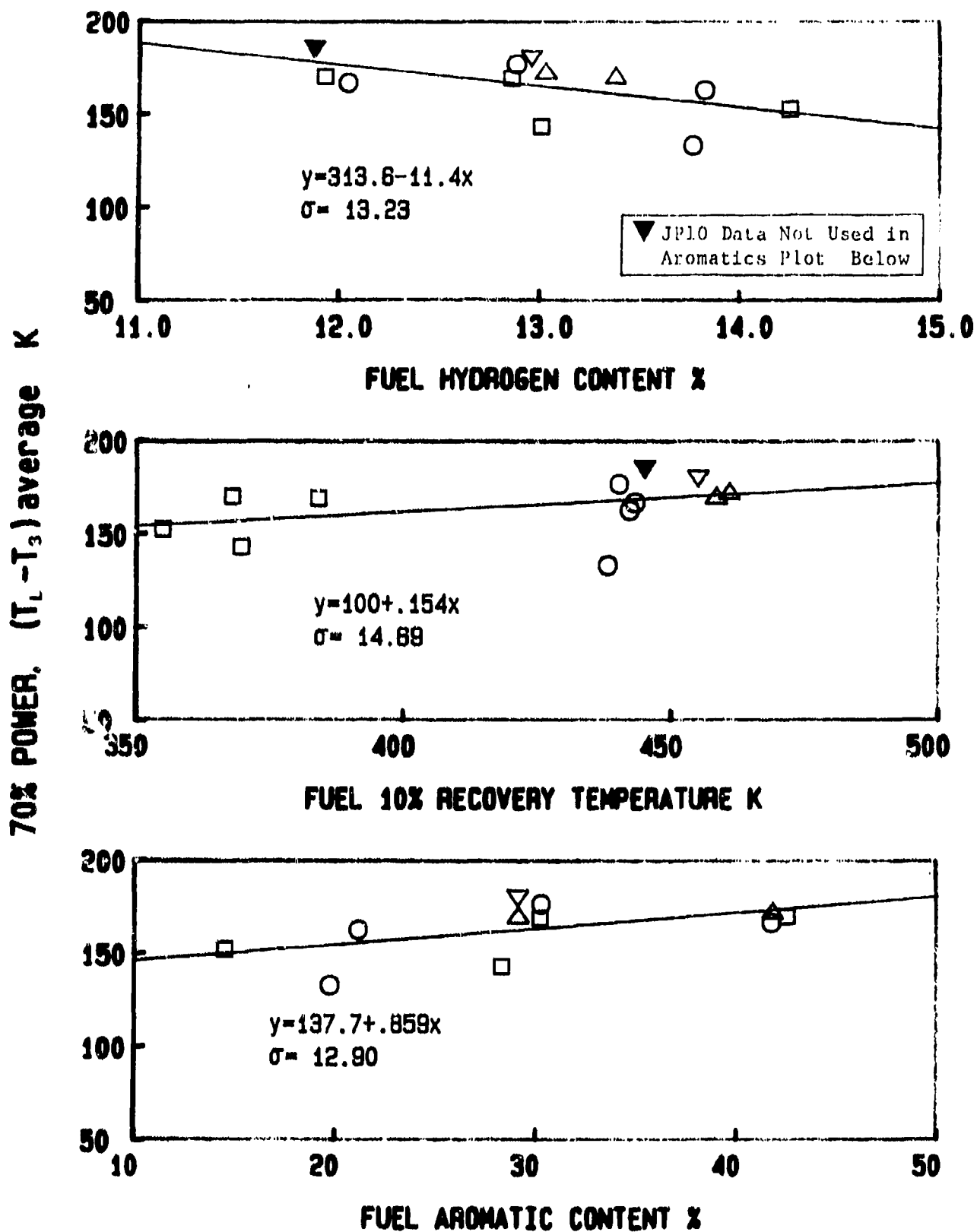


Figure 6.49: Effects of Fuel Properties on 70% Power Liner Temperatures (PT6A-65 Atmospheric, Lean P.Z., Simplex 1.1 FN)

LINER TEMPERATURE PARAMETER (average)

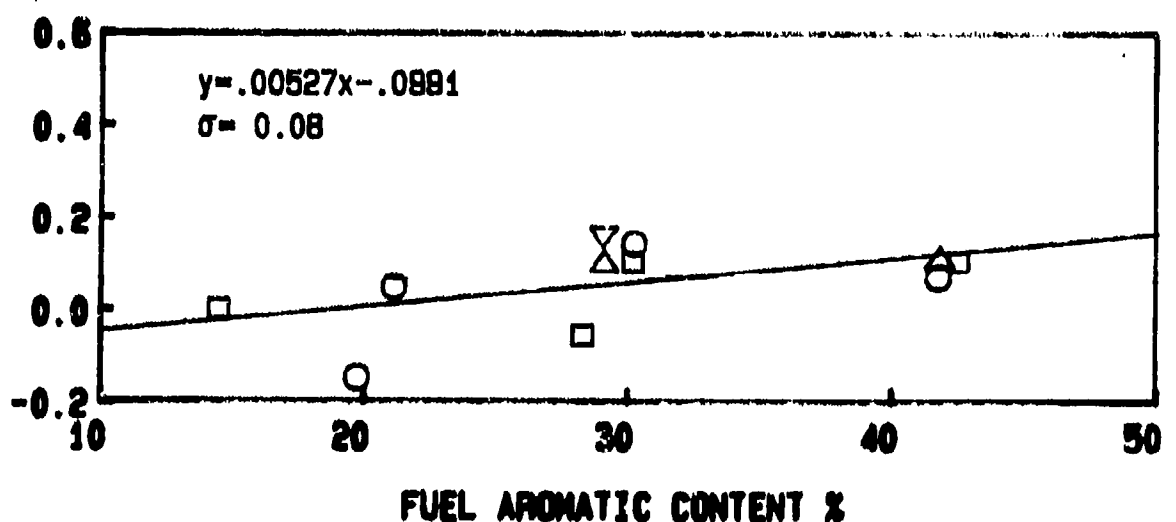
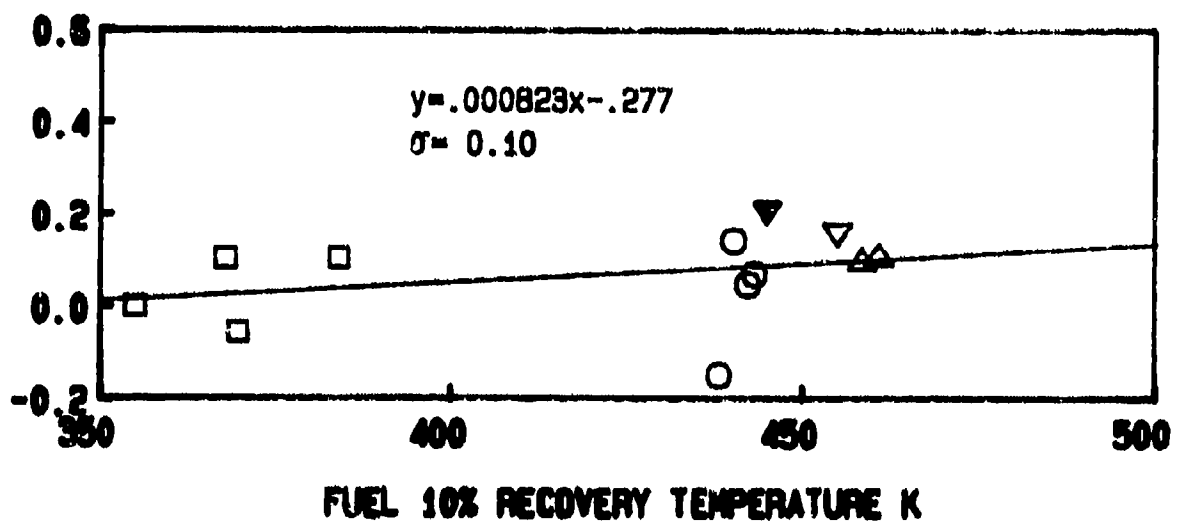
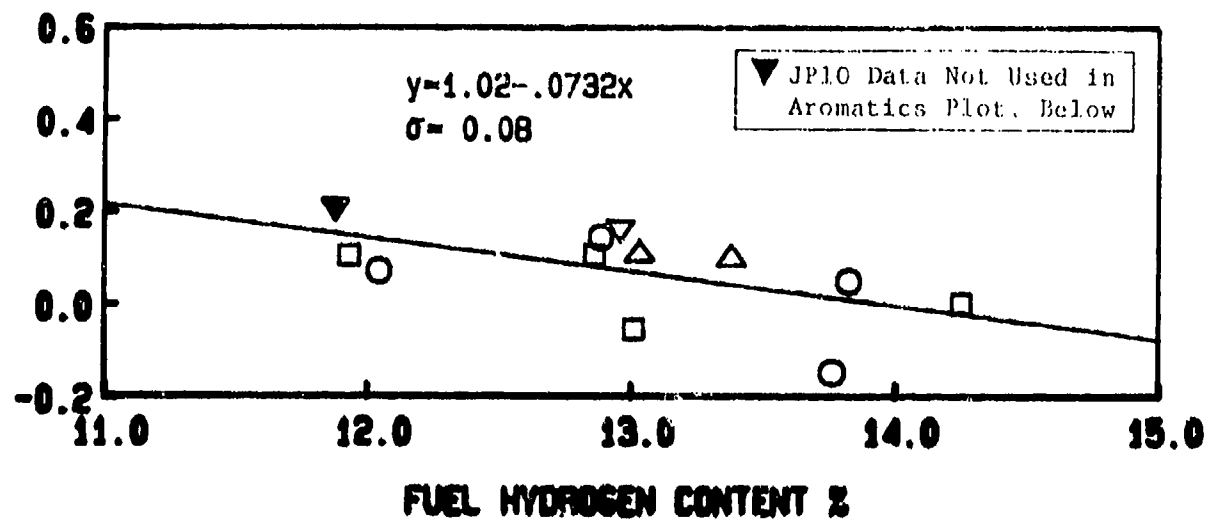


Figure 6.50: Effects of Fuel Properties on Liner Temperatures (PT6A-65 Atmospheric, Lean P.Z, Simplex 1.1 FN)

70% POWER, $(T_L - T_3)$ peak K

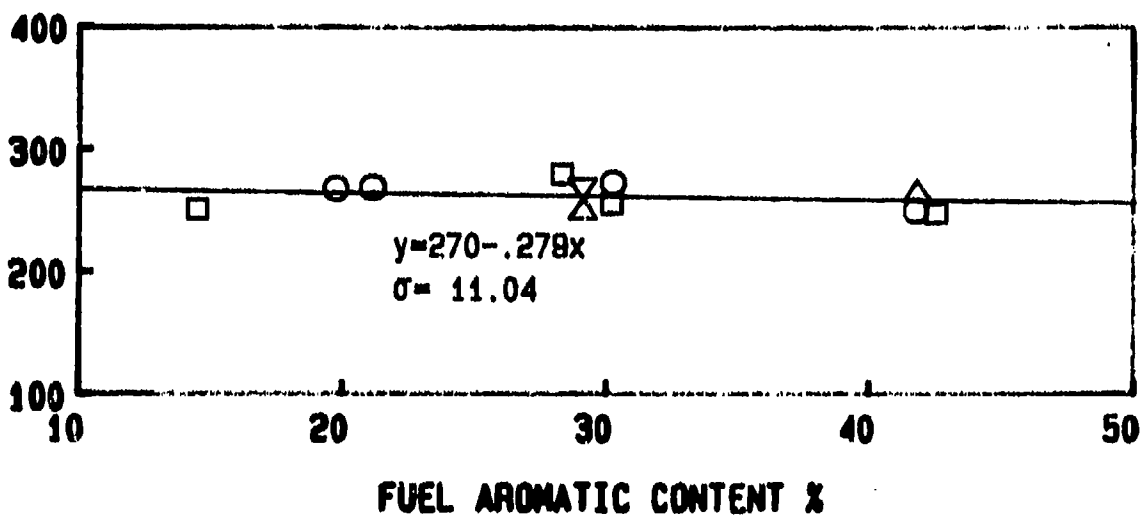
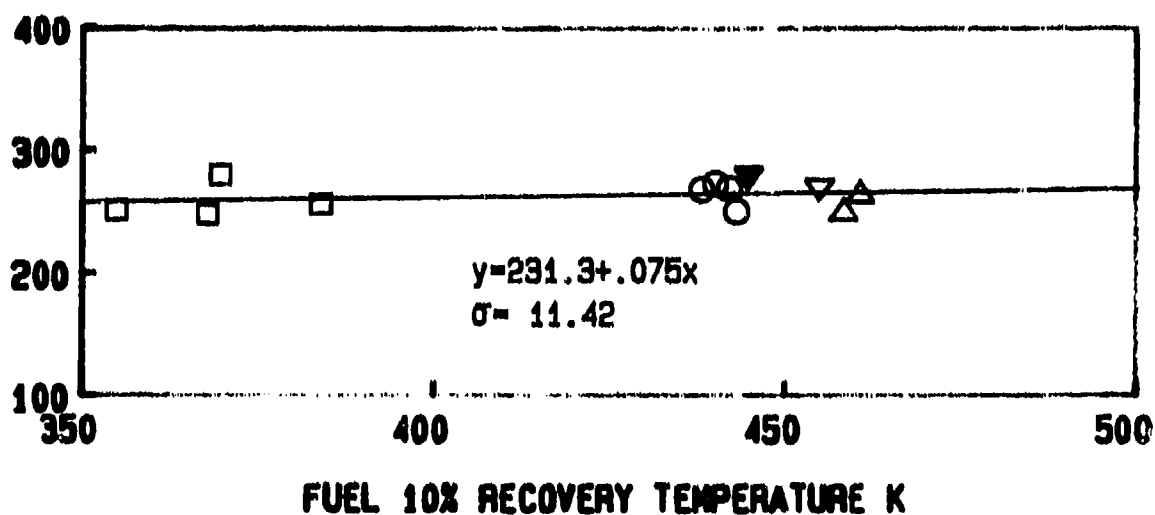
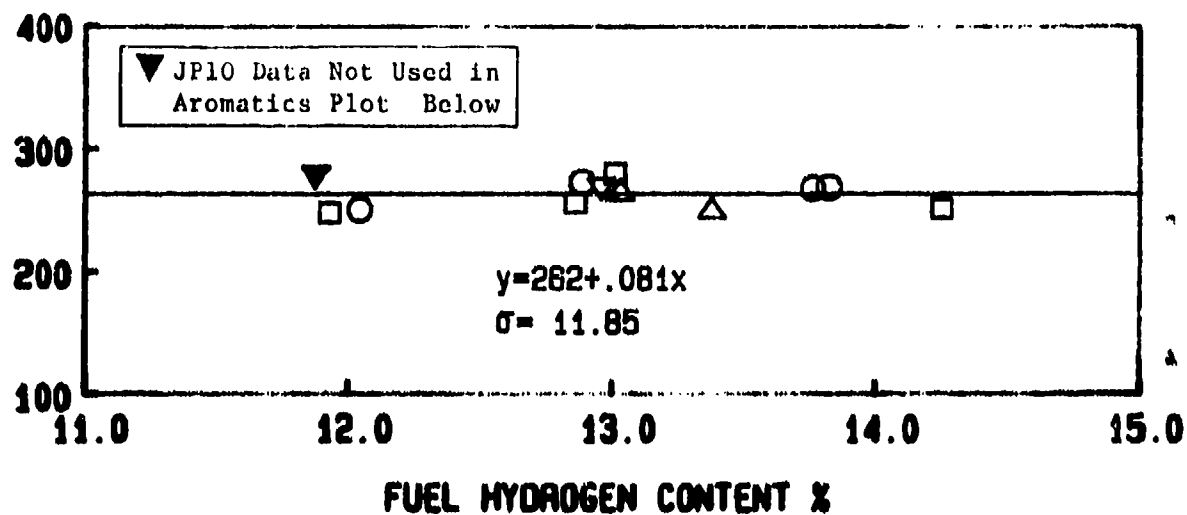


Figure C.51: Effects of Fuel Properties on 70% Power Liner Temperatures (PT6A-65 Atmospheric, Lean P.Z., Simplex 1.1 FN)

LEAN LIMIT FUEL-AIR RATIO (g/kg)

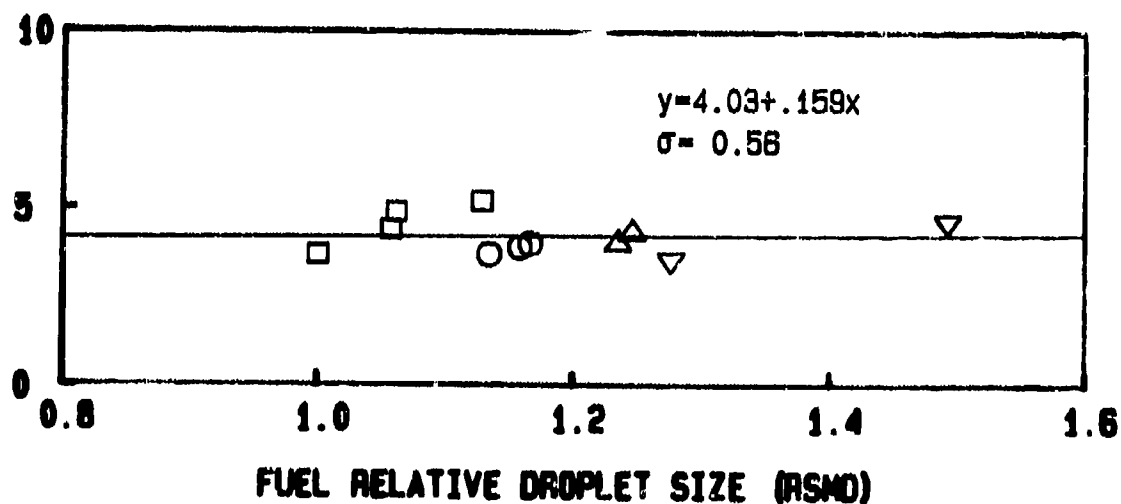
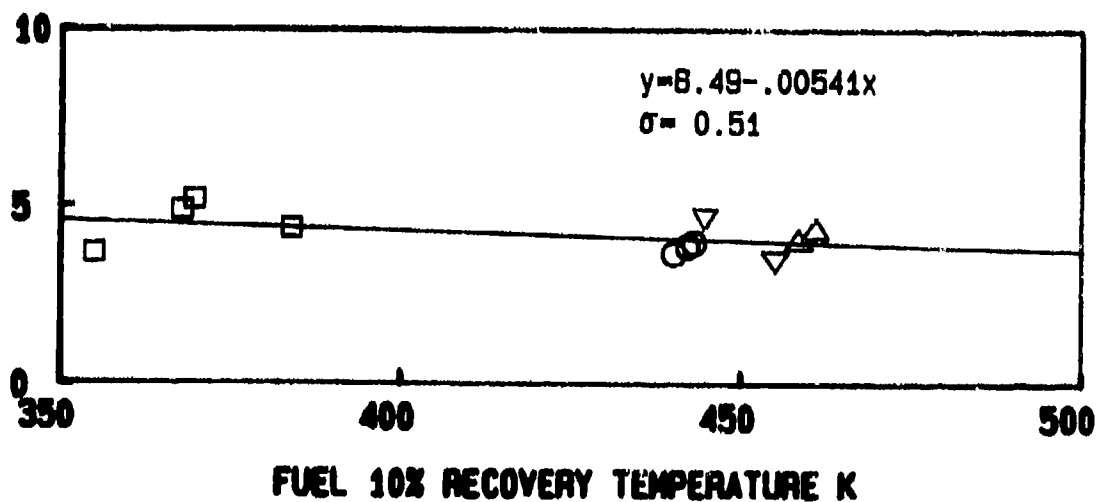
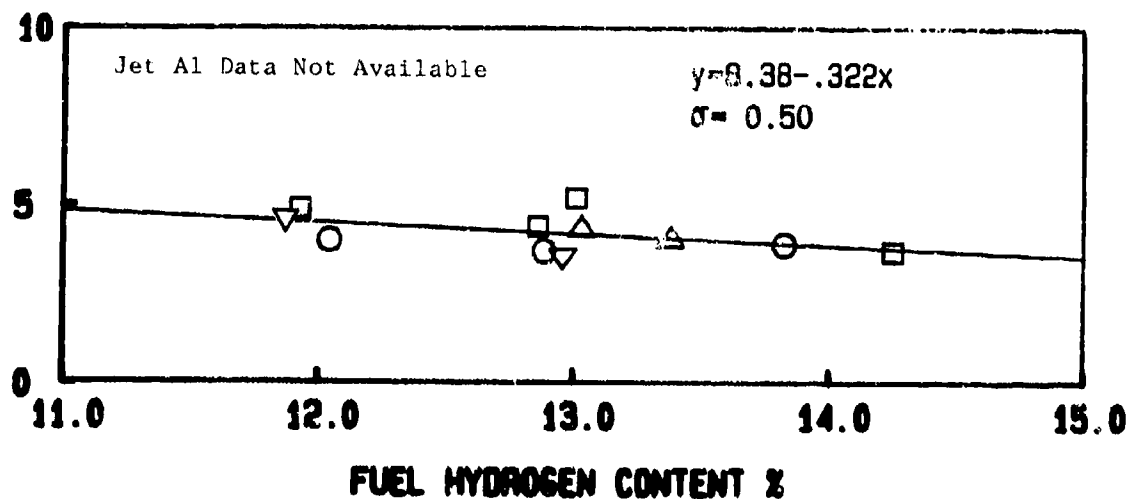


Figure 6.52: Effects of Fuel Properties on Lean Limit Fuel-Air Ratio (PT6A-65 Atmospheric, BOM, Simplex 0.65 FN)

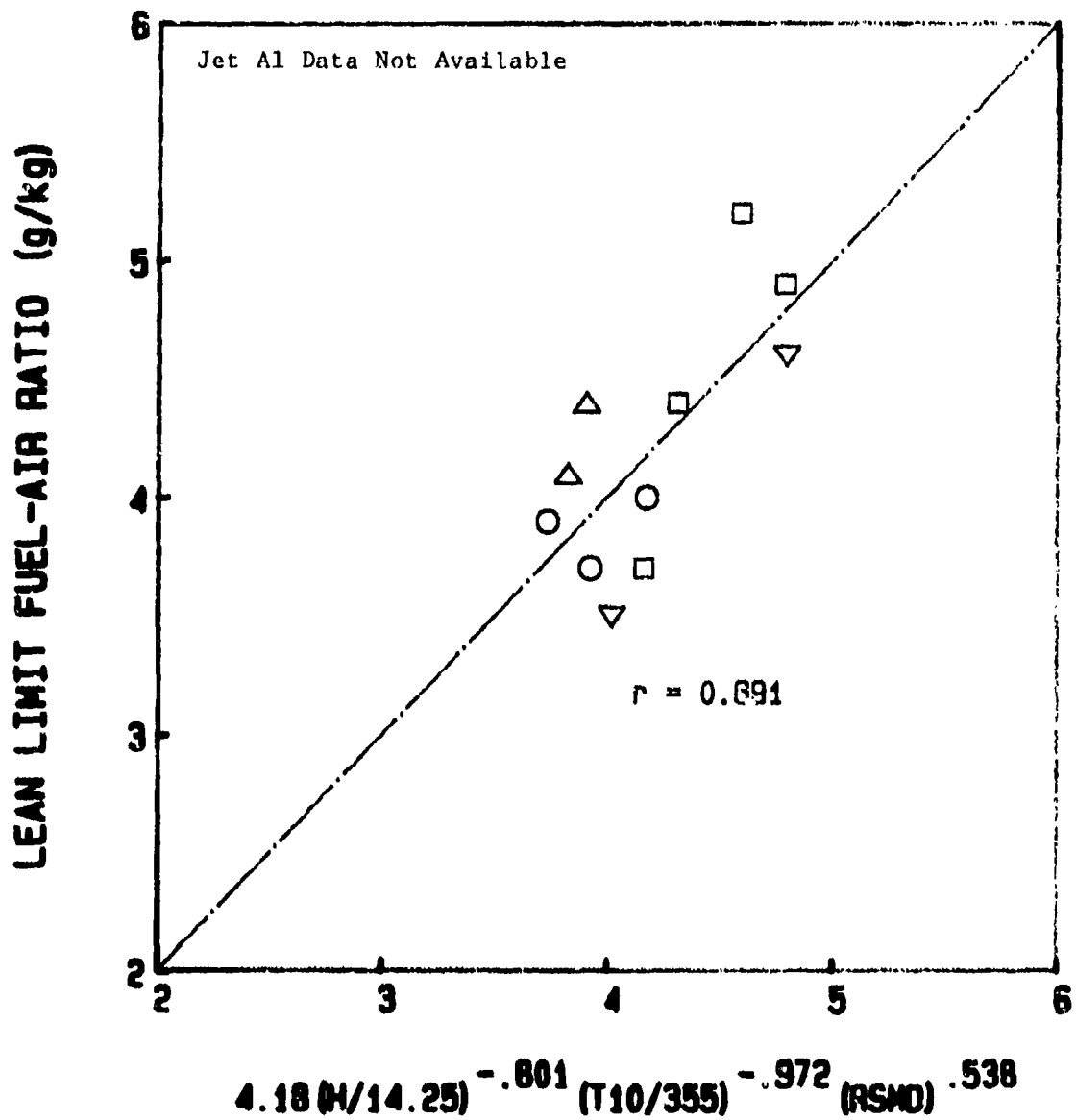


Figure 6.53: Lean Limit Fuel-Air Ratio vs Multiple Parameter Correlation (PT6A-65 Atmospheric, BOM, Simplex 0.65 FN)

LEAN LIMIT FUEL-AIR RATIO (g/kg)

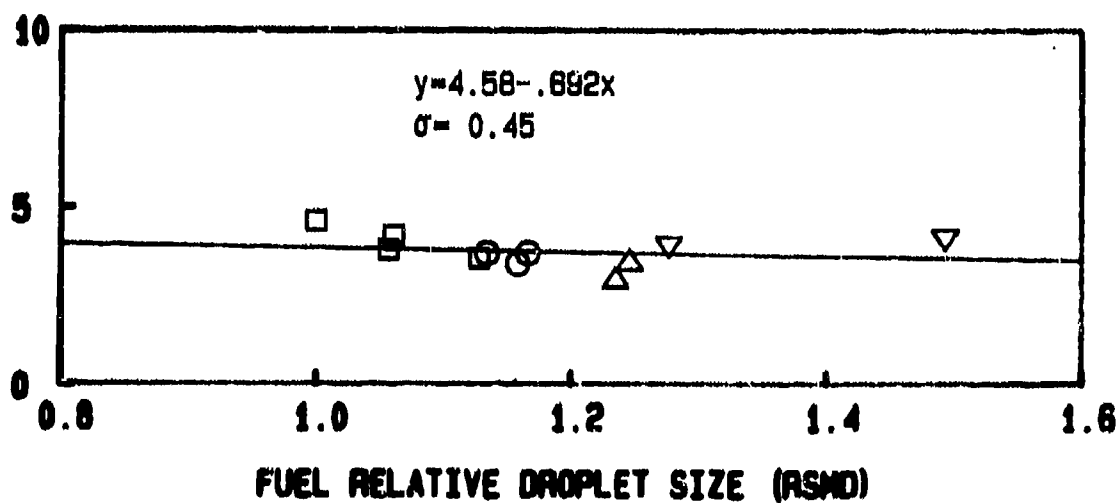
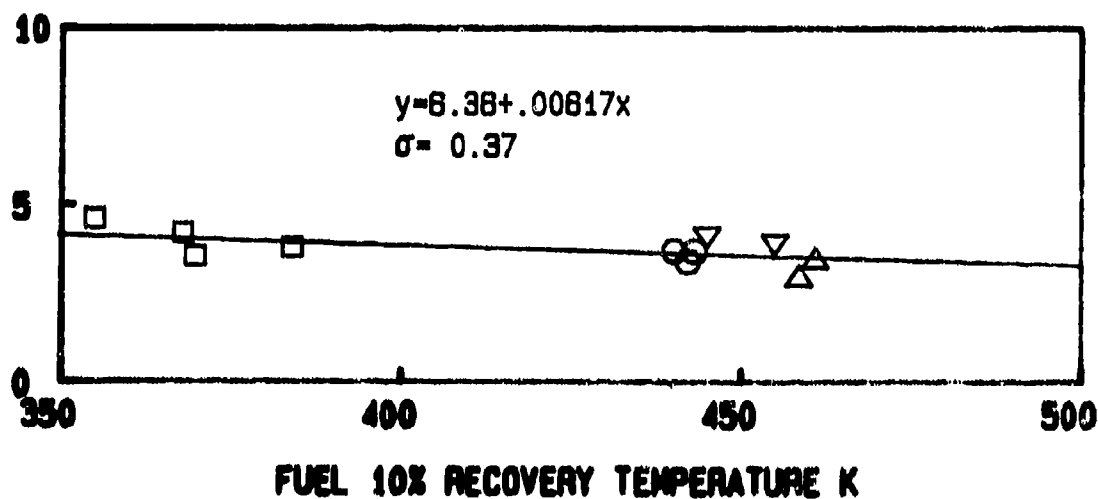
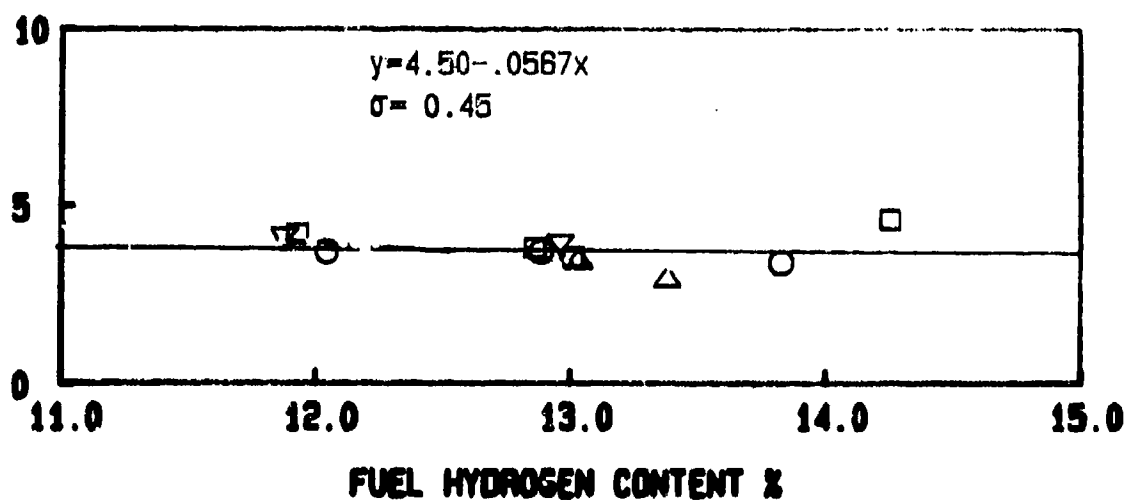


Figure 6.54: Effects of Fuel Properties on Lean Limit Fuel-Air Ratio (PT6A-65 Atmospheric, Lean P.Z., Simplex 0.65 FN)

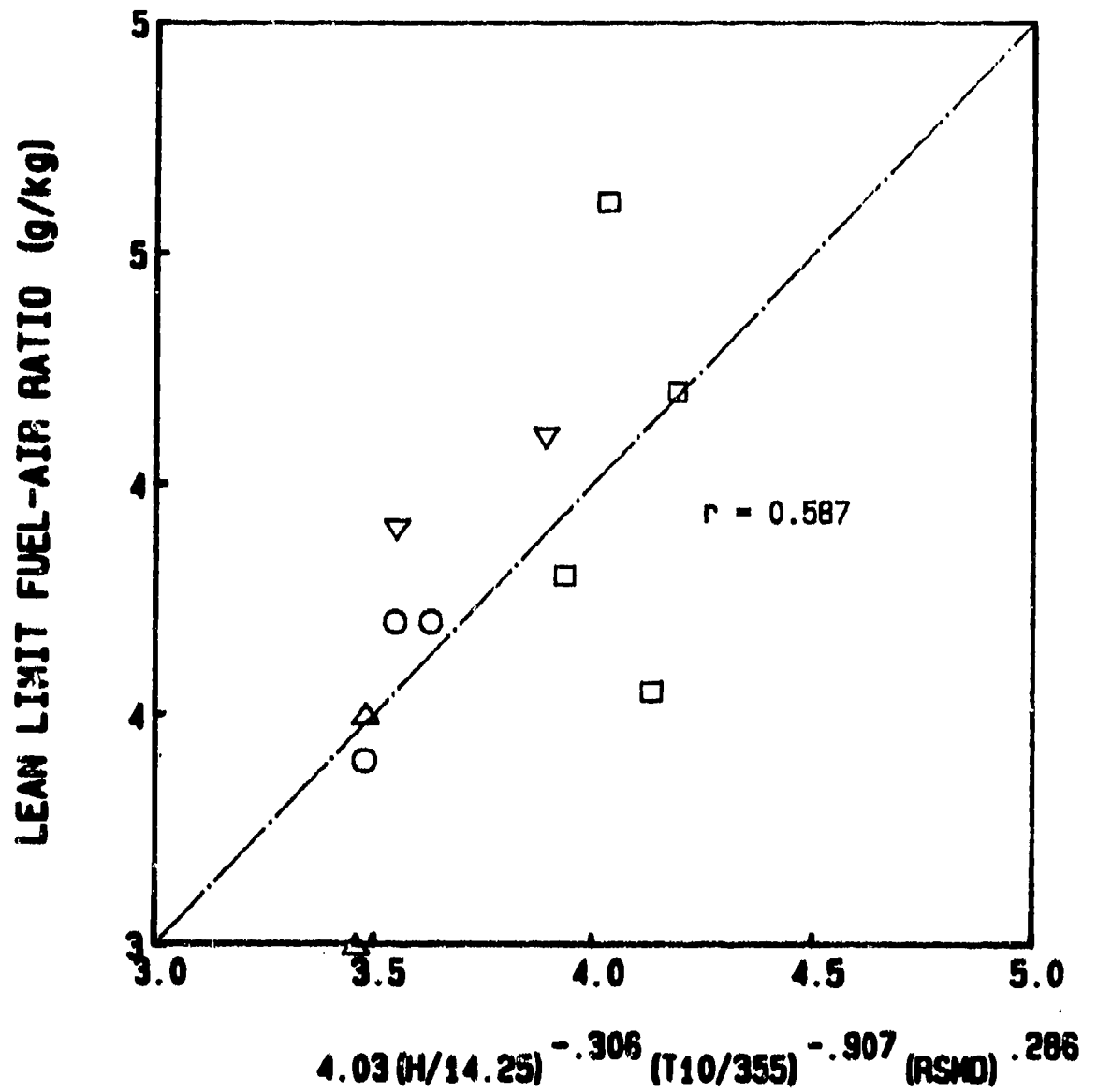


Figure 6.55: Lean Limit Fuel-Air Ratio vs Multiple Parameter Correlation (PT6A-65 Atmospheric, Lean P.Z, Simplex 0.65 FN)

LEAN LIMIT FUEL-AIR RATIO (g/kg)

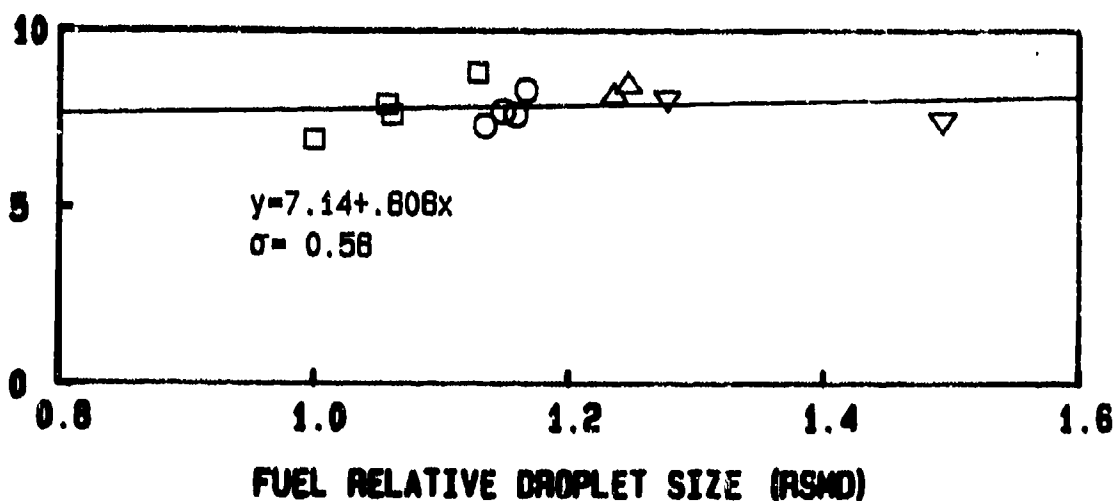
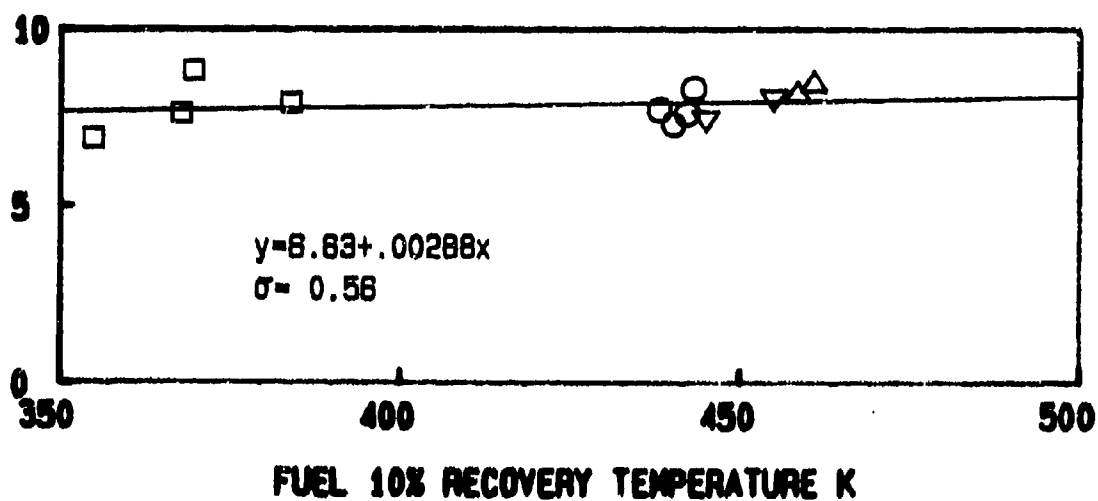
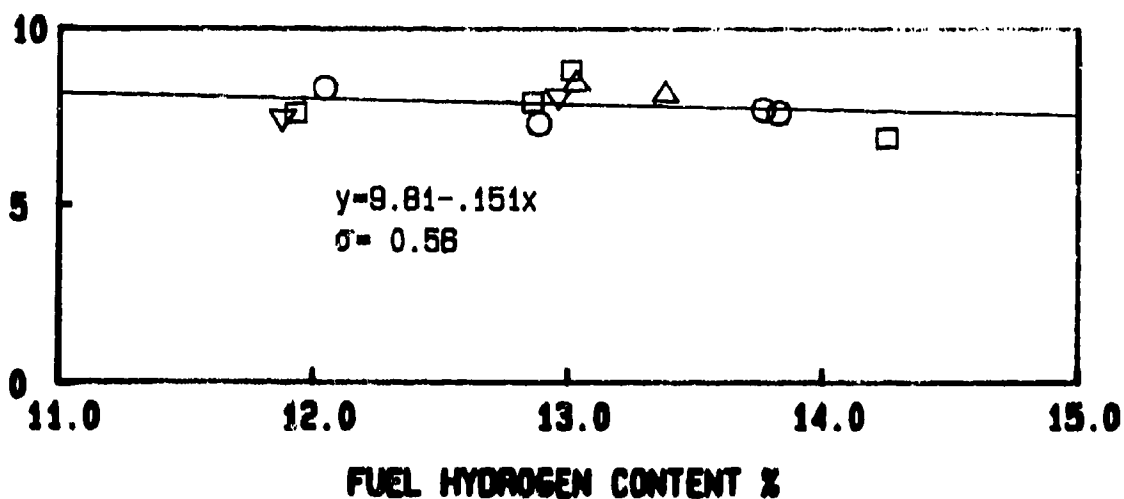


Figure 6.56: Effects of Fuel Properties on Lean Limit Fuel-Air Ratio (PT6A-65 Atmospheric, BOM, Simplex 1.1 FN)

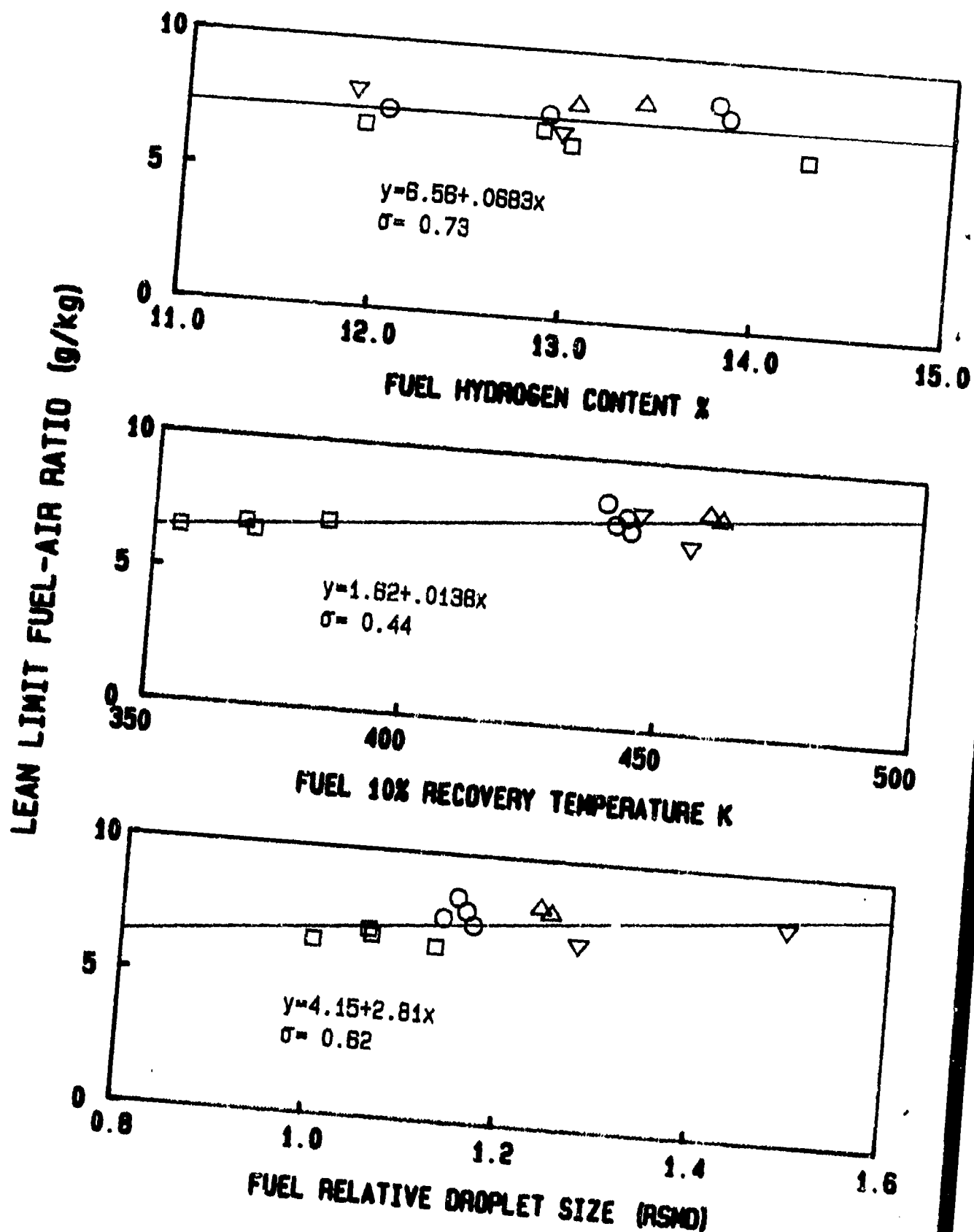


Figure 6.57: Effects of Fuel Properties on Lean Limit Fuel-Air Ratio (PT6A-65 Atmospheric, Lean P.Z., Simplex 1.1 FN)

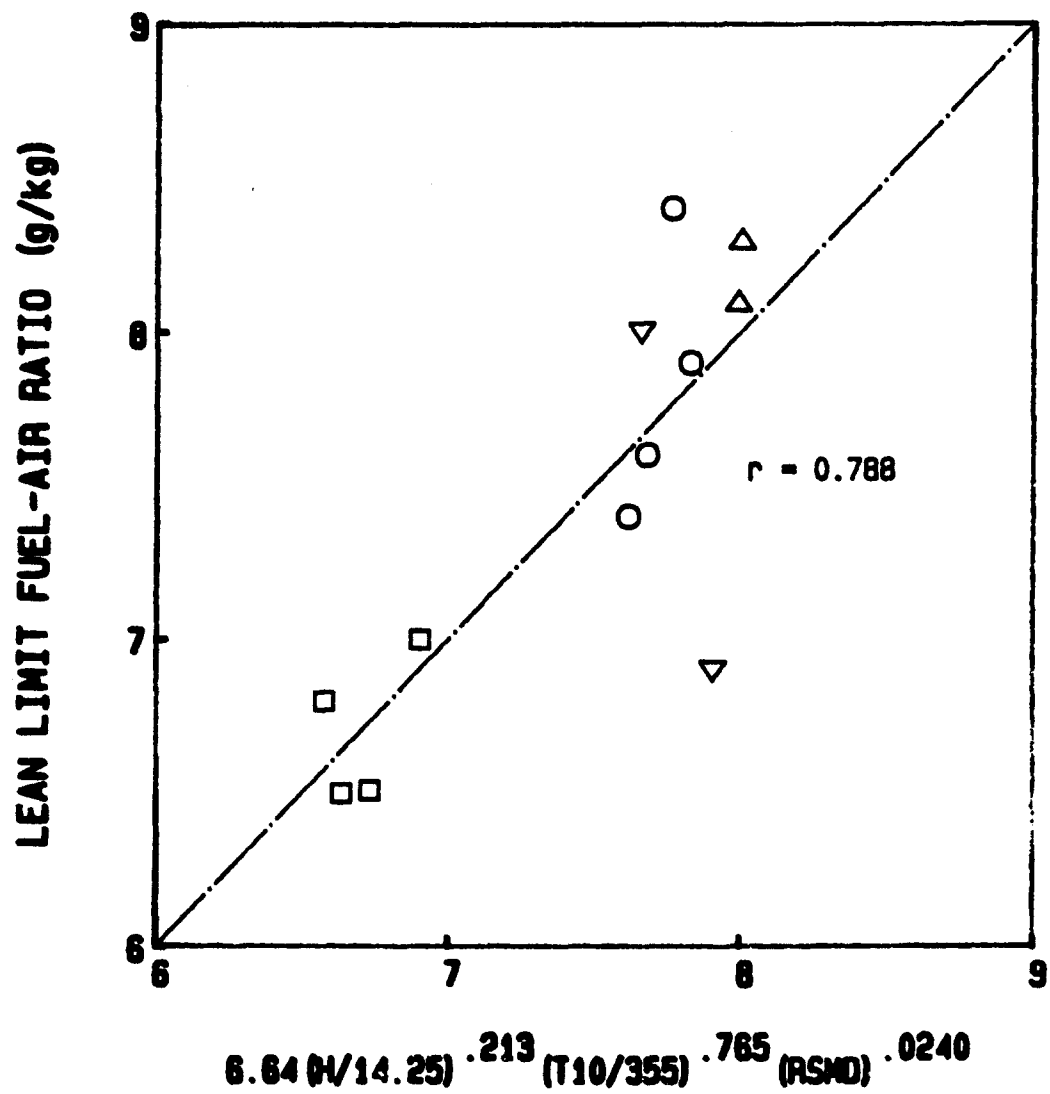


Figure 6.58: Lean Limit Fuel-Air Ratio vs Multiple Parameter Correlation (PT6A-65 Atmospheric, Lean P.Z., Simplex 1.1 FN)

RELATIVE PROFILE FACTOR

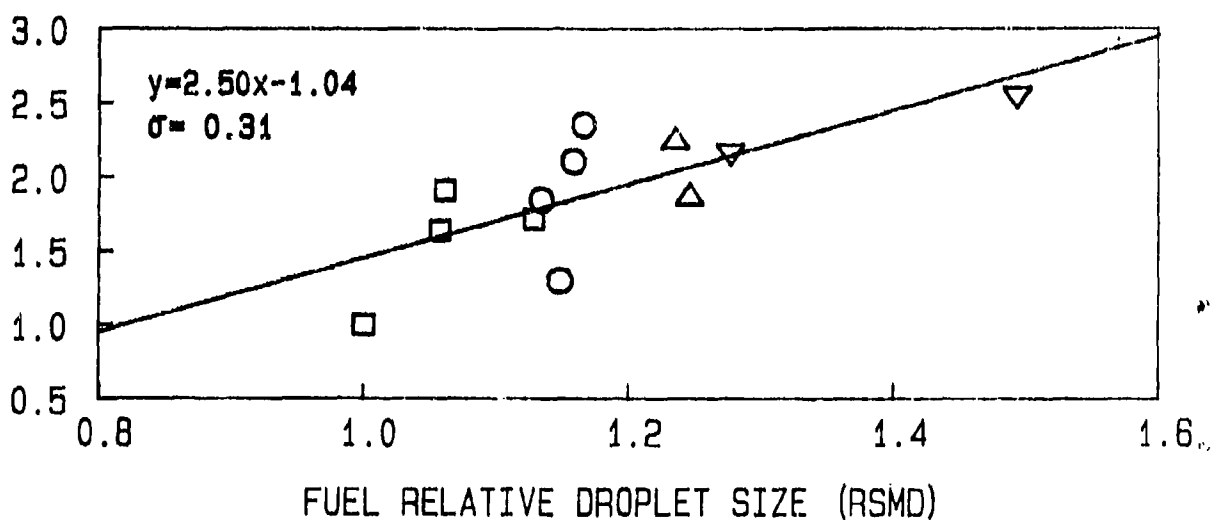
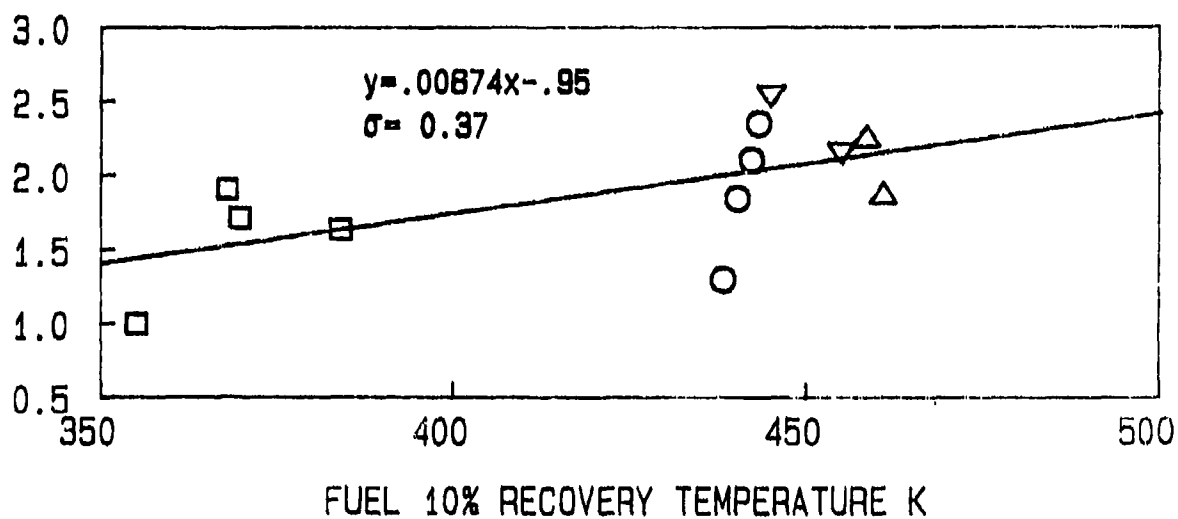
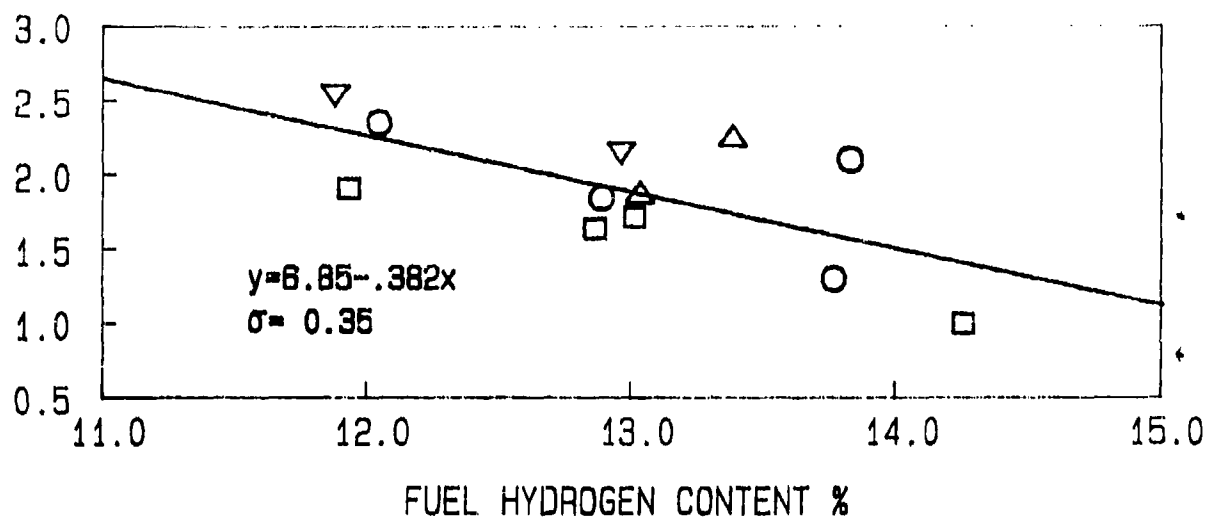


Figure 6.59: Effects of Fuel Properties on Relative Profile Factors
(PT6A-65 Atmospheric, BOM, Simplex 0.65 FN)

RELATIVE PATTERN FACTOR

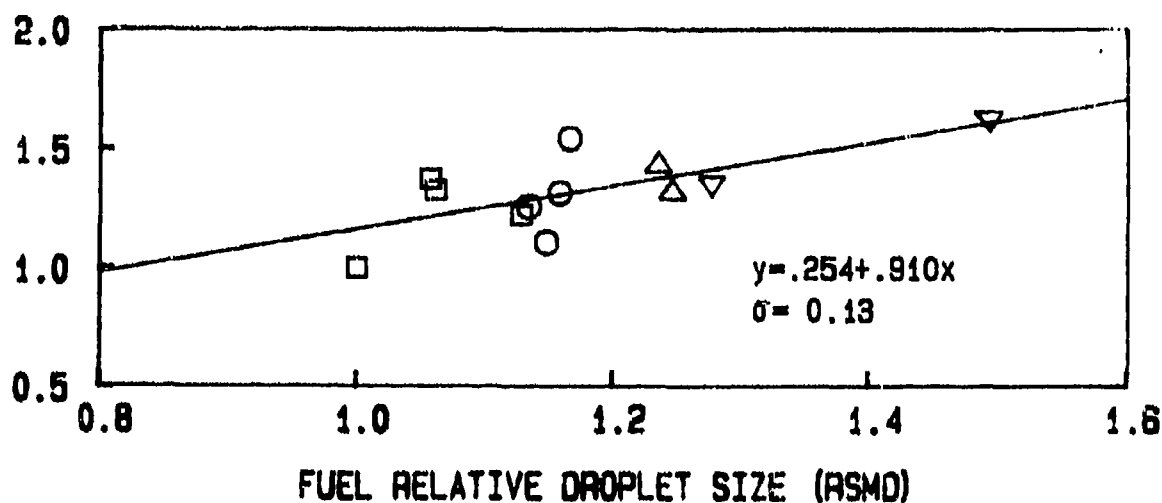
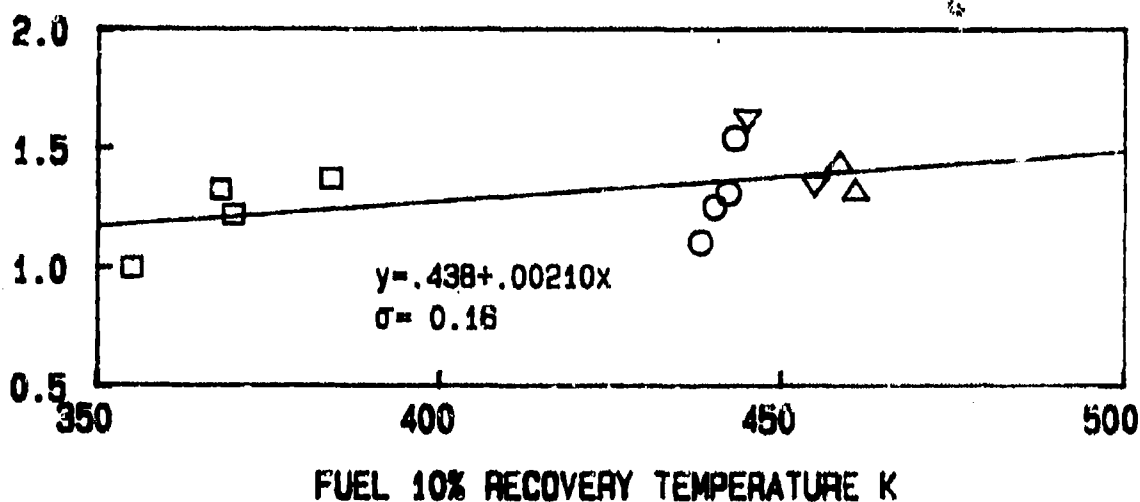
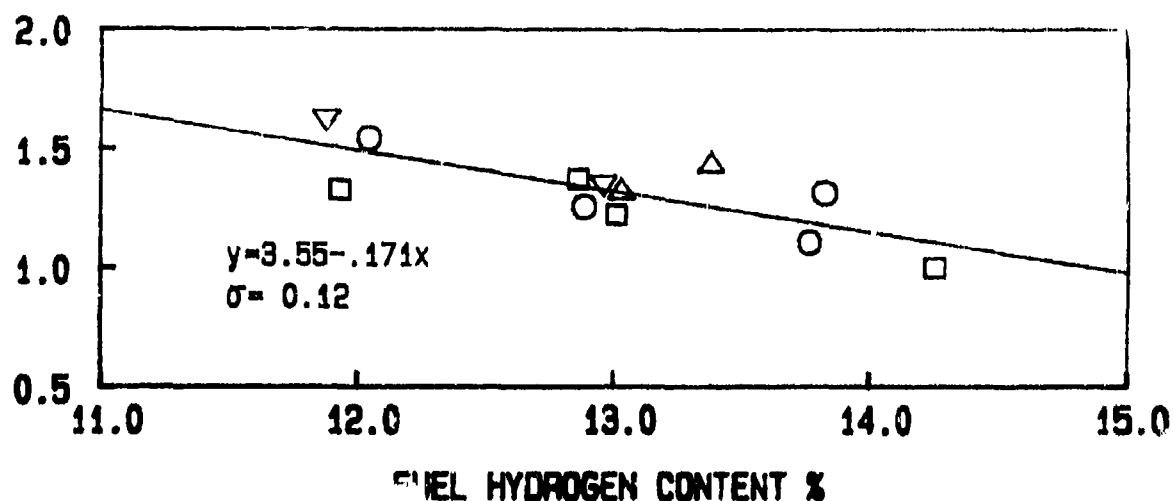


Figure 6.60: Effects of Fuel Properties on Relative Pattern Factors
(PT6A-65 Atmospheric, BOM, Simplex 0.65 FN)

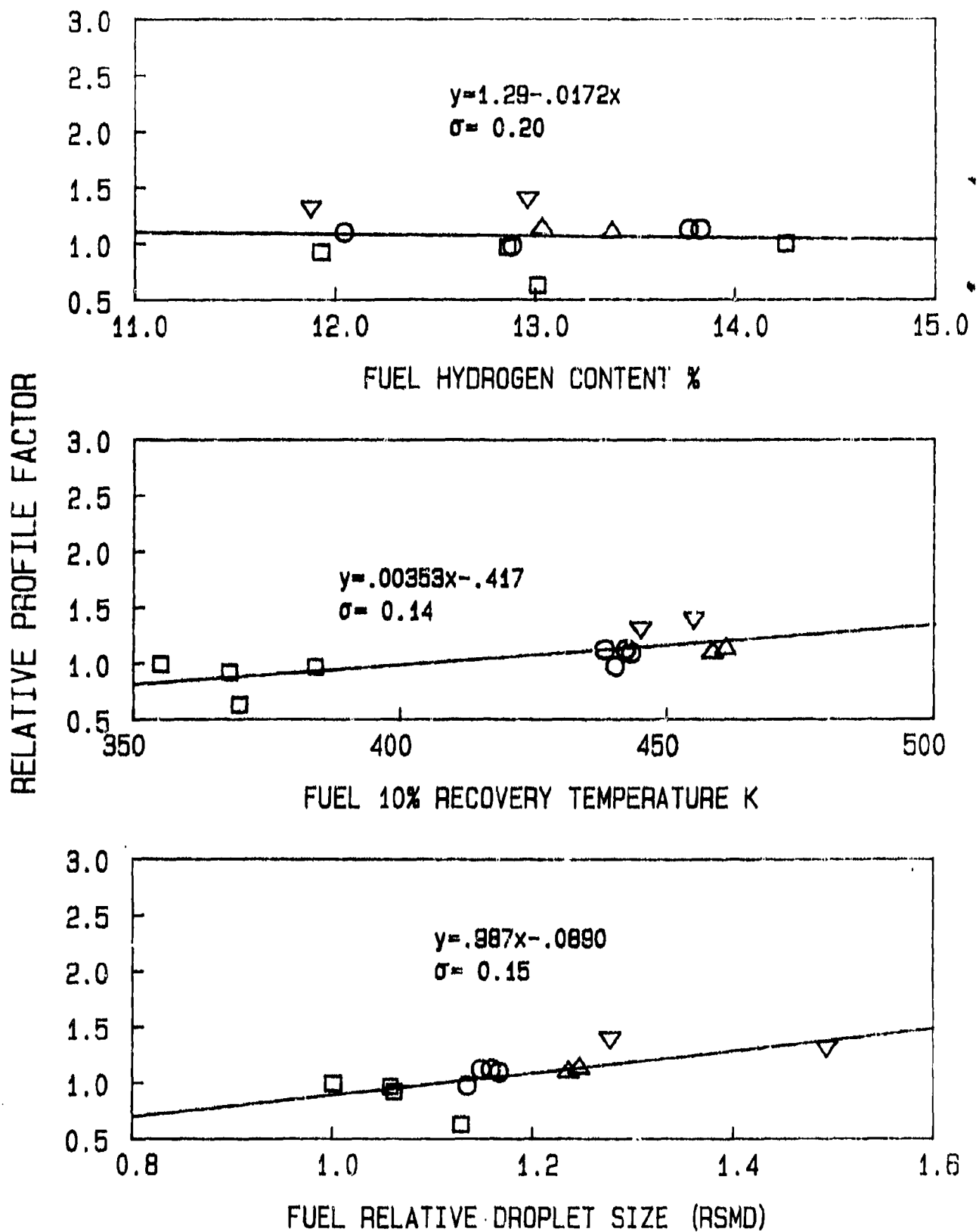


Figure 6.61: Effects of Fuel Properties on Relative Profile Factors
(PT6A-65 Atmospheric, Lean P.Z., Simplex 0.65 FN)

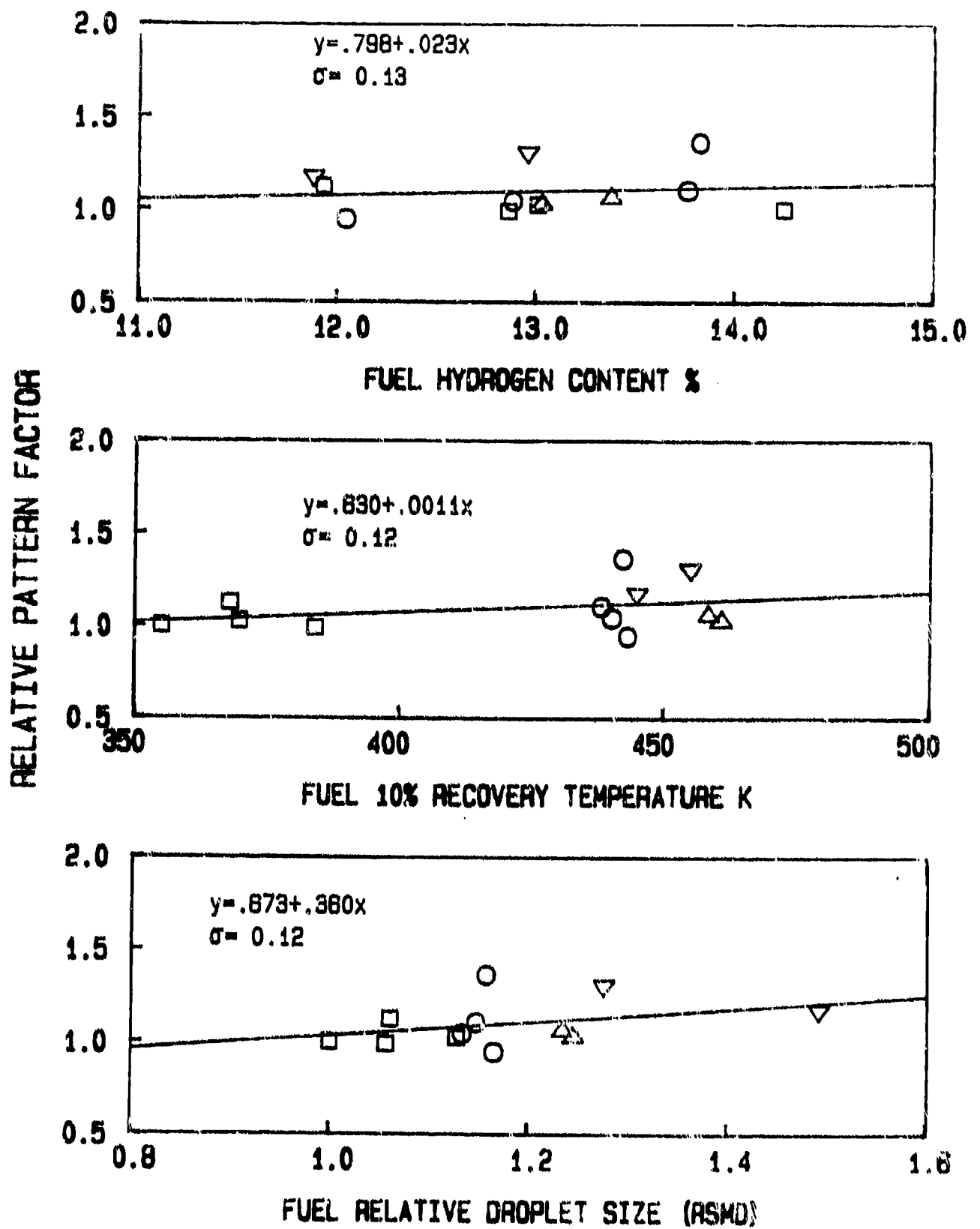


Figure 6.62: Effects of Fuel Properties on Relative Pattern Factor
(PT6A-65 Atmospheric, Lean P.Z., Simplex 0.65 FN)

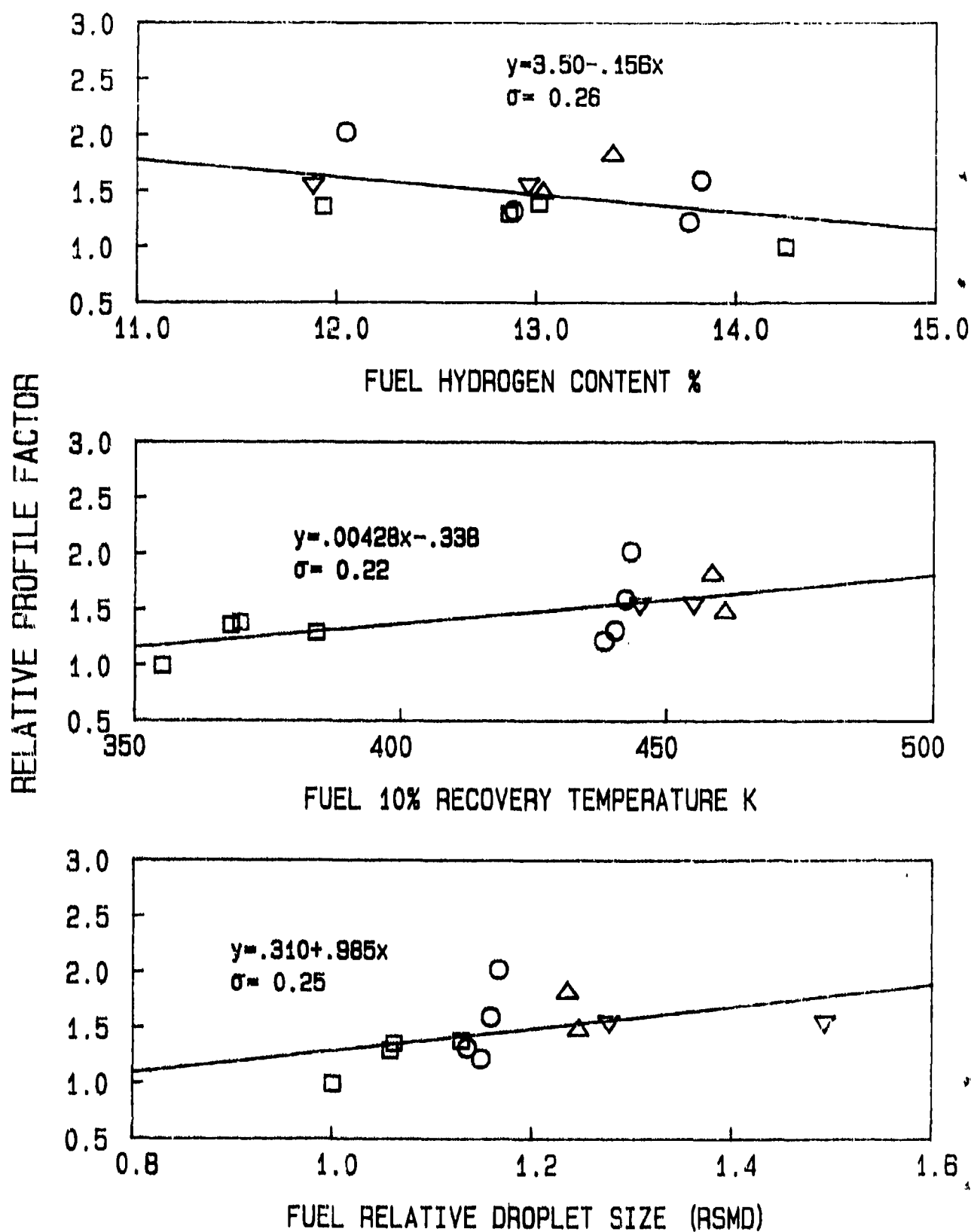


Figure 6.63: Effects of Fuel Properties on Relative Profile Factors
 (PT6A-65 Atmospheric, BOM, Simplex 1.1 FN)

RELATIVE PATTERN FACTOR

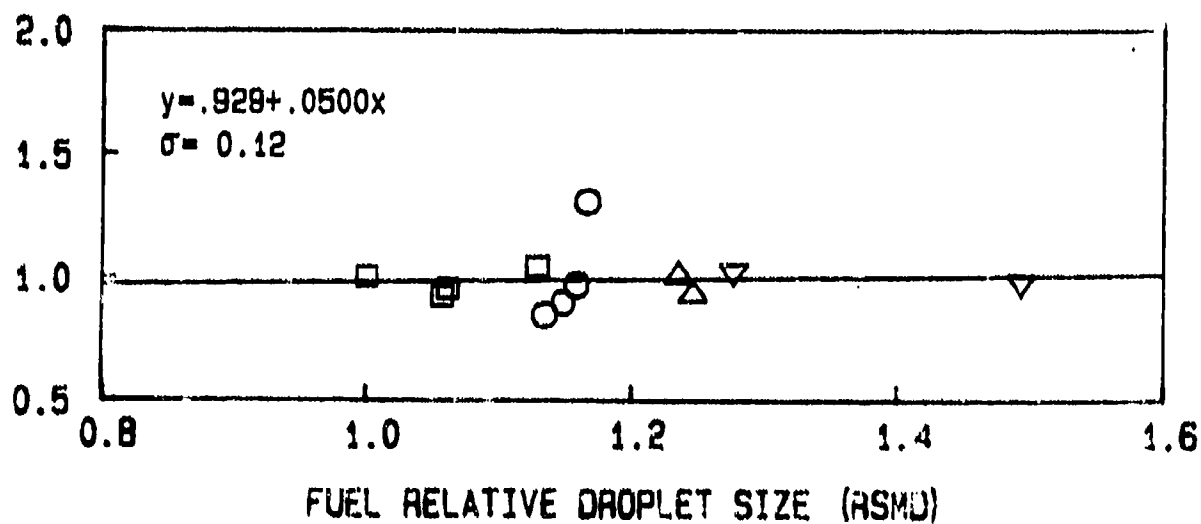
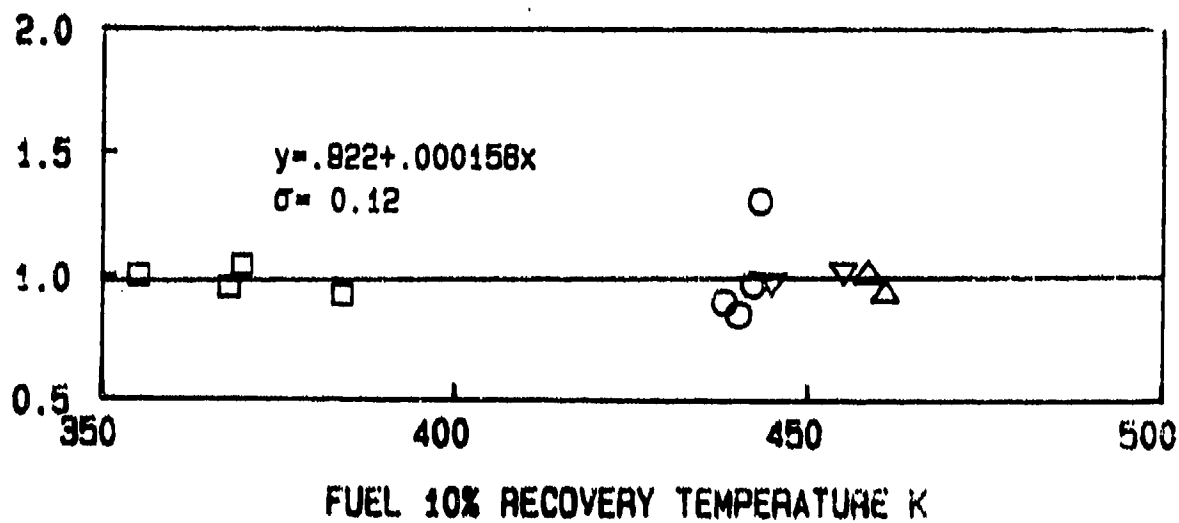
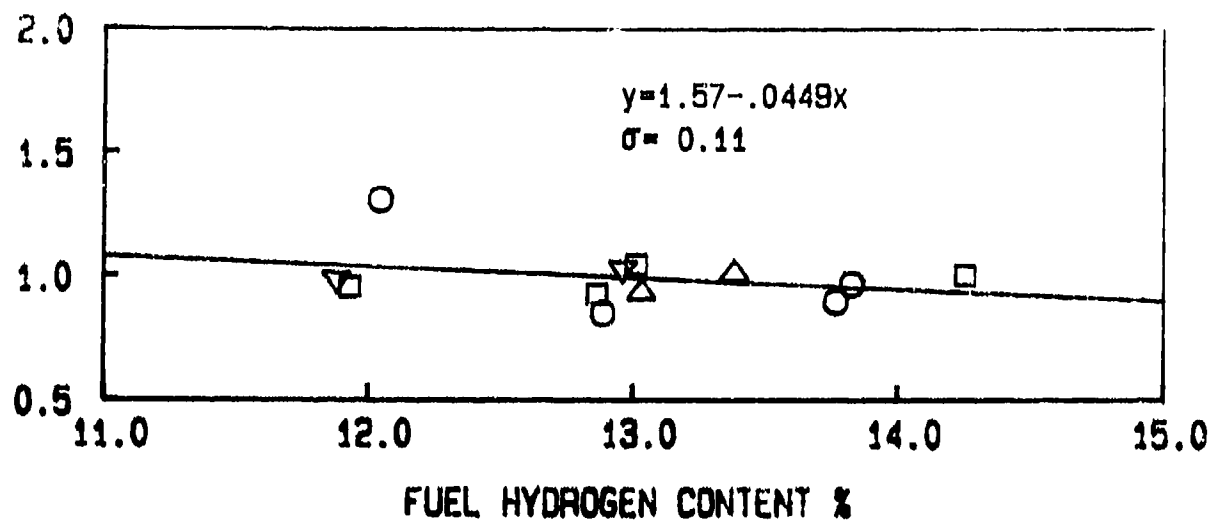


Figure 6.64: Effects of Fuel Properties on Relative Pattern Factor (PT6A-65 Atmospheric, BOM, Simplex 1.1 FN)

RELATIVE PROFILE FACTOR

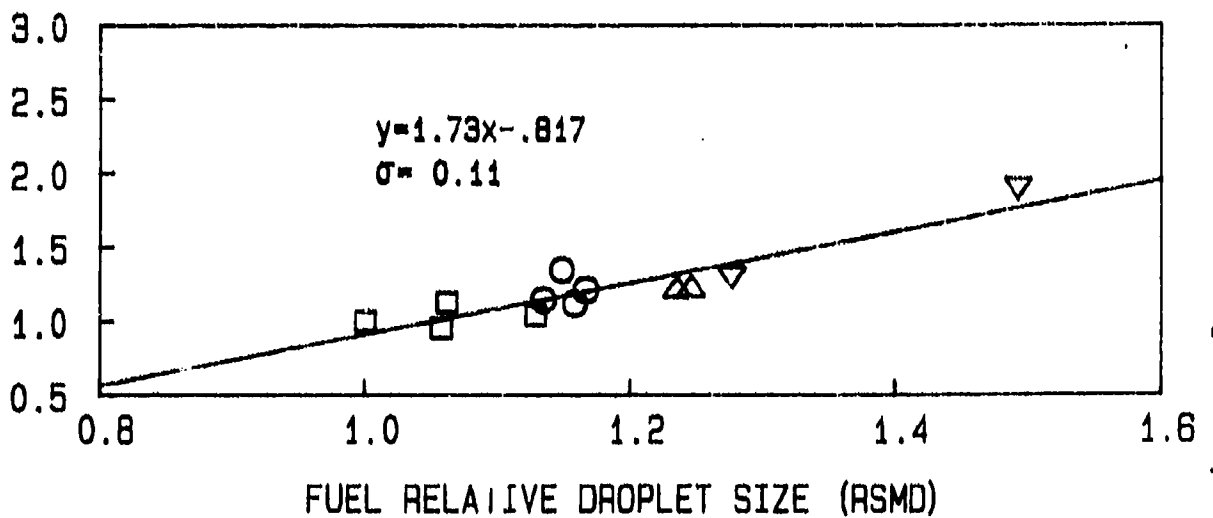
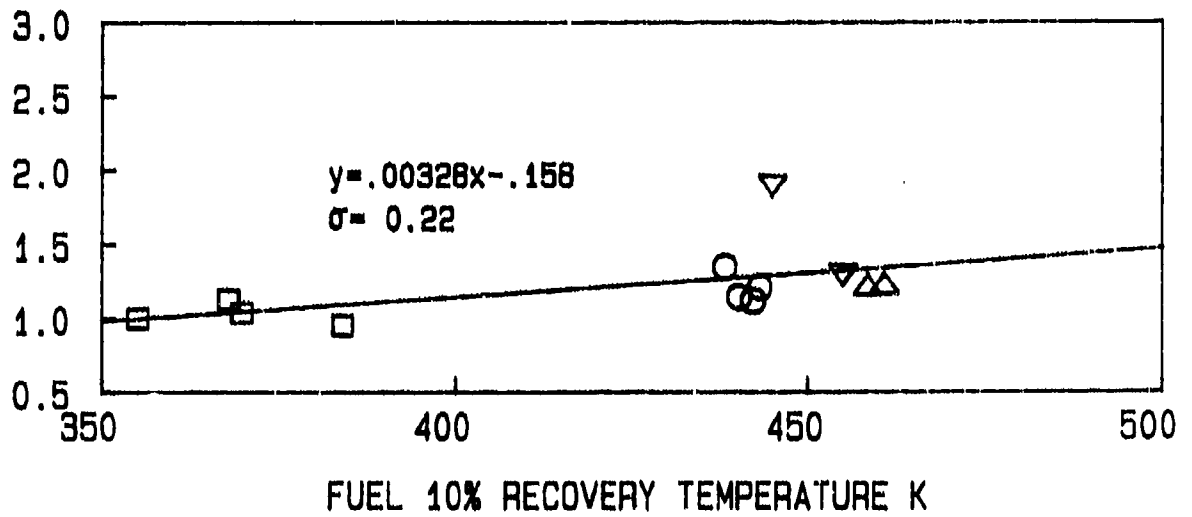
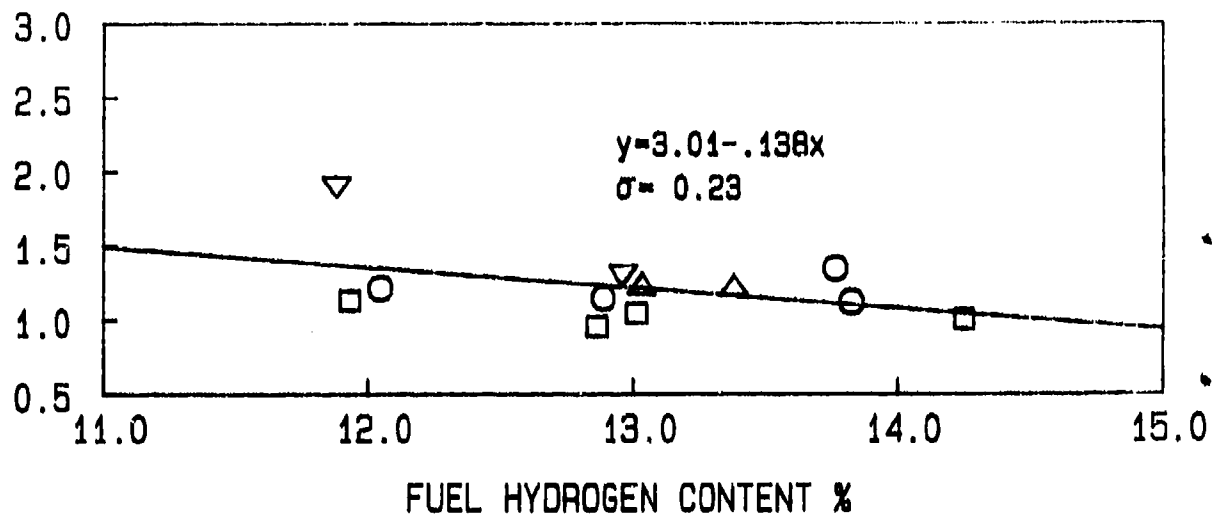


Figure 6.65: Effects on Fuel Properties on Relative Profile Factor (PT6A-65 Atmospheric, Lean P.Z., Simplex 1.1 FN)

RELATIVE PATTERN FACTOR

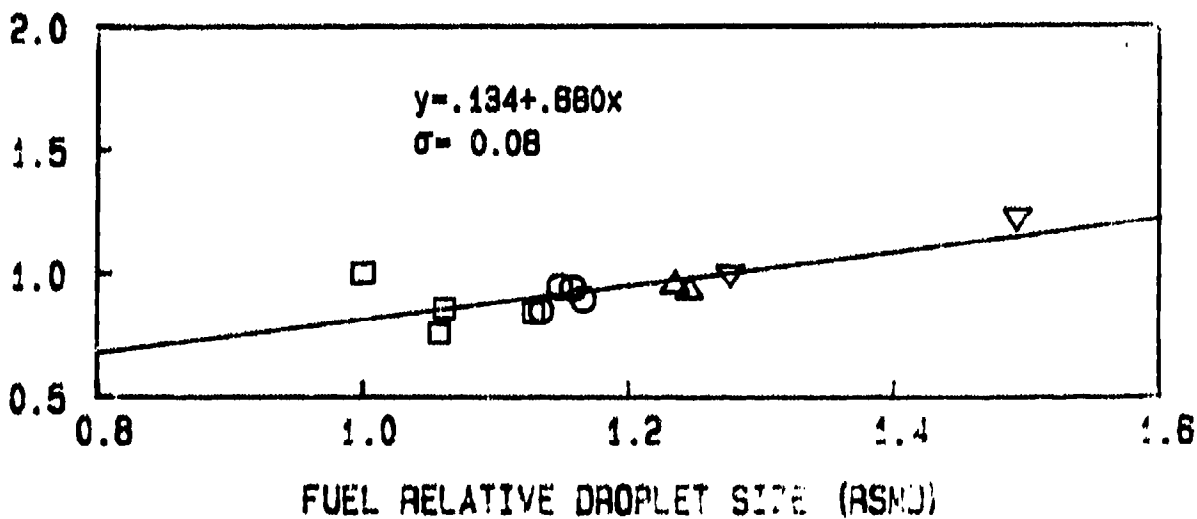
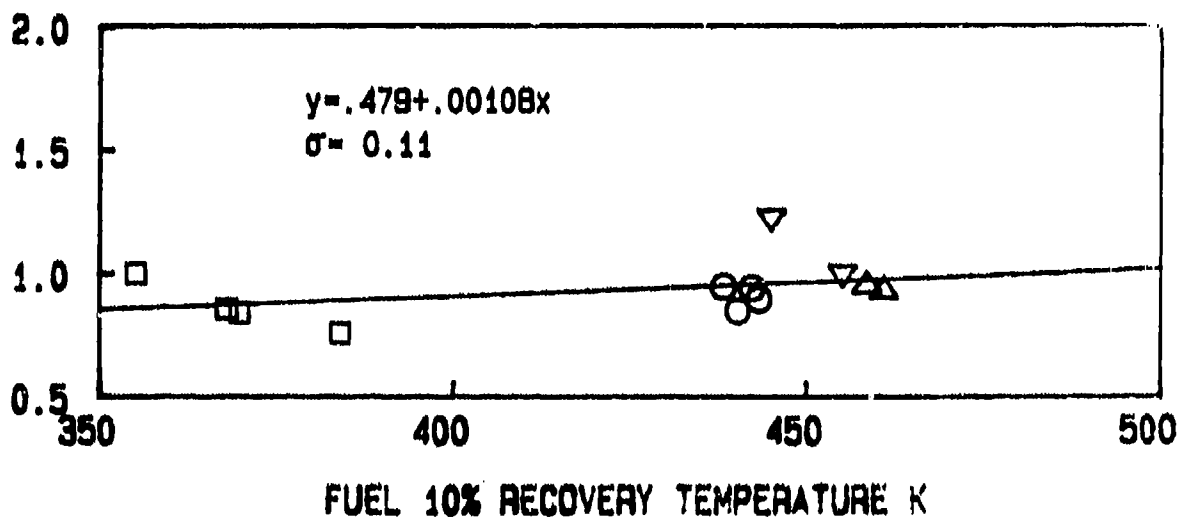
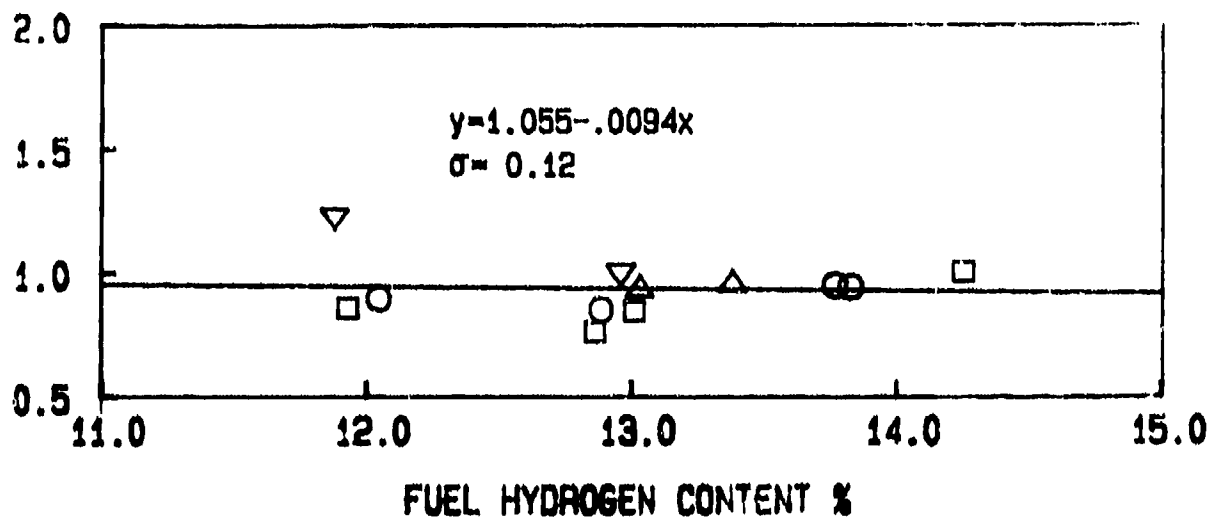


Figure 6.66: Effects of Fuel Properties on Relative Pattern Factors
(PT6A-65 Atmospheric, Lean P.2., Simplex 1.1 FN)

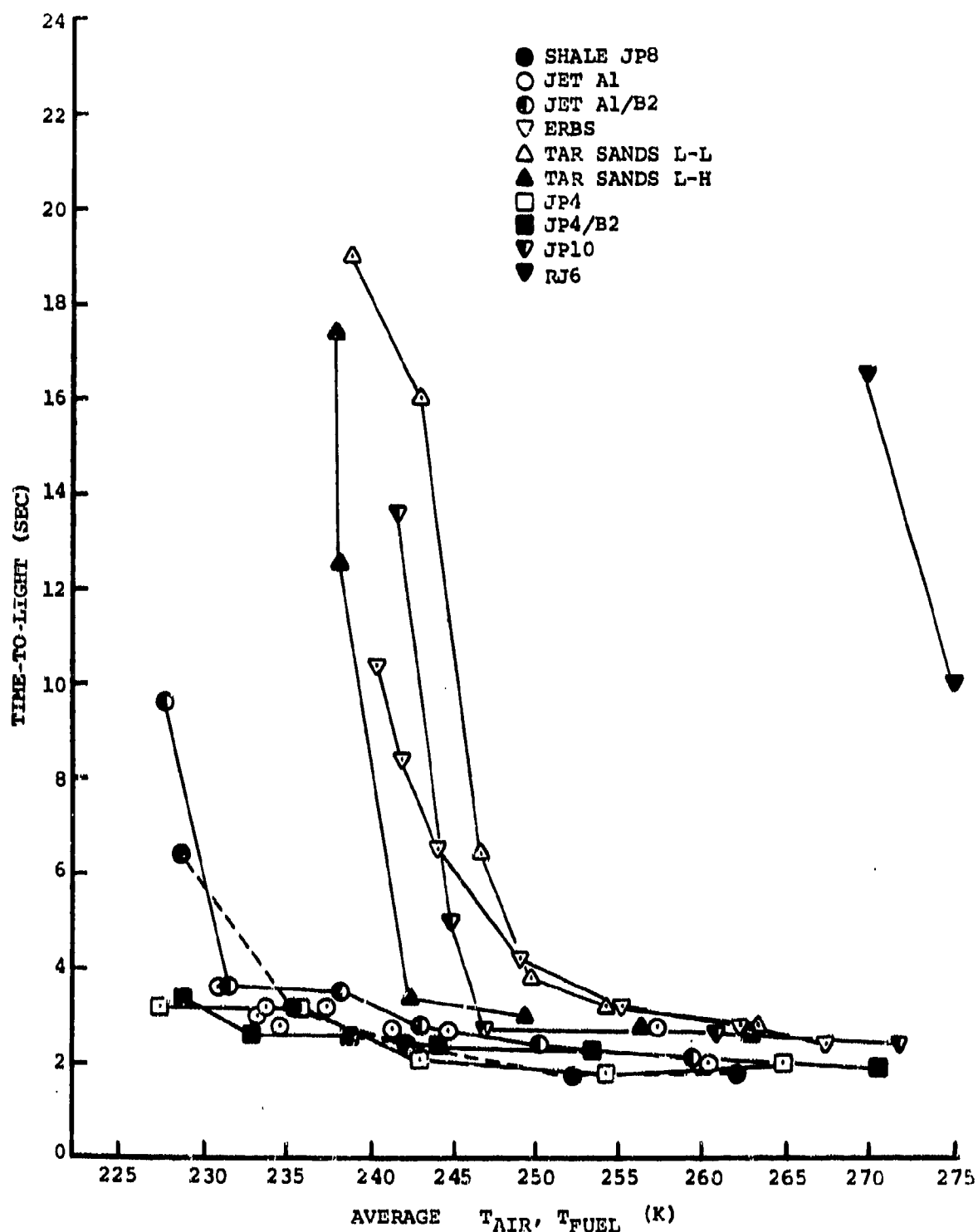


Figure 6.67: Effects of Fuel and Air Inlet Temperatures on Time to Light (PT6A-65 Cold Start Tests)

TIME-TO-LIGHT (T₁-T_f=244K) sec.

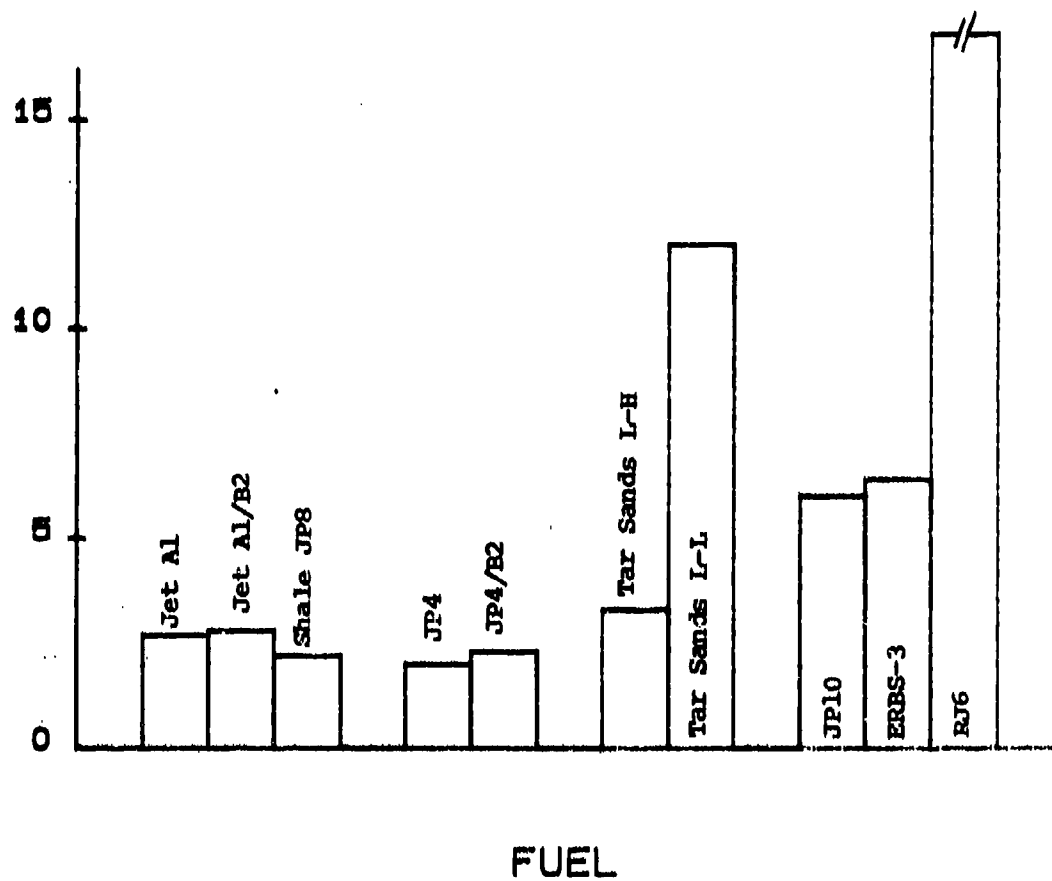


Figure 6.68: Comparison of Times to Light at Fuel and Air Inlet Temperature of 244K (PT6A-65 Cold Start Tests)

TIME-TO-LIGHT ($T_1=T_f=244K$), sec

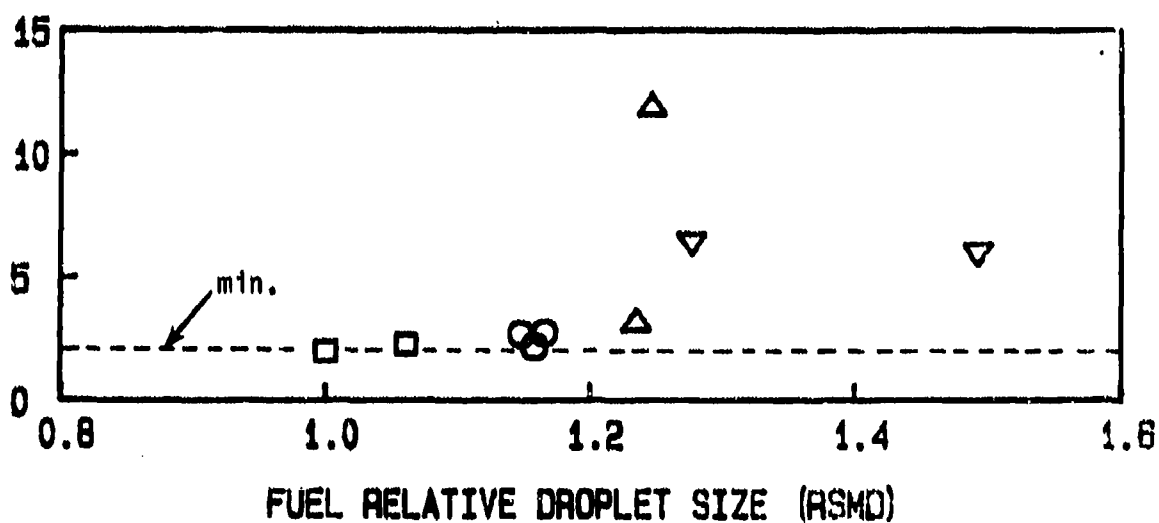
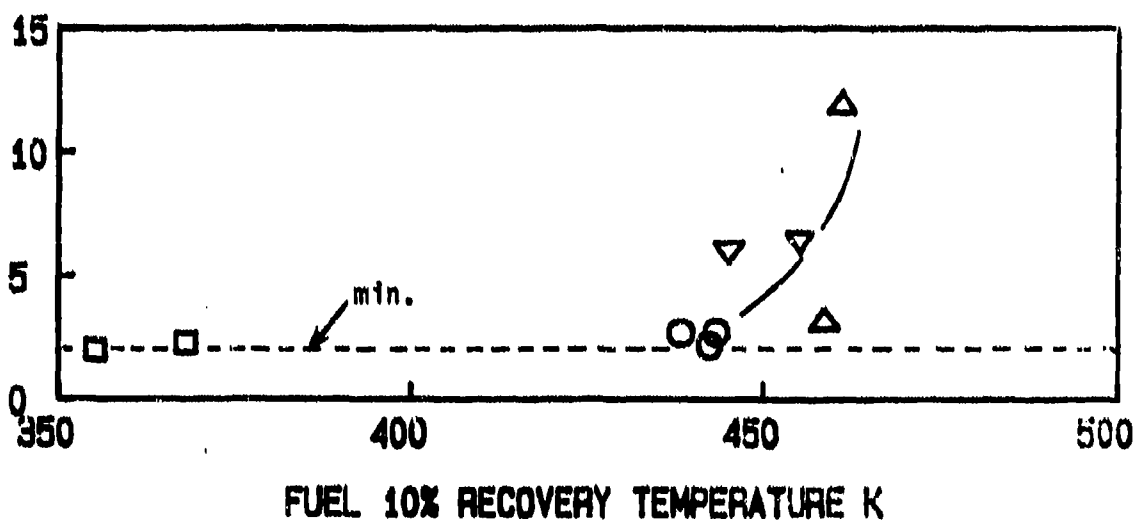
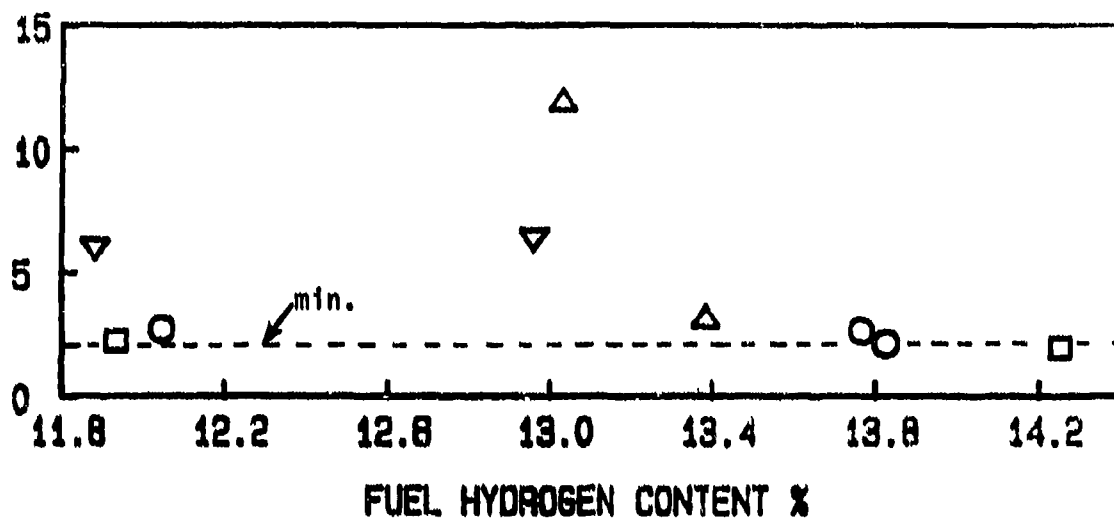


Figure 6.69: Effects of Fuel Properties on Time-to-Light (PT6A-65 Cold Start Tests)

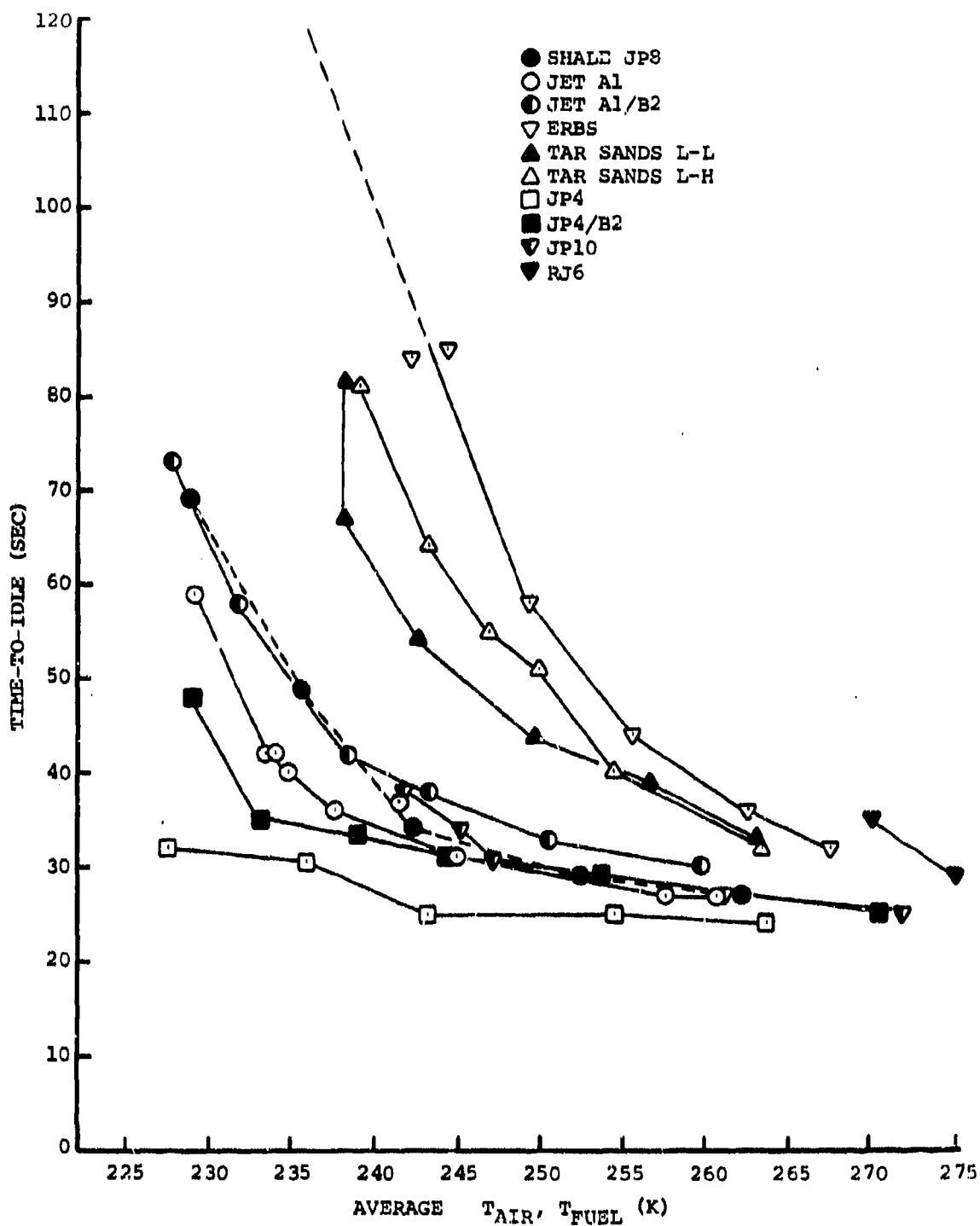


Figure 6.70: Effects of Fuel and Air Inlet Temperatures on Time to Idle (PT6A-65 Cold Start Tests)

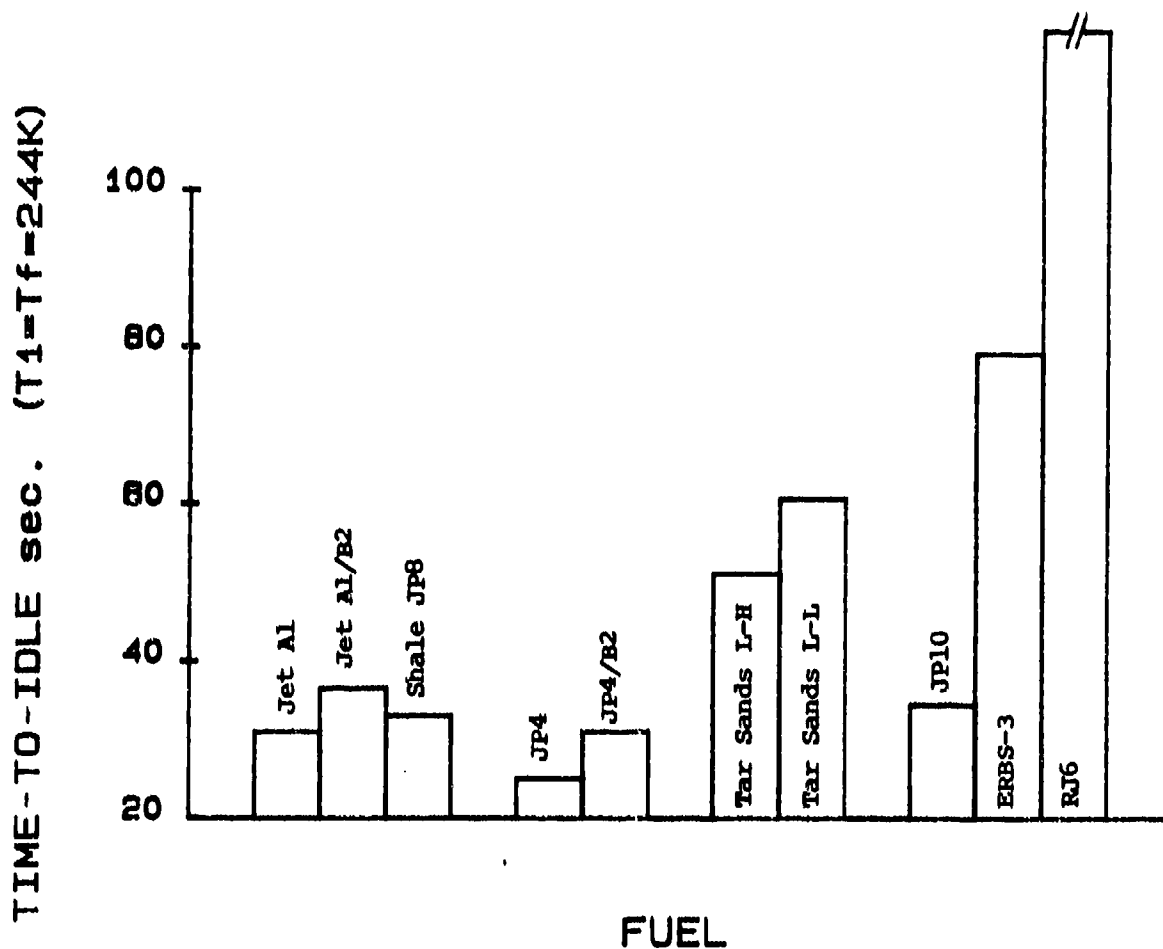


Figure 6.71: Comparison of Times to Idle at Fuel and Air Inlet Temperature of 244K (PT6A-65 Cold Start Tests)

TIME-TO-IDLE ($T_1=T_2=244K$), sec

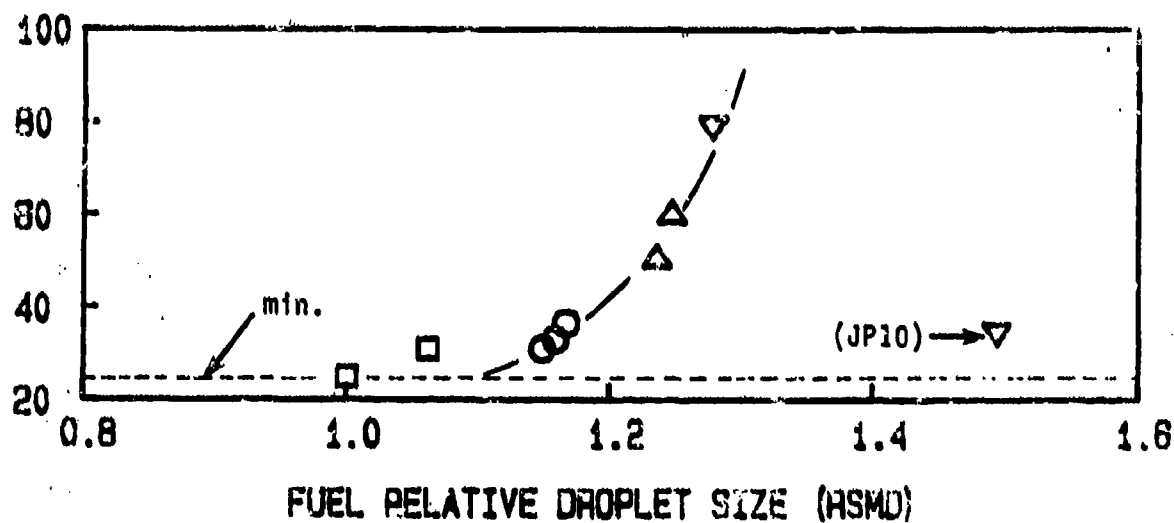
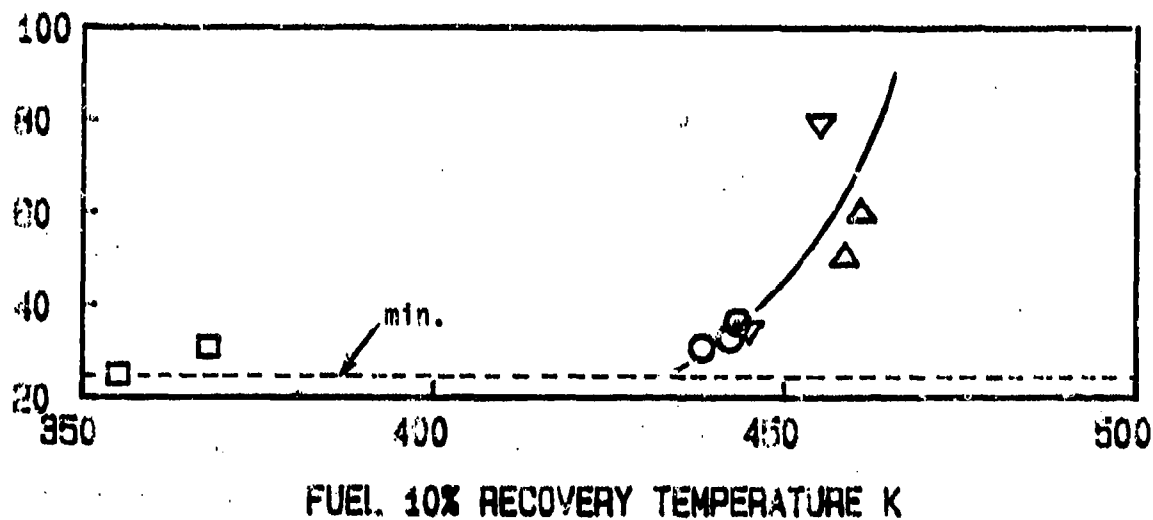
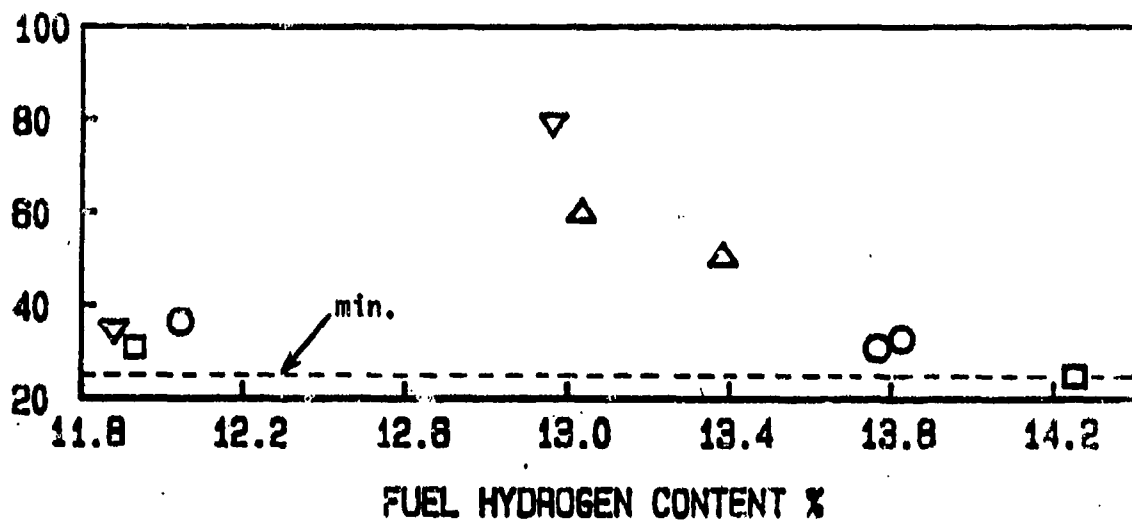


Figure 6.72: Effects of Fuel Properties on Time-to-Idle

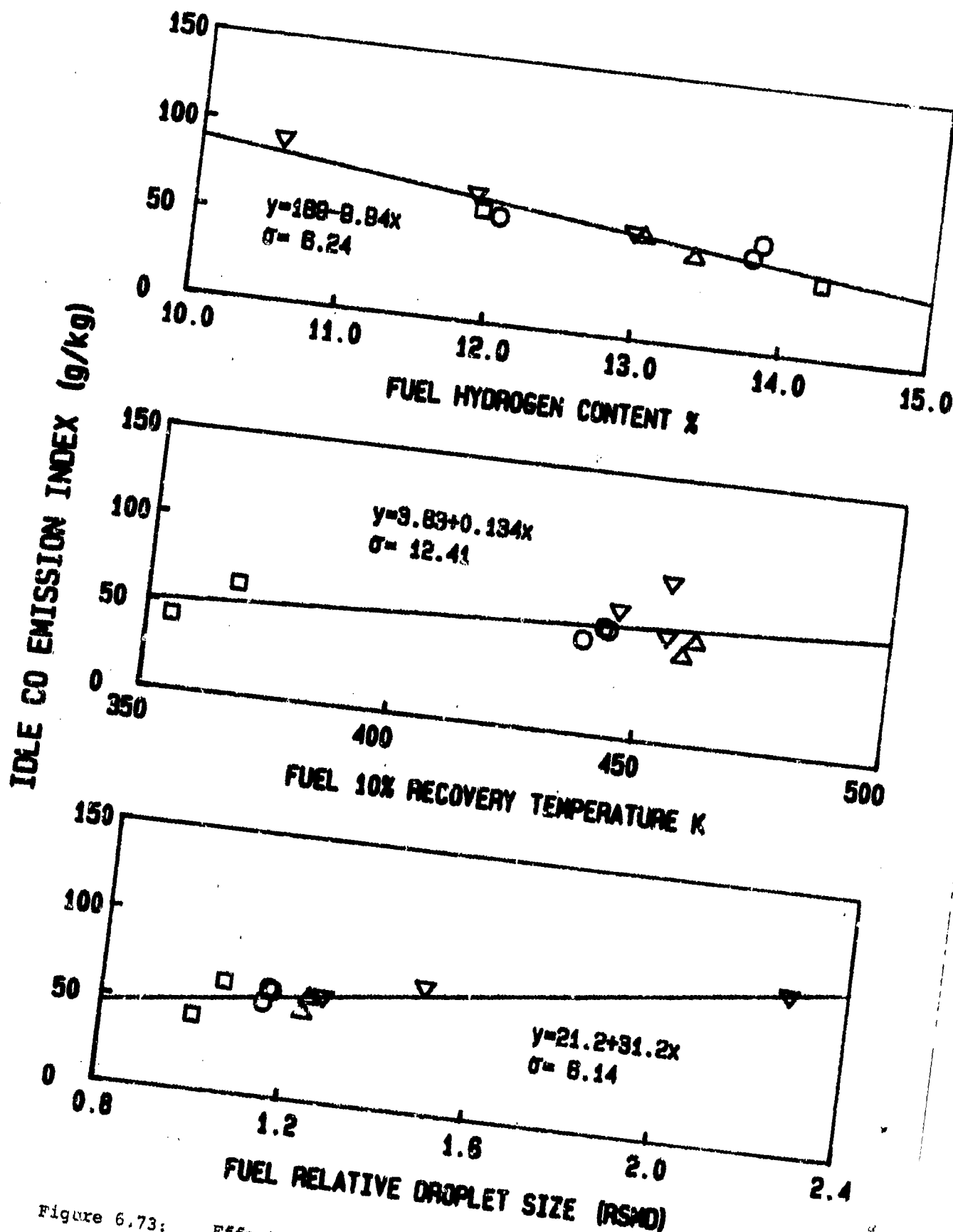


Figure 6.73: Effects of Fuel Properties on Idle CO Emissions
(PT6A-65 Gas Generator, BOM, Simplex 1.9 FN)

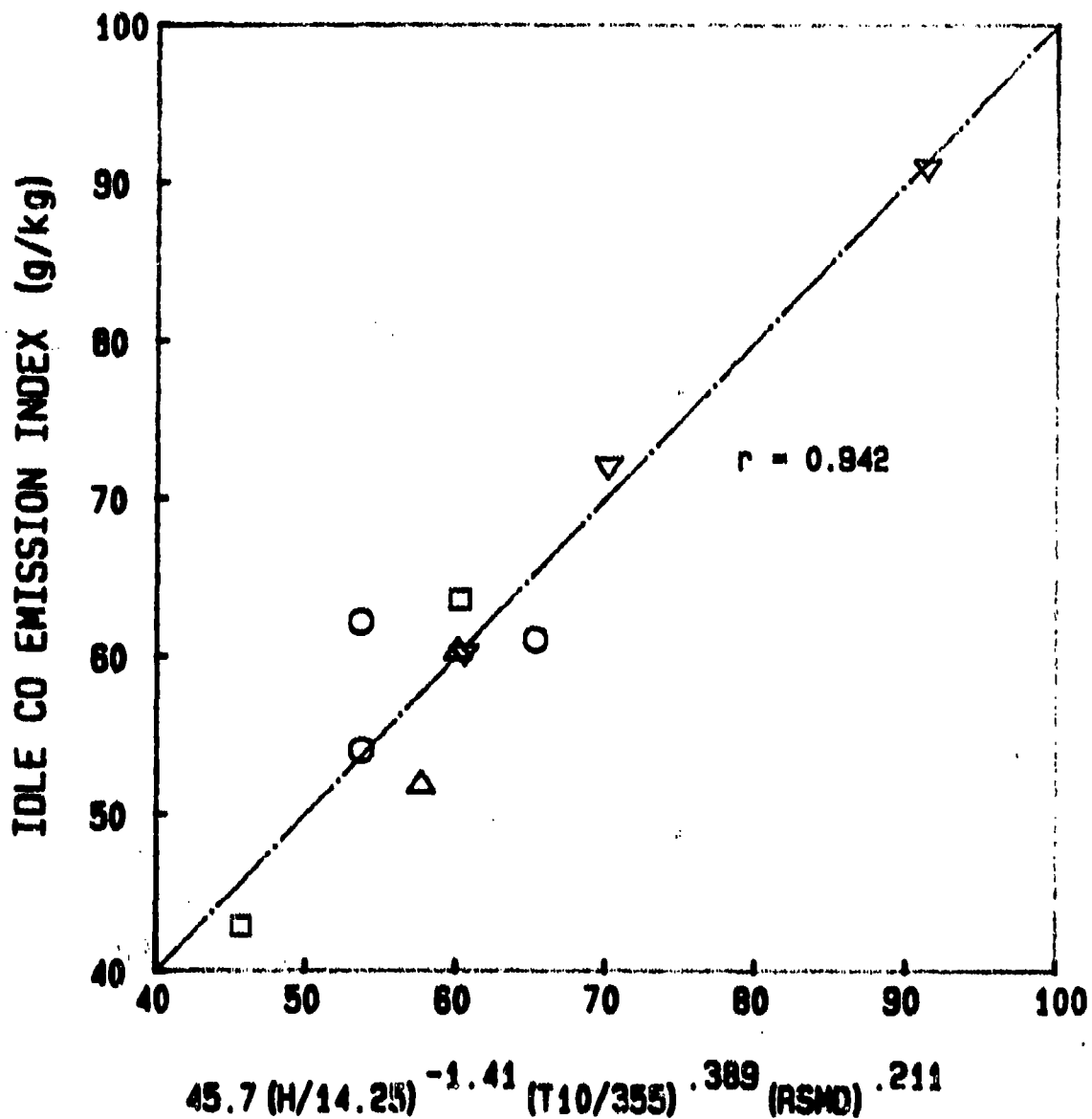


Figure 6.74: Idle CO Emissions vs Multiple Parameter Correlation
(PT6A-65 Gas Generator, BOM, Simplex 1.9 FN)

Idle HC Emission Index (g/kg)

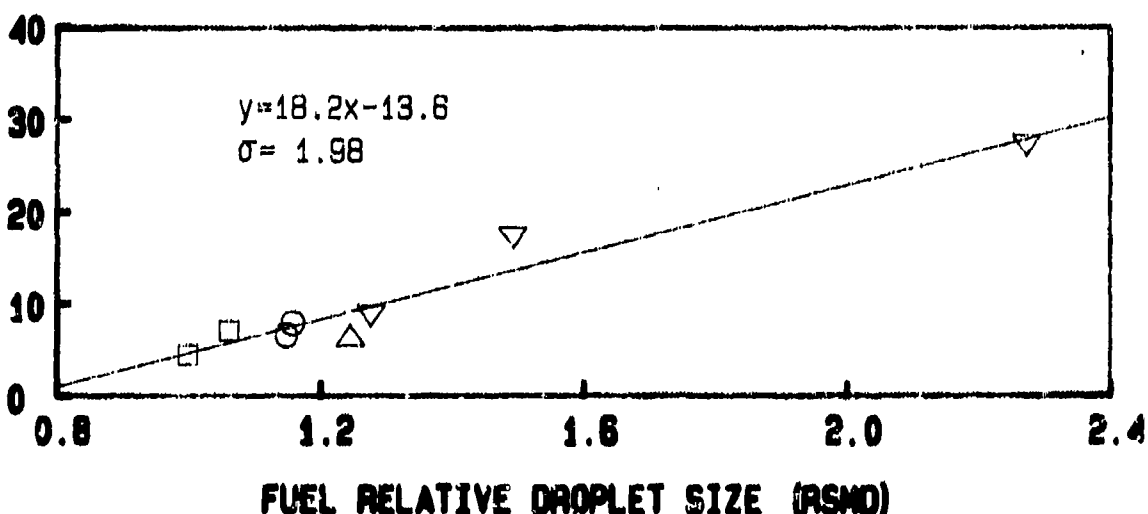
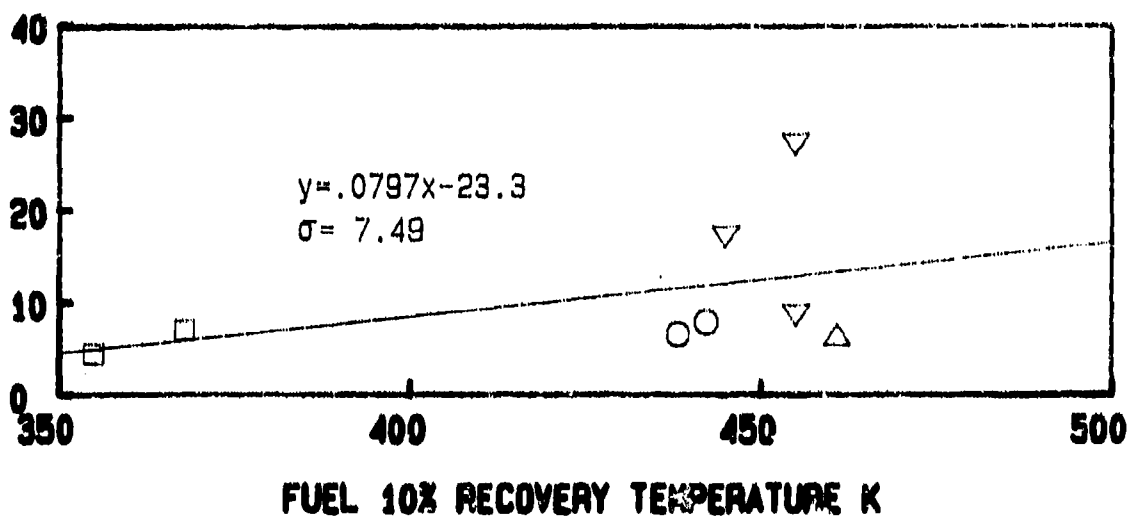
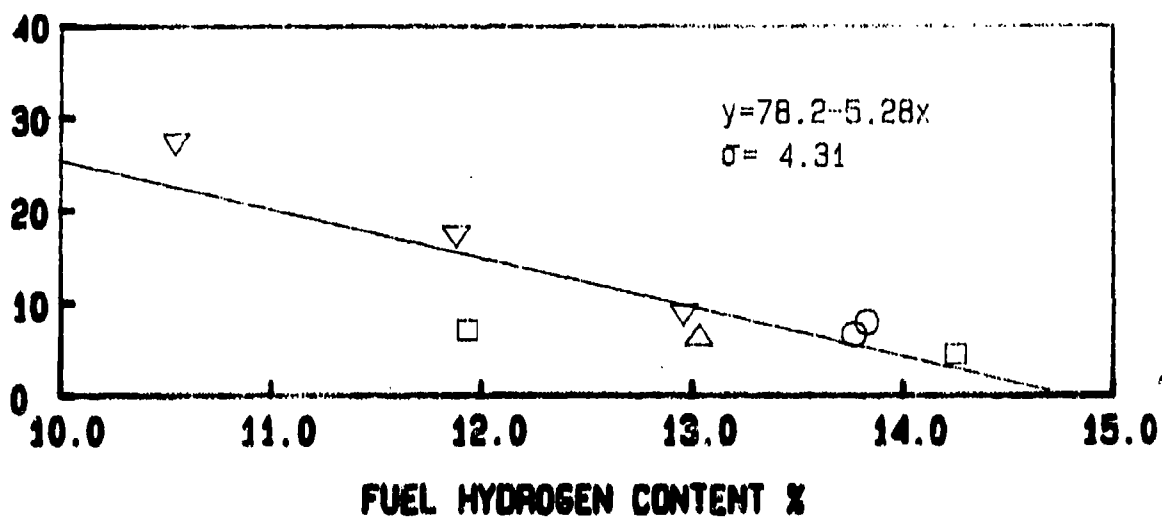
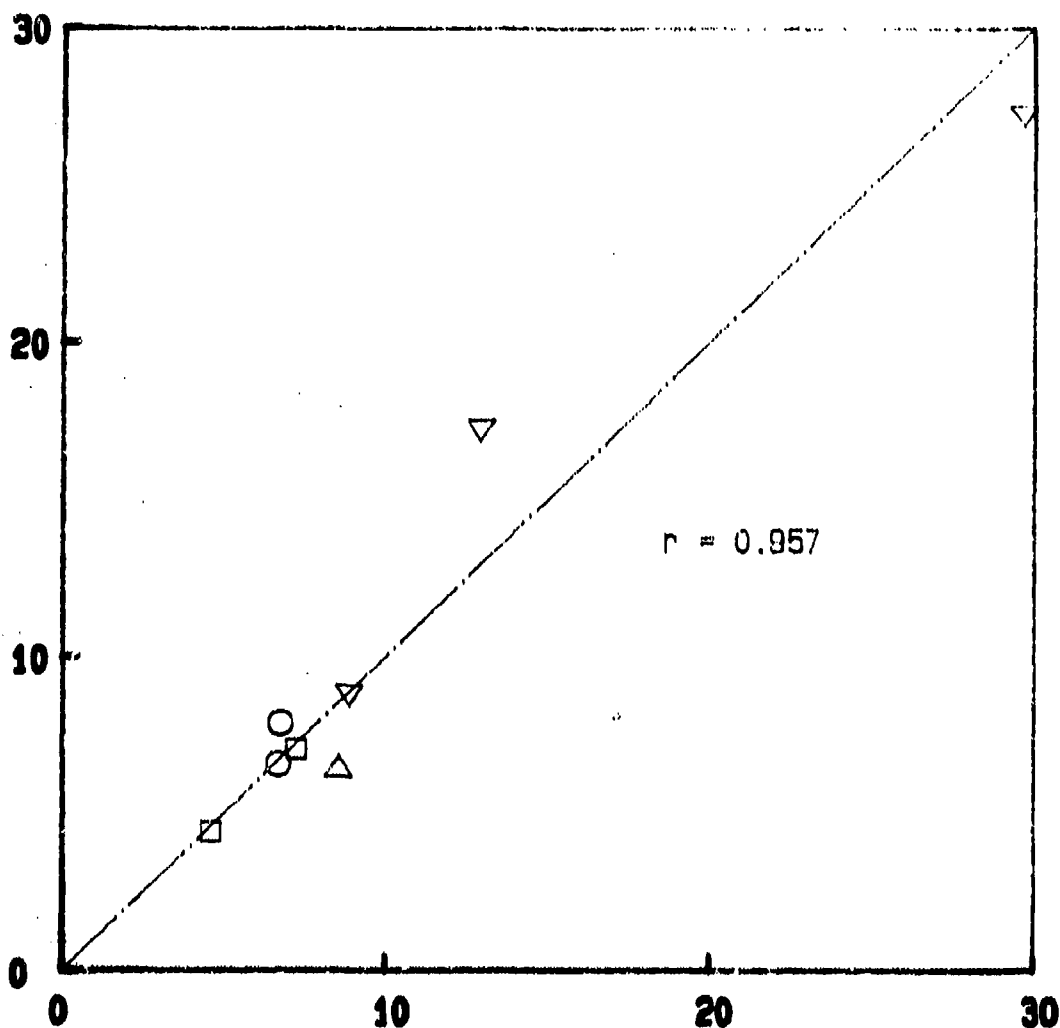


Figure 6.75: Effects of Fuel Properties on Idle HC Emissions
(FT6A-65 Gas Generator, BOM, Simplex 1.9 FN)

Idle HC Emission Index (g/kg)



$$2.13 (H/14.25)^{-1.98} (T10/355)^{0.528} (RSMO) 1.38$$

Figure 6.76: Idle HC Emissions vs Multiple Parameter Correlation (PT6A-65 Gas Generator, BOM, Simplex 1.9 FN)

IDLE CO EMISSION INDEX (g/kg)

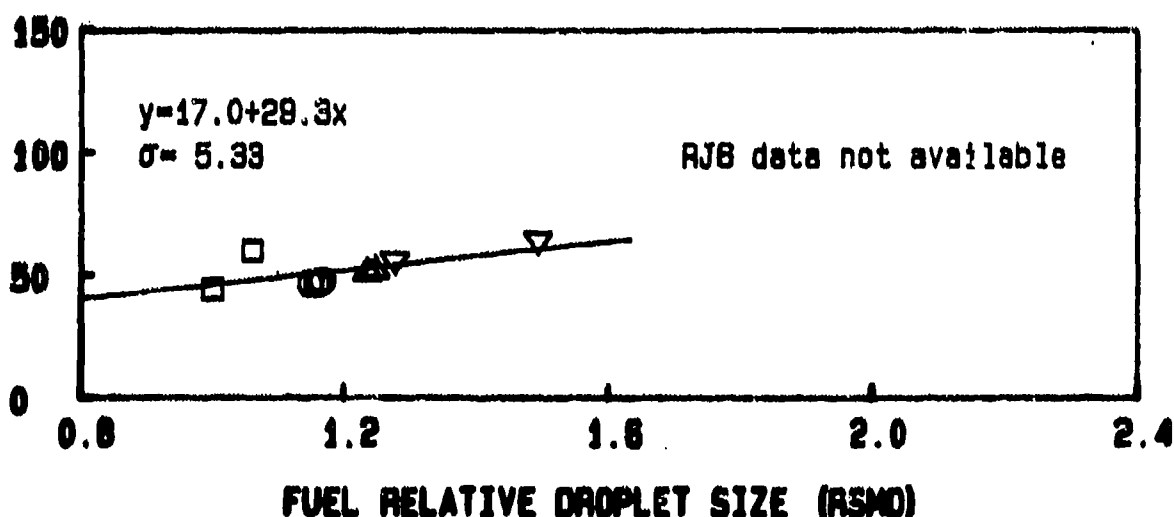
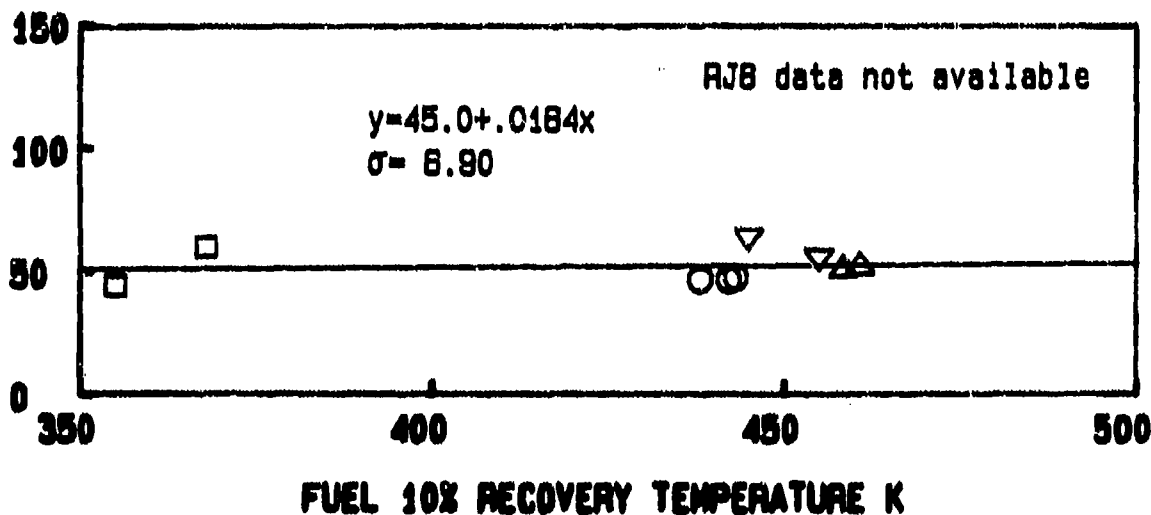
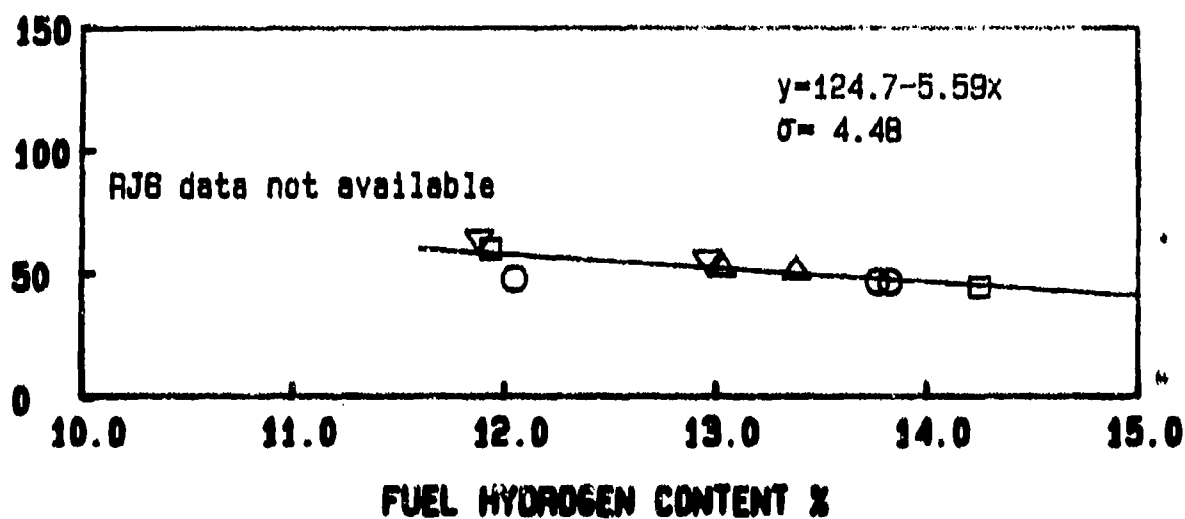


Figure 6.77: Effects of Fuel Properties on Idle CO Emissions
(PT6A-65 Gas Generator, 5% Bleed, Simplex 1.9 FN)

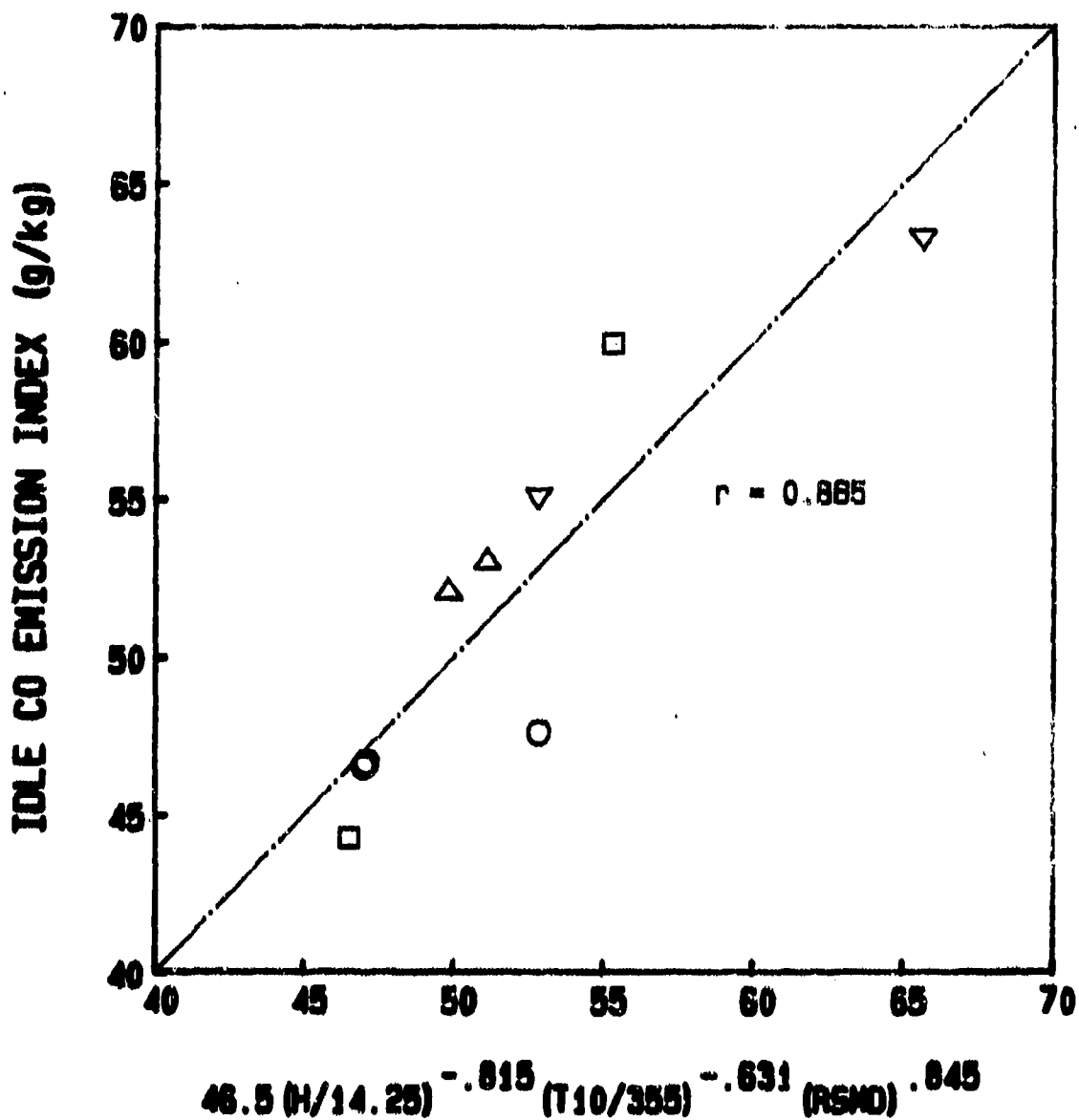


Figure 6.78: Idle CO Emissions vs Multiple Parameter Correlation
(PT6A-65 Gas Generator, 5% Bleed, Simplex 1.9 FN)

IDLE HC EMISSION INDEX (g/kg)

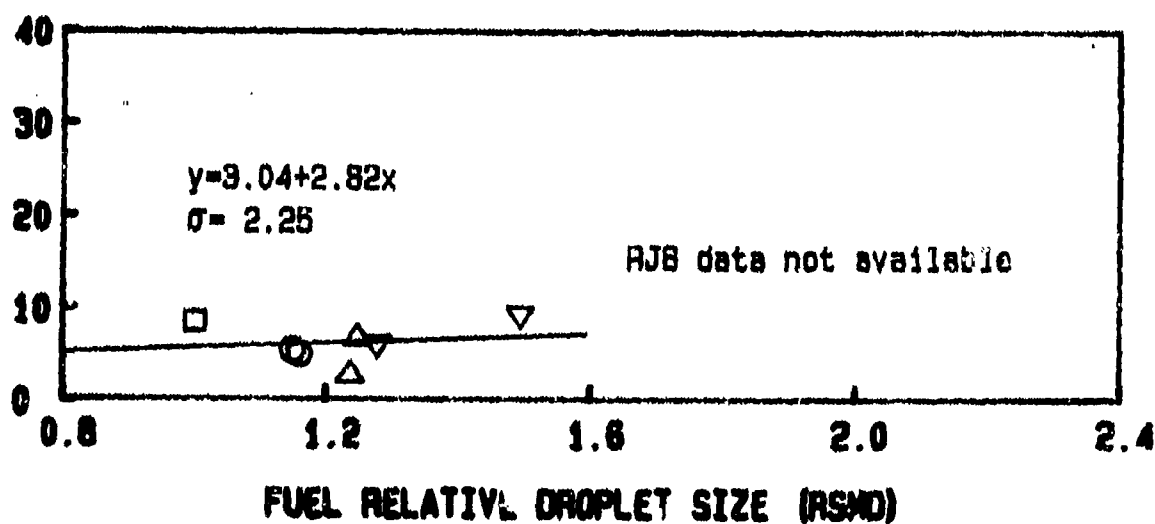
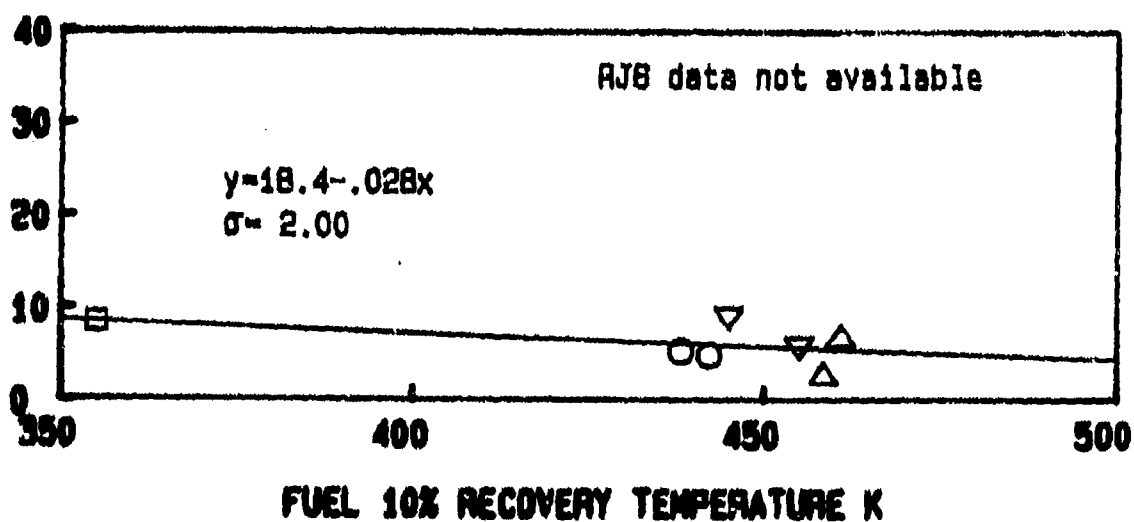
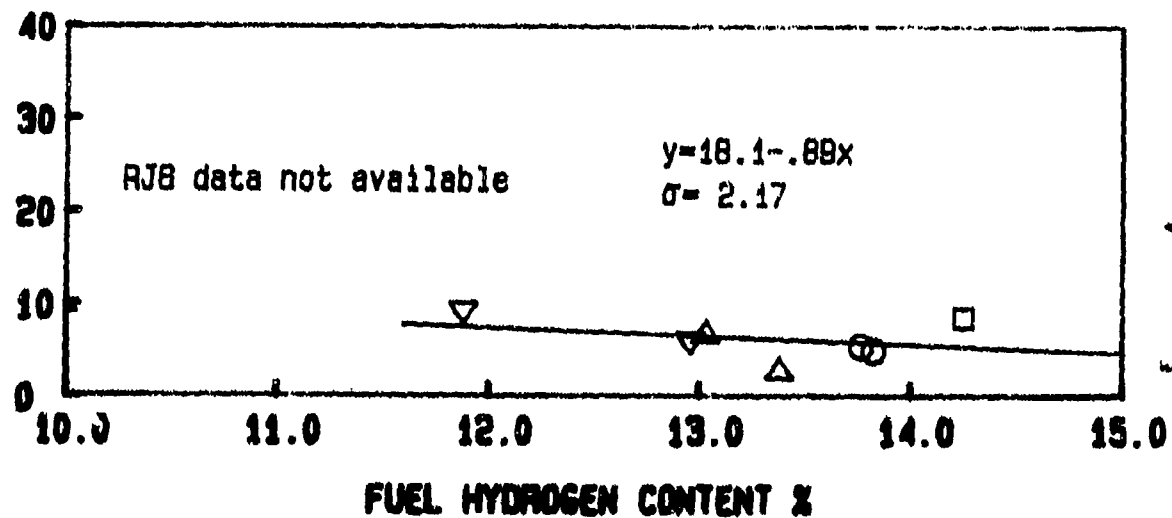


Figure 6.79: Effects of Fuel Properties on Idle HC Emissions
 (PT6A-65 Gas Generator, 5% Bleed, Simplex 1.9 FN)

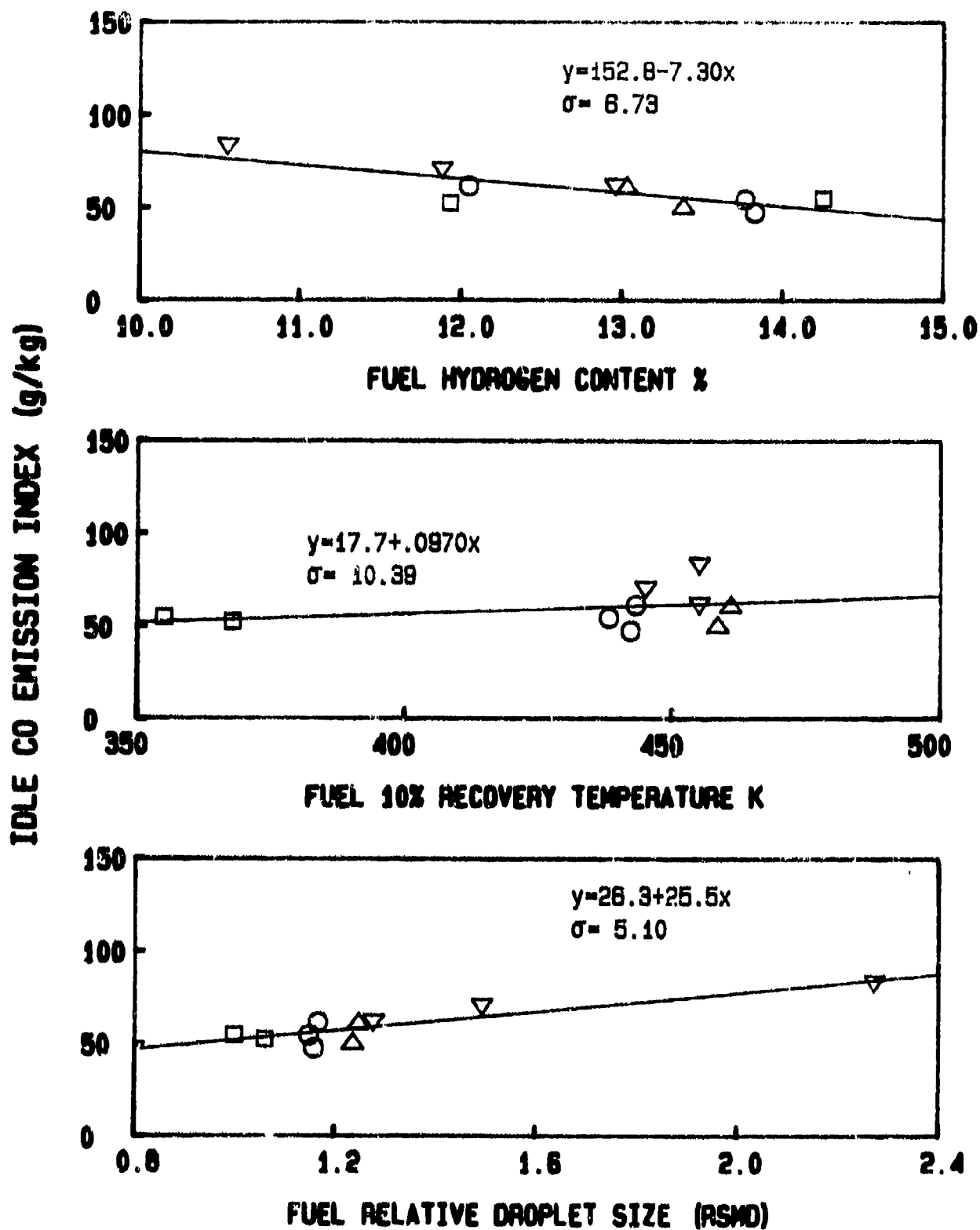


Figure 6.80: Effects of Fuel Properties on Idle CO Emissions
 (PT6A-65 Gas Generator, BOM, Simplex 2.2 FN)

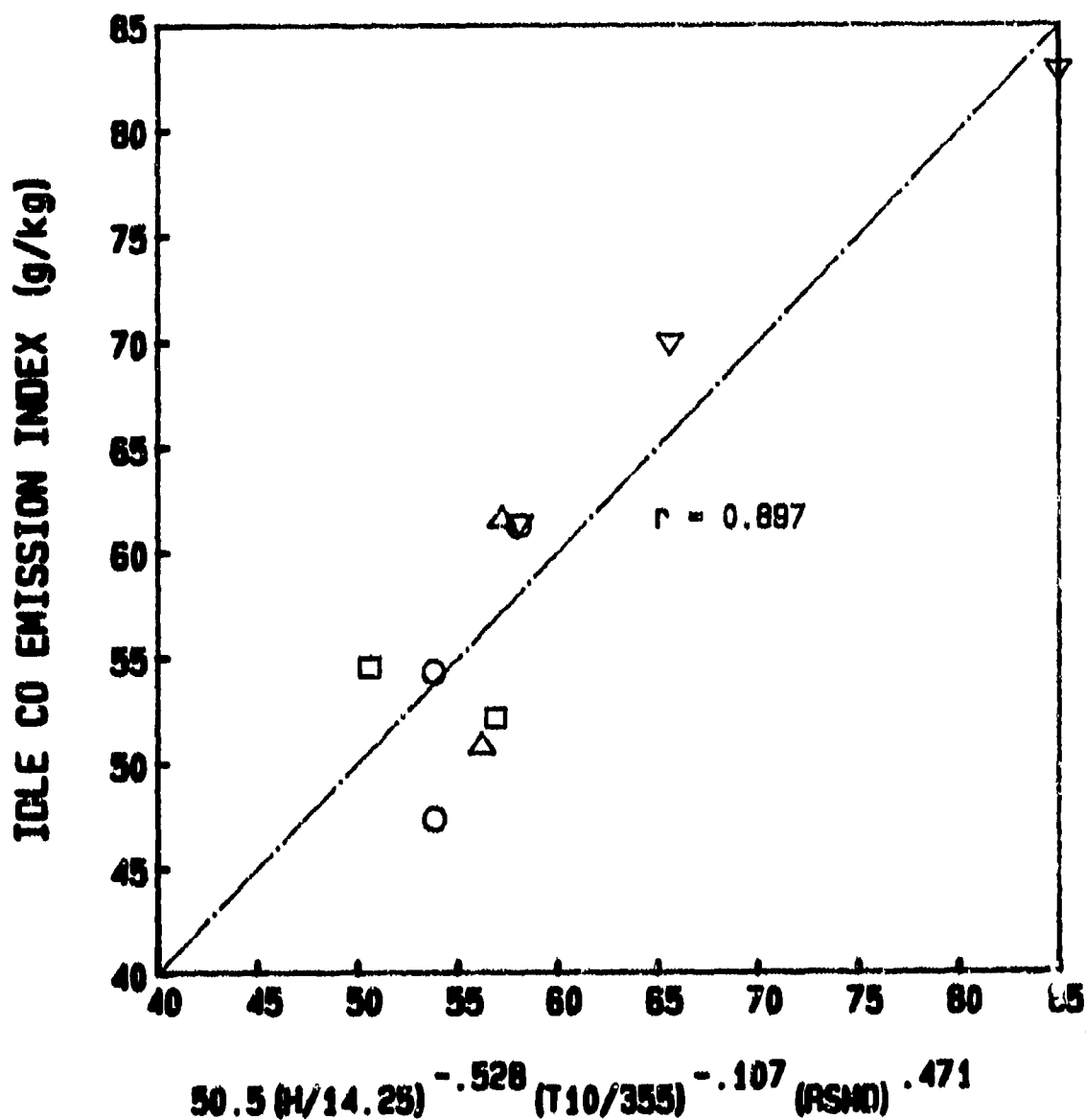


Figure 6.81: Idle CO Emissions vs Multiple Parameter Correlation
(PT6A-65 Gas Generator, BOM, Simplex 2.2 FN)

Idle HC Emission Index (g/kg)

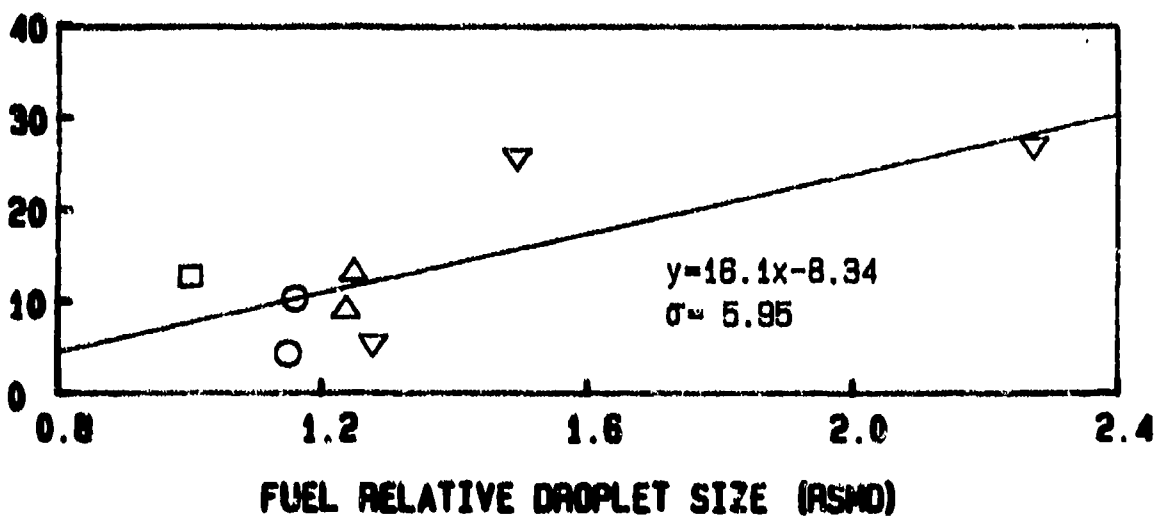
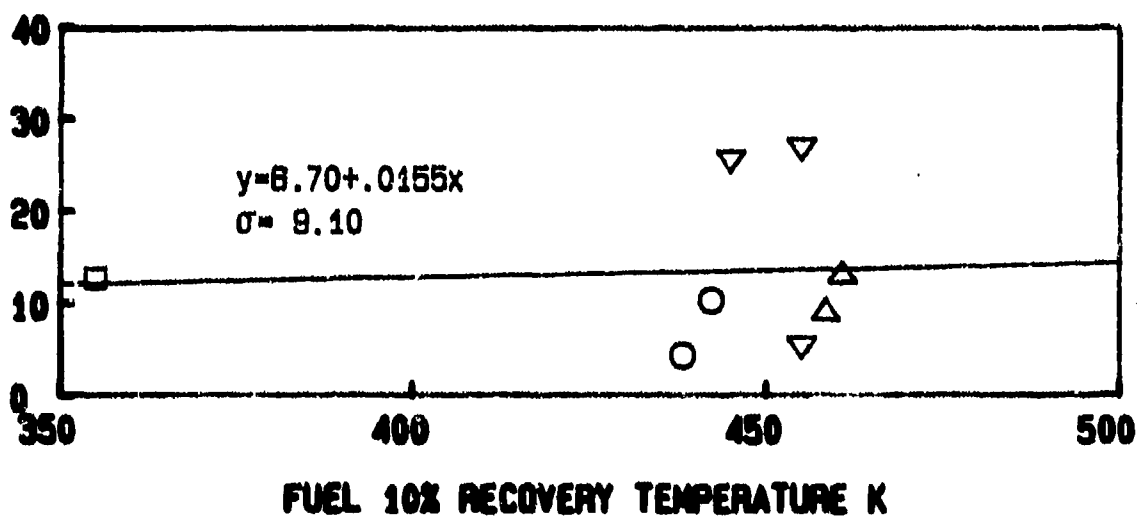
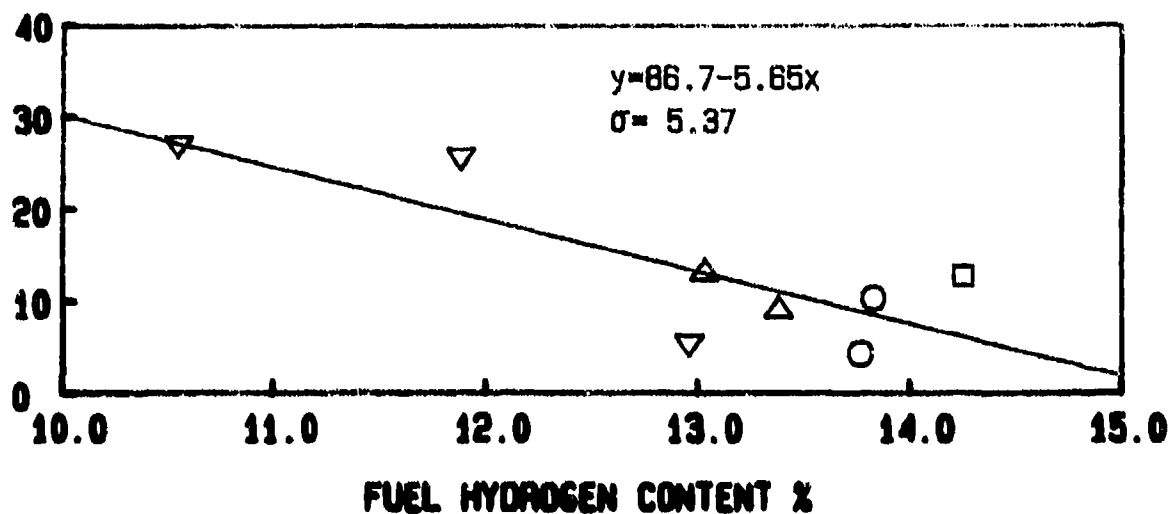


Figure 6.82: Effects of Fuel Properties on Idle HC Emissions (PT6A-65 Gas Generator, BOM, Simplex 2.2 FN)

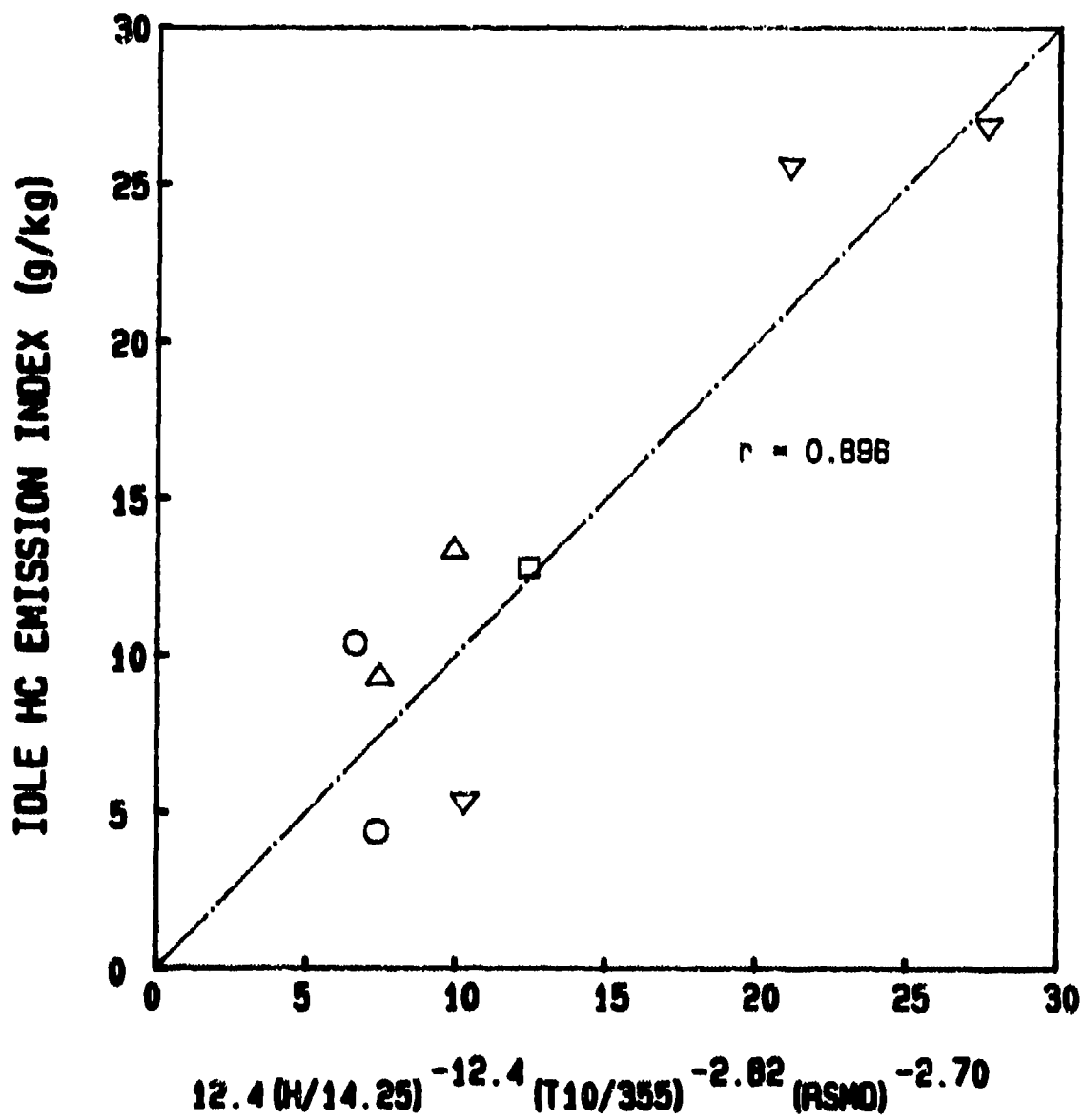


Figure 6.83: Idle HC Emissions vs Multiple Parameter Correlation
(PT6A-65 Gas Generator, BOM, Simplex 2.2 FN)

Idle CO Emission Index (g/kg)

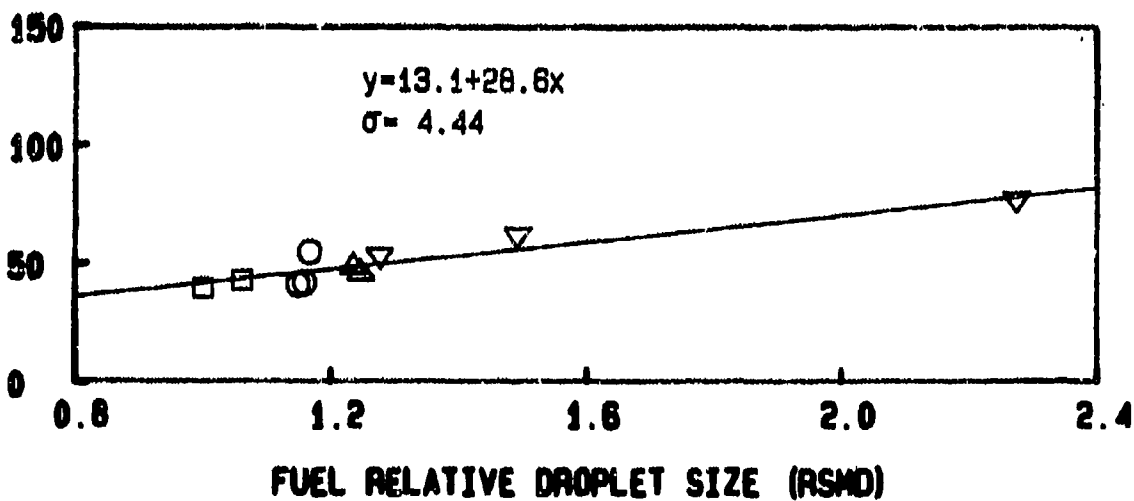
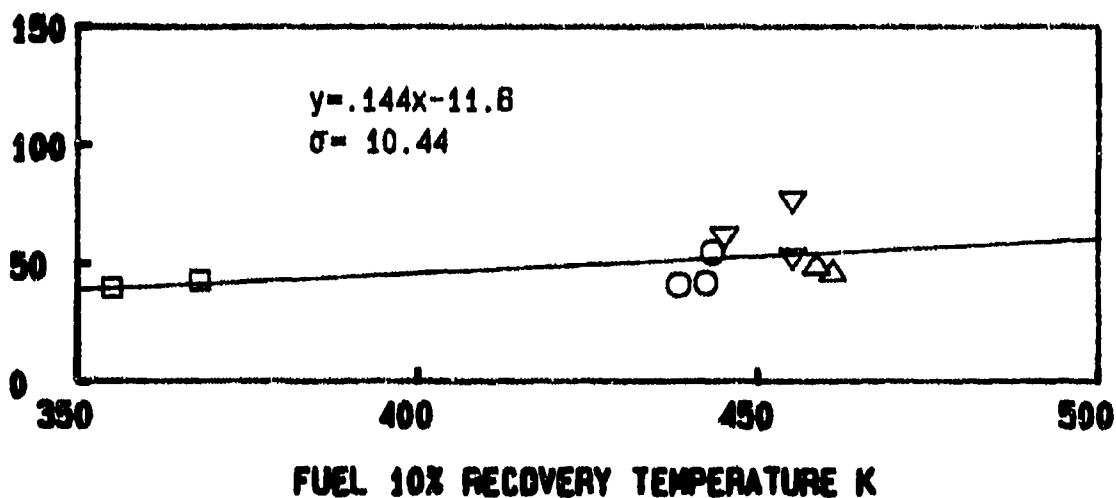
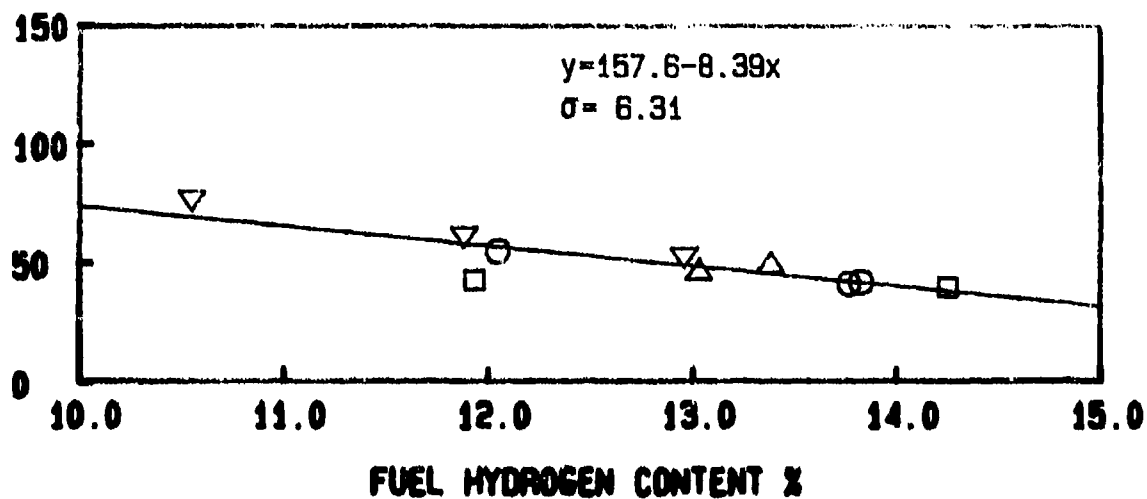


Figure 6.84: Effects of Fuel Properties on Idle CO Emissions
 (PT6A-65 Gas Generator, 5% Bleed, Simplex 2.2 FN)

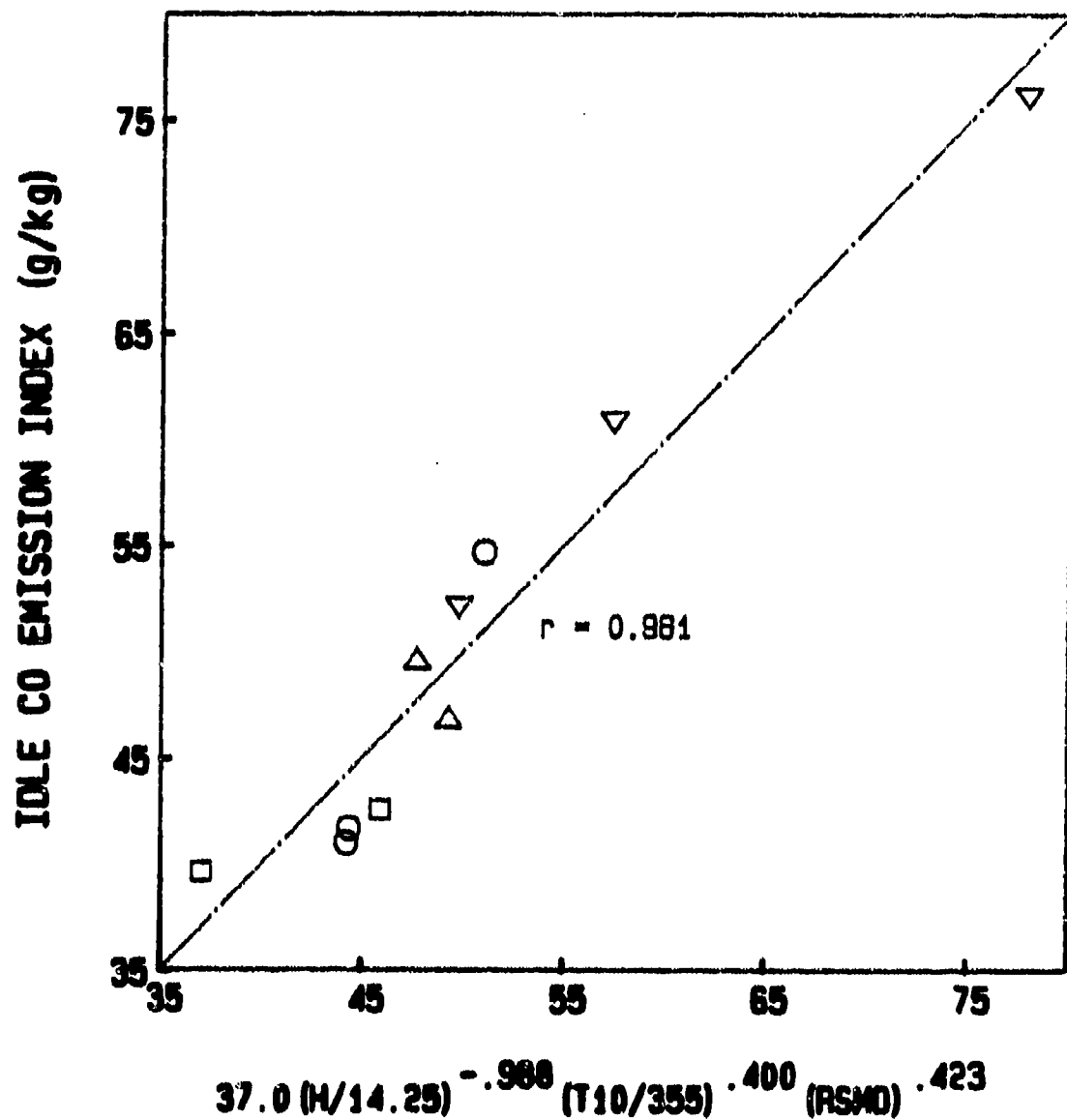


Figure 6.85: Idle CO Emissions vs Multiple Parameter Correlation
(PT6A-65 Gas Generator, 5% Bleed, Simplex 2.2 FN)

Idle HC Emission Index (g/kg)

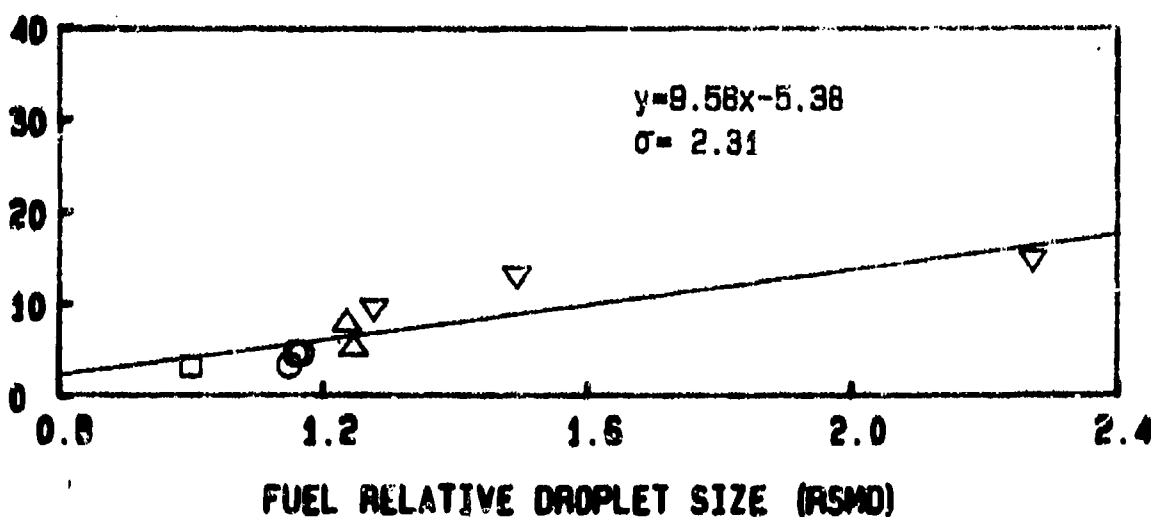
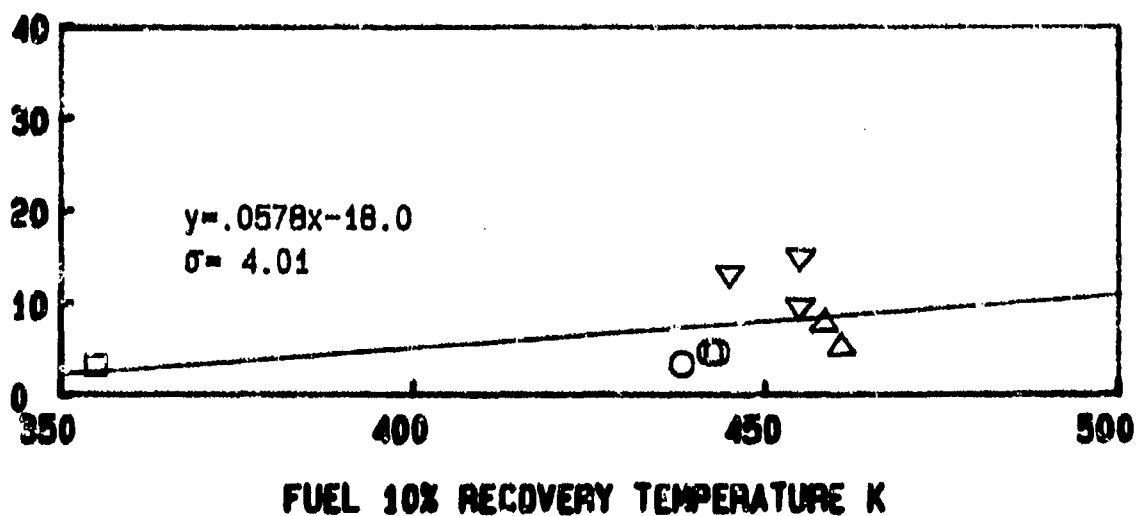
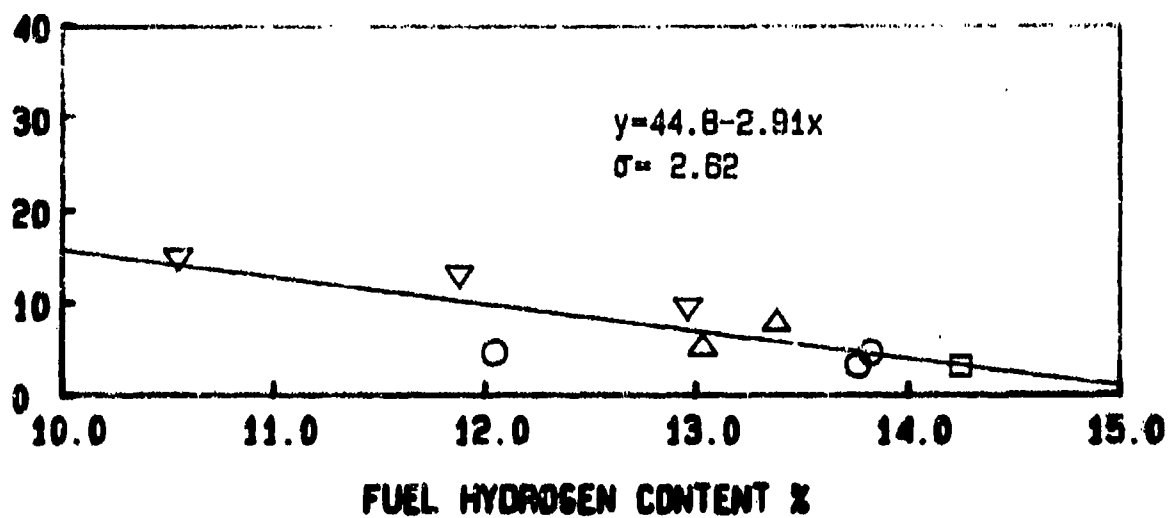


Figure 6.86: Effects of Fuel Properties on Idle HC Emissions
 (PT6A-65 Gas Generator, 5% Bleed, Simplex 2.2 FN)

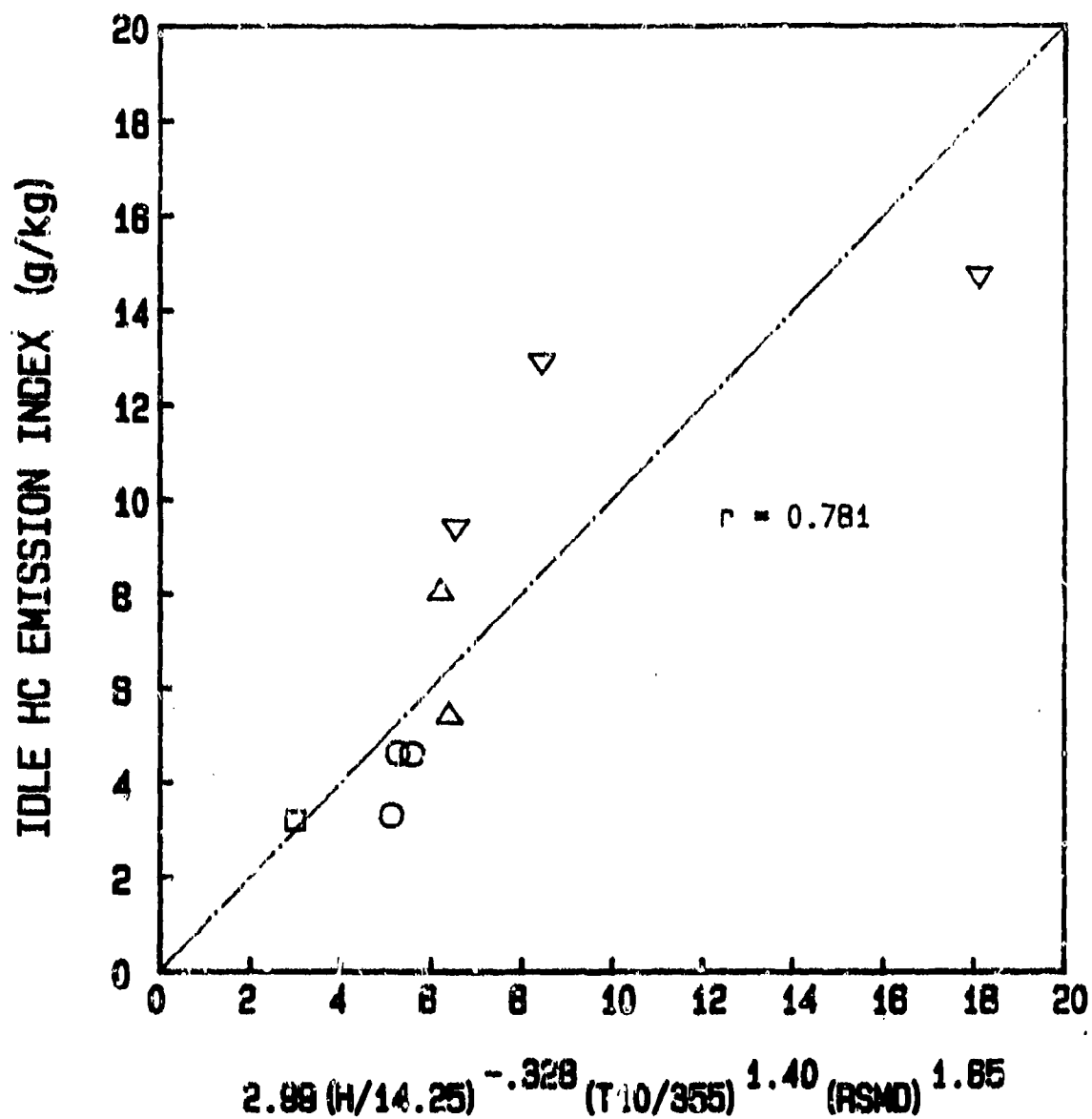


Figure 6.87: Idle HC Emissions vs Multiple Parameter Correlation
(PTGA-65 Gas Generator, 5% Bleed, Simplex 2.2 FN)

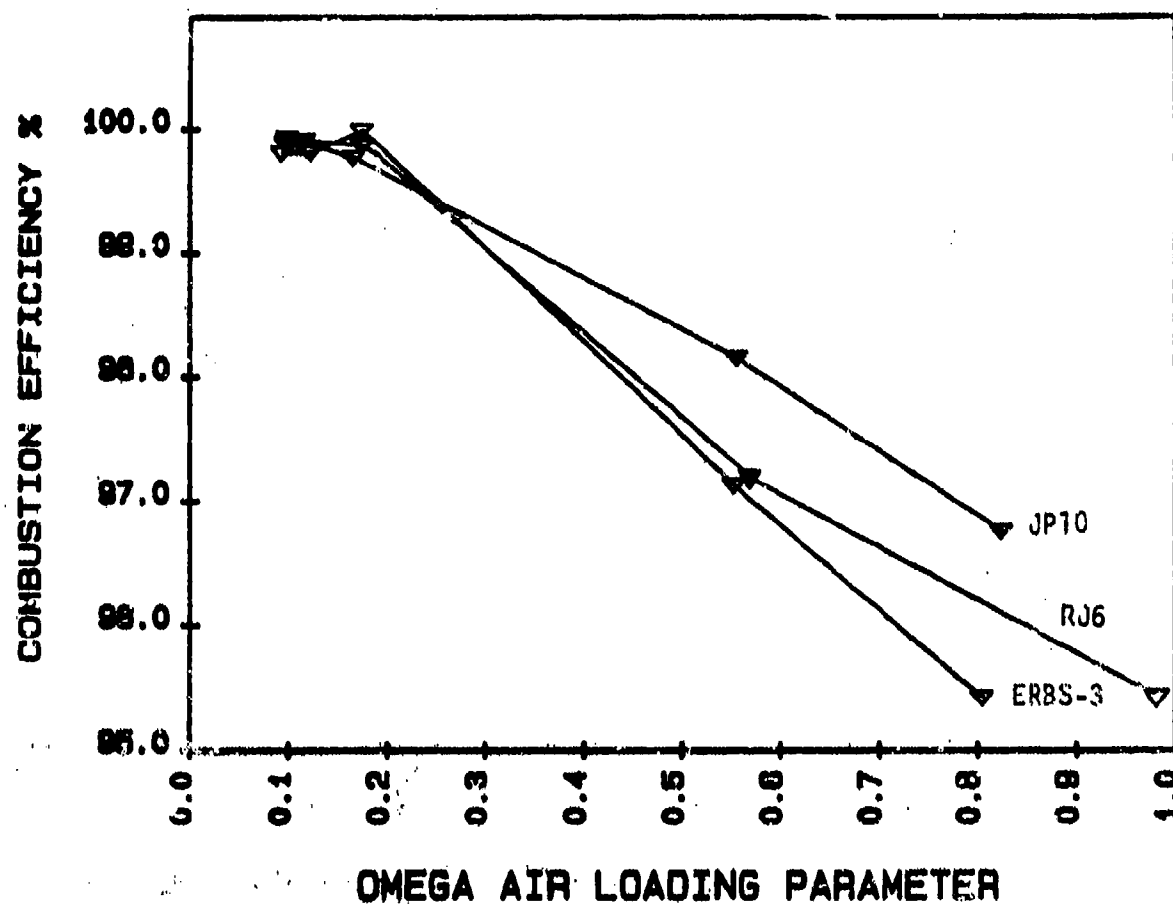


Figure 6.88: Combustion Efficiency Variations Over Operating Range
(PT6A-65 Gas Generator, BOM, Simplex 1.9 FN)

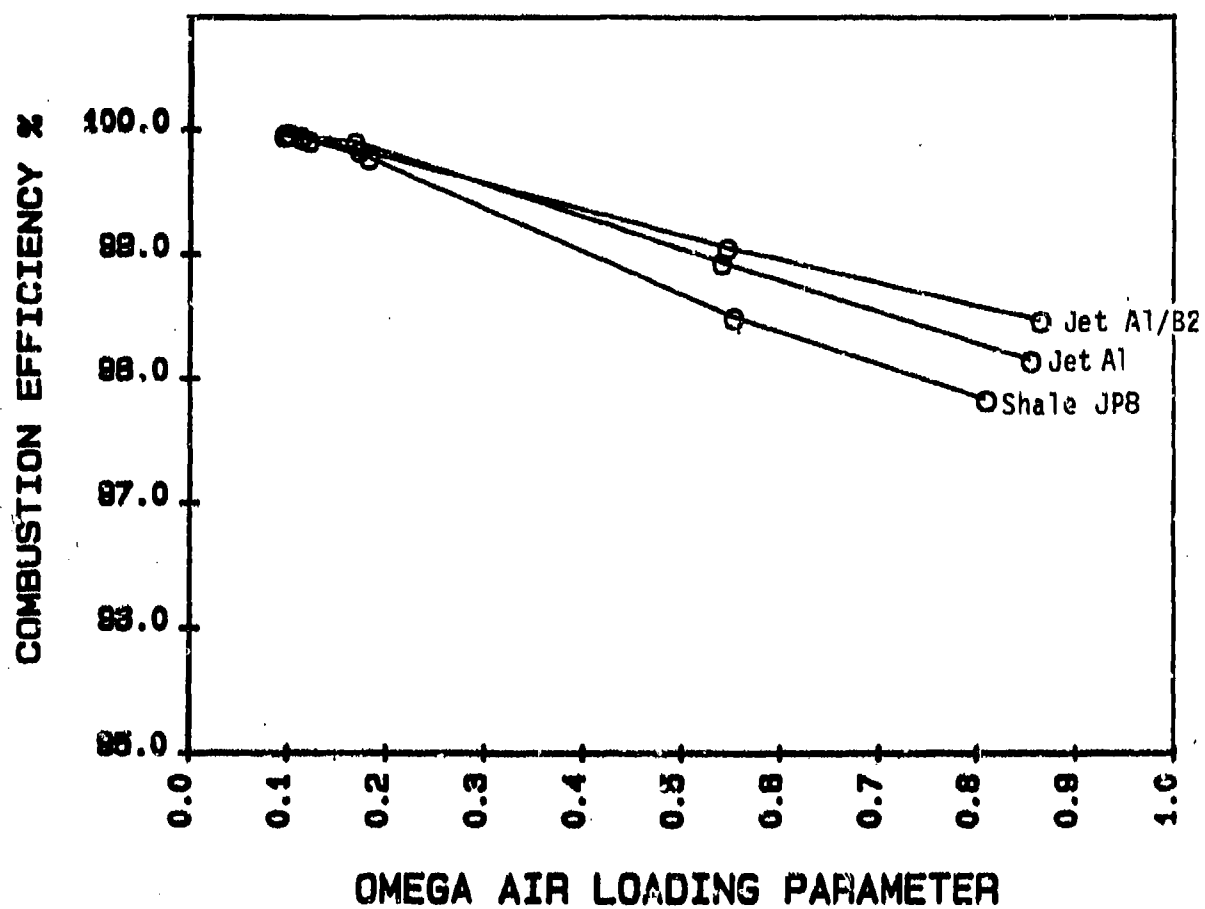


Figure 6.89: Combustion Efficiency Variations Over Operating Range (PT6A-65 Gas Generator, BOM, Simplex 1.9 FN)

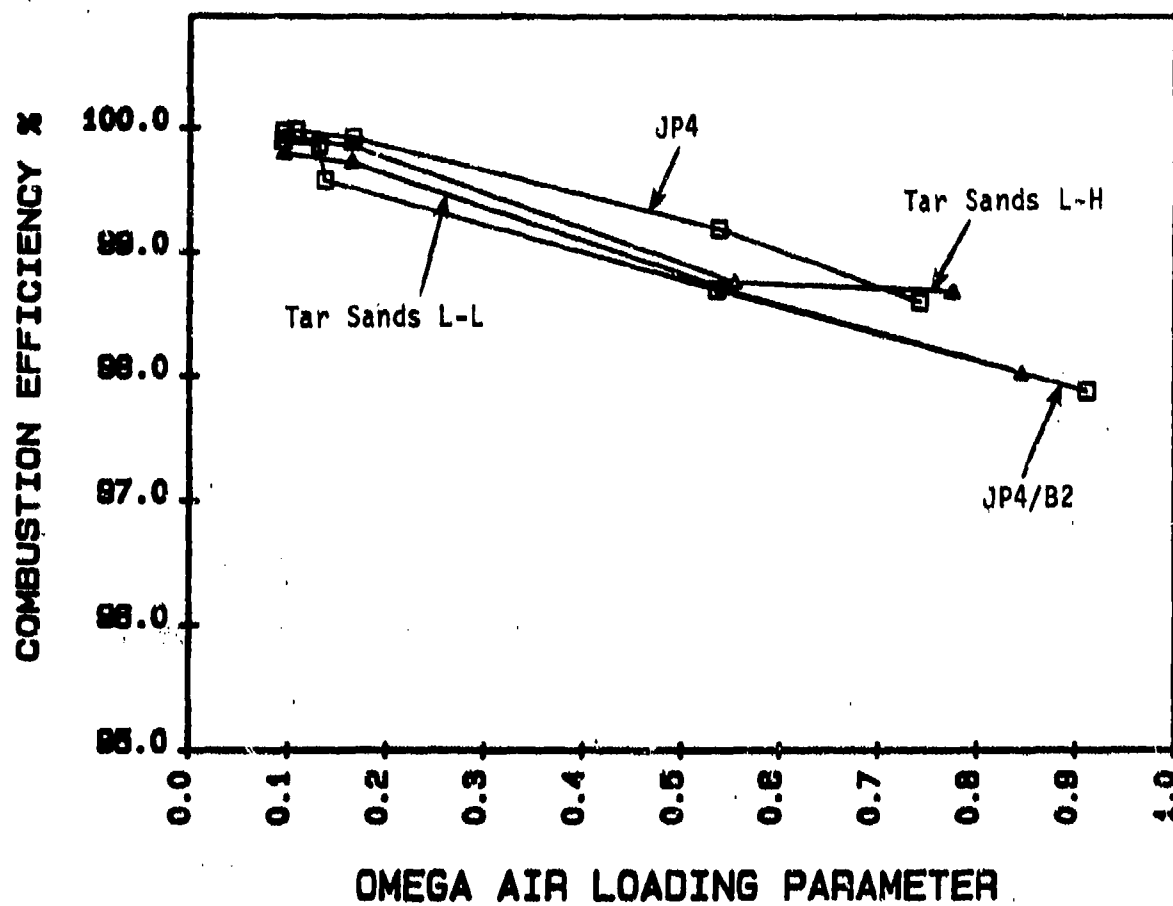


Figure 6.90: Combustion Efficiency Variations Over Operating Range
(PT6A-65 Gas Generator, BOM, Simplex 1.9 FN)

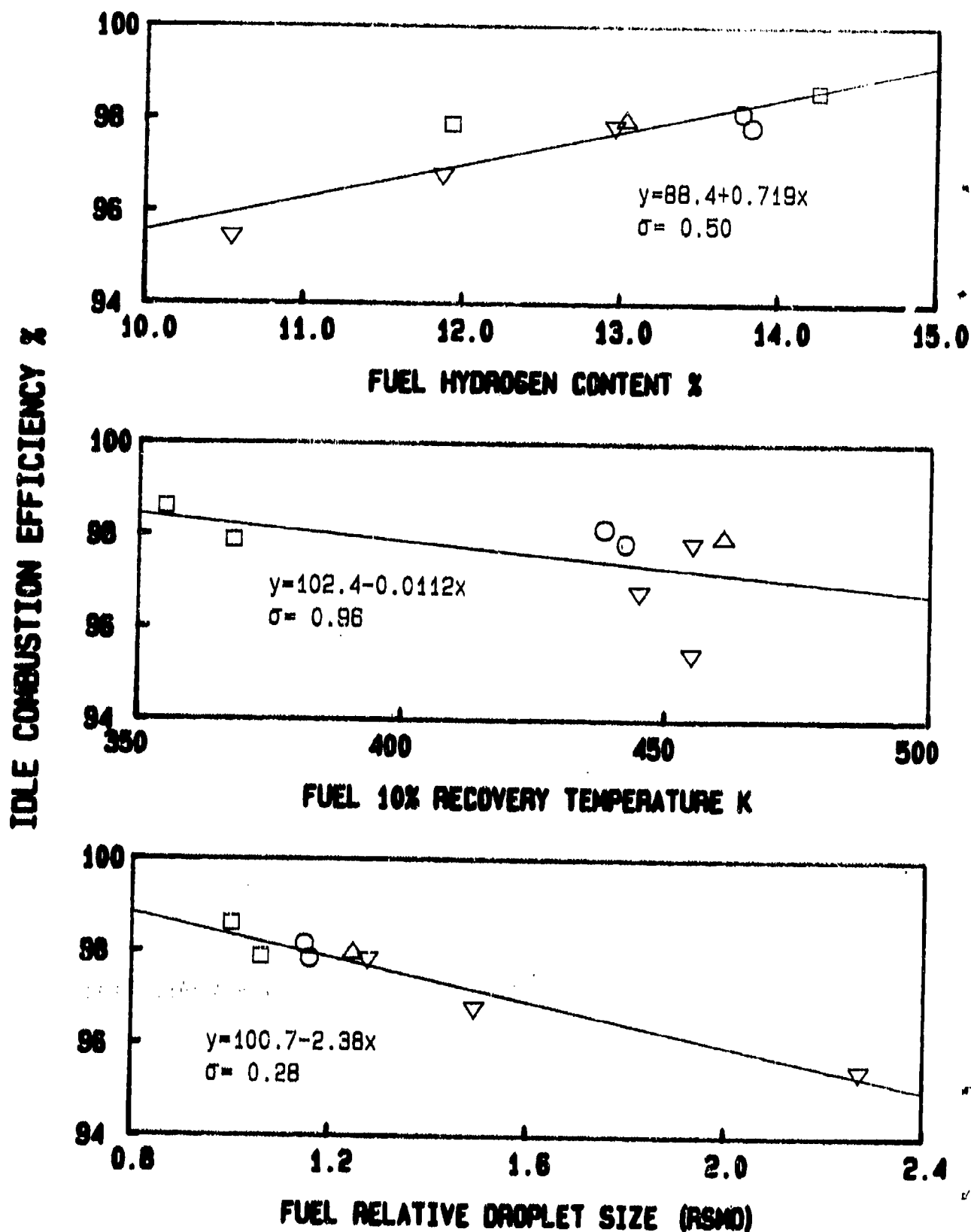


Figure 6.91: Effects of Fuel Properties on Idle Combustion Efficiency
(PT6A-65 Gas Generator, BOM, Simplex 1.9 FN)

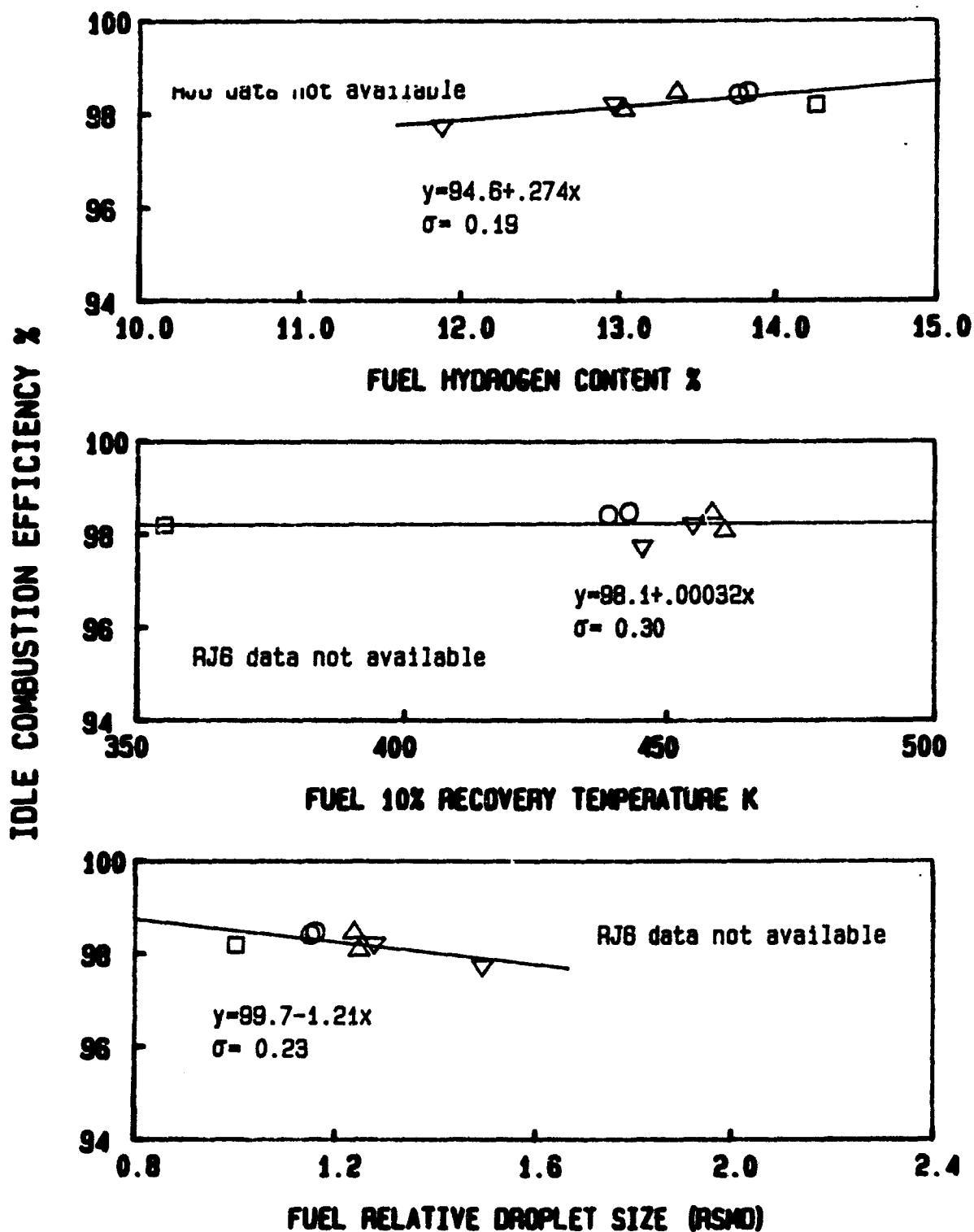


Figure 6.95: Effects of Fuel Properties on Idle Combustion Efficiency
 (PT6A-65 Gas Generator, 5% Bleed, Simplex 1.9 FN)

7% POWER COMBUSTION EFFICIENCY %

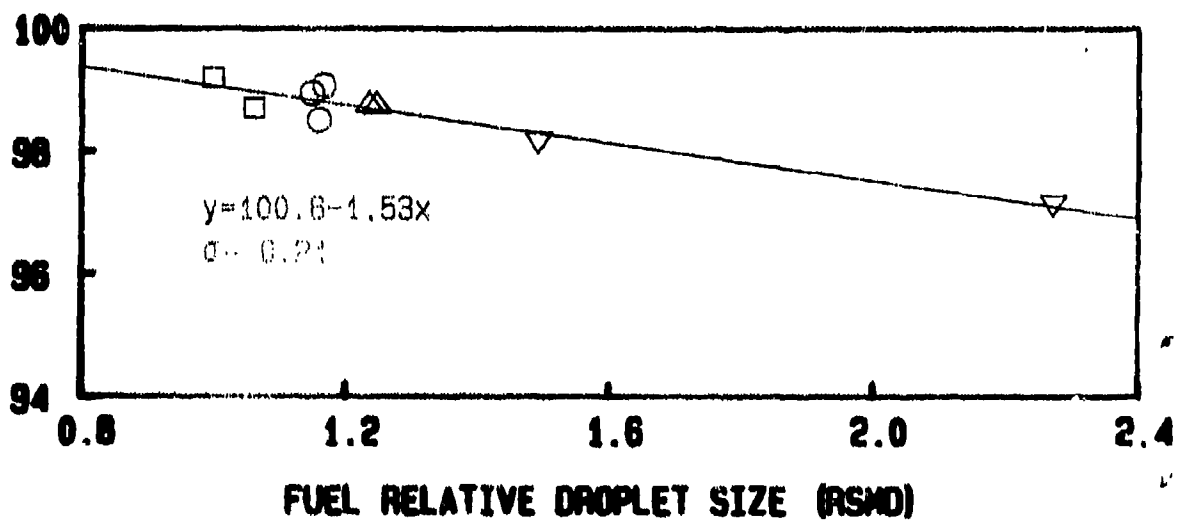
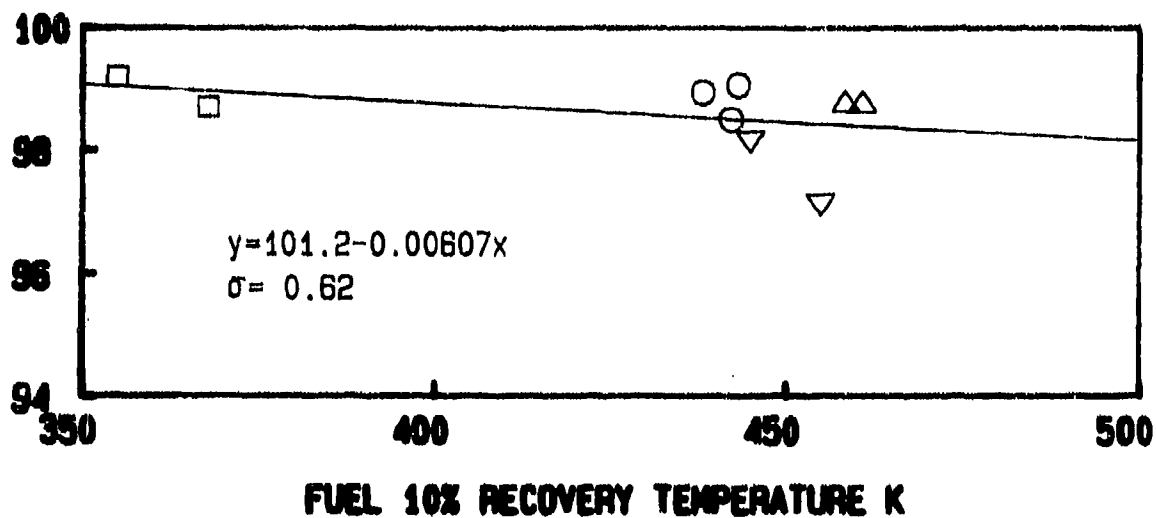
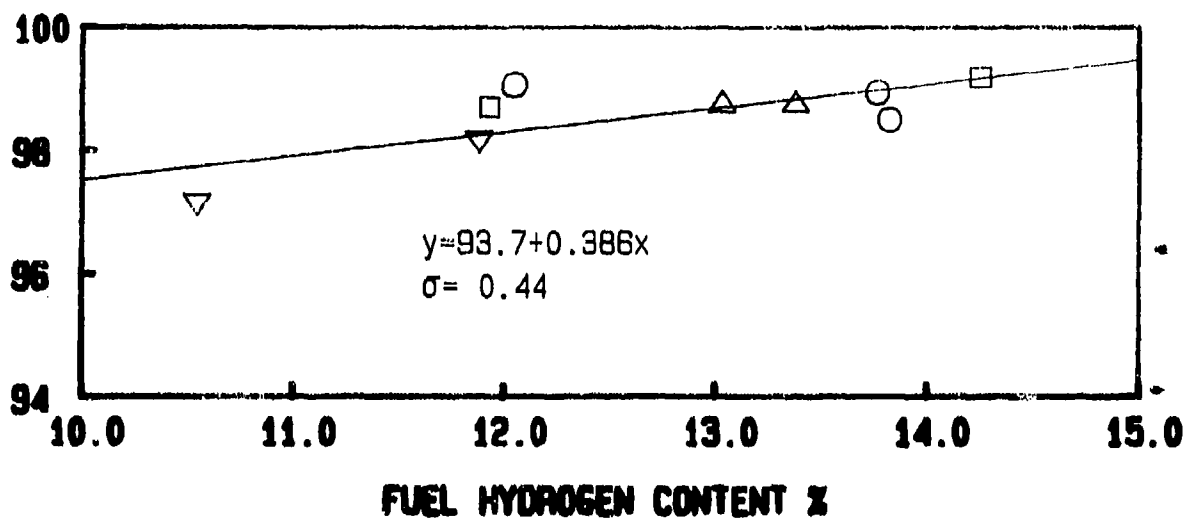


Figure 6.93: Effects of Fuel Properties on 7% Power Combustion Efficiency (PT6A-65 Gas Generator, BOM, Simplex 1.9 FN)

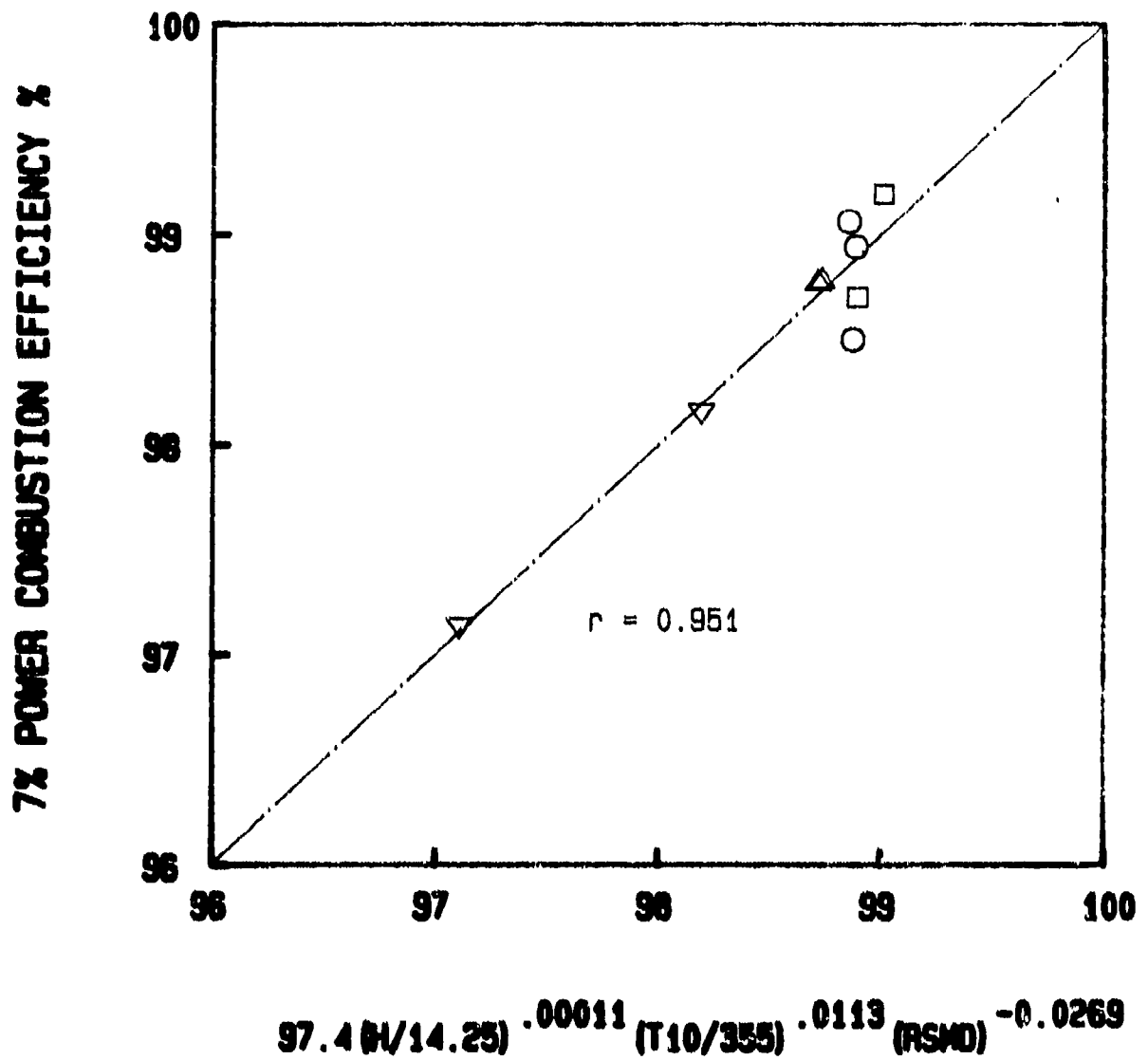


Figure 6.94: 7% Power Combustion Efficiency vs Multiple Parameter Correlation (PT6A-65 Gas Generator, BOM, Simplex 1.9 FN)

Idle Combustion Efficiency %

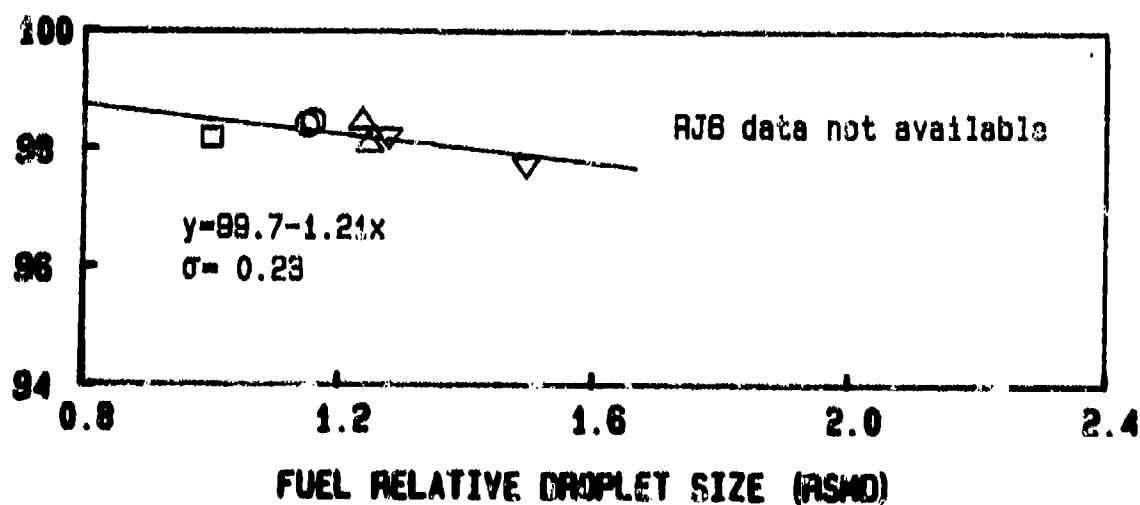
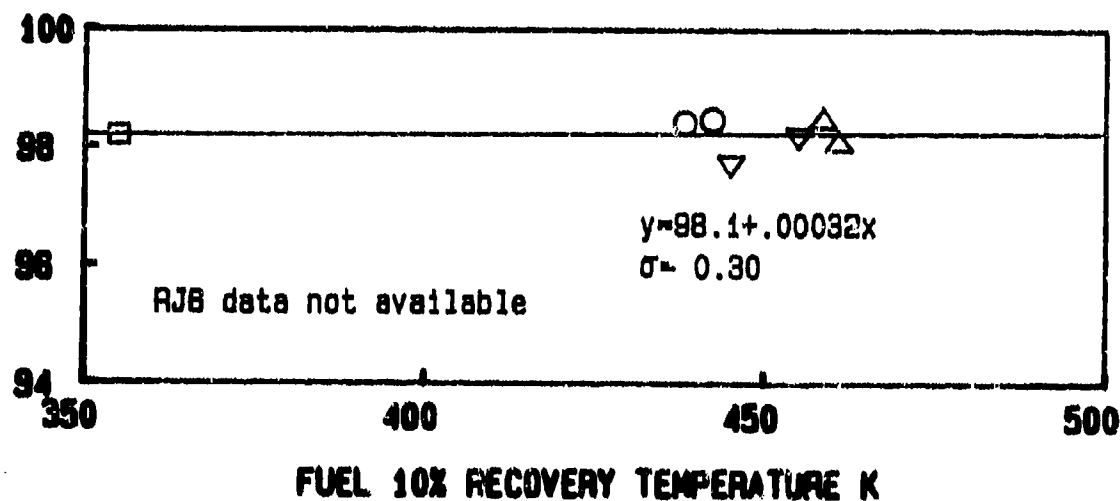
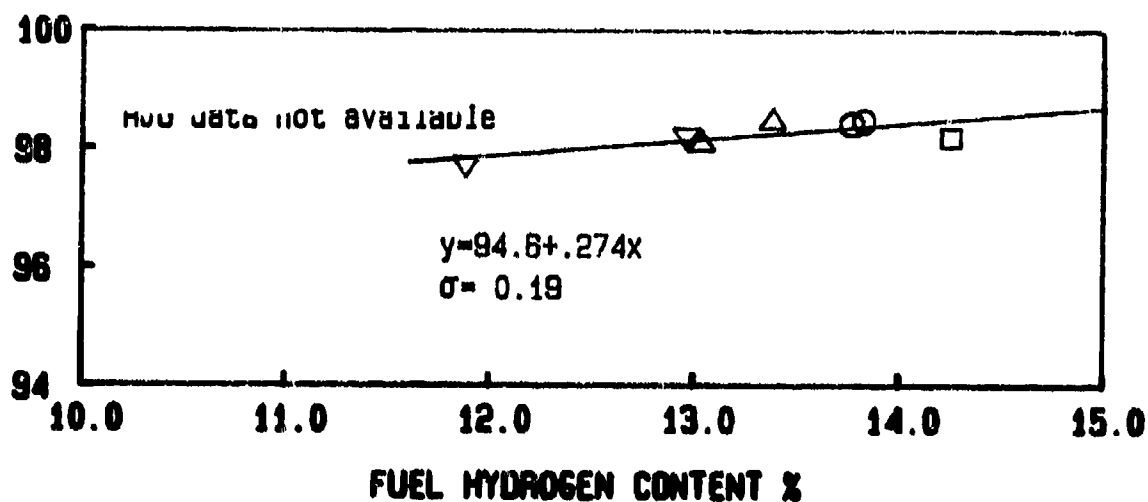


Figure 6.95: Effects of Fuel Properties on Idle Combustion Efficiency (PT6A-65 Gas Generator, 5% Bleed, Simplex 1.9 FN)

Idle Combustion Efficiency %

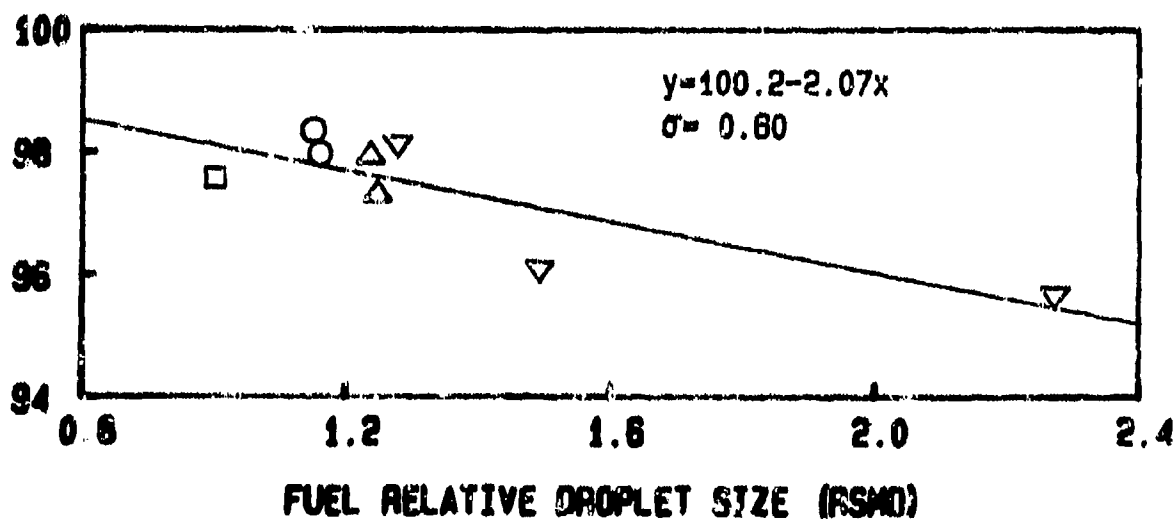
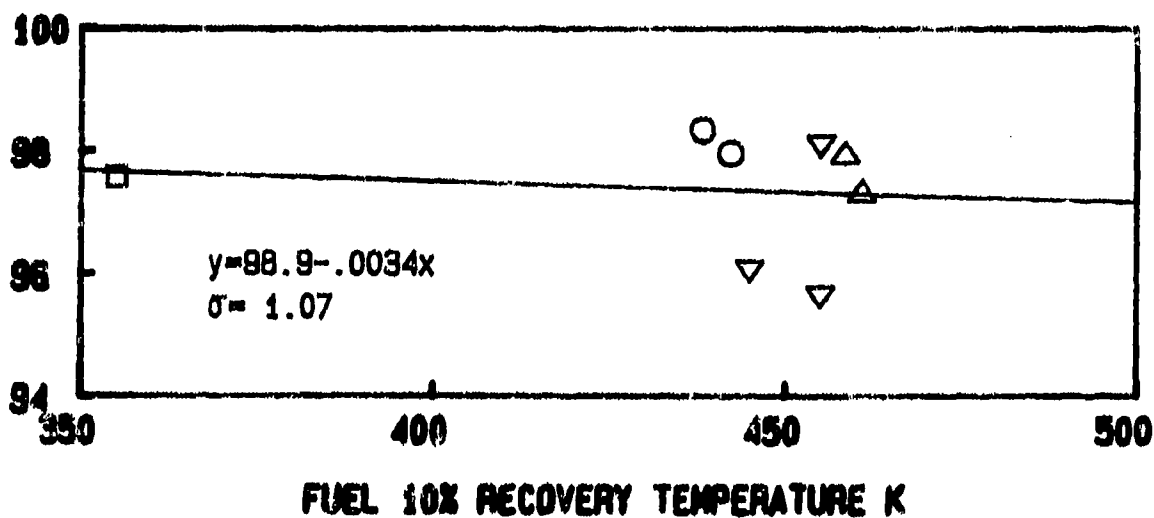
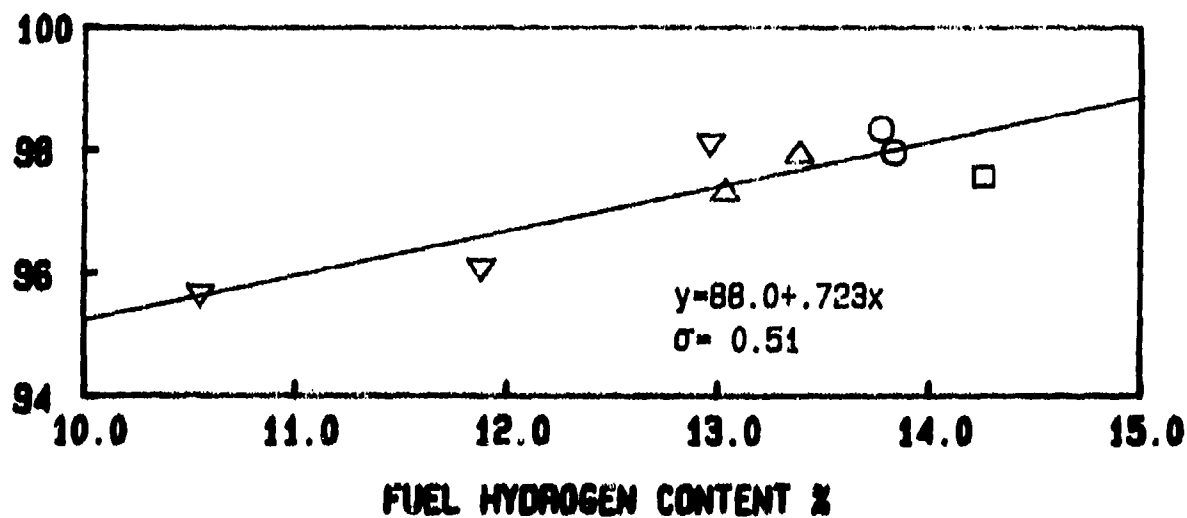


Figure 6.96: Effects of Fuel Properties on Idle Combustion Efficiency (PT6A-65 Gas Generator, BOM, Simplex 2.2 FN)

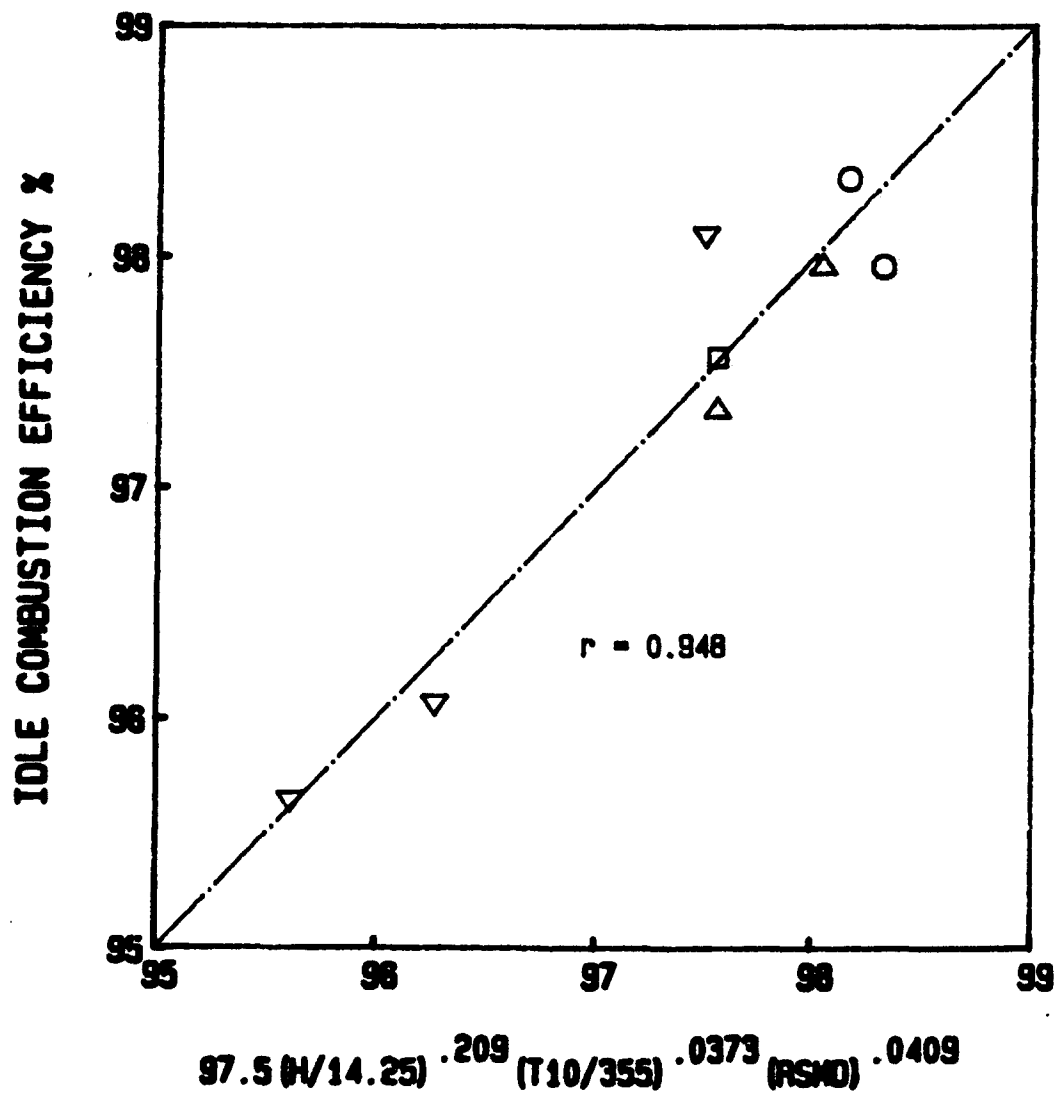


Figure 6.97: Idle Combustion Efficiency vs Multiple Parameter Correlation (PT6A-65 Gas Generator, BOM, Simplex 2.2 FN)

Idle Combustion Efficiency %

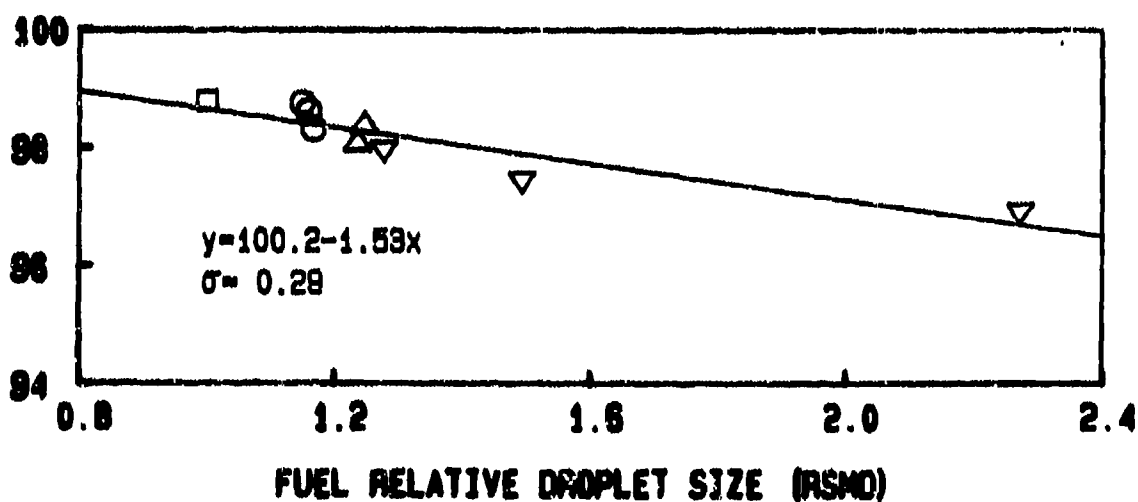
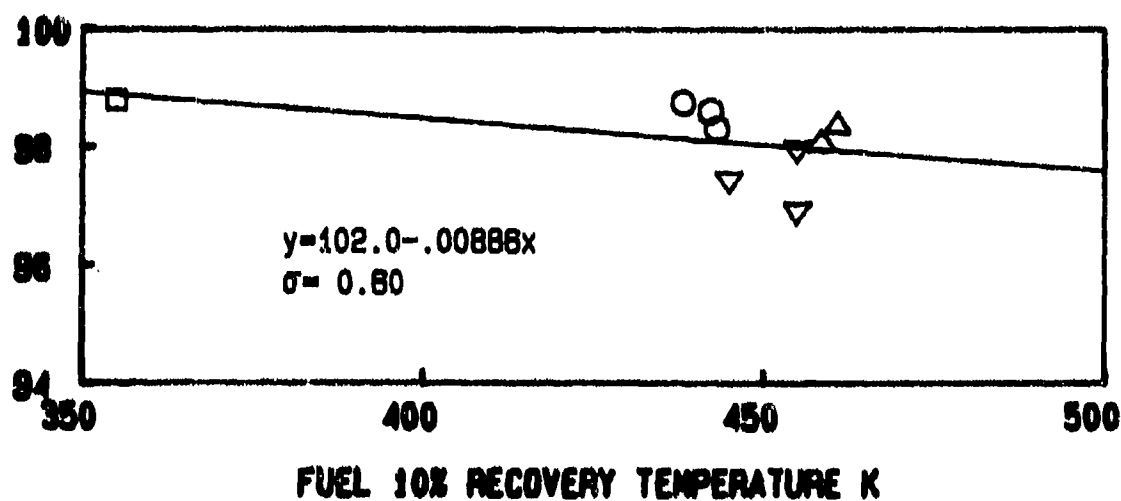
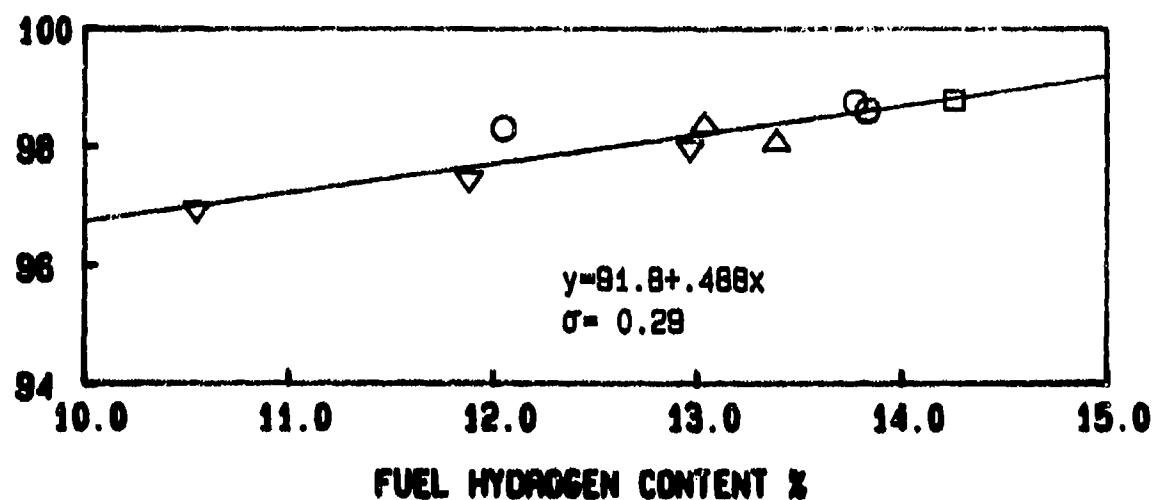


Figure 6.98: Effects of Fuel Properties on Idle Combustion Efficiency (PT6A-65 Gas Generator, 5% Bleed, Simplex 2.2 FN)

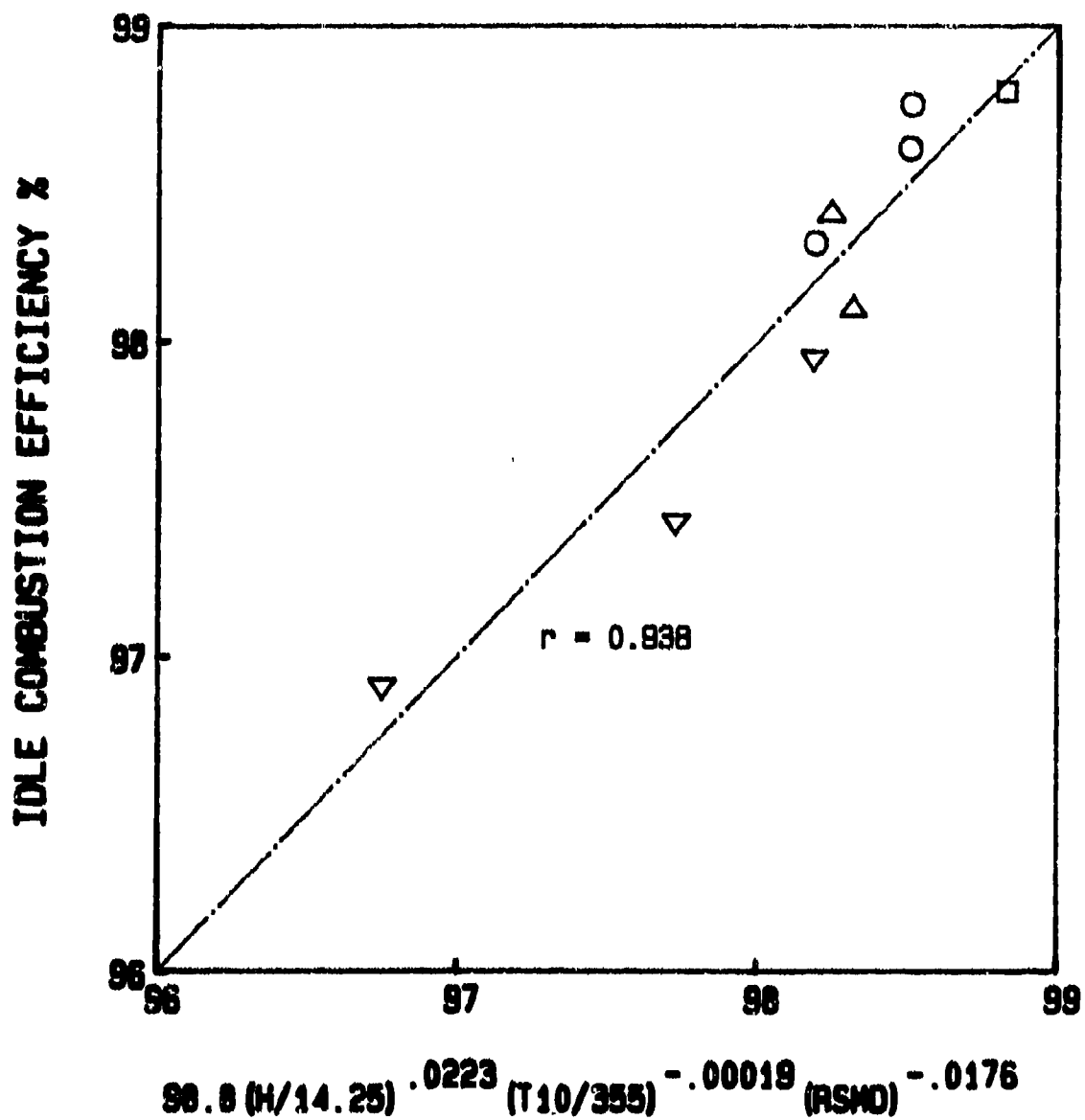


Figure 6.99: Idle Combustion Efficiency vs Multiple Parameter Correlation (PT6A-65 Gas Generator, 5% Bleed, Simplex 2.2 FN)

CORRECTED NOx EMISSION INDEX (g/kg)

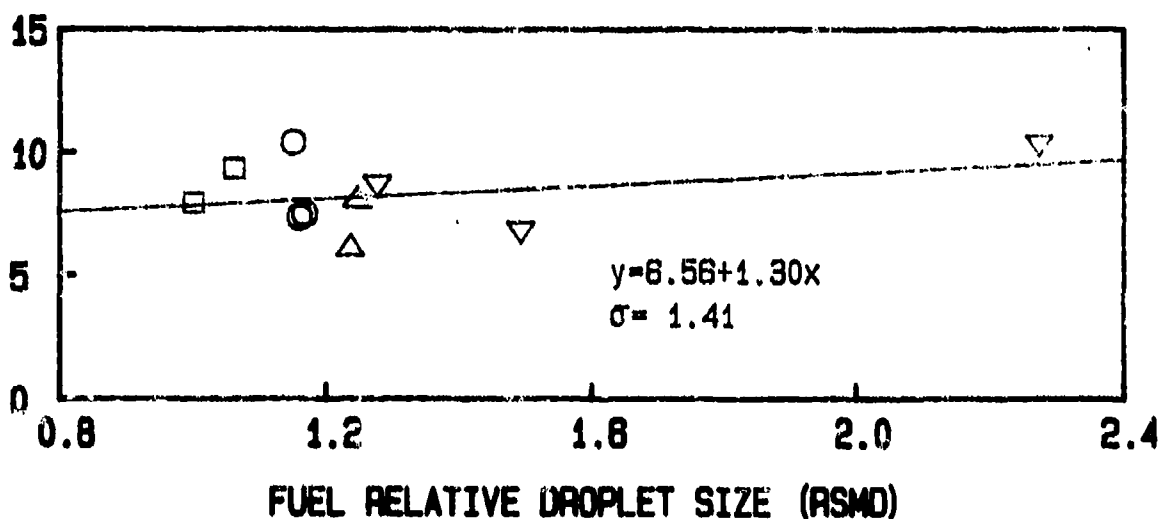
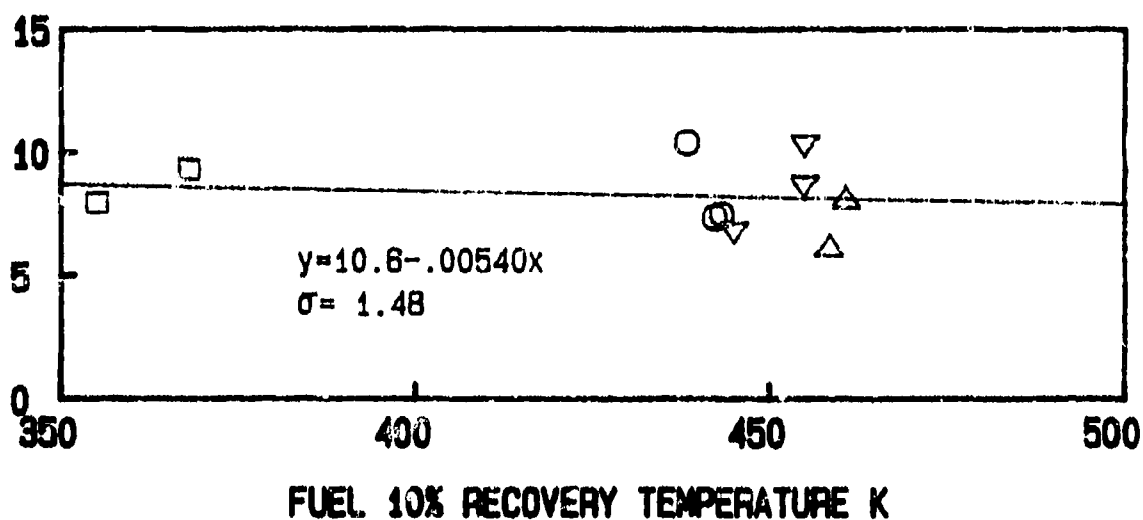
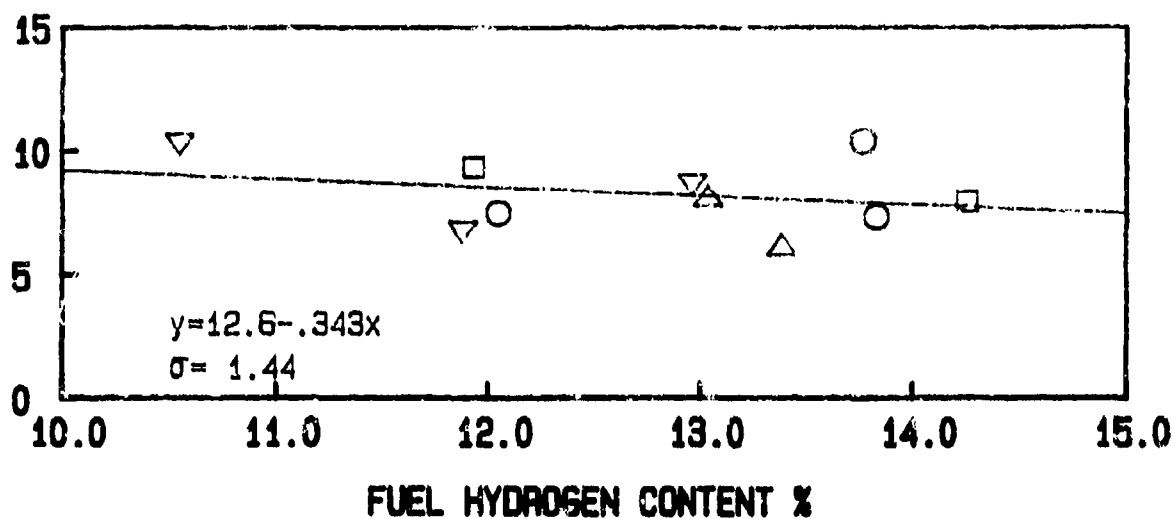


Figure 6.100: Effects of Fuel Properties on Corrected NOx Emissions (FT6A-65 Gas Generator, BOM, Simplex 1.9 FN)

CORRECTED NOx EMISSION INDEX (g/kg)

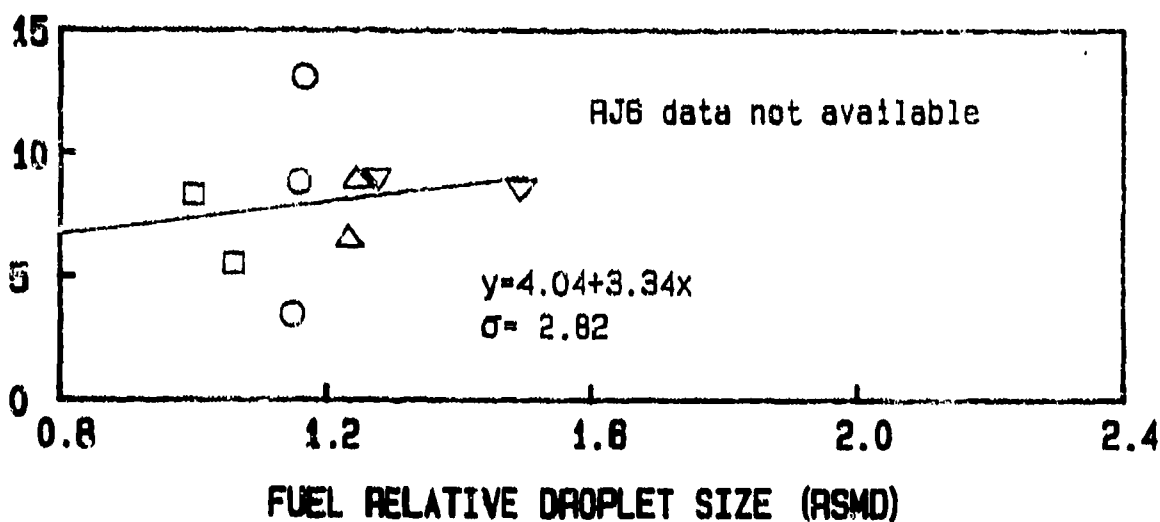
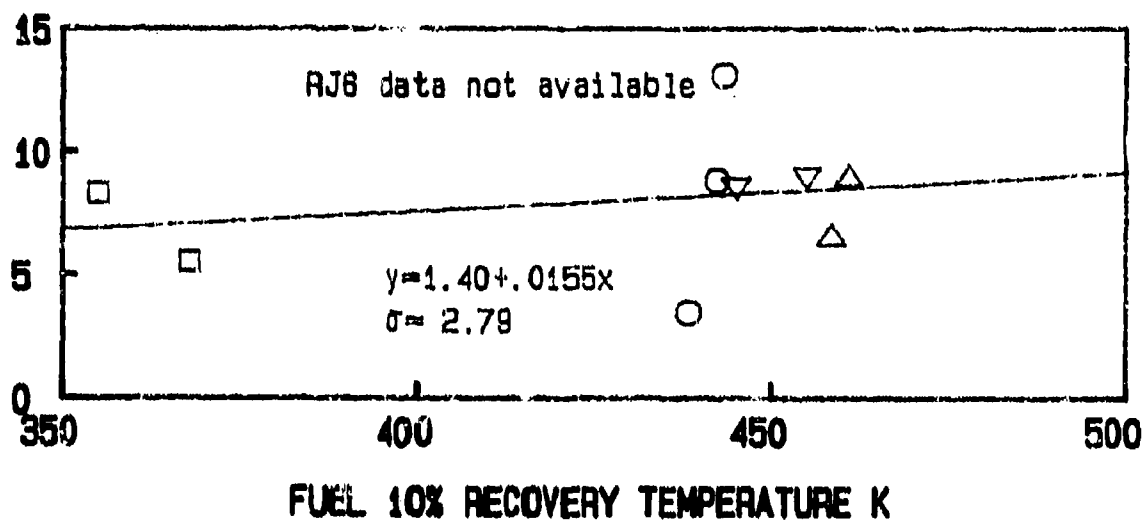
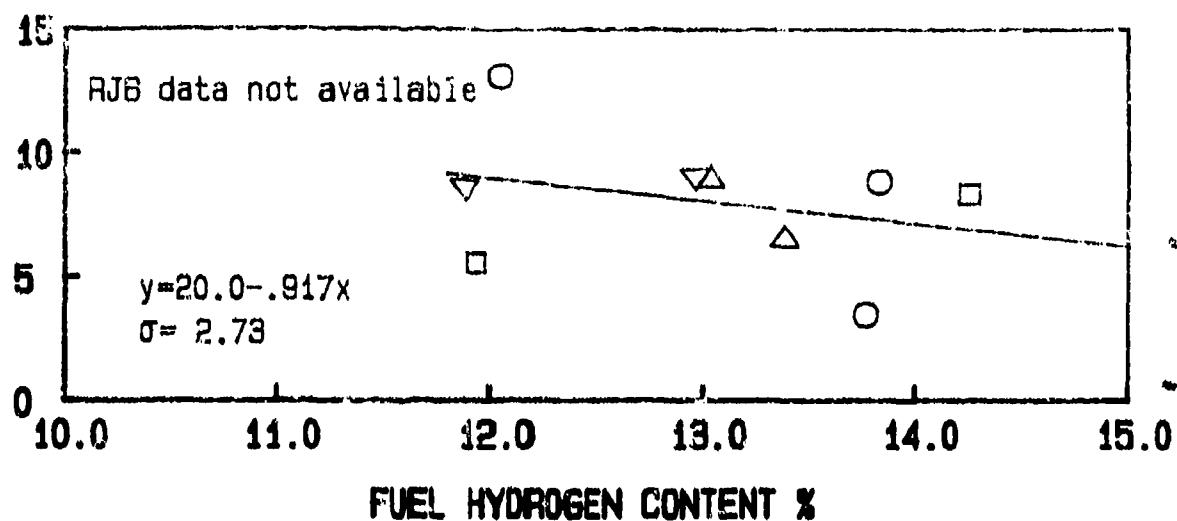


Figure 6.101: Effects of Fuel Properties on Corrected NOx Emissions (PT6A-65 Gas Generator, 5% Bleed, Simplex 1.9 FN)

CORRECTED NOx EMISSION INDEX (g/kg)

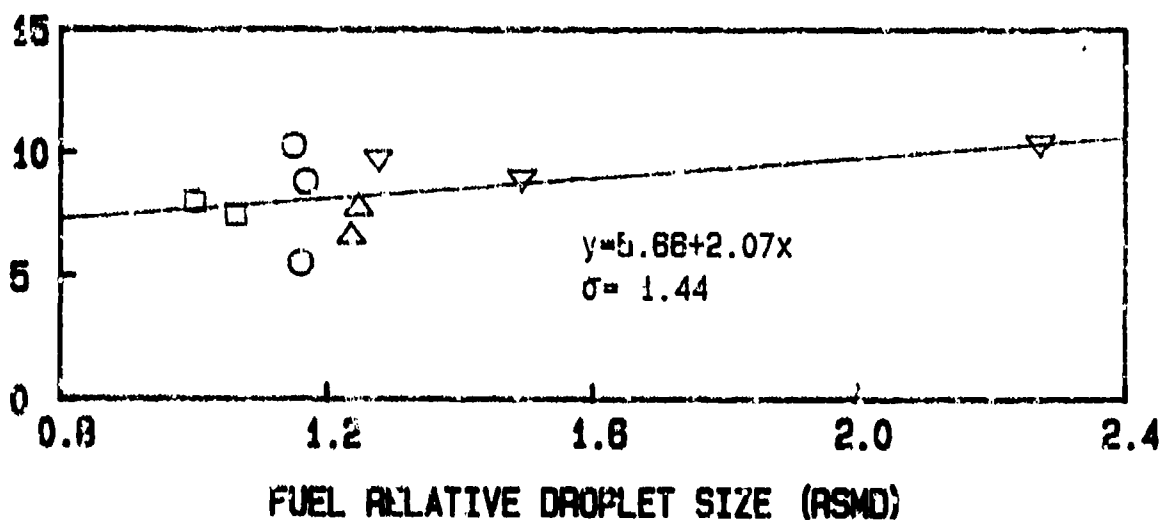
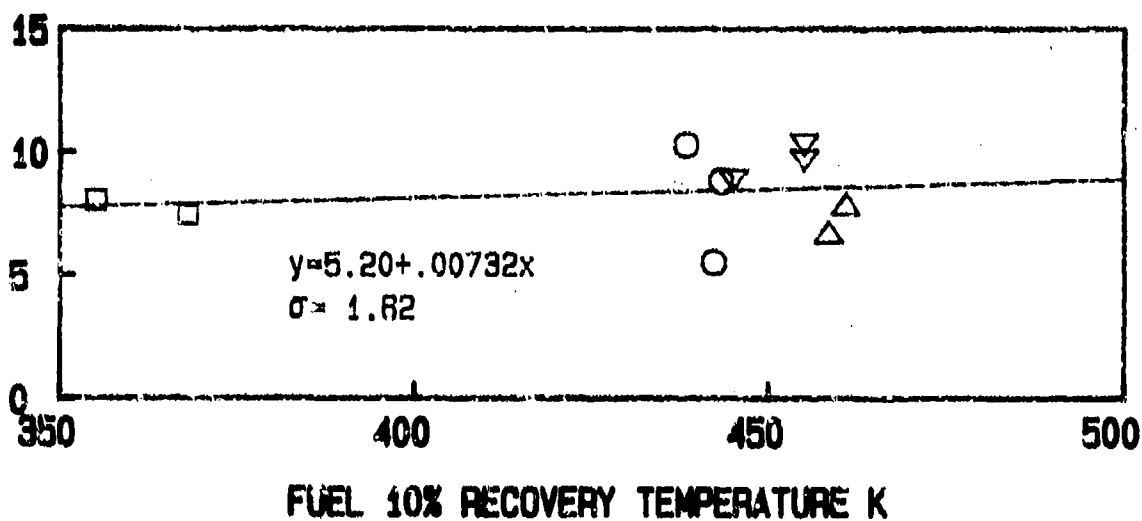
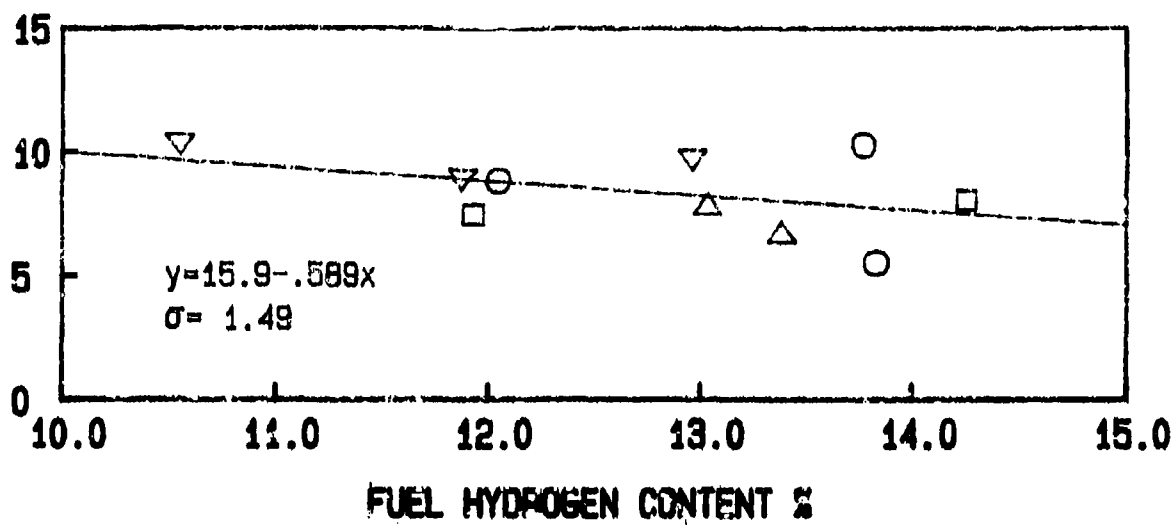


Figure 6.102: Effects of Fuel Properties on Corrected NOx Emissions
(PT6A-65 Gas Generator, BOM, Simplex 2.2 FN)

CORRECTED NOx EMISSION INDEX (g/kg)

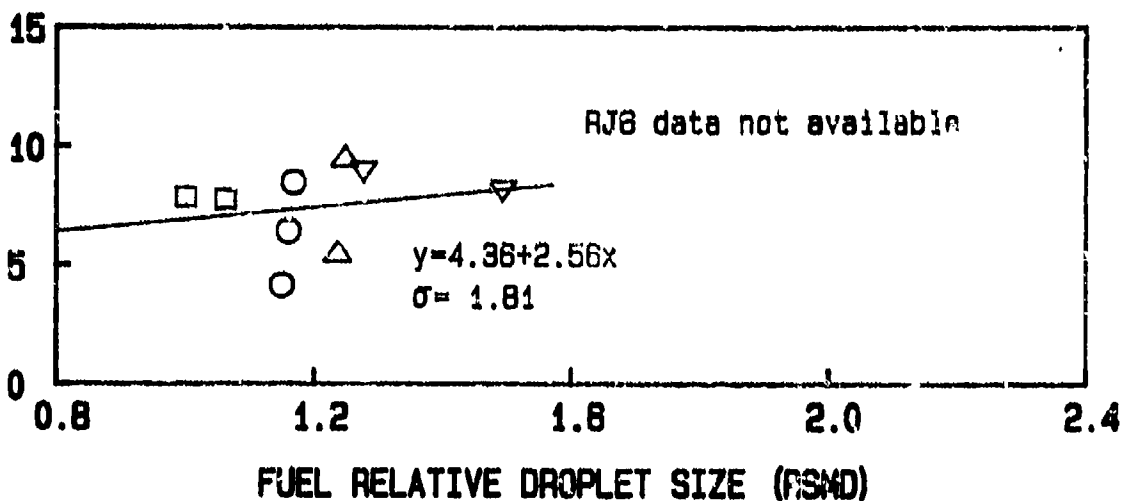
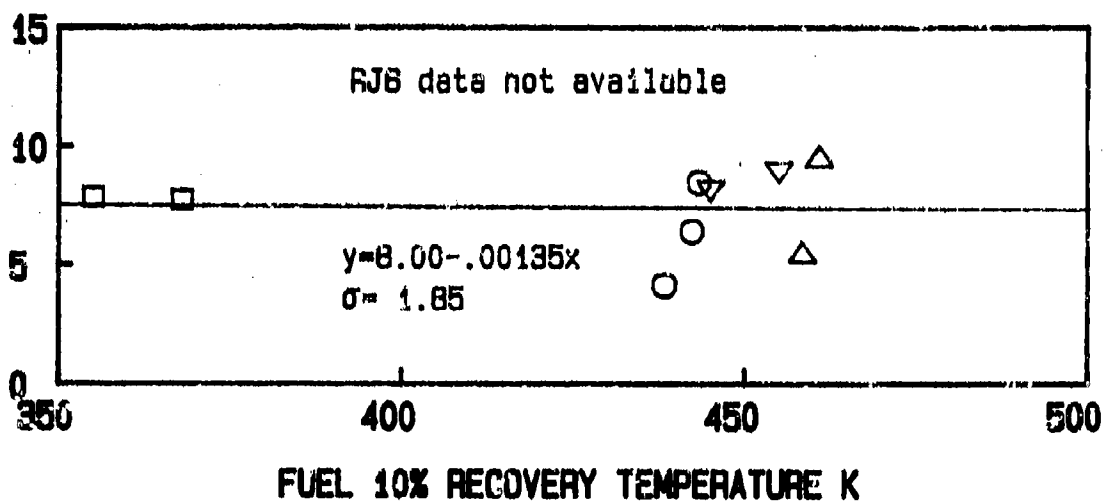
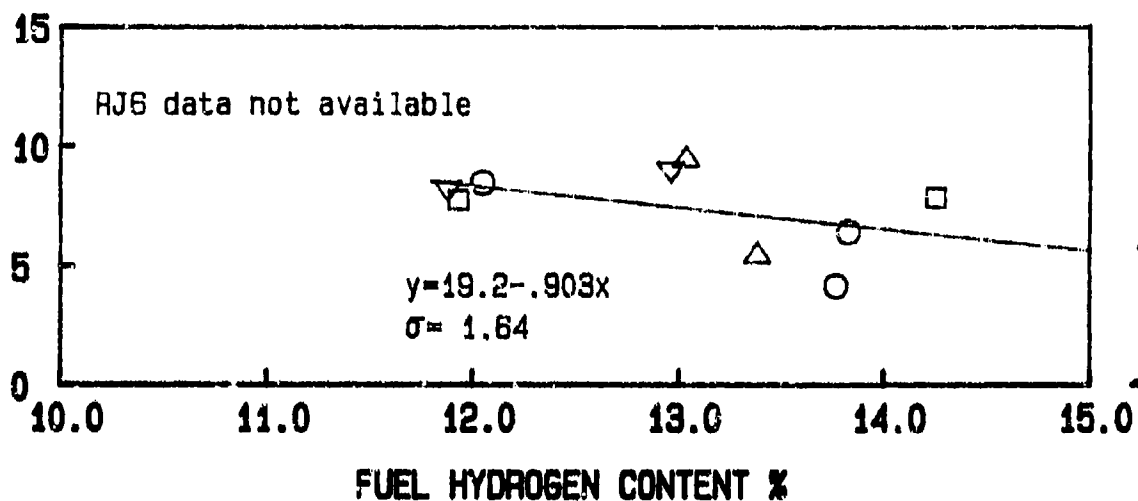


Figure 6.103: Effects of Fuel Properties on Corrected NOx Emissions
(PT6A-65 Gas Generator, 5% Bleed, Simplex 2.2 FN)

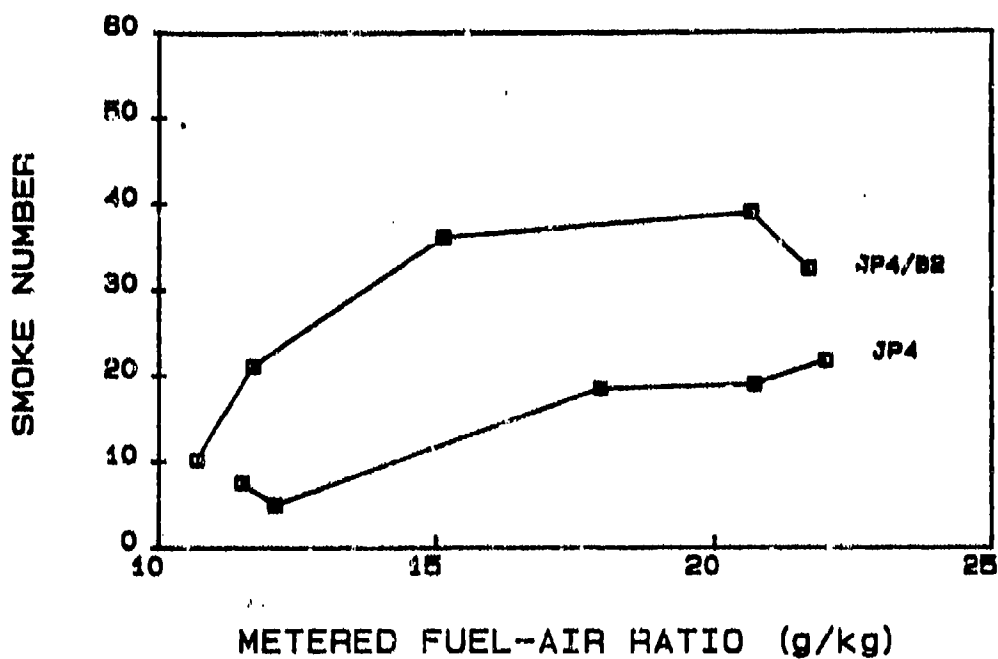
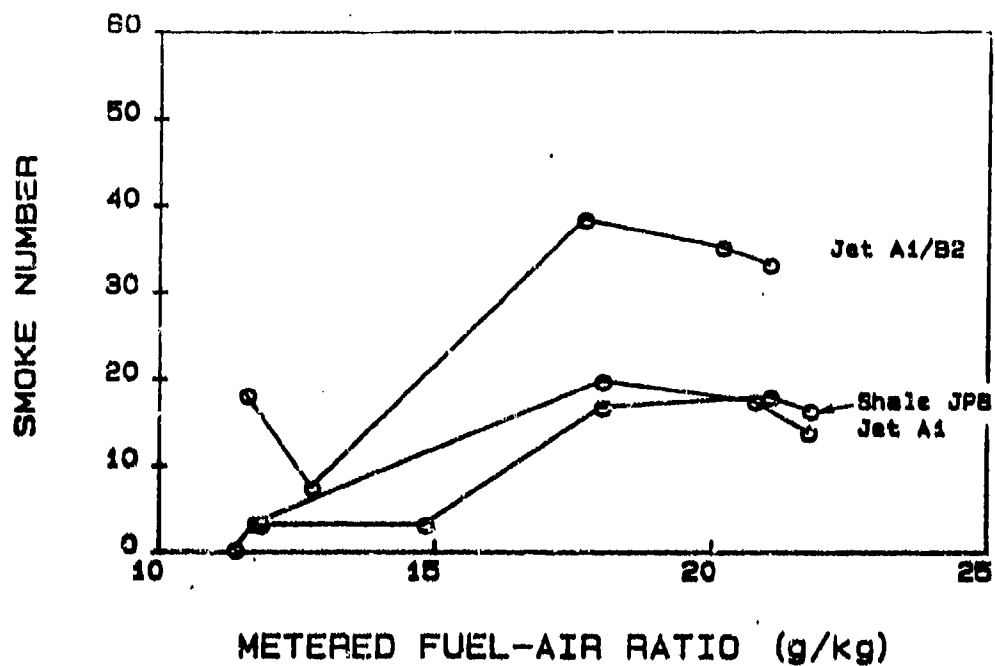


Figure 6.104: Smoke Emission Variations Over Operating Range
(PT6A-65 Gas Generator, BOM, Simplex 1.9 FN)

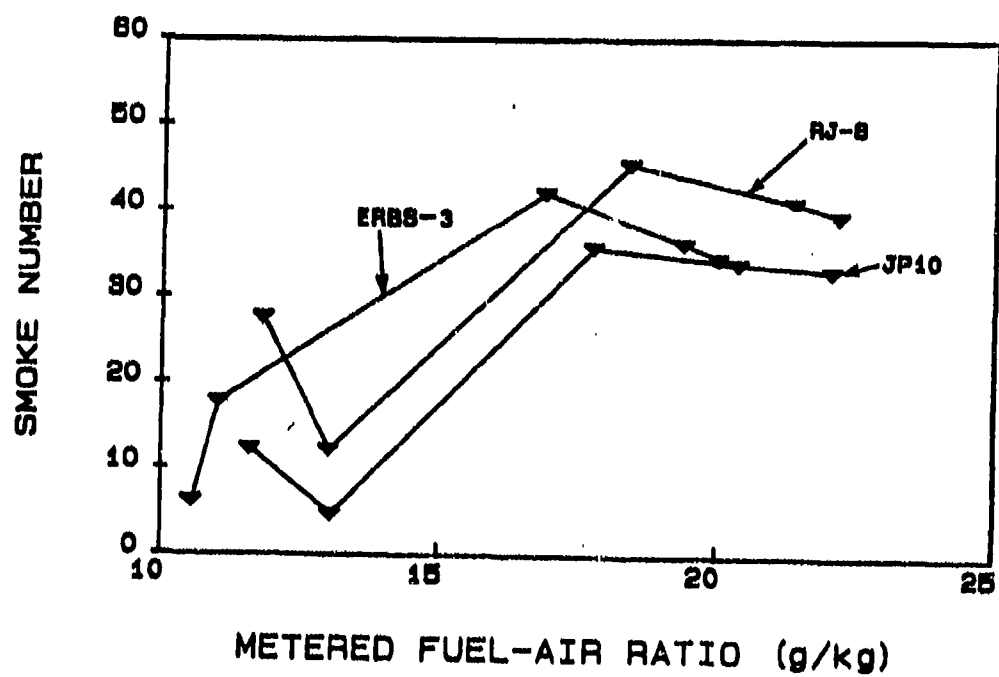
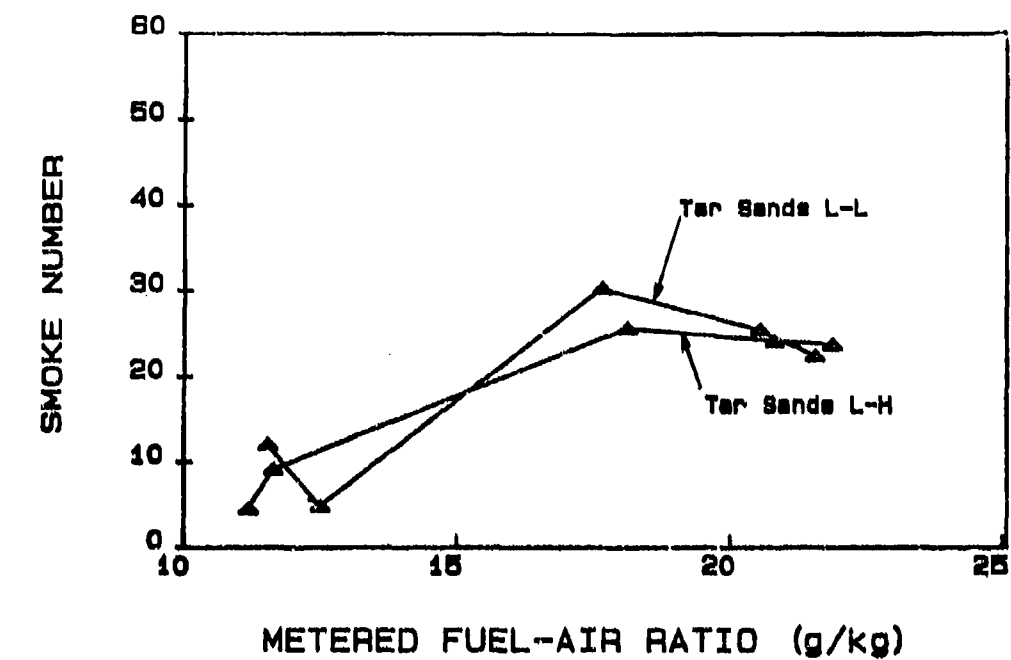


Figure 6.105: Smoke Emission Variations Over Operating Range
(PT6A-65 Gas Generator, BOM, Simplex 1.9 FN)

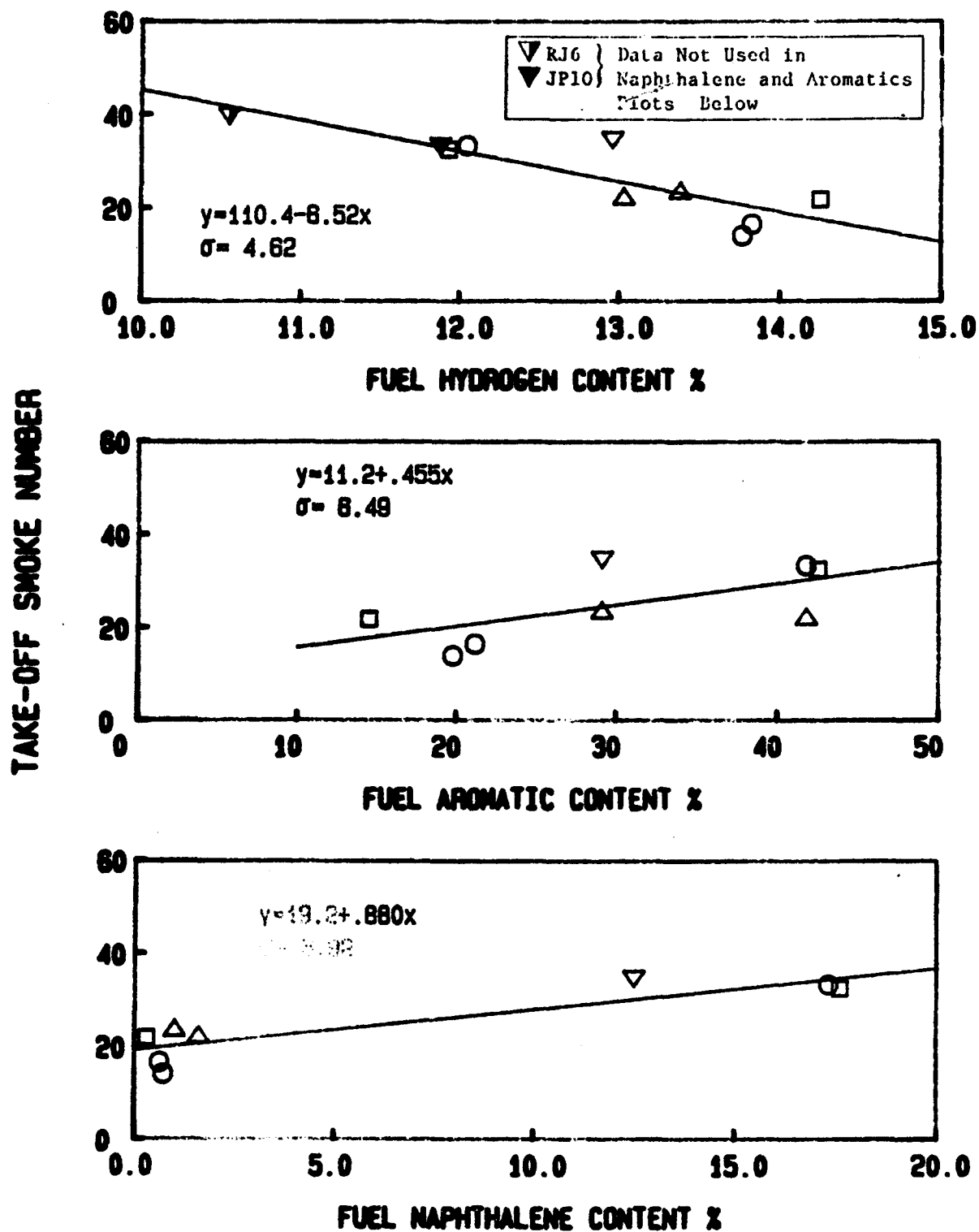


Figure 6.106: Effects of Fuel Properties on Take-Off Smoke Number
 (PT6A-65 Gas Generator, BOM, Simplex 1.9 FN)

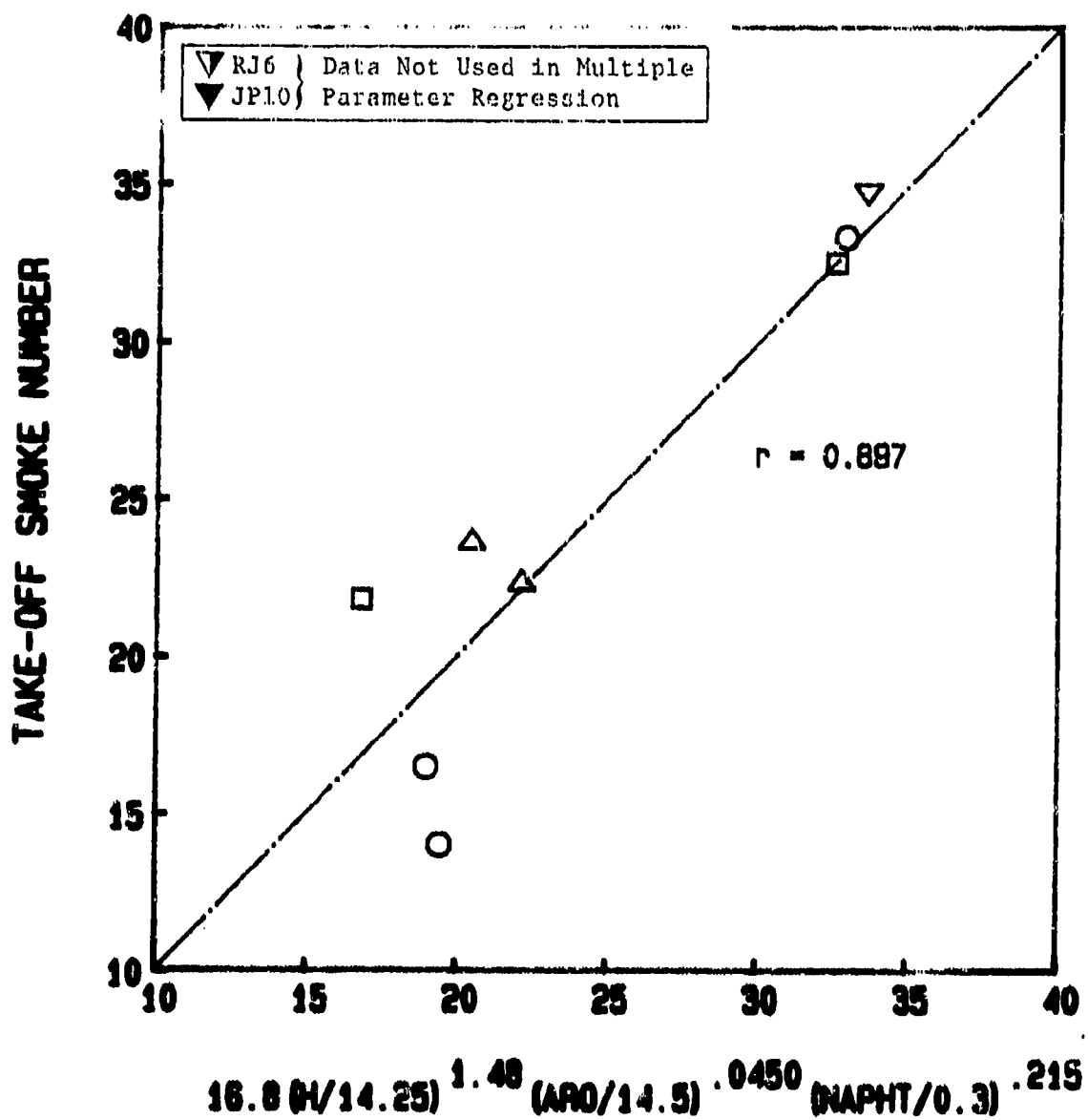


Figure 6.107: Take-Off Smoke Number vs Multiple Parameter Correlation (PT6A-65 Gas Generator, BOM, Simplex 1.9 FN)

TAKE-OFF SMOKE NUMBER

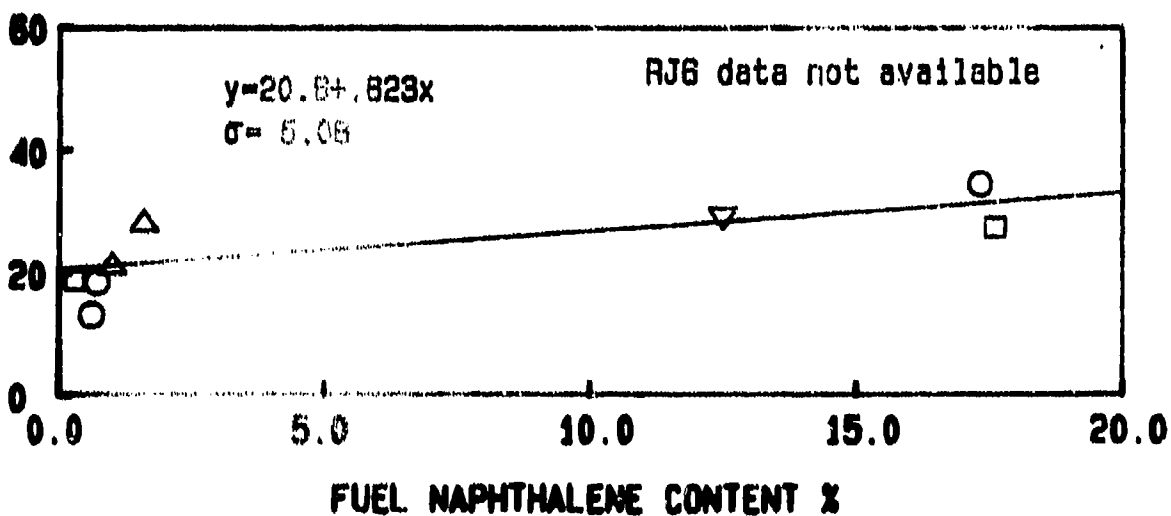
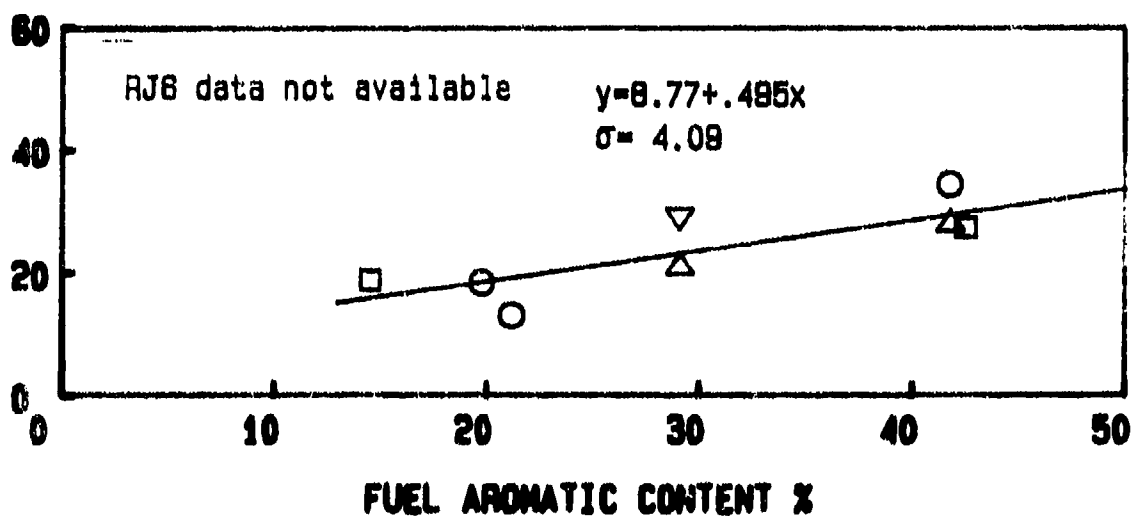
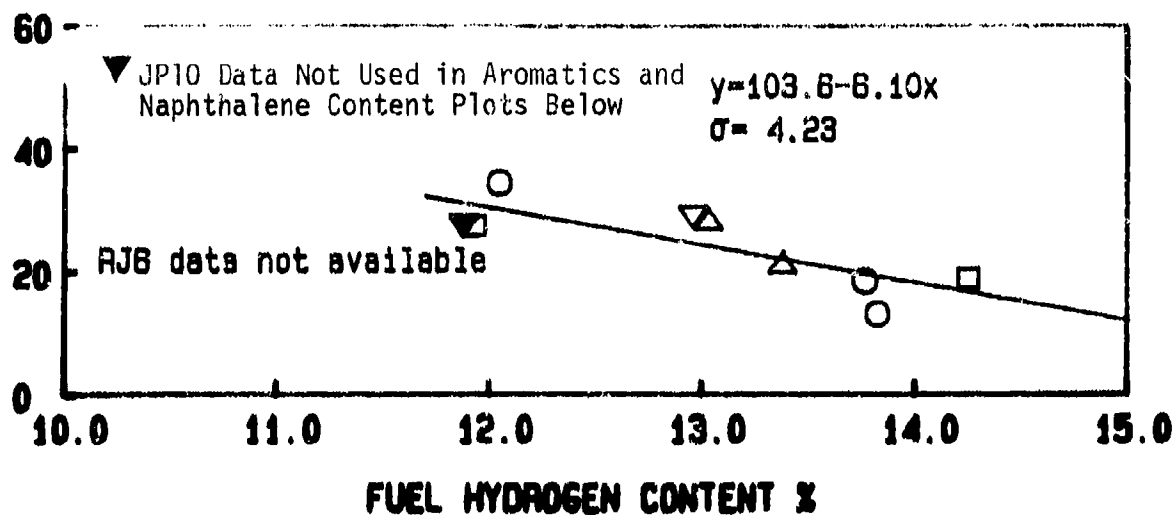


Figure 6.108: Effects of Fuel Properties on Take-Off Smoke Number (PT6A-65 Gas Generator, 5% Bleed, Simplex 1.9 FN)

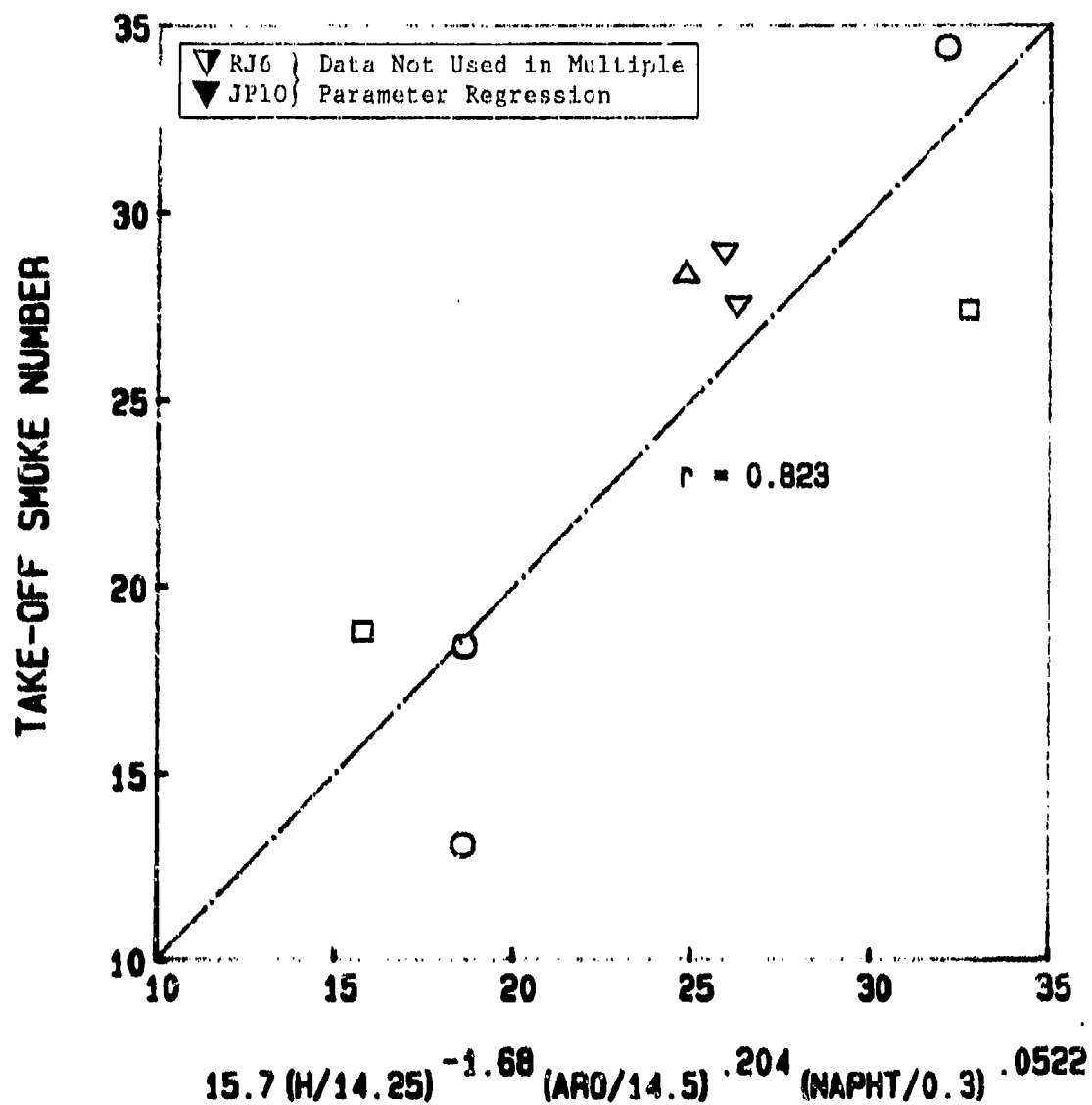


Figure 6.109: Take-Off Smoke Number vs Multiple Parameter Correlation
 (PT6A-65 Gas Generator, 5% Bleed, Simplex 1.9 FN)

TAKE-OFF SMOKE NUMBER

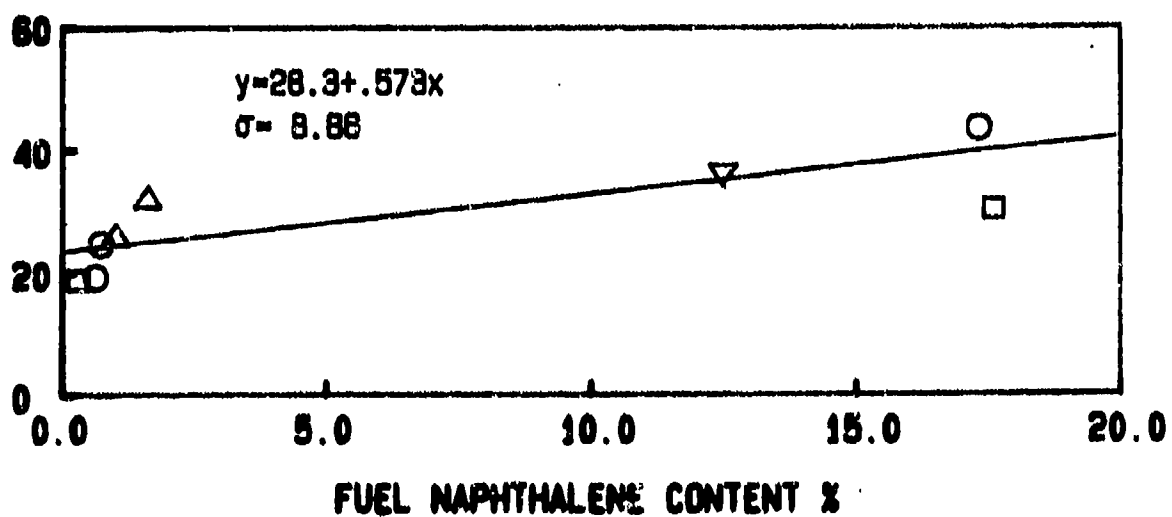
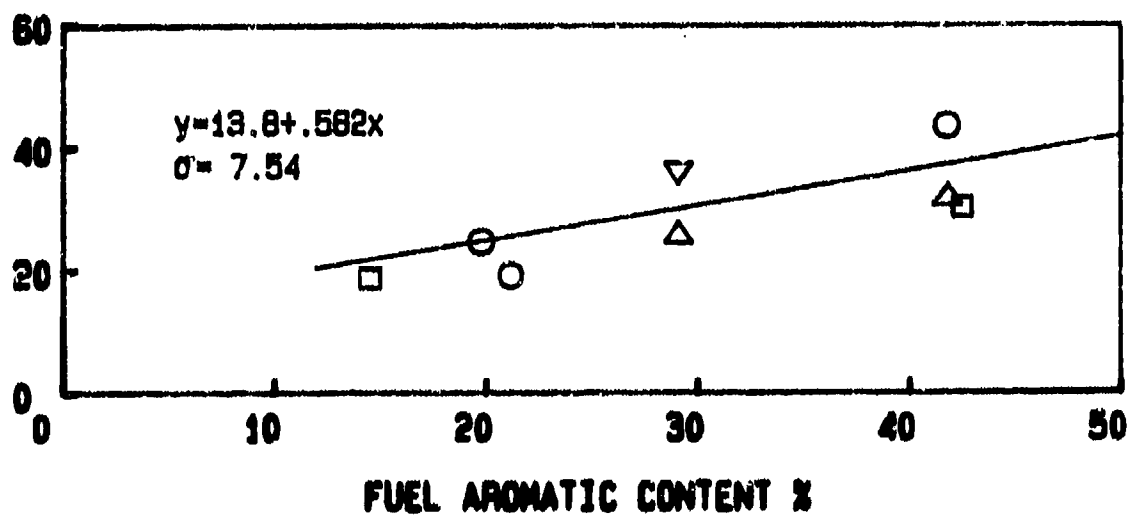
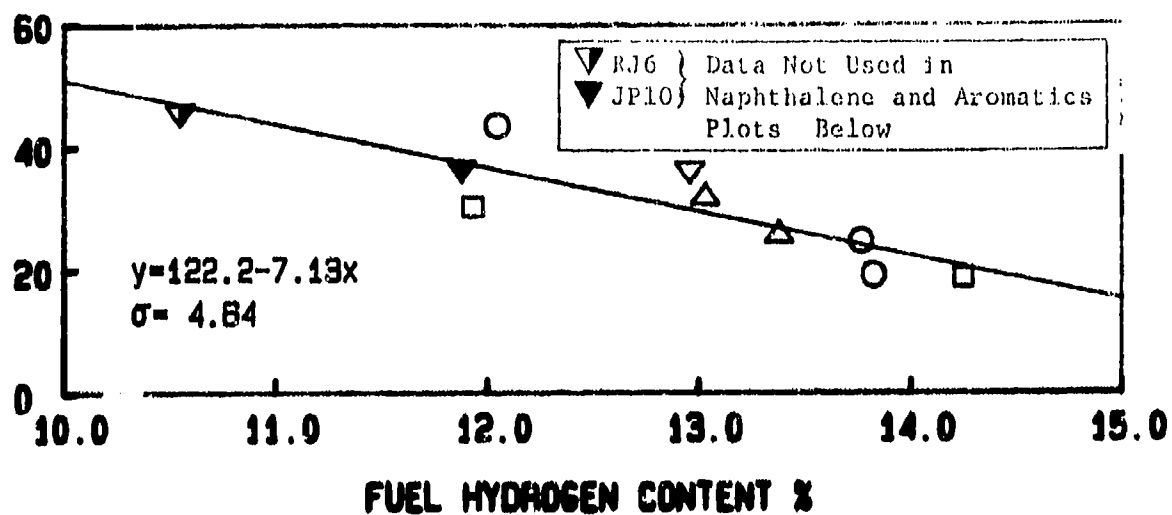


Figure 6.110: Effects of Fuel Properties on Take-Off Smoke Number (PT6A-65 Gas Generator, BOM, Simplex 2.2 FN)

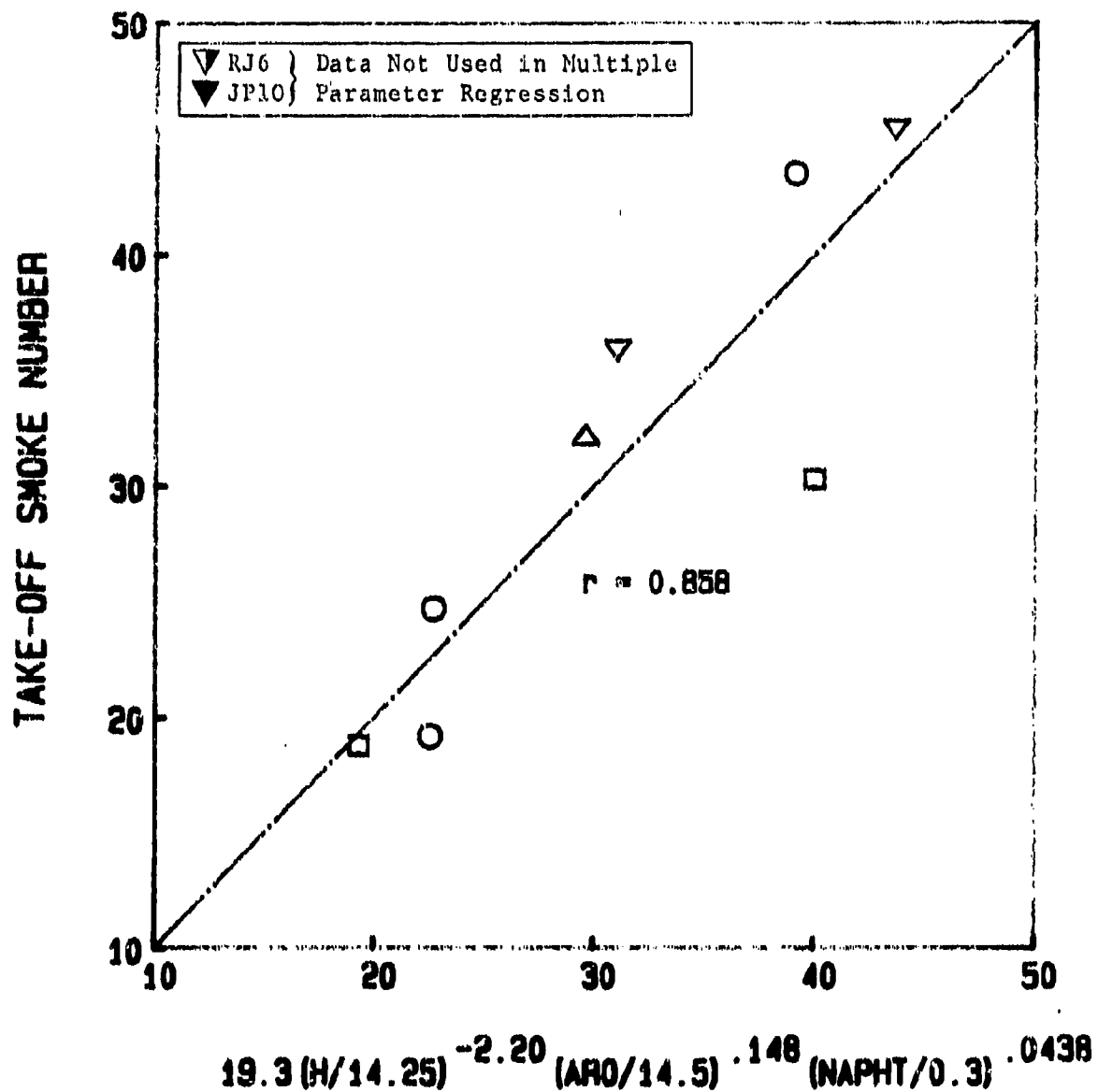


Figure 6.111: Take-Off Smoke Number vs Multiple Parameter Correlation
(PT6A-65 Gas Generator, BOM, Simplex 2.2 FN)

TAKE-OFF SMOKE NUMBER

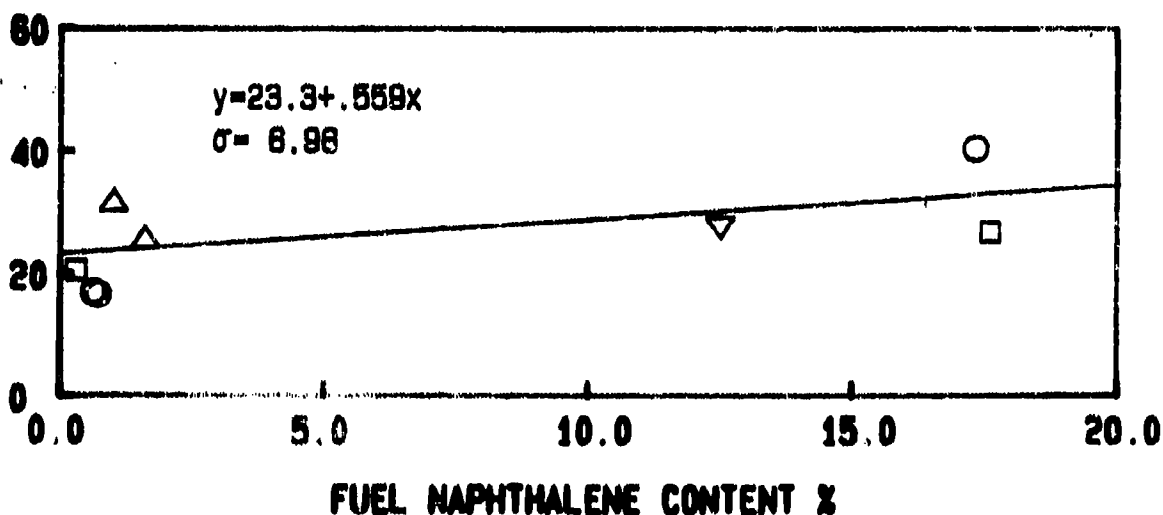
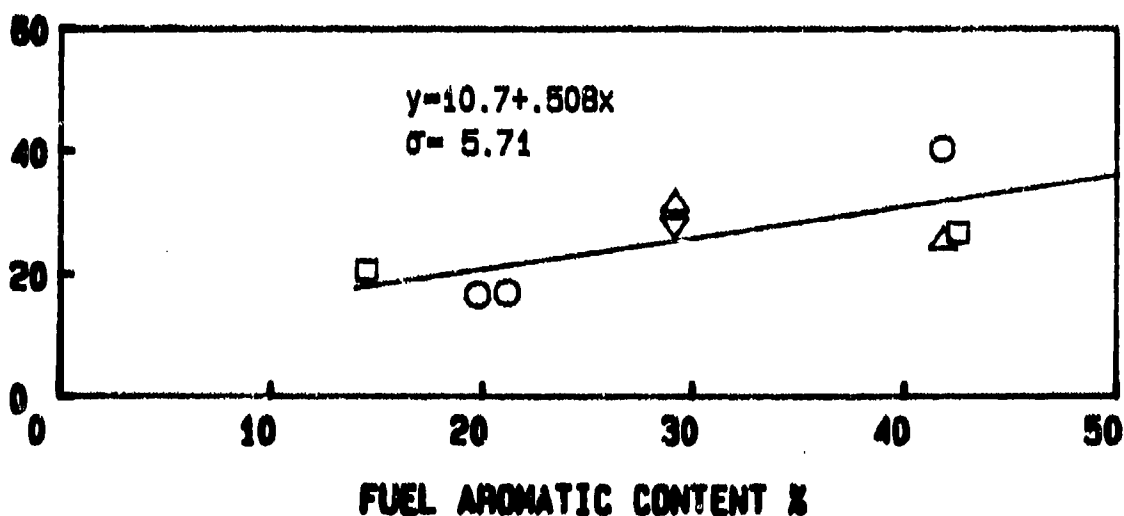
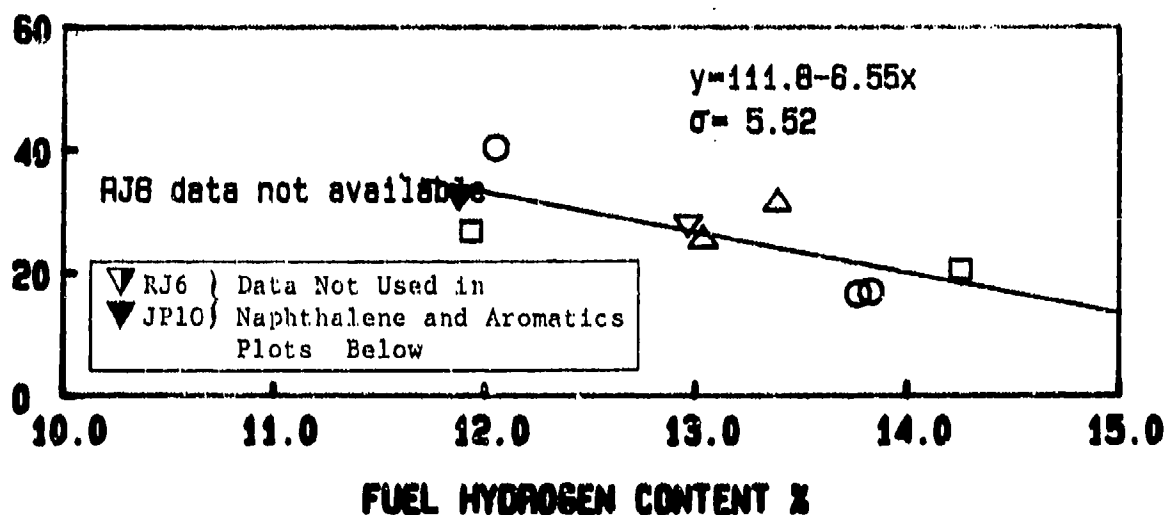


Figure 6.112: Effects of Fuel Properties on Take-Off Smoke Number (PT6A-65 Gas Generator, 5% Bleed, Simplex 2.2 FN)

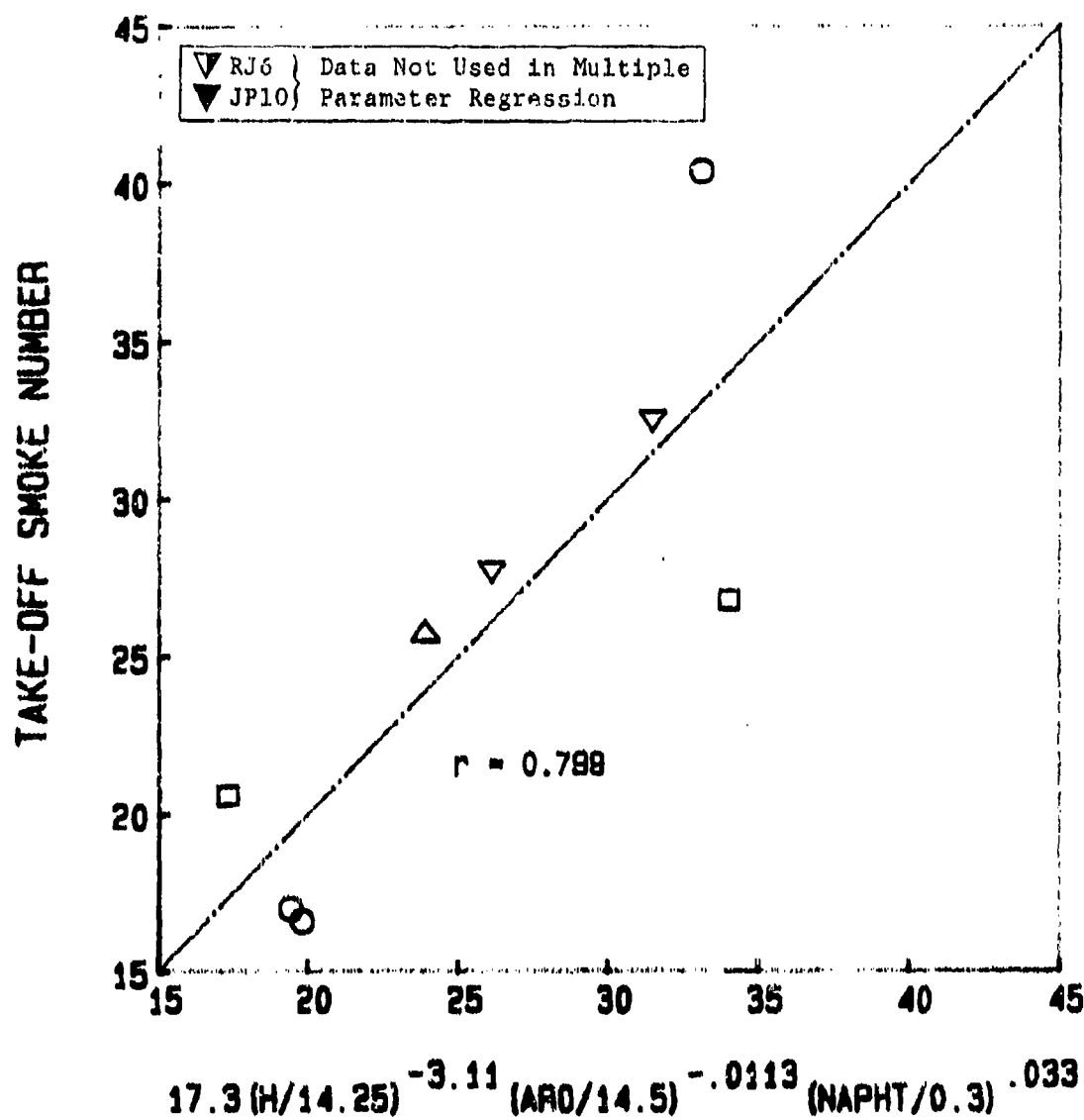


Figure 6.113: Take-Off Smoke Number vs Multiple Parameter Correlation
(PT6A-65 Gas Generator, 5% Bleed, Simplex 2.2 FN)

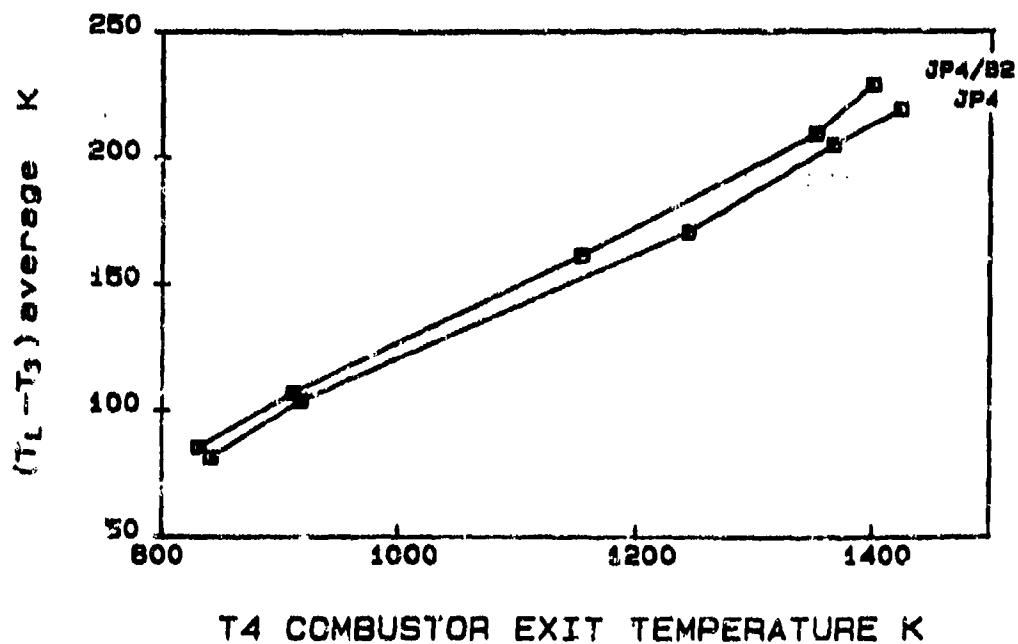
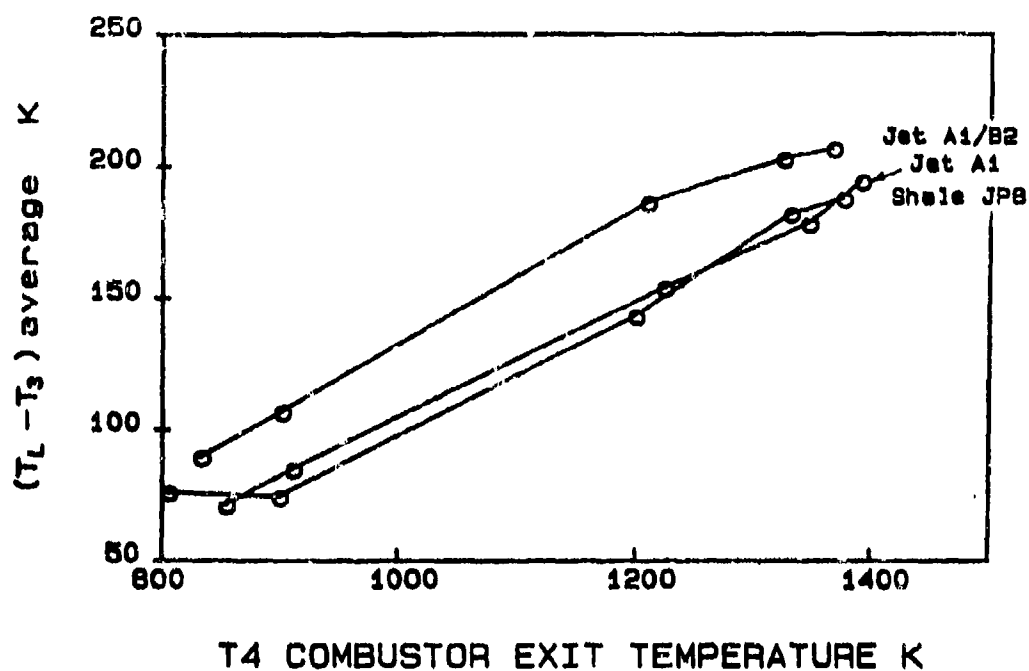


Figure 6.114: Linex Temperature Variations Over Operating Range
(PT6A-65 Gas Generator, BOM, Simplex 1.9 FN)

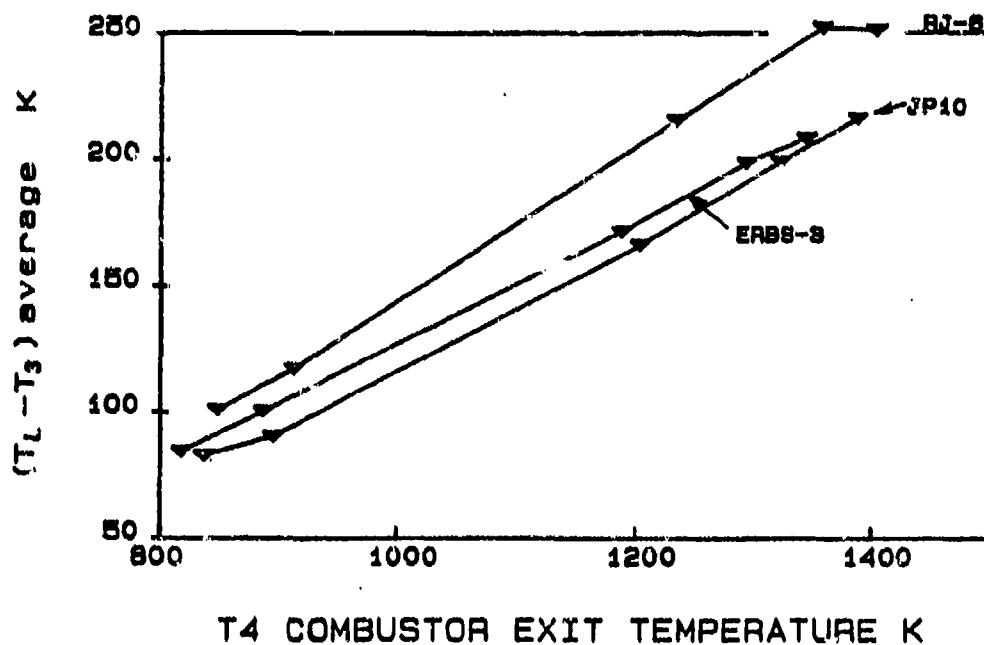
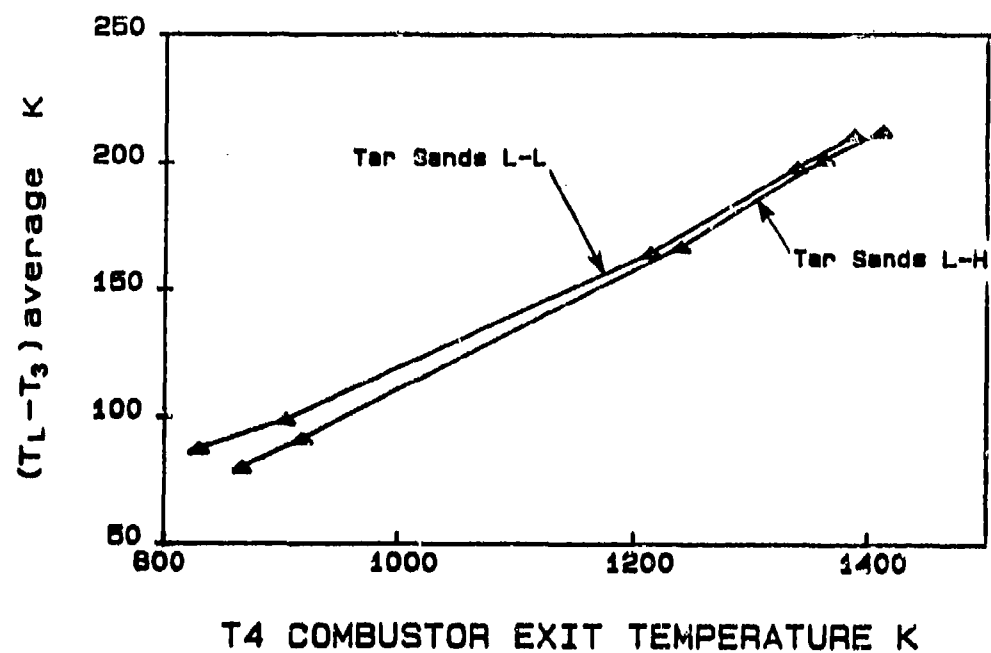


Figure 6.115: Liner Temperature Variations Over Operating Range
(PT6A-65 Gas Generator, BOM, Simplex 1.9 FN)

$(T_L - T_3)$ average K. $T_4 = 1326K$

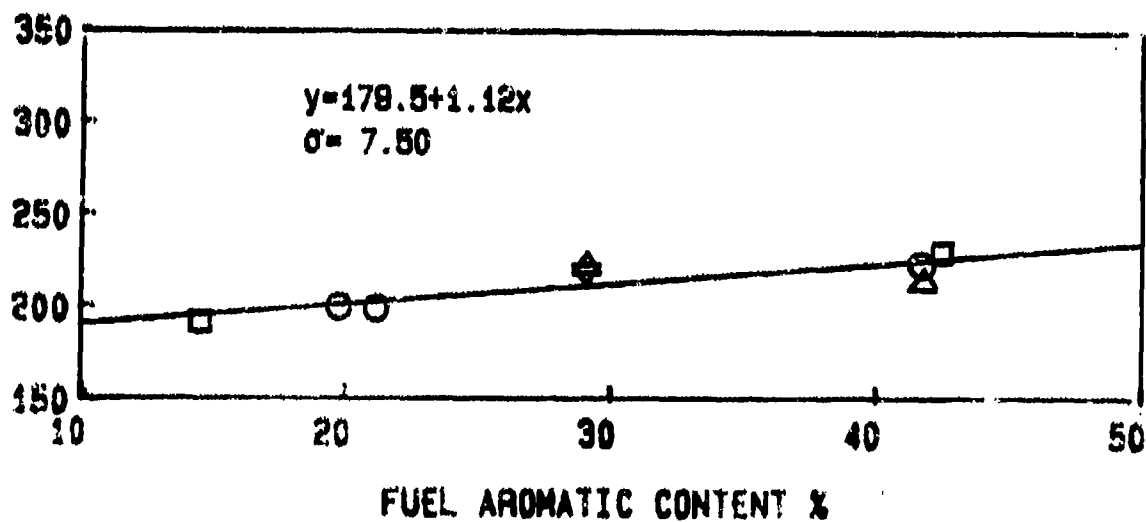
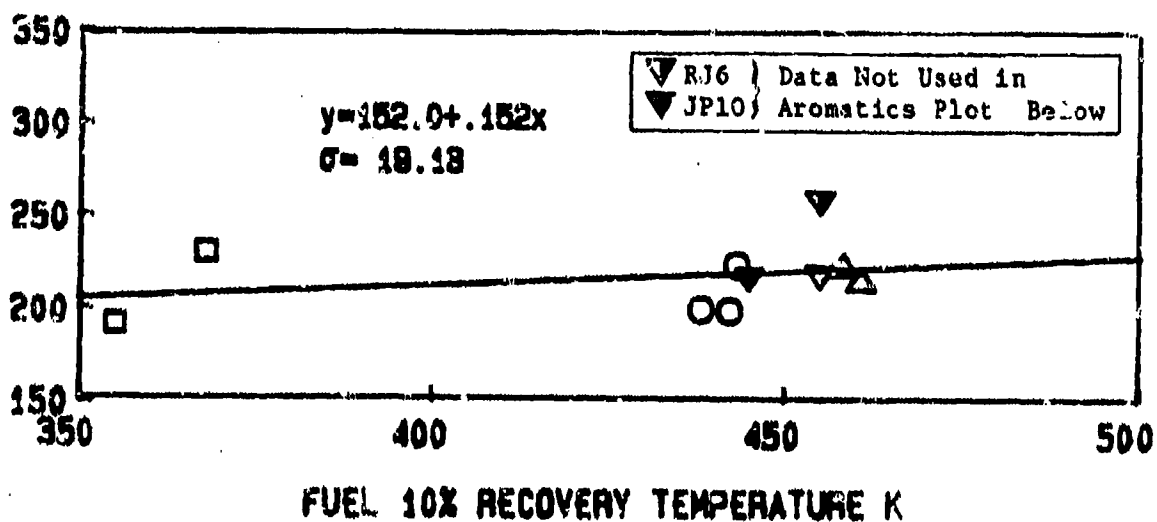
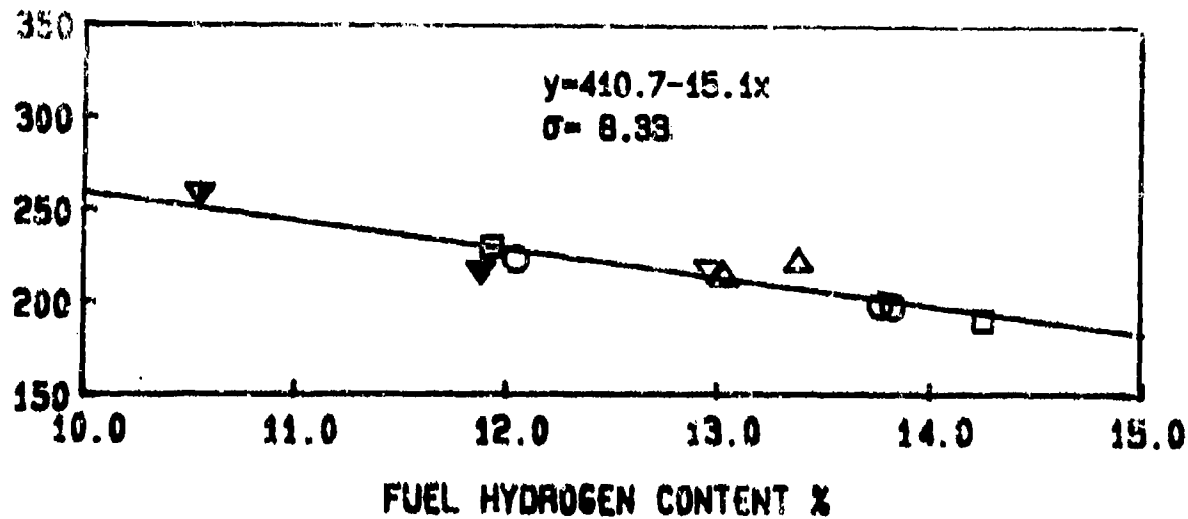


Figure 6.116: Effects of Fuel Properties on Average liner Temperatures
 (PT6A-65 Gas Generator, BOM, Simplex 1.9 FN)

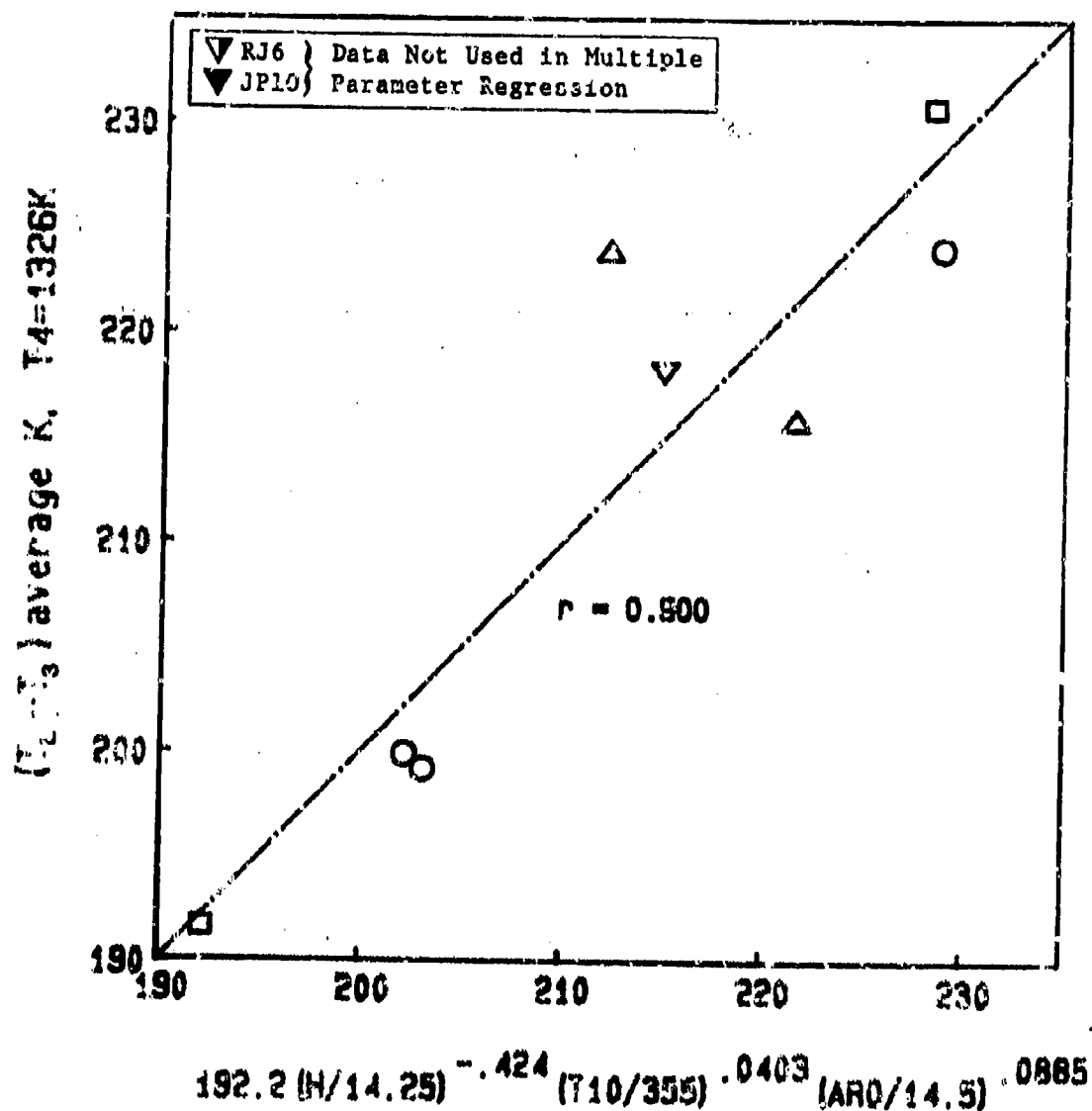


Figure 6.117: Average Liner Temperature vs Multiple Parameter Correlation
(PT6A-65 Gas Generator, BOM, Simplex 1.9 FN)

LINER TEMPERATURE PARAMETER (average)

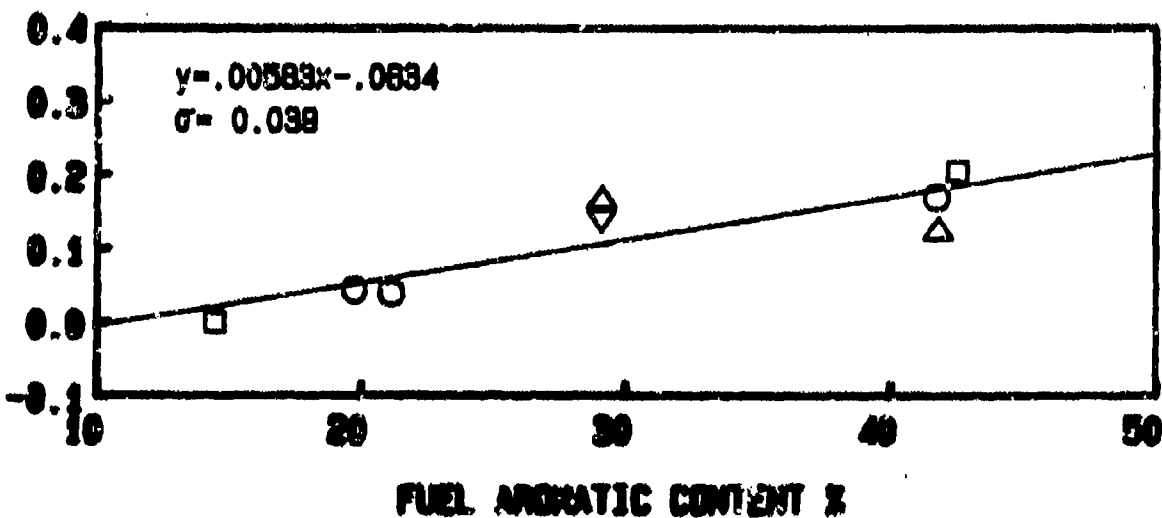
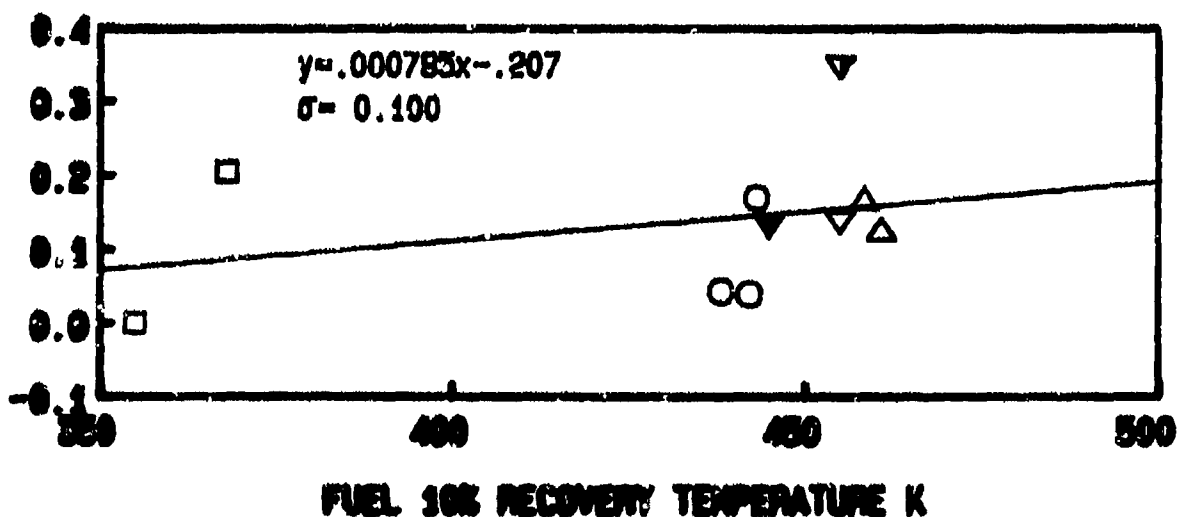
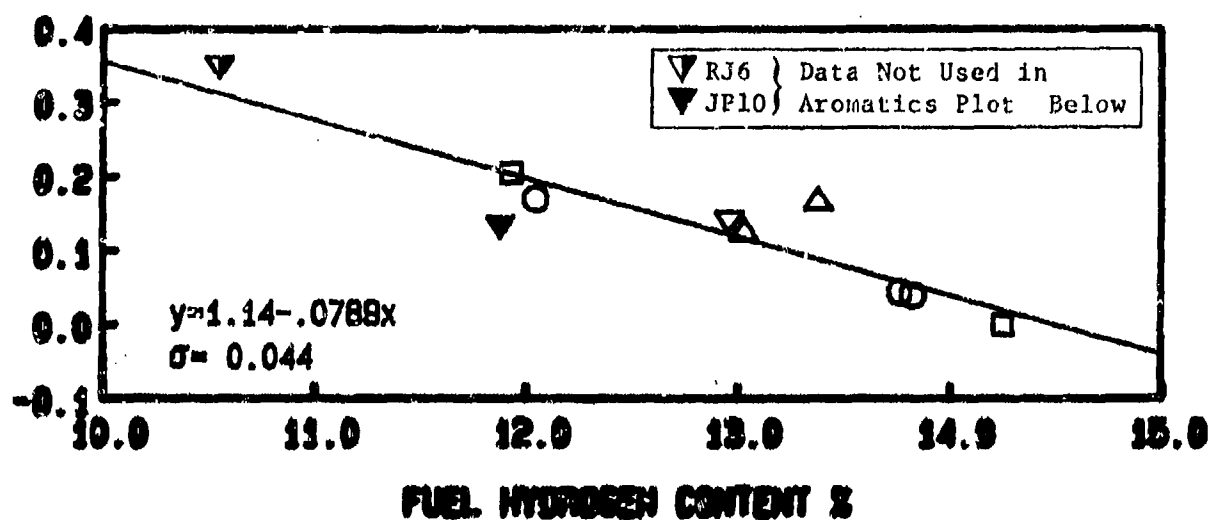


Figure 6.118: Effects of Fuel Properties on Liner Temperature Parameter (PT6A-65 Gas Generator, BOM, Simplex 1.9 FN)

$(T_1 - T_3)$ peak K. $T_4 = 1326K$

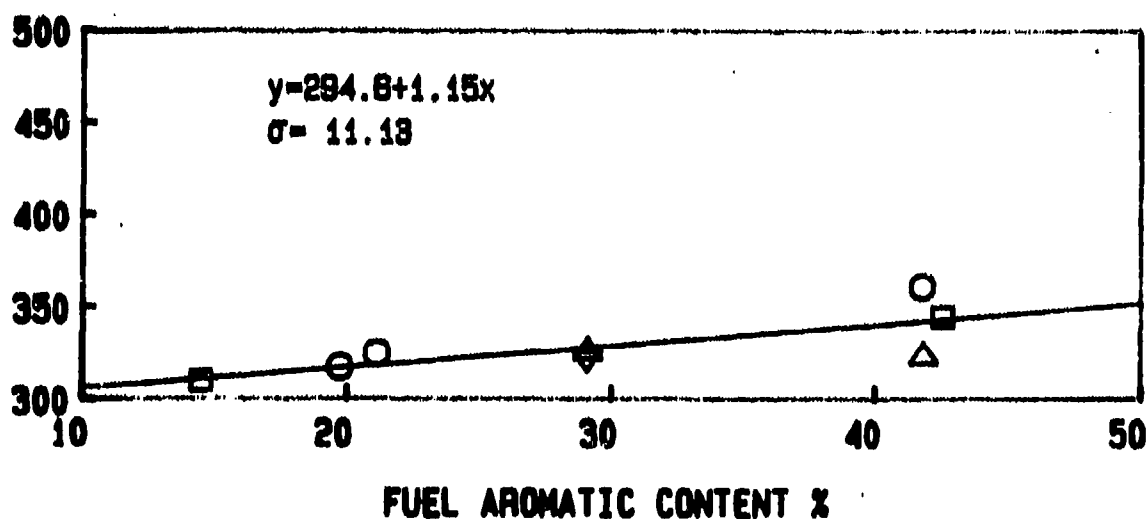
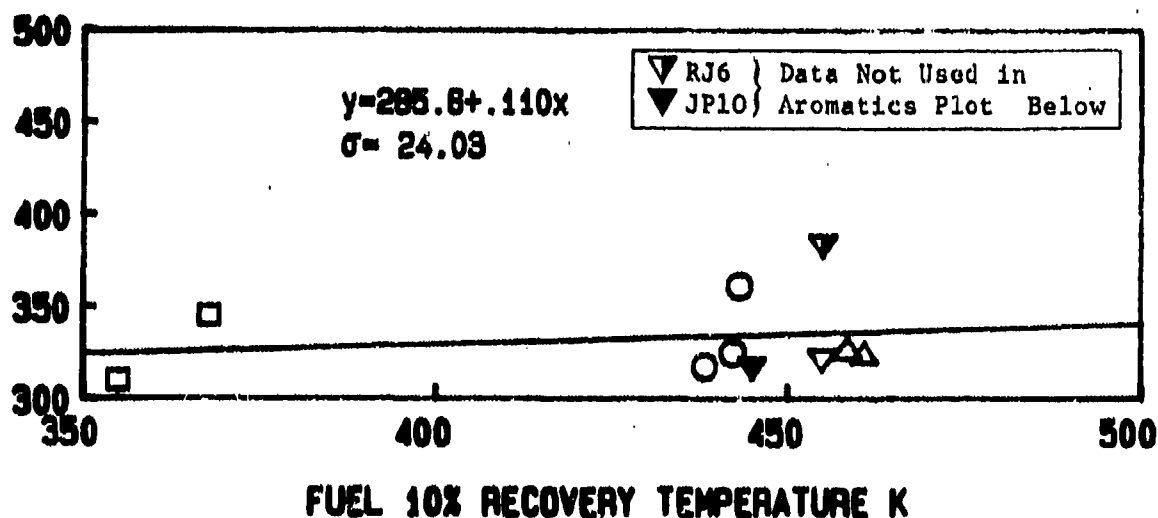
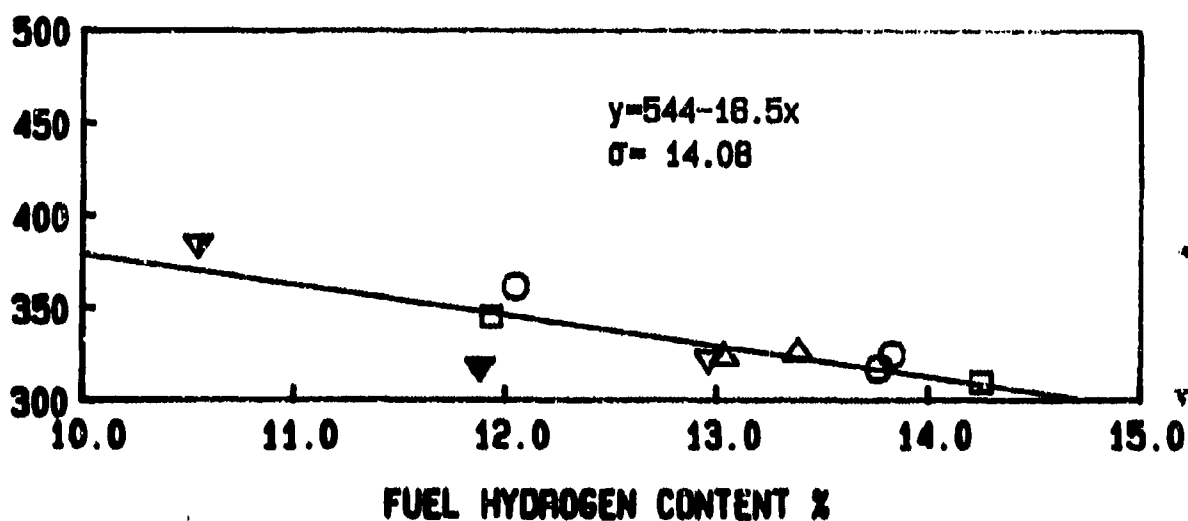


Figure 6.119: Effects of Fuel Properties on Peak Linear Temperatures (PT6A-65 Gas Generator, BOM, Simplex 1.9 FN)

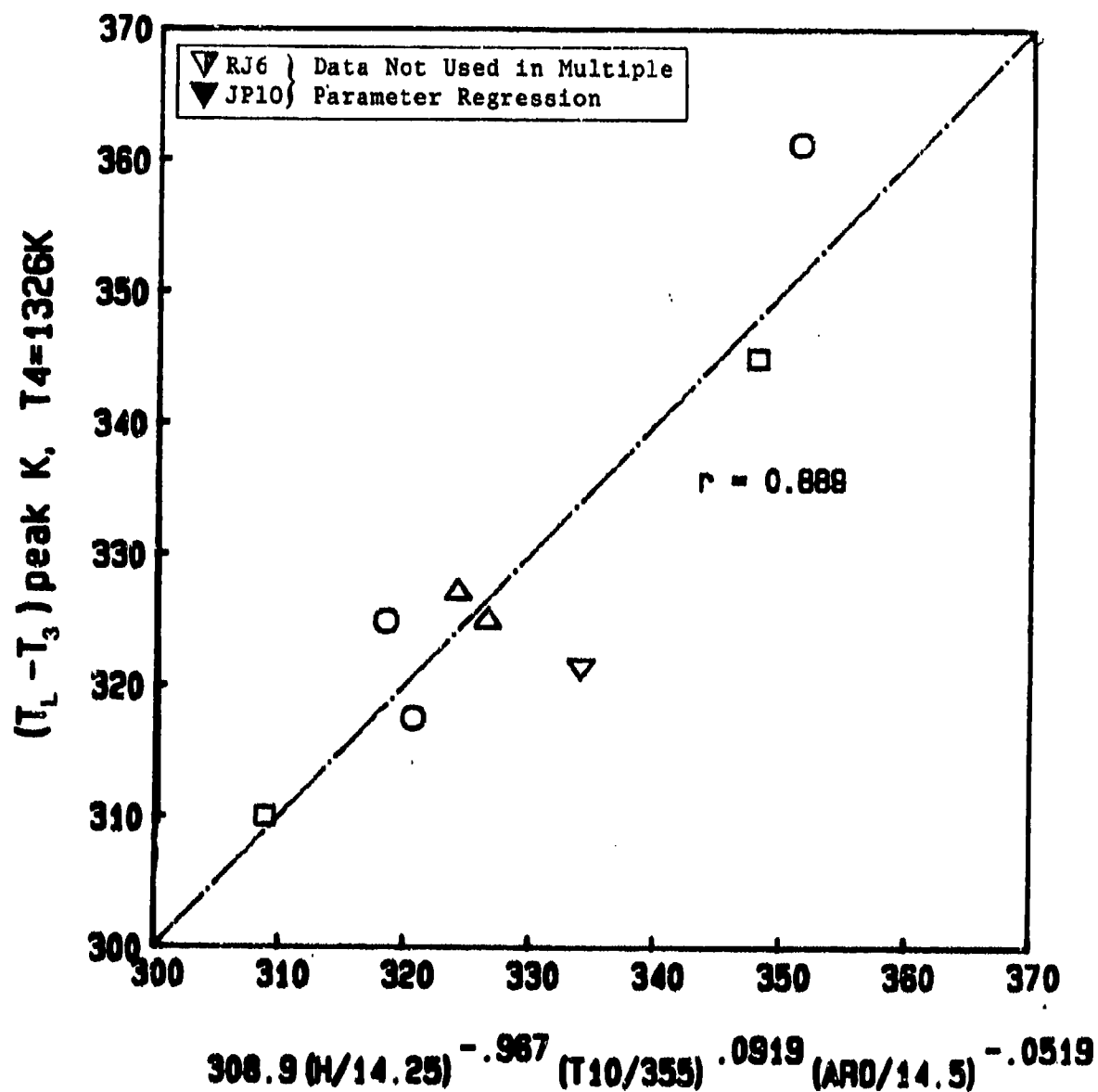


Figure 6.120: Peak Linear Temperature vs Multiple Parameter Correlation (PT6A-65 Gas Generator, BOM, Simplex 1.9 FN)

$(T_L - T_3)$ average K, $T_4 = 1326K$

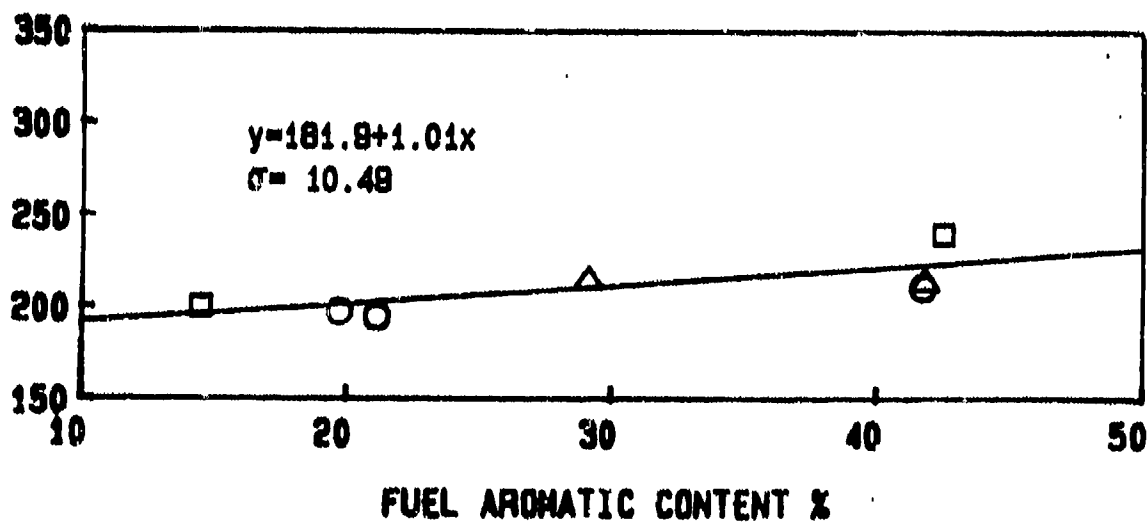
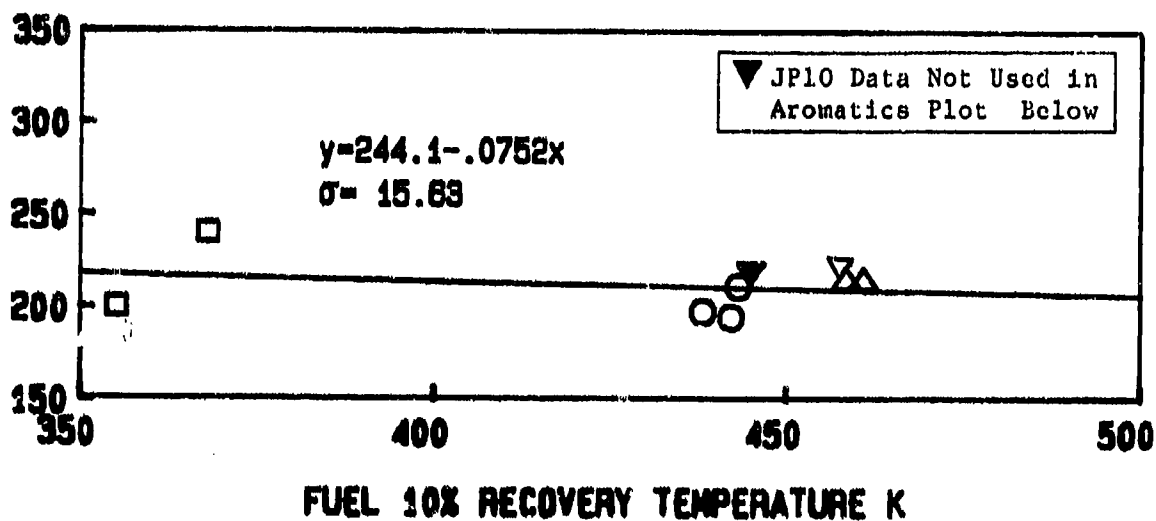
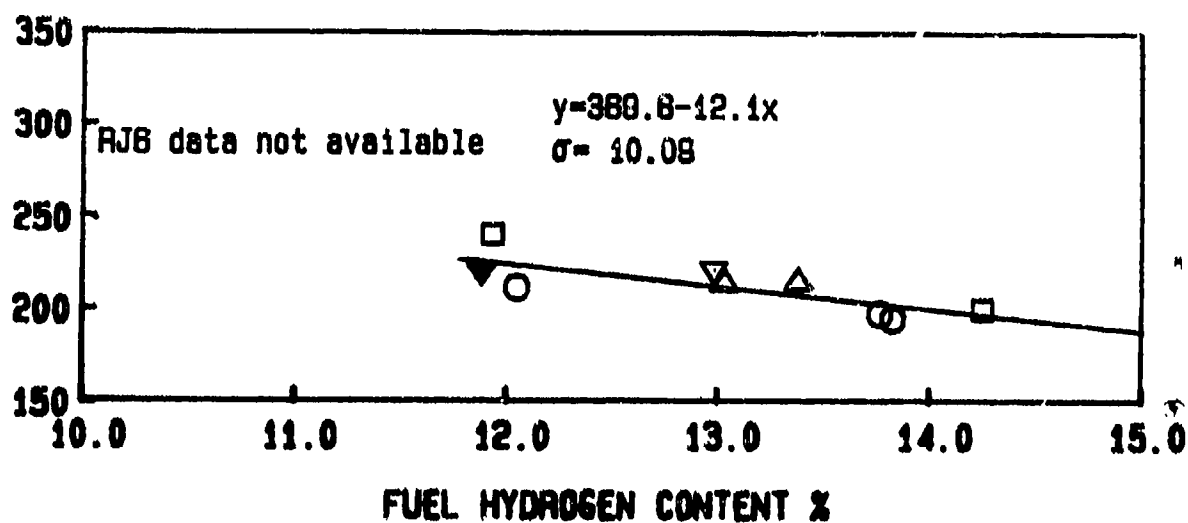


Figure 6.121: Effects of Fuel Properties on Average Liner Temperatures (PT6A-65 Gas Generator, 5% Bleed, Simplex 1.9 FN)

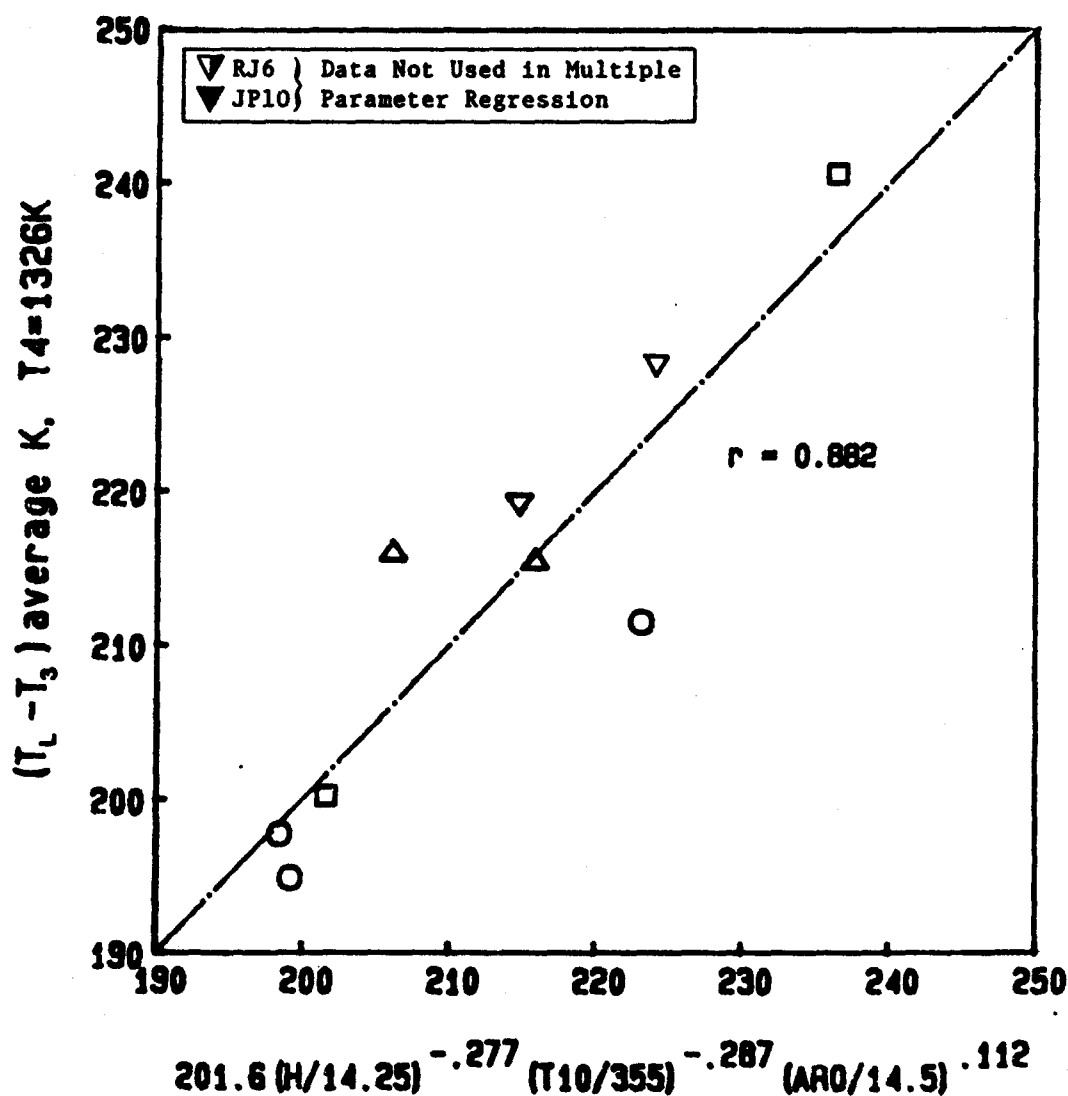


Figure 6.122: Average Liner Temperatures vs Multiple Parameter Correlation
(PT6A-65 Gas Generator, 5% Bleed, Simplex 1.9 FN)

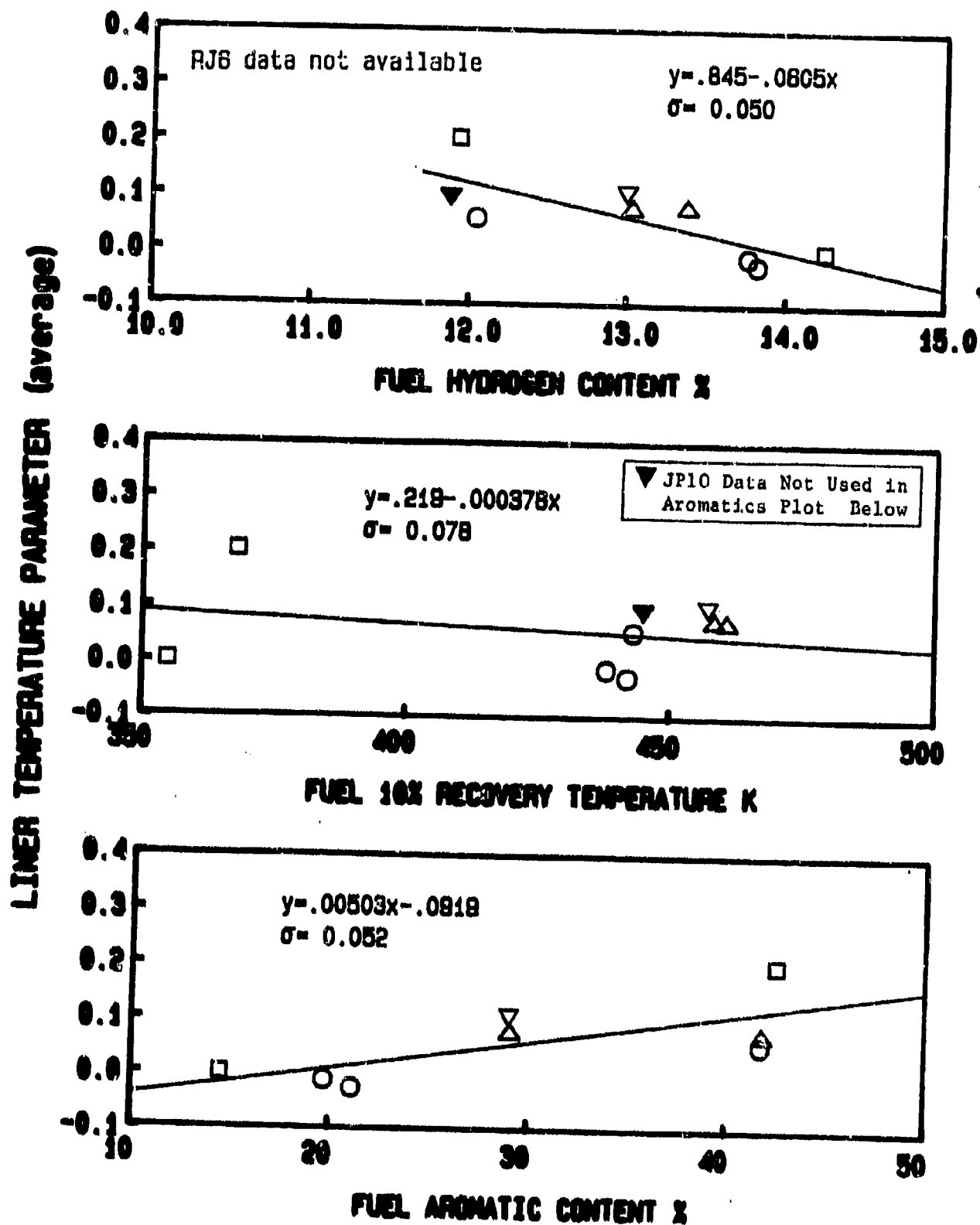


Figure 6.123: Effects of Fuel Properties on Liner Temperature Parameter (PT6A-65 Gas Generator, 5% Bleed, Simplex 1.9 FN)

$(T_L - T_3)$ peak K, $T_4 = 1326K$

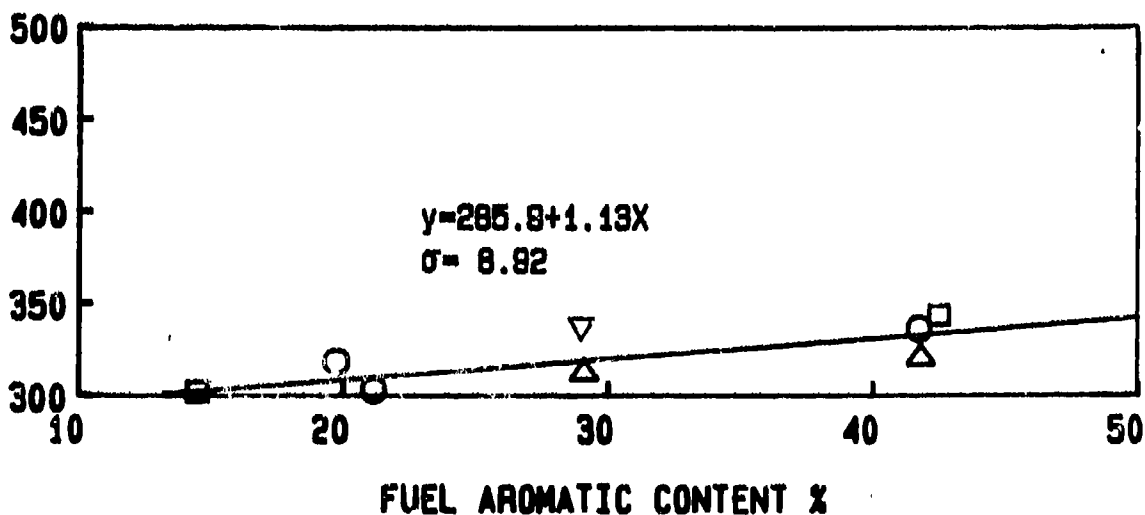
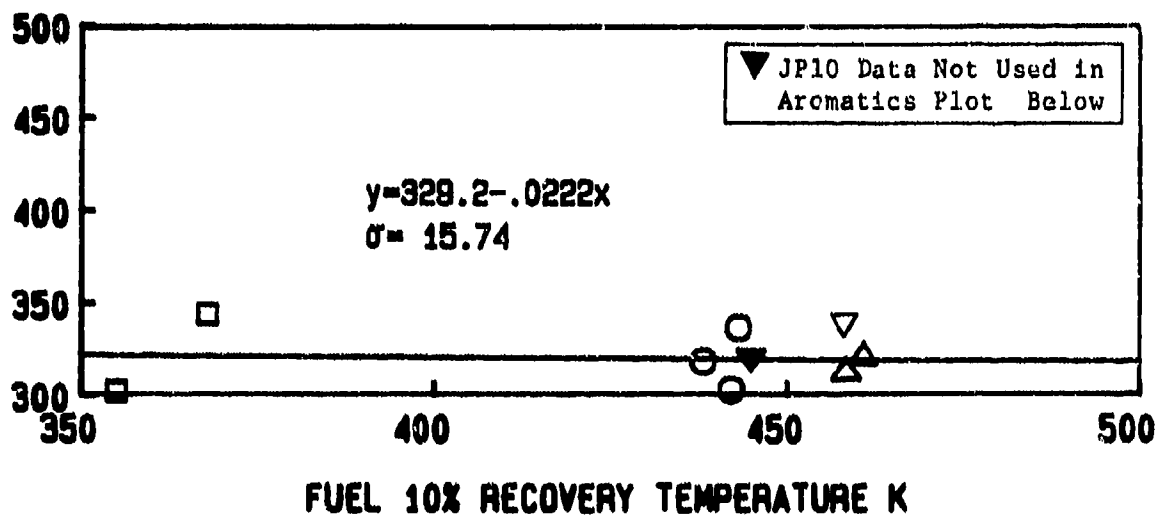
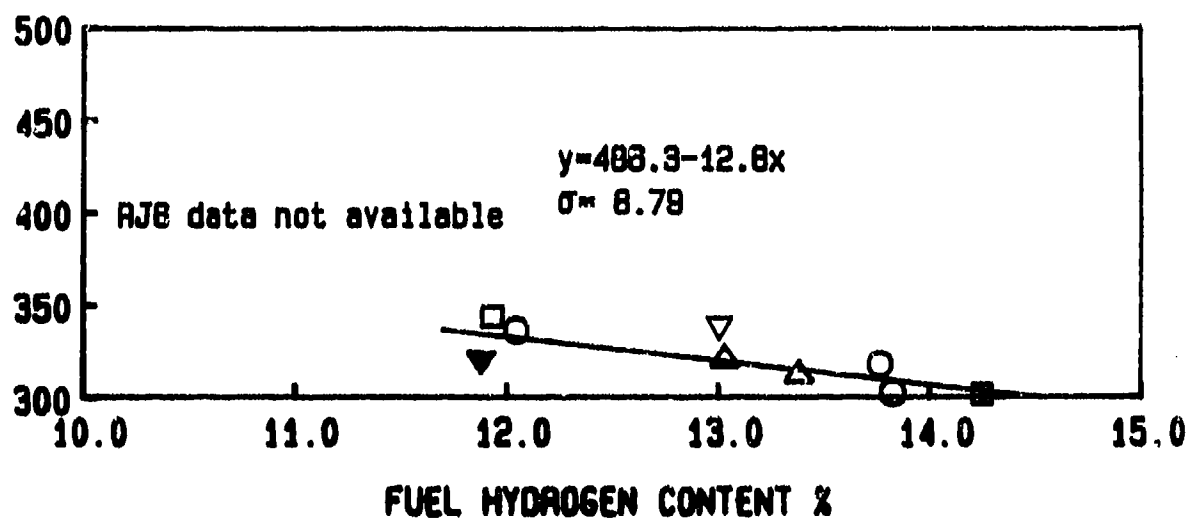


Figure 6.124: Effects of Fuel Properties on Peak Liner Temperatures (PT6A-65 Gas Generator, 5% Bleed, Simplex 1.9 FN)

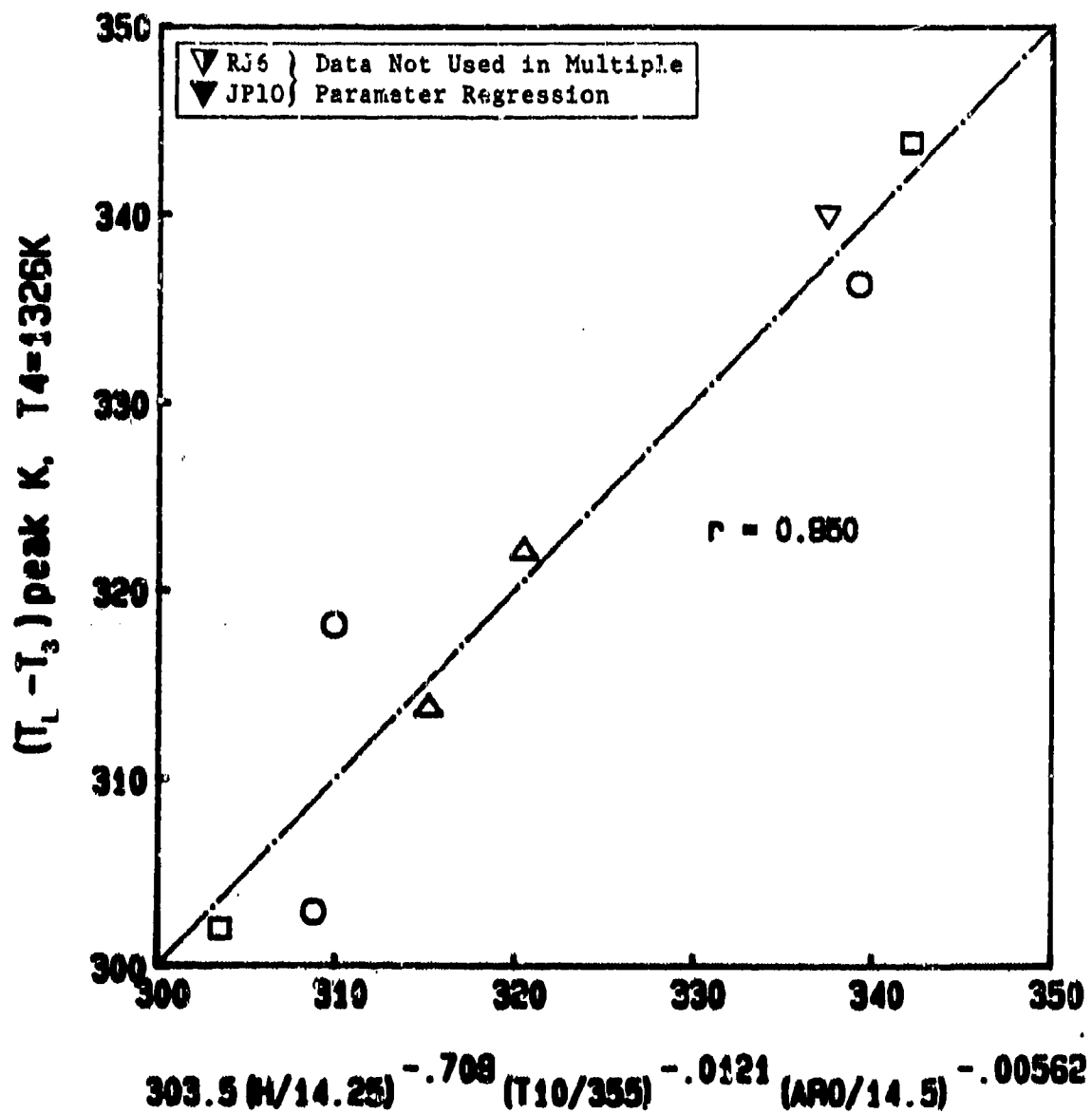


Figure 6.125: Peak Liner Temperatures vs Multiple Parameter Correlation
(PT6A-65 Gas Generator, 5% Bleed, Simplex 1.9 FN)

$(T_L - T_3)$ average K, $T_4 = 1326K$

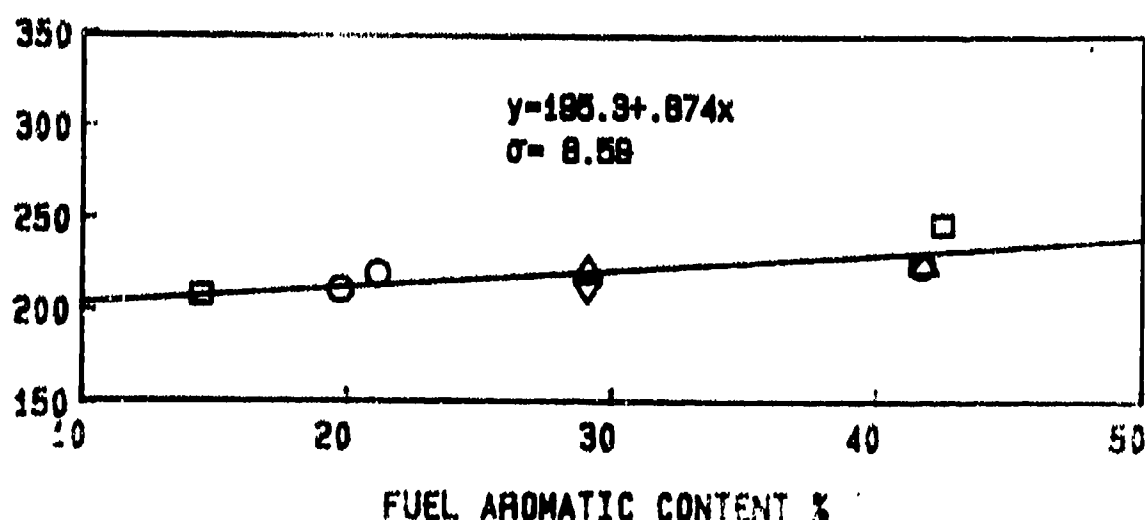
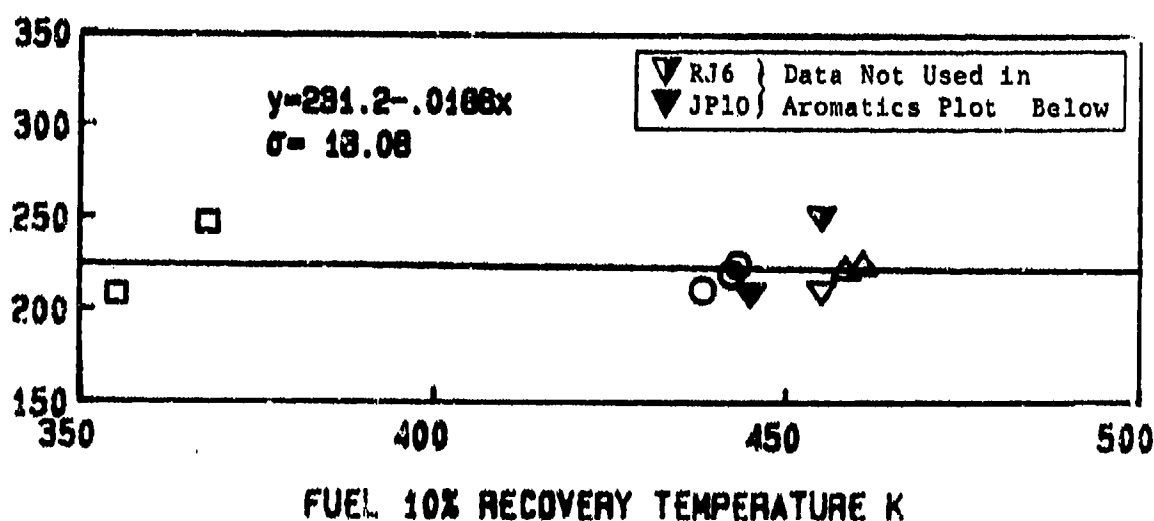
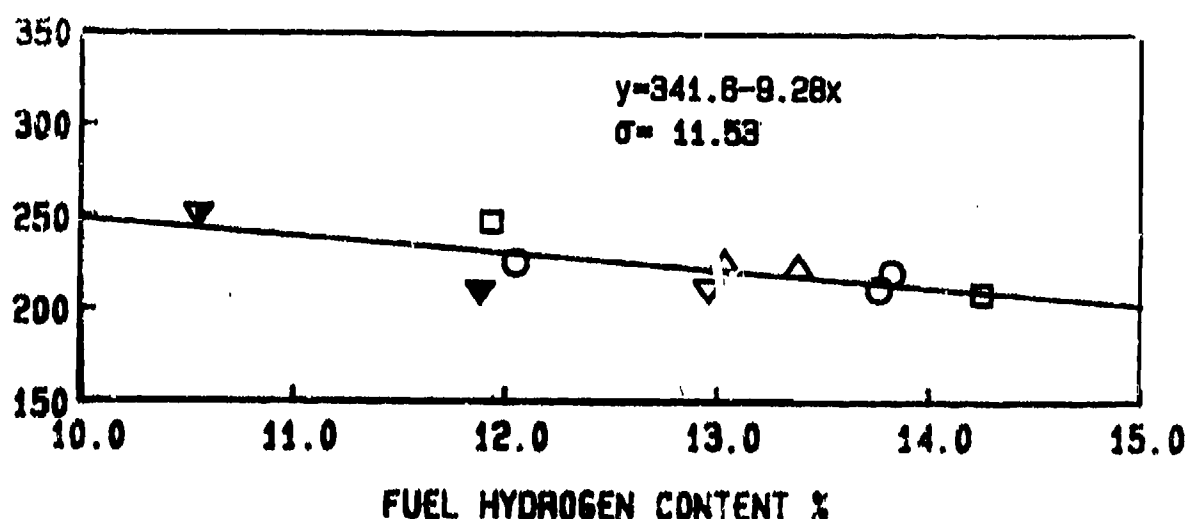


Figure 6.126: Effects of Fuel Properties on Average Line) Temperatures (PT6A-65 Gas Generator, BOM, Simplex 2.2 FN)

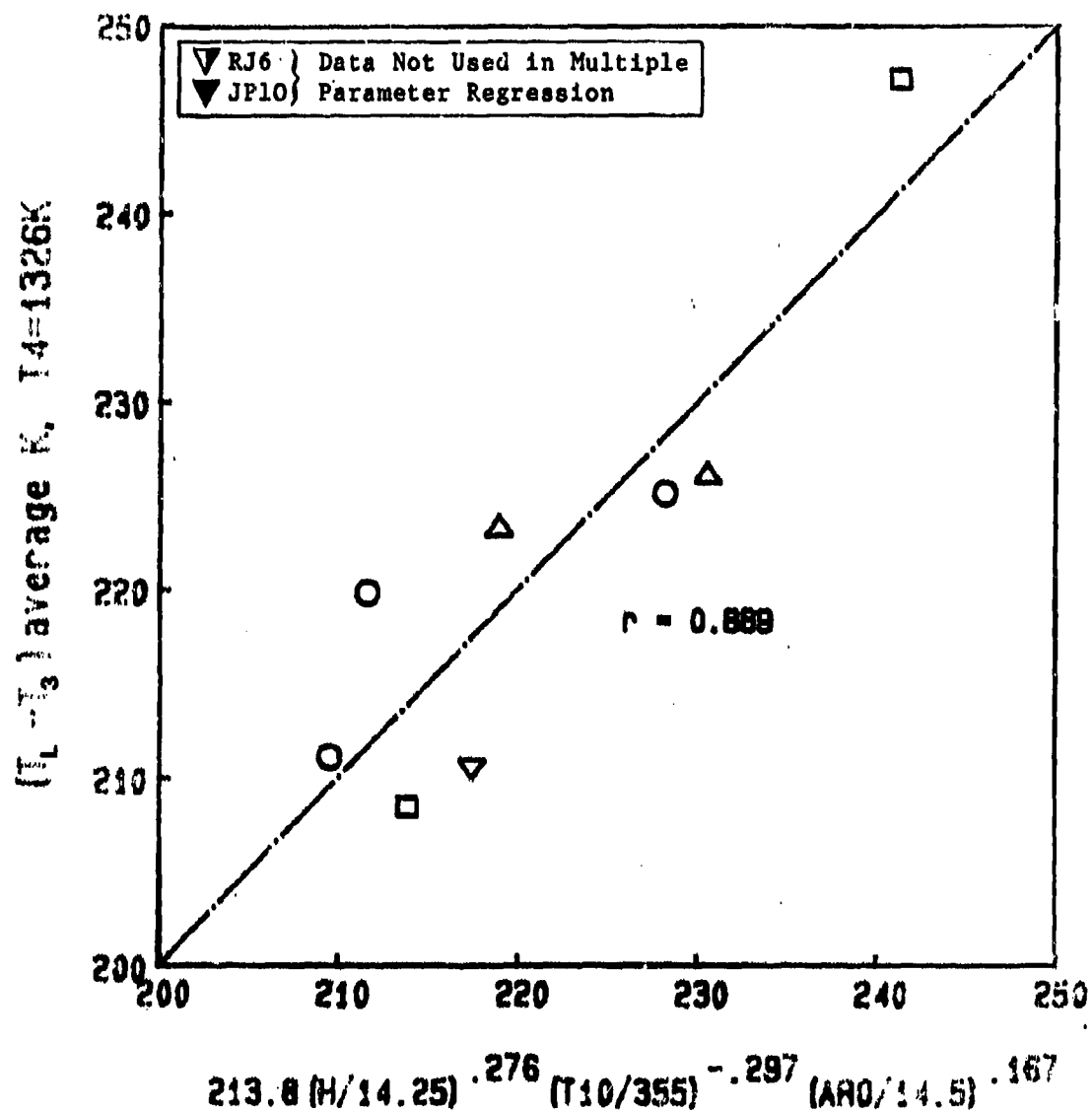


Figure 6.127: Average Liner Temperature vs Multiple Parameter Correlation (PT6A-65 Gas Generator, BCM, Simplex 2.2 FN)

LINEAR TEMPERATURE PARAMETER (average)

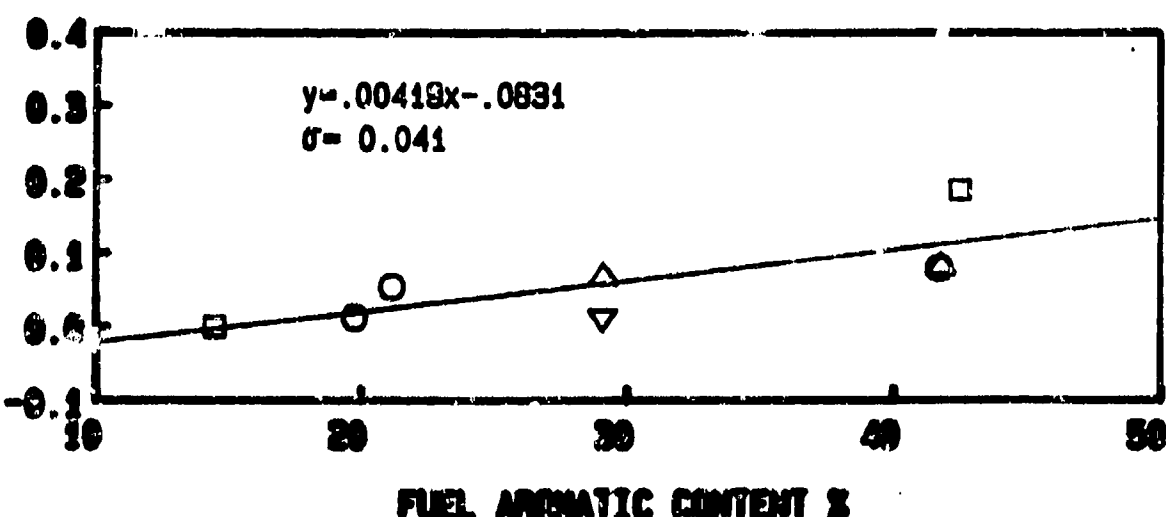
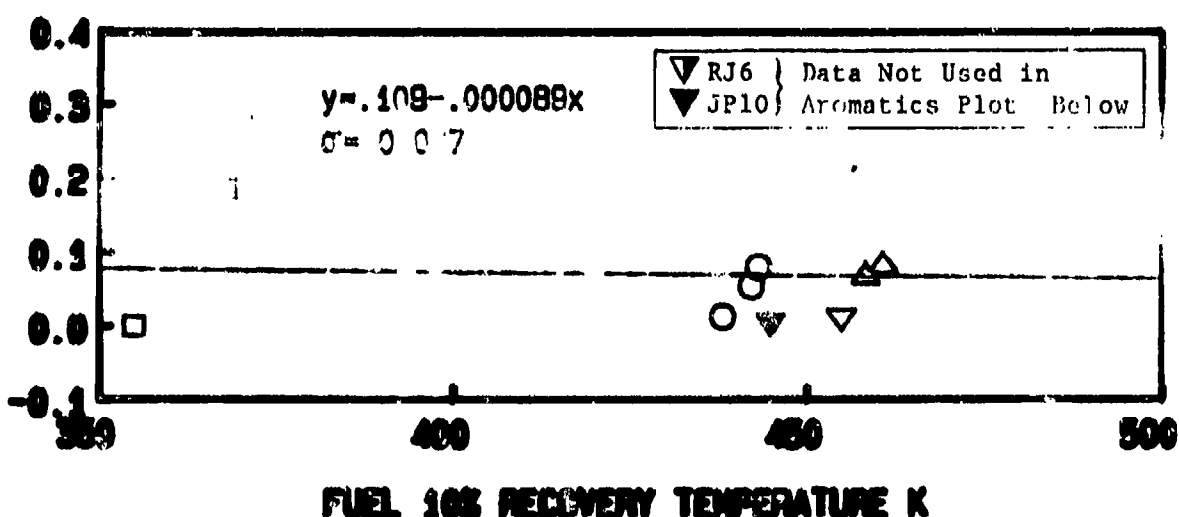
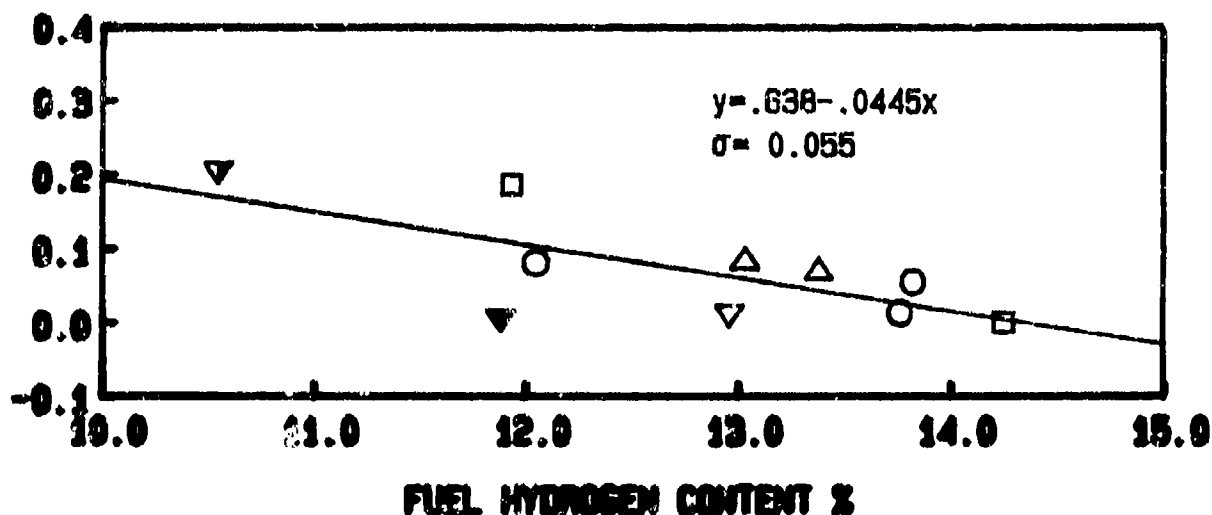


Figure 6.128: Effects of Fuel Properties on Linear Temperature Parameter (PT6A-65 Gas Generator, ROM, Simplex 2.2 FN)

$(T_L - T_3)$ peak K, $T_4 = 1326K$

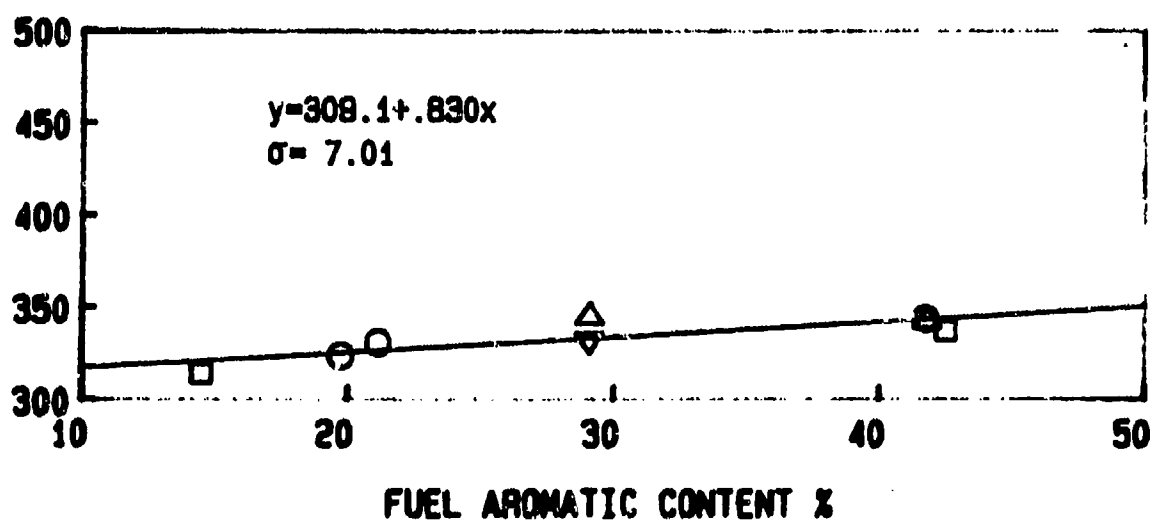
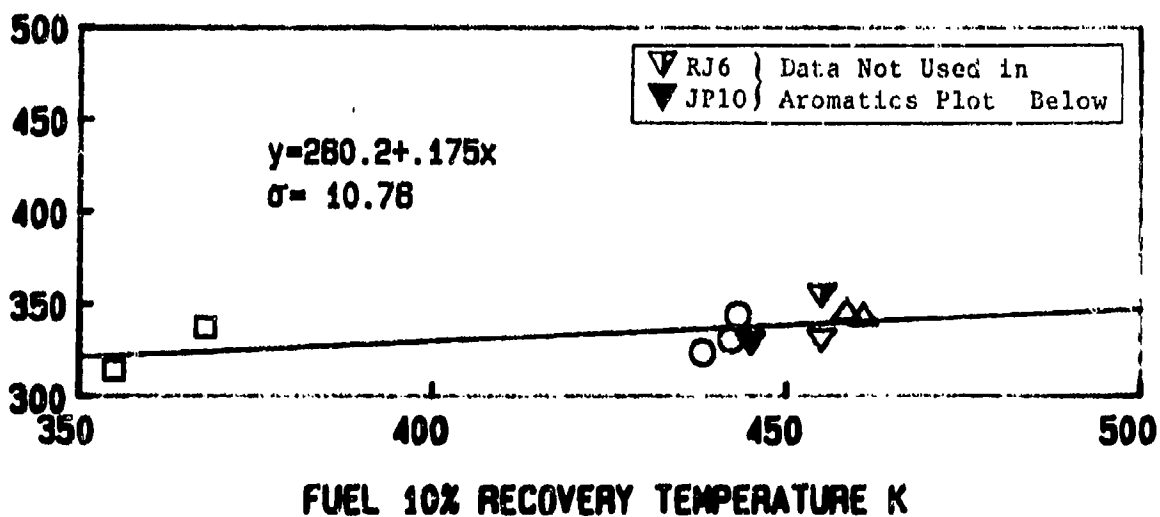
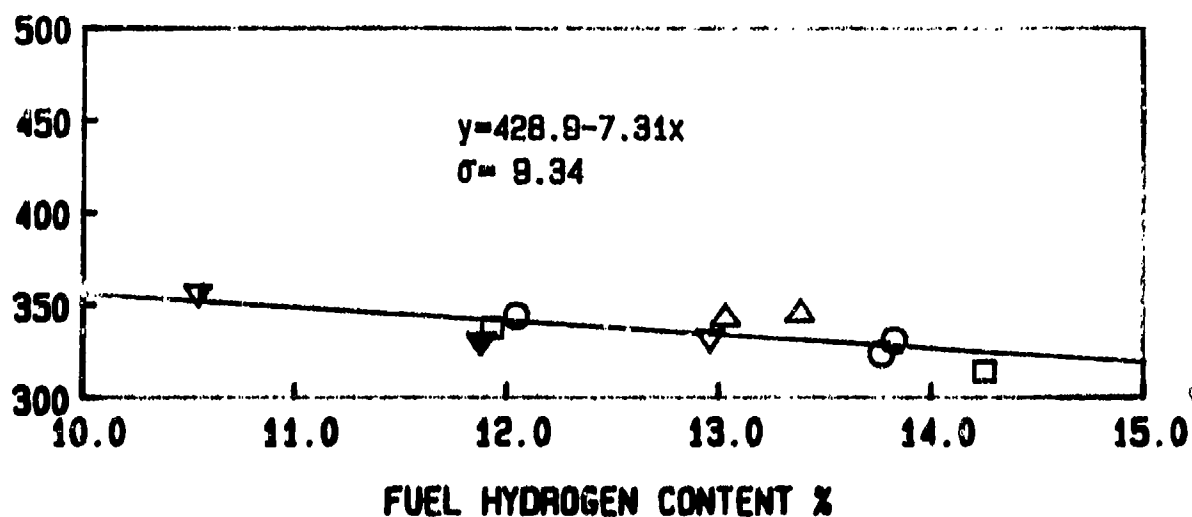


Figure 6.129: Effects of Fuel Properties on Peak Liner Temperatures (PT6A-65 Gas Generator, BOM, Simplex 2.2 FN)

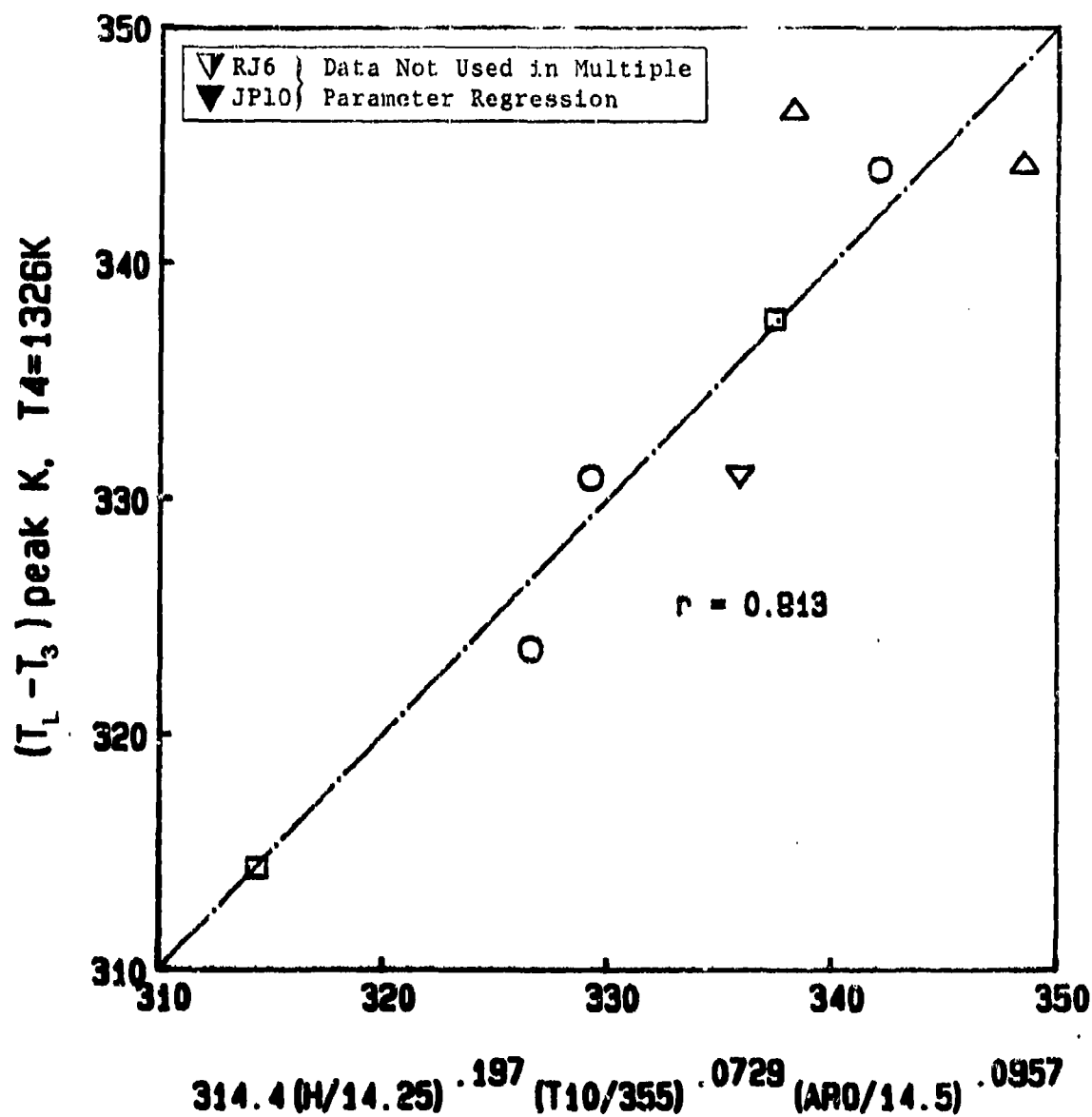


Figure 6.130: Peak Linear Temperatures vs Multiple Parameter Correlation (PT6A-65 Gas Generator, BQM, Simplex 2.2 FN)

(T₁-T₃) average K, 14-1326K

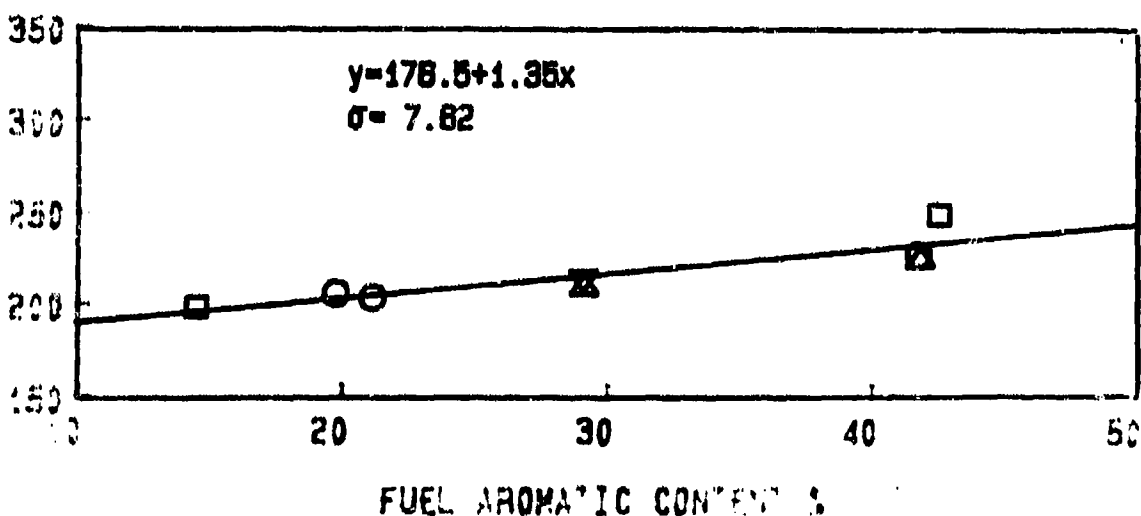
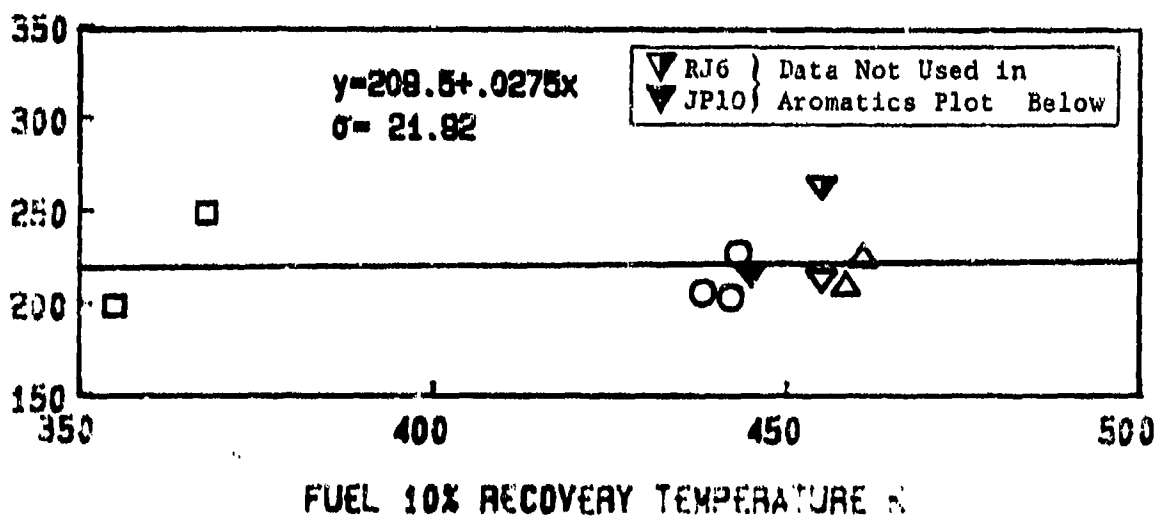
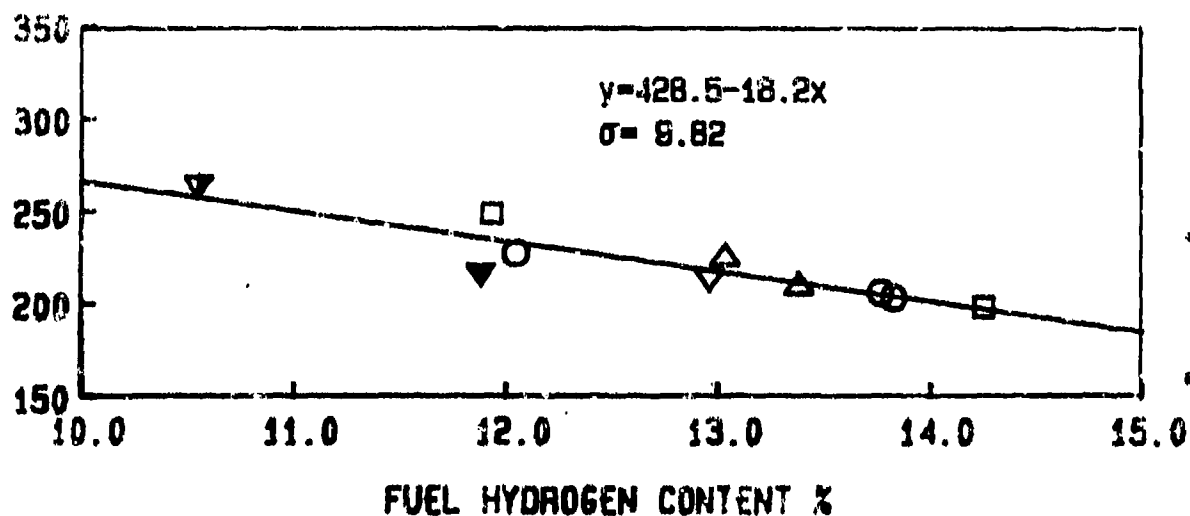


Figure 6.131: Effects of Fuel Properties on Average Liner Temperatures
 (PT6A-65 Gas Generator, 5% Bleed, Simplex 2.2 FN)

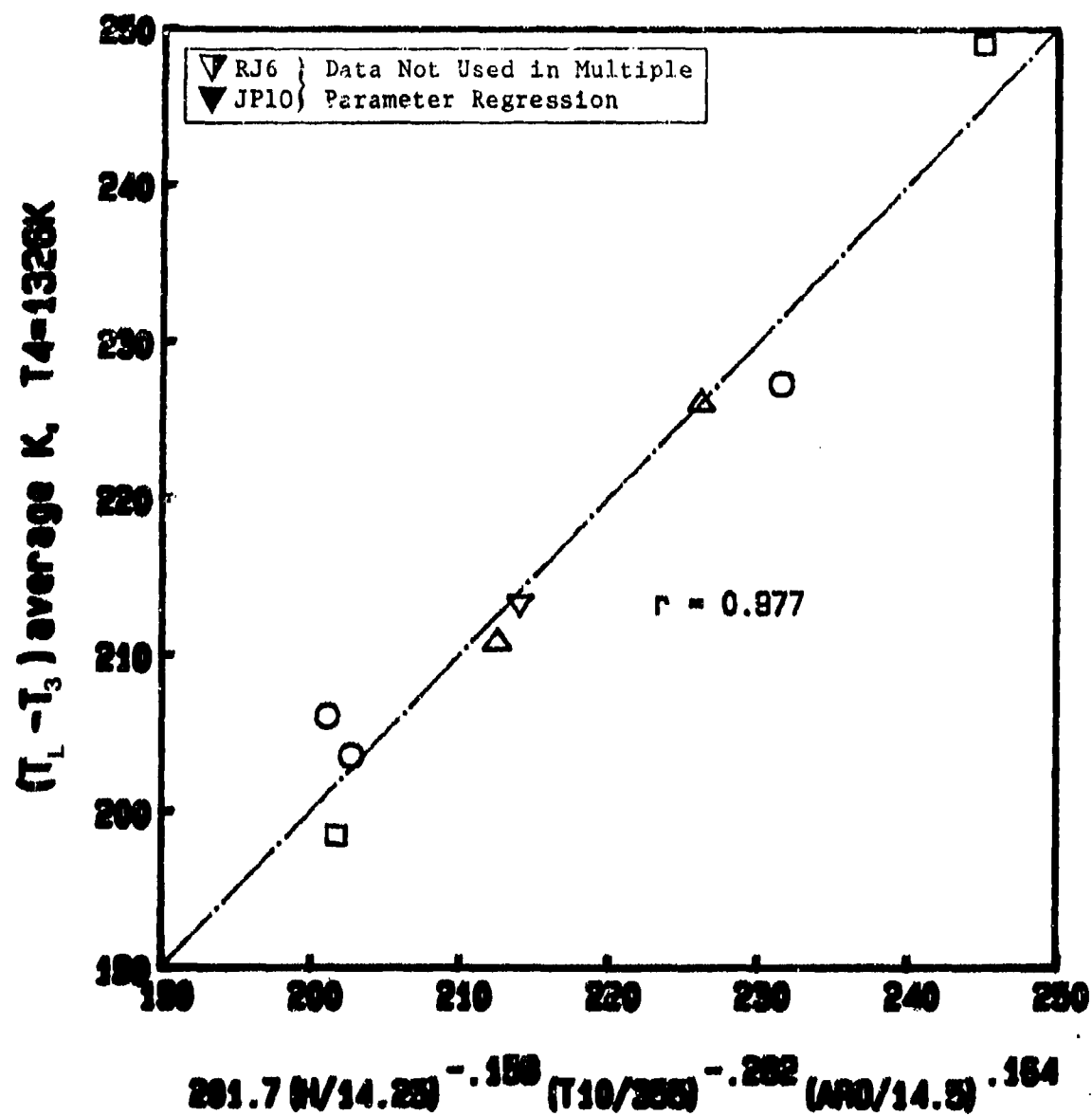


Figure 6.132: Average Liner Temperatures vs Multiple Parameter Correlation
(PT6A-65 Gas Generator, 5% Bleed, Simplex 2.2 FN)

LINER TEMPERATURE PARAMETER (average)

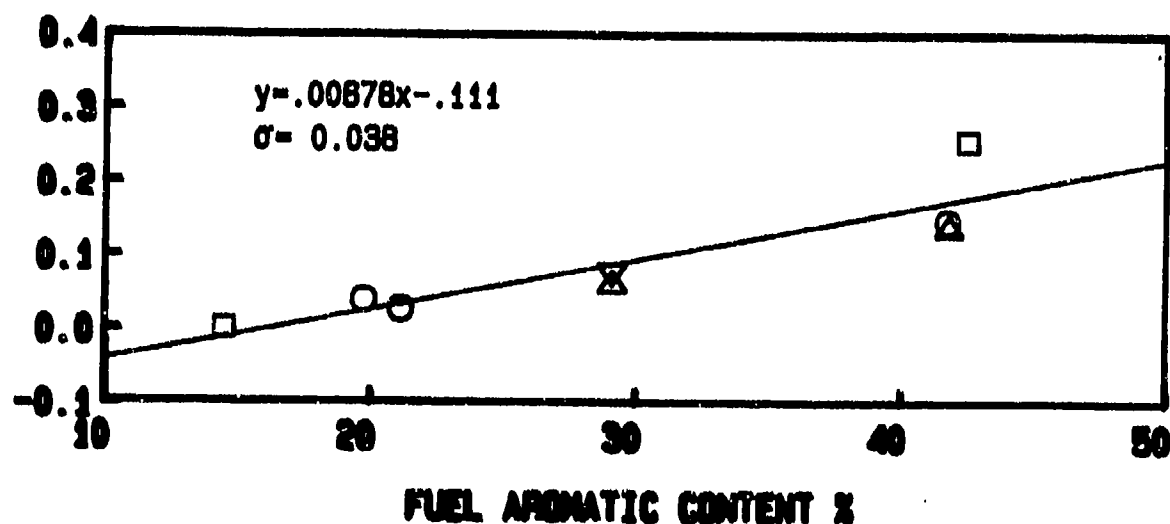
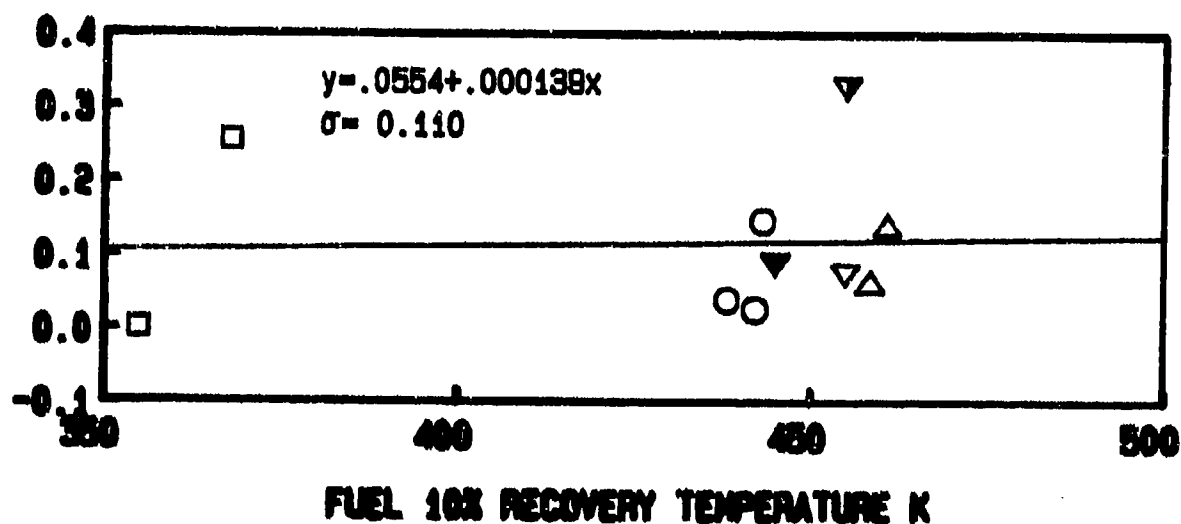
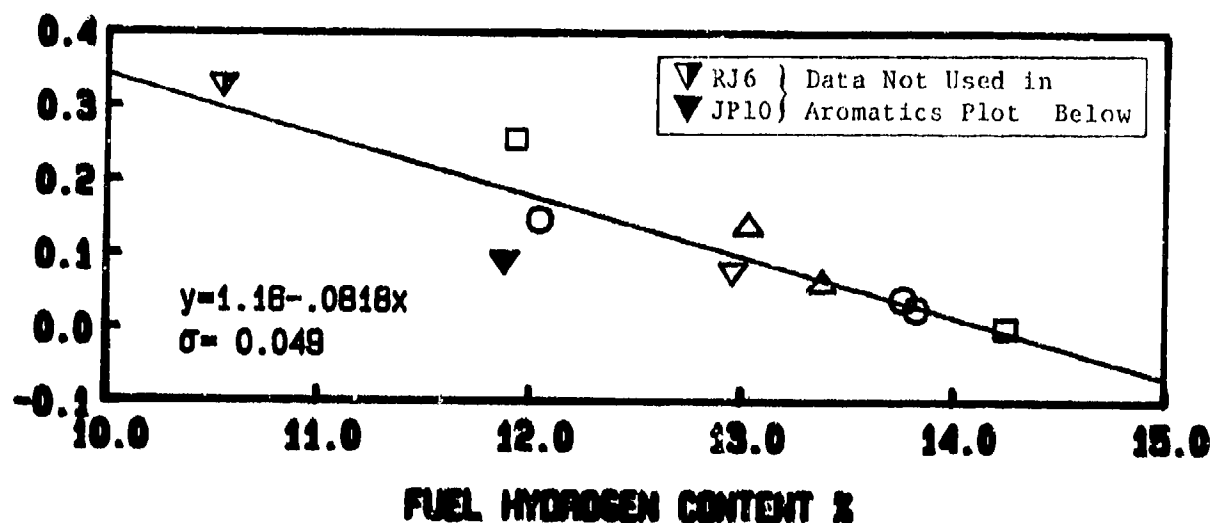


Figure 6.133: Effects of Fuel Properties on Liner Temperature Parameter (PT6A-65 Gas Generator, 5% Bleed, Simplex 2.2 FN)

$(T_L - T_3)$ peak K, $T_4 = 1328K$

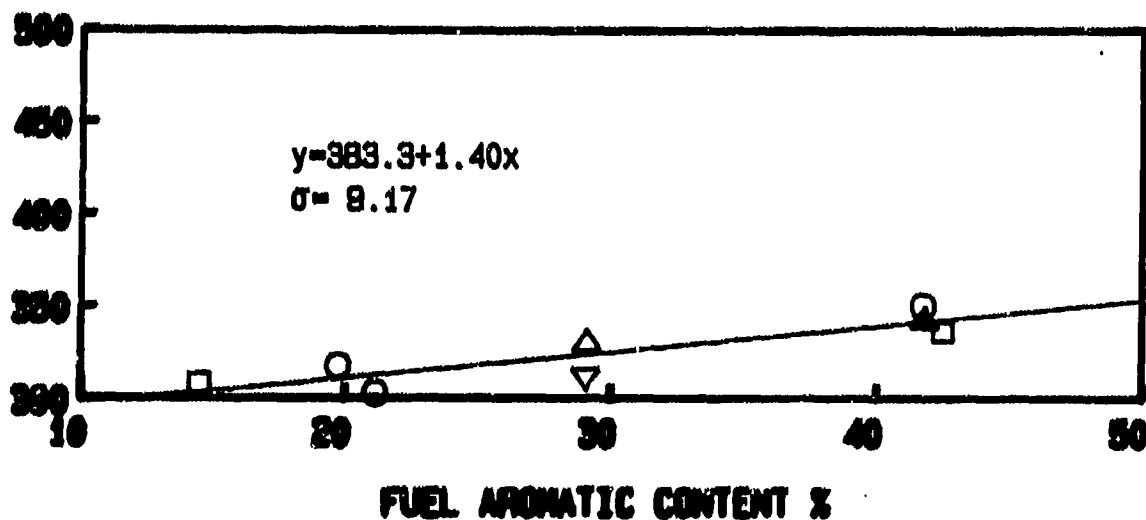
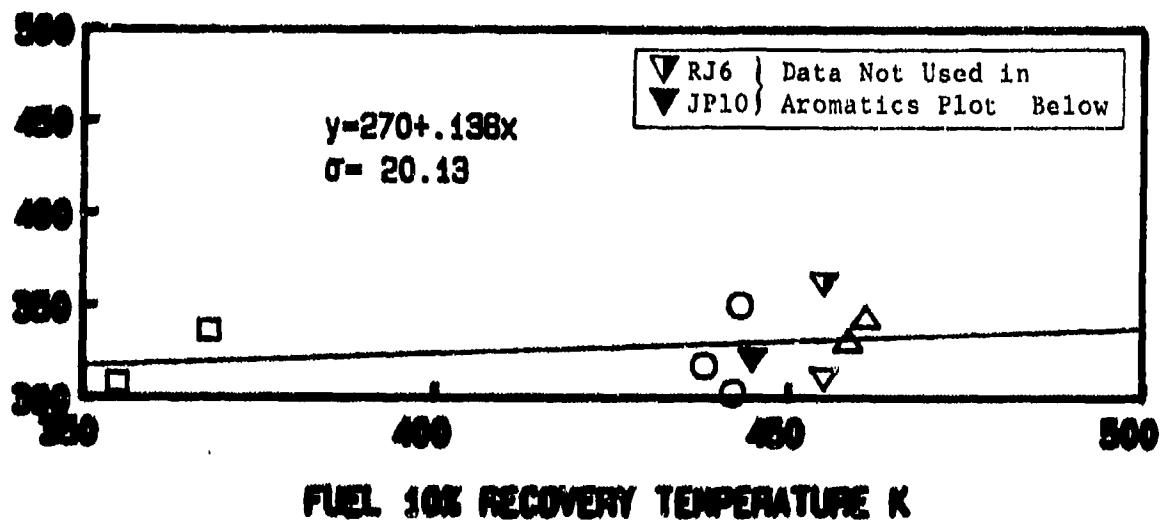
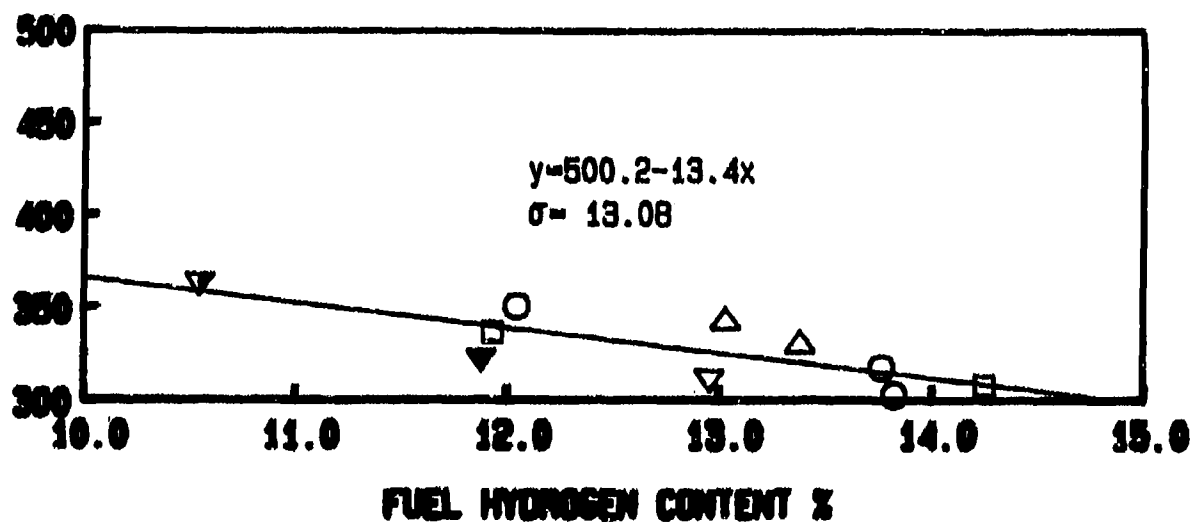


Figure 6.134: Effects of Fuel Properties on Peak Liner Temperatures (PT6A-65 Gas Generator, 5% Bleed, Simplex 2.2 FN)

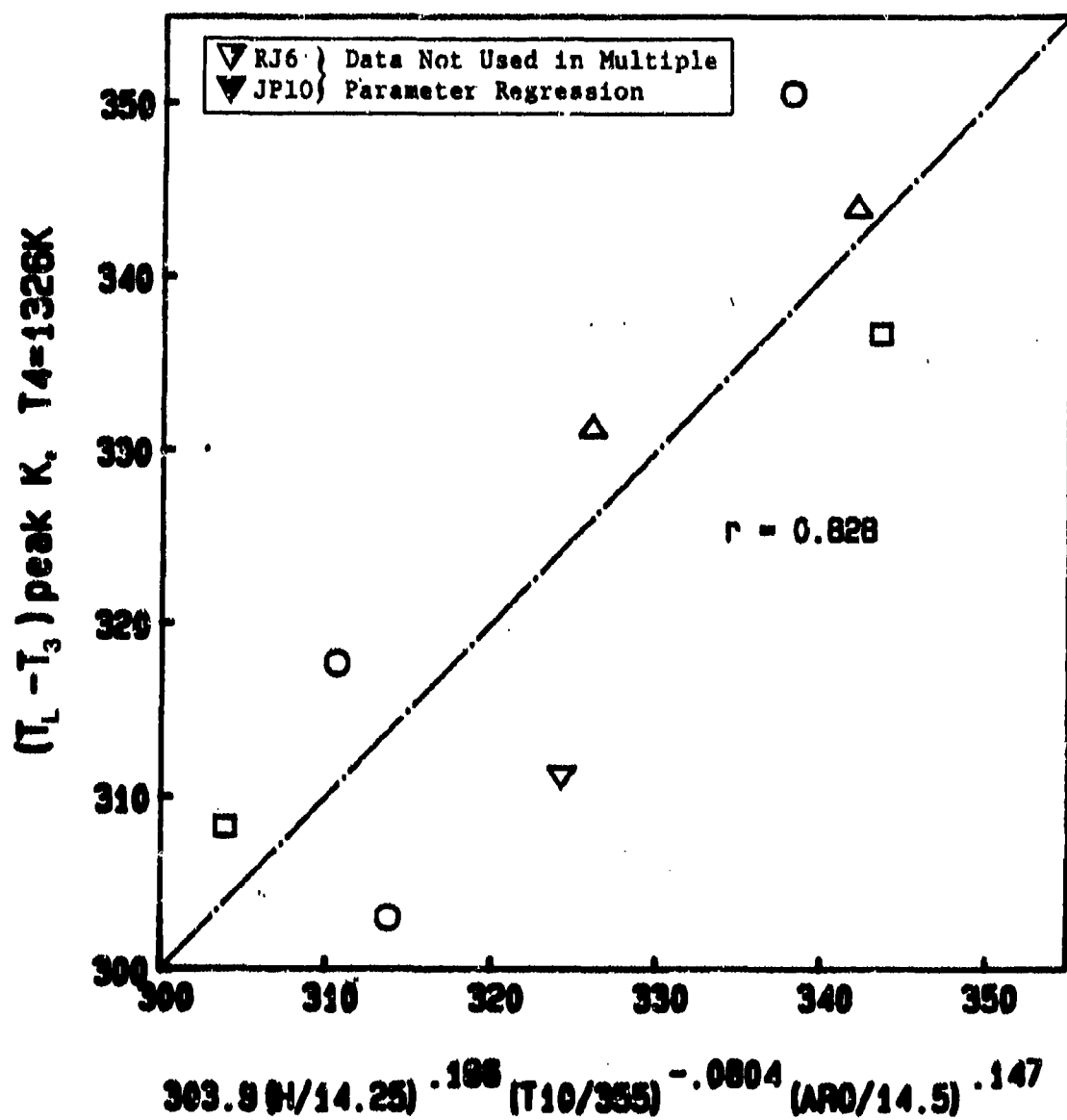


Figure 6.135; Peak Liner Temperatures vs Multiple Parameter Correlation (PT6A-65 Gas Generator, 5% Bleed, Simplex 2.2 FN)

TAKE-OFF RELATIVE PROFILE FACTOR

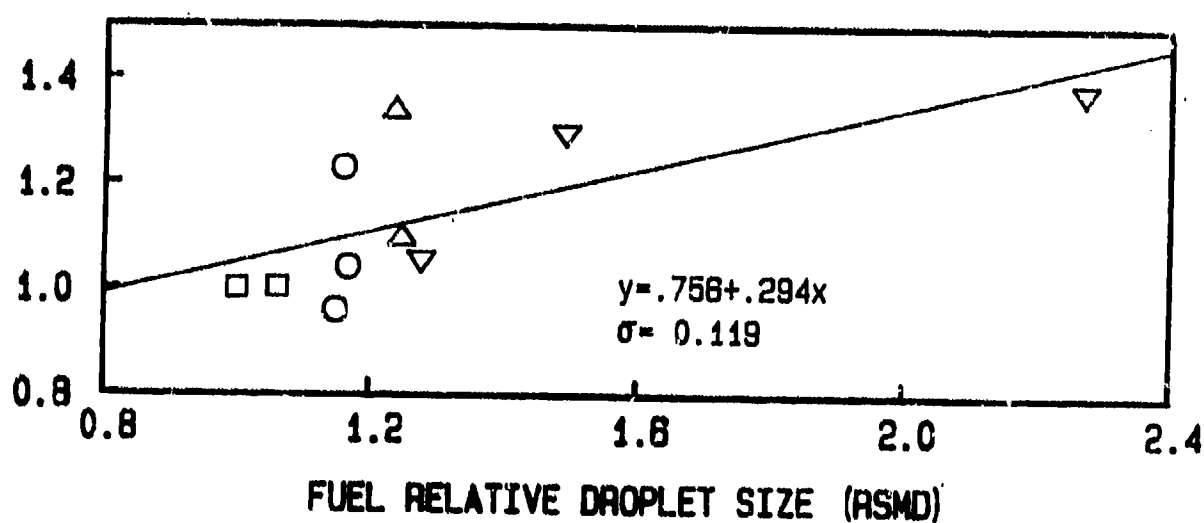
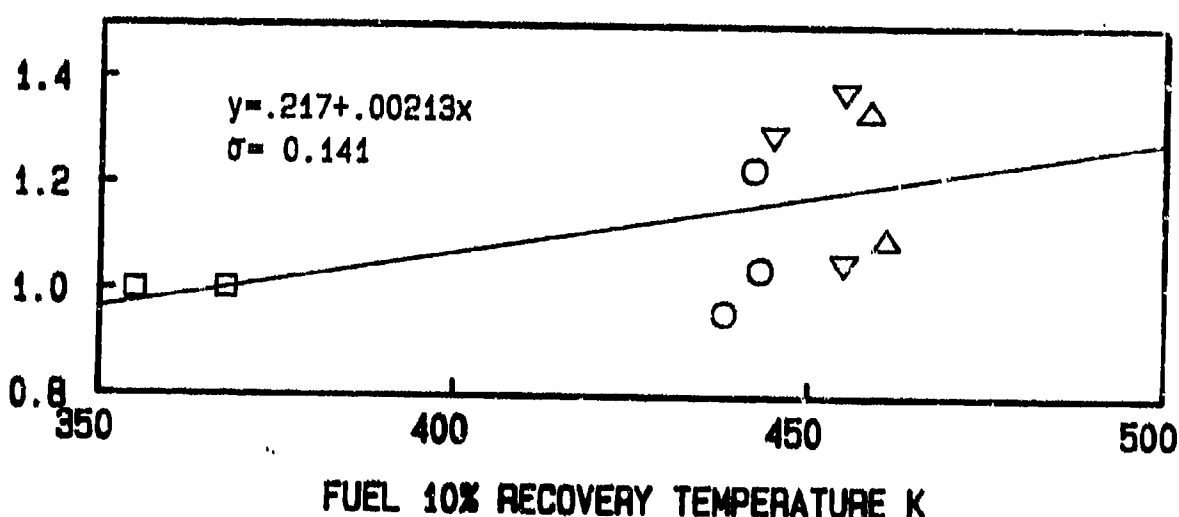
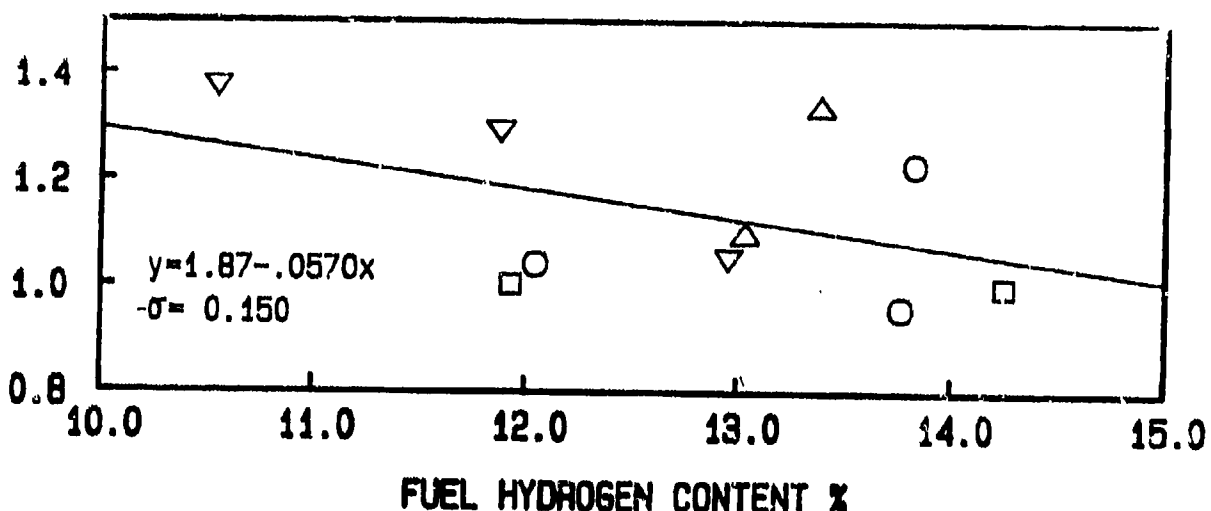


Figure 6.136: Effects of Fuel Properties on Take-Off Relative Profile Factor (PT6A-65 Gas Generator, BOM, Simplex 1.9 FN)

TAKE-OFF RELATIVE PATTERN FACTOR

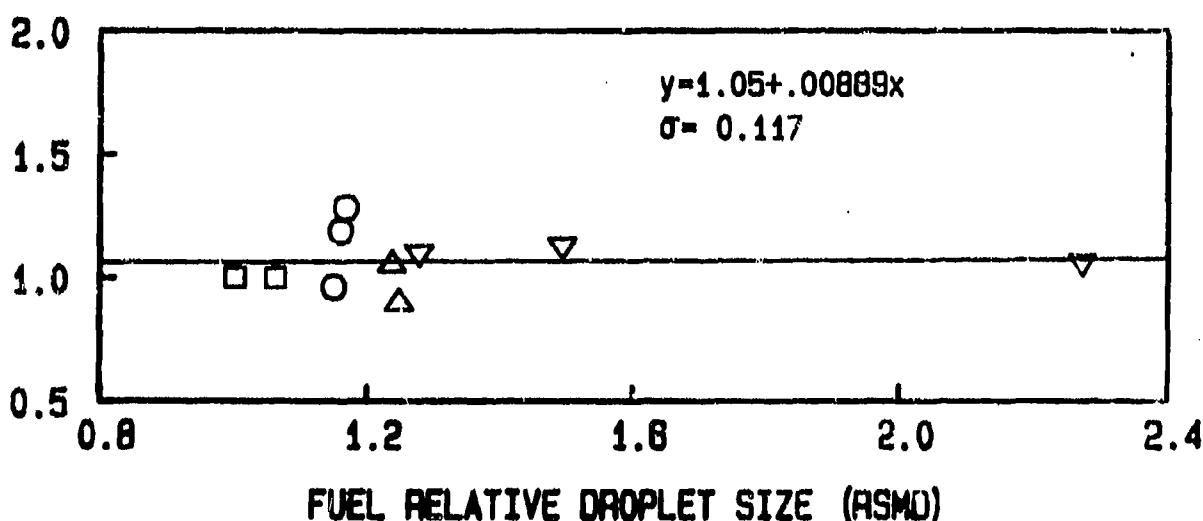
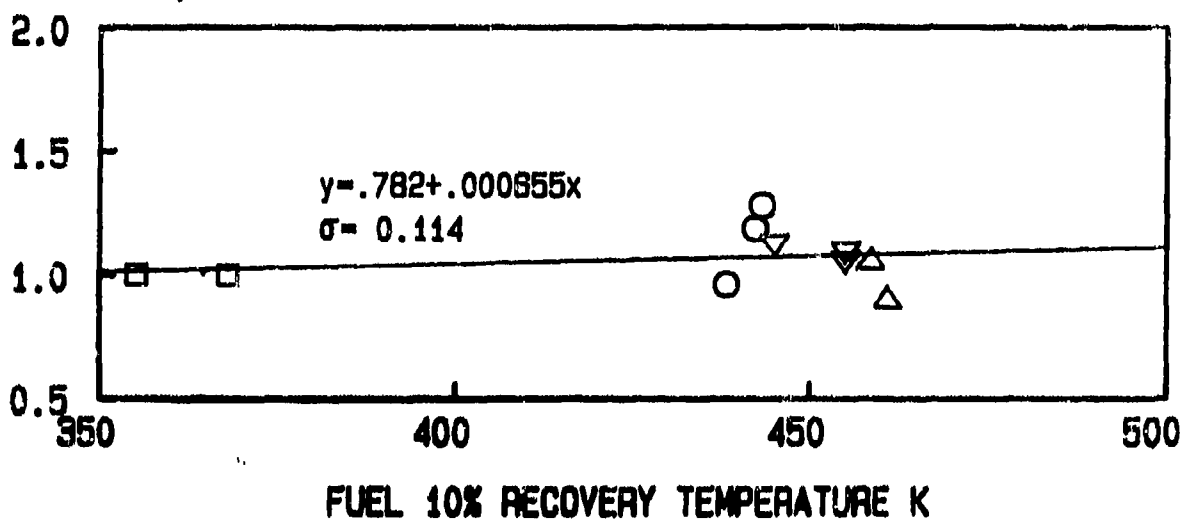
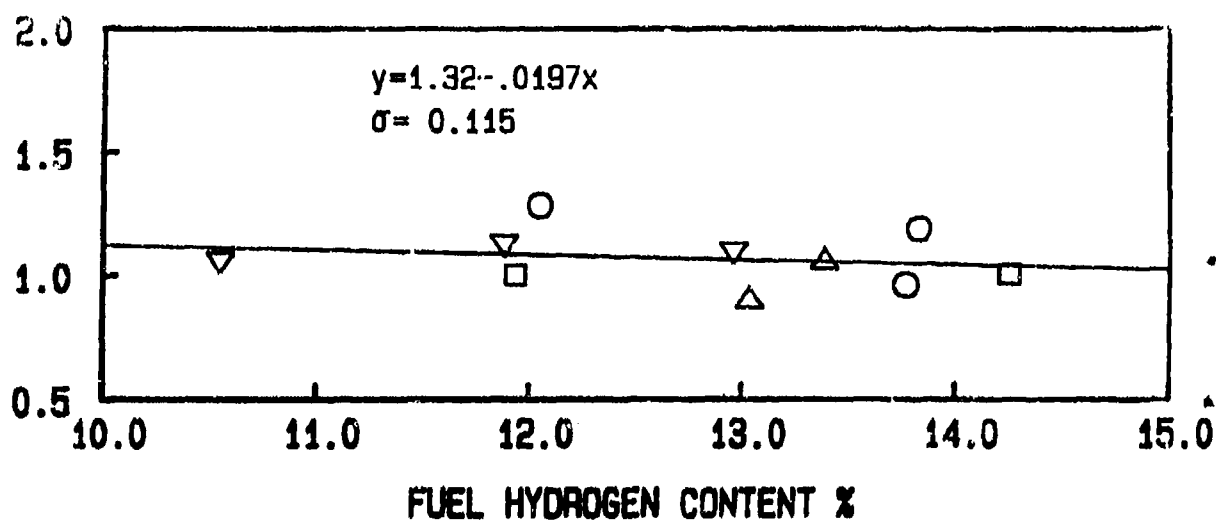


Figure 6.137: Effects of Fuel Properties on Take-Off Relative Pattern Factor (PT6A-65 Gas Generator, BOM, Simplex 1.9 FN)

TAKE-OFF RELATIVE PROFILE FACTOR

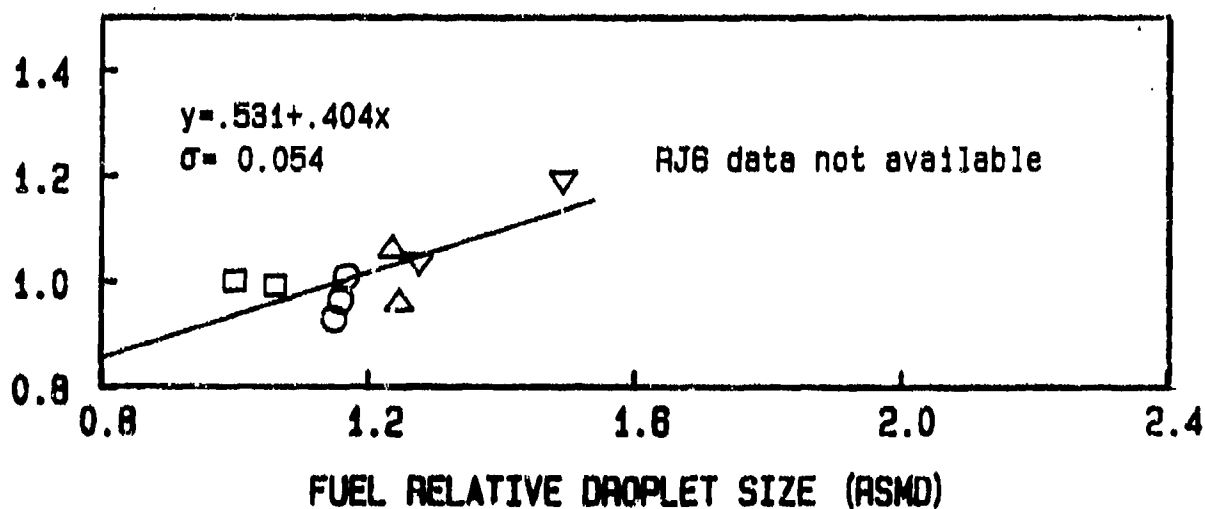
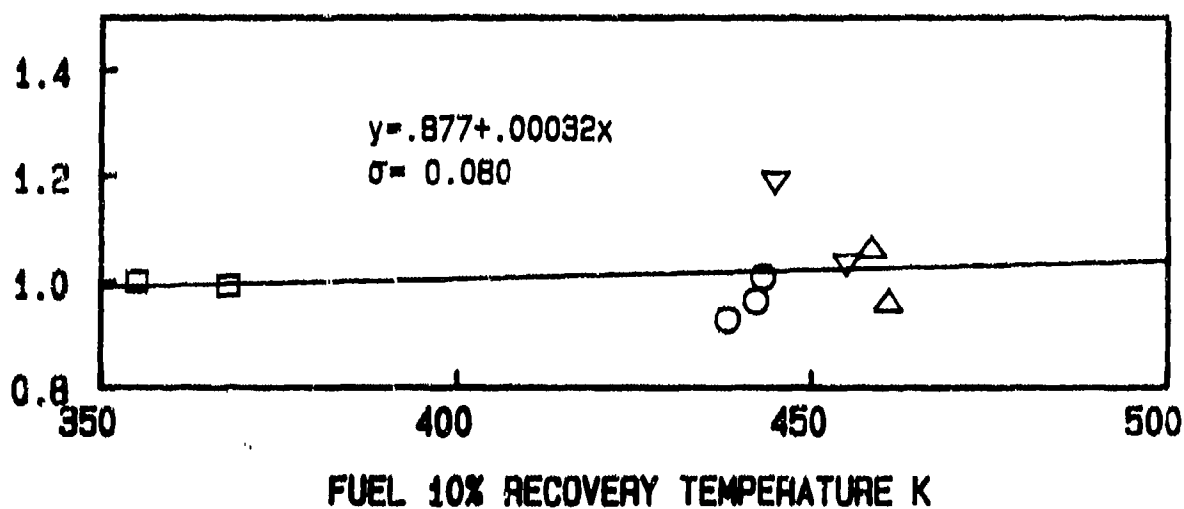
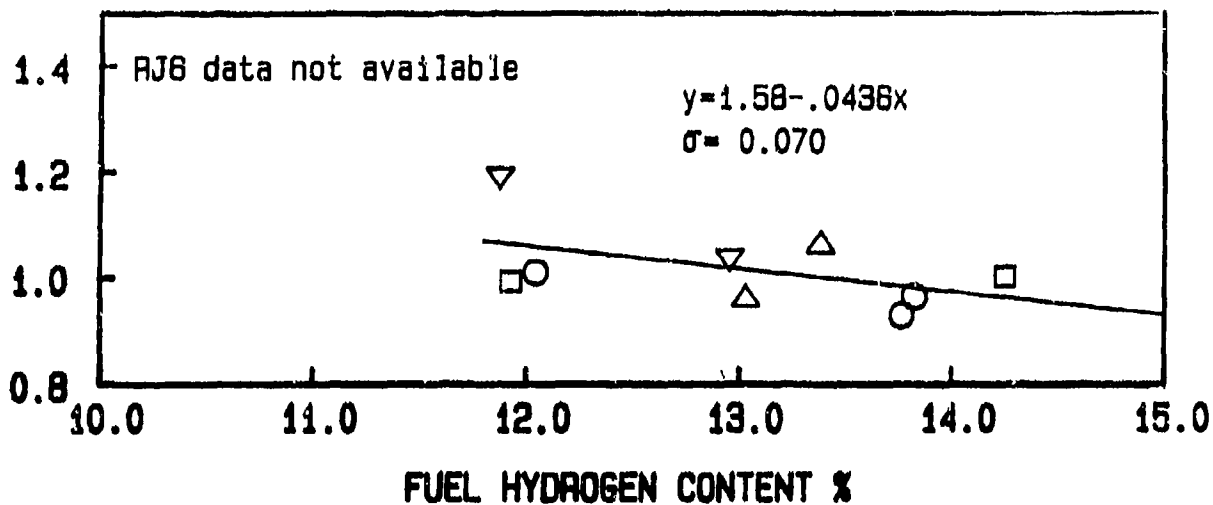


Figure 6.138: Effects of Fuel Properties on Take-Off Relative Profile Factor (PT6A-65 Gas Generator, 5% Bleed, Simplex 1.9 FN)

TAKE-OFF RELATIVE PATTERN FACTOR

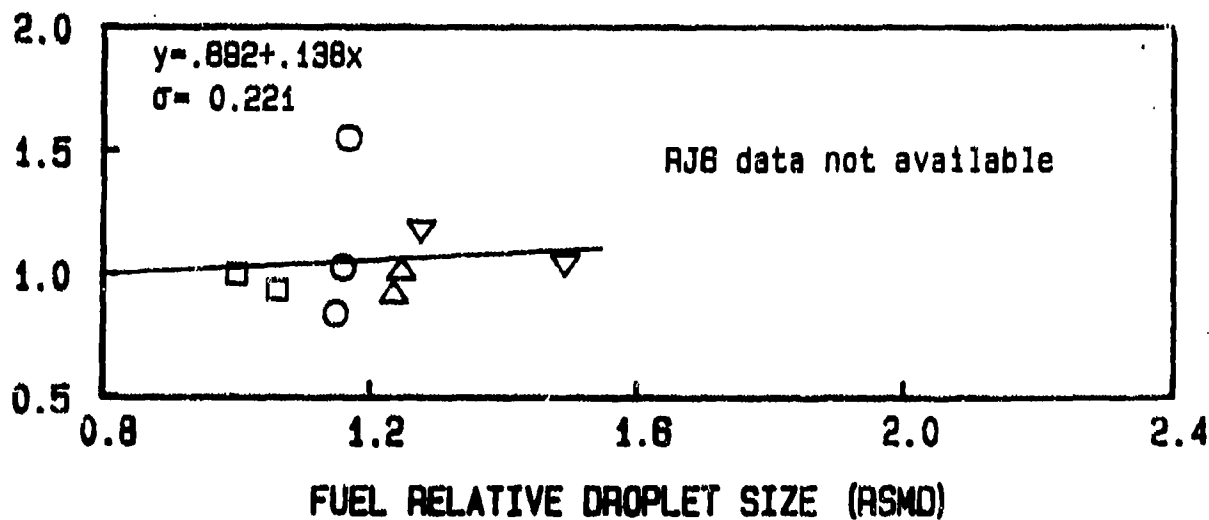
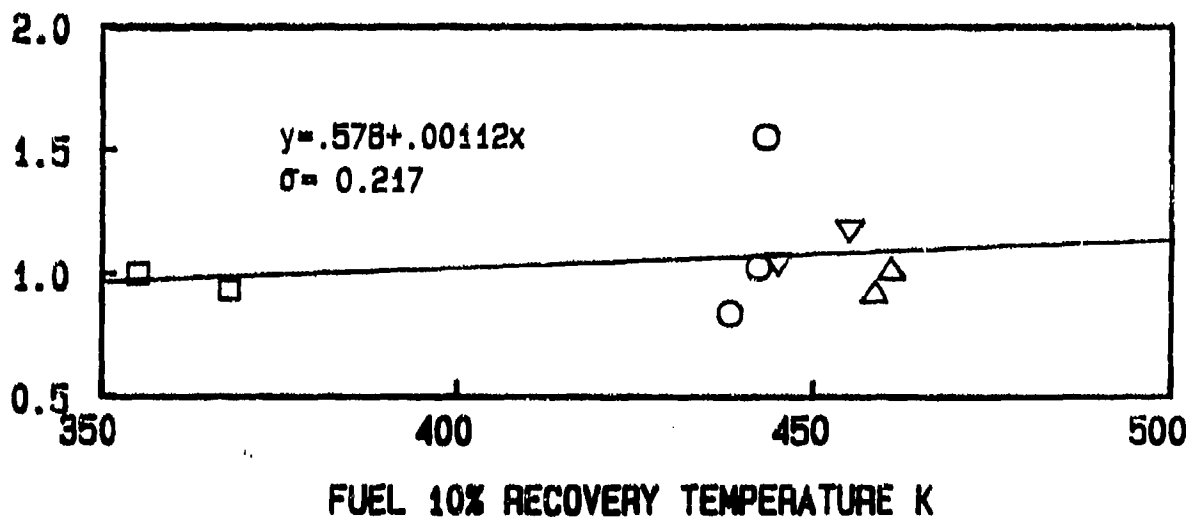
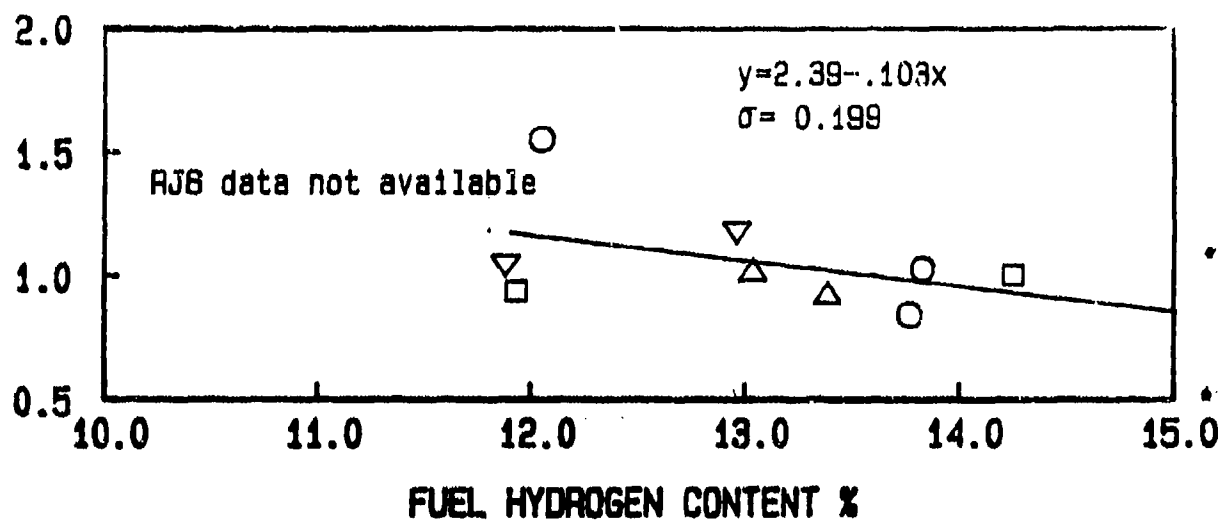


Figure 6.139: Effects of Fuel Properties on Take-Off Relative Pattern Factor (PT6A-65 Gas Generator, 5% Bleed, Simplex 1.9 FN)

TAKE-OFF RELATIVE PROFILE FACTOR

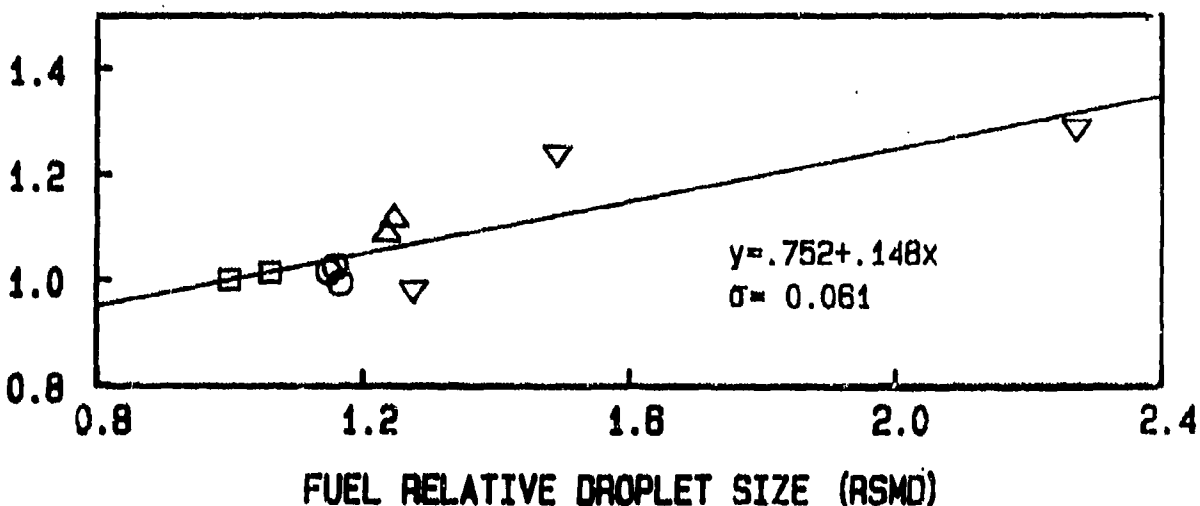
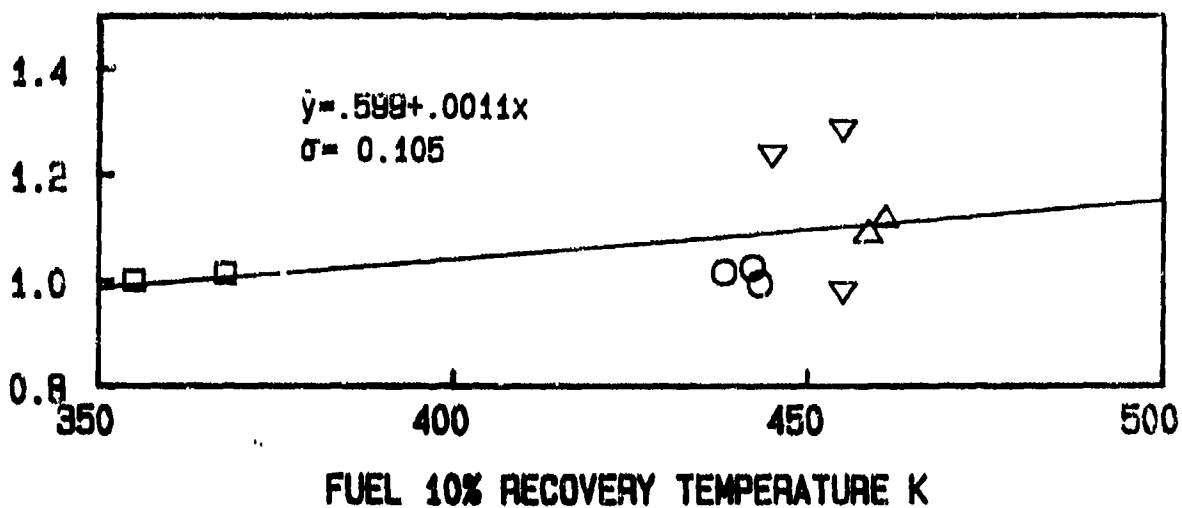
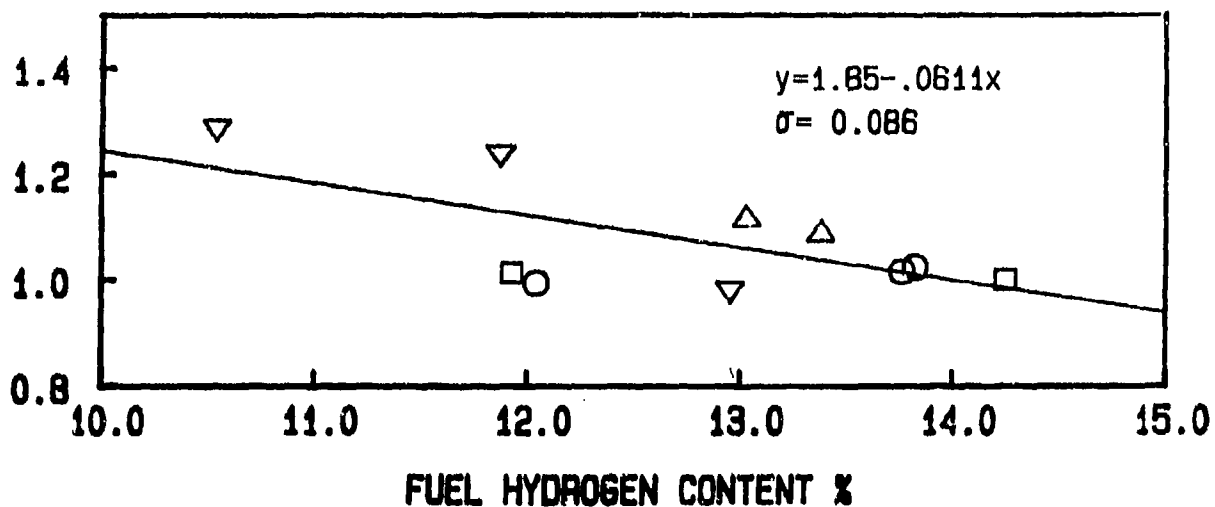


Figure 6.140: Effects of Fuel Properties on Take-Off Relative Profile Factor (PT6A-65 Gas Generator, BOM, Simplex 2.2 FN)

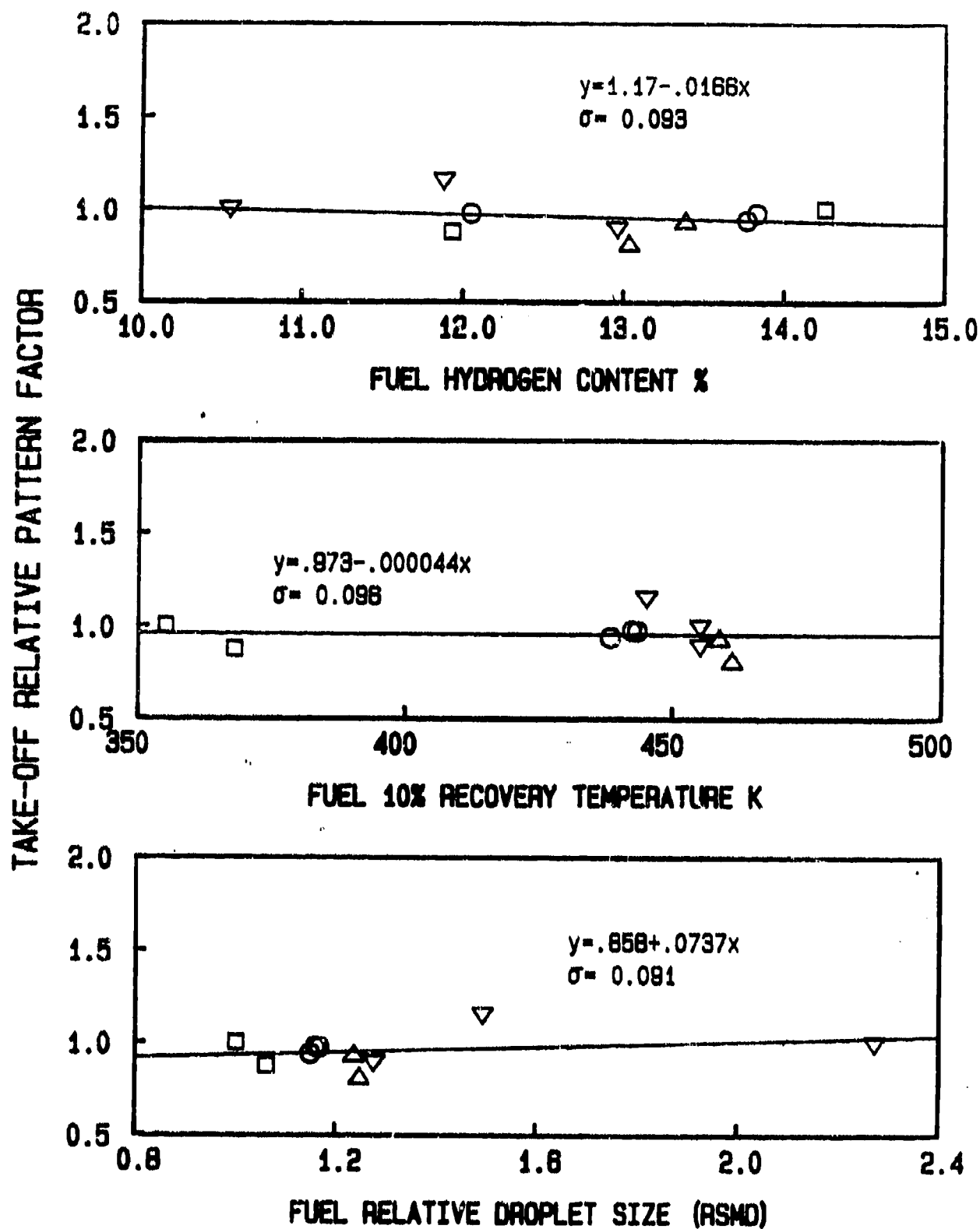


Figure 6.141: Effects of Fuel Properties on Take-Off Relative Pattern Factor (PT6A-65 Gas Generator, BOM, Simplex 2.2 FN)

TAKE-OFF RELATIVE PROFILE FACTOR

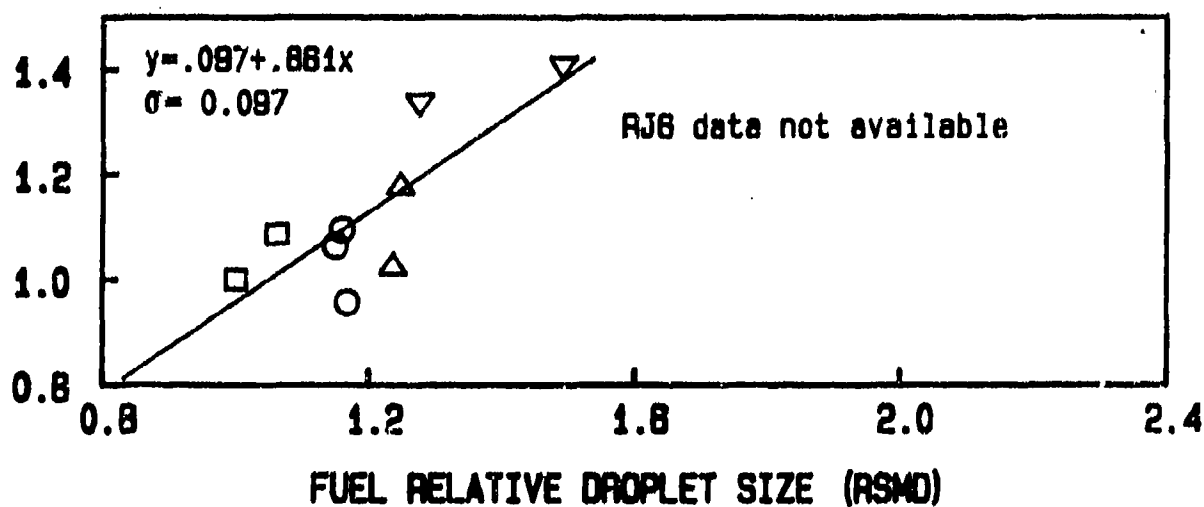
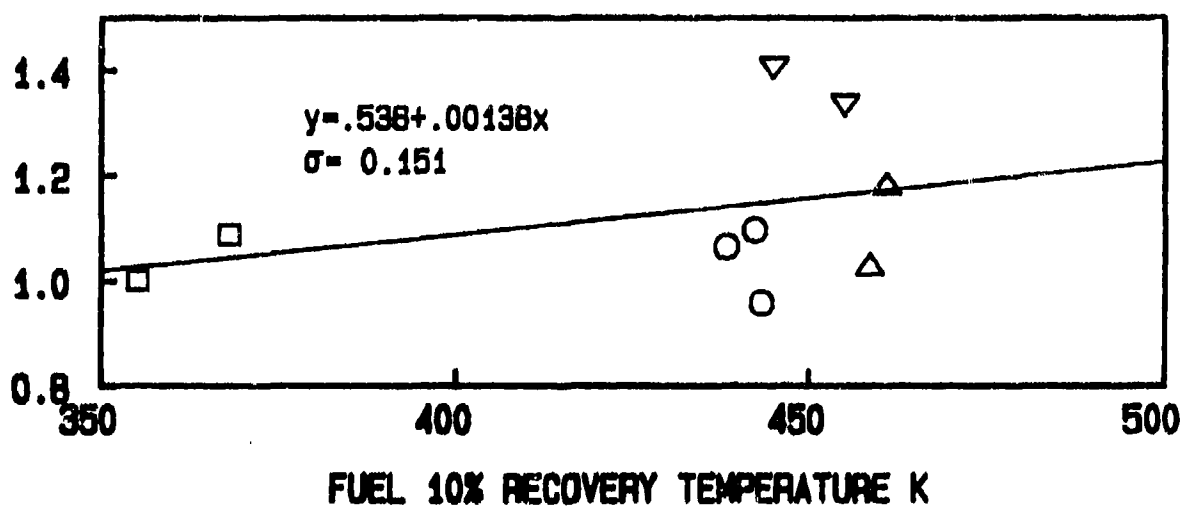
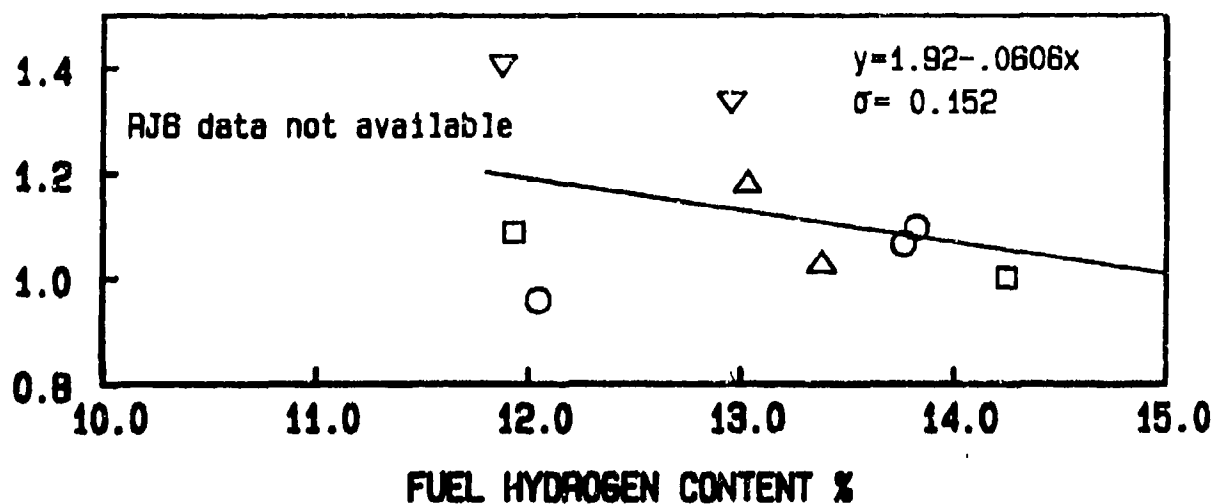


Figure 6.142: Effects of Fuel Properties on Take-Off Relative Profile Factor - 6A-65 Gas Generator, 5% Bleed, Simplex 2.2 FN)

TAKE-OFF RELATIVE PATTERN FACTOR

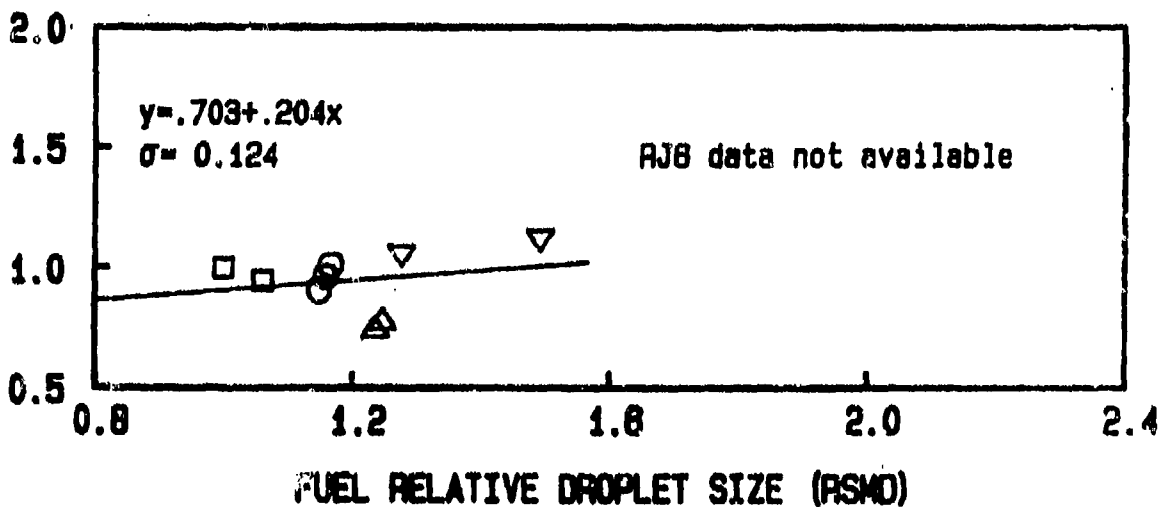
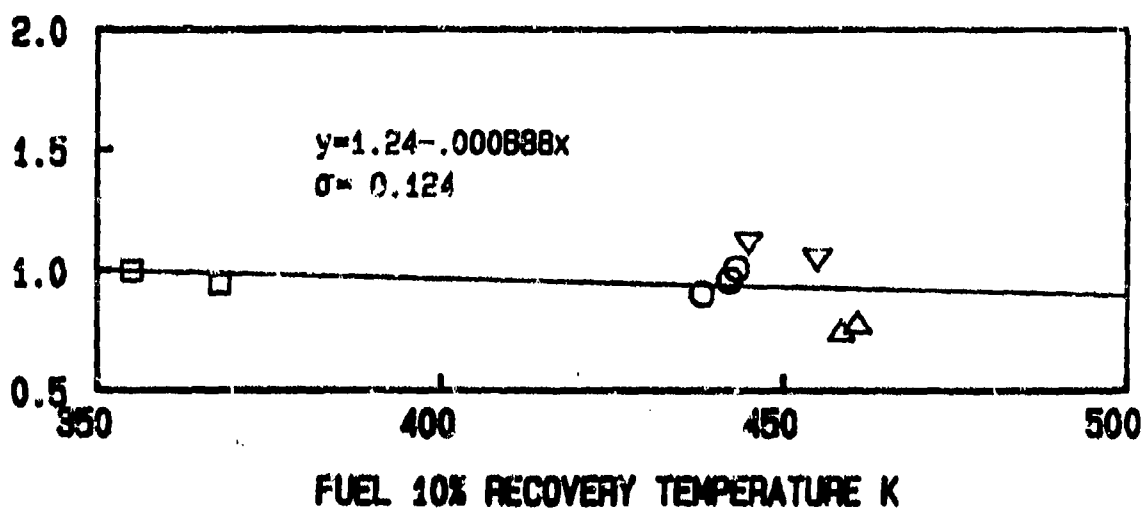
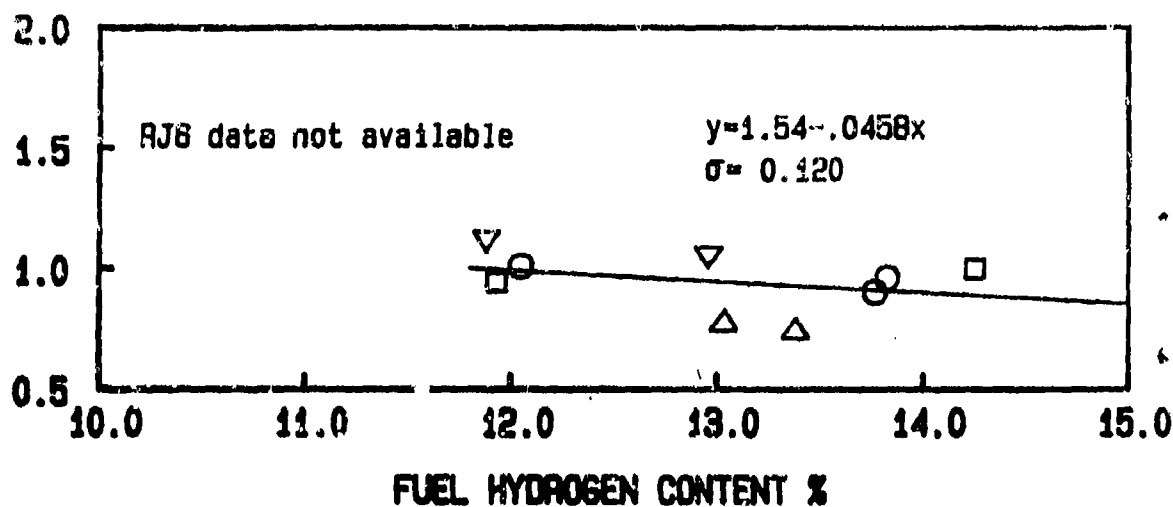


Figure 6.143: Effects of Fuel Properties on Take-Off Relative Pattern Factor (PT6A-65 Gas Generator, 5% Bleed, Simplex 2.2 FN)

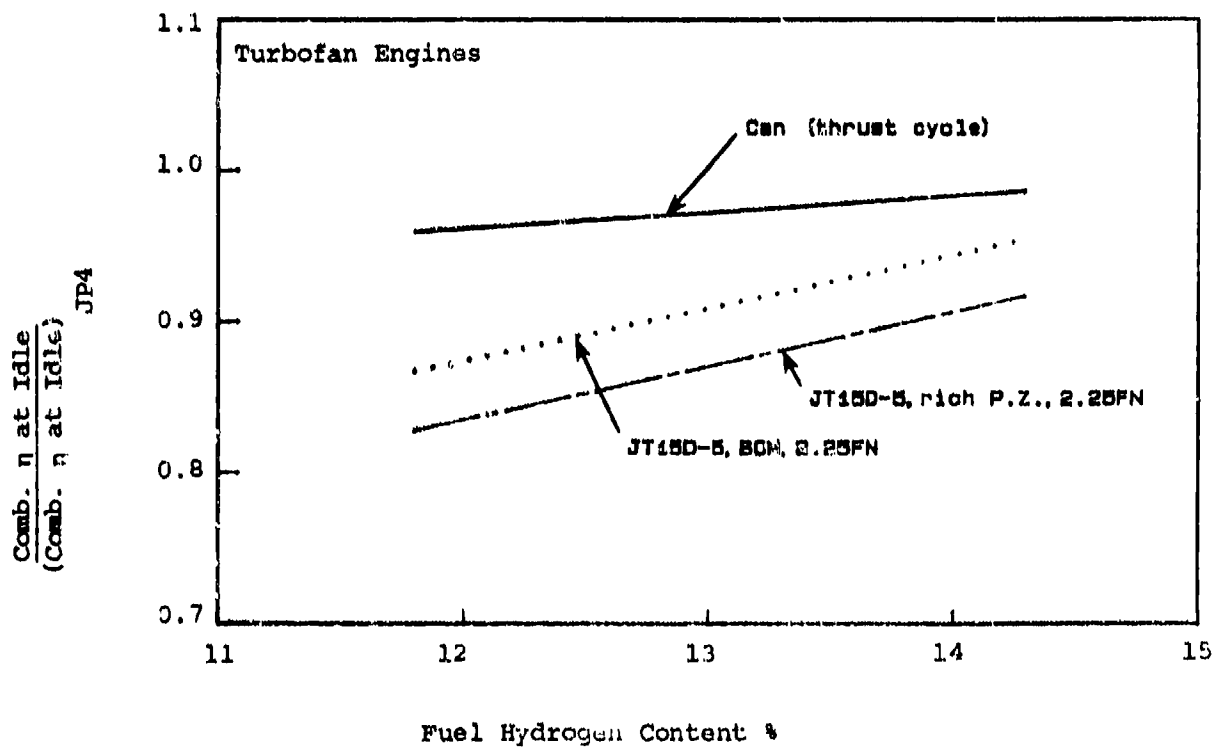
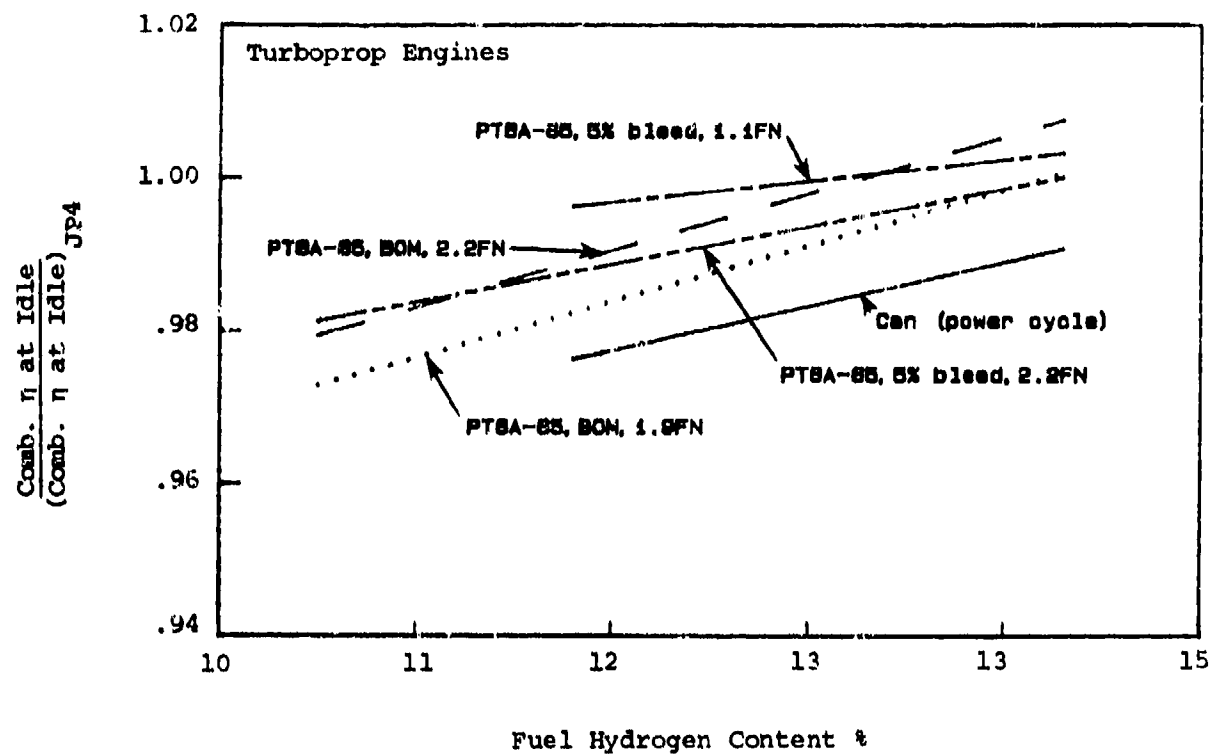


Figure 6.144: Effects of Fuel Hydrogen Content on Relative Idle Combustion Efficiency

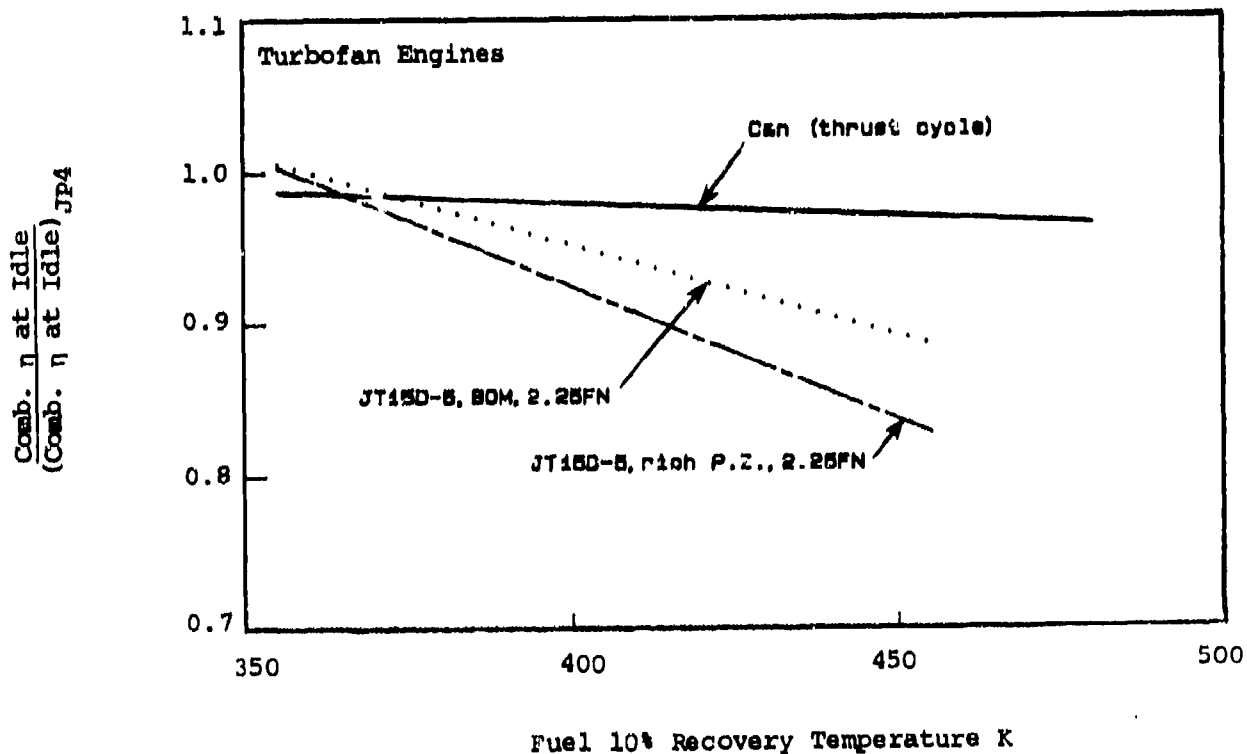
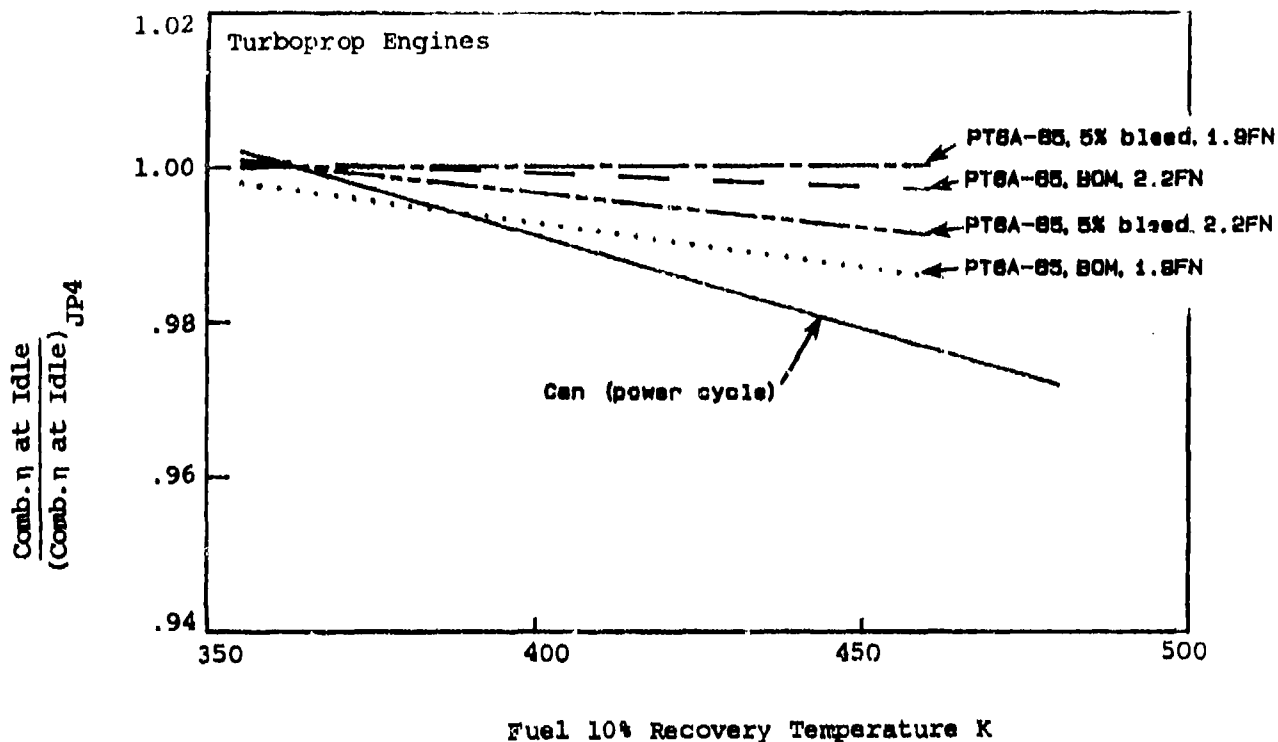


Figure 6.145: Effects of Fuel Volatility on Relative Idle Combustion Efficiency

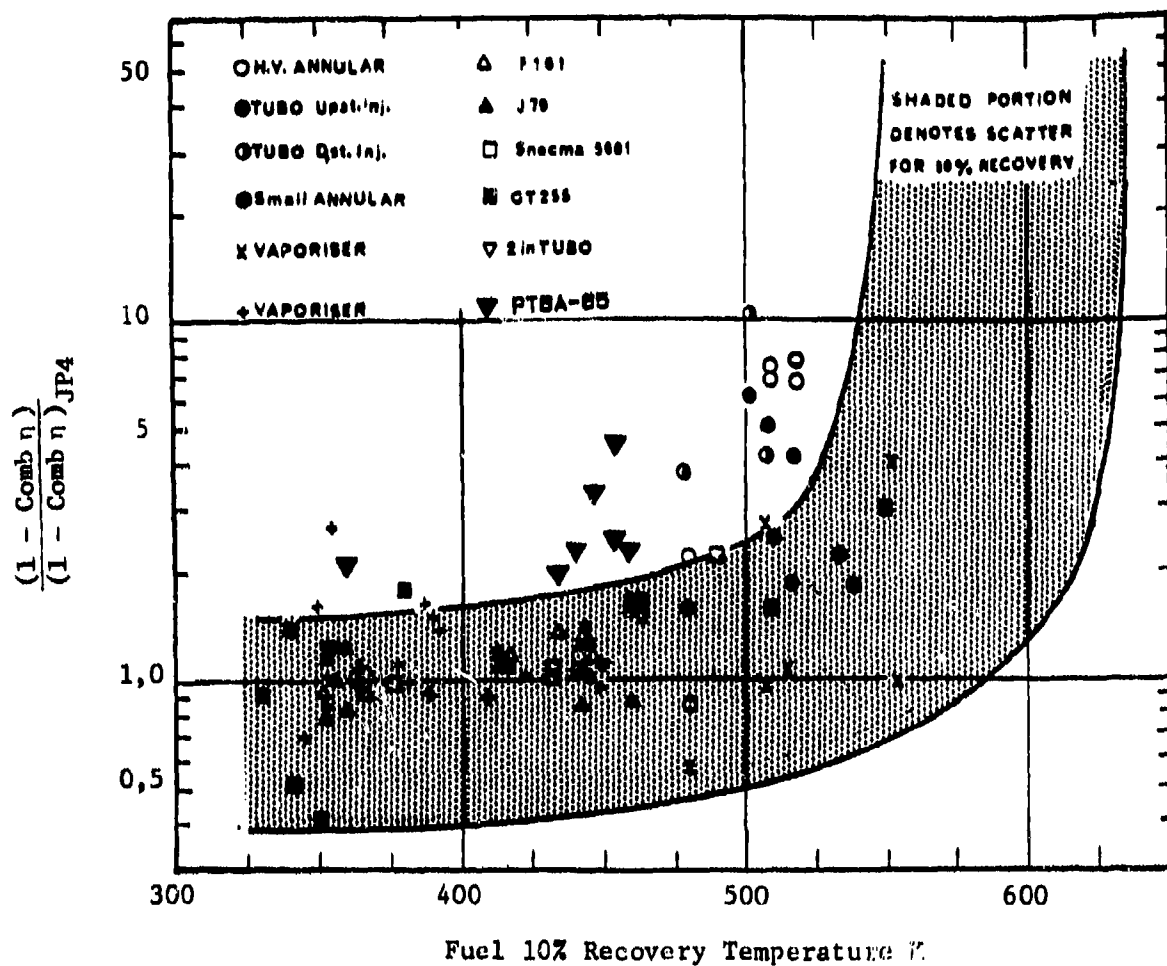


Figure 6.146: Effect of Fuel Volatility on Relative Combustion Inefficiency

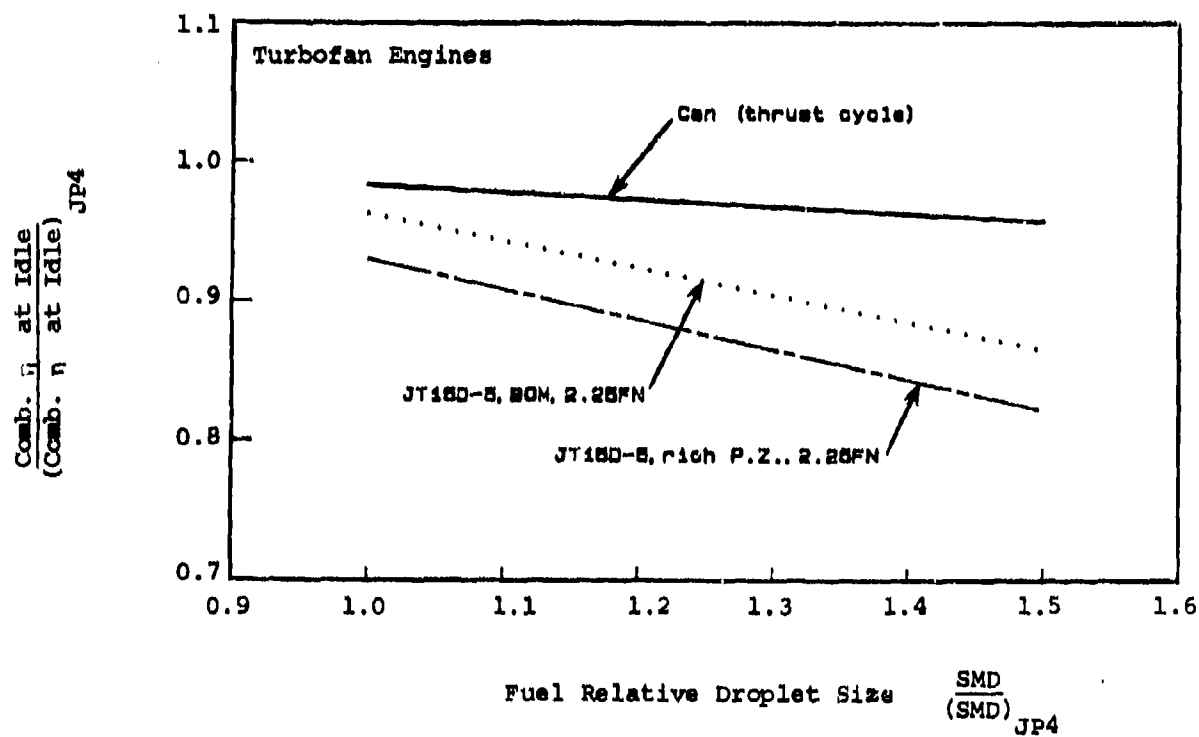
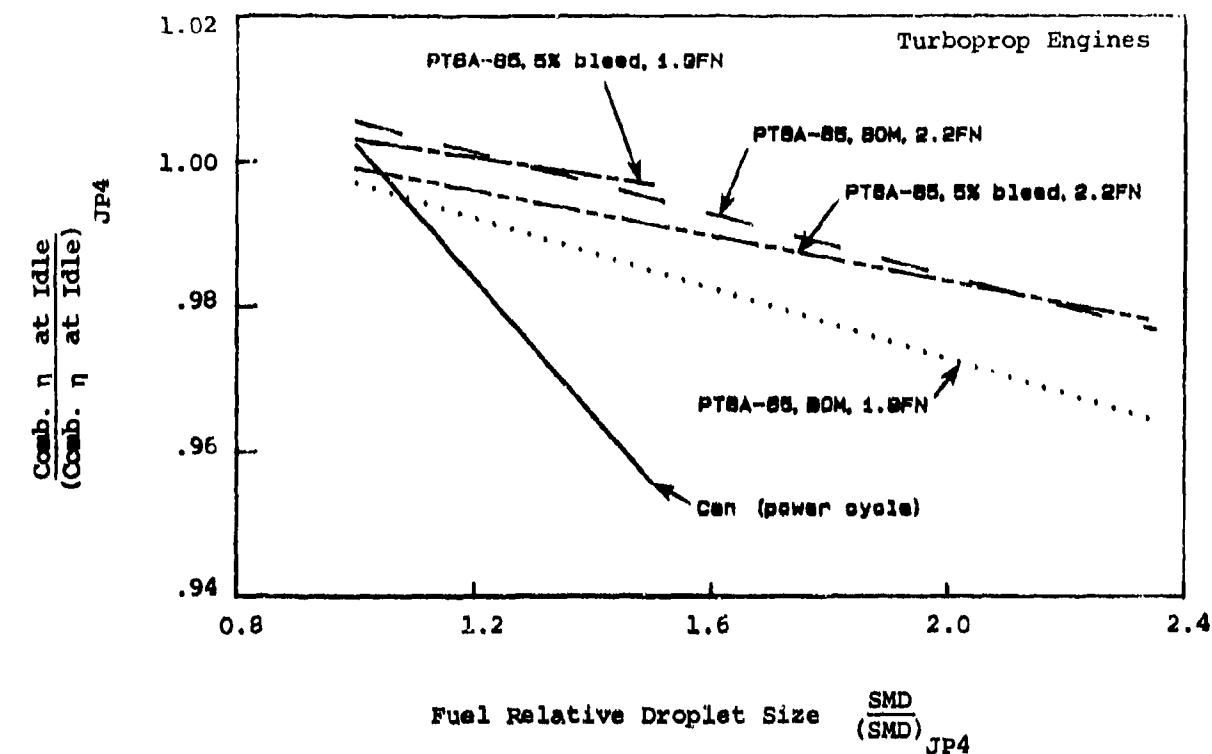


Figure 6.147: Effects of Fuel Droplet Size on Relative Idle Combustion Efficiency

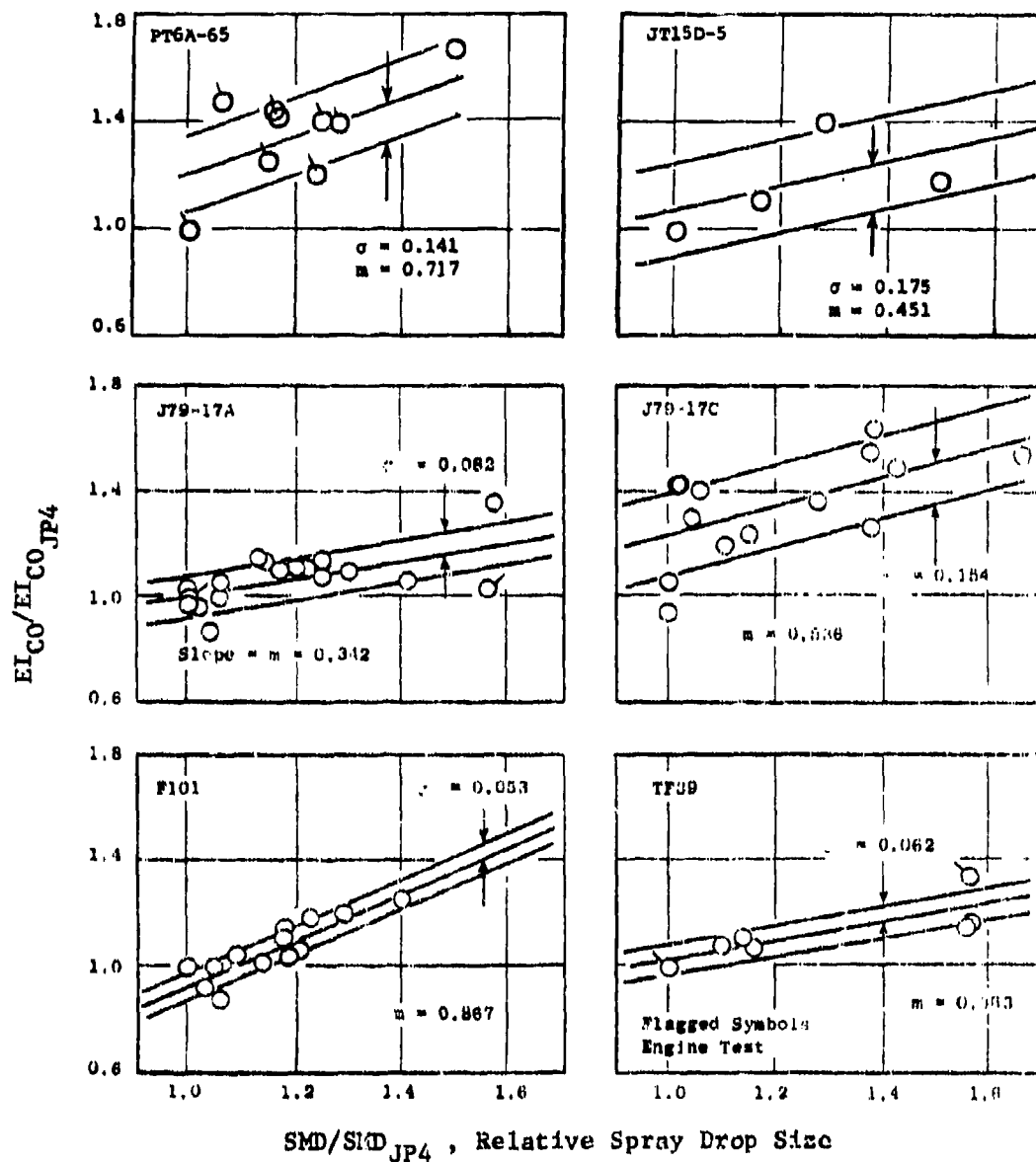


Figure 6.148: Effects of Relative Spray Droplet Size on Idle Emissions

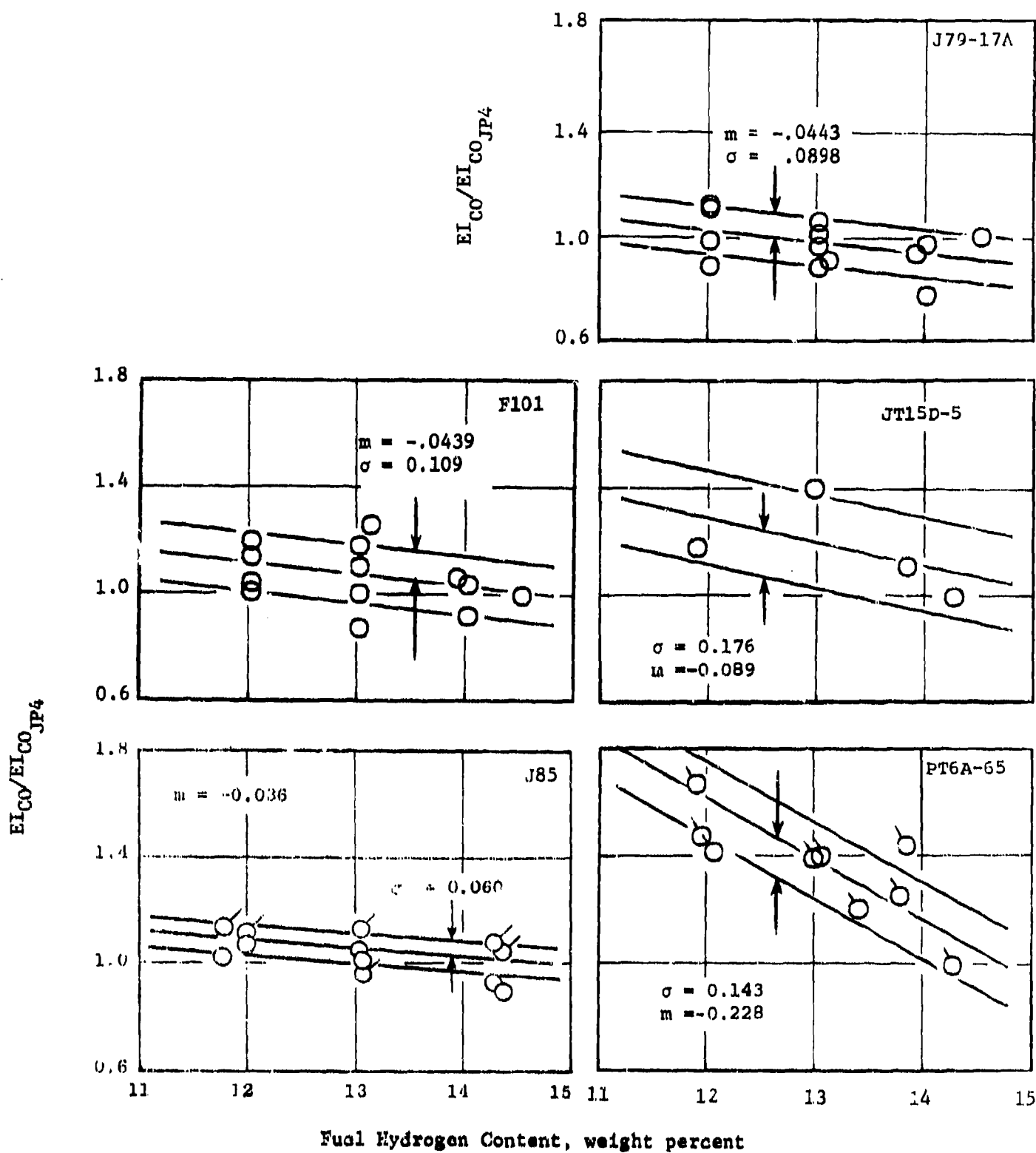


Figure 6.149: Effect of Fuel Hydrogen Content on Idle CO Emissions

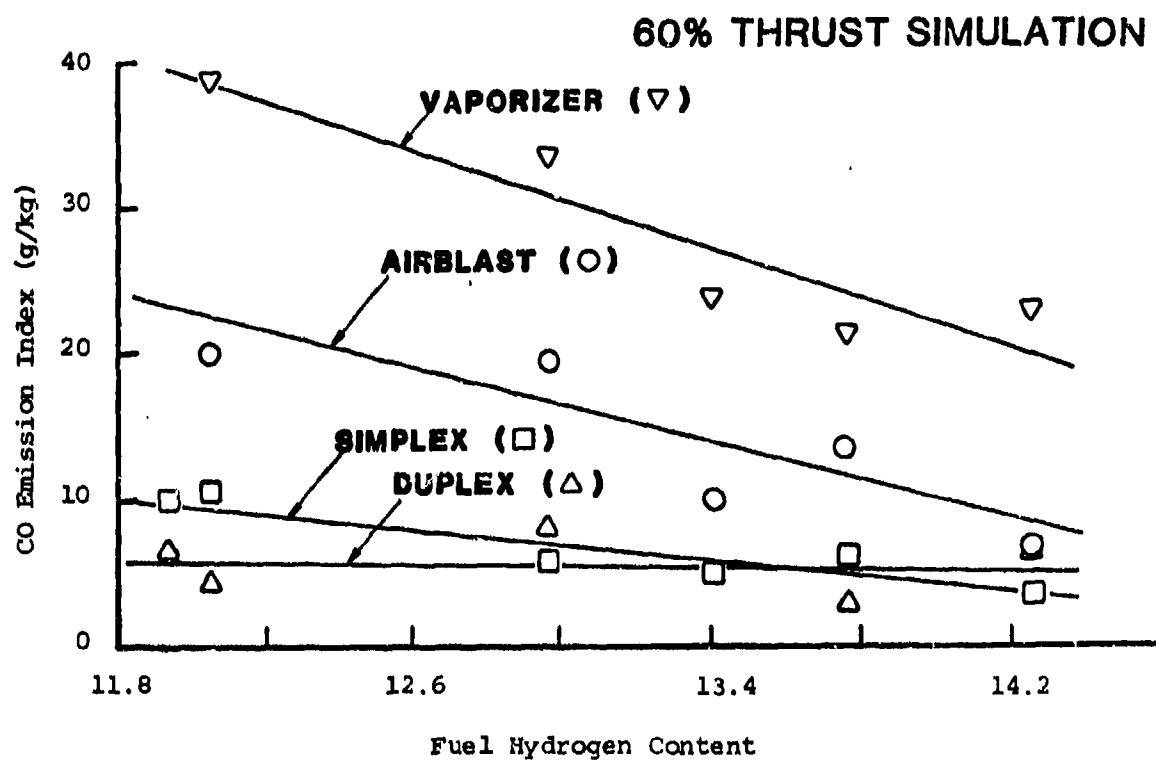


Figure 6.150: Effect of Fuel Hydrogen Content on CO Emission Index
(Can Combustor Tests, Nozzle Comparison)

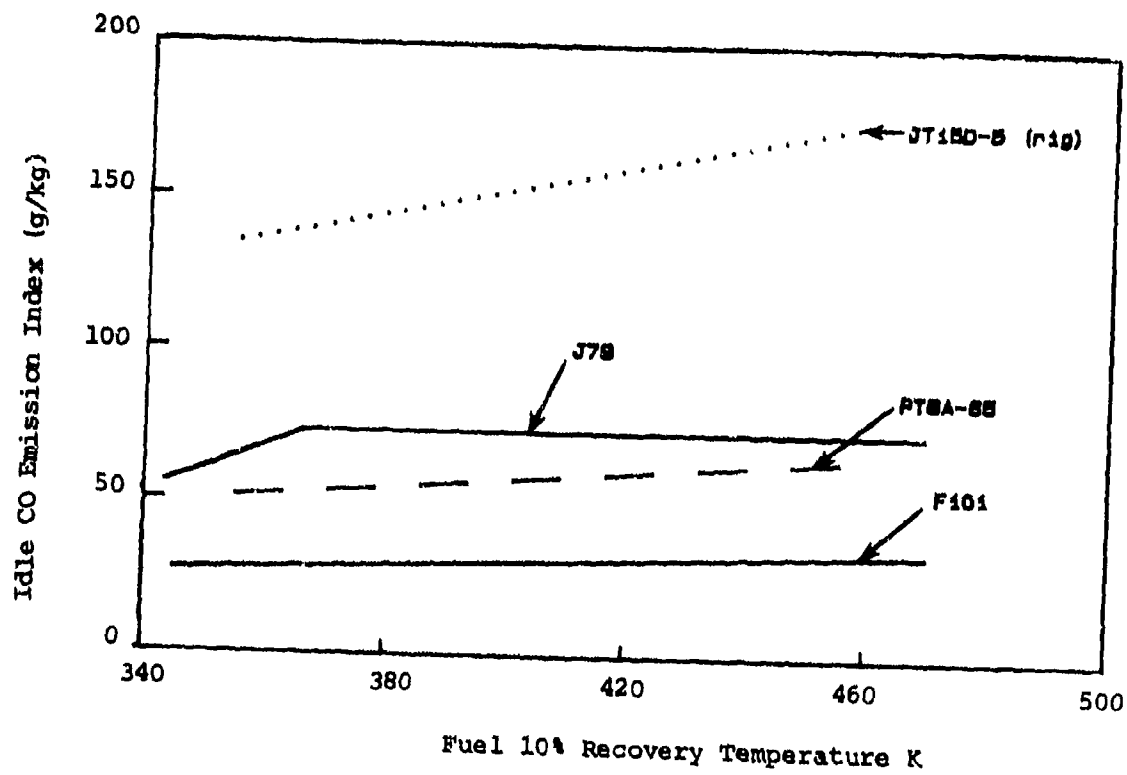


Figure 6.151: Effect of Fuel Volatility on Idle CO Emissions

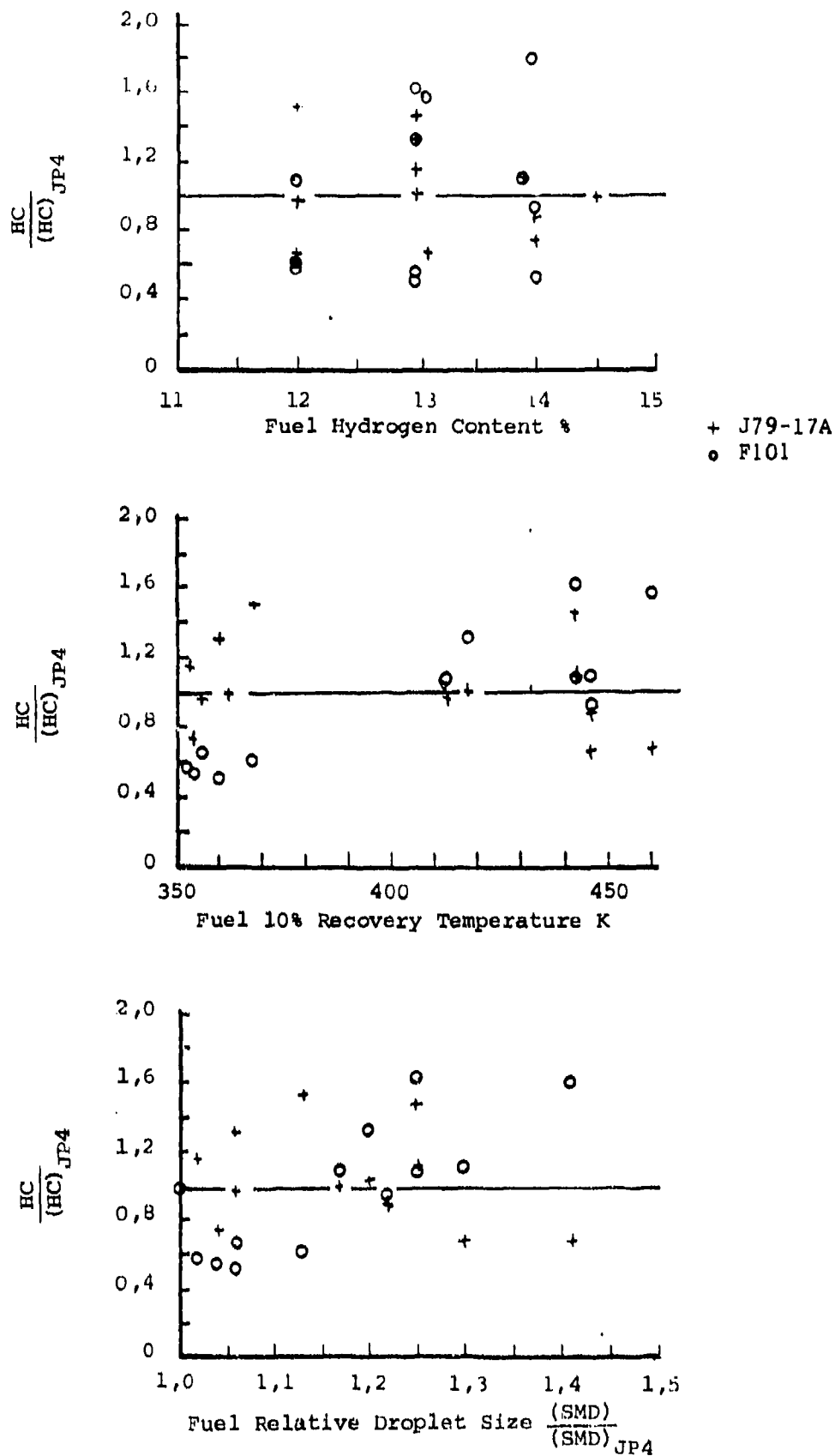


Figure 6.152: Effects of Fuel Properties on Relative HC Emissions

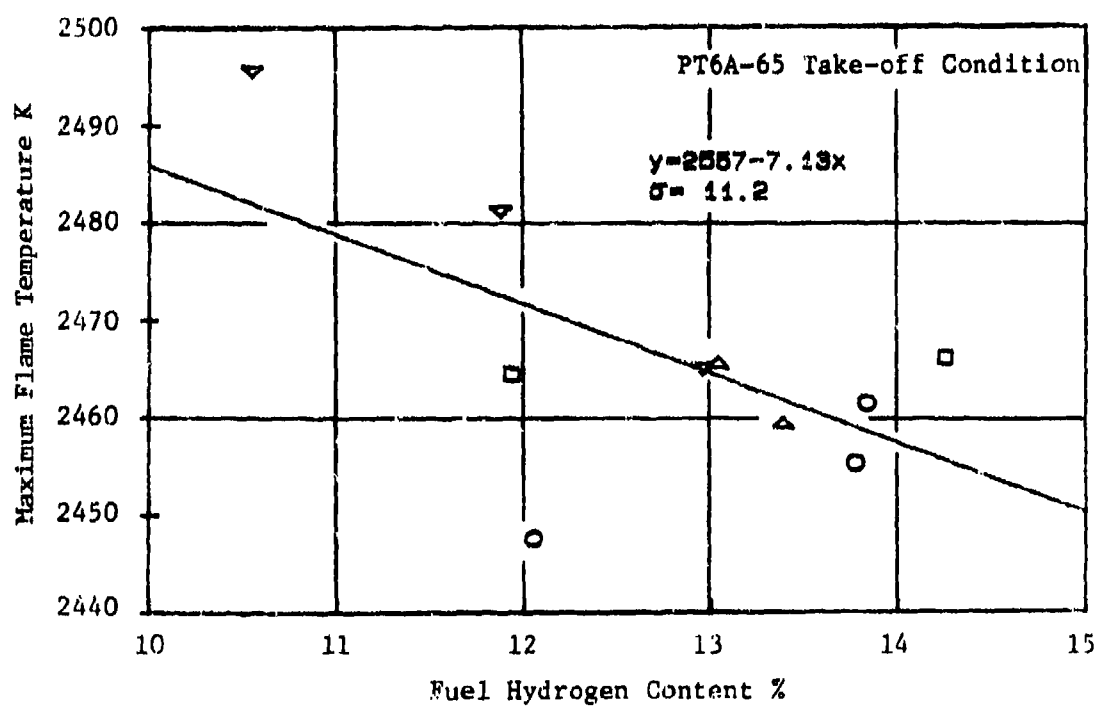


Figure 6.153: Effect of Fuel Hydrogen Content on Maximum Flame Temperature

EI_{NO_x}/EI_{NO_x} JP4

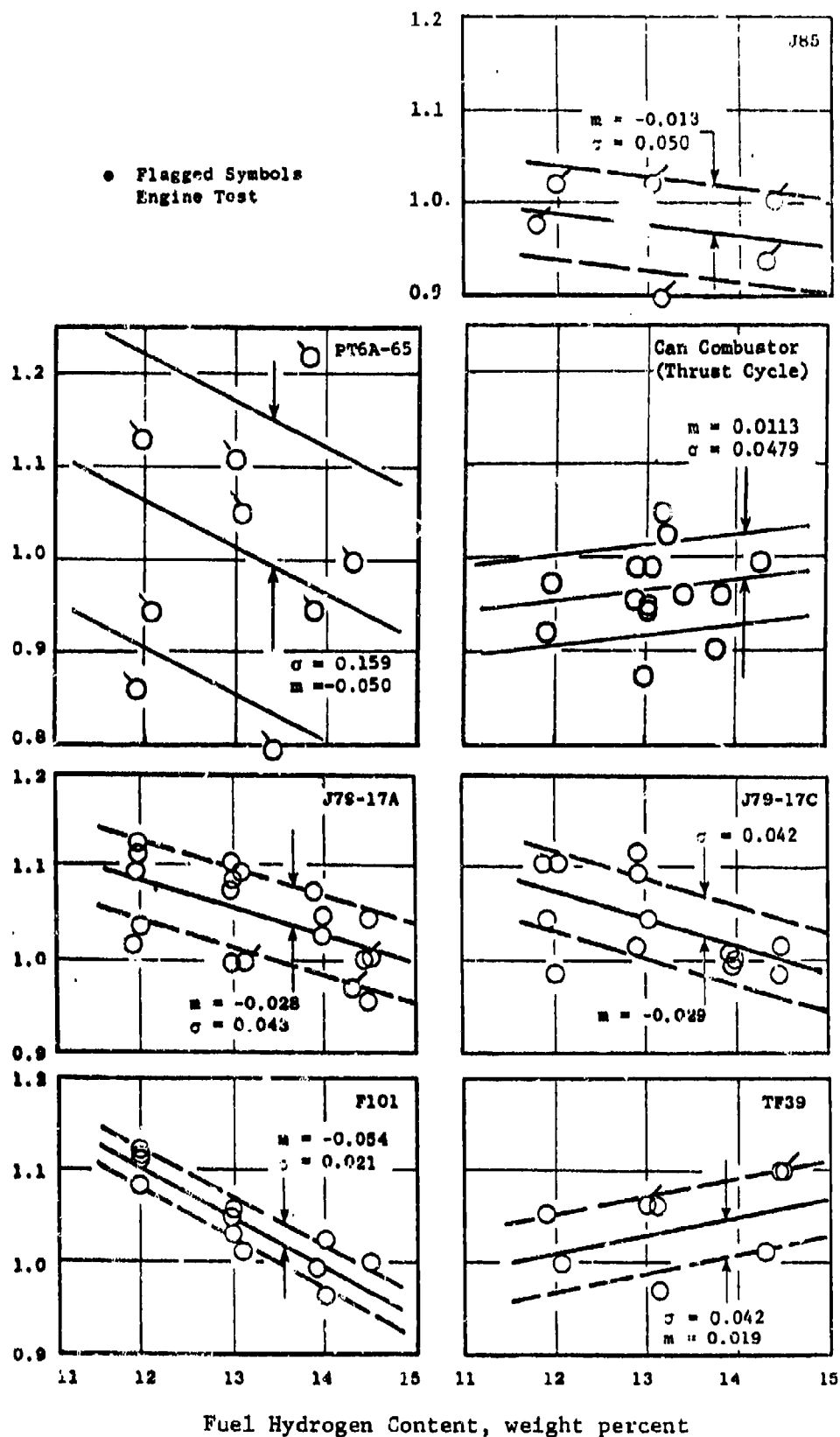


Figure 6.154: Effect of Fuel Hydrogen Content on Take-Off NO_x Emissions

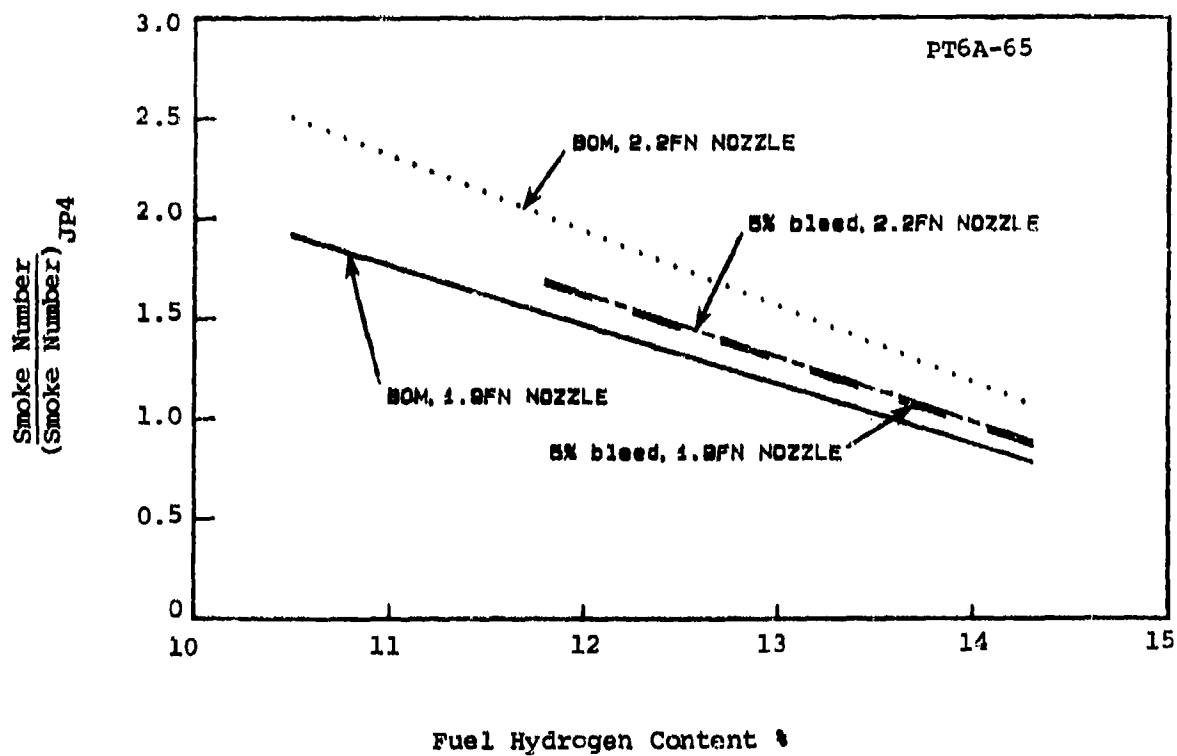


Figure 6.155: Effect of Fuel Hydrogen Content on Relative Smoke Number (PT6A-65 Nozzle/Stoichiometry Comparison)

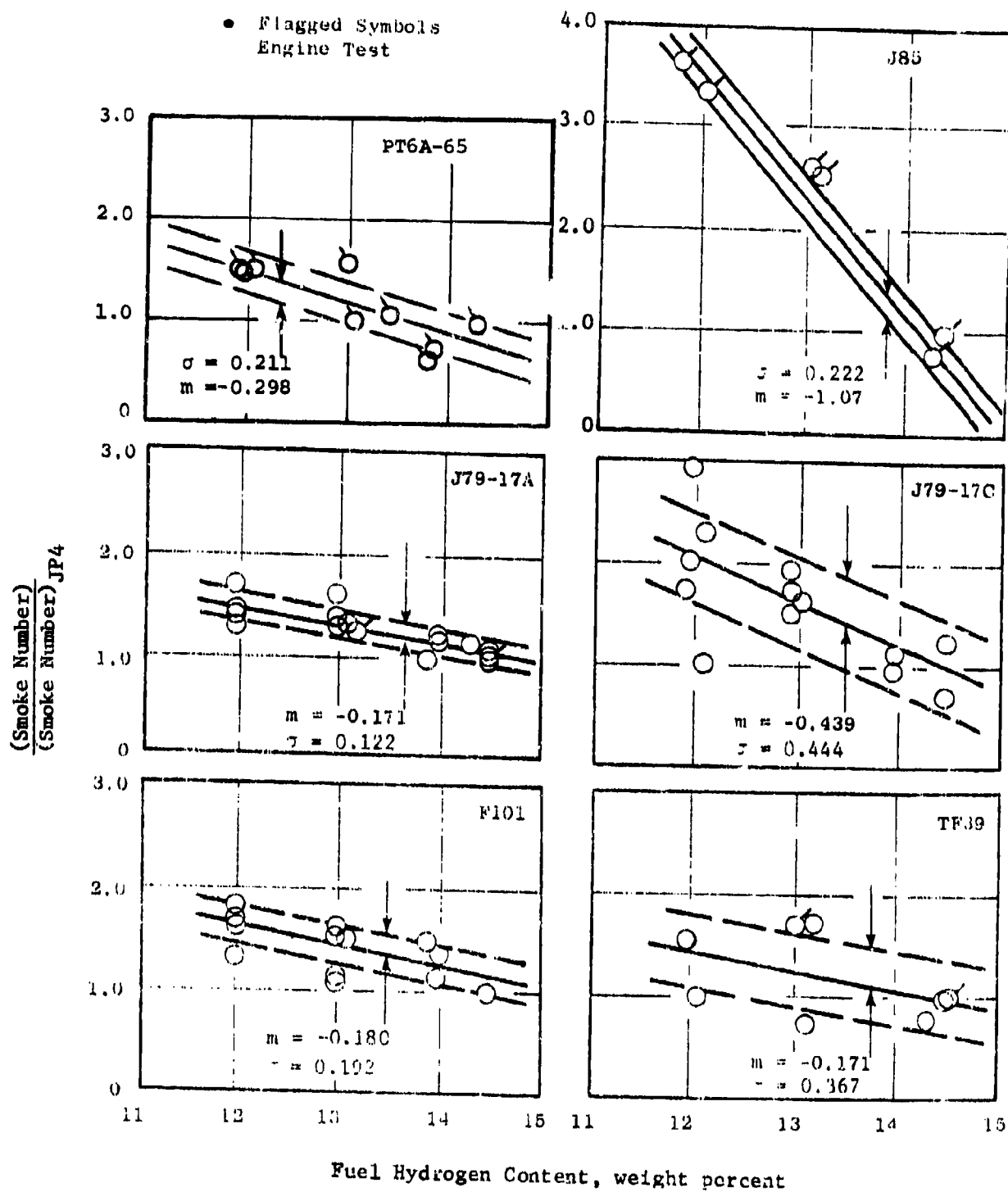


Figure 6.156: Effect of Fuel Hydrogen Content on Take-Off Smoke Emissions

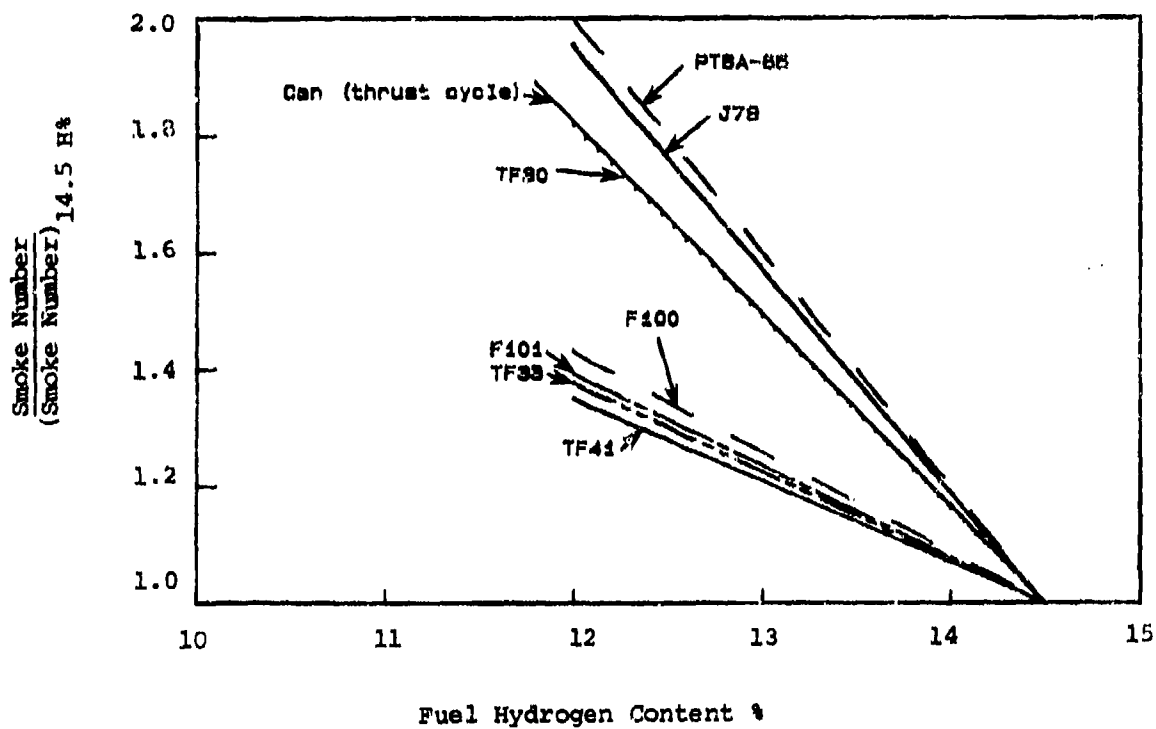


Figure 6.157: Effect of Fuel Hydrogen Content on Relative Smoke Number

T_{Amb} , Minimum Lightoff Temperature, K (Nominal Fuel Schedule)

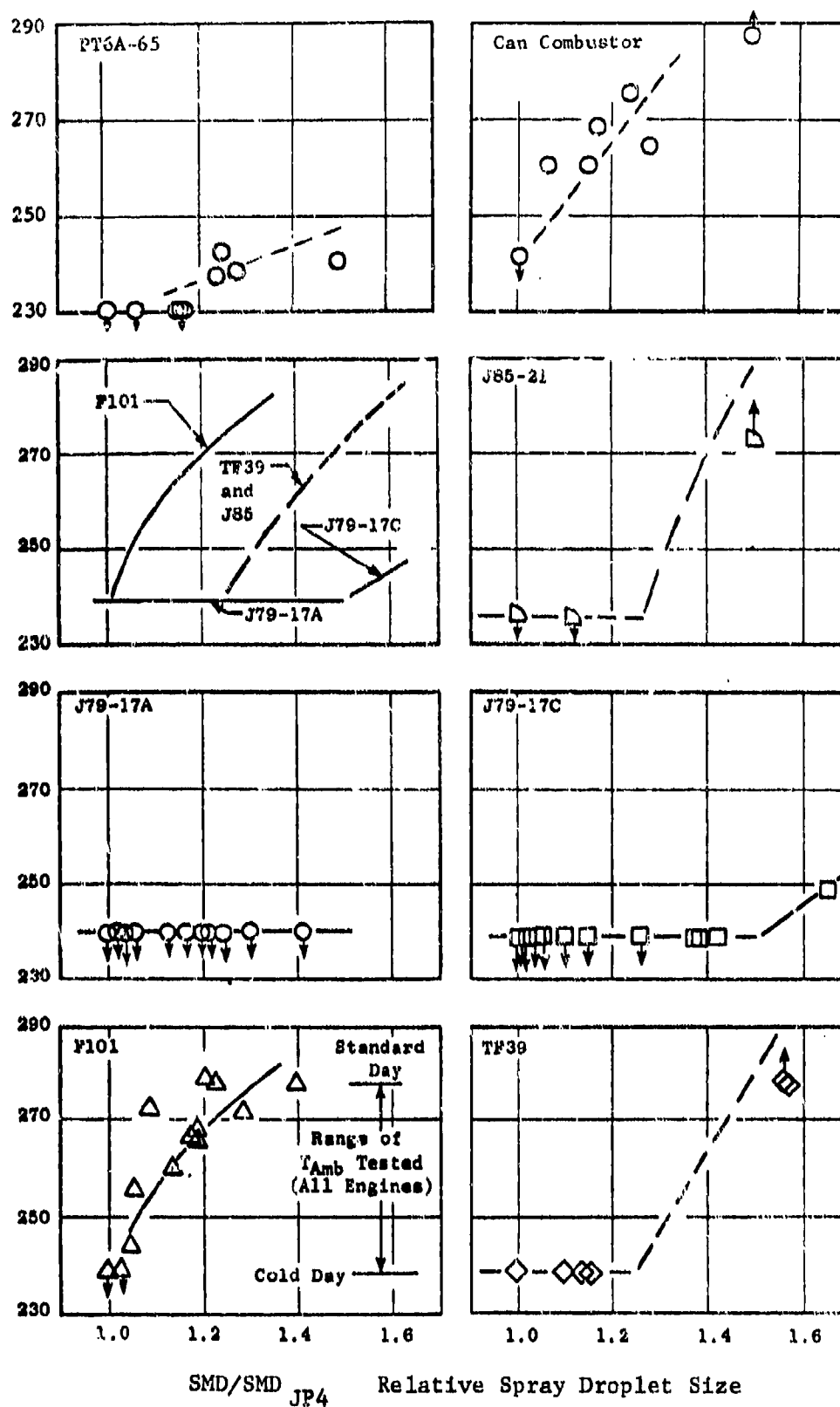


Figure 6.158: Effect of Relative Spray Droplet Size on Starting Characteristics

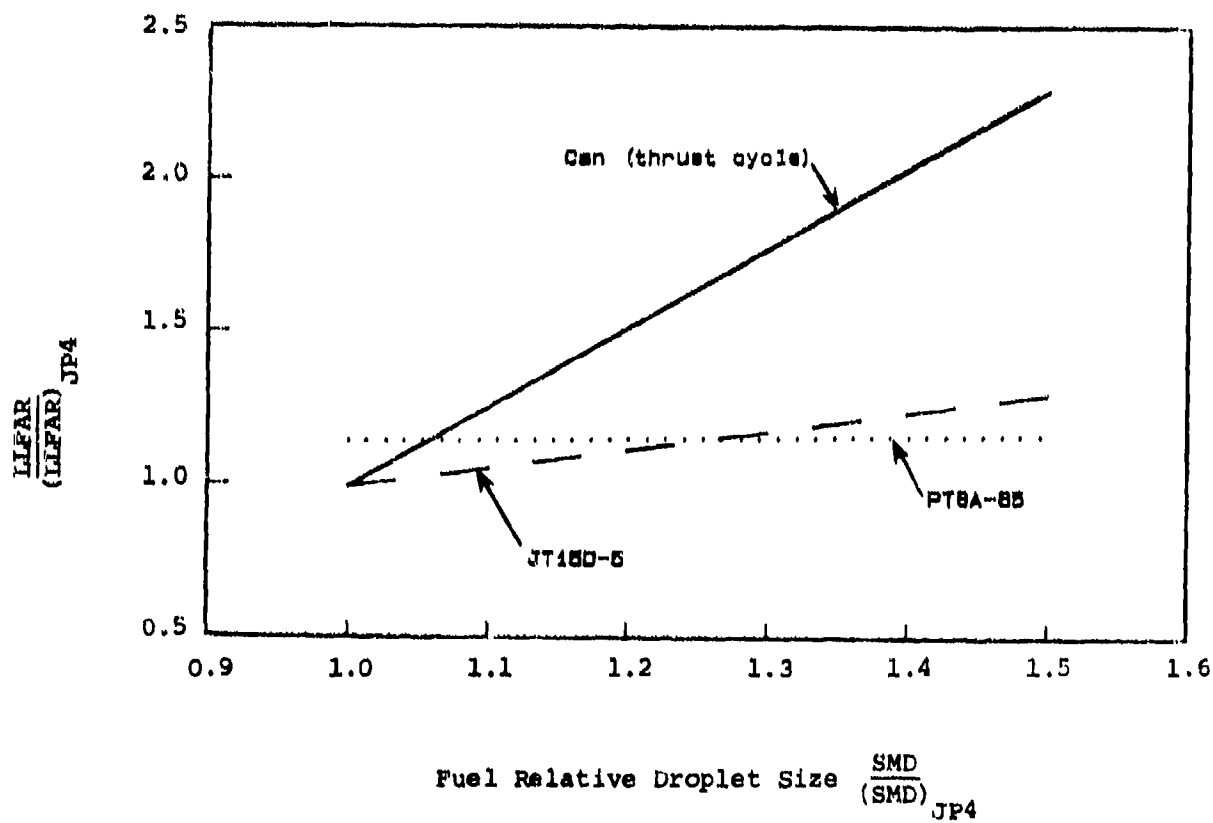
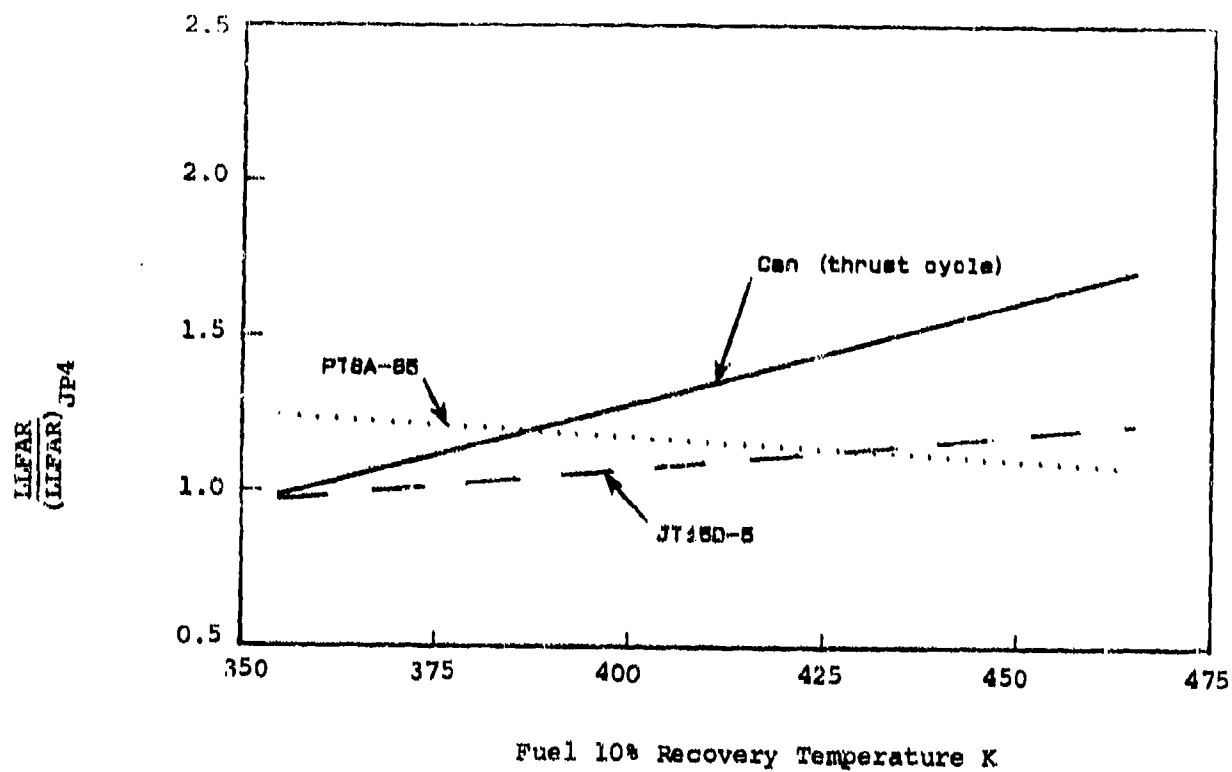


Figure 6.159: Effects of Fuel Properties on Relative Lean Stability Limits

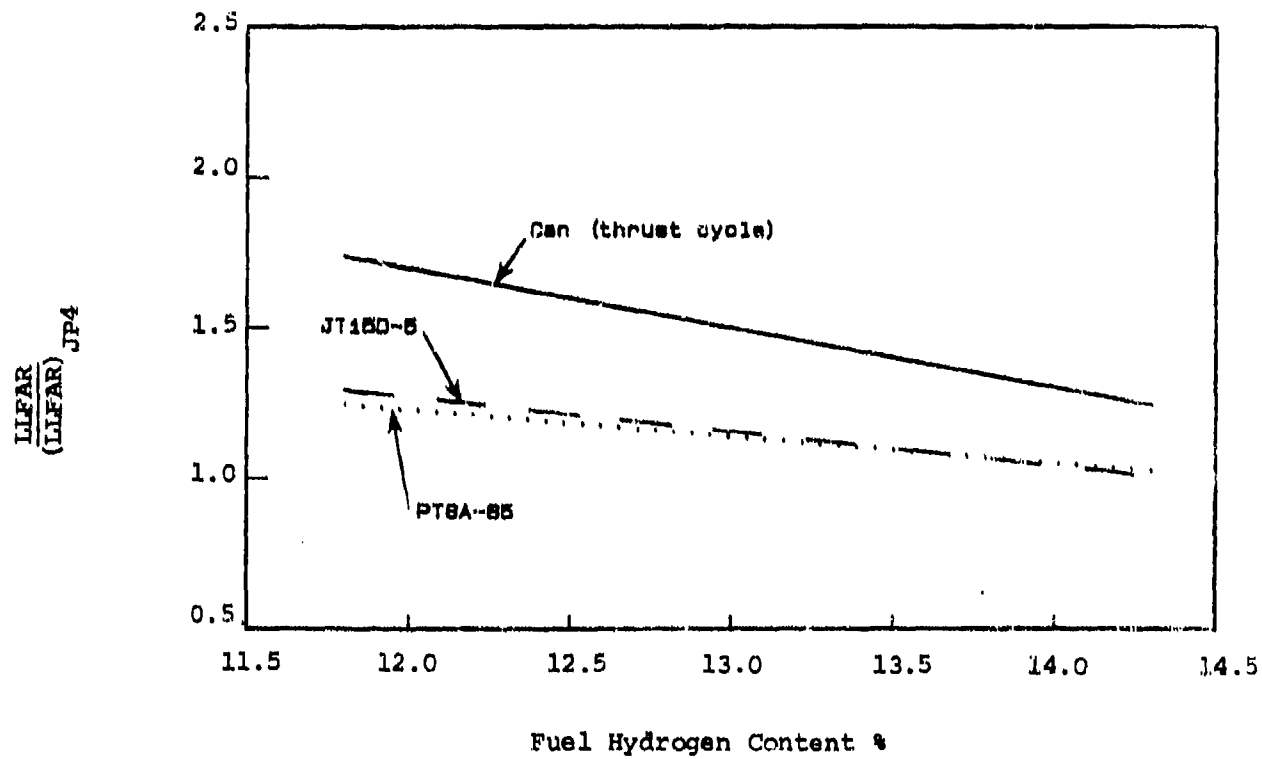


Figure 6.160: Effect of Fuel Hydrogen Content on Relative Lean Stability Limits

Peak Liner Temperature Rise
 $\frac{(T_L - T_3)}{(T_L - T_3)_{JP4}}$

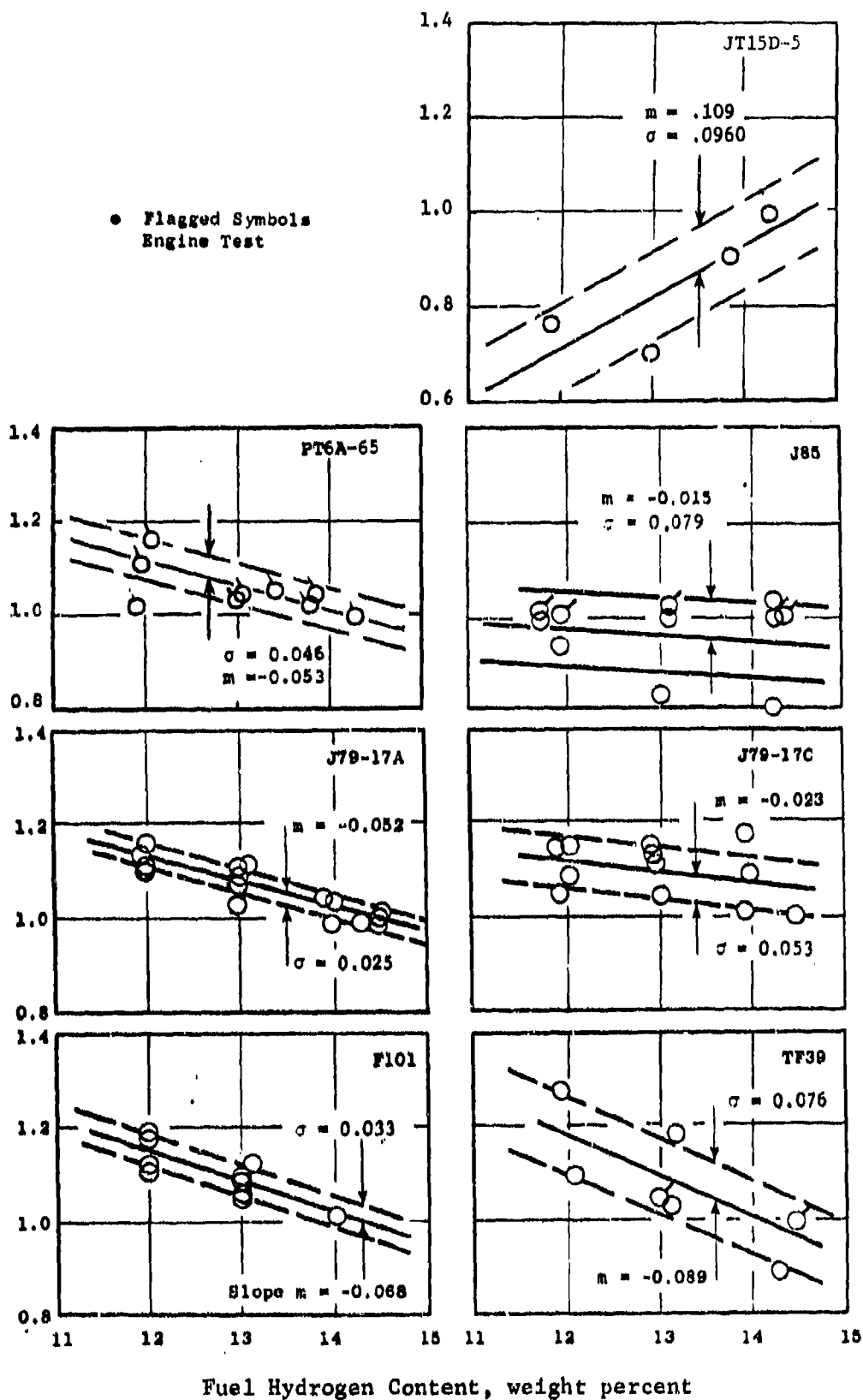


Figure 6.161: Effect of Fuel Hydrogen Content on Peak Liner Temperatures

$\frac{(T_L - T_3)}{(T_L - T_3)_{JP4}}$ Average Liner Temperature Rise

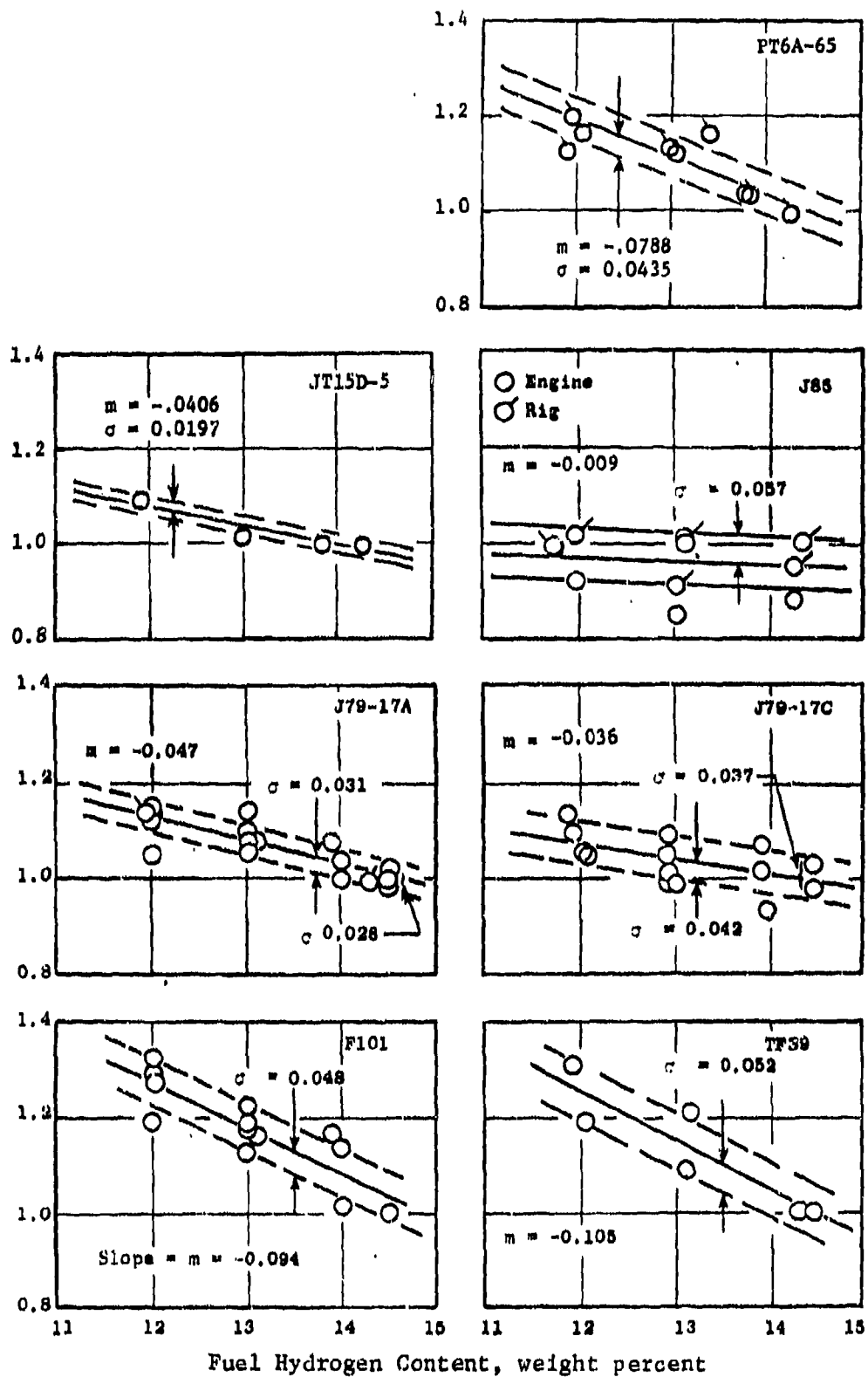


Figure 6.162: Effect of Fuel Hydrogen Content on Average Liner Temperatures

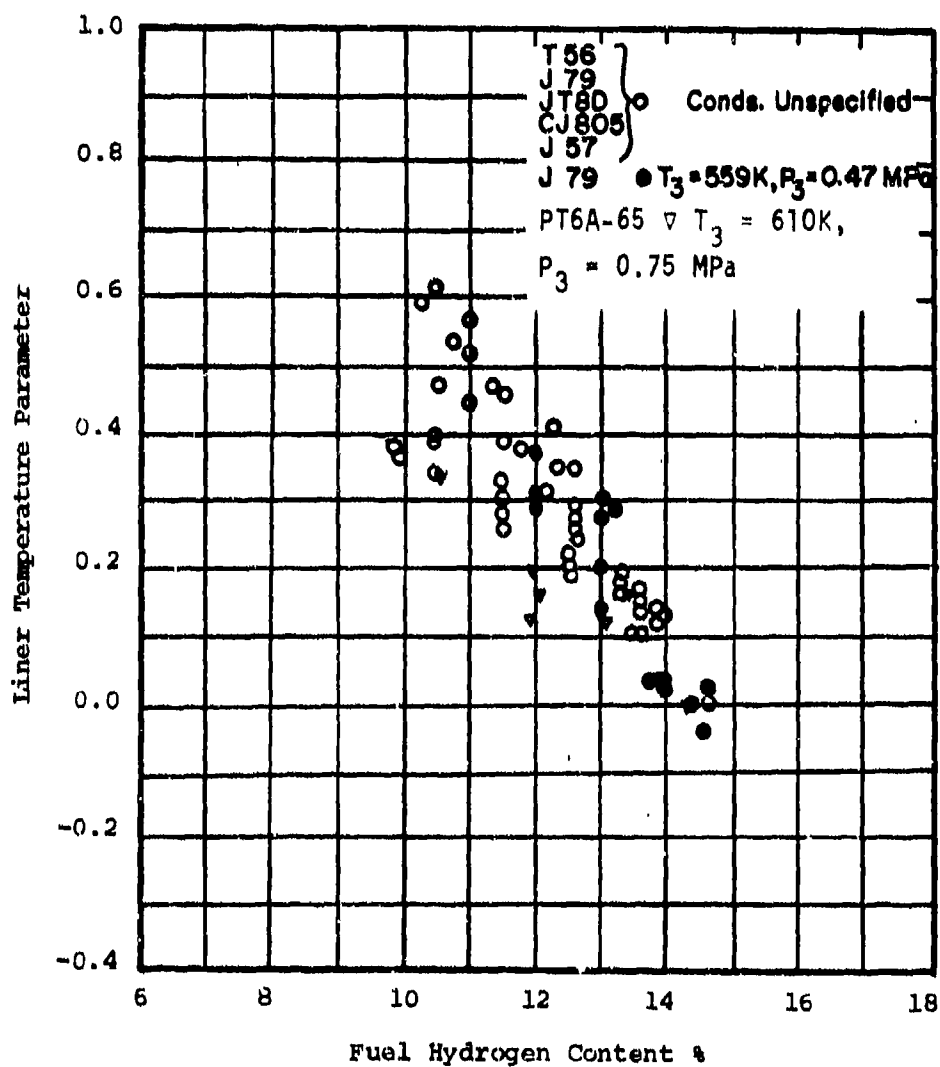


Figure 6.163: Effect of Fuel Hydrogen Content on Liner Temperature

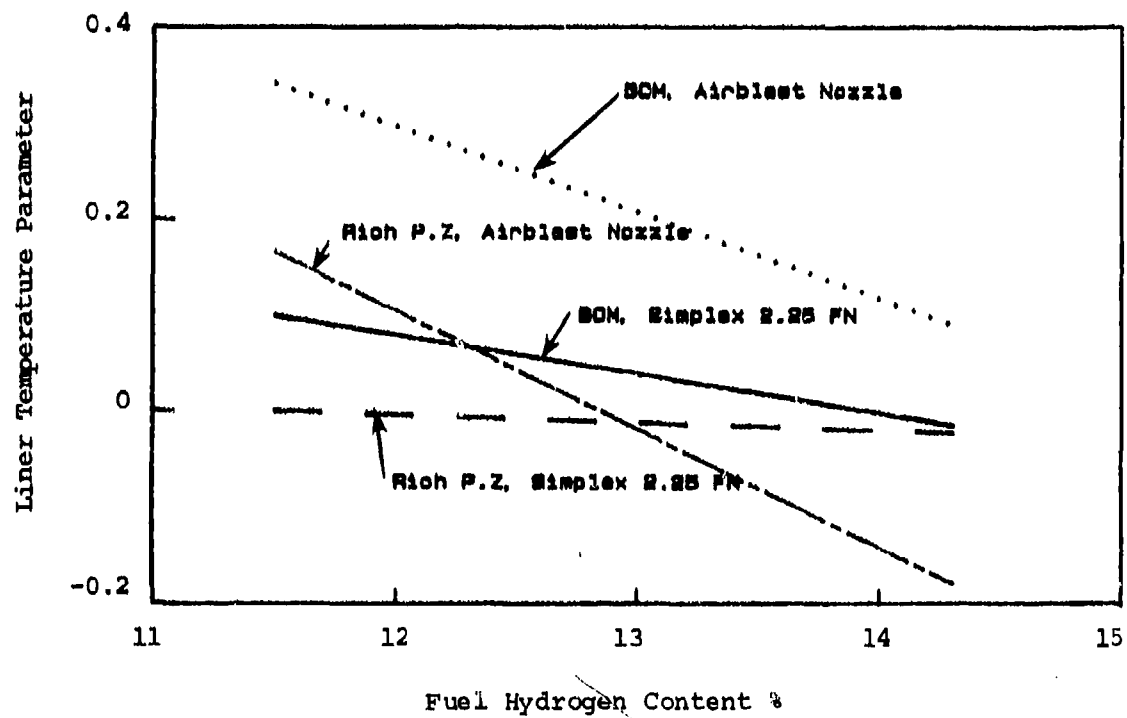
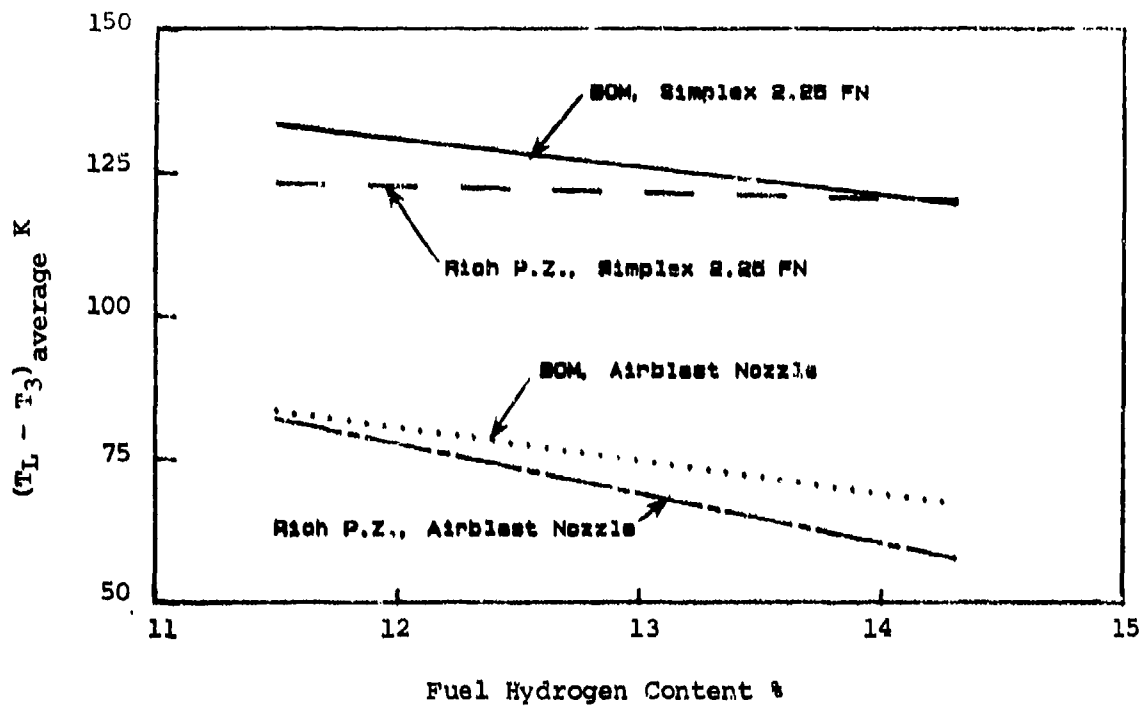


Figure 6.164: Effects of Fuel Hydrogen Content on Liner Temperatures (JT15D-5 Nozzle/Stoichiometry Comparison)

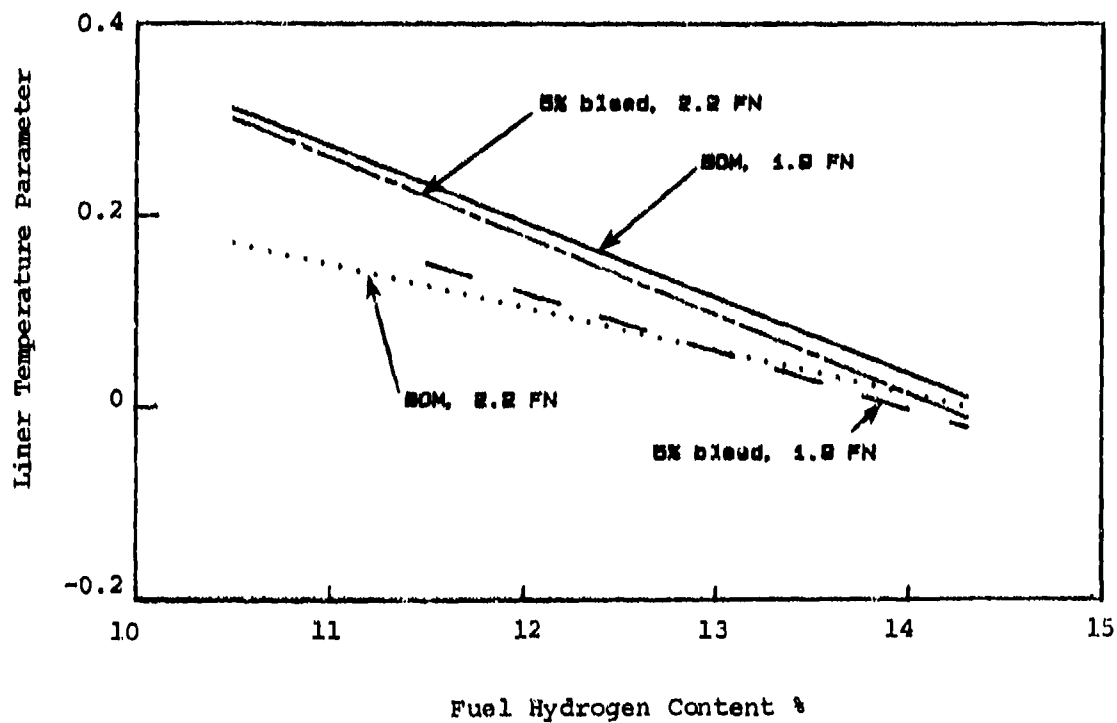
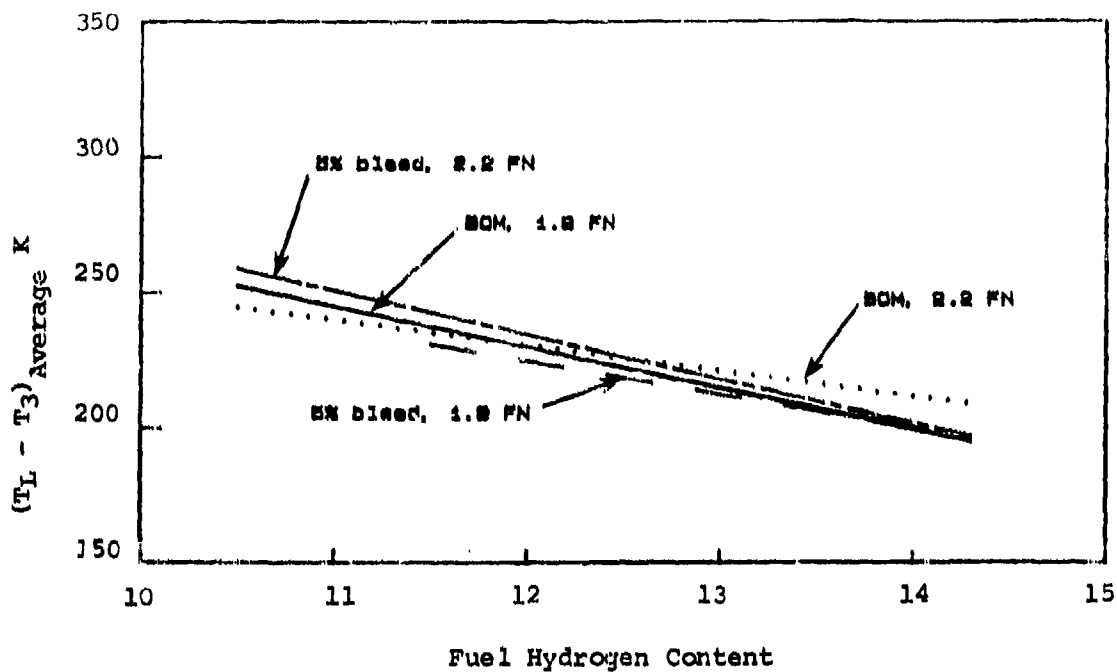


Figure 6.165: Effects of Fuel Hydrogen Content on Liner Temperatures (PT6A-65 Nozzle/Stoichiometry Comparison)

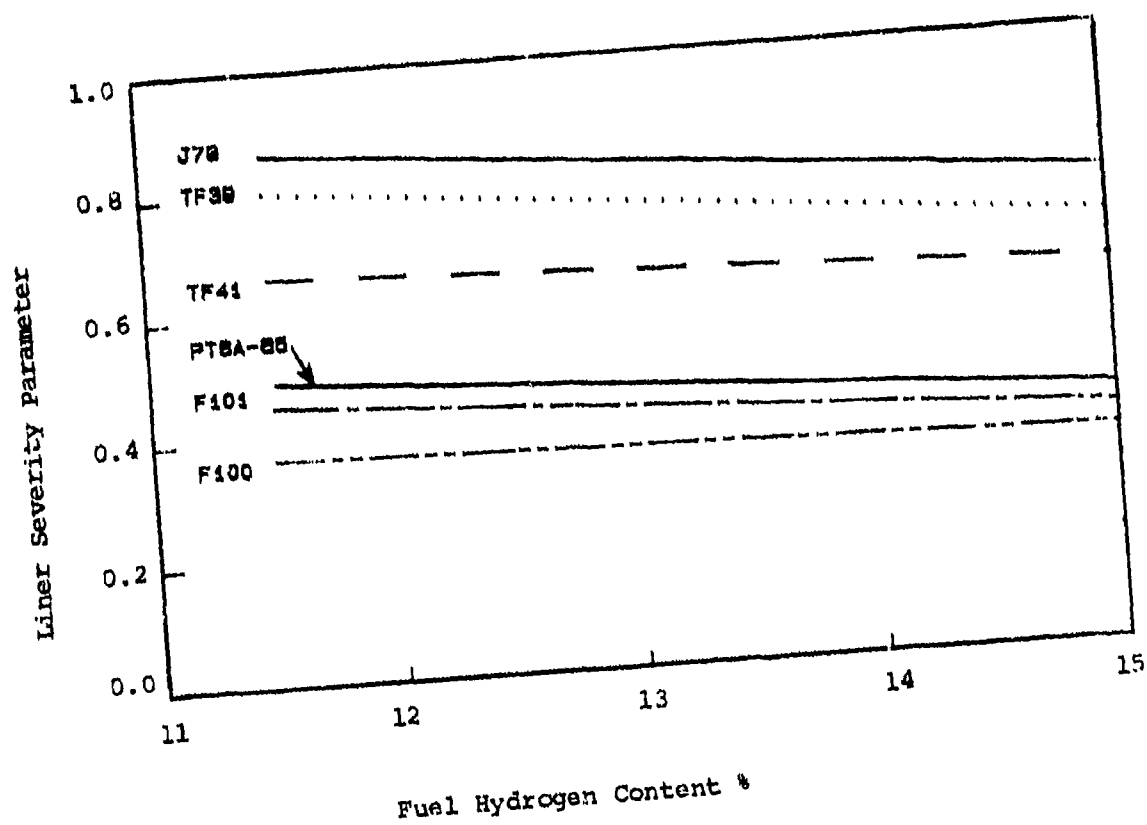


Figure 6.166: Effect of Fuel Hydrogen Content on Liner Severity Parameter

SECTION VII

CONCLUSIONS AND RECOMMENDATIONS

Based on the test programs involving the 'can' and reverse-flow-annular combustion systems, several conclusions and recommendations are presented.

7.1 Conclusions

- a) Fuel properties such as volatility, viscosity and hydrogen content have significant impact on the performance of the small gas turbine combustors tested. The effects are influenced by the type of combustor and also by the type and performance of the fuel injection system.
- b) Lean blow out stability is influenced by fuel hydrogen content and spray quality. The effects are particularly strong with the can and JT15D reverse-flow-annular combustion systems which both have axial fuel injectors. However with the PT6A reverse-flow-annular combustion system, which has tangentially spraying fuel nozzles, the effects of fuel hydrogen content and spray quality on lean blow out stability are less dominant, possibly because of stronger interaction between fuel sprays in the front of the liner, thereby maintaining more uniform thermal gradients around the liner circumference.

Volatility effects are mixed: for JP4 based fuels volatility appears to have little effect on lean blow out performance, whereas for other fuels volatility has a stronger effect. During can combustor evaluation, airblast and vaporizer nozzles had worse lean blow-out limits than pressure atomizing nozzles; during JT15D-5 evaluation, airblast nozzles displayed poorer stability than pressure atomizing nozzles.

- c) Ignition performance is strongly influenced by fuel properties. With the can combustor, minimum light off fuel-air ratio and minimum light-up temperatures are strongly influenced by volatility and by properties affecting fuel atomization. The same evaluation indicates fuel hydrogen content has a relatively weak influence on light-up characteristics. PT6A engine start-up tests indicate both ignition and propagation (light-around) performance are influenced by fuel properties.
- d) Low end combustion efficiencies are significantly influenced by both the chemical and physical properties of the fuel with all tested combustion systems.
- e) CO emissions are strongly influenced by fuel hydrogen content, but correlations with relative droplet size are stronger with reverse-flow annular combustion systems than with straight-through annular combustion systems.
- f) Hydrocarbon emissions are strongly influenced by fuel hydrogen content and relative droplet size.

- g) NO_x emissions at take-off are relatively insensitive to fuel properties and with the can combustion system, variations were within the range of data repeatability. NO_x emissions at idle appear to be influenced by combustion efficiency which affects reaction zone temperatures.
- h) Smoke levels are strongly affected by fuel hydrogen content, aromatic content and atomizer design. The nature of the aromatics appears to influence smoke emissions as well.
- i) Radiation heat loads and liner temperatures are strongly influenced by fuel hydrogen content and by factors affecting fuel atomization characteristics.
- j) Carbon check tests with the can combustion system were inconclusive, possibly because of carbon shedding with several fuels. Similar checks were not made with the reverse-flow-annular combustion system but there was no evidence of turbine blade erosion from the limited gas generator testing. No fuel spray deterioration was observed with any of the nozzles or test fuels.
- k) Combustor exit temperature distribution was influenced by changes in fuel composition and physical properties.

7.2

Recommendations

- a) Life prediction analysis based on observed liner temperature effects are recommended so that comparisons can be made with such predictions for other combustion systems.
- b) Combustion model studies are recommended to establish fuel property effects analytically. Test results from this program should be compared in detail with other published models so that more up-to-date correlations can be derived. Such models could be used to estimate fuel property effects on different types of combustion systems.
- c) Effects of parametric variations of aromatics, naphthalenes and hydrogen contents need further evaluation. Fuels chosen for the current program did not provide such a selective variation, hence the effects of fuel properties on performance parameters such as smoke were not clearly established.
- d) Additional work is required to evaluate fuel system fouling tendencies. Fuels with low thermal stability can have significant effects especially with the small passage sizes of fuel injectors used in small engines.

REFERENCES

1. Gratton, M., Sampath, P., "Alternate Fuels Combustion Research Phase II", Pratt & Whitney Canada, AFWAL-TR-83-2057, October 1983.
2. Coleman, J.R., Gallop, L.D., "Properties of Fuels Employed in a Gas Turbine Combustor Program", DREO Technical Note No. 82-42, September 1982.
3. Jackson, T. A., "The Evaluation of Fuel Property Effects in Air Force Gas Turbine Engines - Program Genesis", ASME 1980.
4. Gleason, C. C., et al., "Evaluation of Fuel Character Effects on J79 Engine Combustion System", General Electric Company, AFAPL-TR-79-2015, CEEDO-TR-79-06, June 1979.
5. Gleason, C. C., et al., "Evaluation of Fuel Character Effects on F101 Engine Combustion System", General Electric Company, AFAPL-TR-79-2018, CEEDO-TR-79-07, June 1979.
6. Jackson, T. A., Blazowski, W. S., "Fuel Hydrogen Content as an Indicator of Radioactive Heat Transfer in an Aircraft Gas Turbine Combustor, Gas Turbine Combustion and Fuels Technology", ASME, 1977.
7. Lohmann, R. P., Szetela, E. J., Vranos, A., "Analytical Evaluation of the Impact of Broad Specification Fuels on High Bypass Turbofan Engine Combustor", United Technologies Corporation, Pratt and Whitney Aircraft Group, Commercial Products Division, NASA CR-159454, PWA 5564-15, December 1978.
8. Demitri, E. P., Topping, R. F., Wilson, R. P., "Study of Research and Development Requirements of Small Gas Turbine Combustor", NASA CR-159796, ADL 83381-1, January 1980.
9. Moffat, R. J., Hunn, B. D., Ayers, J. F., "Development of a Transpiration Radiometer", Trans. Instrument Society of America, v. 9, 1971.
10. Blazowski, W. S., "Combustion Considerations for Future Jet Fuels", Proceedings of Sixteenth International Symposium on Combustion, August 1979.
11. Simmons, H. C., "The Prediction of Sauter Mean Diameter for Gas Turbine Fuel Nozzles of Different Types", Parker Hanfin, ASME Paper No. 79-WA/GT-5, 1979.
12. Olier, T. L., et al., "Fuel Mainburner/Turbine Effects", General Electric Company, AFWAL-TR-81-2100, 1981.

13. Advisory Group for Aerospace Research & Development (AGARD), "Propulsion and Energetics Panel Working Group 13 on Alternative Jet Engine Fuels", AGARD-AR-181-VOL.II.
14. Mosier, S. A., "Fuel Effects on Gas Turbine Combustion Systems", Pratt & Whitney Aircraft, AGARD Conference on Combustion Problems in Turbine Engines, AGARD-CPP-353, 1983.

APPENDIX A

JT15D-5 ATMOSPHERIC TEST DATA

Simplex 2.25 FN Nozzle, Bill of Material

FUEL	COND No.	T3 (K)	P3 (kPa)	Wf kg/hr	W3 (kg/s)	T4 Ideal (K)	Smoke Number	EI (NOx) (g/kg)	EI (CO) (g/kg)	EI (HC) (g/kg)	EI (CO2) (g/kg)	TL (ave) (K)	TL (peak) (K)	Profile Factor	LLFAR (g/kg)
Shale JF8	Idle	409.4	103.0	39.6	1.224	761.1	0.2	3.8	153.5	210.2	2338.1	444.7	487.2		6.36
	30 %	508.9	103.8	42.7	1.135	904.8	0.0	5.6	109.4	91.6	2733.5	568.9	649.2		
	70 %	607.2	103.9	53.6	1.008	1142.0	0.0	8.3	31.2	4.1	3097.1	719.7	843.8		
	100%	651.7	104.0	61.4	0.976	1266.9	0.0	12.9	6.7	3.1	3146.3	773.3	939.2	0.035	0.235
JP10	Idle	409.4	103.4	40.8	1.249	764.9	1.5	3.8	163.3	214.5	2381.8	443.5	508.3		7.14
	30 %	507.8	104.0	44.2	1.161	908.4	1.1	3.8	125.4	62.0	2860.7	574.9	654.0		
	70 %	606.7	104.5	55.4	1.036	1144.7	0.7	3.6	33.8	0.4	3173.9	722.3	829.9		
	100%	651.7	104.3	61.8	0.979	1272.8	1.1	4.0	3.4	0.4	3221.7	784.8	890.6	0.063	0.273
EP8S-3	Idle	409.4	103.0	40.3	1.223	766.9	2.0	5.4	193.5	237.9	2230.4	446.8	498.3		6.07
	30 %	508.3	103.9	43.9	1.152	908.2	1.3	2.7	138.0	95.6	2736.3	572.0	659.4		
	70 %	607.8	104.1	54.6	1.024	1143.6	1.5	2.7	74.3	13.6	3034.5	711.3	823.1		
	100%	651.7	104.1	61.1	0.969	1271.8	1.5	4.3	6.5	3.5	3165.8	775.4	873.6	0.031	0.217
JP4	Idle	410.0	103.5	39.4	1.235	757.5	0.7	4.8	137.6	127.6	2573.9	454.9	508.3		5.50
	30 %	507.8	103.9	42.4	1.138	900.3	0.3	5.9	102.9	38.0	2872.2	586.1	647.3		
	70 %	606.1	104.1	53.1	1.017	1132.2	1.0	3.2	24.1	6.6	3065.2	707.5	849.9		
	100%	651.7	104.0	59.4	0.963	1259.5	0.5	3.1	6.0	3.2	3123.0	773.1	968.7	0.022	0.209

Airblast Nozzle, Bill of Material

FUEL	COND No.	T3 (K)	P3 (kPa)	Wf kg/hr	W3 (kg/s)	T4 Ideal (K)	Smoke Number	EI (NOx) (g/kg)	EI (CO) (g/kg)	EI (HC) (g/kg)	EI (CO2) (g/kg)	TL (ave) (K)	TL (peak) (K)	Profile Factor	LLFAR (g/kg)
Shale JF8	Idle	409.4	103.4	40.1	1.240	760.8	2.5	0.4	160.4	75.1	2698.7	444.7	489.7		4.76
	30 %	507.9	104.1	44.0	1.160	906.7	1.3	1.4	97.2	28.9	2825.2	551.8	629.8		
	70 %	606.1	104.2	54.6	1.028	1140.7	0.7	2.6	40.5	4.8	3080.5	666.1	766.7		
	100%	652.1	104.1	61.2	0.976	1268.3	0.0	2.5	7.4	1.4	3141.9	722.5	834.7	0.043	0.314
JP10	Idle	409.4	103.4	40.1	1.238	762.0	0.7	0.5	166.6	147.2	2561.9	446.0	515.2		5.14
	30 %	508.9	103.9	43.6	1.147	910.9	1.0	0.9	123.6	37.7	2930.3	554.0	640.4		
	70 %	606.4	104.2	54.9	1.024	1145.0	1.0	4.1	57.3	1.6	3133.9	687.2	770.1		
	100%	651.7	104.4	61.5	0.975	1271.7	1.0	2.5	11.4	0.4	3209.2	726.1	839.1	0.061	0.344
EP8S-3	Idle	408.9	103.3	40.4	1.238	763.5	4.4	0.5	158.1	107.2	2645.5	445.5	509.1		5.74
	30 %	507.9	104.3	43.9	1.183	899.2	1.5	0.9	98.5	31.6	2947.0	554.7	643.3		
	70 %	606.1	104.1	54.7	1.026	1142.6	0.7	2.5	59.2	3.8	3085.0	678.1	802.0		
	100%	652.2	104.2	62.1	0.976	1277.6	0.2	2.2	8.6	0.9	3172.4	740.0	878.2	0.035	0.288
JP4	Idle	410.0	103.3	38.7	1.209	757.9	0.1	0.2	86.1	109.0	2706.0	436.7	503.2		7.14
	30 %	509.6	103.7	42.2	1.119	906.4	0.1	1.0	87.7	69.8	2811.3	547.3	600.0		
	70 %	607.1	104.1	52.9	0.996	1141.5	0.1	2.0	34.7	8.7	3062.6	659.8	723.7		
	100%	652.2	104.0	59.1	0.945	1267.3	0.0	1.3	11.2	2.1	3117.7	714.1	794.0	0.051	0.285

Simplex 2.25 FN Nozzle, Rich Primary Zone

FUEL	COND No.	T3 (K)	P3 (kPa)	WE kg/hr	W3 (kg/s)	T4 Ideal (K)	Smoke Number	EI (NOx) (g/kg)	EI (CO) (g/kg)	EI (HC) (g/kg)	EI (CO2) (g/kg)	TL (ave) (K)	TL (peak) (K)	Profile Factor	Pattern Factor	LLFAR (g/kg)
Shale JP8	Idle	409.4	103.1	39.6	1.232	759.1	0.2	4.6	152.7	232.1	2279.2	437.0	491.1			6.97
	30 %	507.8	103.8	43.2	1.145	905.0	0.8	3.6	104.8	62.4	2821.0	546.4	626.9			
	70 %	605.6	104.0	53.3	1.012	1135.9	0.8	3.9	62.2	4.8	3045.3	709.7	822.1			
	100%	651.1	104.0	60.0	0.957	1268.5	2.4	2.9	12.2	2.9	3130.1	773.0	874.1	0.028	0.229	
JP10	Idle	508.5	103.1	40.6	1.236	766.7	0.6	2.3	154.9	189.4	2464.1	463.9	725.2			
	30 %	507.8	103.1	42.7	1.119	909.4	0.8	2.1	105.4	49.5	2926.6	572.4	665.5			5.77
	70 %	606.1	104.1	54.8	1.027	1142.0	0.2	2.6	60.4	1.4	3129.6	708.0	824.4			
	100%	651.7	104.1	61.5	0.976	1271.7	6.2	3.5	6.8	0.9	3215.0	778.1	942.7	0.039	0.303	
ENBS-3	Idle	409.4	102.5	39.8	1.228	761.7	1.6	4.4	176.0	262.2	2189.6	436.3	495.9			
	30 %	507.8	103.7	43.2	1.137	906.7	1.6	2.9	119.6	40.3	2890.0	547.3	631.8			5.87
	70 %	606.1	104.1	54.1	1.016	1141.7	1.4	2.3	67.9	8.5	3058.4	722.3	857.8			
	100%	651.7	104.0	60.5	0.962	1269.4	1.3	2.7	10.6	4.1	3160.7	766.6	893.7	0.023	0.228	
JP4	Idle	409.4	103.4	39.5	1.237	756.9	0.3	2.3	150.3	72.7	2705.0	451.6	502.6			
	30 %	507.8	103.9	42.8	1.131	899.8	1.6	2.6	97.9	21.6	2928.1	567.7	652.1			5.30
	70 %	606.7	104.0	53.3	1.025	1130.5	0.2	3.1	64.5	2.2	3033.8	755.2	966.9			
	100%	652.2	104.0	60.6	0.973	1259.3	0.6	4.1	34.9	1.2	3082.9	774.9	1038.6	0.023	0.315	

Airblast Nozzle, Rich Primary Zone

FUEL	COND No.	T3 (K)	P3 (kPa)	WE kg/hr	W3 (kg/s)	T4 Ideal (K)	Smoke Number	EI (NOx) (g/kg)	EI (CO) (g/kg)	EI (HC) (g/kg)	EI (CO2) (g/kg)	TL (ave) (K)	TL (peak) (K)	Profile Factor	Pattern Factor	LLFAR (g/kg)
Shale JP8	Idle	409.4	103.3	39.7	1.224	761.9	1.8	7.9	157.9	104.8	2621.0	434.8	493.6			4.74
	30 %	508.3	103.9	42.8	1.135	905.1	1.9	4.1	95.6	26.7	2933.7	534.5	629.5			
	70 %	606.1	104.0	53.6	1.016	1136.9	2.9	4.3	43.6	4.8	3075.5	640.0	776.9			
	100%	651.7	104.0	60.1	0.960	1267.8	1.9	4.6	10.8	2.5	3133.4	702.8	859.0	0.031	0.339	
JP10	Idle	408.9	103.3	40.6	1.239	764.4	1.2	4.6	89.9	260.2	2536.3	428.5	523.1			
	30 %	508.3	104.1	44.0	1.148	910.6	0.9	3.5	133.1	37.4	3026.7	524.6	649.3			5.38
	70 %	606.1	104.3	54.9	1.030	1142.2	1.6	3.6	18.0	4.8	3186.8	652.9	797.4			
	100%	651.7	104.3	61.4	0.971	1273.9	1.0	3.5	13.2	1.8	3202.6	736.3	858.0	0.058	0.365	
ENBS-3	Idle	409.4	103.1	39.6	1.217	763.5	2.4	7.3	201.0	188.4	2354.8	433.3	520.9			5.48
	30 %	507.8	103.9	43.0	1.134	906.7	1.0	4.7	103.8	50.7	2886.1	542.0	639.1			
	70 %	606.7	104.1	53.8	1.011	1142.1	1.2	3.5	61.9	10.6	3062.2	661.1	811.8			7.50
	100%	651.7	104.0	60.3	0.957	1270.6	1.6	4.0	9.8	5.9	3157.0	714.0	864.9	0.000	0.000	
JP4	Idle	408.9	103.4	39.5	1.233	757.2	1.3	3.1	149.4	92.4	2652.4	461.6	781.6			
	30 %	505.6	103.9	42.6	1.147	897.2	0.6	2.5	89.7	12.7	2965.4	564.8	916.8			
	70 %	606.7	104.0	53.4	1.022	1132.8	0.6	2.5	35.4	2.1	3079.6	675.8	946.0			
	100%	651.7	104.2	59.8	0.965	1261.1	0.6	2.9	13.2	0.6	3118.6	722.1	806.3	0.054	0.301	

APPENDIX B

PT6A-65 ATMOSPHERIC TEST DATA

Simpler .65 FN Nozzle, Bill of Material

FUEL	CORD No.	T3 (K)	P3 (MPa)	WE kg/hr	W3 (kg/s)	T4 Ideal (K)	Smoke Number	SI(NOx) (g/kg)	EI(CO) (g/kg)	EI(HC) (g/kg)	EI(CO2) (g/kg)	TL(ave) (K)	TL(peak) (K)	Profile Factor	Pattern Factor	ILFAR (g/kg)
State J78	Idle	417.4	106.4	16.9	0.566	742.3	2.5	2.8	105.8	50.1	2853.4	478.3	540.1			3.90
	40 %	556.5	106.5	21.6	0.479	1020.6	1.9	3.6	22.7	0.0	3121.6	661.2	737.0			
	55 %	575.2	106.5	24.4	0.469	1082.0	1.7	3.8	9.8	0.0	3141.8	693.5	771.8	0.370	0.135	
JP10	70 %	588.2	106.4	23.9	0.469	1113.1	1.0	4.1	5.2	0.0	3149.0	714.7	794.2			
	Idle	417.6	105.8	24.6	0.566	830.9	3.5	4.1	93.3	15.4	3039.3	512.8	602.7			4.60
	40 %	556.3	106.8	32.4	0.492	1228.5	2.9	5.3	1.2	0.0	3226.3	721.7	851.2			
FP9S-3	55 %	573.0	106.8	34.0	0.469	1290.6	2.5	5.3	0.4	0.0	3227.5	751.5	887.6	0.457	0.163	
	70 %	587.4	106.7	36.5	0.526	1274.5	1.7	4.9	0.4	0.2	3226.9	775.9	921.7			
	Idle	416.7	106.6	21.0	0.565	817.8	4.3	2.2	96.2	22.5	2975.5	499.1	564.3			3.50
JP4	40 %	556.7	106.7	27.1	0.478	1131.7	2.1	3.6	6.1	0.5	3177.7	700.2	816.2			
	55 %	574.1	106.7	28.9	0.467	1195.0	3.1	4.0	2.0	0.9	3183.1	734.4	856.3	0.380	0.138	
	70 %	586.3	106.8	30.7	0.460	1248.5	2.9	1.6	1.3	3.0	3178.2	771.2	910.7			
JP4/B1	Idle	419.4	106.6	20.5	0.561	1069.0	0.0	1.8	91.6	16.8	2951.1	477.5	556.4			3.70
	40 %	555.4	106.6	26.5	0.479	1372.6	0.0	3.5	9.1	0.6	3125.2	678.1	795.0	0.282	0.064	
	55 %	573.5	106.6	28.1	0.464	1436.6	0.0	3.7	2.4	8.3	3136.4	707.4	830.9			
JP4/B2	70 %	585.9	106.6	29.3	0.459	1477.5	0.0	3.9	2.1	0.3	3137.0	727.6	857.4			
	Idle	417.2	106.6	25.1	0.553	909.6	5.7	2.0	88.3	12.5	3019.4	493.2	573.2			4.40
	40 %	556.9	106.4	26.5	0.465	1133.3	4.2	4.0	7.2	0.0	3181.1	687.0	798.0	0.387	0.105	
JP4/2840/DF	55 %	576.3	106.6	28.5	0.457	1200.8	3.0	4.7	3.3	1.9	3184.5	722.4	847.7			
	70 %	580.9	106.9	30.8	0.458	1242.6	3.7	4.4	1.6	0.6	3188.1	743.3	875.0			
	Idle	418.3	106.6	23.1	0.559	860.8	4.2	1.9	88.6	12.9	3051.7	505.0	585.4			4.90
JET A1	40 %	555.3	106.7	28.1	0.475	1153.7	4.4	3.6	4.4	1.0	3216.7	705.7	821.2	0.374	0.122	
	55 %	575.0	106.6	29.3	0.457	1215.2	4.1	4.1	2.1	0.6	3221.3	737.4	853.7			
	70 %	587.4	106.7	31.1	0.453	1266.7	4.5	3.9	2.0	0.0	3223.2	758.8	885.3			
JET A1/B1	Idle	420.0	106.8	21.3	0.570	1099.1	0.0	1.8	116.8	18.3	2952.9	486.3	574.9			5.20
	40 %	558.7	106.7	28.6	0.479	1417.8	0.0	3.9	4.7	0.0	3179.4	672.4	829.2	0.345	0.110	
	55 %	573.0	106.6	29.3	0.460	1465.0	0.0	4.3	1.8	0.0	3183.8	701.3	875.7			
JET A1/B2	70 %	586.5	106.7	30.4	0.454	1507.4	0.0	4.7	1.0	0.0	3185.2	718.3	901.8			
	Idle	420.0	106.8	21.3	0.571	1076.7	1.6	4.0	83.9	27.0	2953.3	490.6	561.8			3.30
	40 %	556.1	106.8	28.3	0.476	1411.2	0.0	5.3	4.2	0.5	3151.3	659.1	771.7	0.312	0.083	
JET A1/B3	55 %	572.4	106.8	29.0	0.465	1198.6	0.0	4.1	0.0	0.0	0.0	0.0	0.0			
	70 %	588.5	106.7	30.1	0.457	1244.2	0.0	4.2	1.3	0.0	3157.3	708.1	841.9			
	Idle	416.9	106.6	20.2	0.559	806.5	2.9	2.4	97.0	18.1	2989.3	493.6	560.8			3.70
JET A1/B4	40 %	557.0	106.7	26.8	0.477	1126.9	3.4	3.8	11.0	1.1	3171.2	694.2	812.8	0.354	0.118	
	55 %	575.2	106.8	29.7	0.480	1139.8	1.4	4.9	6.4	0.0	3212.2	702.2	792.1			4.60
	70 %	587.4	106.5	29.3	0.483	1209.5	2.4	5.1	2.3	0.0	3218.7	738.3	843.1	0.435	0.150	
Tar Sands IL	Idle	417.2	106.6	21.7	0.547	843.2	1.2	3.7	92.0	17.7	2992.9	500.3	561.6			4.40
	40 %	556.1	106.9	27.6	0.486	1136.9	2.4	5.4	4.3	1.3	3175.7	703.1	827.8	0.374	0.120	
	55 %	574.3	106.9	29.3	0.471	1197.7	2.4	5.3	2.1	1.2	3179.5	736.7	876.6			
Tar Sands LP	70 %	586.3	106.6	28.4	0.460	1203.3	2.7	4.4	2.5	1.8	3177.2	741.1	856.1	0.405	0.190	
	Idle	417.2	106.7	22.0	0.561	839.1	2.7	0.9	98.6	57.8	2859.4	497.5	571.0			4.10
	40 %	556.1	106.7	29.0	0.475	1171.8	2.7	3.7	3.5	3.7	3157.6	697.5	825.7	0.374	0.120	
Tar Sands LP	55 %	574.4	106.7	31.5	0.463	1233.8	2.0	3.8	1.7	3.9	3159.9	727.5	875.3			
	70 %	587.5	106.7	33.3	0.449	1237.1	2.5	4.0	1.1	6.3	3154.3	751.7	904.3			

Simplex L-1 FN Nozzle, Bill of Material

FUEL	COND No.	T3 (K)	P3 (kPa)	WF kg/hr	W3 (kg/s)	T4 Ideal (K)	Smoke Number	EI(MON) (g/kg)	EI(CO) (g/kg)	EI(HC) (g/kg)	EI(CO2) (g/kg)	TL(ave) (K)	TL(peak) (K)	Profile Pattern Factor	LLPFR (g/kg)
Shale JP8	Idle	418.3	106.4	21.2	0.562	823.4	2.6	2.4	123.0	173.2	2487.8	485.7	527.9		7.60
	40 %	555.6	106.6	26.6	0.481	1117.3	1.9	3.7	29.8	1.0	3109.2	676.1	766.1		
	55 %	573.9	106.7	25.4	0.469	1182.6	2.5	4.3	5.6	1.0	3145.8	710.6	810.3		
JP10	Idle	417.4	106.6	29.8	0.461	1230.0	1.8	4.3	2.0	3.0	3145.8	733.5	836.6	0.304	0.116
	40 %	556.5	106.6	27.0	0.564	925.0	3.1	2.0	157.7	101.6	2701.0	470.3	541.0		7.40
	55 %	573.9	106.5	26.5	0.464	1189.4	2.2	3.9	3.5	0.0	3211.5	687.3	775.2		
ERAS-3	Idle	416.9	106.7	29.6	0.456	1233.6	1.7	4.0	1.5	0.0	3225.9	742.1	840.2	0.306	0.112
	40 %	555.2	106.7	22.7	0.566	846.8	3.1	1.6	162.0	78.7	2717.8	472.4	524.3		8.60
	55 %	574.4	106.6	23.9	0.466	1195.1	3.1	3.7	7.9	6.4	3158.7	698.9	784.7		
JP4	Idle	418.7	106.4	20.0	0.558	1061.5	0.9	0.6	176.0	129.2	2509.3	459.7	507.9	0.320	0.112
	40 %	554.4	106.7	26.2	0.482	1362.3	1.4	3.5	32.8	4.4	3077.5	666.4	799.2		6.90
	55 %	566.5	106.6	27.6	0.465	1418.4	0.6	4.4	11.5	1.2	3119.9	690.8	822.7		
JP4/BI	Idle	417.6	106.4	21.5	0.552	836.5	3.2	1.3	129.5	154.4	2564.5	471.7	544.4	0.315	0.073
	40 %	555.9	106.8	15.8	0.471	907.0	4.0	3.0	50.9	19.7	3058.2	678.7	788.1		7.90
	55 %	575.7	106.7	23.2	0.463	1188.2	3.6	3.9	10.9	3.1	3166.7	716.3	840.9		
JP4/B2	Idle	418.2	106.4	21.9	0.554	842.6	2.0	0.8	144.8	123.6	2659.0	478.3	527.1	0.290	0.094
	40 %	556.1	106.6	29.7	0.476	1183.8	1.4	4.1	7.3	22.4	3153.4	702.3	792.4		7.60
	55 %	575.2	106.5	31.6	0.459	1259.5	1.6	4.5	1.8	7.1	3263.8	738.3	832.5		
JP4/2040/DE	Idle	416.7	106.5	22.9	0.565	851.1	0.0	1.3	167.9	84.2	2691.5	459.8	566.7	0.299	0.099
	40 %	555.4	106.8	28.3	0.481	1151.1	0.0	4.1	14.9	1.2	3160.1	663.8	810.7		8.80
	55 %	573.3	106.8	30.5	0.470	1221.1	0.4	4.5	4.1	0.3	3179.5	699.3	856.7		
JET A1	Idle	417.8	106.3	21.5	0.561	1084.8	0.2	0.8	124.2	312.0	2106.2	440.2	517.2	0.327	0.101
	40 %	556.7	106.7	28.6	0.475	1419.5	0.0	4.4	7.9	0.0	3146.9	654.3	773.8		7.70
	55 %	587.2	106.6	30.4	0.452	1510.3	0.0	4.8	2.1	0.0	3156.0	704.0	844.8	0.281	0.089
JET A1/EI	Idle	418.0	106.3	21.9	0.559	838.8	0.8	4.5	149.6	118.5	2645.7	472.9	531.3	0.266	0.096
	40 %	556.7	106.5	26.4	0.477	1119.4	0.6	4.7	43.9	1.4	3118.8	681.7	761.2		7.30
	55 %	573.2	106.5	31.6	0.459	1245.3	0.4	4.9	7.3	0.9	3177.5	717.0	808.1		
JET A1/B2	Idle	417.0	106.1	19.4	0.554	795.5	2.1	1.8	153.3	149.5	2570.2	456.5	530.8	0.410	0.147
	40 %	555.0	106.7	25.5	0.475	1101.4	1.1	2.6	54.8	1.0	3133.4	684.6	800.5		8.30
	55 %	575.0	106.8	28.8	0.478	1178.7	0.4	4.3	5.3	0.9	3211.5	729.7	861.1		
Tar Sands II	Idle	415.6	106.1	21.2	0.559	823.3	4.1	3.2	167.8	141.0	2534.6	458.4	511.0	0.296	0.109
	40 %	555.0	106.6	27.0	0.474	1131.7	1.1	4.0	27.8	0.5	3141.0	682.2	771.1		8.50
	55 %	573.5	106.6	29.0	0.462	1219.9	1.8	4.3	4.3	0.4	3178.1	720.2	817.0		
Tar Sands IE	Idle	416.9	106.1	20.5	0.553	817.0	3.4	5.4	116.9	384.3	1333.0	445.5	502.1	0.320	0.134
	40 %	556.6	106.6	27.0	0.473	1136.2	1.0	4.7	15.9	2.8	3140.6	677.6	785.4		8.20
	55 %	573.0	106.7	28.8	0.457	1203.1	2.1	4.8	2.5	4.3	3157.6	713.7	826.7		
	Idle	416.9	106.7	30.0	0.453	1266.5	2.5	4.6	1.2	0.5	3169.2	736.7	846.6		

Simplex .65 FN Nozzle, Lean Primary Zone

FUEL	COND No.	T3 (K)	P3 (kPa)	WF kg/hr	W3 (kg/s)	T4 Ideal (K)	Stroke Number	EI (NOx) (g/kg)	EI (CO) (g/kg)	EI (HC) (g/kg)	EI (CO2) (g/kg)	TL (ave) (K)	TL (peak) (K)	Profile Factor	Pattern Factor	LIPAF (g/kg)
Shale JP8	Idle	417.0	106.6	20.2	0.564	803.5	1.3	3.5	112.5	20.8	2923.4	488.1	557.4			3.40
	40 #	555.6	106.6	26.1	0.478	1111.0	0.4	4.6	4.2	0.0	3150.6	688.2	776.4			
	55 #	574.1	106.6	27.9	0.466	1174.8	1.4	4.6	1.7	0.0	3154.6	718.2	809.5	0.450	0.124	
JP10	70 #	587.6	106.6	29.0	0.457	1220.6	2.2	4.7	0.8	0.0	3156.0	743.7	842.1			
	Idle	417.8	106.7	21.1	0.561	822.1	3.5	1.7	128.8	36.8	2924.8	499.5	572.0			4.10
	40 #	556.9	106.9	27.1	0.479	1130.6	1.8	4.0	1.7	0.3	3224.7	705.4	795.7			
JP10	55 #	574.4	106.7	28.8	0.459	1203.6	0.5	4.1	1.5	0.0	3225.8	739.5	835.2			
	70 #	586.3	106.6	29.8	0.453	1241.1	2.5	4.5	1.0	0.0	3226.7	759.6	864.7	0.386	0.144	
JP10	Idle	416.7	106.8	22.4	0.567	841.1	6.2	2.2	77.2	12.9	3031.8	509.2	559.0			3.90
	40 #	556.3	106.8	29.5	0.482	1173.2	0.8	4.0	2.7	0.0	3184.4	709.5	849.0			
	55 #	574.3	106.9	28.0	0.470	1173.8	0.7	4.1	1.2	0.0	3186.7	748.6	902.4			
JP4	70 #	585.7	106.7	30.0	0.461	1234.8	0.8	4.3	1.9	0.4	3184.5	765.6	907.4	0.429	0.153	
	Idle	417.2	106.7	20.2	0.418	929.6	1.4	2.0	88.9	10.1	2973.7	484.9	559.6			4.61
	40 #	555.2	107.0	25.8	0.475	1107.3	0.6	3.6	8.0	0.0	3128.6	678.0	779.4			
JP4/B1	55 #	574.4	106.7	27.7	0.460	1179.8	1.9	3.9	2.2	0.0	3137.6	710.0	815.2			
	70 #	587.4	106.7	28.4	0.451	1215.6	2.0	4.3	1.0	0.0	3139.6	732.8	838.8	0.331	0.110	
	Idle	418.0	106.7	20.5	0.559	813.9	2.3	2.2	114.9	11.1	2981.3	490.3	552.7			3.80
JP4/B2	40 #	553.7	106.8	26.6	0.477	1119.0	2.6	3.2	7.0	1.1	3178.4	686.7	769.0			
	55 #	574.4	106.8	28.6	0.467	1188.1	1.6	3.9	2.8	0.3	3186.8	716.2	803.7			
	70 #	587.8	106.9	30.4	0.457	1247.9	0.0	3.8	2.0	0.9	3186.8	741.9	831.1	0.327	0.107	
JP4/2040/BF	Idle	417.6	106.6	19.0	0.551	790.1	4.3	2.7	102.0	2.7	3058.7	503.0	593.1			4.20
	40 #	556.7	106.9	29.9	0.471	1194.9	1.3	4.4	3.3	0.9	3218.6	708.3	821.7			
	55 #	577.0	106.8	31.1	0.446	1268.3	1.9	4.6	1.5	0.9	3221.5	738.5	852.3			
JP4/2040/BF	70 #	587.8	106.9	32.3	0.459	1282.9	0.5	4.8	1.4	0.3	3223.3	759.2	867.2	0.371	0.102	
	Idle	417.8	106.9	22.4	0.563	844.6	1.2	1.8	107.3	6.1	3001.3	483.4	567.7			3.55
	40 #	556.1	106.9	27.6	0.468	1152.2	0.2	4.4	2.4	0.0	3182.9	668.0	809.3			
JET A1	55 #	574.1	106.9	29.0	0.460	1200.0	0.0	0.0	0.0	0.0	0.0	0.0	0.0			
	70 #	587.2	106.7	31.6	0.454	1275.7	0.2	5.0	0.5	0.0	3186.0	726.7	835.5	0.339	0.070	
	Idle	419.4	106.4	20.3	0.541	824.1	0.0	3.5	93.8	10.1	2984.3	482.4	571.5			3.08
JET A1/B1	40 #	553.1	106.5	27.0	0.468	1137.0	0.0	4.4	3.5	0.0	3153.7	652.3	792.8			
	55 #	574.1	106.5	29.0	0.460	1200.0	0.0	0.0	0.0	0.0	0.0	0.0	0.0			
	70 #	587.4	106.5	30.8	0.452	1262.5	0.0	4.4	1.0	0.1	3157.4	710.0	834.6	0.365	0.124	
JET A1/B2	Idle	417.4	106.6	21.4	0.558	829.8	2.8	5.4	114.1	26.4	2939.6	496.0	568.0			3.70
	40 #	556.9	106.8	27.6	0.478	1146.7	1.7	5.5	4.8	0.0	3183.8	698.6	801.5			
	55 #	575.6	106.7	30.9	0.466	1236.6	3.5	5.5	3.3	0.0	3186.3	730.0	834.4			
JET A1/B2	70 #	587.6	106.7	30.6	0.452	1258.5	3.2	4.9	1.9	0.0	3188.5	759.8	872.1	0.345	0.108	
	Idle	416.3	106.6	20.6	0.551	818.7	6.7	1.4	121.3	43.0	2911.3	491.8	567.7			3.70
	40 #	554.4	106.8	26.5	0.472	1124.2	1.2	2.8	9.1	5.7	3192.2	700.5	801.3			
Tar Sands LL	55 #	575.0	106.8	29.7	0.461	1217.7	2.2	3.6	2.9	3.7	3237.4	746.5	871.4			
	70 #	587.4	106.8	31.0	0.459	1258.4	2.0	3.5	1.5	6.2	3197.3	769.8	903.0	0.312	0.121	
	Idle	417.0	106.7	21.1	0.561	821.2	3.1	2.5	113.2	30.4	2924.6	499.1	572.9			3.50
Tar Sands LH	40 #	555.9	106.9	29.4	0.479	1174.8	1.2	4.5	2.9	3.0	3173.1	709.0	851.1			
	55 #	573.0	106.7	29.4	0.464	1202.5	1.3	4.6	1.9	3.5	3173.5	739.9	875.9			
	70 #	586.5	106.8	32.5	0.458	1267.5	0.4	4.5	0.8	5.7	3169.1	772.5	937.7	0.344	0.127	
Tar Sands LH	Idle	416.5	106.6	21.7	0.550	840.3	0.0	2.5	111.1	24.2	2932.2	492.6	584.3			3.00
	40 #	556.1	106.8	27.6	0.470	1152.5	0.0	4.0	3.3	7.7	3146.9	699.2	803.3			
	55 #	575.2	106.8	29.3	0.458	1213.6	0.0	1.6	1.6	6.6	3152.5	732.5	836.6			
Tar Sands LH	70 #	586.9	106.8	29.3	0.446	1241.3	0.0	3.6	1.4	0.8	3168.9	755.4	858.2	0.355	0.123	
	Idle	416.5	106.6	21.7	0.550	840.3	0.0	2.5	111.1	24.2	2932.2	492.6	584.3			3.00
	40 #	556.1	106.8	27.6	0.470	1152.5	0.0	4.0	3.3	7.7	3146.9	699.2	803.3			
	55 #	575.2	106.8	29.3	0.458	1213.6	0.0	1.6	1.6	6.6	3152.5	732.5	836.6			
	70 #	586.9	106.8	29.3	0.446	1241.3	0.0	3.6	1.4	0.8	3168.9	755.4	858.2	0.355	0.123	

Simplex 1.1 FN Nozzle, Lean Primary Zone

FUEL	COND No.	T3 (°F)	P3 (kPa)	WE (kg/hr)	W3 (kg/ε)	T4 Ideal (K)	Smoke Number	EI(NOX) (g/kg)	EI(CO) (g/kg)	EI(HC) (g/kg)	EI(CO2) (g/kg)	TL(ave) (K)	TL(peak) (K)	Profile Factor	Extinction Factor	LIFAF (g/kg)
Stale JP8	Idle	417.0	106.5	20.9	0.566	814.0	1.0	2.2	146.0	155.2	2509.9	472.4	515.3			7.90
	40 %	555.9	106.7	27.4	0.483	1130.1	0.8	3.7	16.9	6.3	3129.7	690.5	769.0			
	55 %	573.9	106.6	29.1	0.469	1194.9	0.6	4.0	2.1	0.3	3153.0	724.5	807.7			
JP10	Idle	417.4	106.7	29.7	0.459	1229.9	0.1	3.5	1.8	0.0	3154.4	749.5	855.3	0.319	0.099	
	40 %	556.7	106.7	27.3	0.479	1135.0	2.2	3.5	7.8	0.0	3215.0	696.0	772.3			8.60
	55 %	574.3	106.7	28.4	0.465	1188.1	0.2	3.8	2.7	0.0	3224.0	727.3	808.0			
JP10-3	Idle	417.2	106.6	29.1	0.455	1224.9	2.9	4.5	0.0	0.0	3178.2	773.3	865.8	0.414	0.167	
	40 %	555.4	106.6	27.2	0.478	1131.5	0.8	4.2	17.8	0.0	3160.5	698.7	781.9			6.90
	55 %	574.1	106.7	28.9	0.466	1195.8	1.2	4.4	3.2	0.5	3182.2	731.5	821.2			
JP4	Idle	417.6	106.5	20.2	0.559	807.0	2.3	1.4	161.9	111.2	2580.9	470.8	507.6			6.50
	40 %	556.7	106.7	26.3	0.474	1118.5	1.8	3.5	39.8	1.1	3075.6	677.9	755.0			
	55 %	573.7	106.7	28.1	0.463	1182.6	1.0	4.1	8.4	0.6	3126.1	713.7	756.8			
JP4/B1	Idle	417.6	106.6	28.6	0.454	1217.7	1.4	4.5	3.9	0.6	3133.3	742.1	840.7	0.340	0.088	
	40 %	554.9	106.8	29.7	0.477	1181.7	4.4	3.6	4.3	0.9	3183.2	705.2	786.1			7.00
	55 %	573.9	106.6	29.4	0.464	1210.0	4.3	4.2	2.5	0.0	3186.5	734.4	816.1			
JP4/B2	Idle	419.1	106.6	22.6	0.450	1251.6	3.6	4.7	1.5	0.3	3185.1	758.0	844.6	0.257	0.084	
	40 %	555.0	106.8	28.7	0.470	1171.4	1.6	4.8	10.4	0.0	3210.0	697.4	776.4			6.80
	55 %	574.4	106.7	29.3	0.456	1216.0	1.6	5.4	3.2	1.4	3217.4	735.2	812.4			
JP4/2046/EF	Idle	417.8	106.9	22.7	0.457	845.6	0.8	1.1	153.8	114.9	2668.7	463.9	528.0			
	40 %	558.3	106.9	27.6	0.477	1143.3	0.4	5.0	18.2	0.5	3156.6	676.1	766.3			6.51
	55 %	574.4	106.9	30.7	0.470	1227.1	0.0	5.1	2.1	0.0	3183.4	714.5	862.9			
JET A1	Idle	417.8	106.5	21.7	0.560	834.1	0.0	1.1	151.5	108.4	2623.2	462.7	525.4			8.40
	40 %	557.2	105.7	28.3	0.473	1159.7	0.0	4.1	5.8	0.5	3148.8	675.7	787.0			
	55 %	574.4	106.6	30.5	0.453	1254.6	0.0	0.0	0.0	0.0	0.0	0.0	0.0			
JET A1/B1	Idle	418.3	106.5	21.4	0.560	811.8	1.0	0.8	168.8	86.8	2687.5	470.7	521.1			7.60
	40 %	556.5	105.8	26.9	0.476	1159.8	0.9	3.5	36.8	0.4	3132.6	694.0	781.2			
	55 %	575.2	106.8	30.6	0.466	1228.8	0.0	3.6	6.0	0.3	3181.1	727.6	817.2			
JET A1/B2	Idle	416.3	106.5	22.1	0.555	844.2	3.1	2.2	161.1	73.6	2756.9	474.8	511.6			7.40
	40 %	556.3	106.8	27.5	0.477	1159.0	2.4	3.1	28.9	4.0	3165.8	690.6	781.4			
	55 %	574.4	106.8	29.5	0.466	1212.0	0.2	3.5	4.0	5.1	3201.8	734.0	824.2			
Tar Sands IN	Idle	416.9	106.6	29.5	0.451	1237.8	0.2	4.6	2.0	19.2	3169.5	752.5	836.4	0.304	0.107	
	40 %	555.6	106.8	29.5	0.476	1159.0	0.5	3.7	10.7	8.2	3146.6	706.8	798.1			8.10
	55 %	574.3	106.7	26.3	0.463	1186.7	1.4	4.4	2.1	0.3	3182.8	730.3	811.4			
Tar Sands IN	Idle	418.2	106.4	20.6	0.552	821.2	2.4	1.1	178.1	100.4	2617.3	464.7	509.7			8.30
	40 %	555.7	106.8	27.8	0.472	1159.0	1.6	3.5	6.1	4.7	3150.9	684.9	761.9			
	55 %	575.2	106.8	29.2	0.458	1213.9	1.5	3.5	1.5	8.5	3147.5	725.7	834.5			
Tar Sands IN	Idle	417.4	106.6	31.0	0.451	1239.6	0.2	3.9	0.3	4.7	3161.2	757.8	838.6	0.326	0.106	

APPENDIX C

PT6A-65 COLD START TEST DATA

Fuel	T _f (K)	T _i (K)	N ₂ (kg/hr)	N ₂ (kg/hr)	T ₅ max (s)	Fuel	T ₅ max (K)	T _i (K)	N ₂ (kg/hr)	N ₂ (kg/hr)	T ₅ max (s)	T ₅ max (K)	
Jet A1	245	244	6.0	6.0	31	Scale JP8	796	285	288	6.0	34	2.0	988
	239	236	6.0	6.0	36		752	239	227	6.0	34	6.4	723
	236	233	6.0	6.0	40		755	237	234	5.8	34	3.2	738
	239	239	6.0	6.0	42		740	243	241	6.0	32	2.4	779
	260	261	6.5	6.0	27		841	253	252	6.0	34	1.7	845
	262	252	6.0	6.0	27		848	262	262	6.0	32	1.8	878
	239	238	6.0	6.0	42		742						
	242	241	6.0	6.0	37		806	287	289	6.0	36	2.1	955
	232	230	5.8	5.8	59		749	256	236	6.0	30	3.2	747
242	242	5.9	5.9	36	790	243	243	6.0	34	2.1	808		
Jet A1/R2	290	292	6.9	6.9	22	JP4	905	254	254	5.9	36	1.8	852
	244	242	6.0	6.0	38		757	263	263	6.0	36	2.0	868
	233	230	5.5	5.5	58		737	229	225	6.0	28	3.2	717
	229	227	5.5	5.5	73		730	299	304	6.2	34	2.8	1011
	238	239	6.0	6.0	42		773	230	228	6.0	34	3.4	735
	250	250	6.0	6.0	33		835	234	232	6.0	32	2.6	746
	260	259	6.0	6.0	30		882	239	239	6.0	34	2.6	764
	290	301	6.6	6.6	24		974	244	244	6.0	34	2.4	797
	244	240	5.8	5.8	84		773	254	253	6.0	32	2.3	870
ERBS-3	250	248	6.0	6.0	58	JP10	788	270	270	6.0	34	1.9	916
	257	254	5.8	5.8	44		843						
	235	235	5.9	5.9	10.2		703	292	310	6.0	32	2.0	1011
	231	231	6.0	6.0	117		780	272	271	6.0	32	2.4	910
	244	241	5.8	5.8	85		789	261	260	6.0	32	2.6	861
	245	243	5.8	5.8	36		877	247	247	5.9	32	2.8	844
	262	262	6.0	6.0	32		890	242	242	6.0	32	13.6	845
	268	266	6.0	6.0	32		890	244	245	6.0	32	5.0	845
					2.4								
Tar Sands L-L	253	300	6.5	6.5	24	R26	970	283	292	6.0	28	2.7	967
	242	242	5.8	5.8	64		778	244	242	6.0	34	N/L	-
	240	240	6.0	6.0	81		787	246	249	6.0	34	N/L	-
	250	250	5.0	5.0	51		840	249	248	6.0	34	N/L	-
	247	247	6.0	6.0	55		820	257	252	6.0	36	N/L	-
	254	255	6.0	6.0	32		826	269	280	6.0	32	6.0	1048
	260	264	6.0	6.0	40		851	269	270	5.9	32	16.5	995
					2.8			275	275	6.0	30	10.0	989
					2.8			278	280	6.0	30	7.0	978
Tar Sands L-H	281	282	6.0	6.0	27		960	289	289	6.0	28	4.3	985
	243	242	5.8	5.8	54		797						
	250	249	6.0	6.0	44		820						
	257	256	6.0	6.0	39		856						
	234	232	6.0	6.0	83		741						
	239	238	6.0	6.0	82		769						
	238	238	6.0	6.0	67		777						
	263	262	5.9	5.9	33		882						
					2.6								

N/L = No-Light

APPENDIX D

PT6A-65 GAS GENERATOR TEST DATA

Simplex 1.9 F Nozzle, Bill of Material

FUEL	COMP No.	T4 (°)	P3 (MPa)	WF (kg/hr)	W3 (kg/s)	H2 (kg/s)	T4 Ideal (K)	Smoke Number	SI/DOX (g/kg)	SI(CO) (g/kg)	SI(HC) (g/kg)	SI(CO2) (g/kg)	TL(ave) (K)	TL(peak) (K)	Profile Factor	Pattern Factor
Shale JP3	Idle	323.6	156.6	51.9	0.975	19.19	804.4	3.3	2.5	62.2	7.9	3037.9	456.2	532.3		
	5 %	451.4	298.9	74.0	1.724	25.54	898.3	3.3	3.1	35.3	7.5	3044.2	525.8	585.5		
	45 %	588.3	607.0	186.0	2.844	33.19	1199.4	16.9	5.7	3.3	1.5	3147.2	701.5	809.9		
	80 %	595.9	781.3	255.3	3.325	35.29	1131.1	18.1	5.5	1.3	0.5	3153.7	777.9	905.0	0.054	0.465
JP10	100%	621.7	880.6	293.3	3.683	36.30	1376.7	16.5	7.1	1.3	0.0	3155.2	809.6	942.6		
	Idle	401.7	288.7	54.8	1.135	20.10	837.8	4.7	2.5	72.0	17.2	3067.8	468.9	546.0		
	5 %	455.7	297.9	73.9	1.737	25.50	896.1	12.3	3.0	43.6	9.2	3134.4	546.3	606.6		
	45 %	567.1	634.3	187.6	2.880	33.02	1294.4	35.9	6.3	7.4	0.6	3215.0	733.6	809.8		
EMSS-3	80 %	606.5	816.7	256.3	3.429	34.98	1322.8	34.1	7.2	3.8	0.0	3222.2	805.1	900.5	0.057	0.435
	100%	621.3	881.6	293.5	3.529	36.09	1383.9	33.3	6.5	4.6	0.0	3221.1	837.9	951.1		
	Idle	395.9	206.7	53.7	1.288	20.01	818.3	6.2	1.8	60.1	6.8	3070.1	465.2	562.6		
	5 %	452.1	303.0	74.2	1.837	25.47	887.8	17.8	2.8	41.3	15.6	3080.8	552.5	654.4		
JP4	45 %	555.4	634.3	187.3	3.030	32.93	1188.9	42.2	6.0	5.7	0.0	3179.6	731.3	843.2		
	80 %	585.8	739.7	292.0	2.839	32.52	1243.3	18.5	6.1	1.4	0.5	3137.4	756.9	876.5		
	80 %	626.0	828.9	261.0	3.370	34.76	1367.2	19.0	7.7	1.1	0.0	3139.4	831.4	978.3	0.044	
	100%	643.4	898.8	301.5	3.629	36.03	1424.4	21.8	7.5	1.1	0.0	3139.3	863.0	1029.7		
JP6	Idle	410.6	210.0	55.6	1.143	20.44	848.9	12.2	2.2	90.8	27.2	3056.6	511.6	566.9		
	5 %	460.8	290.9	75.0	1.715	25.39	913.3	27.6	2.6	32.3	15.6	3136.7	574.3	631.0		
	45 %	576.7	608.0	189.0	2.776	32.98	1234.4	45.6	4.5	11.4	2.9	3243.0	786.5	933.9		
	80 %	605.1	765.0	250.7	3.270	34.93	1358.9	41.2	7.6	6.9	0.4	3262.2	857.7	1054.8	0.061	0.412
JP4/B2	100%	630.5	897.8	297.7	3.629	36.13	1404.4	39.7	5.9	8.1	0.0	3261.3	882.1	1096.1		
	Idle	412.5	217.8	53.8	1.352	20.61	831.1	10.2	3.4	63.6	7.1	3107.0	480.3	554.9		
	5 %	463.0	303.0	73.1	1.728	25.52	911.1	21.1	3.9	34.8	5.4	3156.9	570.0	633.9		
	45 %	581.6	739.7	198.9	3.357	34.74	1153.3	36.1	6.5	4.9	3.3	3209.4	763.2	855.8		
JET A1	80 %	619.6	739.7	261.5	3.402	34.93	1352.2	39.0	7.1	3.3	0.8	3219.1	829.5	943.6	0.044	0.391
	100%	636.5	907.9	297.8	3.679	36.09	1400.6	32.5	8.5	3.1	6.3	3220.4	855.7	993.4		
	Idle	412.5	215.8	53.7	1.275	20.93	833.3	0.4	2.3	54.1	5.6	3056.3	468.4	542.7		
	5 %	462.4	302.0	74.7	1.724	25.45	910.0	3.4	3.1	30.1	3.9	3101.0	547.4	624.5		
JET A1/B2	45 %	574.4	634.3	189.5	2.848	33.02	1231.9	19.9	5.9	4.0	0.0	3153.1	728.3	830.0		
	80 %	614.1	815.7	259.0	3.370	34.96	1347.2	17.6	7.0	1.9	0.0	3156.2	782.6	908.0	0.042	0.376
	100%	631.3	905.9	296.8	3.688	36.16	1392.2	14.0	9.2	1.4	0.0	3157.1	825.8	957.1		
	Idle	404.7	202.7	53.9	1.143	20.20	832.2	7.6	2.6	61.1	1.2	3123.0	477.1	583.8		
Tar Sands LL	5 %	458.6	303.0	74.9	1.755	25.51	906.6	18.3	3.4	32.0	2.2	3168.0	569.4	648.9		
	45 %	570.2	639.4	190.8	2.903	32.95	1210.0	38.5	3.0	3.9	0.8	3214.1	757.3	863.6		
	80 %	608.8	811.7	261.0	3.420	34.84	1337.6	25.4	9.4	2.6	0.0	3181.9	814.2	948.4	0.046	0.302
	100%	626.0	904.8	298.9	3.733	36.11	1386.7	22.4	7.9	1.9	0.0	3219.3	836.4	963.4		
Tar Sands LH	Idle	455.1	207.7	54.3	1.166	20.59	828.9	4.8	2.6	50.5	6.5	3073.2	476.4	554.7		
	5 %	459.2	298.9	75.4	1.755	25.48	903.9	12.0	3.0	31.2	5.5	3122.0	558.6	616.3		
	45 %	570.2	639.4	190.8	2.908	33.04	1212.2	30.2	6.4	3.2	0.5	3179.6	735.2	818.2		
	80 %	608.8	811.7	261.0	3.420	34.84	1337.6	25.4	9.4	2.6	0.0	3181.9	814.2	948.4	0.048	0.355
Tar Sands RH	100%	626.0	904.8	298.9	3.733	36.11	1386.7	22.4	7.9	1.9	0.0	3181.9	836.4	963.4		
	Idle	457.7	228.0	56.1	1.138	21.82	846.1	4.5	2.4	53.0	1.1	3085.5	490.3	565.1		
	5 %	469.2	303.0	76.0	1.756	25.64	917.8	9.1	2.6	36.4	4.0	3165.2	569.5	646.1		
	45 %	580.4	625.2	190.1	2.917	32.99	1237.8	25.6	4.8	10.3	0.4	3156.0	747.2	833.7	0.055	0.448
Tar Sands RH	80 %	623.6	813.7	262.1	3.379	34.97	1362.1	24.1	6.2	8.4	0.0	3159.5	825.1	948.7		
	100%	640.8	899.8	299.3	3.685	36.14	1413.0	23.7	6.5	7.9	0.0	3161.0	853.1	963.2		

Simplex 2.2 FN Nozzle, Bill of Material

FUEL	CC-10 No.	23 (K)	P3 (KPa)	WF (kg/hr)	W1 (kg/s)	N2 (KPa)	T4 (K)	Stroke Number	EI(50X) (g/kg)	EI(CO) (g/kg)	EI(HC) (g/kg)	EI(CO2) (g/kg)	TL(ave) (K)	TL(peak) (K)	Profile Factor	Pattern Factor
Snale J98	Idle	414.7	202.7	53.8	0.971	20.01	842.8	3.7	2.2	47.3	10.4	3054.4	456.3	564.8		
	5 %	471.5	297.9	75.0	1.665	25.48	922.8	5.7	3.1	23.5	5.4	3105.6	558.7	536.8		
	45 %	579.7	607.0	189.7	2.743	33.05	1239.4	20.7	5.7	0.0	1.0	3154.5	736.2	839.1		
	80 %	617.2	763.0	259.2	3.743	34.96	1366.7	19.4	5.1	0.0	0.0	3157.2	818.1	923.4		
JP-10	Idle	638.9	887.7	296.7	3.579	36.15	1421.1	19.2	5.2	0.0	0.0	3157.2	850.6	936.8	0.047	0.450
	5 %	351.2	195.6	54.0	0.993	19.63	805.6	6.2	2.0	69.9	25.5	3048.4	475.9	545.7		
	45 %	451.1	303.0	75.1	1.774	25.51	832.2	14.2	2.8	45.5	12.2	3123.4	567.6	628.2		
	80 %	556.9	601.9	187.4	2.799	33.01	1212.2	35.1	6.2	6.4	0.9	3215.7	725.5	830.7		
EROS-3	Idle	616.1	883.6	294.7	3.660	36.11	1380.0	36.1	8.5	5.2	0.0	3220.0	824.7	942.2	0.057	0.577
	5 %	397.9	208.7	53.6	1.161	20.27	818.3	4.4	2.0	61.3	5.3	3077.8	484.6	553.6		
	45 %	451.1	303.0	74.6	1.774	25.47	837.8	14.1	2.9	34.0	7.7	3114.1	550.9	630.6		
	80 %	552.3	603.4	187.2	2.917	32.95	1189.4	38.8	6.4	3.4	2.4	3176.6	745.7	852.2		
JP4	Idle	615.0	924.1	295.6	3.860	36.23	1345.6	35.9	9.3	1.9	0.0	3185.7	820.6	944.3	0.045	0.477
	5 %	356.9	196.6	54.4	0.962	19.40	860.0	2.2	2.0	54.5	12.8	3020.3	471.6	546.7		
	45 %	461.4	302.0	75.2	1.733	25.48	805.6	16.5	6.1	3.7	0.0	3100.5	542.9	632.2		
	80 %	566.8	612.0	187.6	2.762	32.91	1236.7	15.5	6.1	2.1	0.0	3135.3	730.7	908.1		
RJ6	Idle	636.5	878.5	299.0	3.611	36.11	1406.7	18.8	7.7	1.8	0.0	3138.3	848.3	926.4	0.046	0.502
	5 %	413.8	207.7	62.1	0.925	20.40	826.7	11.9	2.7	82.8	26.8	2977.9	580.3	567.0		
	45 %	461.2	305.0	74.4	1.751	25.49	805.6	16.5	6.1	59.5	17.5	3047.0	575.1	624.4		
	80 %	566.8	612.0	187.6	2.762	32.91	1236.7	15.5	6.1	2.1	0.0	3135.3	730.7	908.1		
JP4/E2	Idle	626.2	896.7	296.0	3.660	36.15	1392.8	45.4	10.0	6.8	0.0	3177.9	870.9	1071.5	0.059	0.499
	5 %	426.3	221.9	55.3	1.306	21.37	858.3	5.4	2.1	52.1	1.3	3140.8	515.0	575.1		
	45 %	471.5	303.0	76.5	1.710	25.42	831.7	25.1	2.2	28.2	2.4	3175.8	584.4	657.9		
	80 %	526.4	639.4	191.8	2.853	33.04	1238.3	41.5	5.3	3.8	0.3	3219.6	782.4	877.5		
JET A1	Idle	623.6	935.0	264.8	3.429	35.64	1362.8	31.9	6.7	2.7	0.0	3222.1	868.2	931.9	0.046	0.439
	5 %	413.2	210.8	54.1	1.134	20.41	835.0	5.5	4.6	54.3	4.4	3062.0	487.1	551.2		
	45 %	465.5	306.0	74.7	1.678	25.27	823.3	8.2	6.0	28.1	3.8	3164.6	549.6	636.0		
	80 %	521.4	623.2	189.9	2.776	32.86	1246.1	24.7	9.3	2.5	0.6	3153.8	730.7	832.8		
JET A1/E2	Idle	639.5	1008.6	297.9	3.611	36.04	1415.6	24.7	9.7	1.6	0.0	3156.8	837.8	925.9	0.047	0.471
	5 %	395.6	201.6	53.9	1.683	19.64	737.2	9.0	2.1	61.2	4.0	3115.1	486.0	554.6		
	45 %	454.4	303.0	74.4	1.819	25.47	878.9	17.9	3.2	33.6	5.0	3155.7	556.4	627.8		
	80 %	563.9	639.4	198.8	3.037	33.08	1171.1	44.7	6.2	2.8	0.9	3215.2	752.1	860.8		
JET A1/E2	Idle	619.4	923.1	246.6	3.583	36.20	1391.1	43.5	8.2	0.9	0.0	3220.8	831.1	951.3	0.046	0.489
	5 %	413.2	210.8	54.1	1.134	20.41	835.0	5.5	4.6	54.3	4.4	3062.0	487.1	551.2		
	45 %	465.5	306.0	74.7	1.678	25.27	823.3	8.2	6.0	28.1	3.8	3164.6	549.6	636.0		
	80 %	521.4	623.2	189.9	2.776	32.86	1246.1	24.7	9.3	2.5	0.6	3153.8	730.7	832.8		
JET A1/E2	Idle	639.5	1008.6	297.9	3.611	36.04	1415.6	24.7	9.7	1.6	0.0	3156.8	837.8	925.9	0.047	0.471
	5 %	395.6	201.6	53.9	1.683	19.64	737.2	9.0	2.1	61.2	4.0	3115.1	486.0	554.6		
	45 %	454.4	303.0	74.4	1.819	25.47	878.9	17.9	3.2	33.6	5.0	3155.7	556.4	627.8		
	80 %	563.9	639.4	198.8	3.037	33.08	1171.1	44.7	6.2	2.8	0.9	3215.2	752.1	860.8		
JET A1/E2	Idle	619.4	923.1	246.6	3.583	36.20	1391.1	43.5	8.2	0.9	0.0	3220.8	831.1	951.3	0.046	0.489
	5 %	413.2	210.8	54.1	1.134	20.41	835.0	5.5	4.6	54.3	4.4	3062.0	487.1	551.2		
	45 %	465.5	306.0	74.7	1.678	25.27	823.3	8.2	6.0	28.1	3.8	3164.6	549.6	636.0		
	80 %	521.4	623.2	189.9	2.776	32.86	1246.1	24.7	9.3	2.5	0.6	3153.8	730.7	832.8		
JET A1/E2	Idle	639.5	1008.6	297.9	3.611	36.04	1415.6	24.7	9.7	1.6	0.0	3156.8	837.8	925.9	0.047	0.471
	5 %	395.6	201.6	53.9	1.683	19.64	737.2	9.0	2.1	61.2	4.0	3115.1	486.0	554.6		
	45 %	454.4	303.0	74.4	1.819	25.47	878.9	17.9	3.2	33.6	5.0	3155.7	556.4	627.8		
	80 %	563.9	639.4	198.8	3.037	33.08	1171.1	44.7	6.2	2.8	0.9	3215.2	752.1	860.8		
JET A1/E2	Idle	619.4	923.1	246.6	3.583	36.20	1391.1	43.5	8.2	0.9	0.0	3220.8	831.1	951.3	0.046	0.489
	5 %	413.2	210.8	54.1	1.134	20.41	835.0	5.5	4.6	54.3	4.4	3062.0	487.1	551.2		
	45 %	465.5	306.0	74.7	1.678	25.27	823.3	8.2	6.0	28.1	3.8	3164.6	549.6	636.0		
	80 %	521.4	623.2	189.9	2.776	32.86	1246.1	24.7	9.3	2.5	0.6	3153.8	730.7	832.8		
JET A1/E2	Idle	639.5	1008.6	297.9	3.611	36.04	1415.6	24.7	9.7	1.6	0.0	3156.8	837.8	925.9	0.047	0.471
	5 %	395.6	201.6	53.9	1.683	19.64	737.2	9.0	2.1	61.2	4.0	3115.1	486.0	554.6		
	45 %	454.4	303.0	74.4	1.819	25.47	878.9	17.9	3.2	33.6	5.0	3155.7	556.4	627.8		
	80 %	563.9	639.4	198.8	3.037	33.08	1171.1	44.7	6.2	2.8	0.9	3215.2	752.1	860.8		
JET A1/E2	Idle	619.4	923.1	246.6	3.583	36.20	1391.1	43.5	8.2	0.9	0.0	3220.8	831.1	951.3	0.046	0.489
	5 %	413.2	210.8	54.1	1.134	20.41	835.0	5.5	4.6	54.3	4.4	3062.0	487.1	551.2		
	45 %	465.5	306.0	74.7	1.678	25.27	823.3	8.2	6.0	28.1	3.8	3164.6	549.6	636.0		
	80 %	521.4	623.2	189.9	2.776	32.86	1246.1	24.7	9.3	2.5	0.6	3153.8	730.7	832.8		
JET A1/E2	Idle	639.5	1008.6	297.9	3.611	36.04	1415.6	24.7	9.7	1.6	0.0	3156.8	837.8	925.9	0.047	0.471
	5 %	395.6	201.6	53.9	1.683	19.64	737.2	9.0	2.1	61.2	4.0	3115.1	486.0	554.6		
	45 %	454.4	303.0	74.4	1.819	25.47	878.9	17.9	3.2	33.6	5.0	3155.7	556.4	627.8		
	80 %	563.9	639.4	198.8	3.037	33.08	1171.1	44.7	6.2	2.8	0.9	3215.2	752.1	860.8		
JET A1/E2	Idle	619.4	923.1	246.6	3.583	36.20	1391.1	43.5	8.2	0.9	0.0	3220.8	831.1	951.3	0.046	0.489
	5 %	413.2	210.8	54.1	1.134	20.41	835.0	5.5	4.6	54.3	4.4	3062.0	487.1	551.2		
	45 %	465.5	306.0	74.7	1.678	25.27	823.3	8.2	6.0	28.1	3.8	3164.6	549.6	636.0		
	80 %	521.4	623.2	189.9	2.776	32.86	1246.1	24.7	9.3	2.5	0.6	3153.8	730.7	832.8		
JET A1/E2	Idle	639.5	1008.6	297.9	3.611	36.04	1415.6	24.7	9.7	1.6	0.0	3156.8	837.8	925.9	0.047	0.471
	5 %	395.6	201.6	53.9	1.683	19.64	737.2									

Simplex 1.9 FM Nozzle, 5% Cabin Bleed

FUEL	COND No.	T3 (K)	P3 (kPa)	Wf (kg/hr)	W3 (kg/s)	E2 (hrpm)	T4 Ideal (K)	Smoke Number	EI (CO) (g/kg)	EI (HC) (g/kg)	EI (CO2) (g/kg)	TL (ave) (K)	TL (peak) (K)	Profile Factor	Fatigue Factor
Shell JP6	Idle	421.5	218.9	61.5	1.111	21.42	914.4	1.4	2.2	46.5	5.0	3070.5	587.8	582.5	
	5 %	462.8	293.9	30.6	1.574	25.40	986.7	3.4	2.2	27.0	2.7	3167.3	559.7	658.9	
	45 %	573.6	626.2	282.5	2.763	33.02	1296.7	16.3	4.9	2.7	0.0	3153.0	735.8	836.3	
	80 %	612.7	809.6	275.3	3.216	34.93	1421.1	14.6	6.4	2.4	0.0	3153.5	836.4	918.2	
JP10	Idle	398.7	203.7	60.6	1.061	19.81	907.2	5.5	2.5	63.2	9.0	3104.1	502.6	572.6	
	5 %	453.8	291.8	30.0	1.406	25.42	965.0	10.3	2.6	42.5	5.9	3125.3	561.5	625.1	
	45 %	570.1	623.2	282.3	2.762	33.02	1279.4	32.9	6.7	5.5	0.0	3222.6	737.8	847.0	
	80 %	610.9	816.7	276.7	3.329	35.21	1398.9	30.6	8.6	3.7	0.0	3222.5	829.2	935.4	
JP4	Idle	409.4	219.9	61.7	1.238	21.03	0.0	0.0	3.8	55.0	5.9	3086.1	514.1	606.0	
	5 %	460.0	298.9	30.3	1.717	25.49	0.0	0.0	3.4	33.4	2.4	3129.5	569.5	679.6	
	45 %	572.2	624.2	281.6	2.844	32.90	0.0	0.0	2.9	2.5	0.0	3184.7	769.3	881.0	
	80 %	608.1	812.7	274.1	3.470	34.81	0.0	0.0	7.6	1.8	0.0	3185.7	816.0	920.2	
JP6	Idle	415.4	216.8	62.7	1.089	20.94	885.6	4.2	2.7	44.3	8.5	3048.2	599.2	592.0	
	5 %	466.3	292.8	31.2	1.560	25.36	988.9	10.2	3.1	23.6	3.3	3094.7	560.5	638.3	
	45 %	566.3	566.4	283.7	2.345	32.17	1308.9	24.6	4.4	2.0	0.3	3137.0	771.5	896.4	
	80 %	611.8	752.9	275.7	3.121	34.95	1416.7	20.2	6.7	2.5	0.0	3137.2	839.8	985.9	
JP6	Idle	415.4	216.8	62.7	1.089	20.94	885.6	4.2	2.7	44.3	8.5	3048.2	599.2	592.0	
	5 %	466.3	292.8	31.2	1.560	25.36	988.9	10.2	3.1	23.6	3.3	3094.7	560.5	638.3	
	45 %	566.3	566.4	283.7	2.345	32.17	1308.9	24.6	4.4	2.0	0.3	3137.0	771.5	896.4	
	80 %	611.8	752.9	275.7	3.121	34.95	1416.7	20.2	6.7	2.5	0.0	3137.2	839.8	985.9	
JP4/B2	Idle	412.4	208.7	62.0	1.043	20.39	936.1	10.4	1.1	59.9	3.3	3123.1	528.0	602.5	
	5 %	462.4	297.9	31.4	1.592	25.43	937.8	22.5	2.0	33.7	1.5	3169.2	584.8	662.2	
	45 %	581.6	623.2	283.3	2.676	32.91	1312.2	34.5	5.1	5.2	0.0	3218.2	787.4	880.0	
	80 %	619.8	794.4	278.5	3.157	34.75	1449.4	28.9	5.0	3.6	0.0	3220.7	857.8	987.0	
JET A1	Idle	417.9	223.9	61.3	1.048	21.50	933.8	2.8	1.5	46.7	5.4	3071.1	501.5	572.6	
	5 %	459.2	293.9	79.4	1.597	25.41	969.2	4.0	1.6	28.5	1.8	3109.5	554.4	636.1	
	45 %	571.4	621.2	282.4	2.640	32.85	1313.4	20.1	2.3	3.0	0.3	3153.9	740.6	855.5	
	80 %	615.8	808.6	276.1	3.262	34.88	1427.2	20.3	3.1	0.0	0.0	3159.3	814.1	942.2	
JET A1/B2	Idle	410.8	221.9	63.1	1.238	21.27	939.4	10.2	2.3	47.6	2.2	3141.5	518.0	625.9	
	5 %	456.4	303.9	31.6	1.683	25.76	955.0	16.0	5.4	28.2	2.3	3171.8	569.3	628.7	
	45 %	567.7	650.5	284.7	2.921	33.36	1247.8	33.0	6.1	3.1	0.0	3217.4	753.3	883.0	
	80 %	607.7	852.2	281.2	3.479	35.53	1375.5	33.3	7.2	0.9	0.0	3220.8	811.5	927.6	
Jet Sands LH	Idle	413.8	225.0	61.8	1.247	21.58	926.7	6.1	2.4	53.1	7.0	3083.4	509.2	552.0	
	5 %	454.0	293.9	30.4	1.633	25.47	960.0	12.8	3.3	32.6	3.6	3125.0	562.5	617.7	
	45 %	566.0	624.2	282.3	2.744	32.93	1320.0	32.5	6.0	5.3	0.0	3177.7	752.0	848.2	
	80 %	605.4	804.6	276.6	3.289	34.94	1401.7	32.5	7.1	4.2	0.0	3179.5	822.8	935.9	
Jet Sands LH	Idle	411.5	211.9	63.6	1.061	20.71	932.2	2.9	2.3	52.1	3.0	3083.1	517.6	585.5	
	5 %	462.5	294.9	31.5	1.686	25.44	964.7	7.3	2.6	27.1	3.6	3111.8	569.7	639.3	
	45 %	579.4	630.3	282.6	2.703	32.53	1332.2	23.7	5.6	1.1	0.0	3171.9	753.3	883.0	
	80 %	614.6	794.4	273.1	3.193	34.64	1421.7	23.7	7.1	2.7	0.0	3179.5	822.8	935.9	
Jet Sands LH	Idle	411.5	211.9	63.6	1.061	20.71	932.2	2.9	2.3	52.1	3.0	3083.1	517.6	585.5	
	5 %	462.5	294.9	31.5	1.686	25.44	964.7	7.3	2.6	27.1	3.6	3111.8	569.7	639.3	
	45 %	579.4	630.3	282.6	2.703	32.53	1332.2	23.7	5.6	1.1	0.0	3171.9	753.3	883.0	
	80 %	614.6	794.4	273.1	3.193	34.64	1421.7	23.7	7.1	2.7	0.0	3179.5	822.8	935.9	

Simplex 2.2 FN Nozzle, 54 Cabin Sled

FUEL	COND No.	T3 (K)	P3 (kPa)	Wf (kg/hr)	X3 (kg/s)	X2 (hr)	T4 (K)	Smoke Number	EF(MOX) (g/kg)	EF(CO) (g/kg)	EF(HC) (g/kg)	EF(CO2) (g/kg)	Wf(ave) (K)	Profile Factor	Pattern Factor
Shale JP8	Idle	403.1	290.6	62.0	0.898	19.97	911.1	2.7	2.1	41.7	4.5	3079.0	508.4	585.6	
	5	465.3	293.9	80.2	1.583	25.46	983.9	4.5	2.3	20.7	5.4	3109.9	561.2	641.8	
	45	574.7	595.8	203.3	2.555	32.94	1320.6	17.7	5.3	1.3	1.7	3150.5	742.5	941.4	
	80	608.5	756.1	275.7	3.107	35.06	1443.3	13.5	6.0	0.5	0.6	3154.8	813.9	941.8	0.442
	100	632.1	822.6	315.5	3.488	36.27	1477.2	17.0	5.6	0.0	0.0	3157.2	846.5	934.2	0.053
JP10	Idle	393.2	199.6	51.2	0.925	19.83	892.2	5.3	2.4	60.8	12.9	3087.2	501.7	584.2	
	5	450.6	287.8	80.1	1.552	25.17	967.2	8.8	3.5	40.4	5.8	3148.7	561.9	641.7	
	45	564.2	609.0	201.2	2.753	33.17	1272.8	33.3	6.2	3.0	0.5	3222.1	774.6	1141.1	
	80	601.1	787.1	276.2	2.189	35.06	1423.4	31.5	5.4	1.9	0.0	3225.2	856.9	1415.5	0.068
	100	627.5	993.7	316.6	3.715	36.67	1429.4	32.5	7.9	1.6	0.0	3225.7	877.1	1371.9	0.513
EPR3-3	Idle	413.6	215.8	62.2	1.089	21.02	921.7	5.6	2.5	52.1	9.4	3081.0	517.5	584.1	
	5	443.4	263.5	75.2	1.429	24.00	982.8	9.6	3.3	36.1	6.8	3113.1	556.9	634.4	
	45	565.3	558.8	189.4	2.585	32.18	1275.6	33.1	6.1	3.1	0.0	3183.8	767.1	1131.5	
	80	602.2	742.7	259.5	3.180	34.95	1378.9	29.1	7.0	1.9	0.0	3185.6	846.0	1389.3	0.065
	100	622.7	862.3	297.1	3.511	36.13	1420.6	27.7	8.7	1.6	0.0	3186.0	865.4	1340.0	0.453
JP4	Idle	415.4	203.7	62.6	1.029	20.91	927.2	2.9	3.0	35.7	3.2	3070.1	521.4	596.4	
	5	464.2	296.9	81.2	1.610	25.40	979.4	8.5	3.4	19.4	1.5	3106.6	574.3	669.0	
	45	577.3	623.2	203.6	2.617	32.73	1324.4	26.0	7.1	2.1	0.0	3137.8	782.6	874.6	
	80	623.4	824.8	281.9	3.266	34.96	1435.5	18.5	6.1	1.7	0.0	3138.4	844.0	936.7	0.049
	100	637.4	932.2	319.9	3.760	36.86	1435.6	20.6	7.2	1.6	0.0	3138.7	856.1	955.7	0.455
JP5	Idle	413.8	207.7	62.1	0.925	20.40	906.1	11.9	2.6	76.1	14.7	3114.1	537.8	609.9	
	5	466.8	292.8	80.9	1.565	25.33	984.4	23.8	3.2	47.7	8.2	3176.5	603.7	667.7	
	45	592.3	648.5	202.5	2.849	33.79	1278.3	45.0	6.3	6.4	2.3	3253.0	817.1	983.9	
	80	628.3	814.7	280.2	3.215	35.26	1446.1	41.5	8.6	7.1	1.4	3258.9	893.1	1195.1	0.000
	100	642.1	931.2	318.0	0.000	0.00	0.0	C.C.	0.0	0.0	0.0	0.0	899.9	1146.0	0.000
JP4/S2	Idle	420.5	218.9	63.0	1.216	21.34	955.6	9.5	2.7	42.6	1.0	3156.6	532.4	600.1	
	5	465.8	295.9	81.4	1.583	25.42	988.9	21.5	3.2	24.2	2.3	3182.1	586.8	661.7	
	45	578.1	624.2	204.2	2.699	33.00	1307.2	42.6	4.9	1.3	0.7	3222.3	797.8	896.8	
	80	619.1	815.7	278.9	3.211	34.95	1436.1	34.1	5.9	0.5	0.4	3244.4	853.4	947.5	0.053
	100	642.1	931.2	318.0	3.656	36.83	1455.6	26.8	7.0	0.1	0.0	3226.1	871.5	957.8	0.434
JET A1	Idle	420.0	220.9	62.2	1.216	21.38	948.9	3.9	2.8	41.0	3.3	3085.8	512.1	587.3	
	5	463.3	296.9	80.8	1.601	25.46	979.4	6.3	2.8	24.5	2.3	3114.4	559.1	650.5	
	45	576.6	628.2	202.8	2.798	33.03	1303.6	18.7	5.1	2.3	0.0	3155.7	745.0	859.4	
	80	616.8	826.6	276.5	3.198	34.85	1431.1	21.0	3.8	1.5	0.0	3156.9	815.4	905.0	0.052
	100	640.5	929.2	318.6	3.665	36.80	1453.9	16.6	4.2	1.5	0.0	3156.9	843.0	940.2	0.415
JET A1/S2	Idle	431.1	238.7	61.6	1.429	20.41	890.6	7.7	2.5	54.7	4.6	3131.7	511.4	599.5	
	5	452.8	299.9	80.0	1.719	25.57	932.2	16.2	3.2	34.5	3.8	3157.6	564.9	655.3	
	45	561.7	620.1	200.6	2.802	32.92	1245.0	43.1	6.0	3.0	0.5	3216.0	763.9	883.8	
	80	601.7	819.8	274.5	3.470	34.95	1456.7	41.2	7.3	2.8	0.0	3217.9	820.0	936.1	0.052
	100	616.7	904.5	315.6	3.751	36.10	1411.7	40.4	7.9	2.0	0.0	3219.1	843.0	940.2	0.415
JET A1/S2	Idle	431.1	238.7	61.6	1.429	20.41	890.6	7.7	2.5	54.7	4.6	3131.7	511.4	599.5	
	5	452.8	299.9	80.0	1.719	25.57	932.2	16.2	3.2	34.5	3.8	3157.6	564.9	655.3	
	45	561.7	620.1	200.6	2.802	32.92	1245.0	43.1	6.0	3.0	0.5	3216.0	763.9	883.8	
	80	601.7	819.8	274.5	3.470	34.95	1456.7	41.2	7.3	2.8	0.0	3217.9	820.0	936.1	0.052
	100	616.7	904.5	315.6	3.751	36.10	1411.7	40.4	7.9	2.0	0.0	3219.1	843.0	940.2	0.415
JET A1/S2	Idle	431.1	238.7	61.6	1.429	20.41	890.6	7.7	2.5	54.7	4.6	3131.7	511.4	599.5	
	5	452.8	299.9	80.0	1.719	25.57	932.2	16.2	3.2	34.5	3.8	3157.6	564.9	655.3	
	45	561.7	620.1	200.6	2.802	32.92	1245.0	43.1	6.0	3.0	0.5	3216.0	763.9	883.8	
	80	601.7	819.8	274.5	3.470	34.95	1456.7	41.2	7.3	2.8	0.0	3217.9	820.0	936.1	0.052
	100	616.7	904.5	315.6	3.751	36.10	1411.7	40.4	7.9	2.0	0.0	3219.1	843.0	940.2	0.415
JET A1/S2	Idle	431.1	238.7	61.6	1.429	20.41	890.6	7.7	2.5	54.7	4.6	3131.7	511.4	599.5	
	5	452.8	299.9	80.0	1.719	25.57	932.2	16.2	3.2	34.5	3.8	3157.6	564.9	655.3	
	45	561.7	620.1	200.6	2.802	32.92	1245.0	43.1	6.0	3.0	0.5	3216.0	763.9	883.8	
	80	601.7	819.8	274.5	3.470	34.95	1456.7	41.2	7.3	2.8	0.0	3217.9	820.0	936.1	0.052
	100	616.7	904.5	315.6	3.751	36.10	1411.7	40.4	7.9	2.0	0.0	3219.1	843.0	940.2	0.415
JET A1/S2	Idle	431.1	238.7	61.6	1.429	20.41	890.6	7.7	2.5	54.7	4.6	3131.7	511.4	599.5	
	5	452.8	299.9	80.0	1.719	25.57	932.2	16.2	3.2	34.5	3.8	3157.6	564.9	655.3	
	45	561.7	620.1	200.6	2.802	32.92	1245.0	43.1	6.0	3.0	0.5	3216.0	763.9	883.8	
	80	601.7	819.8	274.5	3.470	34.95	1456.7	41.2	7.3	2.8	0.0	3217.9	820.0	936.1	0.052
	100	616.7	904.5	315.6	3.751	36.10	1411.7	40.4	7.9	2.0	0.0	3219.1	843.0	940.2	0.415
JET A1/S2	Idle	431.1	238.7	61.6	1.429	20.41	890.6	7.7	2.5	54.7	4.6	3131.7	511.4	599.5	
	5	452.8	299.9	80.0	1.719	25.57	932.2	16.2	3.2	34.5	3.8	3157.6	564.9	655.3	
	45	561.7	620.1	200.6	2.802	32.92	1245.0	43.1	6.0	3.0	0.5	3216.0	763.9	883.8	
	80	601.7	819.8	274.5	3.470	34.95	1456.7	41.2	7.3	2.8	0.0	3217.9	820.0	936.1	0.052
	100	616.7	904.5	315.6	3.751	36.10	1411.7	40.4	7.9	2.0	0.0	3219.1	843.0	940.2	0.415
JET A1/S2	Idle	431.1	238.7	61.6	1.429	20.41	890.6	7.7	2.5	54.7	4.6	3131.7	511.4	599.5	
	5	452.8	299.9	80.0	1.719	25.57	932.2	16.2	3.2	34.5	3.8	3157.6	564.9	655.3	
	45	561.7	620.1	200.6	2.802	32.92	1245.0	43.1	6.0	3.0	0.5	3216.0	763.9	883.8	
	80	601.7	819.8	274.5	3.470	34.95	1456.7	41.2	7.3	2.8	0.0	3217.9	820.0	936.1	0.052
	100	616.7	904.5	315.6	3.751	36.10	1411.7	40.4	7.9	2.0	0.0	3219.1	843.0	940.2	0.415
JET A1/S2	Idle	431.1	238.7	61.6	1.429	20.41	890.6	7.7	2.5	54.7	4.6	3131.7	511.4	599.5	
	5	452.8	299.9	80.0	1.719	25.57	932.2	16.2	3.2	34.5	3.8	3157.6	564.9	655.3	
	45	561.7	620.1	200.6	2.802	32.92	1245.0	43.1	6.0	3.0	0.5	3216.0	763.9	883.8	
	80	601.7	819.8	274.5	3.470	34.95	1456.7								